WELL COMPLETION REPORT
INTERPRETATIVE

THYLACINE-2

T/30P

OFFSHORE OTWAY BASIN

June 2004

Origin Energy Resources Ltd
339 Coronation Drive
MILTON, 4064
Brisbane, Queensland
Australia

TABLE OF CONTENTS

1. *WELL INDEX SHEET* 1

2. *WELL SUMMARY* 3

3. *HYDROCARBONS* 4

4. *STRATIGRAPHY* 8

5. *PETROPHYSICAL AND CORE SUMMARY* 18

   5.1 *Petrophysical Summary* 18

   5.2 *Core Analysis Summary* 18

6. *GEOPHYSICAL DISSCUSSION* 20

   6.1 *Seismic Data* 20

   6.2 *Structure* 20

   6.3 *Seismic Amplitudes* 26

   6.4 *Actual versus Predicted depths* 26

7. *GEOLOGICAL DISCUSSION* 29

   7.1 *Previous Exploration* 30

   7.2 *Regional Geology* 31

   7.3 *Contributions to Geological Concepts and Conclusions* 33

8. *REFERENCES* 35

TABLES

1. Thylacine-2 Reservoir Summary
2. Predicted versus Actual Formation tops
3. Previous drilling history, eastern offshore Otway Basin

FIGURES

1. Thylacine-2 Location Map
2. Top Porosity depth structure map over Thylacine Prospect
3. Offshore Otway Stratigraphic Section
4. Predicted versus Actual Stratigraphy
5. Investigator 3D and 2D Seismic Survey Location Map
6. Composite 3D seismic traverse through Thylacine-1 and Thylacine-2
7. Close-up composite 3D seismic traverse through the reservoir section in Thylacine-1 and Thylacine-2
8. Variance Cube Time Slice (1512 ms TWT) through Thylacine Prospect
9. 3D Inline 1150 showing Top Porosity seismic amplitude anomaly at Thylacine-2
10. Thylacine-2 Time-Depth curve
11. Tectonic Elements of the Otway Basin

APPENDICES

1. Petrophysics Report
2. MDT Report
3. DST Interpretation Report
4. Geochemistry Report
5. Palynological Report
6. Petrology Report
7. Core Interpretation
8. Special Core Analysis

ENCLOSURES

1. Composite Log

1. WELL INDEX SHEET

Permit Interests:	Origin Energy Resources Ltd (30%) - OPERATOR Woodside Energy Ltd (50%) Benaris International NV (20%)	
Rig on Location:	18:20hrs	17/08/2001
Spud:	01:45hrs	28/08/2001
Reached TD:	12:00hrs	08/09/2001
Rig Released:	07:30hrs	28/09/2001
Total Rig Days:	27.8 days	
Rig Name:	Ocean Bounty (Semi-submersible)	
Drilling Contractor:	Diamond Offshore General Co.	
Total Depth:	2525.0 mMDRT (Driller) 2535.2 mMDRT (Schlumberger)	
Well Status:	Plugged & Abandoned	

Well Name:	Thylacine-2
Basin:	Offshore Otway
Permit:	T/30P
Type:	Vertical Appraisal Well
Water Depth:	101.2m LAT
Elevation:	25m (RT-sea level)
Latitude:	039° 13' 42.675" South
Longitude:	142° 50' 55.000" East
Easting:	659 564.5 metres
Northing:	5 656 220.4 metres
	(AGD 84; AMG Zone 54, Central Meridian 141° East) Deviation from intended location = 1.7m toward 247°
Seismic Reference:	Inline 1150, CDP 1250
Actual Well Cost:	A$21,287,481

Formation Tops:

FORMATION / *SEISMIC MARKER*	**TOPS (m)**				**REMARKS/SHOWS**
	MDRT	SUBSEA	THICK	TWT(ms)	
Port Campbell Limestone / *Seabed*	126.2	101.2	193.8	0.132	No returns 126.2 – 557 mMDRT
Gellibrand Marl			1005.7		
Upper Gellibrand Marl	320.4	295.4	(410.5)	-	Below 557 mMDRT, calcareous claystone grading to argillaceous calcilutite with lesser argillaceous calcisiltite and rare calcarenite
Middle Miocene Seismic Marker	-	-		0.345	
Lower Gellibrand Marl *Base Miocene Seismic Marker*	730.9	705.9	(595.2)	-	calcareous claystone with lesser argillaceous calcisiltite, argillaceous calcilutite and rare sandstone
Narrawaturk Marl	1326.1	1301.1	123.1	1.079	calcareous claystone and argillaceous calcilutite with minor calcareous sandstone
Mepunga Formation	1449.2	1424.2	14.4	1.161	sandstone
Paaratte Formation / *Base Tertiary*	1463.6	1438.6	361.8	1.171	claystone and silty claystone with minor interbedded sandstone and trace argillaceous calcilutite
Belfast Formation	1825.0	1800.0	411.9	1.407	claystone with occasional siltstone and sandstone stringers
Thylacine Member	2143.3	2118.3	(94.0)	1.595	interbedded sandstone, siltstone and claystone **Gas shows**
Flaxman Formation	2237.3	2212.3	116.8	1.646	interbedded argillaceous siltstone and sandstone **Gas shows**
Waarre Formation			170.9+		
Upper Waarre Formation	2354.1	2329.1	(170.9+)	1.708	sandstone and minor siltstone
TD (Logger)	**2535.2**	**2515.2**			

Formation Evaluation While Drilling:

Suite #	Run #	Interval (mMDRT)	Logs Acquired
1	1	557 – 2109m	Powerpulse/CDR/MVC/IWOB

Wireline Logs:

Suite #	Run #	Interval (mMDRT)	Logs Acquired
1	1	2103.5 - 2530.0	PEx (HRLA)-GPIT-DSI
1	2	2103.5 - 2530.0	FMI-GR-LEH-QT-GPIT
1	3	2144.0 - 2493.0	MDT-GR
1	4	1197.0 - 2530.0	CSI-GR

Cores:

Conventional:

Core #	Interval (mMDRT)	Cut (m)	Recovered (m)	Formation
1	2150.0 – 2203.5	53.5	49.87m (93%)	Thylacine Member
2	2203.5 – 2258.5	55.0	53.9m (98%)	Thylacine Member & Flaxman Fm
3	2258.5 – 2316.0	57.5	56.05m (97.5%)	Flaxman Fm

Sidewall:
No sidewall cores were taken.

Pressure Testing and Fluid Sampling:

Suite#	Run#	Type	Interval (mMDRT)	Total Tests	Valid Tests	Supercharged	Tight	Samples Collected
1	3	MDT	2144.0 – 2206.5	47	26	4	5	4

Hole & Casing Details:

Hole Size	Interval (mMDRT)	Casing Size	Shoe Setting Depth (mMDRT)
36”	126.0 – 185.0	30” x 20”	183.9
17.5”	185.0 – 557.0	$13^{3/8}$”	550.7
12.25”	557.0 – 2109.0	$10^{3/4}$ “ x $9^{5/8}$”	2101.3
8.5”	2109.0 – 2525.0	7”	2524.0

Abandonment Plugs:

Abandonment Plug #	Interval (mMDRT)
1	2146.0 - 2262.0
2	1800.0 - 1890.0
3	153.0 - 233.0

2. WELL SUMMARY

Thylacine-2 is a vertical appraisal well located in the Tasmanian part of the offshore Otway Basin in the northwest corner of petroleum exploration permit T/30P, approximately 240 km southwest of Melbourne, 70 km south of Port Campbell, and 150 km southeast of Portland (Figure 1). The well was designed to test the western flank of the Thylacine Gas Field, approximately 5.7 km west-northwest of the discovery well, Thylacine-1.

Thylacine-2 spudded on the 28th August 2001 in 101.2 m of water. It was drilled by the semi submersible rig Ocean Bounty and reached a total depth of 2525 mMDRT. The Thylacine Structure (Figure 2) is a large, triangular, composite horst developed on a major N-NW trending ridge. The structure is fault-bounded to the northeast, south, and east, and pitches to the west. Prior to drilling, the primary objectives were the Turonian age Flaxman Formation and Upper Waarre Formation, but only the Flaxman Formation proved to be hydrocarbon bearing, with the gas column extending upwards into a previously unknown, younger Santonian reservoir unit called the Thylacine Member of the Belfast Formation. The well is interpreted to have encountered a 182.4 m gas column with a net gas-bearing sand pay of 80.2 m (N:G = 44%), average effective porosity of 14.8%, and average gas permeability of 1 mD. Production testing resulted in a maximum flow rate of 28 MMscfd. Thylacine-2 was plugged and abandoned and the rig released at 07:30 hrs on the 28th September 2001.

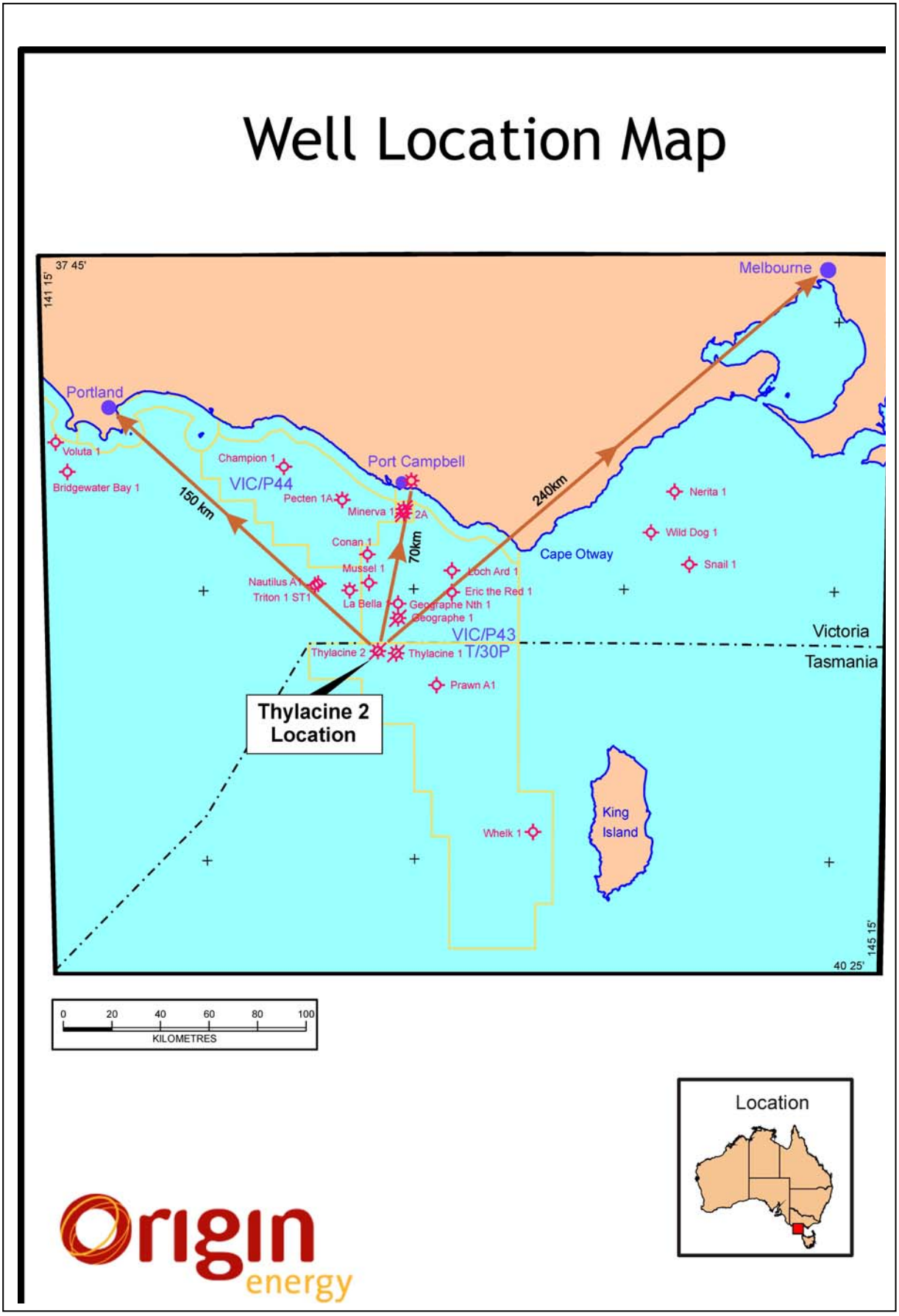


Figure 1 – Thylacine 2 Location Map

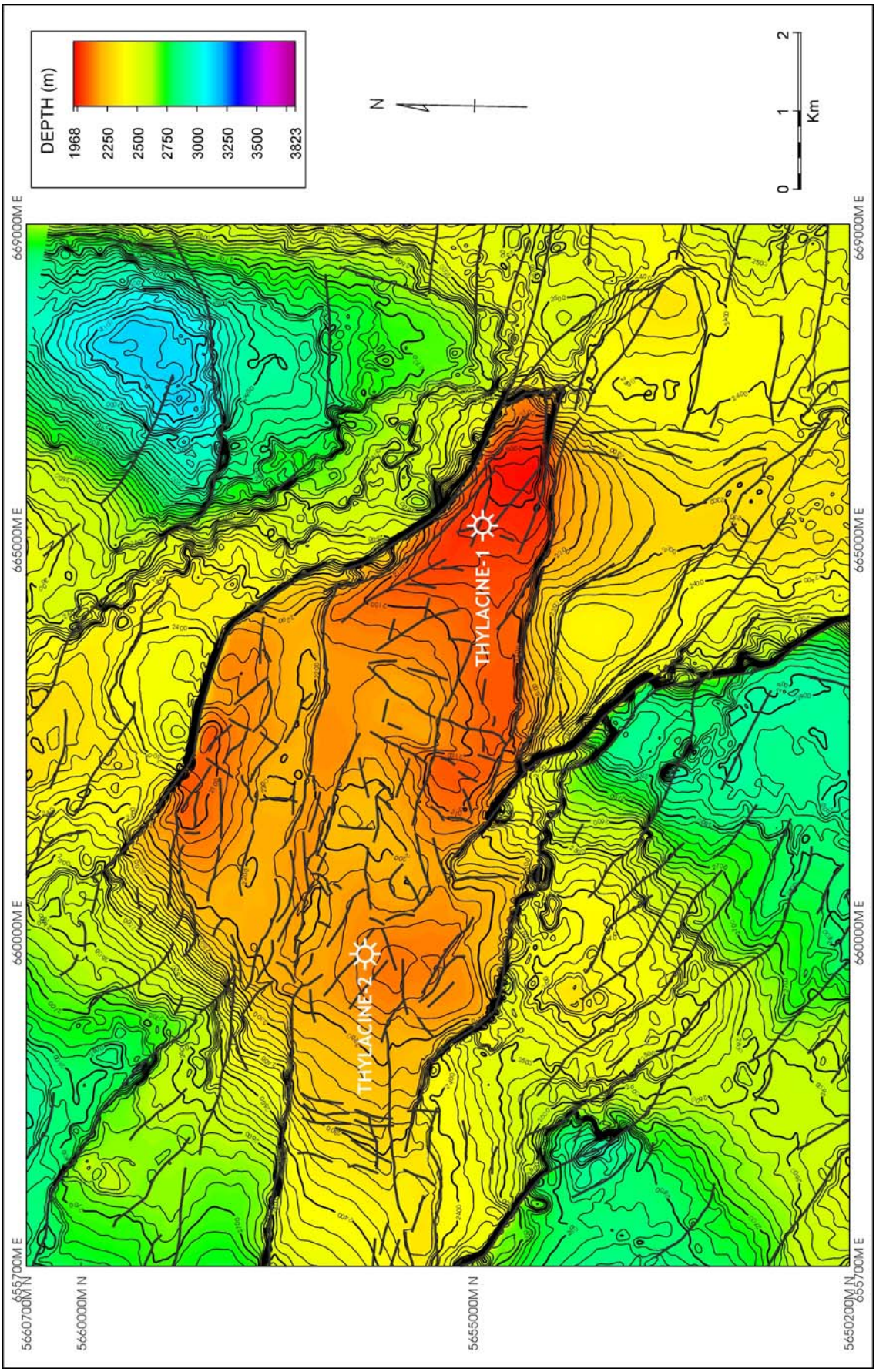


Figure 2 – Top Porosity depth structure map over Thylacine Prospect

3. HYDROCARBONS

Background gas readings in Thylacine-2 remained fairly steady down to the base of the Tertiary (range 0.02 - 0.22%). No significant gas peaks were recorded and no fluorescence was observed.

Immediately upon entering the Late Cretaceous section, background gas readings in the well increased slightly to between 0.018 – 0.30%, and then remained fairly steady down through the Paaratte and Belfast Formations to the top of the Thylacine Member. No fluorescence was observed over this interval.

Immediately prior to entering the Thylacine Member (2141.5 – 2237.0 mMDRT), the gas readings rose sharply, increasing from 0.3% at 2039 mMDRT to 4.4% at 2243 mMDRT, and then dropped back slightly before peaking again at 4.0% at 2146 mMDRT. The gas reading then dropped back sharply below background levels at 2151 mMDRT, and over the next 25 m fluctuated between 0.02 and 0.15% before gradually rising again, reaching 3.4% in the middle of the Thylacine Member at about 2188 mMDRT. The high gas readings then continued down in to the lower part of the Thylacine Member, peaking at 6.8% before dropping back down to between 0.1 and 0.5% near the base of the unit. The gas readings in the well then began to climb again upon approaching the top of the Flaxman Formation at 2237 mMDRT, peaking slightly above 5.0% at 2242 mMDRT and 2255 mMDRT, after which the readings started to decline, fluctuating between 0.07 and 1.0% from 2258 mMDRT down to TD.

No fluorescence was observed in any of the cuttings or core recovered from the Thylacine Member or Flaxman Formation. However, Core 1 (2150.0 – 2203.5 mMDRT) did have a slight hydrocarbon odour, as did the top of Core 2 (2203.5-2258.5 mMDRT) and base of Core 3 (2258.5-2316 mMDRT) (see Appendix 2 of Thylacine-2 Basic WCR). The odour was primarily associated with core from the Thylacine Member of the Belfast Formation.

Log analysis (Appendix 1) indicates a 182.4 m gross gas column was intersected in Thylacine-2 extending down from the top of the Thylacine Member into the Flaxman Formation. MDT measurements (Appendix 2) indicate the presence of at least four, possibly five, separate hydraulic systems over the reservoir interval in Thylacine-2, with significant pressure offsets between the various sands within the Thylacine Member and Flaxman Formation. The MDT data suggest the Flaxman Formation sands encountered in

Thylacine-2 are not in communication with the equivalent Flaxman Formation sequence in Thylacine-1, as they also have significantly deeper interpreted Free Water Levels. In addition, the Upper Sand within the Thylacine Member is also interpreted to be a separate system to both the Flaxman Formation sands in Thylacine-2 and equivalent Thylacine Member sequence in Thylacine-1. Insufficient valid pressure data was obtained from the Lower Sand within the Thylacine Member to make any conclusions about this reservoir at Thylacine-2.

Two production tests were run on Thylacine-2 (see Appendix 3). DST1 (2176 – 2226 mMDRT) tested the Thylacine Member and recorded a maximum flow rate of 7.6 MMscfd on a 1" choke. DST2 tested both the Thylacine Member (2176 – 2226 mMDRT) and underlying Flaxman Formation (2296 – 2302 mMDRT) and recorded a maximum commingled flow rate of 28 MMscfd on a 1.5" choke.

Analysis of gas recovered from Thylacine-2 (Appendix 2) indicates it has a slightly lower CO_2 content (8 - 9 %) than the gas in Thylacine-1. The average liquids content is, however, similar to that in Thylacine-1, although a large variation in LPG content (10 – 20 bbl/MMscf) was observed between the two samples recovered from Thylacine-2. High Temperature Gas Chromatographic analysis of dead condensate recovered from DST2 (Appendix 4) indicates there is no risk of wax precipitation from the Thylacine fluid during production.

4. STRATIGRAPHY

The generalised stratigraphy of the eastern offshore Otway Basin is illustrated in Figure 3 and the stratigraphic section intersected by Thylacine-2 in Figure 4. As can be seen in Figure 4, the actual stratigraphy differs from the prognosed stratigraphy in a number of areas. Key differences include: 1) a thicker-than-expected Narrawaturk Marl, 2) a thinner-than-expected Mepunga Formation, 3) the absence of the Pember Mudstone and Dilwyn Formation, 4) the presence of an unexpected sandy interval at the base of the Belfast Formation, and 5) a thinner-than-expected Flaxman Formation.

A report by Dr Roger Morgan (Morgan Palaeo Associates) on the age and palaeoenvironment of the sediments penetrated in Thylacine-2 is included in Appendix 5. The detailed palynological sampling programme conducted during the drilling of Thylacine-2 (45 core and cuttings samples) has, in co-ordination with the Thylacine-1 and Geographe-1 sampling programmes, allowed Dr Morgan to significantly refine the existing Late Cretaceous spore-pollen and dinoflagellate zonation schemes for the Otway Basin, thereby dramatically increasing their resolution. As a result, it is now possible to correlate units between wells within the Shipwreck Trough far more accurately than before.

Lithological descriptions from ditch cuttings, sidewall core and conventional core, together with the MWD and wireline log interpretation, provide the basis for the stratigraphic breakdown in Enclosure 1.

HEYTESBURY GROUP

Port Campbell Limestone (126.2 – 320.4 mMDRT)

The Port Campbell Limestone in Thylacine-2 is approximately 194 m thick. Its presence in Thylacine-2 is inferred from seismic ties to nearby wells including La Bella-1, Mussel-1 and Conan-1, as first returns in the well were not established until 557.0 mMDRT. To the north of the Shipwreck Trough, onshore, the Port Campbell Limestone is a light grey to white, medium-hard, poorly sorted, shallow marine calcarenite with abundant fossils (corals, bryozoans, foraminifera) and is Miocene in age.

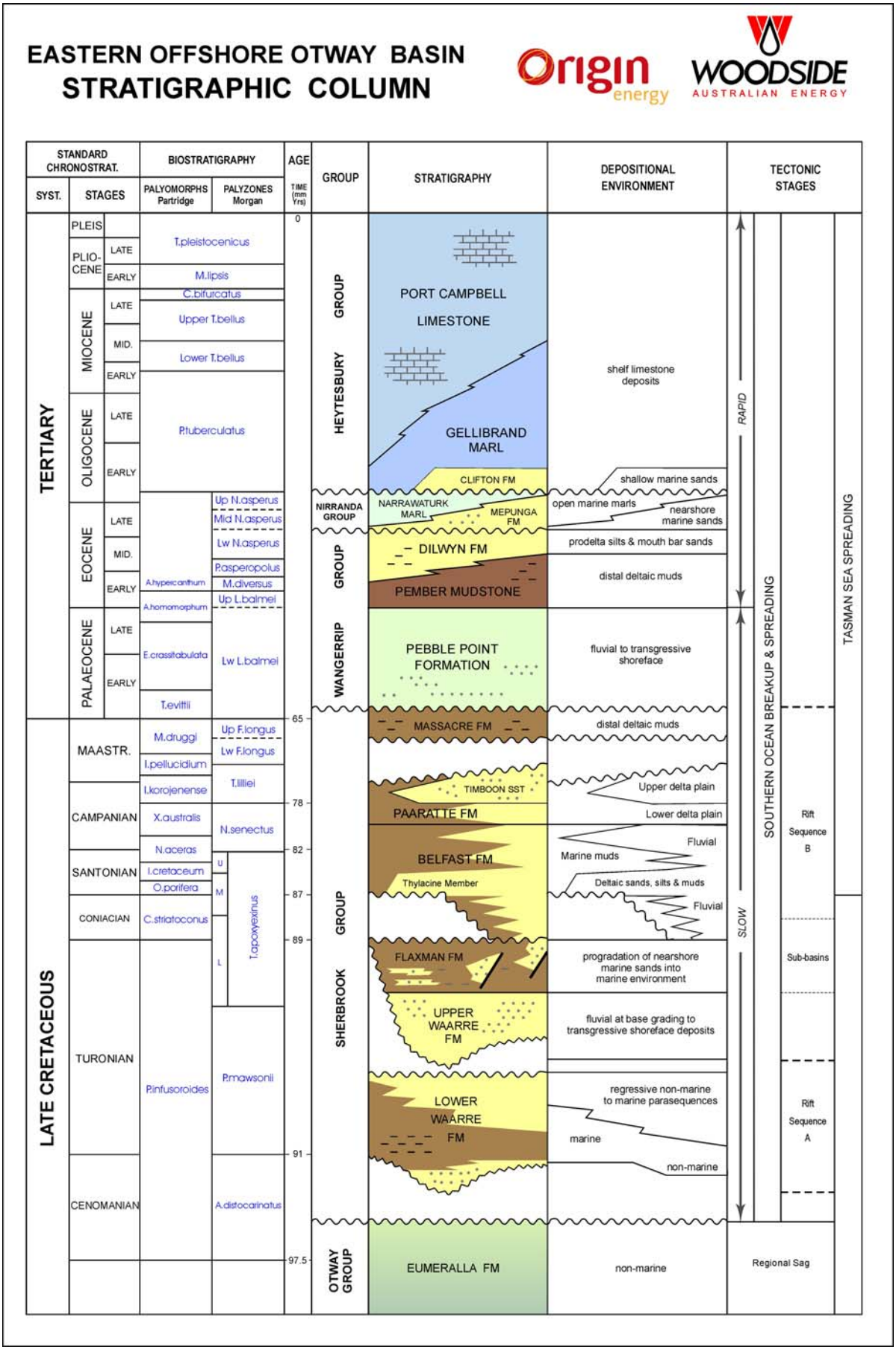


Figure 3 – Offshore Otway Stratigraphic Section

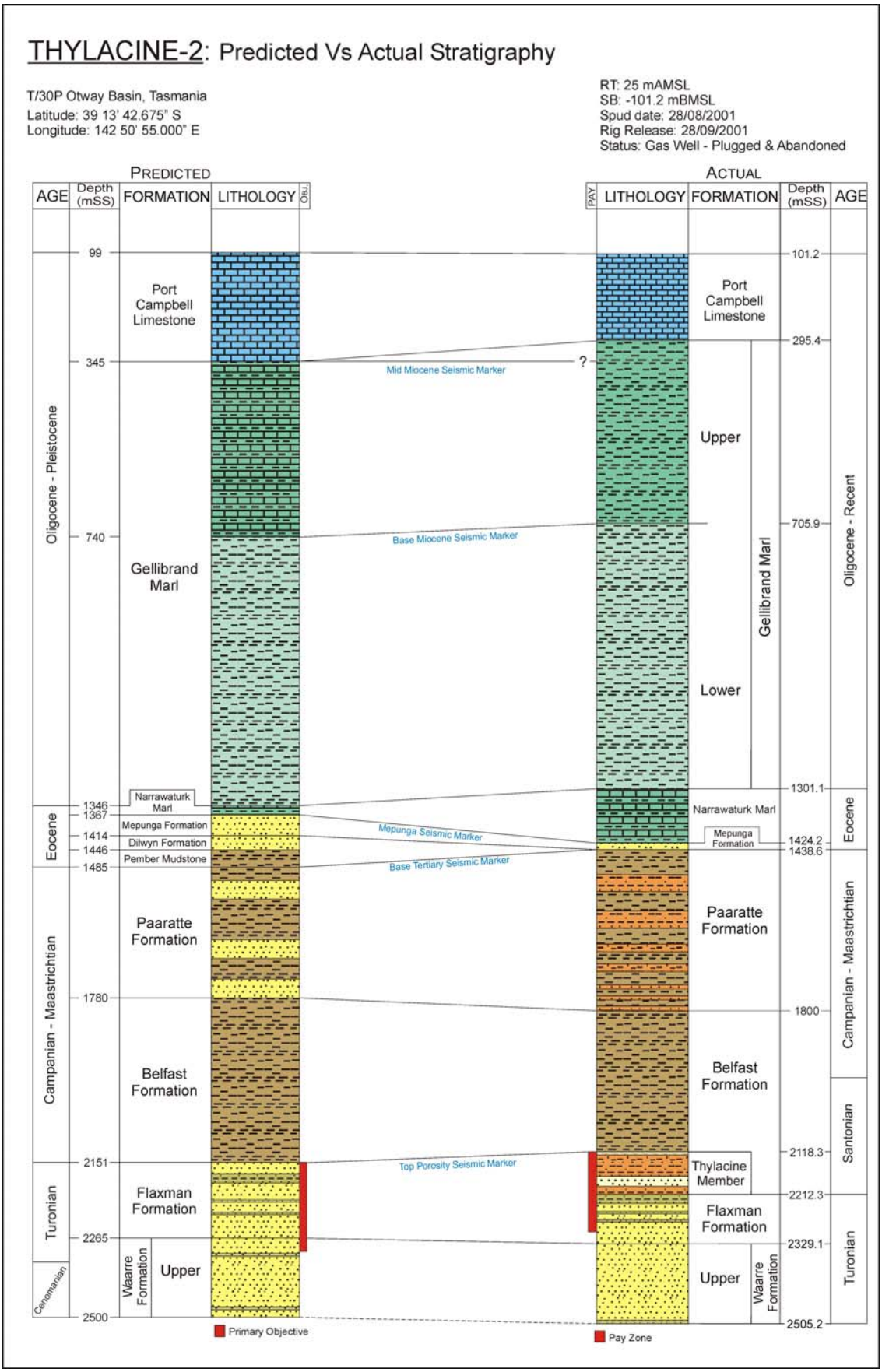


Figure 4 – Predicted versus Actual Stratigraphy

Gellibrand Marl (320.4 – 1326.1 mMDRT)

The Gellibrand Marl is a shallow marine calcareous claystone that gradationally underlies the Port Campbell Limestone. In the Shipwreck Trough, the Gellibrand Marl can be seismically divided into two units separated by a prominent seismic marker called the 'Base Miocene Seismic Marker'. The two units are here called the Upper Gellibrand Marl and Lower Gellibrand Marl. Both units are present in Thylacine-2 where they have a combined thickness of approximately 1006 m.

Upper Gellibrand Marl (320.4 – 730.9 mMDRT)

The Upper Gellibrand Marl in Thylacine-2 is approximately 410 m thick. Prior to drilling, the top of the Gellibrand Marl in the Shipwreck Trough was correlated with a prominent seismic marker called the 'Mid Miocene Seismic Marker'. This event is an unconformity surface with local canyon development that is mappable across the entire Shipwreck Trough area. In this report, the top of the Upper Gellibrand Marl in Thylacine-2 is tied to a drop in ROP like in Thylacine-1 and Geographe-1. In Thylacine-2, the drop in ROP occurs approximately 50 m stratigraphically above the predrill depth estimate for the Mid Miocene Seismic Marker (370 mMDRT).

The lithology of the upper half of the Upper Gellibrand Marl in Thylacine-2 is unknown since first returns were not established until 557 mMDRT. Below this point, the Upper Gellibrand Marl consists largely of calcareous claystone with bands of calcarenite common between 557.0 – 620.0 mMDRT. The calcareous claystone ranges from very light grey to olive grey in colour, and is soft, sub-blocky to amorphous, with rare fine-grained glauconite and pyrite nodules. The interbedded calcarenite, in contrast, is also generally very light grey to olive grey in colour, but ranges from soft to moderately hard, with occasional grains of fine quartz, occasional to common glauconite, and rare to trace specks of carbonaceous matter.

The age of the Upper Gellibrand Marl in Thylacine-2 is not known since it was not sampled for dating purposes. In Thylacine-1, the top of the Lower Gellibrand Marl is mid to late Late Oligocene in age, which suggests the Upper Gellibrand Marl in Thylacine-2 is probably the same age or younger.

Lower Gellibrand Marl / Base Miocene Seismic Marker (730.9 – 1326.1 mMDRT)

The 'Base Miocene' seismic event defines the top of the Lower Gellibrand Marl in Thylacine-2. This event is another unconformity surface with local canyon development that is mappable across the entire Shipwreck Trough area.

In Thylacine-2, the Lower Gellibrand Marl is approximately 596m thick and is composed largely of calcareous claystone, with minor interbedded argillaceous calcisiltite and argillaceous calcilutite near the top and base of the formation respectively. The calcareous claystone is light / medium grey to olive grey in colour, soft to firm, amorphous to sub-blocky, with abundant calcareous clay, rare to minor calcareous silt, and trace foraminifera, skeletal fragments, lithics, glauconite and pyrite. The argillaceous calcisiltite, which occurs near the top of the formation, is very light grey to medium grey in colour, soft to moderately hard, with abundant to very abundant calcareous clay and trace skeletal fragments, lithics and pyrite. The argillaceous calcilutite, in comparison, is very light grey to light grey in colour, soft and amorphous, with a minor component of calcareous silt.

According to cuttings descriptions, sandstone (5%) was also observed in the well between 1260 and 1320 mMDRT (see Appendix 1 Thylacine-2 Basic Data Report). The sandstone is described as loose, very-fine to fine-grained, quartzose, with a yellow - orange – brown staining, very good visual porosity (25%), and trace mica, glauconite and rare lithics.

The age of the Lower Gellibrand Marl in Thylacine-2 is not known since it was not sampled for dating purposes. However, the close proximity of Thylacine-2 to Thylacine-1, where there is some control on the age of the formation, suggests it is most likely mid – late Early Oligocene to mid – late Late Oligocene in age as well.

NIRRANDA GROUP

Narrawaturk Marl (1326.1 – 1449.2 mMDRT)

The Narrawaturk Marl in Thylacine-2 is represented by 123.1 m of interbedded calcareous claystone and argillaceous calcilutite. The calcareous claystone is light / medium grey to olive grey in colour, soft to slightly firm, amorphous to sub-blocky, with minor to abundant quartz silt, minor calcareous silt, rare grains of very fine-grained quartz, and trace pyrite, foraminifera, glauconite and lithics. The interbedded argillaceous calcilutite is very light to light-grey in colour, soft, amorphous, with abundant argillaceous material and minor calcareous silt.

The top of the Narrawaturk Marl in Thylacine-2 is picked on a lithological change coincident with a drop in ROP. It is possible the top of the formation could be as deep as 1417.3 mMDRT, where there are significant breaks in the GR, resistivity and DT logs, but the higher pick (1326.2 mMDRT) is favoured as it ties better with the preferred seismic pick, plus there is a drop in ROP at this depth coincident with a break in the resistivity logs.

Palynological analysis of cutts from 1410 – 1420 mMDRT (Appendix 5) indicate the lower part of the Narrawaturk Marl in Thylacine-2 is Middle Eocene in age based on the presence of *D.heterophylcta* Zone dinoflagellate and *N.asperus* Zone spore-pollen. The predominance of dinoflagellate over spore-pollen suggests the formation was deposited in an offshore marine environment.

Mepunga Formation (1449.2 – 1463.6 mMDRT)

The Mepunga Formation in Thylacine-2 is represented by 14.4 m of light olive-grey, fine- to medium-grained quartz sandstone with an argillaceous calcareous matrix, abundant glauconite, and poor visual porosity. The top of the formation was picked on a break on the GR log at 1449.2 mMDRT coinciding with a sharp increase in the percentage of sandstone cuttings at approximately 1450 mMDRT.

Palynological analysis of cutts from 1450 – 1460 mMDRT (Appendix 5) yielded Early Eocene (*P.asperopolus* Zone) spore-pollen and late Middle Eocene (*D.heterophylcta* Zone) dinoflagellate. The similarity in the size of the spore-pollen and dinoflagellate populations suggests the sediments were deposited in a shelfal marine environment. However, the disparity in ages suggests the dinoflagellate assemblage has been contaminated by cavings.

If correct, then the dinoflagellate content has also been enhanced, which suggests a more nearshore environment of deposition is likely.

SHERBROOK GROUP

Paaratte Formation (1463.6 – 1825.0 mMDRT)

The Paaratte Formation in Thylacine-2 is represented by 361.4 m of claystone and silty claystone with occasional bands of very fine- to fine-grained sandstone and silty sandstone above 1690 mMDRT. The claystones range from dark greyish-brown to medium to dark-grey in colour, while the silty claystones are medium to dark olive-grey in colour. Both lithologies range from soft to firm, and slightly sticky in places to sub-blocky, with trace amounts of glauconite and pyrite present, and trace to rare specks of carbonaceous matter.

The very fine- to fine-grained sandstones vary from greenish-grey in colour near the top of the formation above 1550 mMDRT, to white and very light grey in the middle between 1600 – 1690 mMDRT. Both sets of sands are loose to friable and poorly to moderately sorted with medium- to very coarse grains common. Cements present include calcite and pyrite, both in trace amounts, along with trace very fine carbonaceous matter and glauconite. Sands between 1600 – 1690 mMDRT also have abundant silt matrix and minor to common argillaceous matrix, with visual porosity described as tight.

Palynological data (Appendix 5) indicates the upper part of the Paaratte Formation in Thylacine-2 is at least Campanian in age based on the presence of *Upper X.australis* Zone dinoflagellate and *Upper N.senectus* Zone spore-pollen in cutts from 1505 – 1540 mMDRT. The predominance of spore-pollen over dinoflagellate suggests the sediments within this interval were deposited in a nearshore marine environment. The presence of *P.asperopolus - lower M.diversus* Zone spore-pollen in cutts (1470 – 1475 mMDRT) immediately below the top of the Paaratte Formation (1463.6 mMDRT) is most likely a result of contamination due to caving.

Belfast Formation (1825.0 – 2237.3 mMDRT)

The Belfast Formation in Thylacine-2 is represented by 412.3 m of claystone with rare bands of silty claystone and siltstone. The claystones are generally olive grey to dusky brown in colour, soft to firm, primarily non-calcareous, with trace amounts of glauconite, mica, carbonaceous matter, disseminated pyrite and occasional very-fine quartz. The silty

claystones are dark grey, soft, generally non-calcareous, with trace glauconite and carbonaceous matter, whereas the siltstones are brownish black to olive black in colour, firm to moderately hard, with trace glauconite, mica and carbonaceous matter.

The formation is undifferentiated except for a sequence of interbedded sandstone, siltstone and claystone at the base of the unit called the Thylacine Member (2143.3 – 2237.3 mMDRT). Palynological analysis of cutts from 2080 – 2137 mMDRT (Appendix 5) indicate the basal part of the Belfast Formation spans the *I.cretaceum (lower b)* to *lower N.aceras* dinoflagellate zones and *upper T.apoxyexinus* to *N.senectus* spore-pollen zones, and is Santonian to early Campanian in age. The dinoflagellate and spore-pollen occur in sub-equal proportions, which suggest the Belfast Formation in Thylacine-2 was deposited in a shelfal marine environment. However, the dinoflagellate content in the cuttings sample may have been enhanced by cavings, which would suggest a more nearshore environment of deposition is likely.

Thylacine Member (2143.3 – 2237.3 mMDRT)

The Thylacine Member in Thylacine-2 is 94 m thick. It consists of a basal 3 m thick glauconitic silty claystone overlain by a 57 m thick package of massive to faintly laminated, moderately well sorted, fine to medium grained sandstone (locally interrupted by thin, bioturbated layers of argillaceous siltstone) followed by a 35 m thick coarsening-upward intensely-bioturbated sandy siltstone. The entire unit was fully cored except for the topmost 8.5 m (see Enclosure 1). A detailed description of this core can be found in Appendix 7. The sandstones have an average QFR ratio of 75.4 : 1.4 : 23.2 and straddle the boundary separating sublitharenites from litharenites (see Appendix 6).

Detailed palynological sampling (Appendix 5) indicates the Thylacine Member in Thylacine-2 is *upper O.porifera* Zone (Early Santonian) in age, with the uppermost two to three metres of the unit possibly extending up into the *I.cretaceum lower 'b'* Zone (Middle Santonian). A nearshore to very nearshore marine environment of deposition is inferred based on the predominance of spore-pollen over dinoflagellate and the moderate to low diversity of the latter. The thick package of sandstone between 2173.9 - 2230.9 mMDRT is interpreted as liquefied gravity flows deposited in a proximal submarine ramp or slope-apron environment based on the massive appearance of the sandstones in core and the almost complete absence of bioturbation structures (see Appendix 7). The overlying coarsening upward sandy

siltstone package, in contrast, is interpreted as a shallow marine shelf succession based on the trace fossil assemblage and sedimentary structures identified in core.

Flaxman Formation (2237.3 – 2354.1 mMDRT)

The Flaxman Formation in Thylacine-2 is approximately 117 m thick. About 79 m of core was recovered from the Flaxman Formation extending from the top of the unit down to 2316.0 mMDRT (see Enclosure 1). A detailed description of this core can be found in Appendix 7. The lower half of the formation consists of a sequence of interbedded argillaceous siltstone and very fine to fine grained sandstone which is overlain by a sequence of stacked beds of argillaceous siltstone coarsening-up to very fine to fine grained sandstone. The two sequences are separated by a six metre thick fine- to coarse-grained sandstone. Bioturbation is common to locally intense throughout the entire Flaxman interval, and the sands (average QFR ratio = 95.0 : 0 : 5.0) are slightly more quartz-rich than the overlying Thylacine Member sands (average QFR ratio = 75.4 : 1.4 : 23.2).

Detailed sampling of the cored interval in combination with cuttings from the lower third of the unit indicates the Flaxman Formation in Thylacine-2 spans the *P.infusorioides upper 'a'* to *upper 'c'* dinoflagellate Zones, and is late Turonian in age (Appendix 5). An overall decrease in the percentage and diversity of dinoflagellate up-section suggests the sediments were deposited in a nearshore marine to shelf environment at the base, shallowing to nearshore to very nearshore marine toward the top.

Waarre Formation (2354.1 – 2525.0 mMDRT [TD])

The Waarre Formation in the Shipwreck Trough can be informally divided into two units based largely on environment of deposition. The two units are called (in ascending stratigraphic order) the Lower Waarre and Upper Waarre, and are separated by a major sequence boundary located within the mid *P.infusoroides* dinoflagellate Zone. The Lower Waarre is interpreted as a largely regressive unit ranging from marine at the base to non-marine near the top, while the Upper Waarre is interpreted as a transgressive unit grading from fluvial at the base to shoreface toward the top. The two units have similar high net : gross values, but the Upper Waarre sand bodies are generally thicker, cleaner, and have a distinctive blocky GR profile.

In Thylacine-2, only the Upper Waarre was intersected before the well reached its target depth.

Upper Waarre Formation (2354.1 – 2525.0 mMDRT [TD])

Thylacine-2 penetrated approximately 170 m into the Upper Waarre, but its true thickness is not known as the base of the unit was not intersected in the well. The Upper Waarre in Thylacine-2 consists largely of very light grey, very poorly sorted, very fine to coarse-grained sandstone with minor interbedded grey-black siltstone (see Enclosure 1). The sands are loose to friable, with a minor argillaceous matrix, trace calcite cement and rare silica cement. The siltstones, in comparison, are firm to hard, sub-blocky to sub fissile, with abundant to very abundant carbonaceous detritus and trace very fine grained quartz, lithic fragments, and disseminated to nodular pyrite.

Palynological analysis of cutts from 2350 – 2356 mMDRT (Appendix 5) indicates the top of the Upper Waarre in Thylacine-2 is late Turonian in age based on the presence of *P.infusorioides upper 'a'* Subzone dinoflagellate and *lower T.apoxyexinus* Zone spore-pollen. No samples were collected below 2356 mMDRT for dating purposes.

5. PETROPHYSICAL SUMMARY

5.1 Petrophysical Summary

This report details a review of the reservoir quality and hydrocarbon saturation of three Late Cretaceous formations intersected whilst drilling the exploration well, Thylacine-2 in T/30P in the Otway Basin, offshore Tasmania. The study entails an analysis of all available lithological data, and a complete petrophysical analysis. A full report is included in Appendix-1 and summarised in Table 2.

The Thylacine Member (2143.3-2237.3 mMDRT) encountered at Thylacine-2 is interpreted to have moderate reservoir quality. The unit has a net to gross of 58.4%, although the sandstones that are present contain high clay volumes, averaging 28.2%. Calculated effective porosities average only 14.8% for these reservoirs. As a result, the log-derived gas permeability is considerably reduced in comparison to other cleaner reservoirs, geometrically averaging only 0.78mD, which will negatively affect this units producibility and recovery factor. The average effective water saturation is 74.9%.

The Flaxman Formation (2237.3-2354.9 mMDRT) has much better reservoir development in part, although the overall net to gross ratio is low. The sandstones present, on average, are cleaner and have an average clay volume of 19.3%. The average effective porosity is similar (14.7%), but the average gas permeability is higher, averaging 1.4mD. This unit has a net reservoir to gross of 27.6%, and an average effective water saturation of 64.3%.

A gas-oil contact cannot be identified from the logs, and it is assumed that the reservoir at the Thylacine-2 location does not contain an oil-leg. The lowermost gas-bearing sandstone is present at 2325.7 mMDRT. A thin sandstone bed at 2334 mMDRT displays inconclusive hydrocarbon saturation. Based upon the Spontaneous Potential log, the GWC may be interpreted as low as 2343 mMDRT. Due to poor reservoir quality across the potential GWC, the FWL should be best defined by the MDT log pass. A full discussion of the petrophysical review is contained in Appendix 1.

5.2 Core Analysis Summary

See Appendix 8 for the Special Core Analysis Report.

FORMATION	TOP (mMDRT)	BASE (mMDRT)	GROSS INTERVAL (mMDRT)	NET RESERV INTERVAL (mMDRT)	AVER VCLAY (%)	AVER PHIE (%)	AVER AIR PERM (mD)	AVER GAS PERM (mD)	AVER H2O PERM (mD)	AVER SWE (%)	NET / GROSS (%)
Thylacine Member	2143.3	2237.3	94	54.92	28.2	14.79	1.04	0.78	0.28	74.88	58.43
Flaxman Fm-GWC	2237.3	2325.7	88.4	25.24	18.86	14.76	2.26	1.73	0.63	57.87	28.55
		TOTAL	**182.4**	**80.16**	**25.26**	**14.78**	**1.32**	**1.01**	**0.36**	**69.53**	**43.95**

Thylacine Member	2143.3	2237.3	94	54.92	28.2	14.79	1.04	0.78	0.28	74.88	58.43
Flaxman Formation	2237.3	2354.9	117.6	32.4	19.27	14.65	1.86	1.42	0.51	64.32	27.55
Upper Waarre Fm	2354.9	2536.24	181.34	98.64	16.9	15.88	1.15	0.87	0.31	94.64	54.4

Cut-offs Applied		
Net Pay	K gas >	0.1mD
	VCl <	40.00%

Table 1: Thylacine-2 Reservoir Summary

6. GEOPHYSICAL DISCUSSION

6.1 Seismic Data

The Investigator 3D seismic survey, acquired in 2000, covers an area of 986.4 km^2 across permits VIC/P43 and T/30P in the central Shipwreck Trough (Figure 5). The Thylacine Structure is located at the southern end of the Investigator 3D area.

Seismic data quality over the Thylacine Structure is generally very good, as the top of the reservoir objective was readily discernible over the prospect and significant stratigraphic detail was apparent (see Figures 6 & 7). The Top Porosity event is represented by a trough or hard kick (negative amplitude) on the 3D data, except within closure at Thylacine where a phase reversal occurs, consistent with a gas accumulation.

Miocene canyoning slightly degrades the seismic quality over the eastern part of the structure (Figure 6) and may be responsible for a minor amount of velocity "pull-up", but this will need to be confirmed later through detailed velocity analysis. Data quality also deteriorates to the northeast of the Thylacine Structure due to high fault frequency. Overall, though, the 3D data is of high standard, which helped reduce the pre-drill exploration risks.

6.2 Structure

The Thylacine Structure is a large composite horst located close to the axis of the Shipwreck Trough. It is fault-bounded to the south and northeast, and is triangular in shape and pitches to the west (Figure 2). The core of the structure is thought to overlie a relatively rigid basement block that has undergone less subsidence than surrounding areas. Fault mapping in the vicinity of the prospect was assisted by high quality Variance Cube™ time slices (Figure 8) combined with amplitude images extracted from the 3D seismic data set.

The Thylacine Structure is interpreted to have developed in response to repeated episodes of rifting during the break-up of Australia and Antarctica in the Late Jurassic to Late Cretaceous. The primary extension direction varied from N-S to NE-SW, resulting in normal

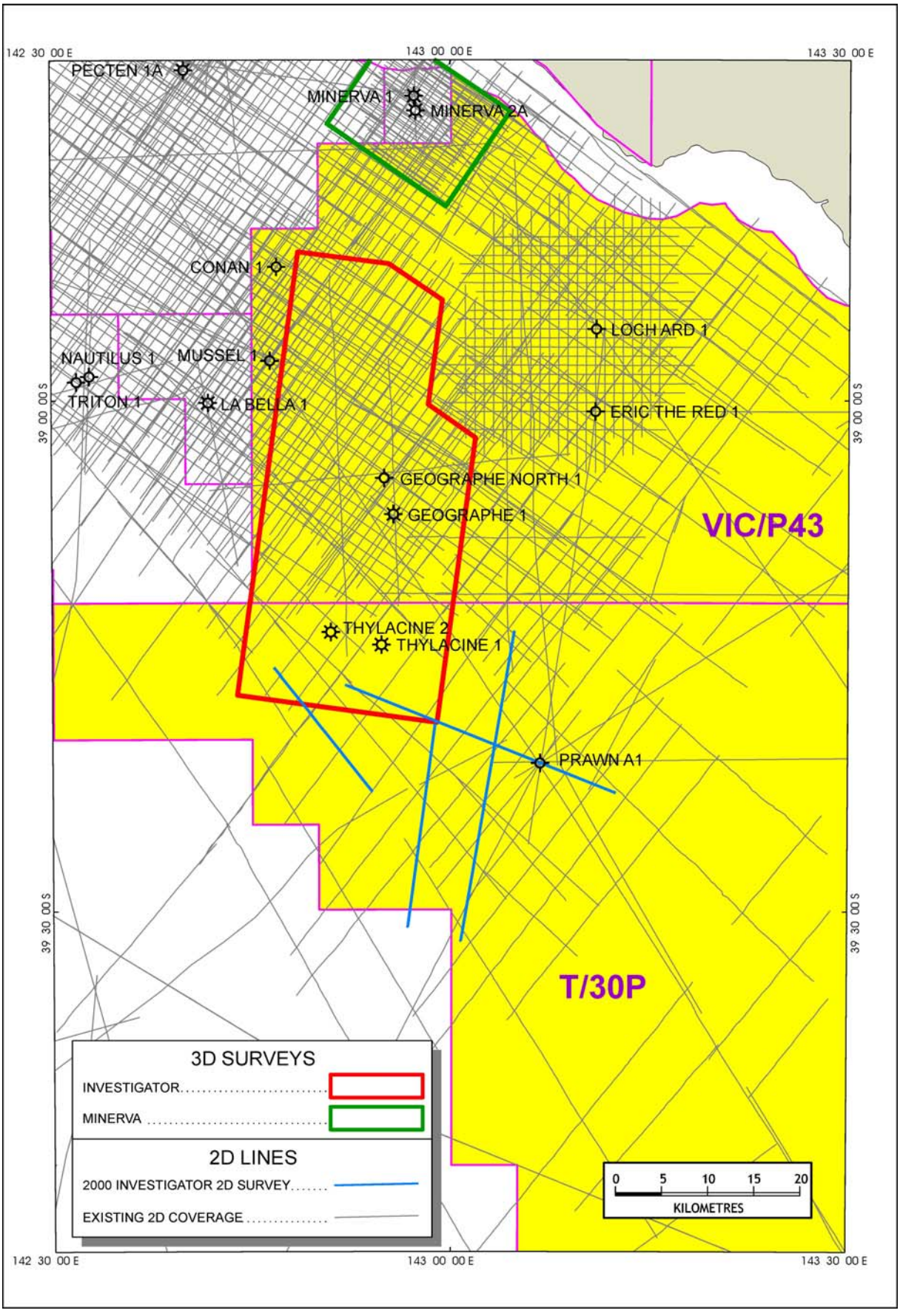


Figure 5 – Investigator 3D and 2D Seismic Survey Location Map

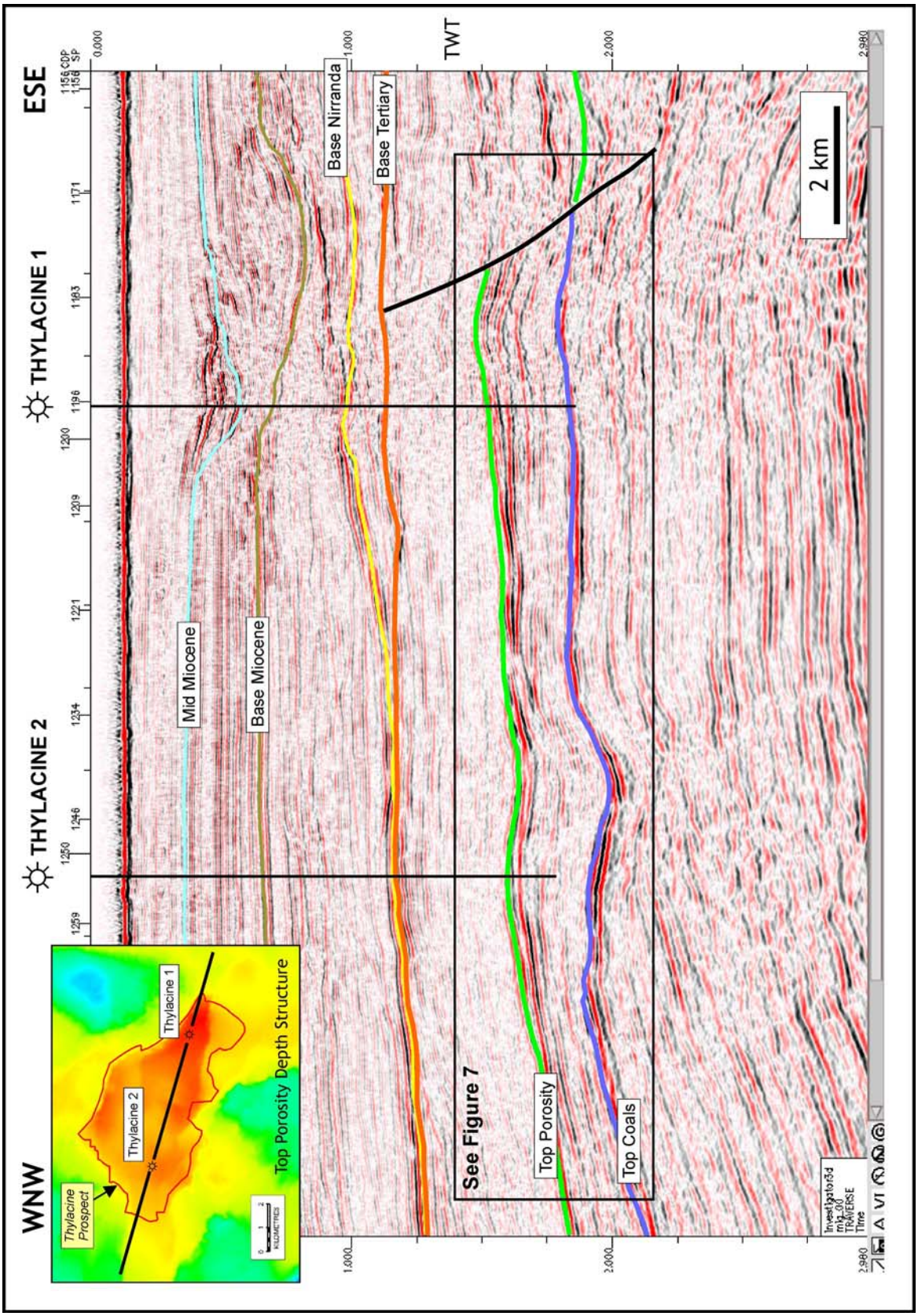


Figure 6 – Composite 3D seismic traverse through Thylacine 1 and Thylacine 2

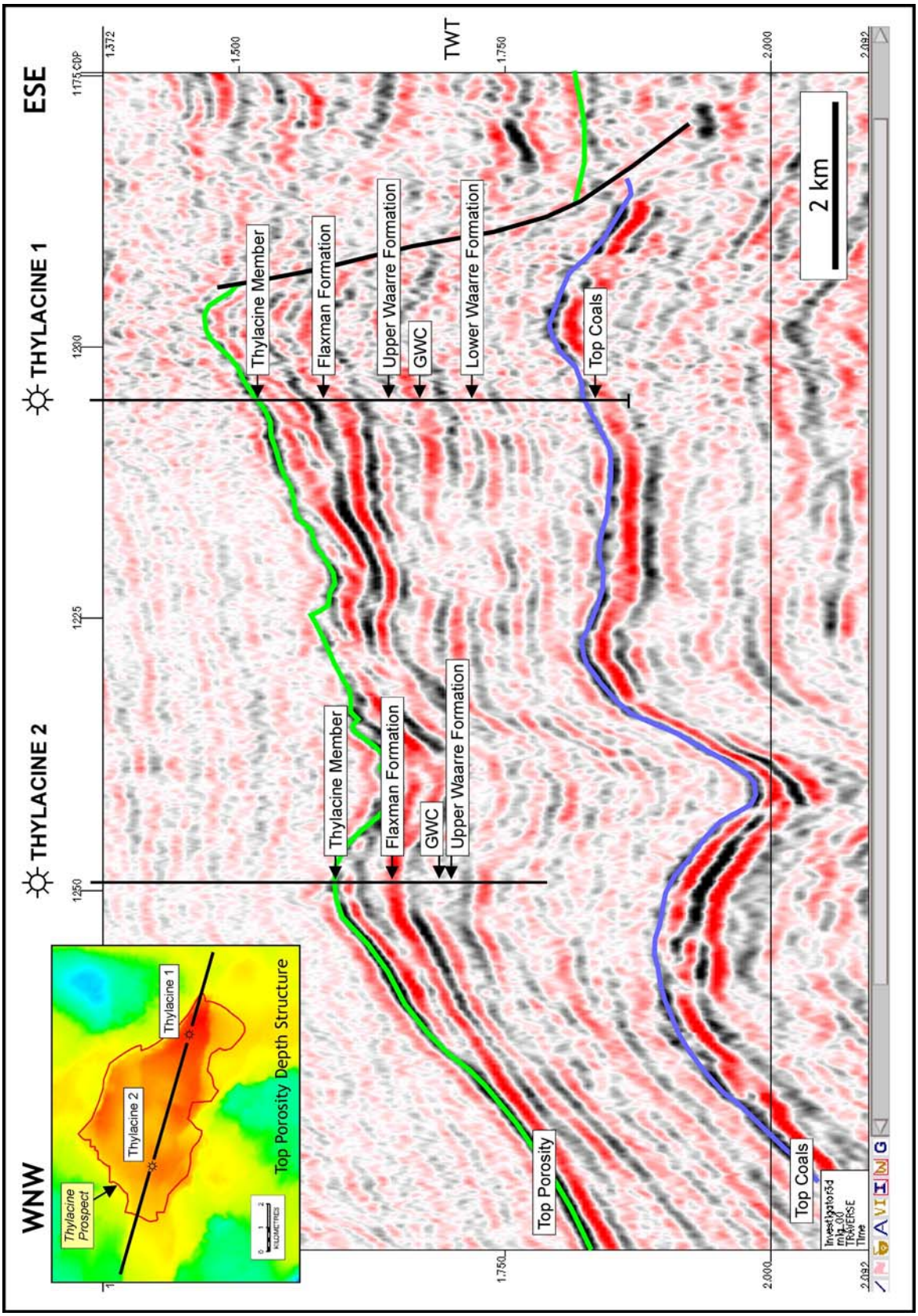


Figure 7 – Close-up composite 3D seismic traverse through the reservoir section in Thylacine 1 and Thylacine 2

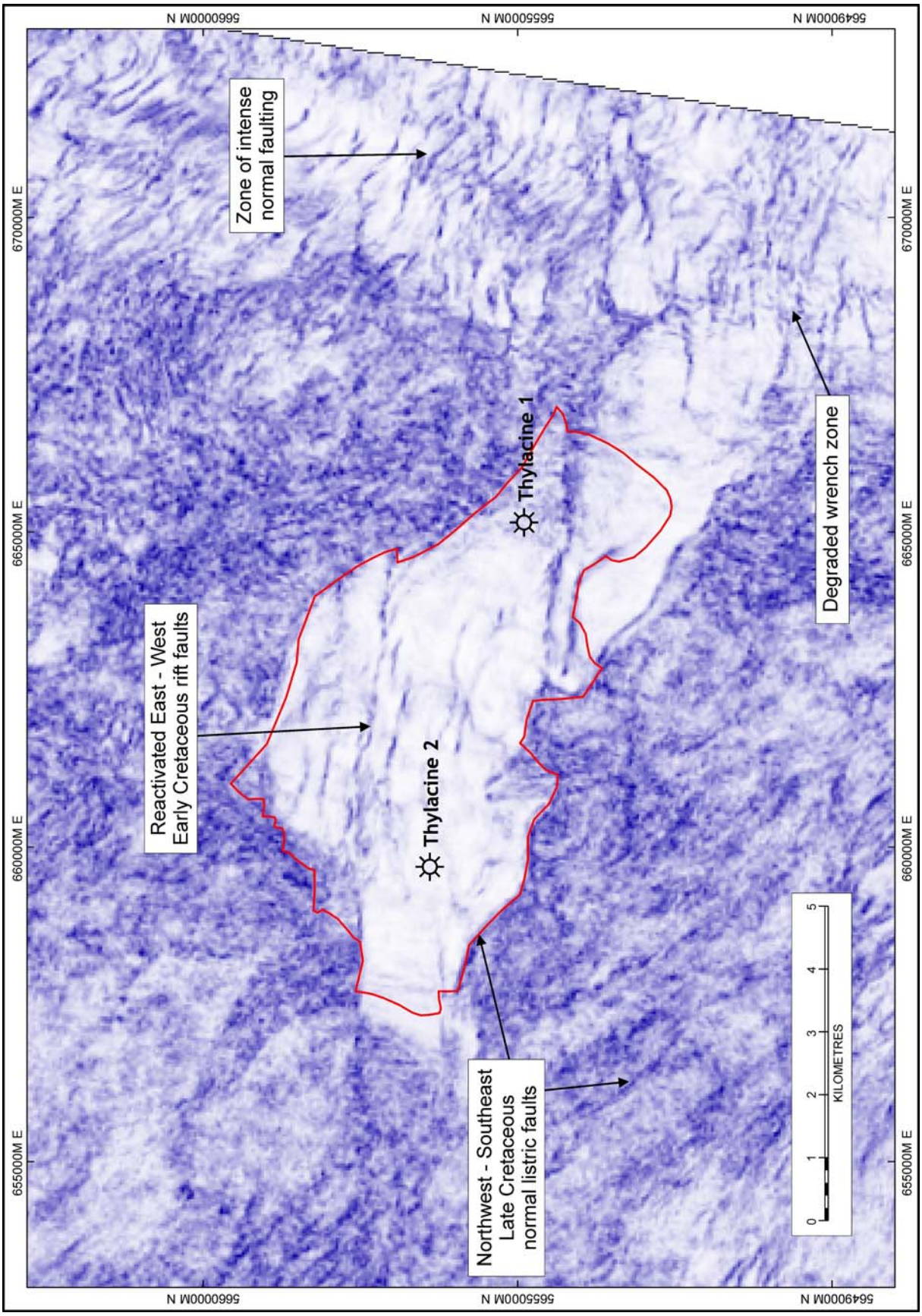


Figure 8 – Variance Cube Time Slice (1512 ms TWT) through Thylacine Prospect

faults orientated E-W to NW-SE. Evidence from elsewhere in the basin suggests that the E-W striking faults are likely to be the oldest and associated with the earliest phase of rifting in the Late Jurassic/Early Cretaceous. These faults tend to be steep and probably extend well into basement. The Late Cretaceous faults predominantly trend ENE to NE and are less steep. Seismic observations indicate many of the Early Cretaceous faults experienced some reactivation during this Late Cretaceous faulting episode. The most recent faulting in the Tertiary section is mainly orientated NNE-SSW.

The eastern end of the Thylacine structure is controlled by the N-S striking Sorrell Transfer Zone, which marks the eastern limit of the west to east rifting associated with the separation of Australia and Antarctica. Fault orientations change abruptly adjacent to the transfer zone due to the long history of repeated strike-slip movement. The Sorrell Transfer Zone is also the primary control on the Shipwreck Trough, which developed in response to the trans-tensional movement. The Thylacine structure is bounded to the south by a large E-W striking normal fault, and to the north by a large NW-SE striking fault. These faults penetrate up to the base of the Tertiary, indicting significant growth of the structure during deposition of the Belfast Formation.

The Thylacine structure contains three main sub-culminations (see Figure 2). Thylacine-1 tested the overall crest at the eastern end of the structure, while Thylacine-2 tested a sub culmination with a small amount of four-way dip closure in the western part of the field. The northern culmination was not tested. Top porosity in Thylacine-2 was intersected approximately 100 m down dip of Thylacine-1, but still 180m above the main gas-water contact (GWC).

Based on the seismic mapping, ultimate structural closure of the Top Porosity horizon is defined by a spill-point across the bounding fault on the northeast side of the prospect. This point is approximately coincident with the GWC in Thylacine-1. However, Thylacine-2 contains multiple gas columns within the Santonian Thylacine Member and Turonian Flaxman Formation reservoir sections. Hence, there is a significant component of stratigraphic control on the gas fluid levels, which is more complex than originally expected based on the results of Thylacine-1.

6.3 Seismic Amplitudes

Seismic amplitudes in both the full and far stack volumes were an essential part of the prospectivity assessment. At the Top Porosity level, there is a distinct amplitude anomaly over the Thylacine structure at the Thylacine-2 location (Figure 9). Based on the calibration of the Thylacine-1 GWC on to the 3D seismic, the evidence for a dimming of seismic amplitudes below the GWC was re-assessed at the Thylacine-2 location. Optical stacking showed that there was strong evidence for amplitudes dimming below the projected Thylacine-1 GWC in Thylacine-2, so the same GWC was predicted in Thylacine-2.

6.4 Actual versus Predicted depths

The depth prognosis for Thylacine-2 was based on the time-depth curve from Thylacine-1. Time picks for each formation were determined by correlating the events on the 3D seismic from Thylacine-1. It was recognized that the Miocene canyoning in Thylacine-1 could produce a mild velocity gradient between the two well locations. Consequently, the uncertainty in the depth estimates was estimated to be in the order of +/- 50m. All final predicted depths together with the actual depths are shown in Table 2.

All tops were within the predicted range of error except for the Mepunga, Flaxman and Waarre formations. The Mepunga Formation was 57.2 m low to prognosis, whereas the Flaxman and Upper Waarre were 61.3 and 64.9 m high to prognosis respectively. The latter two horizons are difficult to pick on seismic, hence the error in depth prediction was mostly a result of uncertain seismic picks and not poor velocity estimation. Time depth curves based on the check-shot surveys from Thylacine-1 and Thylacine-2 (Figure 10) shows the velocity trend for each well is very similar and close to the trend in nearby wells. Details of the Thylacine-2 velocity survey are included in Appendix 7 of the Thylacine-2 Basic Data Report.

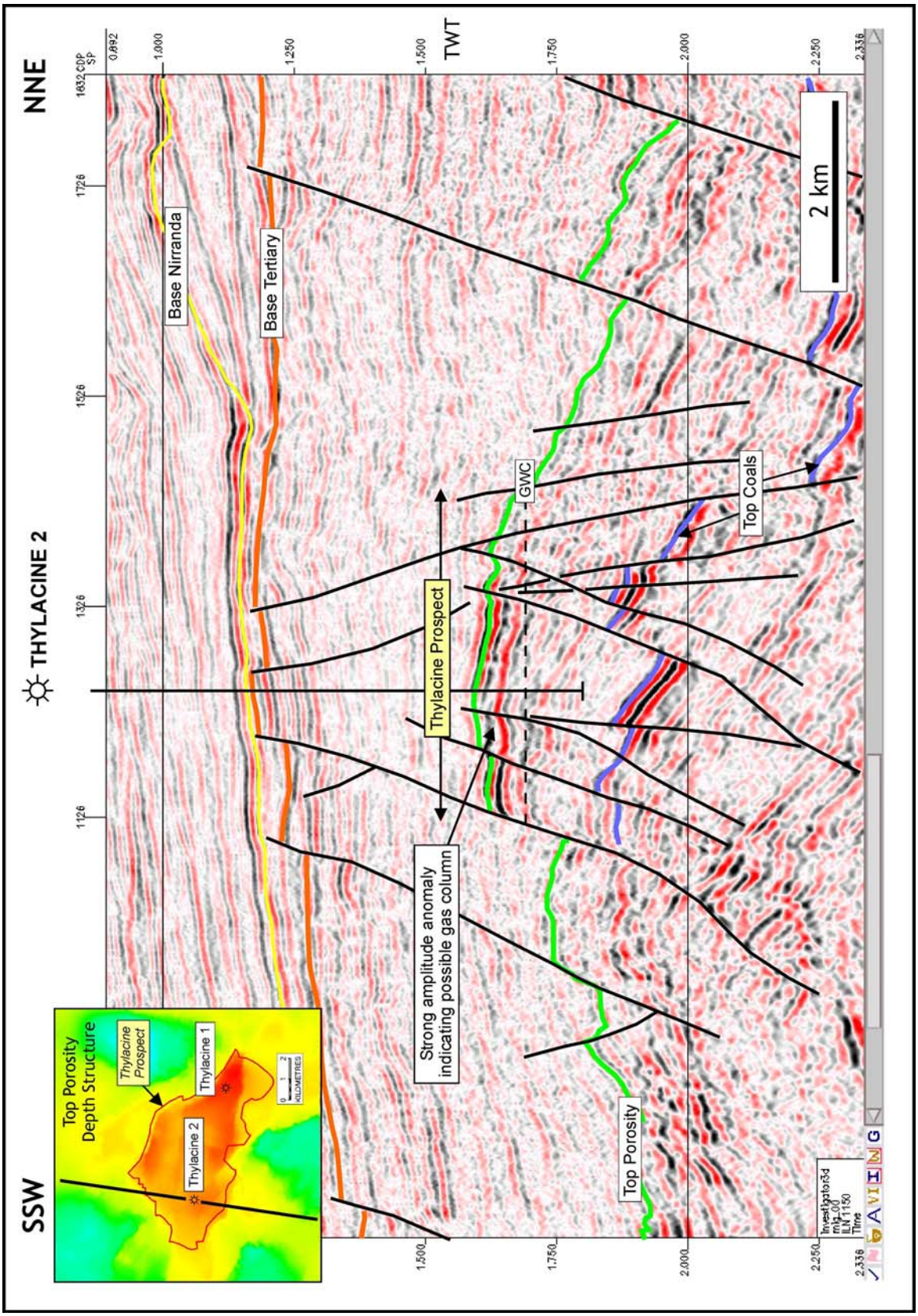


Figure 9 – 3D inline 1150 showing Top Porosity seismic amplitude anomaly at Thylacine 2

Table 2. Predicted vs Actual Formation Tops

Thylacine 2 (Inline 1150 CDP 1250)
RT = 25 m ASL
Water Depth = 101.2 m

	Formation / *Seismic Marker*	Two-way time (ms)	Predicted Depth (mKB)	Actual Depth (mKB)	Actual Depth (mSS)	Thickness (m)	High/Low (-ve = high)
TERTIARY	Port Campbell Limestone / Sea bed	132	124.0	126.2	101.2	194.2	2.2
	Upper Gellibrand Marl	345	370.0	320.4	295.4	410.5	-49.6
	Mid Miocene Seismic Marker	345	370.0	-	-	-	-
	Lower Gellibrand Marl / *Base Miocene Seismic Marker*	740	765.0	730.9	705.9	595.2	-34.1
	Narrawaturk Marl	1137	1371.0	1326.1	1301.1	123.1	-44.9
	Mepunga Formation	1150	1392.0	1449.2	1424.2	14.4	57.2
	Dilwyn Formation	Not Picked	1439.0	Not Intersected	Not Intersected	-	-
	Pember Mudstone	1197	1471.0	Not Intersected	Not Intersected	-	-
CRETACEOUS	Paaratte Formation / *Base Tertiary*	1220	1510.0	1463.6	1438.6	361.8	-46.4
	Belfast Formation	1390	1805.0	1825.4	1800.4	411.9	20.4
	Thylacine Member	Not Prognosed	Not Prognosed	2143.3	2118.3	(94.0)	-
	Flaxmans Formation	1590	2176	2237.3	2212.3	116.8	61.3
	Waarre Formation					181.1 +	
	Upper Waarre Formation	1650	2290.0	2354.1	2329.1		64.1
	TD		**2525.0**	**2535.2**	**2510.2**	-	

NB: Actual TD = Logger

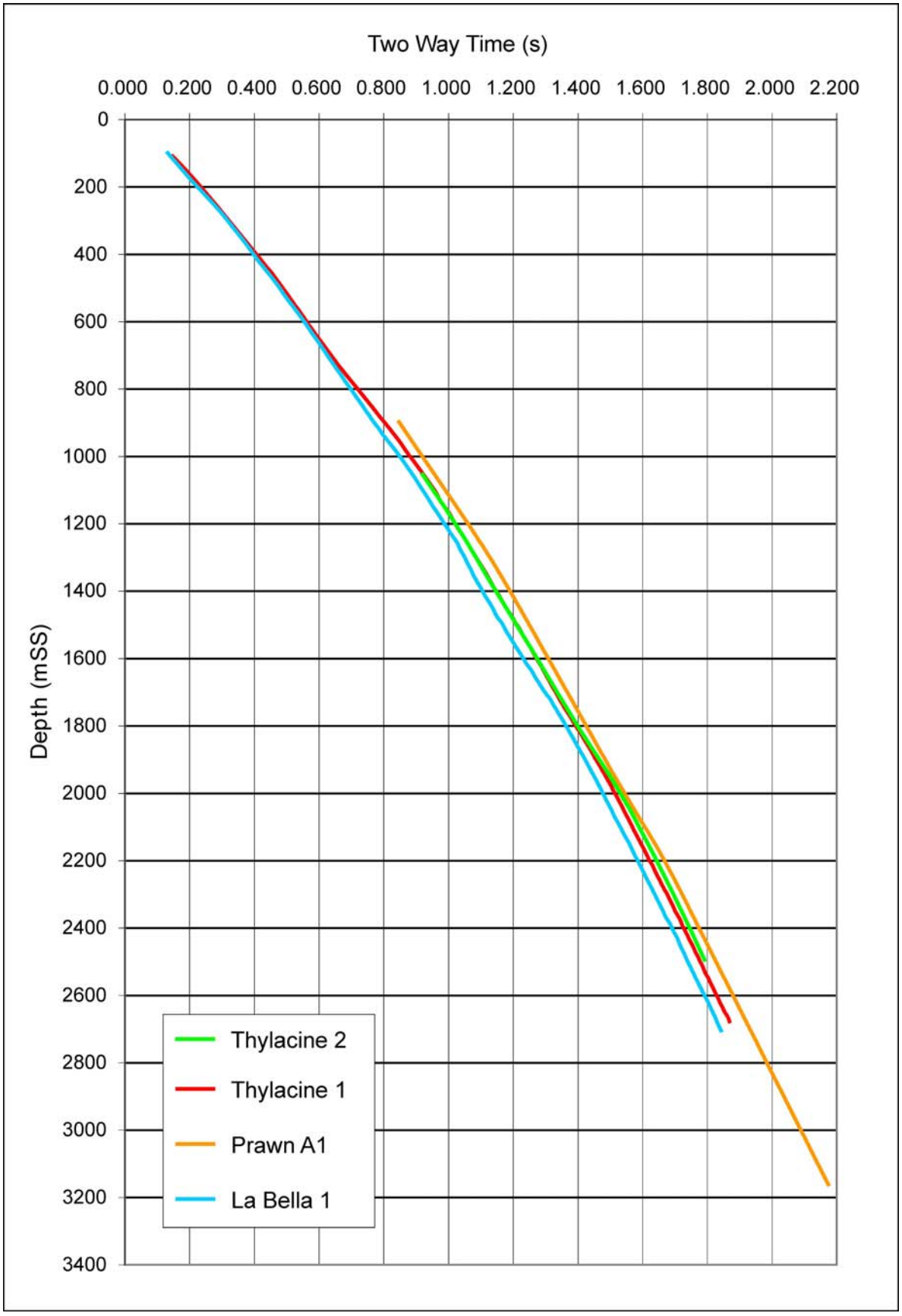


Figure 10 – Thylacine 2 Time Depth curve

7. GEOLOGICAL DISCUSSION

7.1 Previous Exploration

The drilling history in the eastern offshore Otway Basin is summarized in Table 3. Prior to Thylacine-2, only three wells had been drilled in T/30P: Prawn A1, Whelk-1 and Thylacine-1. Prawn-A1 and Whelk-1 were drilled by ESSO over thirty years ago, but no hydrocarbon shows were reported. Thylacine-1 was drilled by Origin Energy in 2001 and was a gas discovery.

Well	Year	Operator	TD (m)	Status	Result
Pecten 1A	1967	Shell	2850	P&A	Gas show, 145 mscfd from 17 m of tight Waarre
Prawn A1	1967	Esso	3193	P&A	No valid closure, good reservoir, poor seal
Nautilus 1A	1968	Esso	2011	P&A	Tertiary wedge play, no reservoir found
Mussel 1	1969	Esso	2450	P&A	Not drilled in crestal location
Whelk 1	1970	Esso	1466	P&A	No seal
Triton 1	1982	Esso	3545	P&A	Poor reservoir, no closure mapped to date
La Bella 1	1993	BHP	2710	GAS	Estimated 210 bcf OGIP
Minerva 1	1993	BHP	2425	GAS	Estimated 575 bcf OGIP
Eric the Red 1	1993	BHP	1875	P&A	No cross fault seal
Minerva 2A	1993	BHP	2170	GAS	Thick Waarre sand development
Loch Ard 1	1993	BHP	1397	P&A	No Top Seal for Waarre reservoir
Conan 1	1995	BHP	2175	P&A	Ineffective fault seal
Champion 1	1995	BHP	1882	P&A	Upper Waarre absent, no cross fault seal
Thylacine 1	2001	Origin	2710	GAS	Estimated 1255 bcf OGIP
Geographe1	2001	Origin	2430	GAS	Estimated 600 bcf OGIP

Table 3: Previous drilling history, eastern offshore Otway Basin.

7.2 Regional Geology

The Otway Basin formed in response to rifting between Australia and Antarctica during the Late Jurassic - Late Cretaceous. The basin has a two-stage rift history. The first stage occurred during the Late Jurassic and Early Cretaceous, followed by the second in the Late Cretaceous. The second event was responsible for the formation of the Shipwreck Trough, which is where all the known gas discoveries in the offshore Otway Basin are located (see Figure 11).

The Shipwreck Trough formed in response to sinistral transtension along the Sorell Transfer Fault during the Late Cretaceous, with significant thickening of Late Cretaceous sediments centred along the axis of the trough. Initial sedimentation commenced in the Cenomanian with the deposition of axially-dispersed marginal marine to fluvial-dominated sediments of the Waarre Formation. This section thickens significantly into the trough and deposition and preservation is dependant on the palaeotopography of the basin, which in turn was dependent upon accommodation created by transpression adjacent to the Sorell Fault.

During the mid Turonian, an increase in rifting resulted in significant growth basinward of the Mussel Fault Zone and Tartwaup Hingeline. This was followed by a major transgression culminating in the deposition of the Flaxman Formation in the late Turonian. A significant increase in structural activity during the Coniacian and Santonian resulted in marked relative uplift east of the Sorell Fault and significant fault movement within the trough itself. This change in structural style resulted in a complete reorganization of sedimentation patterns within the Shipwreck Trough. On high parts of fault blocks, this period of structural reorganisation is marked by a depositional hiatus recorded by the absence of the *C.striatoconus* dinoflagellate zone concomitant with bathyl sedimentation in low areas. Subsequent progradation from the east during the middle and late Santonian resulted in the deposition of deltaic sediments within the trough such as those intersected at the Thylacine and Geographe Fields (i.e. the Thylacine Member of the Belfast Formation). A final widespread regional transgression in the Late Santonian (lower *I.cretaceum* dinoflagellate zone) resulted in the blanket deposition of thick mudstone (Belfast Formation) throughout most areas of the basin west of the Sorell Fault Zone. This mudstone forms the regional seal to the reservoir section in the Thylacine and Geographe Fields, and is also the top seal at other gas fields within the Shipwreck Trough (i.e. La Bella, Minerva).

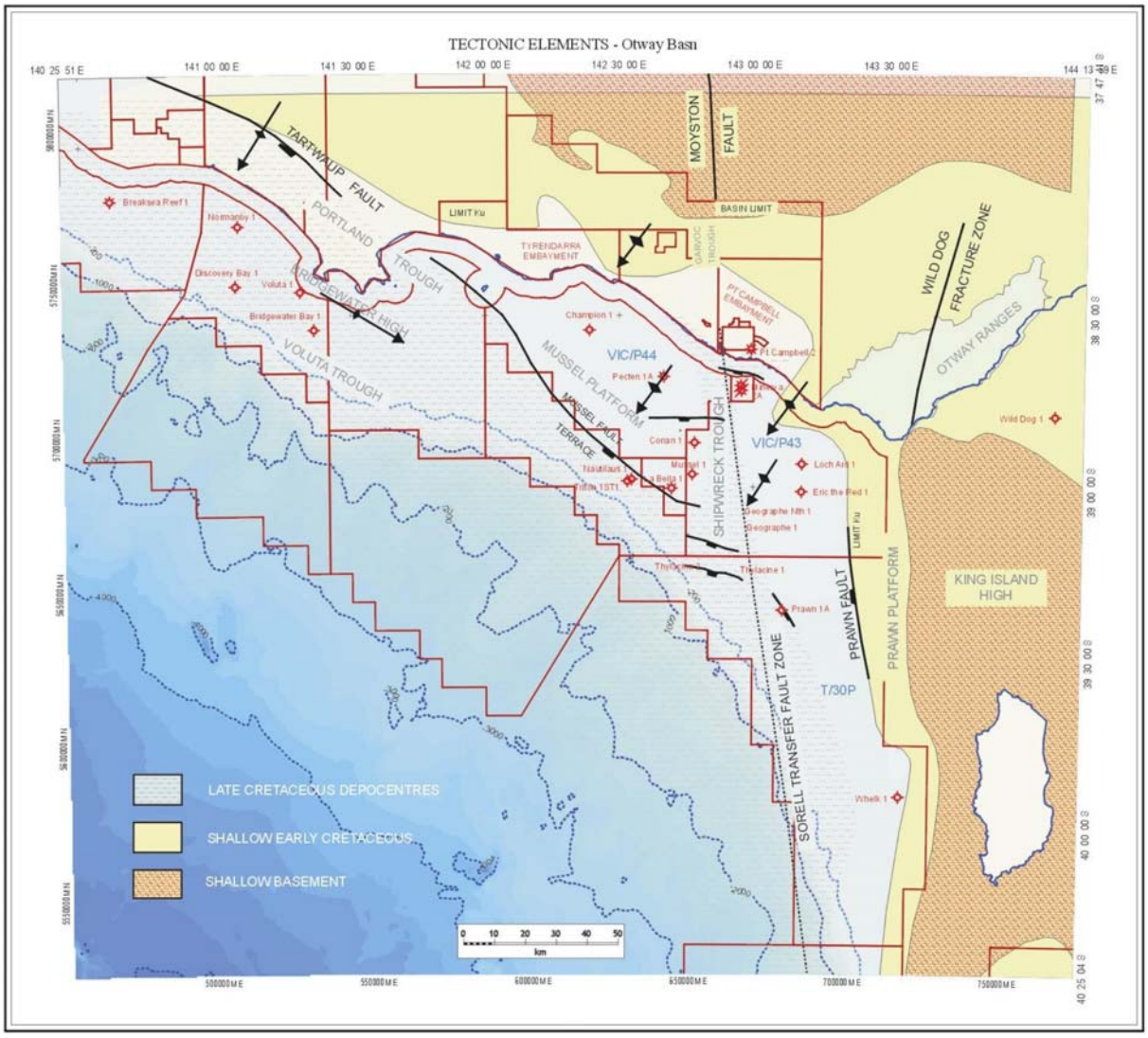


Figure 11 – Tectonic Elements of the Otway Basin

Directly adjacent to, and to the east of the Sorell Fault Zone, the Cenomanian through to the base Tertiary was dominated by continental and nearshore sedimentation reflecting higher palaeotopography and proximity to sediment source areas. These areas provided vast volumes of sediment into the low area adjacent to the Sorell Fault Zone. This is particularly evident within the Late Cretaceous (Santonian to Campanian) sedimentary sections intersected in Prawn-A1 and Whelk-1, which are sandstone-dominated fluvial sequences. Within T/30P, these sand-dominated depositional sequences are clearly evident on seismic data and extend westward off the Prawn Platform and into the Shipwreck Trough.

Regional fold trends that plunge to the southwest are essential to defining prospectivity within the Shipwreck Trough. The Investigator 3D covers three such fold trends within the Shipwreck Trough play fairway. The 'Geographe Anticline', which plunges to the southwest, underlies the Geographe and Thylacine prospects, and is interpreted to control the migration of hydrocarbons from source kitchens to the southwest. The folding and stress field orientations are a composite of at least three different phases of deformation. The first phase began in the Albian/Cenomanian with the initial uplift of the Otway Ranges (crustal kink) in response to rift propagation from the west. This was followed by a second episode of folding and uplift in the Santonian associated with the opening of the Tasman Sea, and a third during the Mid to Late Miocene in response to sea floor spreading inertia following the collision of Australian northern plate margin with the Banda Arc.

Major east-west trending rift faults occur along the Shipwreck Trough together with the transfer fault deformations. The Albian to Turonian east-west striking rift faults are inferred to be perpendicular to the direction of extension. The rift and post rift deformations mean there are three main fault sets that dominate the Shipwreck Trough, with extensional tectonics accentuated towards the shelf margin by gravitational effects.

The northwest-southeast striking listric normal faulting commenced in the middle of the Late Cretaceous and terminated at the end of the Cretaceous with very little penetration above the Base Tertiary unconformity. These faults commonly sole out on the earlier fault sets. Secondary synthetic and antithetic faulting and rollover anticline development is also present. Inversion due to north-northwest transpression is inferred to have affected most structures in the eastern Otway, especially at Minerva.

A degraded north-south oriented wrench zone is present in the east of the Investigator 3D and is best shown on the Variance Cube data (see Figure 8). This wrenching, which is the result of crustal transtension, is manifest as a prominent north-south striking fault that splays vertically with keystone development.

7.3 Contributions to Geological Concepts and Conclusions

Thylacine-2 was drilled as a vertical appraisal well to constrain the size of the Thylacine discovery. Prior to drilling, it was anticipated Thylacine-2 would intersect reservoir in the Late Cretaceous (Turonian) Flaxman Formation and Upper Waarre Formation. Instead, Thylacine-2 encountered gas-saturated sandstones in the basal sandy unit of the Belfast

Formation, the Thylacine Member, and underlying Flaxman Formation. The stratigraphically deeper Upper Waarre proved water saturated.

MDT data indicates the hydraulic system in Thylacine-2 is not as simple as in Thylacine-1, with at least four different hydraulic systems present, resulting in significant pressure offsets between the sands with an 86 m difference in Free Water Levels. The shales within the Thylacine Member and Flaxman Formation at Thylacine-2 must therefore be acting as seals separating the various gas-bearing sands within these units from each other.

The newly encountered Thylacine Member comprises a series of coarsening-upwards progradational sequences that form the distal edge of a larger fluvio-deltaic sequence sourced from the Prawn Platform to the east. Palynological data confirms the presence of a time break between it and the underlying Flaxman Formation observed previously in Thylacine-1. Thylacine-2 also demonstrated significant thickening of the Flaxman and Waarre Formations compared with the equivalent section intersected in wells on the flanks of the Shipwreck Trough such as Minerva-1 and La Bella-1. Core data confirms the Flaxman Formation has fair to excellent reservoir quality in this part of the basin.

Fluid Inclusion Screening (Appendix 4) of cuttings from Thylacine Member and Flaxman Formation in Thylacine-2 revealed both units had strong gas inclusion signals consistent with the presence of gas. Moreover, the screening indicated the inclusions ha a minor liquids component, which was consistent with the low (< 10) CGR of the gas in Thylacine-1 (see Appendix 3 of the Thylacine-1 Interpretative WCR). The overlying Belfast Formation, on the other hand, had no gas- inclusion signal, confirming the effectiveness of this unit as a top seal. No evidence for early oil migration or a palaeo GWC was observed in Thylacine-2.

8. REFERENCES

(Origin Energy) Thylacine-2 Basic Data Report, T/30P, November 2002.

Bal A.A.
(Baker Atlas Geoscience) Thylacine-1 and Thylacine-2 Structural and Sedimentological Interpretation of FMI Images. Volumes 1 & 2, April 2002

APPENDIX 1
PETROPHYSICS REPORT

T30/P, OTWAY BASIN, TASMANIA

THYLACINE - 2

PETROPHYSICAL REPORT

THYLACINE MEMBER, FLAXMAN FORMATION, AND WAARRE FORMATION

2115-2535 mMDRT

Origin Energy Resources Limited
Second Floor, South Court, John Oxley Centre
339 Coronation Drive
MILTON QLD 4064

Chris Shield, January 2004
N:\chris\otway\thylacine\thylacine-2\reports\petrophysics_2003-07\Thylacine-2 Petro Report.doc

EXECUTIVE SUMMARY

This report details a review of the reservoir quality and hydrocarbon saturation of three Late Cretaceous formations intersected whilst drilling the exploration well, Thylacine-2 in T30/P in the Otway Basin, offshore Tasmania. The study entails an analysis of all available lithological data, and a complete petrophysical analysis (Table 1).

The Thylacine Member (2143.3-2237.3 mMDRT) encountered at Thylacine-2 is interpreted to have moderate reservoir quality. The unit has a net to gross of 58.4%, although the sandstones that are present contain high clay volumes, averaging 28.2%. Calculated effective porosities average only 14.8% for these reservoirs. As a result, the log-derived gas permeability is considerably reduced in comparison to other cleaner reservoirs, geometrically averaging only 0.78mD, which will negatively affect this unit's producibility and recovery factor. The average effective water saturation is 74.9%.

The Flaxman Formation (2237.3-2354.9 mMDRT) has much better reservoir development in part, although the overall net to gross ratio is low. The sandstones present, on average, are cleaner and have an average clay volume of 19.3%. The average effective porosity is similar (14.7%), but the average gas permeability is higher, averaging 1.4mD. This unit has a net reservoir to gross of 27.6%, and an average effective water saturation of 64.3%.

A gas-oil contact cannot be identified from the logs, and it is assumed that the reservoir at the Thylacine-2 location does not contain an oil-leg. The lowermost gas-bearing sandstone is present at 2325.7 mMDRT. A thin sandstone bed at 2334 mMDRT displays inconclusive hydrocarbon saturation. Based upon the Spontaneous Potential log, the GWC may be interpreted as low as 2343 mMDRT. Due to poor reservoir quality across the potential GWC, the FWL should be best defined by the MDT log pass.

Based upon the learning from the petrophysical analysis of both Thylacine-1 and Geographe-1, only an Indonesian water saturation equation was applied in this well. It was originally thought that with the benefit of a detailed special core analysis data, the Waxman-Smits equation should result in more realistic values. Unfortunately, this was not the case, as the Waxman-Smits equation encountered problems in argillaceous reservoirs, and under-estimated the gas saturation in comparison with the Indonesian equation. The Indonesian Equation is therefore applied in all reported values.

FORMATION NAME	TOP FROM	BASE TO	GROSS INTERVAL	NET RESERV INTERVAL	AVERAGE VCL	AVERAGE PHIE	AVERAGE AIR PERM	AVERAGE GAS PERM	AVERAGE H_2O PERM	AVERAGE SWE	NET RES / GROSS
	mMDRT	mMDRT	mMDRT	mMDRT	%	%	mD	mD	mD	%	%
Thylacine Member	2143.30	2237.30	94.00	54.92	28.20	14.79	1.04	0.78	0.28	74.88	58.43
Flaxman Fm-GWC	2237.30	2325.70	88.40	25.24	18.86	14.76	2.26	1.73	0.63	57.87	28.55
		TOTAL	**182.40**	**80.16**	**25.26**	**14.78**	**1.32**	**1.01**	**0.36**	**69.53**	**43.95**
Thylacine Member	2143.30	2237.30	94.00	54.92	28.20	14.79	1.04	0.78	0.28	74.88	58.43
Flaxman Formation	2237.30	2354.90	117.60	32.40	19.27	14.65	1.86	1.42	0.51	64.32	27.55
Upper Waarre Fm	2354.90	2536.24	181.34	98.64	16.90	15.88	1.15	0.87	0.31	94.64	54.40

Cut-offs Applied		
Net Pay	K_gas >	0.1mD
	VCl <	40.0%

Table-1. Petrophysical Reservoir Summary

TABLE OF CONTENTS

INTRODUCTION 3

DATA AVAILABILITY AND QUALITY 4

Lithological Data 4
Mudlog Data 5
Electric Log Data 5
Formation Test Data 6
Routine and Special Core Analysis Data 6

BOREHOLE DATA 7

Hole Conditions 7
Mud Properties 7
Bottom Hole Temperature 7

RESERVOIR QUALITY 10

LOG ANALYSIS METHODOLOGY 10

Preparation 10
Environmental Corrections 11
Zonation 11
Clay Volume and Porosity 12
Lithology 12
Formation Water Resistivity 15
Water Saturation 16
Permeability 18
Reservoir Summary Parameters 19
Fluid Contacts 20

DISCUSSION 22

CONCLUSIONS / RECOMMENDATIONS 23

Figures

Figure 1. Location Map 3
Figure-2. Suite-1 Extrapolated Borehole Temperature Plot 10
Figure 3. Clay volume determination. Comparison of results from the RHOB-NPHI, RHOB-DT, and GR techniques for the Flaxman Formation, 2237.2-2347.5 mMDRT. 14
Figure 4. Hydrocarbon density derivation from cross-plot of effective porosity versus apparent grain density. 15
Figure 5. Hingle cross-plot defining formation water resistivity from Upper Waarre Formation below the GWC. Sand petrofacies displayed. 16
Figure 6. Pickett cross-plot defining formation water resistivity from lower Waarre Formation below the GWC. Sand petrofacies displayed. 17
Figure 7. Clay resistivity derivation as applied in the Indonesian water saturation equation. Clay petrofacies displayed. 18
Figure-8. Log-derived permeability derivation via multiple linear regression. 20
Figure-9. Relationship between core-derived overburden air permeability and gas permeability 21
Figure-10. Relationship between core-derived overburden air permeability and water permeability 21

Tables

Table-1. Petrophysical Reservoir Summary
Table 2. Stratigraphic Table
Table-3. Log Data Acquired
Table-4. Mud Properties
Table-5. Waarre Formation water chemistry data
Table-6. Summary of electrical properties applied in the Indonesian Equation
Table-7. Cut Off Parameters
Table-8. Reservoir Summary

Appendices

A. Log depth-matching Summary
B. Mudlog Summary
C. Field Print Summary
D. Core Analysis cross-plots
E. Petrophysical Model and Constant Listing

Enclosures

1. Composite and petrophysical summary plot, 2113-2542 mMDRT 1:500
2. Composite and petrophysical summary plot, 2128-2382 mMDRT 1:200

INTRODUCTION

Thylacine-2 is an appraisal well drilled in 2001, and is located within the current T30/P permit (Figure-1).

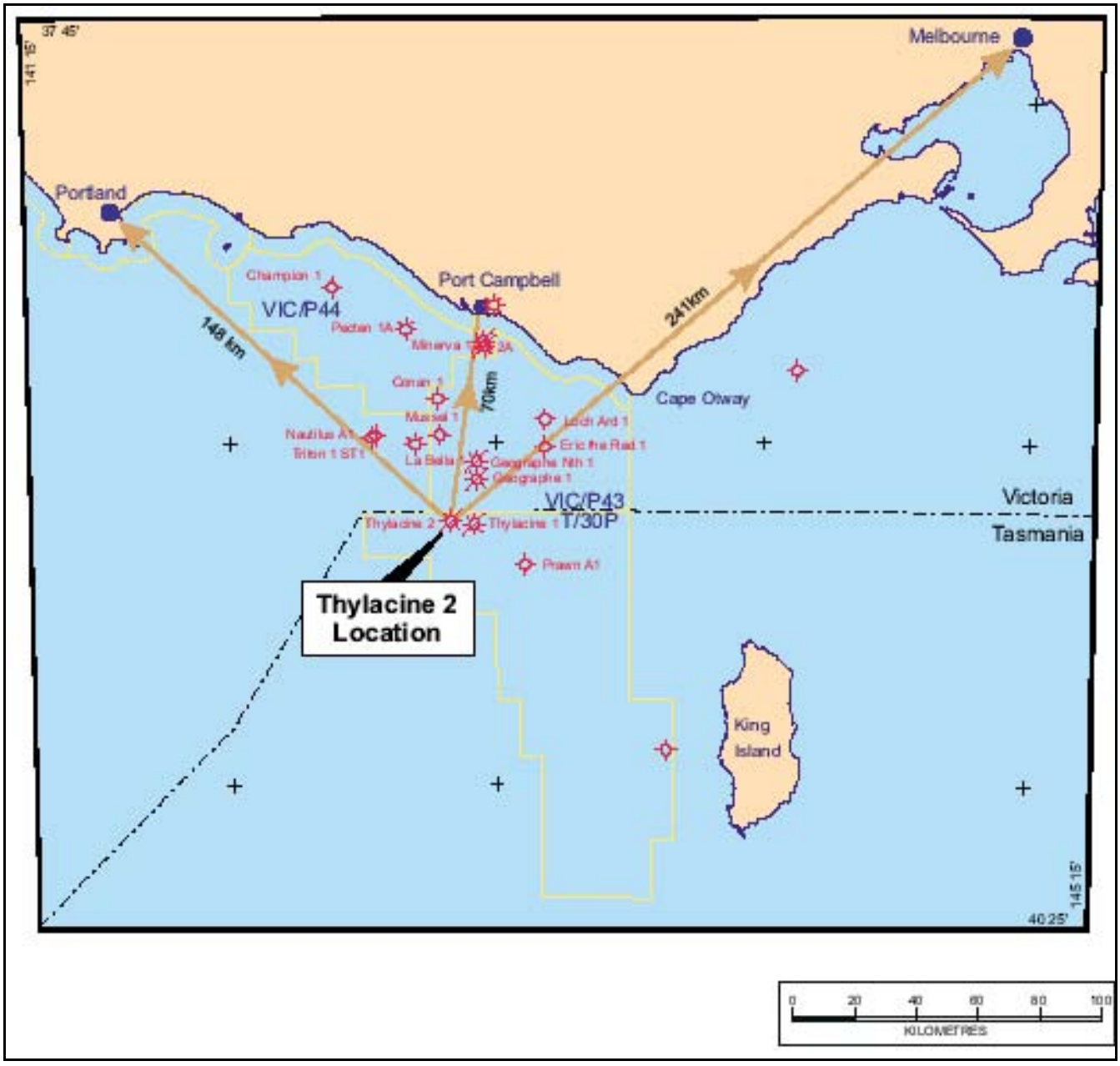


Figure 1. Location Map

The well intersected interbedded claystones, siltstones, and poor to excellent quality sandstones displaying weak to nil fluorescence and very good gas shows within the Thylacine Member and Flaxman Formation, and moderate to excellent quality sandstones displaying nil hydrocarbon shows in the Waarre Formation (Table-2). This report addresses the reservoir

and hydrocarbon-producing potential of all strata intersected between 2115.0 metres and the base of complete log coverage at 2535.0 mMDRT.

FORMATION / *SEISMIC MARKER*	TOPS (m)				REMARKS/SHOWS
	MDRT	SUBSEA	THICK	TWT(ms)	
Port Campbell Limestone / *Seabed*	126.2	101.2	193.8	0.132	No returns 126.2 – 557 mMDRT.
Gellibrand Marl			1005.7		
Upper Gellibrand Marl	320.4	295.4	(410.5)	-	Below 557 mMDRT, mostly calcareous claystone with lesser argillaceous calcisiltite and argillaceous calcilutite and rare calcarenite.
Middle Miocene Seismic Marker	-	-		0.345	
Lower Gellibrand Marl *Base Miocene Seismic Marker*	730.9	705.9	(595.2)	-	Predominantly calcareous claystone with lesser argillaceous calcisiltite, argillaceous calcilutite and rare sandstone.
Narrawaturk Marl	1326.1	1301.1	123.1	1.079	Calcareous claystone and argillaceous calcilutite.
Mepunga Formation	1449.2	1424.2	14.4	1.161	Sandstone.
Paaratte Formation / *Base Tertiary*	1463.6	1438.6	361.4	1.171	Claystone and silty claystone with minor interbedded sandstone and trace argillaceous calcilutite.
Belfast Formation	1825.0	1800.0	316.5	1.407	Claystone with occasional siltstone and sandstone stringers.
Thylacine Member	2143.3	2118.3	(94.0)	1.595	Interbedded sandstone, siltstone and claystone. **Gas shows.**
Flaxman Formation	2237.3	2212.3	117.6	1.647	Interbedded sandstone, siltstone and claystone. **Gas shows.**
Waarre Formation			170.1+		
Upper Waarre Formation	2354.9	2329.9	(170.1+)	1.709	Interbedded sandstone, siltstone, claystone & minor coal.
TD (Logger)	**2535.0**	**2510.0**			

Table 2. Stratigraphic Table

DATA AVAILABILITY AND QUALITY

Lithological Data

Three conventional cores were cut (2150.0-2203.5 mMDRT, 2203.5-2258.5 mMDRT, 2258.5-2316.0 mMDRT), which had 93%, 98%, and 97.5% recoveries respectively. In order to allow

comparison of routine and special core analysis data with the results of the log analysis, it was necessary to depth match the core to wireline depths.

To allow for the fine scale variations in wireline depth, the process was performed by depth-matching the core plug total porosity to the log-derived total porosity and using the gamma ray curves as a guide. The resultant and final depth-match applied was 0.19 metres for Core-1, varies between –0.48 and 0.19 metres for Core-2, and varies between –1.10 and –1.74 metres for Core-3. A listing on the depth shifts applied is included in Appendix-A.

Lithological information is provided by core and cuttings description summaries.

Mudlog Data

Baker Hughes Inteq were contracted to provide mudlogging services. Appendix-B contains a copy of the mudlog encompassing the potential reservoir intervals discussed herein. A variable depth match was applied to this mudlog data to conform to wireline log depths. The ROP and total gas curves were used as the seed to depth match the mudlog data to the wireline gamma ray and density curve data. The depth match applied varied between –2.5 and 2.9 metres. A listing of the depth shifts applied is included in Appendix-A. The raw and depth-shifted data are available in LAS ASCII format on a CD-ROM adjoining this report.

Electric Log Data

MWD and LWD services were provided by Anadrill. These data were matched to wireline depths. The LWD gamma ray was variably depth matched to the wireline gamma ray, which varied between -2.94 and 3.12 metres. The LWD data was not utilised in this interpretation. A summary of the tools and intervals acquired is in Table-3, and a listing of the depth shifts applied is included in Appendix-A. The raw and depth-shifted data are available in LAS ASCII format on a CD-ROM adjoining this report.

Schlumberger, which provided wireline services, logged the well in one suite in 8.5 inch hole. Table-3 contains a summary of the logging tools run. Comments upon log quality, herein discussed, are limited to the first run in the hole as this is the super-combo run. The raw, edited, and merged data are available in LAS ASCII format on a CD-ROM adjoining this report.

Suite/Run	Tool String	Interval (mMDRT)	BHT (degC)
1/1	DGR-ARC5 (LWD)	557.0-2109.0	
1/1	PEx(HRLA)-DSI-HNGS-SP-GPIT	2103.5-2530.0	109
1/2	FMI-GR-GPIT	2103.5-2530.0	114.5
1/3	MDT-GR	2144.0-2493.0	115.5
2/4	CSI-GR	1197.0-2530.0	

Table-3. Log Data Acquired

Copies of all sections of the Schlumberger field prints relevant to a petrophysical evaluation are included as Appendix-C. This appendix includes the log header details, remarks, results, and a complete parameter listing that provides the settings, constants, and environmental corrections applied at the wellsite.

Overall, the data is of a high quality, although the PEF log must be considered to have a lesser quality. This hole was drilled with a mud containing barite. Barite settles out as a solid, and therefore tends to concentrate in the mudcake. In a hole displaying limited wash out, such as this one, the thickness of the mudcake build-up opposite porous sandstones can be estimated by the difference between the bit size and the caliper, although there is always a degree of uncertainty in the environmental barite concentration correction applied. The optimal method of correcting the PEF log for the variable affects of barite is to calibrate and bulk shift the PEF to ensure that the clean quartzose sandstones coincide with the quartz point on a Rhomaa-Umaa cross plot. For the PEF log acquired in Thylacine-2, this required a –0.55 bulk shift.

Formation Test Data

One successful Modular Dynamics Tester (MDT) run resulted in the acquisition of 54 valid pressure tests and four samples, plus a number of tight and super-charged pressure points. These data are discussed in Appendix-2 of the Interpretive Well Completion Report, and thus will not be considered further here.

Routine and Special Core Analysis Data

A comprehensive routine (RCA) and special (SCAL) core analysis programme was undertaken from horizontal and vertical plugs taken from Cores-1-3. The range of analyses

were measured including ambient and overburden helium porosities; ambient, overburden, and Klinkenburg-corrected horizontal and vertical air permeabilities; probe permeabilities; grain densities; cation exchange capacities; porous-plate capillary pressures; relative permeabilities; cementation exponents; and saturation exponents. The results of many of these analyses are utilised in the petrophysical model discussed herein, and for calibration and quality control of the results of the petrophysical model. A selection of the cross-plots relevant to this petrophysical evaluation is included in Appendix-D

Details of the acquisition, measurement and quality control of these data are discussed in Appendix-3 of the Basic Well Completion Report and Appendix-8 of the Interpretive Well Completion Report, and thus will not be considered here further.

As discussed earlier, these core analysis results have been depth matched to wireline depths using the total porosity. The raw and depth shifted core analysis data are available in LAS ASCII on a CD-ROM adjoining this report.

BOREHOLE DATA

Hole Conditions

Apart from the upper 10 metres directly beneath the 9.625-inch casing shoe, the hole condition within 8.5-inch hole section is excellent. The caliper generally does not exceed the bitsize by any more than 0.5 inch, mudcake build-up is limited to less than 0.2 inch, and hole rugosity is minimal, except for one peak at 2315.0 metres.

Mud Properties

The section encompassing the Thylacine Member, Flaxman and Waarre Formations reservoirs was drilled with a KCl-PHPA-Glycol-barite mud. The mud and logging details are summarised in Table-4.

Bottom Hole Temperature

A Horner temperature plot generated for Suite-1 (Figure-2) yielded an extrapolated bottom hole temperature of 117.2 degree Celsius at 2528.0 mMDRT. The maximum-recorded

temperatures from the individual logging runs were used to environmentally correct the wireline log data.

Run number	1
Log date	8-Sep-2001
Depth-Driller	2525
Depth-Logger	2529
Bottom log interval	2530
Top log interval	2103.5
Casing-Driller	2101
Casing-Logger	2103.5
Casing Diameter	9.625
Bit Size	8.5
Hole Fluid type	KCl PHPA Glycol
Fluid Density	1.16
Fluid Viscosity	16
Fluid PH	9
Fluid Loss	3.7
Mud Sample Source	Active Pit
RM @ Surface	0.103
Mud temp Surface	15.0
RMF @ Surface	0.09
MF temp Surface	15.0
RMC @ Surface	0.24
MC Temp Surface	15.0
Source of RMF/RMC	PRESS
Time circ. stopped	13:15
Date circ. stopped	8-Sep-2001
Time logger at btm	00:15
Date logger at btm	9-Sep-2001
Surface hole temp	26.67
Surface temperature	15
Max recorded temp	109
Recorded by	F.Marcano,M.Van
Witness	M.Bilek,G.Weste
Filtrate Cl	43,000 ppm
PV	16
YP	20
% Solids	8
% Sand	Trace
% Oil	0
% KCl	KCl: 6.0%
% NaCl	NaCl: 2.9%
% Barite	Barite: 1.5%

Table-4. Mud Properties

HORNER TEMPERATURE PLOT

Thylacine-2 Suite-1

WELL:	Thylacine-2	**LOG SUITE:**	Suite-1	
PERMIT:	T/30P	**LOG DATE:**	08-Sep-01	
NOTES:	Sensor measure points estimated.	**T.D.:**	2530.0	(Logger)
		Geologist:	Chris Shield	

LOG TYPE	BOTTOM DEPTH OF LOGGED INTERVAL mRT {Sensor Measure Point}	Tx (hrs)	T (hrs)	T/(Tx+T)	Max. TEMP Deg C	Eq. Max TEMP Deg C
PEx(HRLA)-DSI-HNGS	2528.0	0.75	11.00	0.936	104	104.00
FMI-GR	2528.0	0.75	19.25	0.963	109	109.00
MDT-GR	2491.2	0.75	33.08	0.978	115	116.70
CSAT	2527.5	0.75	54.25	0.986	116	116.02

Where: Tx = CIRCULATION TIME
T = TIME SINCE CIRCULATION STOPPED

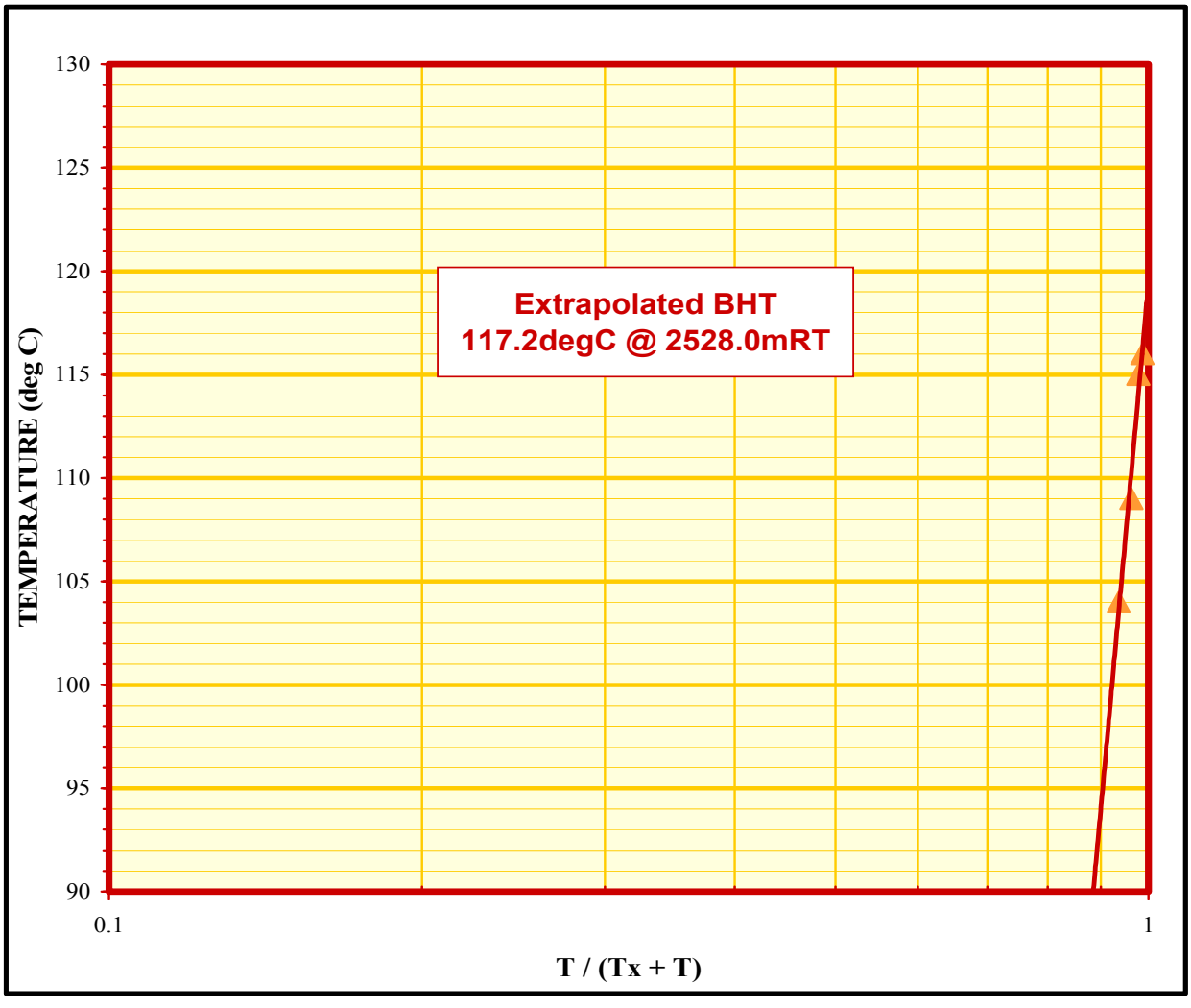


Figure-2. Suite-1 Extrapolated Borehole Temperature Plot

RESERVOIR QUALITY

The upper part of the interpreted interval (2115-2143.3 mMDRT) is described as argillaceous grey-olive brown, moderately hard to hard, sub-blocky, non-calcareous siltstone interbedded with rare siliceous cement and carbonaceous material, and forms part of the Belfast Formation.

The Thylacine Member (2143.3–2237.3mMDRT) is described as colourless to light grey, fine to medium-grained, well-sorted quartzose sandstone with rare calcareous cement and fair to poor visual porosity, and is interbedded with siltstone and minor claystone.

Between 2237.3 and 2354.9mMDRT, the Flaxman Formation is described as colourless to very light grey, very fine to medium-grained, moderately well to poorly sorted quartzose sandstone with trace siliceous and pyritic cement, carbonaceous material and fair visual porosity, interbedded with siltstone.

The upper Waarre Formation between 2354.9 and 2535.0mMDRT is described as very fine to coarse-grained, poorly sorted quartzose sandstone with trace siliceous cement and carbonaceous material, and exhibiting fair to good visual porosity, and is interbedded with siltstone.

LOG ANALYSIS METHODOLOGY

A complete listing of all reservoir zonations, petrophysical models, constants, and parameters applied in the interpretation are included in Appendix-E.

Preparation

The final Schlumberger wireline data were loaded from Origin Energy's master digital well log database into the Crocker Data Processing (CDP) Petrolog v9.2 software. As there were data of various resolutions, wireline data at 5 and 15cm, mudlog data at 50cm, and core plug data at 1cm spacings, all available data were re-sampled to the finest 1cm resolution. This

ensured that the core plug data could be accurately depth-matched, and maximised the degree of correlation between core and log-derived results.

Environmental Corrections

With the Platform Express tool, many environmental corrections are applied at the wellsite. The field prints (Appendix-C) contain a parameter listing, that details which environmental corrections that have been applied by the wireline engineer. This section summarises which corrections were applied, and whether they were applied at the wellsite, or in the Petrolog software in the office.

The gamma ray (GR) curve was corrected for borehole size using the density caliper, and KCl concentration at the wellsite. For the purposes of creating a composite log suite, the GR was corrected for casing thickness, where necessary, in the Petrolog software.

The borehole size and bed thickness corrections were applied to the laterolog data via inverse resistivity modelling at the wellsite. Invasion corrections were applied at the wellsite, resulting in a true formation resistivity (Rt) and invaded zone resistivity (Rxo) curve provided by Schlumberger. Mudcake thickness corrections were applied to the microlaterolog data at the wellsite.

The density (RHOB) log data were corrected for borehole size and mud density at the wellsite. The compensated neutron (NPHI) log was corrected for borehole size and salinity, formation temperature and pressure, mudcake thickness, and mud density at the wellsite. Formation salinity and barite corrections were applied in the Petrolog software.

Zonation

The well was zoned according to the formation tops listed in Table-1. These formational zones were further subdivided into petrophysical facies zones, thus enabling the recognition of sand, silt, and clay-dominated rock types. This procedure was performed by zoning areas of a density-neutron cross-plot for each formation.

This subdivision enabled different inputs and constants to be applied to the different petrological facies within each formational unit. The identification of clay volume parameters

and of clay resistivity values was made more accurate as these parameters were determined from only those points dominated by clay. In a similar fashion, the identification of formation water resistivity and hydrocarbon density could now be evaluated using only sandstone dominated petrophysical facies.

Clay Volume and Porosity

Clay volume (VCl) was defined by application of a linear GR, RHOB-NPHI cross-plot, RHOB-DT cross-plot, and sonic (DT) models (Figure-3). The minimum VCl calculated from all techniques was applied as the final VCl in this interpretation. VCl parameters were set to ensure that the average values calculated from logs matched the core, sidewall cores and cuttings descriptions.

A linear density-neutron model was applied to derive total porosity (PHIT), with a Wyllie sonic porosity model being applied in badhole areas. Badhole was defined using cut-offs for differential caliper, DRHO, and hole rugosity. The density and neutron data were corrected for hydrocarbon density prior to determining the log-derived total porosity. The total porosity was then matched to the overburden helium core porosity, prior to the correction for clay volume and the subsequent derivation of effective porosity.

$$PHIT = \frac{((\rho_{ma} - \rho_b)/(\rho_{ma} - \rho_f)) + \varphi_N}{2}$$

The log derived hydrocarbon density was calculated at 0.51 g/cc, by cross plotting effective porosity versus the apparent grain density (Figure-4). The MDT samples suggest that the hydrocarbon in these reservoirs is gas, and therefore significantly less dense than 0.51 g/cc. There are two possible explanations for this, it is possible that the area of investigation of the density tool was affected by the presence of mud filtrate, or that the density log is responding to the hydrocarbon density of both the movable and immovable hydrocarbon phases in the reservoir, whereas the MDT is only reporting the hydrocarbon density of the movable gaseous hydrocarbon.

Lithology

Petrological studies, detailed in Appendix-6 of the Interpretive Well Completion Report, and conducted on core and sidewall cores samples from Thylacine-1 and Geographe-1, indicate that some of the sandstone reservoirs contained significant amounts of carbonate cements and argillaceous matter. To allow for this variable mineralogy, particularly the carbonate cementation, a complex lithology petrophysical model was applied in preference to a silty sand petrophysical model. The application of this complex lithology model aims to optimise the calculation of total porosity for subtle changes in the matrix density as a result of changing concentration in carbonate cement.

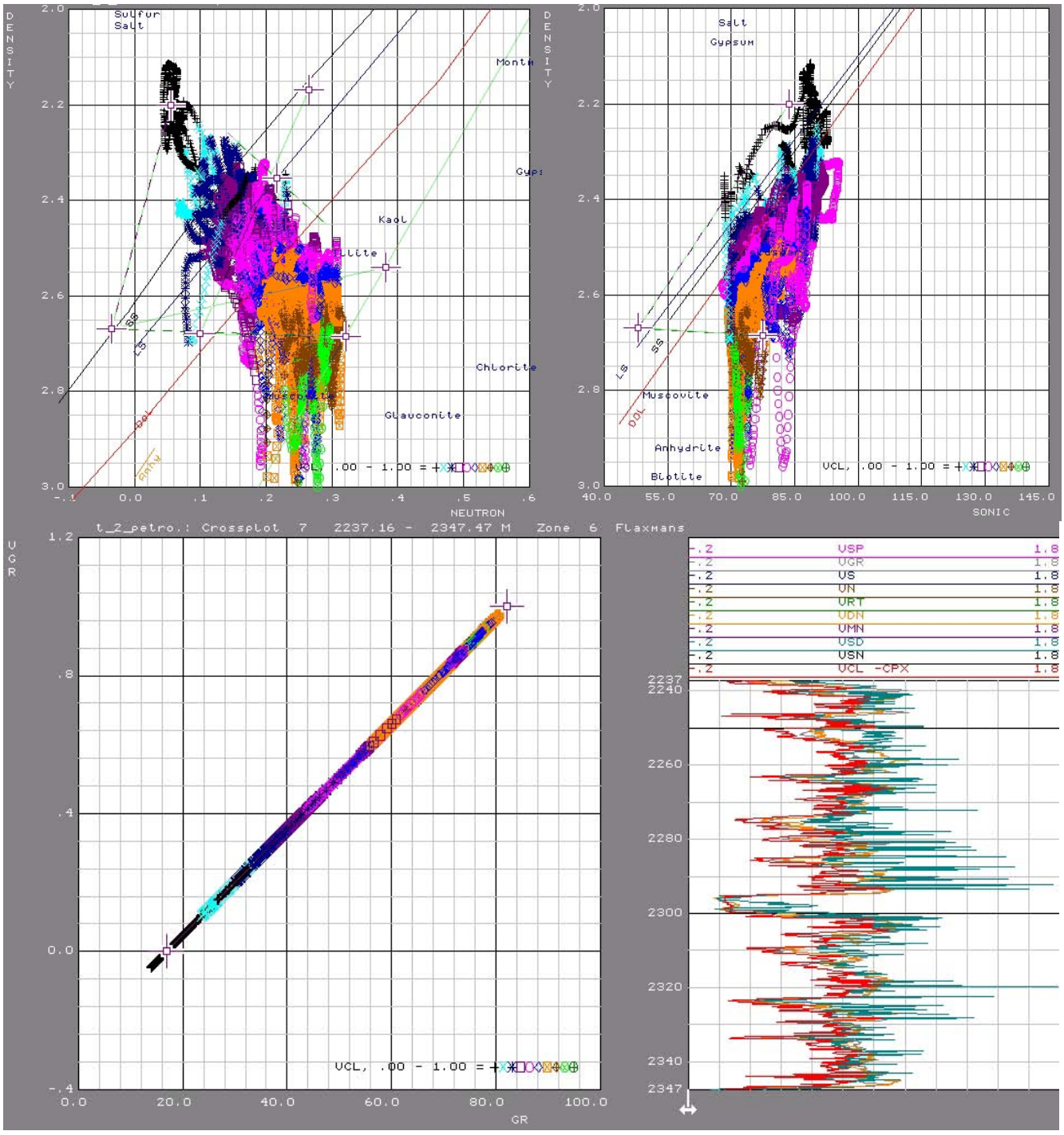


Figure 3. Clay volume determination. Comparison of results from the RHOB-NPHI, RHOB-DT, and GR techniques for the Flaxman Formation, 2237.2-2347.5 mMDRT.

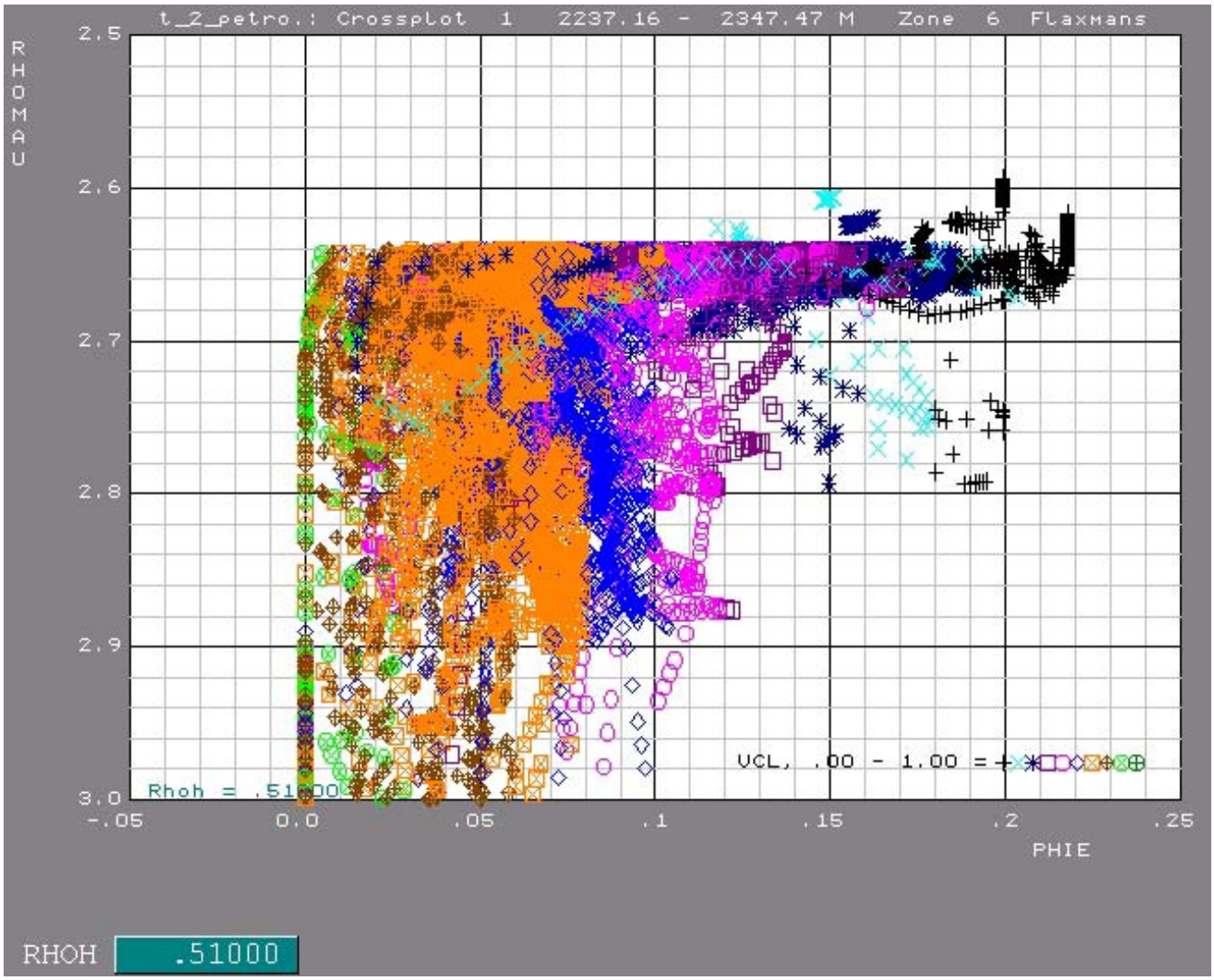


Figure 4. Hydrocarbon density derivation from cross-plot of effective porosity versus apparent grain density.

This model however, does have its drawbacks. As previously discussed, the PEF log, which is an essential component of the complex lithology model, required a bulk correction of –0.55 to the PEF data in order to optimise the distinction between quartz and carbonate cements.

Formation Water Resistivity

The formation water resistivity was defined using the Rwa technique by the application of Hingle (Figure-5) and Pickett (Figure-6) crossplots of sandstone-dominated zones beneath the gas water contact.

A review of offset well data with reliable formation water chemistries was conducted prior to the drilling of Thylacine-2. The results of this study are compared with formation water resistivity data from nearby offset wells in Table-5.

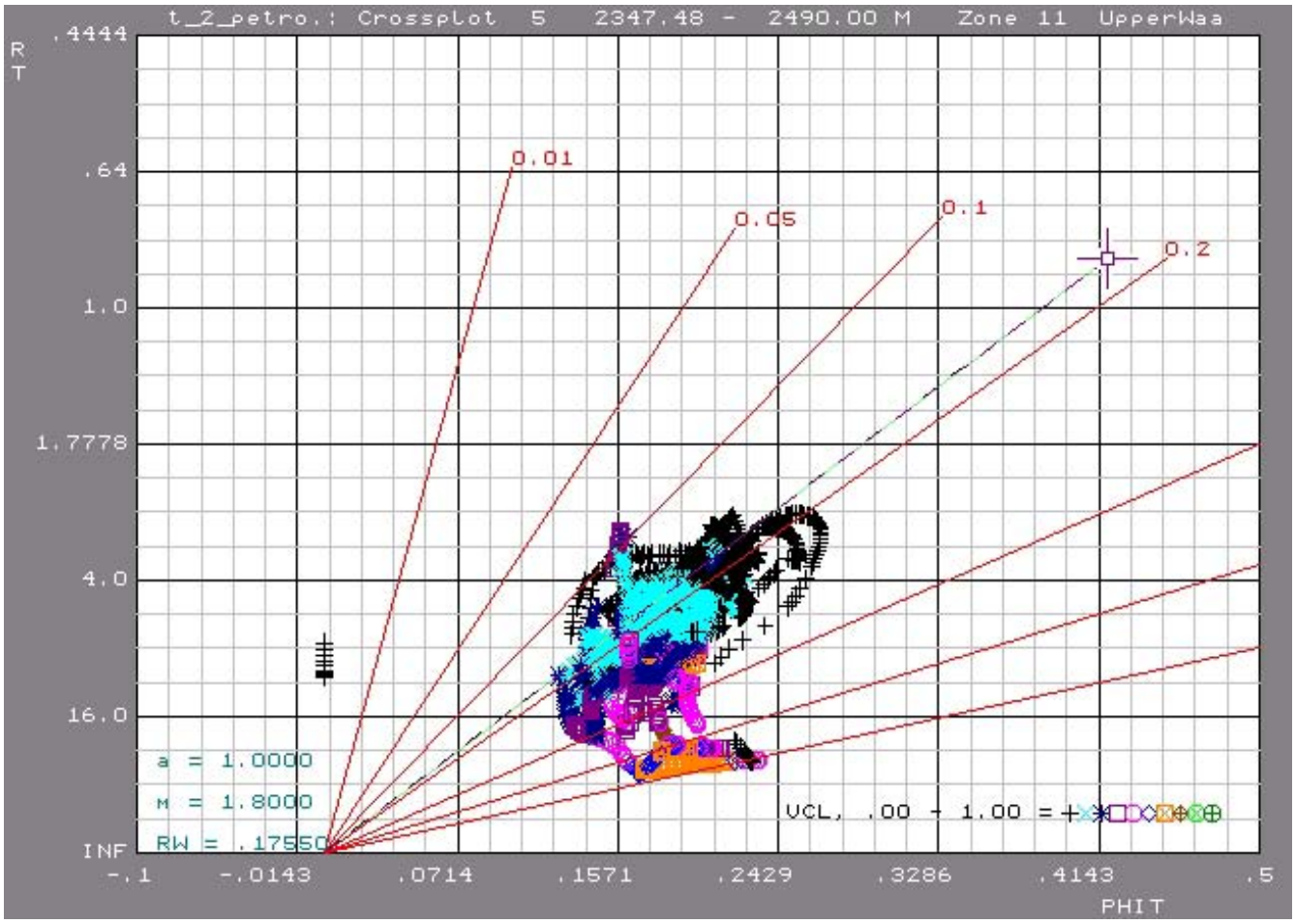


Figure 5. Hingle cross-plot defining formation water resistivity from Upper Waarre Formation below the GWC. Sand petrofacies displayed.

Water Saturation

Based upon the results of the petrophysical analyses of both Thylacine-1 and Geographe-1, where more realistic results were obtained by application of an Indonesian equation than a Waxman-Smits equation, only an Indonesian equation hydrocarbon saturation was calculated for Thylacine-2.

The tortuosity factor (a) was kept constant at one. Values for the cementation exponent (m) and the saturation factor (n) were determined from the results of the special core analysis study. These values remained constant for each petrophysical facies, and across the various lithostratigraphic units (Table-6).

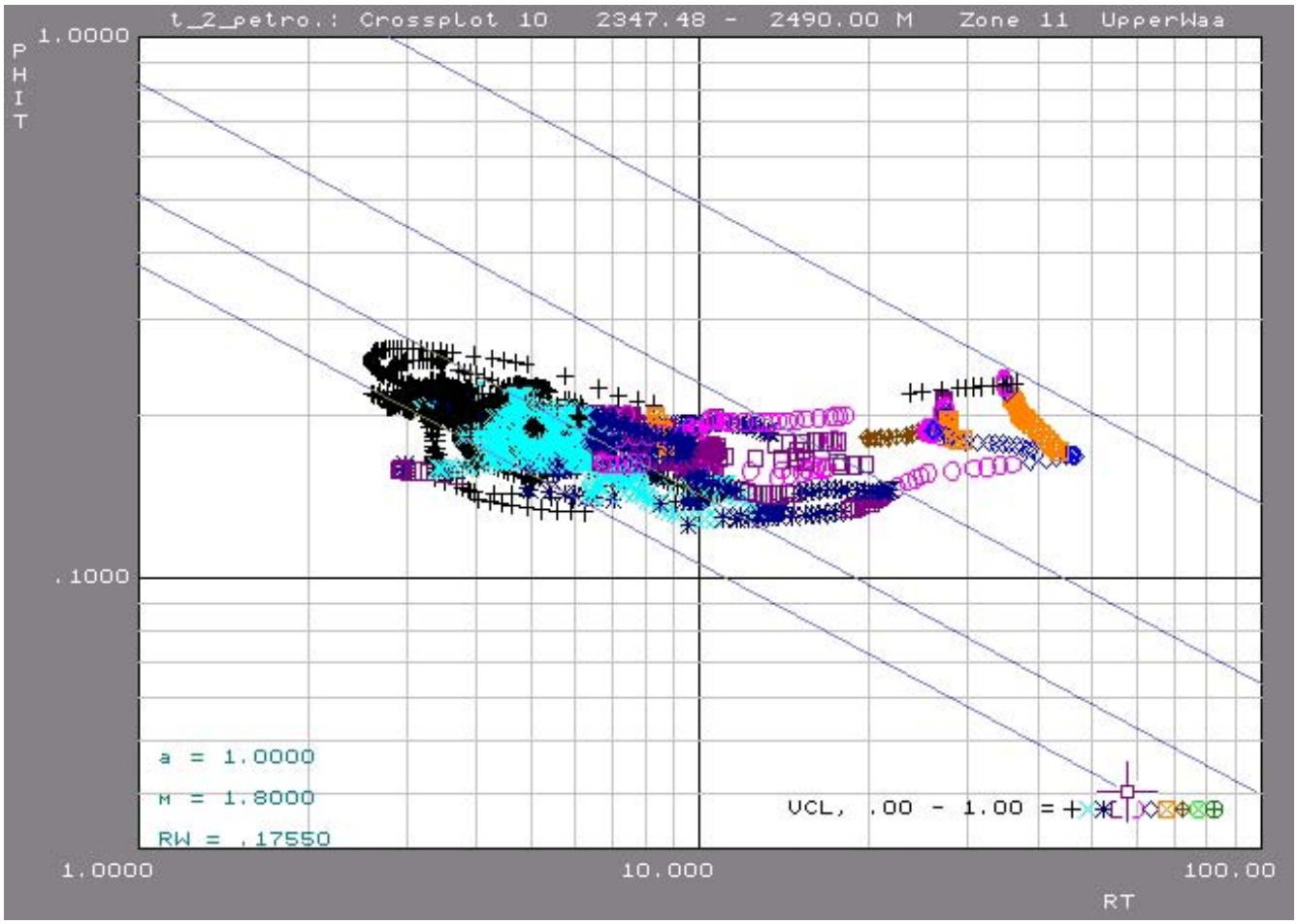


Figure 6. Pickett cross-plot defining formation water resistivity from lower Waarre Formation below the GWC. Sand petrofacies displayed.

Well	Depth (m)	Rw@ Temp (Ωm @ °C)	Salinity (ppm NaCl Eq)	Source
Thylacine-2	2115-2530	0.46 @ 25	13,000	Rwa derived from logs
Geographe-1	2050-2403	0.42 @ 25	14,280	Rwa derived from logs
Thylacine-1	2335-2613	0.46 @ 25	13,000	Rwa derived from logs
Minerva-1	1816-1838	0.48 @ 25	13,800	DST-1 fluid recovery
Pecten-1A	1771-1784	0.32 @ 25	20,700	Production test fluid recovery
Conan-1	1830-1950	0.50 @ 25	11,700	Rwa derived from logs

Table-5. Waarre Formation water chemistry data

Petro-facies	Tortuosity Factor (a)	Cementation Exponent (m)	Saturation Exponent (n)	Clay Resistivity (RCl)
Sandstone	1.00	1.80	1.75	50.0 ohmm
Siltstone	1.00	2.00	1.95	50.0 ohmm
Claystone	1.00	2.35	2.15	50.0 ohmm

Table-6. Summary of electrical properties applied in the Indonesian Equation

The Indonesian equation, which is an effective porosity system that calculates an effective water saturation, derives its shale conductivity factor from the resistivity log-derived Rt. A log-derived clay resistivity (RCl) is defined by cross-plotting the apparent formation water resistivity (Rwa) versus GR for the clay-rich petrophysical facies (Figure-7). This RCl value remains a constant across all zones that are deemed to contain similar clay properties.

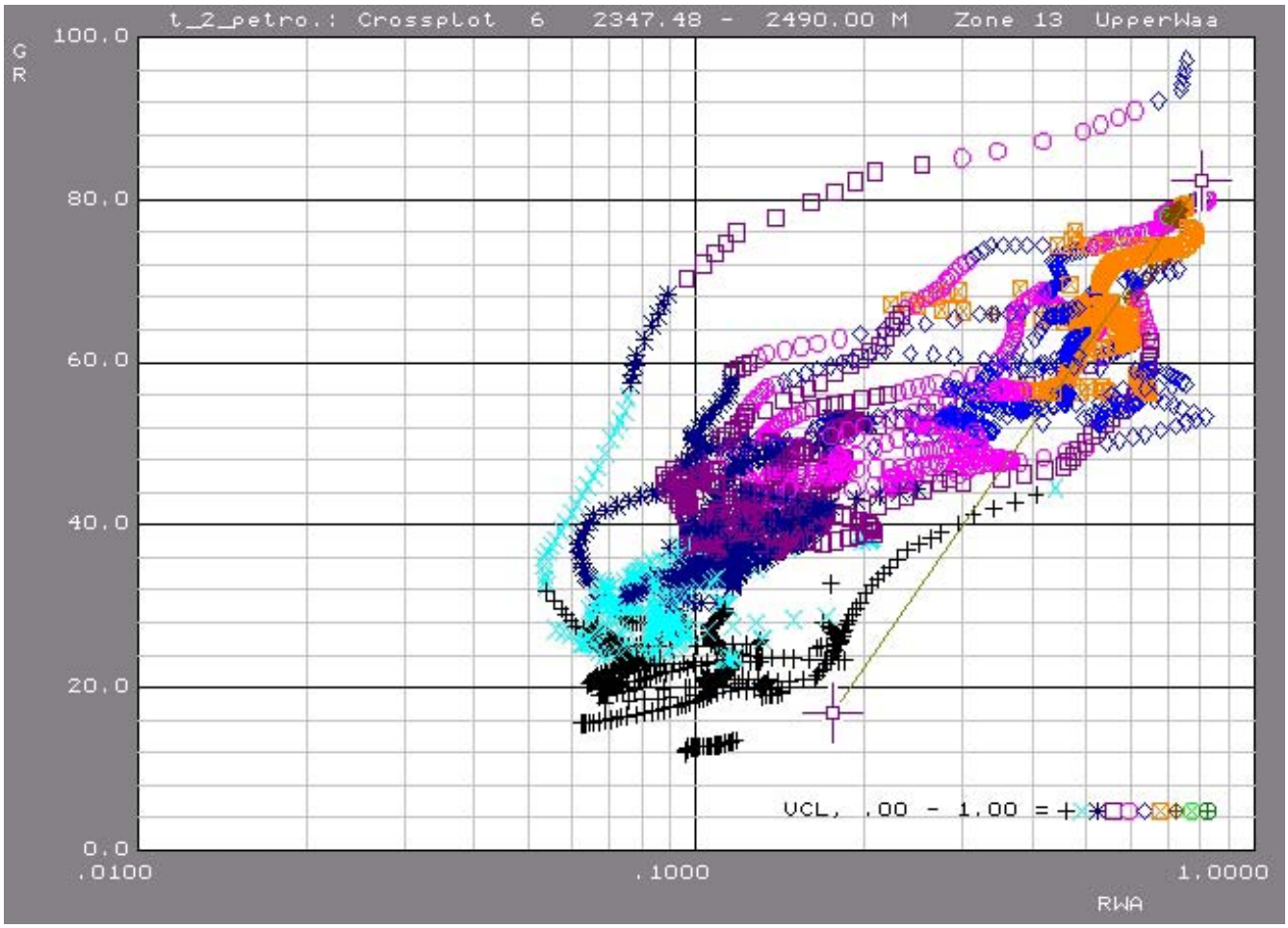


Figure 7. Clay resistivity derivation as applied in the Indonesian water saturation equation. Clay petrofacies displayed.

Permeability

As a component of the special core analysis study, gas-slippage and Klinkenburg-corrected overburden permeabilities were measured from both horizontal and vertical core plugs. These data act as a reference for any log-derived permeability equation. Permeability is often correlated to porosity alone, but this correlation is fraught with inaccuracy, as there are other rock parameters that can affect permeability. The intrinsic permeability of a rock is affected by its clay content, as increasing clay content in the pore space will decrease the flow rate at which a fluid can pass, and also increase the pressure gradient required to make the fluid

flow. A useful qualitative indicator of the distance which a fluid has been able to flow into a formation is given by the difference between the true formation resistivity and the invaded zone resistivity (Rt-Rxo). With decreasing flow rates of mud filtrate into a formation, the difference between these values diminishes to the point that in a claystone, the Rt and Rxo have the same value as the mud filtrate cannot enter the formation as there is no permeability.

As the core analysis data have been accurately depth-matched to wireline depths, it is possible to conduct a multiple linear regression of VCl, PHIT, and Rt-Rxo to derive an effective overburden air permeability curve. This log-derived permeability is displayed on Enclosures-1and 2, and is derived as

$$K_{Air} = 10\text{^}(13.824 \times PHIT - 1.240 \times VCl + 0.638 \times \log(Rt - Rxo) - 2.281)$$

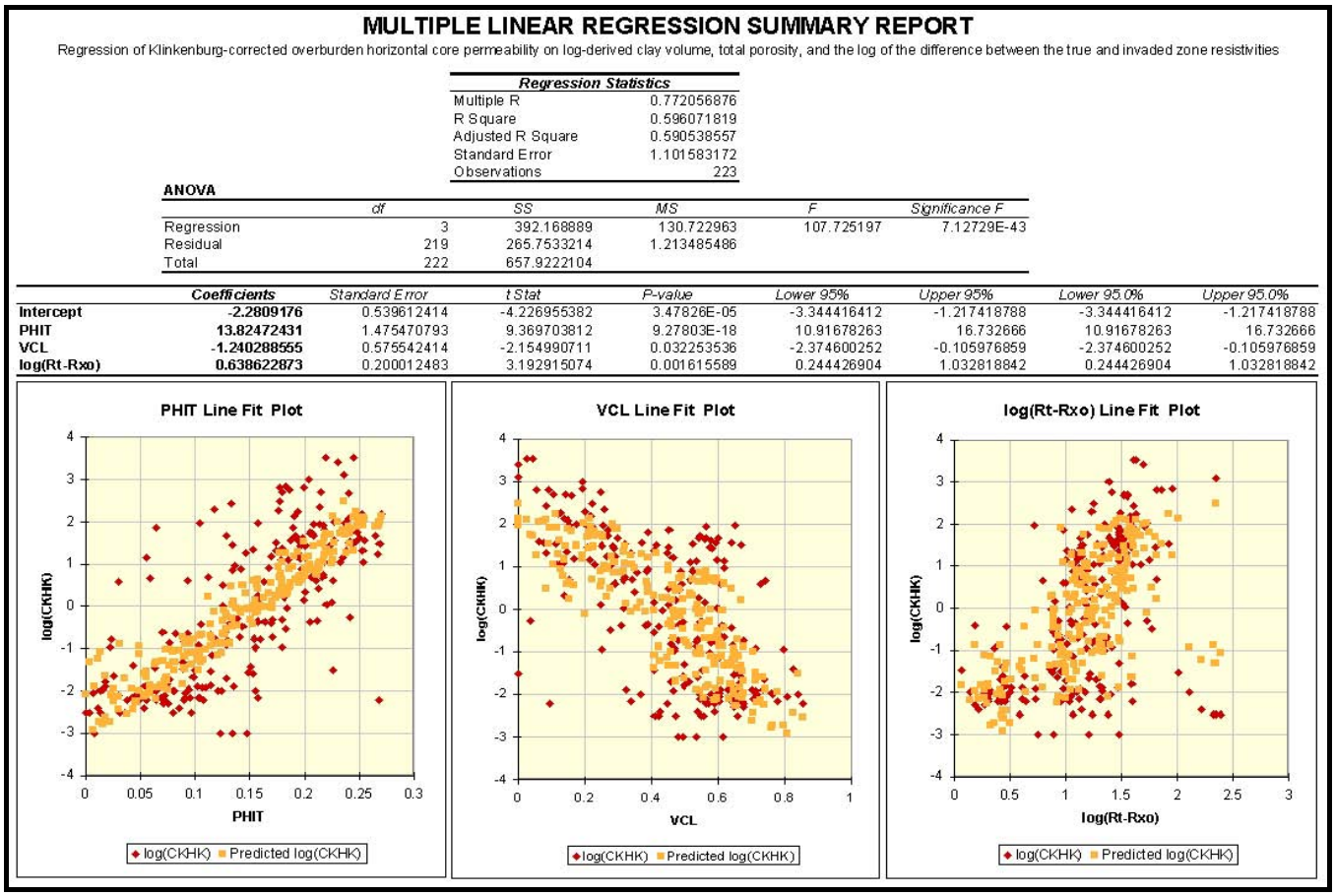
This technique produces a 77% correlation co-efficient between the measured overburden Klinkenburg-corrected permeabilities and the log-derived air permeabilities (Figure-8). This equation incorporates all available routine and special core analysis data for all four wells drilled on the Thylacine and Geographe structures drilled to date. This equation is only quantitatively valid for reservoirs above the gas water contact (GWC), as the values for Rt and Rxo are affected by the nature of the fluid in the pore space. Although average permeabilities have been quoted for rocks below the GWC in subsequent sections of this report, it should be remembered that any reported average log-derived permeabilities in water-bearing strata should be considered qualitatively and would be expected to under-estimate true values.

The SCAL data were used to derive a correlation between the overburden air, and both gas and water permeabilities (Figures-9, 10). These relationships were used to generate gas and water permeability curves, which are also only quantitative above the GWC.

Reservoir Summary Parameters

The cut-off limits for petrophysical parameters are detailed in Table-8. A maximum clay volume of 40% is the basis of the net rock calculation. Net reservoir is defined as those net rocks having a log-derived overburden Klinkenburg-corrected horizontal gas permeability of

greater than 0.1mD. Average effective water saturations are reported for zones above the gas-water contact. The petrophysical results are summarised in Table-9.



MULTIPLE LINEAR REGRESSION SUMMARY REPORT

Regression of Klinkenburg-corrected overburden horizontal core permeability on log-derived clay volume, total porosity, and the log of the difference between the true and invaded zone resistivities

Regression Statistics	
Multiple R	0.772056876
R Square	0.596071819
Adjusted R Square	0.590538557
Standard Error	1.101583172
Observations	223

ANOVA

	df	*SS*	*MS*	*F*	*Significance F*
Regression	3	392.168889	130.722963	107.725197	7.12729E-43
Residual	219	265.7533214	1.213485486		
Total	222	657.9222104			

	Coefficients	*Standard Error*	*t Stat*	*P-value*	*Lower 95%*	*Upper 95%*	*Lower 95.0%*	*Upper 95.0%*
Intercept	**-2.2809176**	0.539612414	-4.226955382	3.47826E-05	-3.344416412	-1.217418788	-3.344416412	-1.217418788
PHIT	**13.82472431**	1.475470793	9.369703812	9.27803E-18	10.91678263	16.732666	10.91678263	16.732666
VCL	**-1.240288555**	0.575542414	-2.154990711	0.032253536	-2.374600252	-0.105976859	-2.374600252	-0.105976859
log(Rt-Rxo)	**0.638622873**	0.200012483	3.192915074	0.001615589	0.244426904	1.032818842	0.244426904	1.032818842

Figure-8. Log-derived permeability derivation via multiple linear regression.

Reservoir	VCl < (%)	Kgas > (mD)
Thylacine Member, Flaxman Formation, Waarre Formation	40	0.1

Table-7. Cut Off Parameters

Fluid Contacts

A gas-oil contact cannot be identified from the logs, and it is assumed that the reservoir at the Thylacine-2 location does not contain an oil-leg. The lowermost gas-bearing sandstone is present at 2325.7 mMDRT. A thin sandstone bed at 2334 mMDRT displays inconclusive hydrocarbon saturation. Based upon the Spontaneous Potential log, the GWC may be interpreted as low as 2343 mMDRT. Due to poor reservoir quality across the potential GWC, the FWL should be best defined by the MDT log pass.

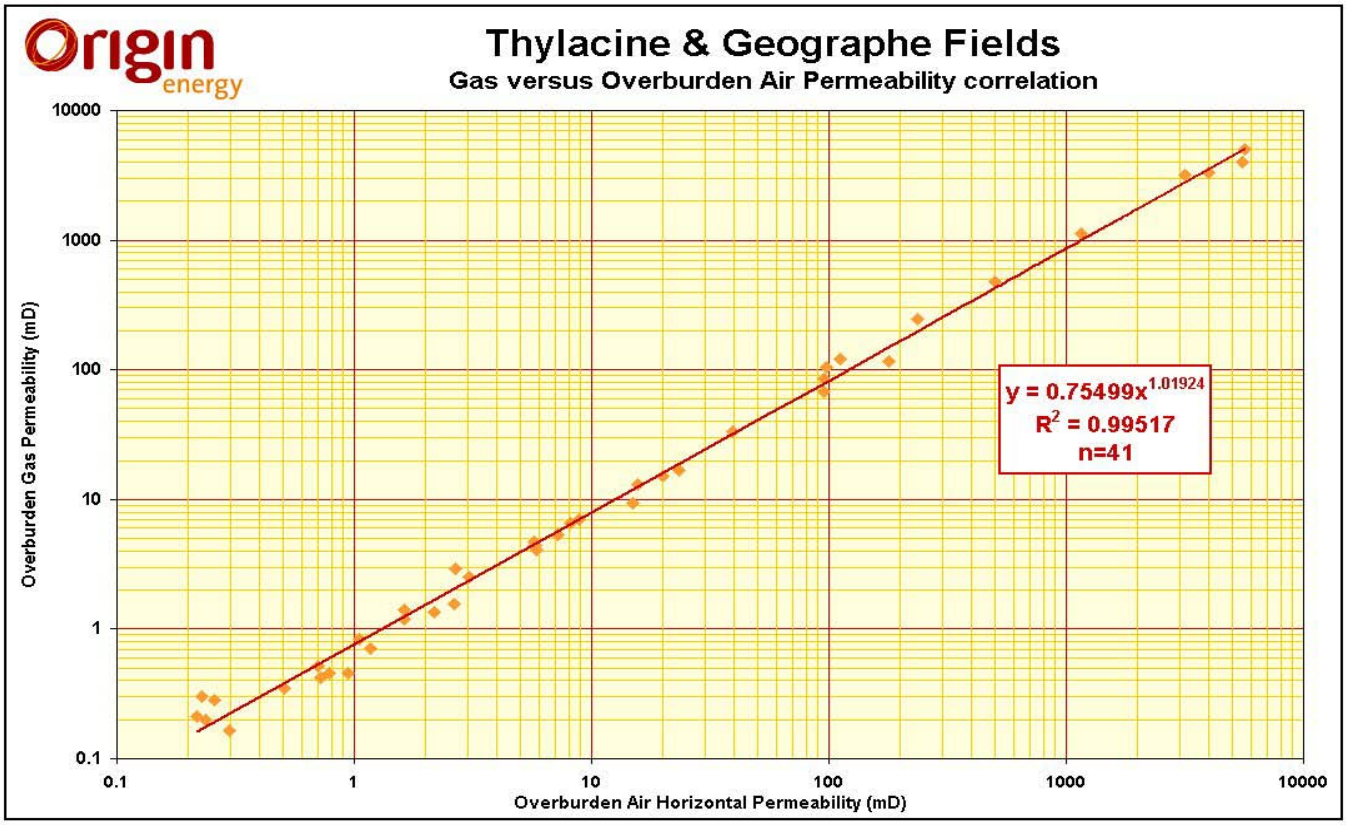


Figure-9. Relationship between core-derived overburden air permeability and gas permeability.

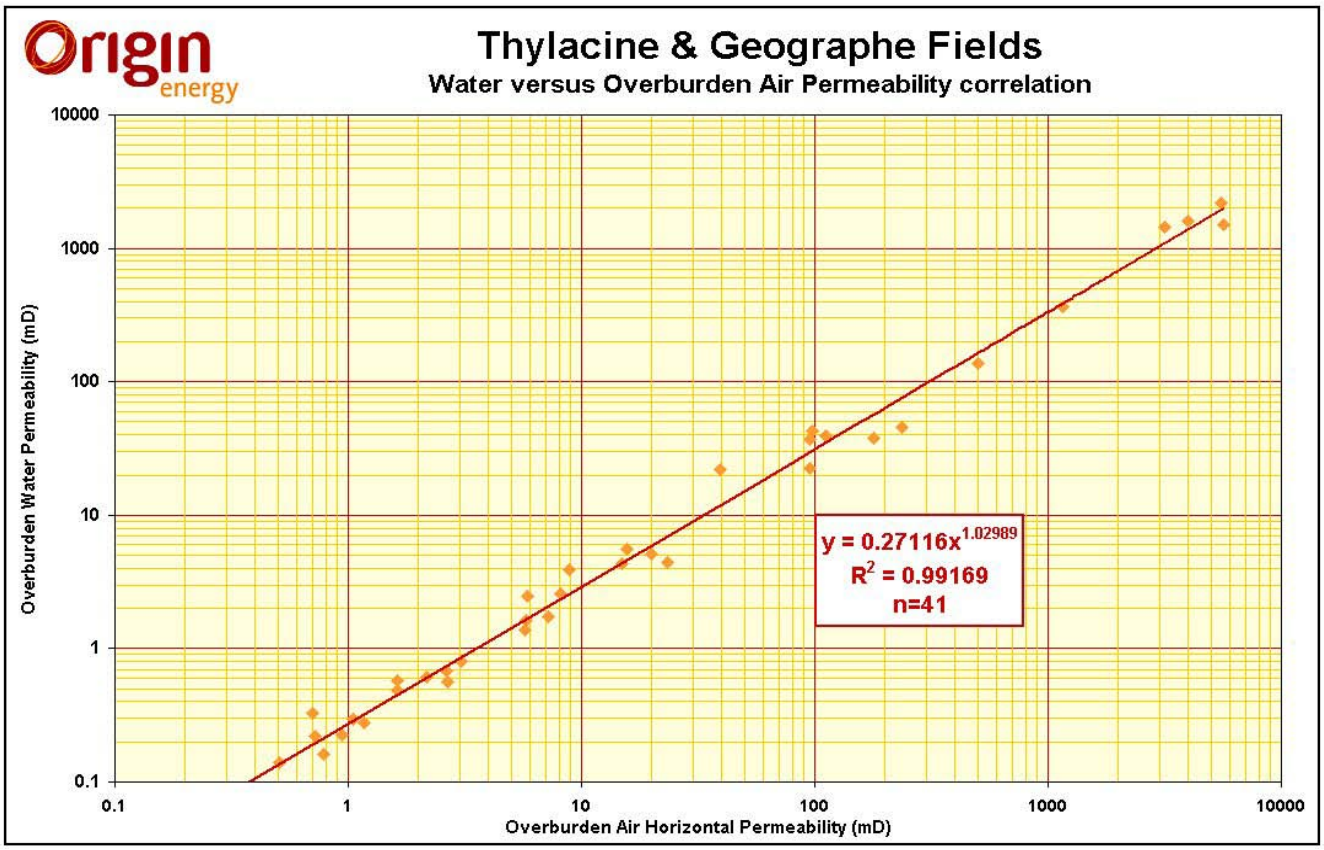


Figure-10. Relationship between core-derived overburden air permeability and water permeability.

FORMATION NAME	TOP FROM	BASE TO	GROSS INTERVAL	NET RESERV INTERVAL	AVERAGE VCL	AVERAGE PHIE	AVERAGE AIR PERM	AVERAGE GAS PERM	AVERAGE H_2O PERM	AVERAGE SWE	NET RES / GROSS
	mMDRT	mMDRT	mMDRT	mMDRT	%	%	mD	mD	mD	%	%
Thylacine Member	2143.30	2237.30	94.00	54.92	28.20	14.79	1.04	0.78	0.28	74.88	58.43
Flaxman Fm-GWC	2237.30	2325.70	88.40	25.24	18.86	14.76	2.26	1.73	0.63	57.87	28.55
		TOTAL	**182.40**	**80.16**	**25.26**	**14.78**	**1.32**	**1.01**	**0.36**	**69.53**	**43.95**

Thylacine Member	2143.30	2237.30	94.00	54.92	28.20	14.79	1.04	0.78	0.28	74.88	58.43
Flaxman Formation	2237.30	2354.90	117.60	32.40	19.27	14.65	1.86	1.42	0.51	64.32	27.55
Upper Waarre Fm	2354.90	2536.24	181.34	98.64	16.90	15.88	1.15	0.87	0.31	94.64	54.40

Cut-offs Applied		
Net Pay	K_gas >	0.1mD
	VCl <	40.0%

Table-8. Reservoir Summary

DISCUSSION

The Thylacine Member (2143.3-2237.3 mMDRT) encountered at Thylacine-2 is interpreted to have moderate reservoir quality. The unit has a net to gross of 58.4%, although the sandstones that are present contain high clay volumes, averaging 28.2%. Calculated effective porosities average only 14.8% for these reservoirs. As a result, the log-derived gas permeability is considerably reduced in comparison to other cleaner reservoirs, geometrically averaging only 0.78mD, which will negatively affect this unit's producibility and recovery factor. The average effective water saturation is 74.9%.

The Flaxman Formation (2237.3-2354.9 mMDRT) has much better reservoir development in part, although the overall net to gross ratio is low. The sandstones present, on average, are cleaner and have an average clay volume of 19.3%. The average effective porosity is similar (14.7%), but the average gas permeability is higher, averaging 1.4mD. This unit has a net reservoir to gross of 27.6%, and an average effective water saturation of 64.3%.

The Upper Waarre Formation is only present below the gas-water contact, but displays average clay volumes of 16.9%, average effective porosities of 15.9%, and an average net to gross ratio of 54.4%

Between the four wells now present on the Thylacine and Geographe fields, sufficient core analysis data is present to calibrate the log responses, and no more core analysis is considered necessary, except for the measurement of CEC on very clean sandstone plugs, to aid in the future application of the Waxman-Smits saturation equation

Given the thinly-bedded nature of the Thylacine Member and Flaxman Formation, it is recommended that all wireline logs are acquired in high resolution mode. To enable consistency in logging responses, and avoid subtle variations in the measurement of different company's logging tools, it is recommended that the same principle logging suite (PEx(HRLA)-DSI-SP) be run in subsequent wells. This is particularly relevant, as core to log correlations have been made using these data, and subsequent wells on these fields are unlikely to contain further cores.

CONCLUSIONS / RECOMMENDATIONS

- The Thylacine Member (2143.3-2237.3 mMDRT) contains sandstones that, due to their argillaceous nature, would be likely to be capable of only moderate producibility.
- The Flaxman Formation (2237.3-2354.9 mMDRT) has a poor net to gross ratio, but contains cleaner and more porous and permeable sandstones that would be expected to achieve high gas production rates.
- Core-to-log correlations of porosity and permeability are adequate to suggest that the acquisition of further core and core analysis data would not significantly increase the confidence level applied to the petrophysical analysis.
- The addition of barite to the mud should be limited or eradicated if possible, in order to improve the quality of density and PEF data in future wells.
- There is no petrophysical requirement to acquire LWD data in future wells, as the wireline resistivity data is considered a more reliable indicator of the nature and volume of the fluids in the pore space.

Appendix – A
Log Depth-matching Summary

SONIC INSIDE CASING TO SURFACE GAMMA RAY PASS

DEPTH MATCH LOGS - MNEMONIC
NPHI GR HCGR HTPR HTUR HUPR DF HURA HFK HSGR SVEL HGR HCFT HTNP CS ETIM TENS HCAL CVEL IHV SCD FCAY FCAZ FTIM HAZIM RB_GPIT P1AZ_GPI PR HAZI P1AZ RB SDEV ITT DTSM DT2 DT4P DT4S ECGR VPVS DT2R DTRP DTRS DTTP DTTS RGR DTCO SSVE EHGR HNPO FCAX TNPH CFTC HTHO HCNT CNTC NPOR

REFERENCE LOGS – MNEMONIC
GR

DEPTH UNITS = M
1354.328 1353.922
1357.478 1357.122
1359.586 1358.748
1361.237 1360.500

MAIN PASS TO SONIC INSIDE CASING

DEPTH MATCH LOGS - MNEMONIC
NPHI GR HCGR HTPR HURA HFK HSGR HTUR HUPR DF.QCPOR HGR HCFT SPAR HAZI CS TIME ETIM TENS SP P1AZ RB SDEV ITT HDAR CVEL IHV SCD HCAL FCAX FCAY FCAZ FTIM HDRA HAZIM RB_GPIT P1AZ_GPI PR HMNO RSOZ RM_HRLT RLA0 RXO_HRLT SDEVM RLA5 RLA4 RLA3 RLA2 RLA1 DSOZ RSO8 EHGR RXO8 RXOI RGR HTNP GR DT4S_MIN DT4S_PLU DT4S VPVS PR RXOZ RHO8 RHOZ PEF8 PEFZ QCRH HPRA DSO8 QCPEF HMIN SVEL TNPH CFTC HTHO HNPO RT_HRLT HCNT DI_HRLT CNTC NPOR DTSM DT1 DTCO DT2 DT4P DT4S DT5 ECGR VPVS DT1R DT2R DTRP DTRS DTTP DTTS QCMCFL SSVE QCRXO

REFERENCE LOGS - MNEMONIC
GR

DEPTH UNITS = M
2091.156 2090.115
2097.507 2096.414
2103.729 2102.866
2108.733 2107.768
2112.543 2111.527
2115.998 2115.058

DSI PROCESSING TO MAIN PASS

DEPTH MATCH LOGS - MNEMONIC
GR DTSM_MIN DTCO DTCO_MIN DTCO_PLU DTSM

REFERENCE LOGS - MNEMONIC
GR

DEPTH UNITS = M
2090.902 2090.344
2096.999 2096.414
2103.806 2102.993

2111.680	2110.740
2122.271	2121.459
2127.885	2127.021
2144.344	2143.480
2163.673	2162.810
2176.729	2175.891
2204.568	2203.704
2282.368	2281.504
2333.752	2332.863
2427.757	2426.919
2484.196	2483.307

LWD TO SONIC INSIDE CASING

DEPTH MATCH LOGS - MNEMONIC
GR_CDR ROP ATR PSR

REFERENCE LOGS - MNEMONIC
GR

DEPTH UNITS = M

160.858	158.064
176.454	173.685
203.556	202.540
222.504	221.818
238.633	237.769
241.503	241.046
252.679	252.832
266.598	265.760
272.517	270.916
284.632	282.677
302.514	299.898
324.485	322.478
340.893	338.353
371.907	368.960
388.569	386.944
398.602	397.510
410.439	409.296
430.530	430.047
437.642	437.286
450.545	450.393
470.560	469.290
500.507	500.659
514.452	514.706
520.624	521.589
530.758	532.130
541.198	542.696
547.751	549.300
557.784	559.054
566.039	566.395
575.335	575.767
578.968	579.349
581.355	581.736
584.251	583.641
585.292	584.657
591.261	589.991
595.300	594.335
598.068	597.459
602.920	603.199

605.663	605.714
607.390	607.720
608.838	609.168
611.454	610.514
613.359	612.394
619.404	618.744
637.057	636.600
643.585	643.280
647.446	647.446
652.678	653.288
656.361	657.987
658.622	659.867
660.629	661.721
662.483	663.651
665.201	666.318
668.452	668.477
672.160	672.109
674.497	674.903
677.418	677.824
684.098	684.505
687.349	687.984
691.388	691.794
692.760	693.191
695.096	695.884
697.967	698.830
700.888	701.827
704.139	704.393
707.873	708.381
712.191	711.937
713.181	712.699
713.994	713.435
715.975	714.578
716.686	715.543
718.134	717.194
720.039	718.845
720.623	719.455
723.595	724.129
724.840	725.373
741.274	741.375
744.703	744.982
746.150	746.481
748.132	748.462
751.891	751.611
753.618	753.110
756.387	757.174
759.308	760.527
761.771	762.686
764.083	764.921
766.089	766.216
770.814	771.119
774.116	774.573
778.713	779.501
781.837	782.803
791.210	793.039
795.655	798.195
799.846	801.802
803.707	805.002
807.314	807.796
810.158	810.209
815.467	815.315
819.404	819.734

823.773	823.747
826.084	826.033
829.285	828.726
841.934	841.781
845.693	845.642
848.360	848.106
852.068	851.103
854.735	853.567
858.622	857.275
862.787	862.101
876.427	875.944
882.980	881.532
905.510	904.469
920.648	922.401
937.514	938.987
945.744	947.141
954.024	955.624
956.513	958.215
962.609	964.641
971.144	974.268
982.116	985.114
986.866	989.533
989.457	991.337
993.572	994.791
995.629	996.848
1005.205	1006.399
1011.885	1013.155
1019.454	1020.089
1026.338	1026.490
1034.136	1034.161
1047.217	1047.572
1072.134	1072.235
1093.597	1093.572
1127.836	1127.912
1143.864	1143.838
1159.789	1159.510
1179.982	1180.160
1192.759	1193.190
1223.772	1223.594
1239.215	1239.342
1268.349	1268.578
1283.818	1284.224
1296.340	1296.721
1323.518	1324.178
1342.390	1342.847
1359.891	1360.627
1361.415	1361.872
1364.539	1364.666
1370.330	1370.203
1379.423	1379.322
1391.056	1390.751
1406.677	1406.601
1417.142	1416.736
1424.737	1424.610
1443.101	1442.999
1459.865	1459.687
1464.767	1464.564
1470.457	1470.431
1487.754	1487.805
1524.584	1524.686
1541.424	1541.551

1578.991	1579.067
1598.651	1599.006
1609.903	1610.487
1617.193	1617.548
1619.199	1620.672
1627.988	1629.486
1629.435	1630.934
1631.137	1631.493
1633.245	1633.728
1639.468	1639.976
1653.845	1654.226
1658.544	1659.509
1670.913	1671.523
1677.873	1678.102
1683.817	1684.579
1687.347	1687.906
1699.666	1700.022
1717.142	1718.081
1727.149	1727.987
1730.883	1731.188
1732.635	1732.813
1741.373	1741.678
1748.663	1749.450
1757.756	1758.493
1772.615	1773.530
1791.081	1791.716
1802.257	1802.968
1818.360	1818.843
1840.078	1840.306
1867.408	1867.205
1890.293	1890.116
1896.059	1895.805
1927.225	1927.479
1929.079	1929.231
1932.178	1932.178
1934.388	1934.413
1936.902	1937.258
1938.731	1939.823
1941.195	1942.058
1950.034	1950.847
1958.111	1959.077
1973.555	1974.520
1991.030	1991.919
2008.911	2009.470
2018.233	2019.046
2037.054	2038.274
2051.075	2052.853
2063.521	2065.325
2079.930	2081.885
2086.839	2088.642

CORE TO WIRELINE

DEPTH MATCH LOGS – MNEMONIC
CPOO CPOR CKHA CKVA CKHO CKVO GDEN SNUM CKHP SNUM COGR CPOR CKHA CKVA CPOO CKHO CKVO GDEN SNUM CKHP SNUM

REFERENCE LOGS - MNEMONIC
PHIT-CPX

```
DEPTH UNITS = M
  2206.900  2207.090
  2230.450  2230.350
  2238.850  2238.370
  2249.650  2249.380
  2256.490  2256.220
  2262.710  2261.510
  2276.030  2274.850
  2280.940  2279.810
  2301.640  2299.900
  2312.480  2311.380
```

MUDLOG TO WIRELINE

```
DEPTH MATCH LOGS – MNEMONIC
DEPT ROP TGAS C1 C2 C3 ic4 nC4 iC5 nC5 CO2 WOB RPM SPP FLOW SPM LAG TPIN TPOT MWIN
MWOT TQAV TQMX TBR DXC BITD BITT CALC DOLO TVD

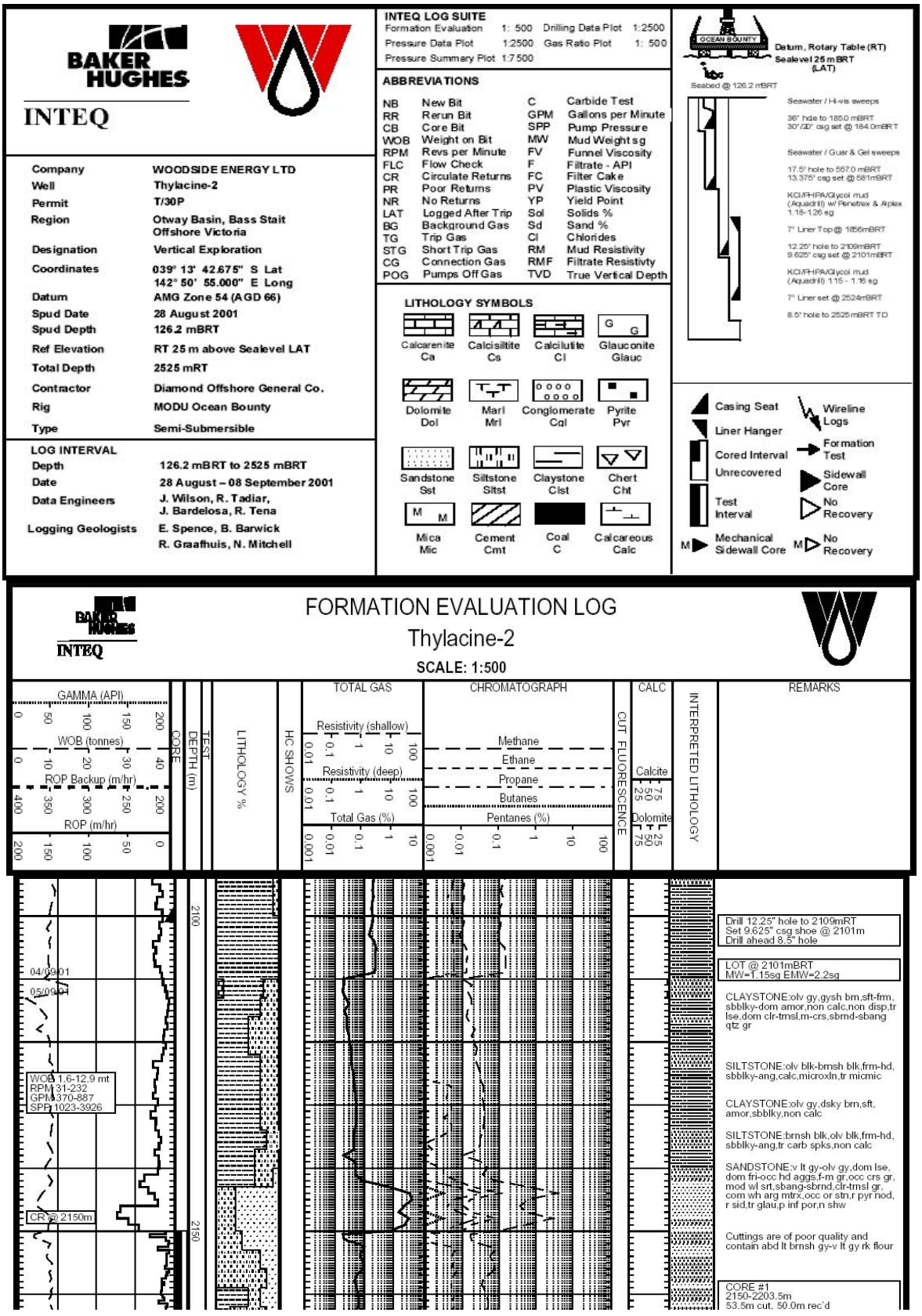
REFERENCE LOGS - MNEMONIC
GR RHO8

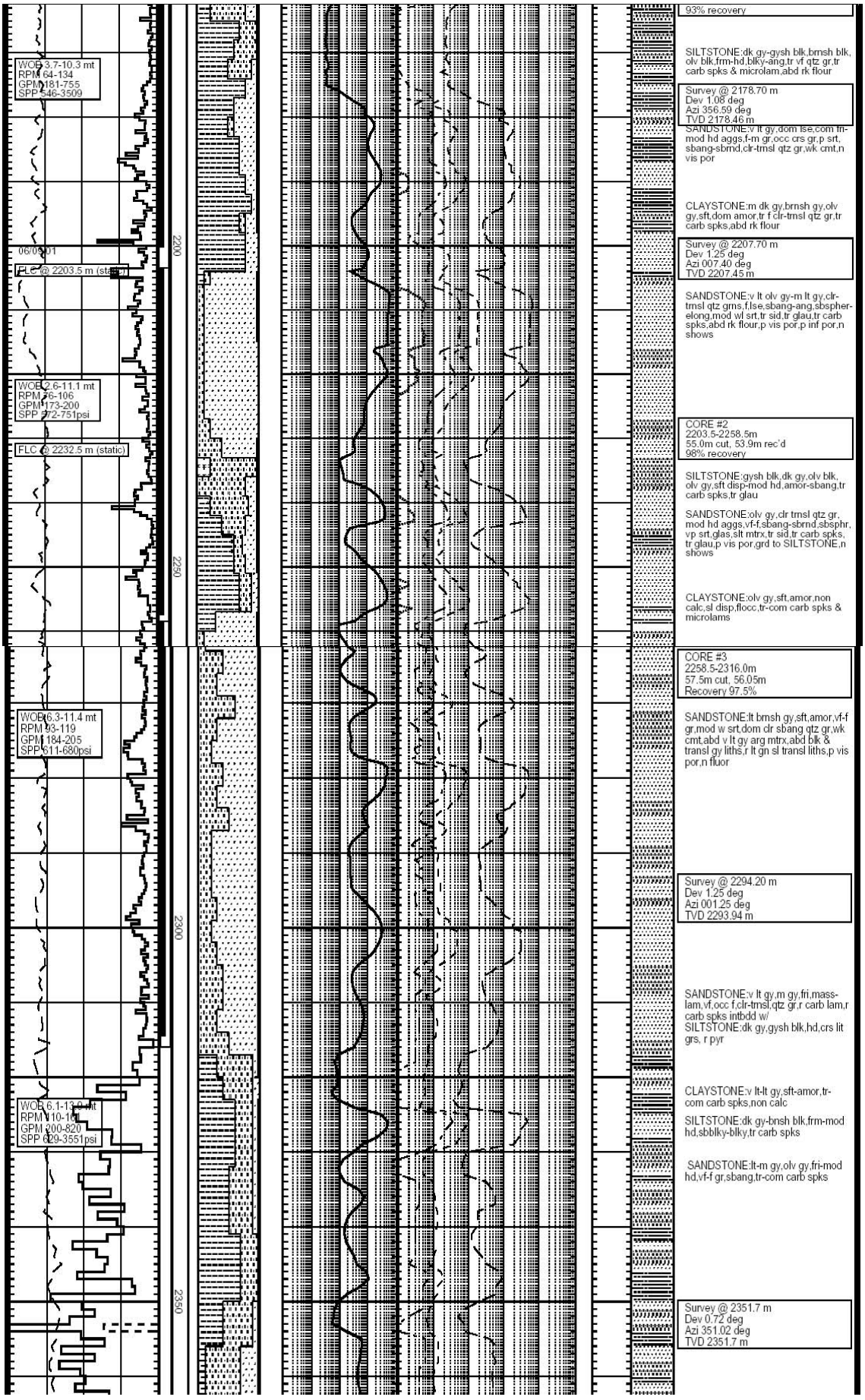
DEPTH UNITS = M
  159.995   162.795
  200.000   201.100
  240.005   240.515
  280.010   281.950
  320.015   322.045
  360.020   362.920
  400.025   401.145
  440.030   440.350
  480.035   480.755
  520.040   519.340
  560.045   558.775
  600.050   600.230
  640.055   640.435
  680.060   679.650
  720.065   720.685
  760.070   759.050
  800.075   797.565
  840.080   840.270
  880.085   881.455
  920.090   918.950
  960.095   958.425
  1000.100  998.900
  1040.105  1040.005
  1080.110  1080.010
```

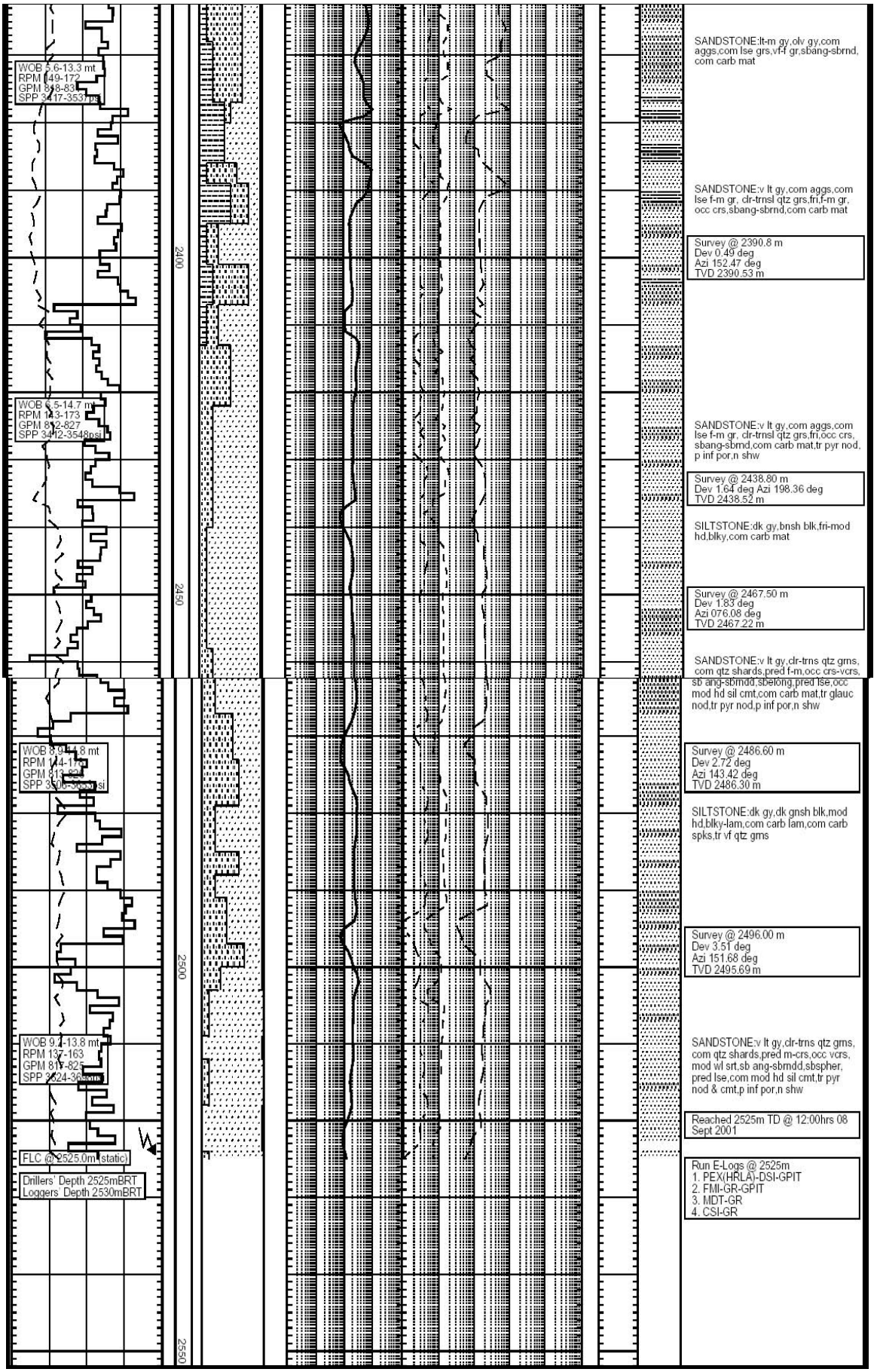
1120.115	1120.115
1160.120	1160.320
1200.125	1199.825
1240.130	1239.930
1280.135	1279.735
1320.140	1319.540
1360.145	1359.445
1400.150	1400.350
1440.155	1440.155
1480.160	1480.160
1520.165	1519.965
1560.170	1560.070
1600.175	1599.775
1640.180	1639.680
1680.185	1679.785
1720.190	1719.290
1760.195	1759.495
1800.200	1799.500
1840.205	1839.905
1880.210	1880.410
1920.215	1920.015
1960.220	1959.220
2000.225	1999.425
2040.229	2039.029
2080.234	2078.334
2120.240	2118.440
2160.244	2158.444
2200.250	2198.450
2240.254	2238.354
2280.260	2278.460
2320.264	2318.464
2360.270	2358.470
2400.274	2398.474
2440.280	2438.480
2480.284	2478.484
2520.290	2518.490

Appendix – B

Mudlog Summary – 1770-2110 mMDRT

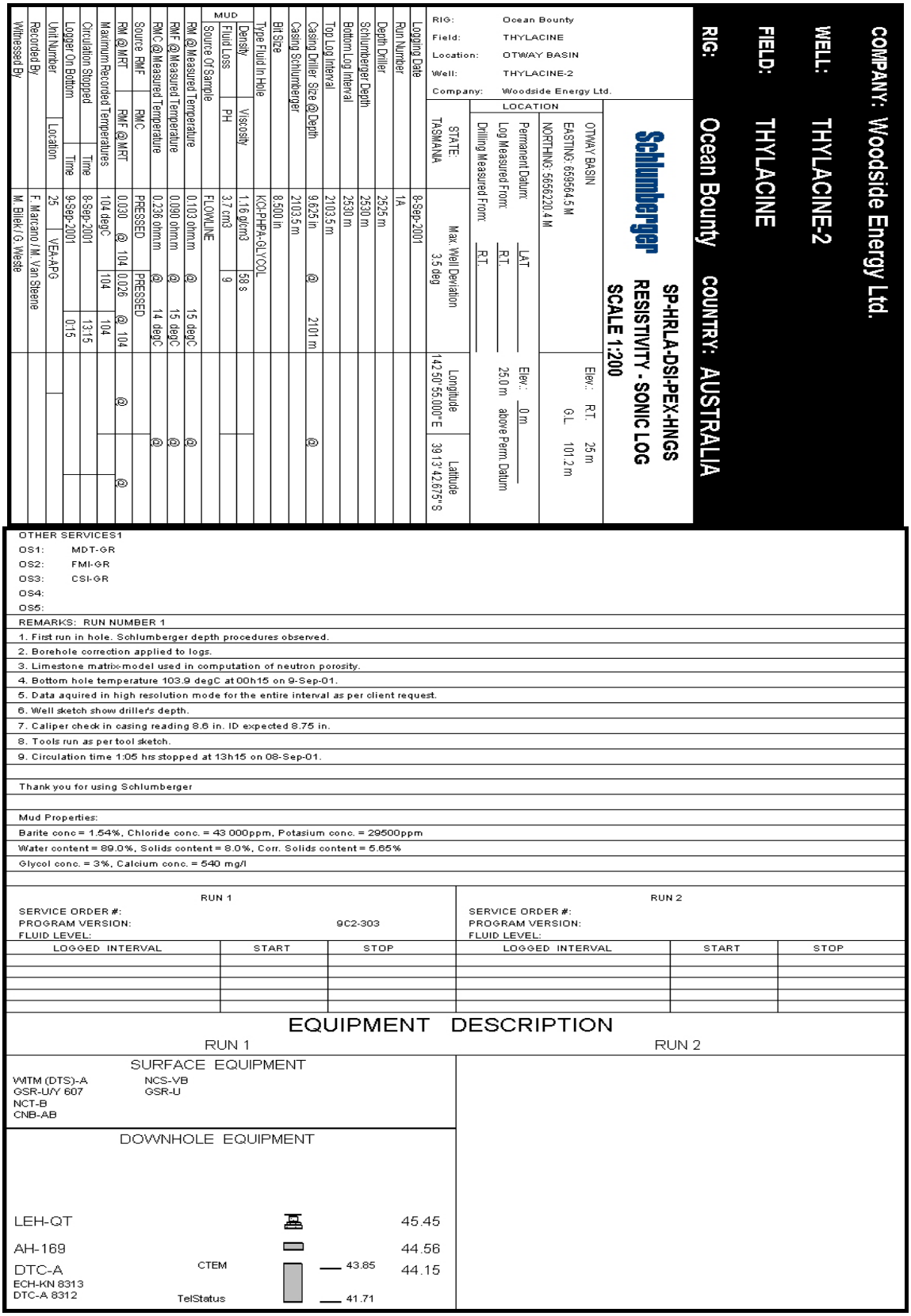



93% recovery
SILTSTONE:dk gy-gysh blk,brnsh blk, olv blk,frm-hd,blky-ang,tr vf qtz gr,tr carb spks & microlam,abd rk flour
Survey @ 2178.70 m
Dev 1.08 deg
Azi 356.59 deg
TVD 2178.46 m
SANDSTONE:v lt gy,dom lse,com fri-mod hd aggs,f-m gr,occ crs gr,p srt, sbang-sbrnd,clr-trnsl qtz gr,wk cmt,n vis por
CLAYSTONE:m dk gy,brnsh gy,olv gy,sft,dom amor,tr f clr-trnsl qtz gr,tr carb spks,abd rk flour
Survey @ 2207.70 m
Dev 1.25 deg
Azi 007.40 deg
TVD 2207.45 m
SANDSTONE:v lt olv gy-m lt gy,clr-trnsl qtz grns,f,lse,sbang-ang,sbspher-elong,mod wl srt,tr sid,tr glau,tr carb spks,abd rk flour,p vis por,p inf por,n shows
CORE #2
2203.5-2258.5m
55.0m cut, 53.9m rec'd
98% recovery
SILTSTONE:gysh blk,dk gy,olv blk, olv gy,sft disp-mod hd,amor-sbang,tr carb spks,tr glau
SANDSTONE:olv gy,clr trnsl qtz gr, mod hd aggs,vf-f,sbang-sbrnd,sbsphr, vp srt,glas,slt mtrx,tr sid,tr carb spks, tr glau,p vis por,grd to SILTSTONE,n shows
CLAYSTONE:olv gy,sft,amor,non calc,sl disp,flocc,tr-com carb spks & microlams
CORE #3
2258.5-2316.0m
57.5m cut, 56.05m
Recovery 97.5%
SANDSTONE:lt brnsh gy,sft,amor,vf-f gr,mod w srt,dom clr sbang qtz gr,wk cmt,abd v lt gy arg mtrx,abd blk & transl gy liths,r lt gn sl transl liths,p vis por,n fluor
Survey @ 2294.20 m
Dev 1.25 deg
Azi 001.25 deg
TVD 2293.94 m
SANDSTONE:v lt gy,m gy,fri,mass-lam,vf,occ f,clr-trnsl,qtz gr,r carb lam,r carb spks intbdd w/
SILTSTONE:dk gy,gysh blk,hd,crs lit grs, r pyr
CLAYSTONE:v lt-lt gy,sft-amor,tr-com carb spks,non calc
SILTSTONE:dk gy-bnsh blk,frm-mod hd,sbblky-blky,tr carb spks
SANDSTONE:lt-m gy,olv gy,fri-mod hd,vf-f gr,sbang,tr-com carb spks
Survey @ 2351.7 m
Dev 0.72 deg
Azi 351.02 deg
TVD 2351.7 m
WOB 3.7-10.3 mt
RPM 64-134
GPM 181-755
SPP 546-3509
06/09/01
FLC @ 2203.5 m (static)
WOB 2.6-11.1 mt
RPM 76-106
GPM 173-200
SPP 672-751psi
FLC @ 2232.5 m (static)
WOB 6.3-11.4 mt
RPM 93-119
GPM 184-205
SPP 611-680psi
WOB 6.1-13.9 mt
RPM 110-161
GPM 200-820
SPP 629-3551psi
2200
2250
2300
2350


WOB 5.6-13.3 mt
RPM 149-172
GPM 818-83
SPP 3417-353
2400
WOB 5.5-14.7 mt
RPM 143-173
GPM 812-827
SPP 3412-3548psi
2450
WOB 8.9-11.8 mt
RPM 144-17
GPM 813-82
SPP 3500-3600psi
2500
WOB 9.4-13.8 mt
RPM 137-163
GPM 817-825
SPP 3524-3
FLC @ 2525.0m (static)
Drillers' Depth 2525mBRT
Loggers' Depth 2530mBRT
2550
SANDSTONE:lt-m gy,olv gy,com aggs,com lse grs,vf-f gr,sbang-sbrnd, com carb mat
SANDSTONE:v lt gy,com aggs,com lse f-m gr, clr-trnsl qtz grs,fri,f-m gr, occ crs,sbang-sbrnd,com carb mat
Survey @ 2390.8 m
Dev 0.49 deg
Azi 152.47 deg
TVD 2390.53 m
SANDSTONE:v lt gy,com aggs,com lse f-m gr, clr-trnsl qtz grs,fri,occ crs, sbang-sbrnd,com carb mat,tr pyr nod, p inf por,n shw
Survey @ 2438.80 m
Dev 1.64 deg Azi 198.36 deg
TVD 2438.52 m
SILTSTONE:dk gy,bnsh blk,fri-mod hd,blky,com carb mat
Survey @ 2467.50 m
Dev 1.83 deg
Azi 076.08 deg
TVD 2467.22 m
SANDSTONE:v lt gy,clr-trns qtz grns, com qtz shards,pred f-m,occ crs-vcrs, sb ang-sbrndd,sbelong,pred lse,occ mod hd sil cmt,com carb mat,tr glauc nod,tr pyr nod,p inf por,n shw
Survey @ 2486.60 m
Dev 2.72 deg
Azi 143.42 deg
TVD 2486.30 m
SILTSTONE:dk gy,dk gnsh blk,mod hd,blky-lam,com carb lam,com carb spks,tr vf qtz grns
Survey @ 2496.00 m
Dev 3.51 deg
Azi 151.68 deg
TVD 2495.69 m
SANDSTONE:v lt gy,clr-trns qtz grns, com qtz shards,pred m-crs,occ vcrs, mod wl srt,sb ang-sbrndd,sbspher, pred lse,com mod hd sil cmt,tr pyr nod & cmt,p inf por,n shw
Reached 2525m TD @ 12:00hrs 08 Sept 2001
Run E-Logs @ 2525m
1. PEX(HRLA)-DSI-GPIT
2. FMI-GR-GPIT
3. MDT-GR
4. CSI-GR

Appendix – C

Field Print Header Summary



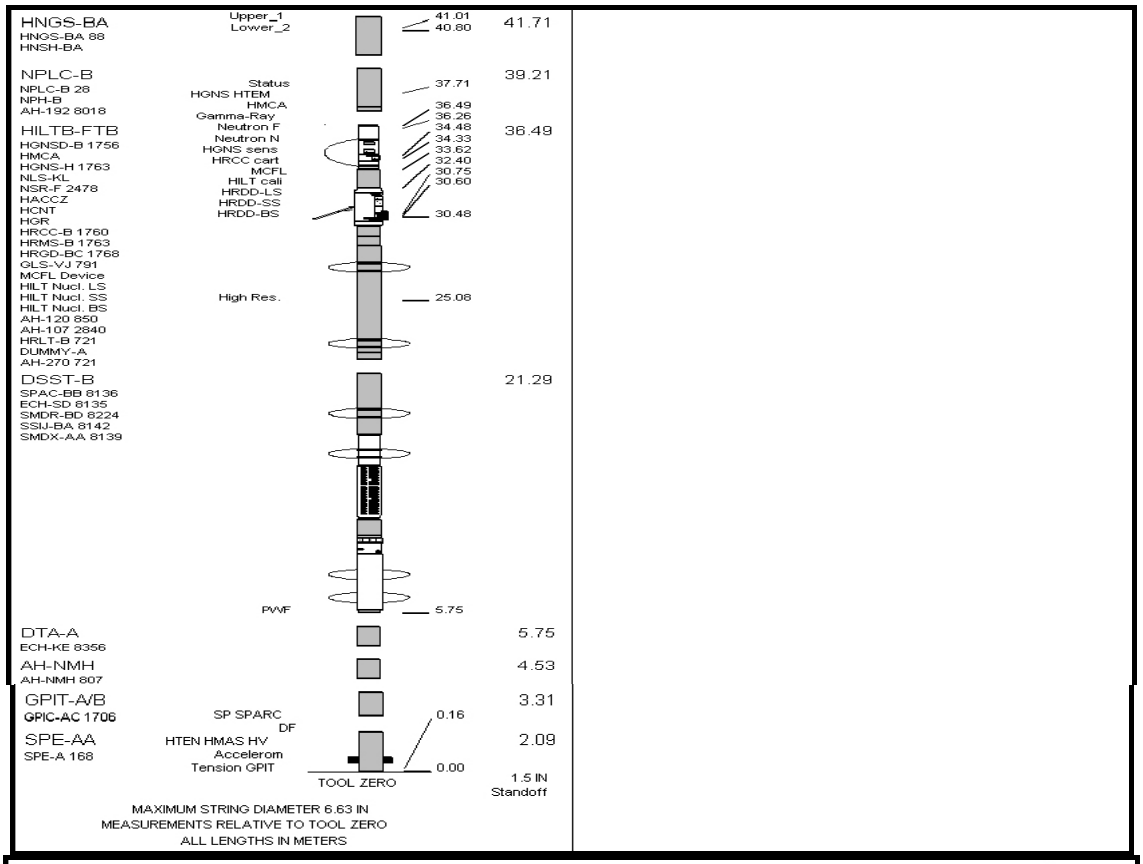
COMPANY: Woodside Energy Ltd.
WELL: THYLACINE-2
FIELD: THYLACINE
RIG: Ocean Bounty COUNTRY: AUSTRALIA

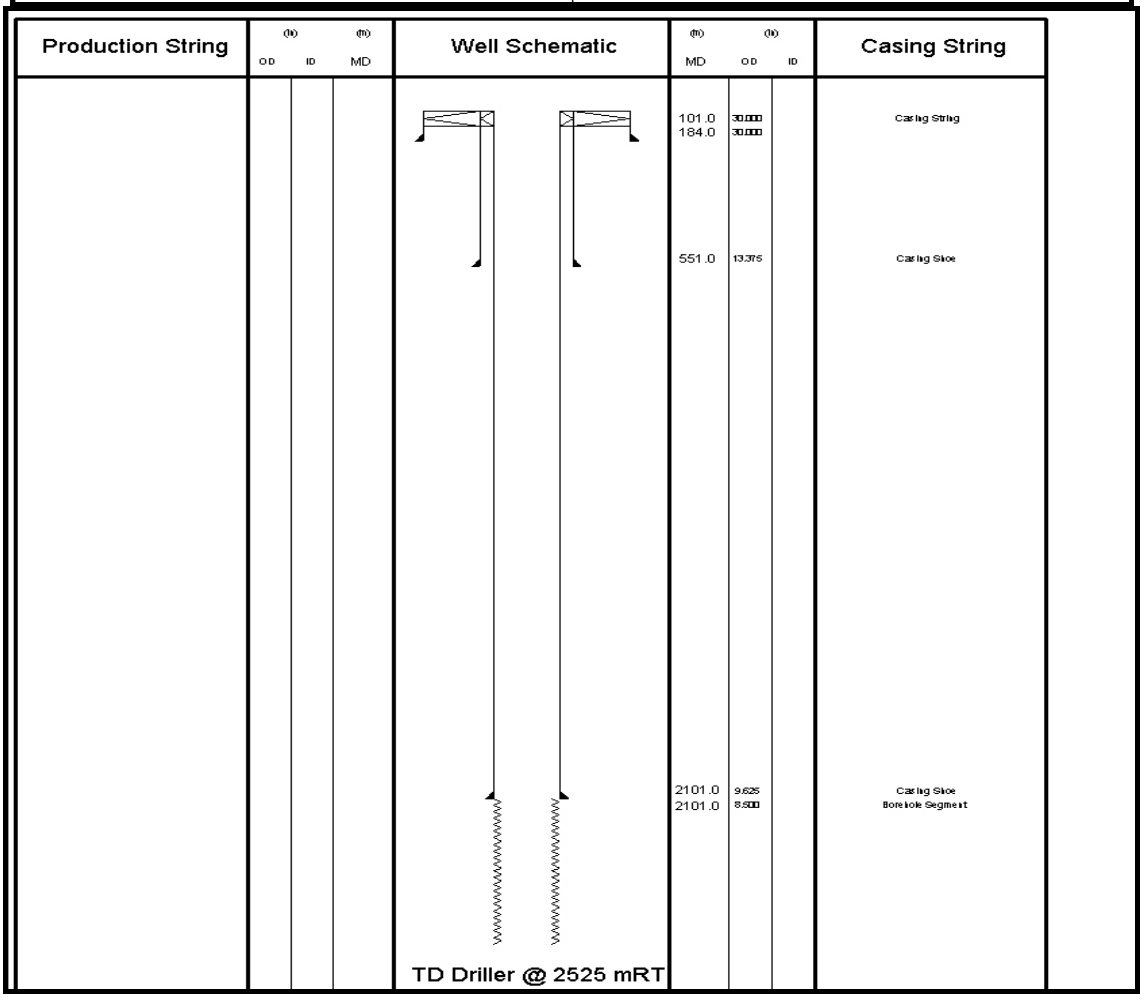
Schlumberger
SP-HRLA-DSI-PEX-HNGS
RESISTIVITY - SONIC LOG
SCALE 1:200

RIG: Ocean Bounty
Field: THYLACINE
Location: OTWAY BASIN
Well: THYLACINE-2
Company: Woodside Energy Ltd.

LOCATION
OTWAY BASIN
EASTING: 659564.5 M
NORTHING: 5666220.4 M
STATE: TASMANIA
Permanent Datum: LAT
Log Measured From: R.T.
Drilling Measured From: R.T.
Elev.: R.T. 25 m
G.L. 101.2 m
Elev.: 0 m
250 m above Perm. Datum
Longitude 142 50' 55.000" E
Latitude 39 13' 42.675" S

| | | |


HNGS-BA
HNGS-BA 88
HNSH-BA
NPLC-B
NPLC-B 28
NPH-B
AH-192 8018
HILTB-FTB
HGNSD-B 1756
HMCA
HGNS-H 1763
NLS-KL
NSR-F 2478
HACCZ
HCNT
HGR
HRCC-B 1760
HRMS-B 1763
HRGD-BC 1768
GLS-VJ 791
MCFL Device
HILT Nucl. LS
HILT Nucl. SS
HILT Nucl. BS
AH-120 850
AH-107 2840
HRLT-B 721
DUMMY-A
AH-270 721
DSST-B
SPAC-BB 8136
ECH-SD 8135
SMDR-BD 8224
SSU-BA 8142
SMDX-AA 8139
DTA-A
ECH-KE 8356
AH-NMH
AH-NMH 807
GPIT-AB
GPIC-AC 1706
SPE-AA
SPE-A 168
Upper_1
Lower_2
41.01
40.80
41.71
Status
HGNS HTEM
HMCA
Gamma-Ray
Neutron F
Neutron N
HGNS sens
HRCC cart
MCFL
HILT cali
HRDD-LS
HRDD-SS
HRDD-BS
37.71
36.49
36.26
34.48
34.33
33.62
32.40
30.75
30.60
30.48
39.21
36.49
High Res.
25.08
21.29
PWF
5.75
5.75
4.53
SP SPARC
DF
HTEN HMAS HV
Accelerom
Tension GPIT
0.16
0.00
3.31
2.09
TOOL ZERO
1.5 IN
Standoff
MAXIMUM STRING DIAMETER 6.63 IN
MEASUREMENTS RELATIVE TO TOOL ZERO
ALL LENGTHS IN METERS


Production String
(in)
OD
ID
(m)
MD
Well Schematic
(m)
MD
(in)
OD
ID
Casing String
101.0
184.0
30.000
30.000
Casing String
551.0
13.375
Casing Shoe
2101.0
2101.0
9.625
8.500
Casing Shoe
Borehole Segment
TD Driller @ 2525 mRT

Parameters

DLIS Name	Description	Value	
ACPP	Accelerometer PROM Presence	PRESENT	
AFMO	Accelerometer Filtering Mode	MOVING_AVERAGE	
ALTDPCHAN	Name of alternate depth channel	SpeedCorrectedDepth	
ART	Accelerometer Reference Temperature	20	DEGC
BAR1	HNGS Detector 1 Barite Constant	0.846629	
BAR2	HNGS Detector 2 Barite Constant	0.85873	
BARS_MTR1	Length for Monopole Transmitter to Receiver 1	2.7432	M
BHFL	Borehole Fluid Type	WATER	
BHK	HNGS Borehole Potassium Correction Concentration	0.02543	
BHS	Borehole Status	OPEN	
BHT	Bottom Hole Temperature (used in calculations)	103.889	DEGC
BILI	Bond Index Level for Zone Isolation	0.8	
BS	Bit Size	8.500	IN
BSAL	Borehole Salinity	43000.00	PPM
BSCO	Borehole Salinity Correction Option	YES	
CALSTAT	HRLTB Calibration Status	SHALLOW_DONE	
CALTEMP	HRLTB Calibration Temperature	96.1409	DEGC
CASF	Label Casing Function - Monopole P&S	50	
CCCO	Casing & Cement Thickness Correction Option	NO	
CDTS	C-Delta-T Shale	100	US/F
COLL	Label Slowness Lower Limit - Monopole P&S Compressional	60	US/F
COUL	Label Slowness Upper Limit - Monopole P&S Compressional	180	US/F
CSD1	Inner Casing Outer Diameter	0	IN
CSD2	Outer Casing Outer Diameter	0	IN
CSIZ	Current Casing Size	9.625	IN
CSTR	Compressive Strength of Cement	0	KPAA
CSW1	Inner Casing Weight	0	LB/F
CSW2	Outer Casing Weight	0	LB/F
CWEI	Casing Weight	47.00	LB/F
DBCC	HNGS Barite Constant Correction Flag	USER	
DDE1	Digitizing Delay 1	0	US
DDE2	Digitizing Delay 2	0	US
DDE3	Digitizing Delay 3	0	US
DDE4	Digitizing Delay 4	0	US
DDE5	Digitizing Delay 5	0	US
DDEX	Digitizing Delay X	0	US
DFD	Drilling Fluid Density	1.16	G/C3
DHC	Density Hole Correction	BS	
DLCS	Label Compressional Source - Dipole Shear	USE	
DLHS	Label Hole Diameter Source for SOBS Channel	AUTO	
DO	Depth Offset for Playback	0.0	M
DPPM	Density Porosity Processing Mode	HIRS	
DSHL	Label Slowness Lower Limit - Dipole Shear	75	US/F
DSHU	Label Slowness Upper Limit - Dipole Shear	475	US/F
DSI1	Digitizer Sample Interval 1	10	US
DSI2	Digitizer Sample Interval 2	40	US
DSI3	Digitizer Sample Interval 3	40	US
DSI4	Digitizer Sample Interval 4	10	US
DSI5	Digitizer Sample Interval 5	10	US
DSIX	Digitizer Sample Interval X	40	US
DTCS	Compressional Delta-T Source for DTCO Channel	PS_COMP	
DTF	Delta-T Fluid	189	US/F
DTM	Delta-T Matrix	56	US/F
DTSS	Shear Delta-T Source for DTSM Channel	PS_SHEAR	
DWC1	Digitizer Word Count 1	512	
DWC2	Digitizer Word Count 2	512	
DWC3	Digitizer Word Count 3	512	
DWC4	Digitizer Word Count 4	512	
DWC5	Digitizer Word Count 5	512	
DWCX	Digitizer Word Count X	512	
EXSICL	External Shale Indicator Clean Value	20	
EXSISH	External Shale Indicator Shale Value	150	
FCD	Future Casing (Outer) Diameter	7	IN
FCF	CBL Fluid Compensation Factor	1	
FD	Fluid Density	1	G/C3
FEXP	Form Factor Exponent	2	
FGM5	First Motion Gate Moveout 5	40	US/F
FILG	Label Fill Gap Control - Monopole P&S	COMP_SHEAR	
FMG5	First Motion Minimum Gate 5	500	US
FMLL	Slowness Lower Limit - FMD	40	US/F
FMRC	Restart Control - FMD	CONTINUE	
FMT5	First Motion Threshold 5	UP	
FMUL	Slowness Upper Limit - FMD	180	US/F
FNUM	Form Factor Numerator	1	
FPHI	Form Factor Porosity Source	DPHZ	
FPM	Processing Mode - FMD	DFMD	
FREQ0	HRLT Frequency Index for Mode 0	32	
FREQ1	HRLT Frequency Index for Mode 1	128	
FREQ2	HRLT Frequency Index for Mode 2	104	
FREQ3	HRLT Frequency Index for Mode 3	86	
FREQ4	HRLT Frequency Index for Mode 4	56	
FREQ5	HRLT Frequency Index for Mode 5	44	
FREQ6	HRLT Frequency Index for Mode 6	116	
FSAL	Formation Salinity	-50000	PPM
FSCO	Formation Salinity Correction Option	NO	
GCSE	Generalized Caliper Selection	HCAL	
GDEV	Average Angular Deviation of Borehole from Normal	0	DEG
GDT1	Gain Delta-T 1	800	US/F
GDT2	Gain Delta-T 2	800	US/F
GDT3	Gain Delta-T 3	800	US/F
GDT4	Gain Delta-T 4	160	US/F
GDT5	Gain Delta-T 5	160	US/F
GDTX	Gain Delta-T X	800	US/F
GGRD	Geothermal Gradient	0.018227	DC/M
GIN1	Gain Interval 1	15360	US
GIN2	Gain Interval 2	15360	US
GIN3	Gain Interval 3	15360	US
GIN4	Gain Interval 4	2560	US
GIN5	Gain Interval 5	1600	US
GINX	Gain Interval X	15360	US
GLM	GPIT Logging Mode	DIPM	
GOBO	Good Bond	2	MV
GRSE	Generalized Mud Resistivity Selection	CHART_GEN_9	
GTSE	Generalized Temperature Selection	LINEAR_ESTIMATE	
H1P	HNGS Detector 1 Allow/Disallow In Processing	ALLOW	
H2P	HNGS Detector 2 Allow/Disallow In Processing	ALLOW	
HABK	HNGS Borehole Potassium Running Average	0.230516	
HACPP	Accelerometer PROM Presence	PRESENT_FILE	
HALF	HNGS Alpha Filter Length	60	IN
HART	Accelerometer Reference Temperature	20	DEGC
HCRB	HNGS Apply Borehole Potassium Correction	USER	
HDCOD	HILT Density Coal detection	2	G/C3
HDSAD	HILT Density Salt detection	2.1	G/C3
HILT_GAS_DENSITY	HILT Gas Downhole Density	0	G/C3
HILT_GAS_OPTION	HILT Gas Computation Option	OFF	

HMWM	Mud Weighting Material	BARI	
HNCOD	HILT Neutron Coal detection	45	PU
HNPE	HNGS Processing Enable	YES	
HNSAD	HILT Neutron Salt detection	5	PU
HPHIECUT	HILT effective Porosity Cutoff	5	PU
HSCO	Hole Size Correction Option	YES	
HSIS	HILT Shale Indicator Selection	GR	
HSWCUT	HILT Water Saturation from AITH cutoff	50	%
HVCS	Integrated Hole Volume Caliper Selection	HCAL	
ICMO	Inclinometry Computation Mode	AUTOMATIC_SELECTION	
ITTS	Integrated Transit Time Source	DTCO	
KFAC_HRLT	HRLT K Factor Option	SONDE	
LFC	Label Formation Character - Monopole P&S	DYNAMIC	
LOOPCOEF_S	HRLT Loop Coefficient for Shallow Modes	LOW	
LOOPMOD0	HRLT Mode 0 Loop Mode	AUTO	
LOOPMOD1	HRLT Mode 1 Loop Mode	AUTO	
LOOPMOD2	HRLT Mode 2 Loop Mode	AUTO	
LOOPMOD3	HRLT Mode 3 Loop Mode	AUTO	
LOOPMOD4	HRLT Mode 4 Loop Mode	AUTO	
LOOPMOD5	HRLT Mode 5 Loop Mode	AUTO	
LOOPMOD6	HRLT Mode 6 Loop Mode	AUTO	
LTXG	Lower Dipole Transmitter Geometry	156	IN
MAI5	Slowness Averaging Interval - FMD	42	IN
MAPP	Magnetometer PROM Presence	PRESENT	
MATR	Rock Matrix for Neutron Porosity Corrections	LIMESTONE	
MCCO	Mud Cake Correction Option	YES	
MCI	Minimum Cemented Interval	4.51523	M
MCOR	Mud Correction	BARI	
MCS	Mean Casing Slowness	57	US/F
MDEC	Magnetic Field Declination	11.0639	DEG
MDEN	Matrix Density	2.71	G/C3
MDS5	Multishot Delta-T Scatter - FMD	20	US
MHC0	MCFL B0 Contrast Correction Coefficient	2.2e-005	OHMS
MHC1	MCFL B1 Contrast Correction Coefficient	3.2e-005	OHMS
MHCC	MCFL High Contrast Correction Switch	NO	
MPOF	MCFL Processing Operation Mode	ON	
MRTE	Magneto Reference Temperature	21	DEGC
MSA	Minimum Sonic Amplitude	19.7824	MV
MST	Mud Sample Temperature	15.00	DEGC
MTXG	Monopole Transmitter Geometry	186	IN
MWCO	Mud Weight Correction Option	YES	
NAAC	HRDD APS Activation Correction	OFF	
NMT	HILT Nuclear Mud Type	BARITE	
NOTS	NPLC Old Temperature Sensor	NO	
NPRM	HRDD Processing Mode	HiRes	
NSAR	HRDD Depth Sampling Rate	1	IN
NWS1	Number Waveforms Stacked 1	1	
NWS2	Number Waveforms Stacked 2	1	
NWS3	Number Waveforms Stacked 3	1	
NWS4	Number Waveforms Stacked 4	1	
NWS5	Number Waveforms Stacked 5	1	
NWSX	Number Waveforms Stacked X	1	
PBVSADP	Use alternate depth channel for playback	YES	
PHIMAX	HILT max porosity	35	PU
PP	Playback Processing	RECOMPUTE	
PROCINV	Inversion Selection	ON	
PROCMFL	Inversion Micro-Resistivity Selection	NO_EXTERNAL_RXO	
PROCMSO	Mechanical Standoff Fin Size	1.5	IN
PROCRM	Processing Mud Resistivity Select	HRLT_Compute	
PROCSPO	Sonde Position	Centered	
PTCO	Pressure/Temperature Correction Option	YES	
RATE	Firing Rate	R3	
RMFS	Resistivity of Mud Filtrate Sample	0.0903	OHMM
RSMN	Label Shear/Compressional Minimum Ratio - Monopole P&S	1.4	
RSMX	Label Shear/Compressional Maximum Ratio - Monopole P&S	2.12	
RW	Resistivity of Connate Water	1.0000	OHMM
RX1G	Receiver 1 Geometry	294	IN
RX2G	Receiver 2 Geometry	300	IN
RX3G	Receiver 3 Geometry	306	IN
RX4G	Receiver 4 Geometry	312	IN
RX5G	Receiver 5 Geometry	318	IN
RX6G	Receiver 6 Geometry	324	IN
RX7G	Receiver 7 Geometry	330	IN
RX8G	Receiver 8 Geometry	336	IN
S1BI	HNGS Detector 1 Calibration Bismuth Count Rate	1.3	CPS
S2BI	HNGS Detector 2 Calibration Bismuth Count Rate	1.3	CPS
SAM1	DSST Sonic Acquisition Mode 1 - Lower Dipole Mode	OFF	
SAM2	DSST Sonic Acquisition Mode 2 - Upper Dipole Mode	ODD	
SAM3	DSST Sonic Acquisition Mode 3 - Low Frequency Monopole Mode for Stoneley	OFF	
SAM4	DSST Sonic Acquisition Mode 4 - High Frequency Monopole Mode for P&S	EVEN	
SAM5	DSST Sonic Acquisition Mode 5 - High Frequency Monopole Mode for FMD	ODD	
SAMX	DSST Sonic Acquisition Mode X - Both Dipoles or Monopole Mode for Expert	BCR	
SAS1	STC Sonic Array Status - Lower Dipole	255	
SAS2	STC Sonic Array Status - Upper Dipole	255	
SAS3	STC Sonic Array Status - Monopole Stoneley	255	
SAS4	STC Sonic Array Status - Monopole P&S	255	
SAS5	Sonic Array Status - FMD	255	
SBO1	STC Search Band Offset - Lower Dipole	3000	US
SBO2	STC Search Band Offset - Upper Dipole	3000	US
SBO3	STC Search Band Offset - Monopole Stoneley	3000	US
SBO4	STC Search Band Offset - Monopole P&S	500	US
SBR4	STC Baseline Removal - Monopole P&S	ON	
SBW1	STC Search Bandwidth - Lower Dipole	8000	US
SBW2	STC Search Bandwidth - Upper Dipole	8000	US
SBW3	STC Search Bandwidth - Monopole Stoneley	8000	US
SBW4	STC Search Bandwidth - Monopole P&S	2000	US
SDAT	Standoff Data Source	SOCN	
SEXP_HILT	HILT Saturation Exponent	2	
SFC1	STC Formation Character - Lower Dipole	SELECTABLE	
SFC2	STC Formation Character - Upper Dipole	SELECTABLE	
SFC3	STC Formation Character - Monopole Stoneley	SELECTABLE	
SFC4	STC Formation Character - Monopole P&S	SELECTABLE	
SFM1	STC Filter - Lower Dipole	B1-3K	
SFM2	STC Filter - Upper Dipole	B1-3K	
SFM3	STC Filter - Monopole Stoneley	B.5-1.5K	
SFM4	STC Filter - Monopole P&S	B3-20K	
SGRC	HNGS Standard Gamma-Ray Correction Flag	YES	
SHLL	Label Slowness Lower Limit - Monopole P&S Shear	75	US/F
SHT	Surface Hole Temperature	20	DEGC
SHUL	Label Slowness Upper Limit - Monopole P&S Shear	180	US/F
SLL1	STC Slowness Lower Limit - Lower Dipole	75	US/F
SLL2	STC Slowness Lower Limit - Upper Dipole	75	US/F
SLL3	STC Slowness Lower Limit - Monopole Stoneley	180	US/F
SLL4	STC Slowness Lower Limit - Monopole P&S	60	US/F

SOCN	Standoff Distance	0.125	IN
SOCO	Standoff Correction Option	NO	
SPFS	Sonic Porosity Formula	RAYMER_HUNT	
SPNV	SP Next Value	0	MV
SPSO	Sonic Porosity Source	DTCO	
SST1	STC Slowness Step - Lower Dipole	4	US/F
SST2	STC Slowness Step - Upper Dipole	4	US/F
SST3	STC Slowness Step - Monopole Stoneley	4	US/F
SST4	STC Slowness Step - Monopole P&S	2	US/F
SSW1	STC Source Waveform - Lower Dipole	EVEN_IN_SAMX	
SSW2	STC Source Waveform - Upper Dipole	WF_SAM2	
SSW4	STC Source Waveform - Monopole P&S	WF_SAM4	
STLL	Label Slowness Lower Limit - Monopole Stoneley	180	US/F
STUL	Label Slowness Upper Limit - Monopole Stoneley	780	US/F
SUL1	STC Slowness Upper Limit - Lower Dipole	475	US/F
SUL2	STC Slowness Upper Limit - Upper Dipole	475	US/F
SUL3	STC Slowness Upper Limit - Monopole Stoneley	780	US/F
SUL4	STC Slowness Upper Limit - Monopole P&S	240	US/F
SWD1	STC Slowness Width - Lower Dipole	40	US/F
SWD2	STC Slowness Width - Upper Dipole	40	US/F
SWD3	STC Slowness Width - Monopole Stoneley	40	US/F
SWD4	STC Slowness Width - Monopole P&S	10	US/F
TBF1	STC Time for Baseline Fill - Lower Dipole	0	US
TBF2	STC Time for Baseline Fill - Upper Dipole	0	US
TBF3	STC Time for Baseline Fill - Monopole Stoneley	0	US
TBF4	STC Time for Baseline Fill - Monopole P&S	300	US
TD	Total Depth	2525	M
TDD	Total Depth - Driller	2525.00	M
TDL	Total Depth - Logger	2530.00	M
TEMS	GPIT Temperature Sensor Used	BOTH	
TLL1	STC Time Lower Limit - Lower Dipole	600	US
TLL2	STC Time Lower Limit - Upper Dipole	600	US
TLL3	STC Time Lower Limit - Monopole Stoneley	600	US
TLL4	STC Time Lower Limit - Monopole P&S	150	US
TPOS	Tool Position	ECCE	
TST1	STC Time Step - Lower Dipole	200	US
TST2	STC Time Step - Upper Dipole	200	US
TST3	STC Time Step - Monopole Stoneley	200	US
TST4	STC Time Step - Monopole P&S	50	US
TUL1	STC Time Upper Limit - Lower Dipole	12462.5	US
TUL2	STC Time Upper Limit - Upper Dipole	12225	US
TUL3	STC Time Upper Limit - Monopole Stoneley	12000	US
TUL4	STC Time Upper Limit - Monopole P&S	3660	US
TWD1	STC Time Width - Lower Dipole	2000	US
TWD2	STC Time Width - Upper Dipole	2000	US
TWD3	STC Time Width - Monopole Stoneley	2000	US
TWD4	STC Time Width - Monopole P&S	1000	US
TWI1	STC Integration Time Window - Lower Dipole	1600	US
TWI2	STC Integration Time Window - Upper Dipole	1600	US
TWI3	STC Integration Time Window - Monopole Stoneley	2400	US
TWI4	STC Integration Time Window - Monopole P&S	500	US
TWRX	Transmitter Waveform Sample Rate X	5	US
TWS	Temperature of Connate Water Sample	37.78	DEGC
TWSX	Transmitter Waveform Select X	0	
UTXG	Upper Dipole Transmitter Geometry	162	IN
VBA1	HNGS Detector 1 Variable Barite Factor Running Average	0.846629	
VBA2	HNGS Detector 2 Variable Barite Factor Running Average	0.85873	
WFDTSP1	SAM1 Waveform Delta for Spectrum	0	US/F
WFDTSP2	SAM2 Waveform Delta for Spectrum	0	US/F
WFDTSP3	SAM3 Waveform Delta for Spectrum	0	US/F
WFDTSP4	SAM4 Waveform Delta for Spectrum	0	US/F
WFDTSPX	SAMX Waveform Delta for Spectrum	0	US/F
WFLLSP1	SAM1 Waveform Lower Limit for Spectrum	0	US
WFLLSP2	SAM2 Waveform Lower Limit for Spectrum	0	US
WFLLSP3	SAM3 Waveform Lower Limit for Spectrum	0	US
WFLLSP4	SAM4 Waveform Lower Limit for Spectrum	0	US
WFLLSPX	SAMX Waveform Lower Limit for Spectrum	0	US
WFM1	Waveform Mode 1	W1	
WFM2	Waveform Mode 2	W1	
WFM3	Waveform Mode 3	W1	
WFM4	Waveform Mode 4	W1	
WFM5	Waveform Mode 5	W1	
WFMX	Waveform Mode X	W1	
WFULSP1	SAM1 Waveform Upper Limit for Spectrum	20000	US
WFULSP2	SAM2 Waveform Upper Limit for Spectrum	20000	US
WFULSP3	SAM3 Waveform Upper Limit for Spectrum	20000	US
WFULSP4	SAM4 Waveform Upper Limit for Spectrum	5000	US
WFULSPX	SAMX Waveform Upper Limit for Spectrum	20000	US

Format: COM_200_SONIC Vertical Scale: 1:200 Graphics File Created: 11-Sep-2001 02:05

OP System Version: 9C2-303

MCM

SPE-AA	9C2-303	GPIT-A/B	9C2-303
DTA-A	OP92-KP2	DSST-B	OP92-KP2
HILTB-FTB	OP92-KP2	NPLC-B	OP92-KP2
HNGS-BA	OP92-KP2	DTC-A	OP92-KP2

Speed Corrected Depth Log

Indexed to Speed Corrected Depth in this Playback

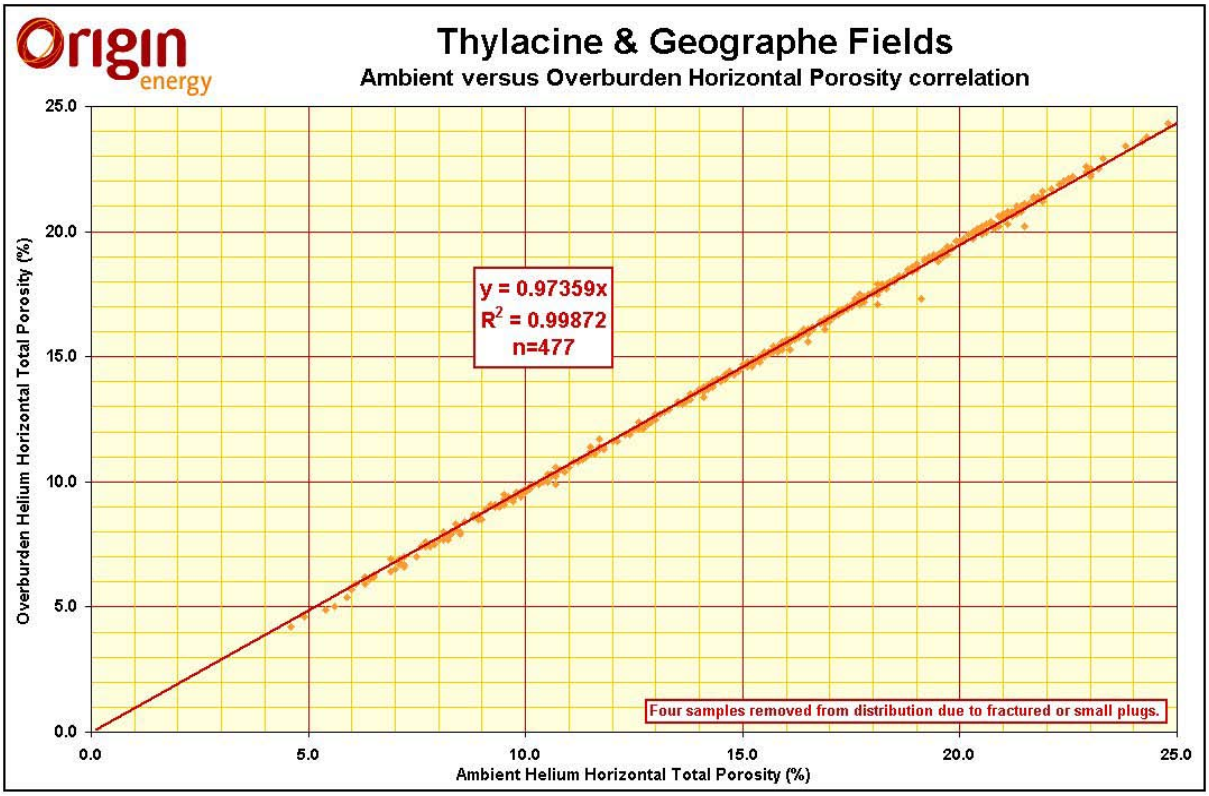
Input DLIS Files

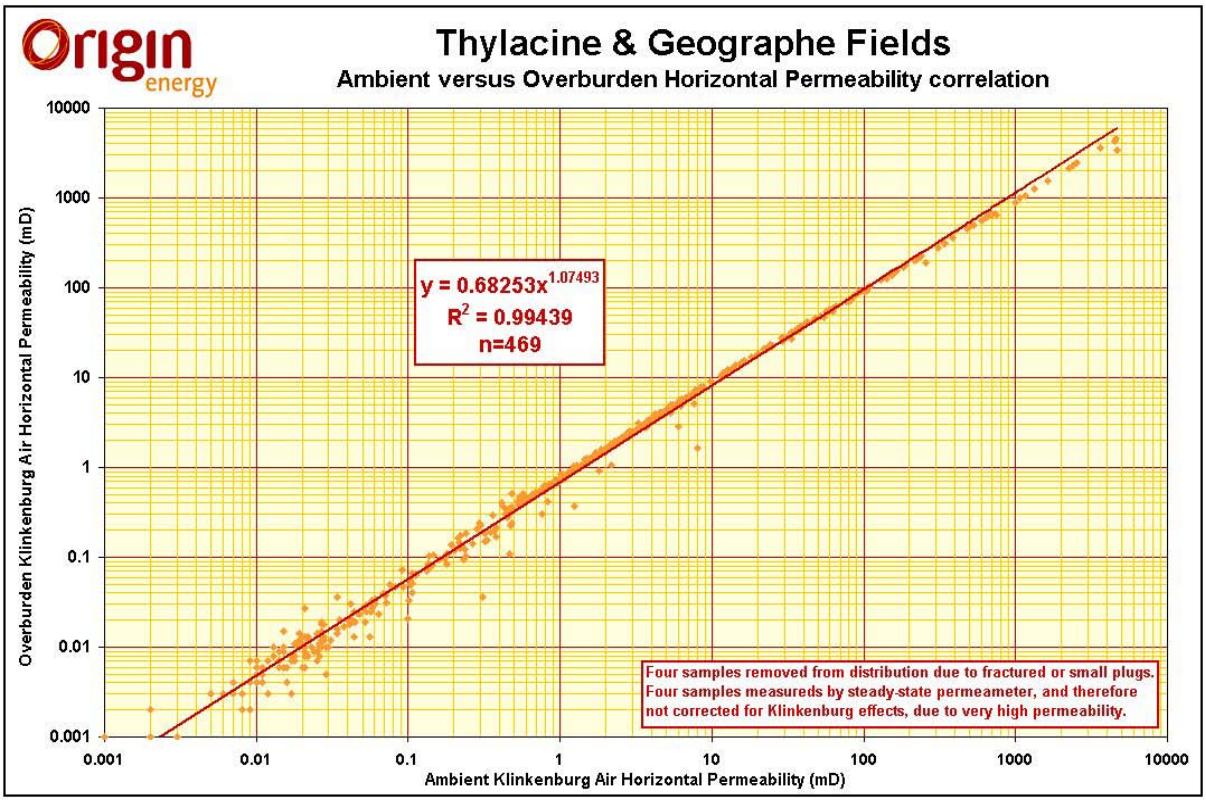
DEFAULT	DSI_TLD_MCFL_CNL_004PUP	FN:80	PRODUCER	09-Sep-2001 05:13	2536.2 M	2088.2 M

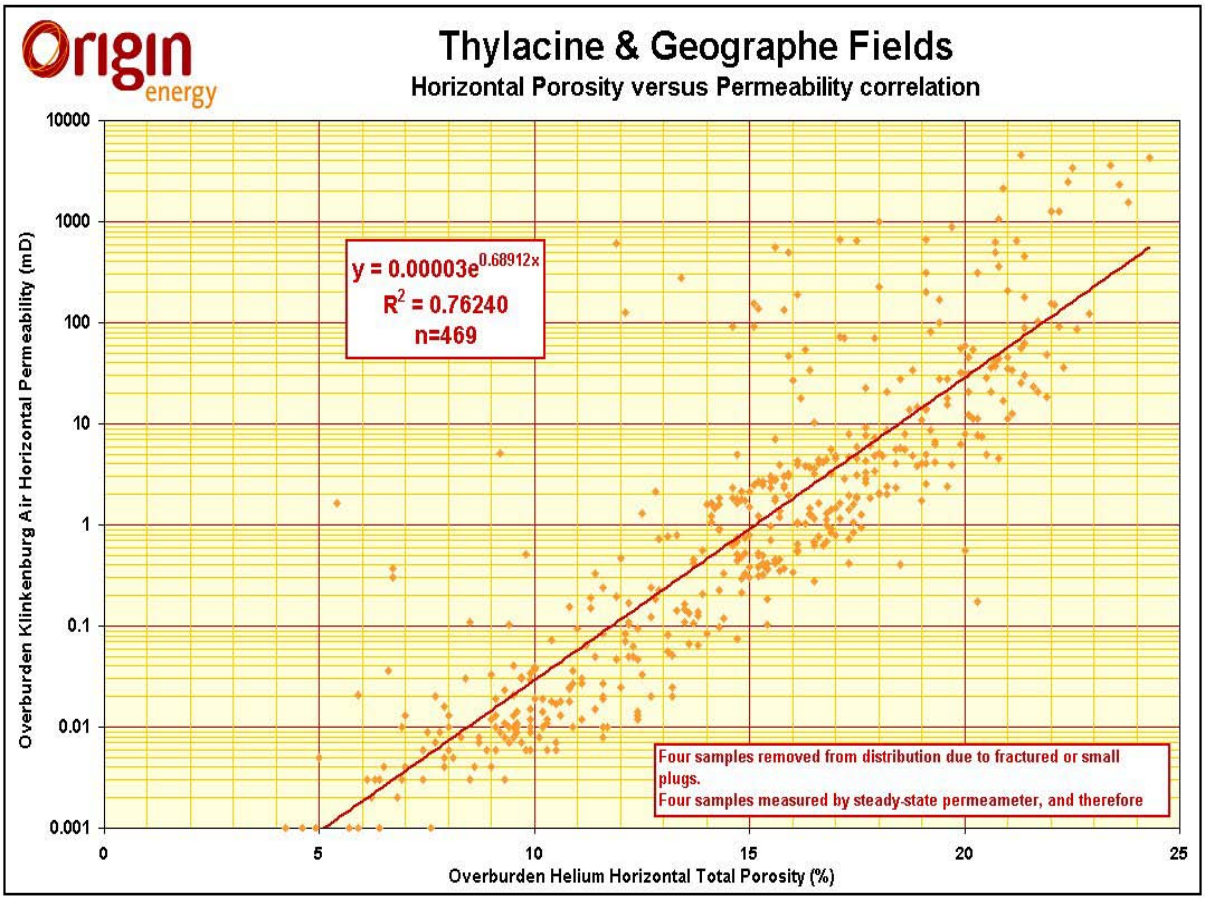
Output DLIS Files

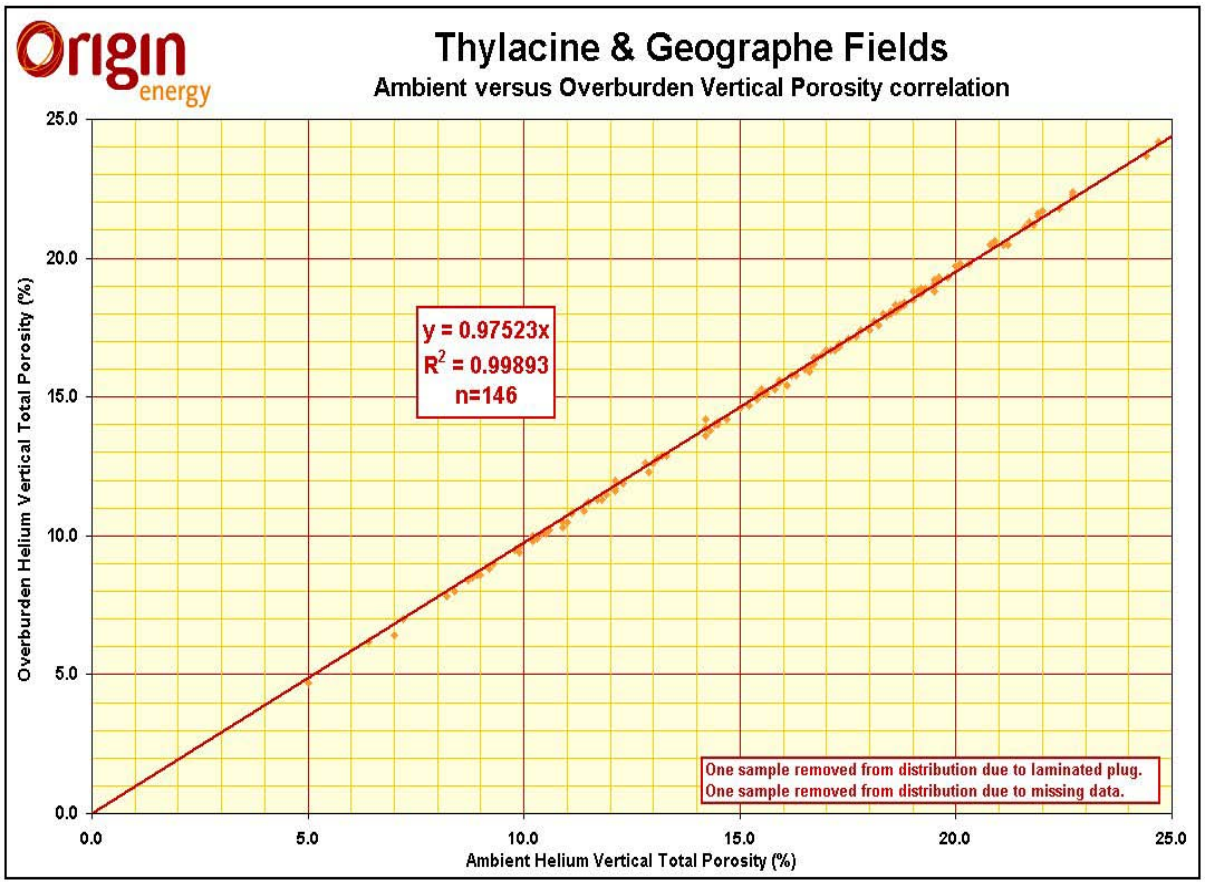
DEFAULT	DSI_TLD_MCFL_CNL_170PUP	FN:297	PRODUCER	11-Sep-2001 02:05

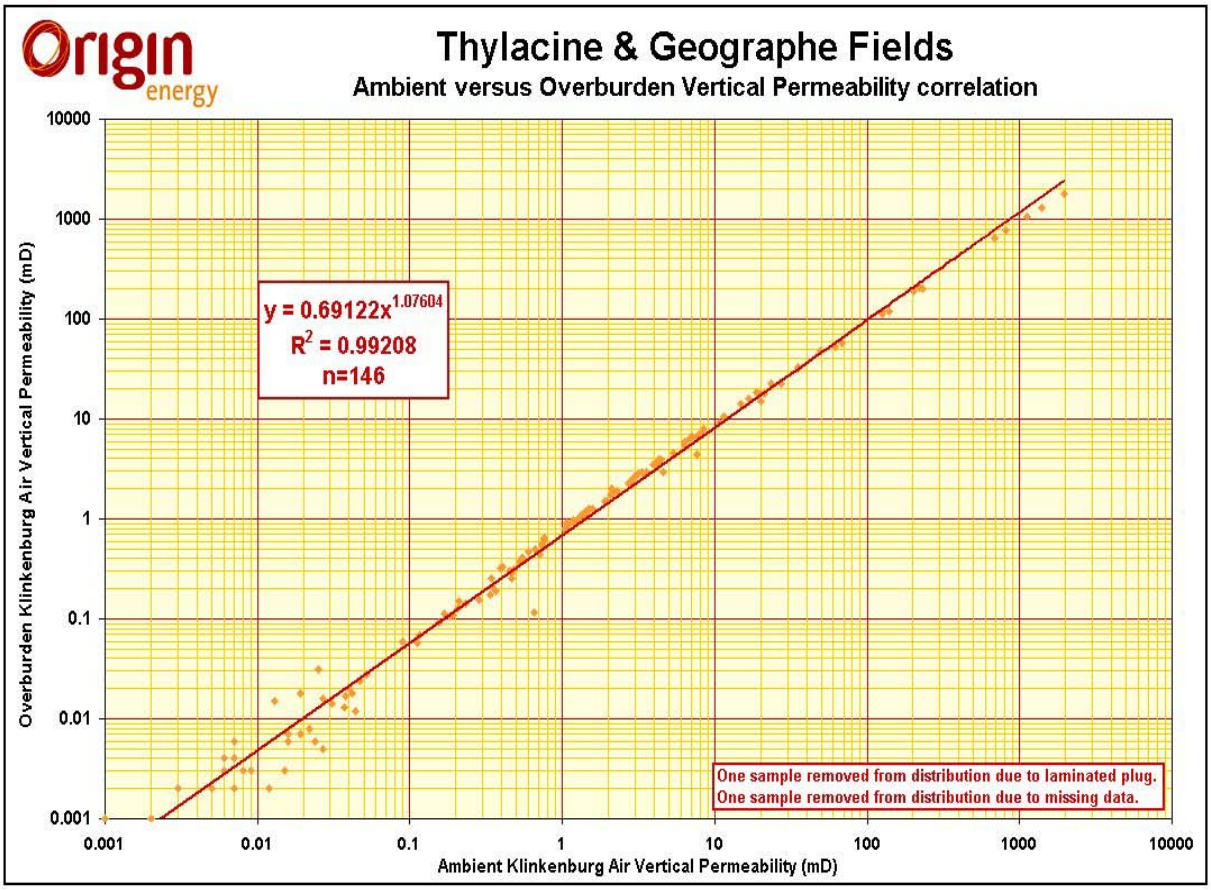
Appendix – D
Core Analysis Cross-plots

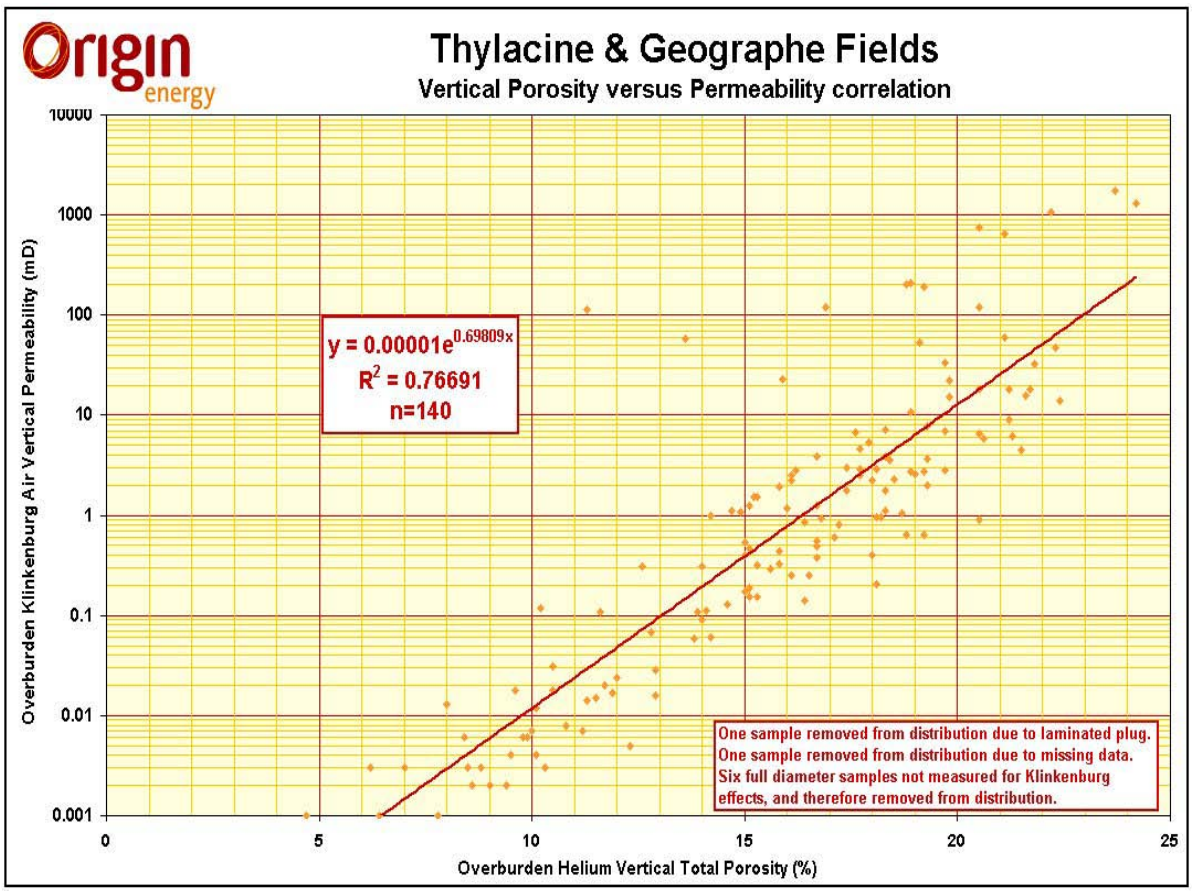


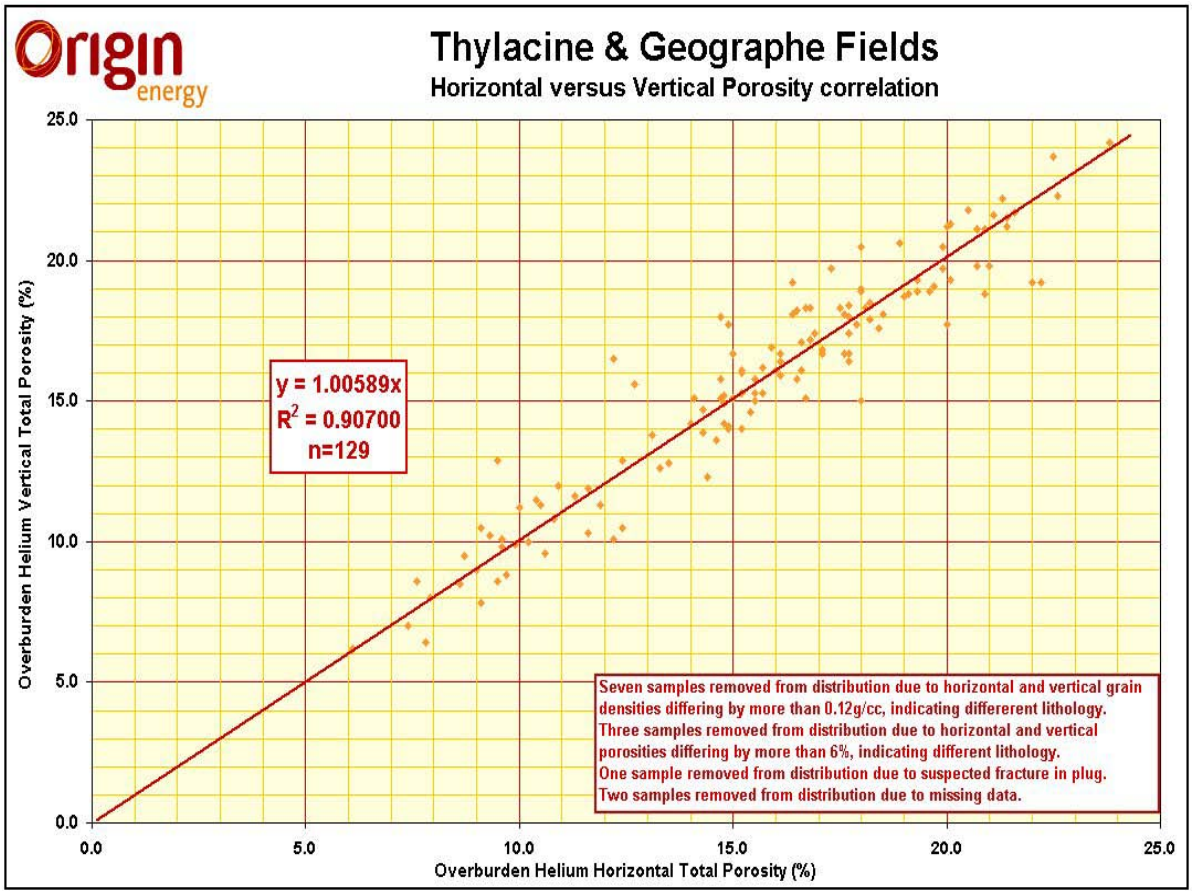


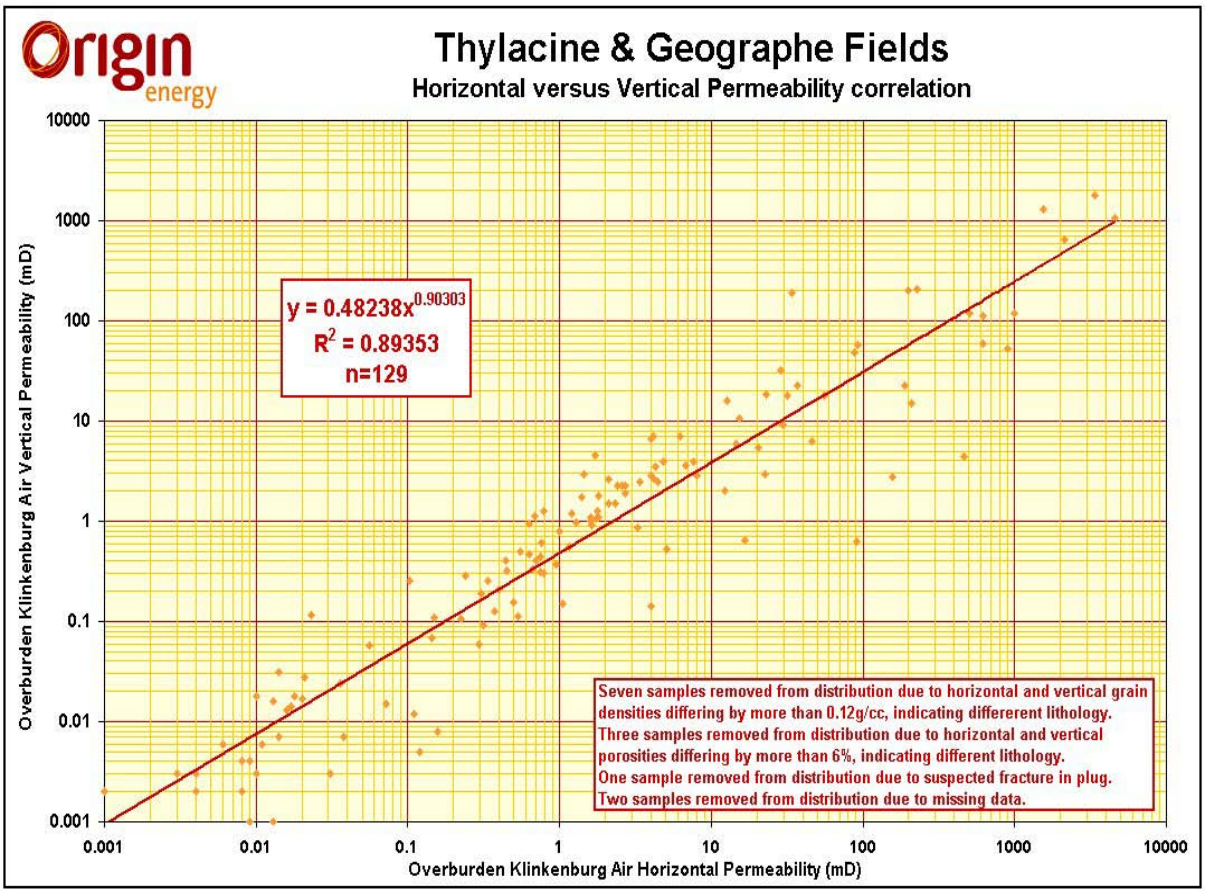

Origin energy
Thylacine & Geographe Fields
Horizontal Porosity versus Permeability correlation
y = 0.00003e^0.68912x
R2 = 0.76240
n=469
Four samples removed from distribution due to fractured or small plugs.
Four samples measured by steady-state permeameter, and therefore
Overburden Klinkenburg Air Horizontal Permeability (mD)
Overburden Helium Horizontal Total Porosity (%)
10000
1000
100
10
1
0.1
0.01
0.001
0
5
10
15
20
25

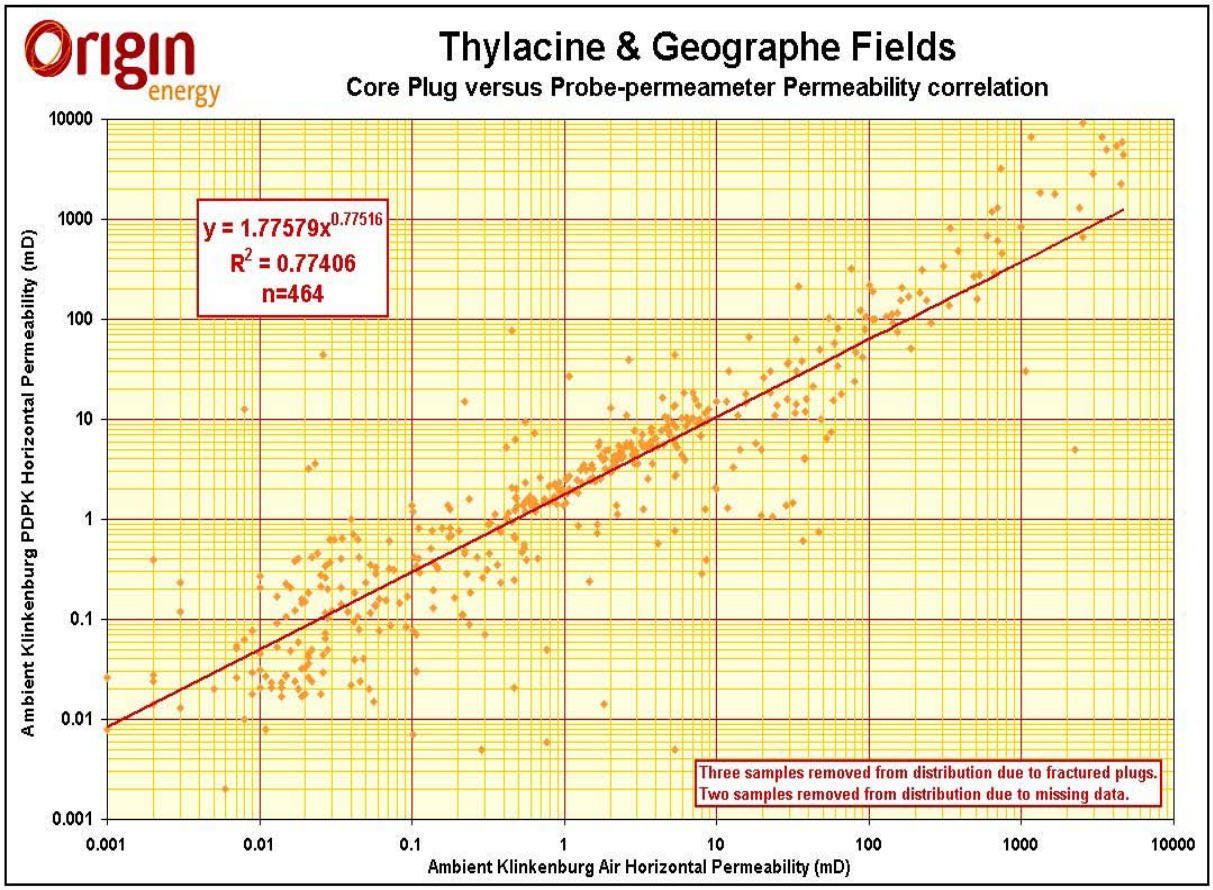

Origin energy
Thylacine & Geographe Fields
Ambient versus Overburden Vertical Porosity correlation
y = 0.97523x
R2 = 0.99893
n=146
One sample removed from distribution due to laminated plug.
One sample removed from distribution due to missing data.
Overburden Helium Vertical Total Porosity (%)
Ambient Helium Vertical Total Porosity (%)
25.0
20.0
15.0
10.0
5.0
0.0
0.0
5.0
10.0
15.0
20.0
25.0

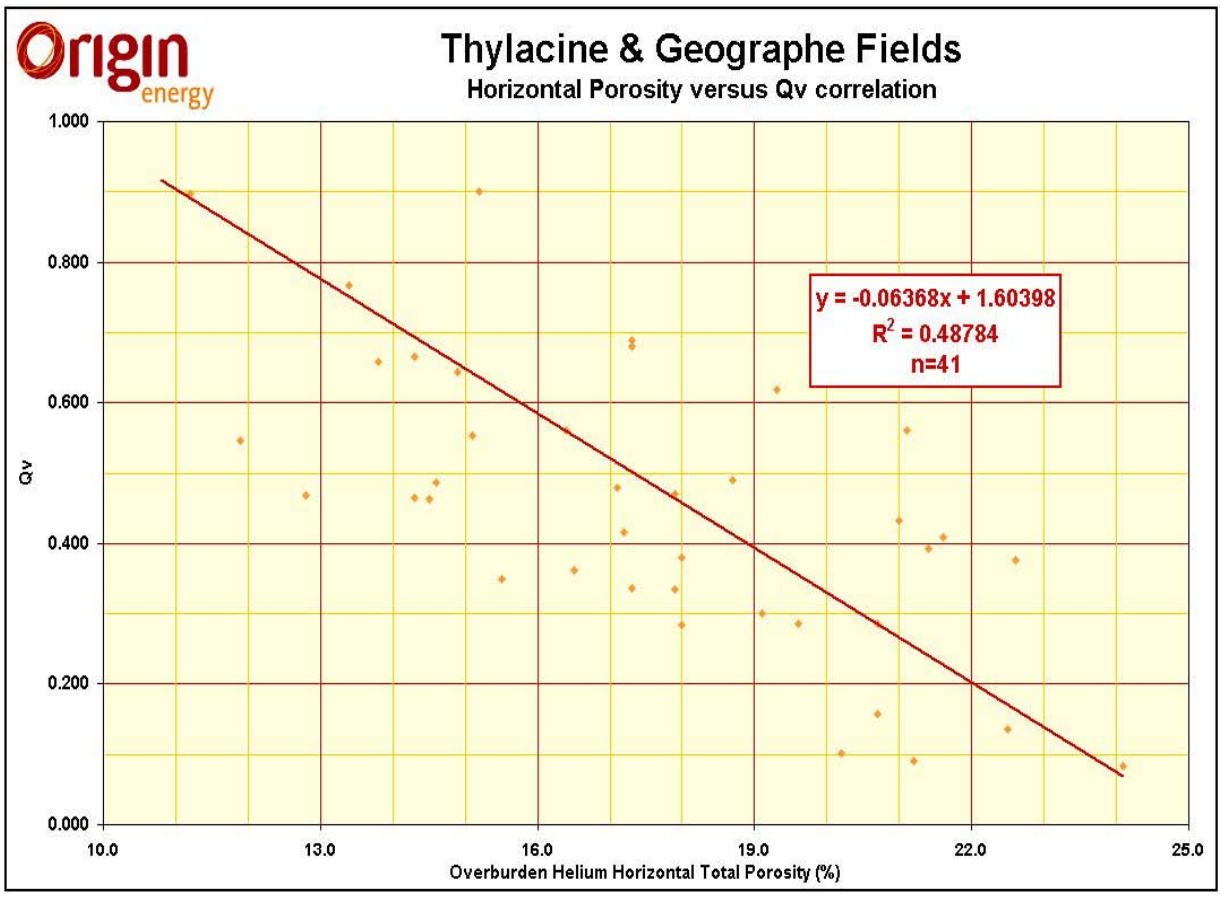

Origin energy
Thylacine & Geographe Fields
Ambient versus Overburden Vertical Permeability correlation
y = 0.69122x^1.07604
R2 = 0.99208
n=146
One sample removed from distribution due to laminated plug.
One sample removed from distribution due to missing data.
Overburden Klinkenburg Air Vertical Permeability (mD)
Ambient Klinkenburg Air Vertical Permeability (mD)
10000
1000
100
10
1
0.1
0.01
0.001
0.001
0.01
0.1
1
10
100
1000
10000

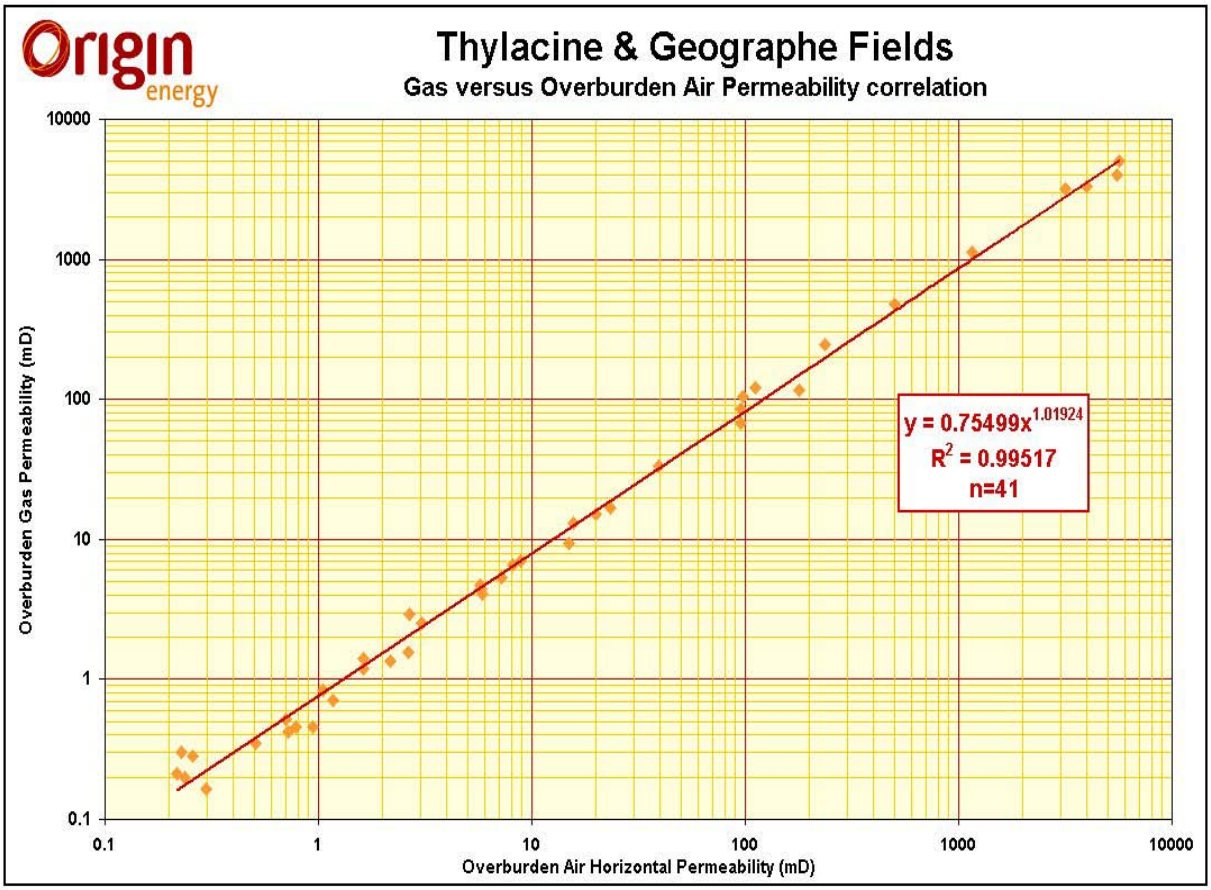

Origin energy
Thylacine & Geographe Fields
Vertical Porosity versus Permeability correlation
y = 0.00001e^0.69809x
R2 = 0.76691
n=140
One sample removed from distribution due to laminated plug.
One sample removed from distribution due to missing data.
Six full diameter samples not measured for Klinkenburg effects, and therefore removed from distribution.
Overburden Klinkenburg Air Vertical Permeability (mD)
Overburden Helium Vertical Total Porosity (%)
10000
1000
100
10
1
0.1
0.01
0.001
0
5
10
15
20
25

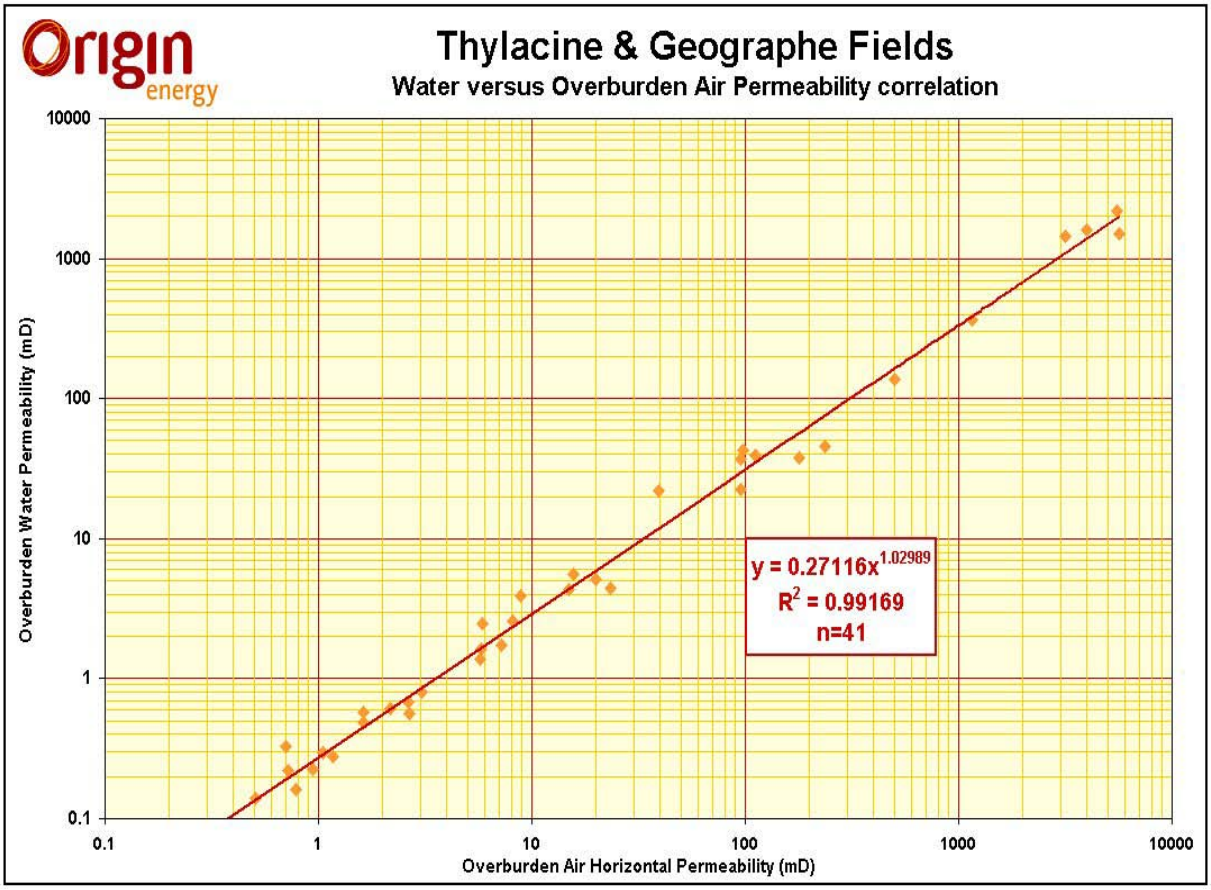

Origin energy
Thylacine & Geographe Fields
Horizontal versus Vertical Porosity correlation
y = 1.00589x
R2 = 0.90700
n=129
Seven samples removed from distribution due to horizontal and vertical grain densities differing by more than 0.12g/cc, indicating differerent lithology.
Three samples removed from distribution due to horizontal and vertical porosities differing by more than 6%, indicating different lithology.
One sample removed from distribution due to suspected fracture in plug.
Two samples removed from distribution due to missing data.
Overburden Helium Vertical Total Porosity (%)
Overburden Helium Horizontal Total Porosity (%)
0.0
5.0
10.0
15.0
20.0
25.0

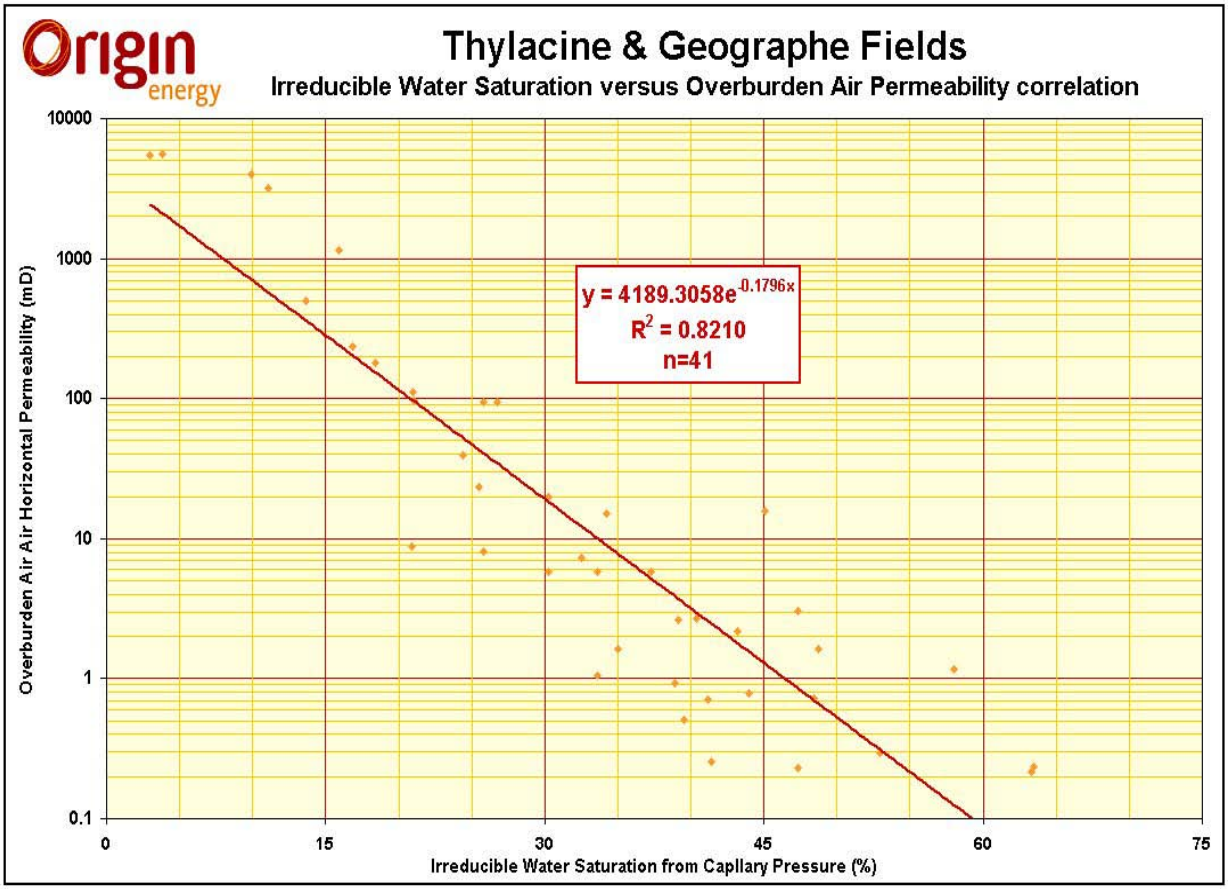

Origin energy
Thylacine & Geographe Fields
Horizontal versus Vertical Permeability correlation
y = 0.48238x0.90303
R2 = 0.89353
n=129
Seven samples removed from distribution due to horizontal and vertical grain densities differing by more than 0.12g/cc, indicating differerent lithology.
Three samples removed from distribution due to horizontal and vertical porosities differing by more than 6%, indicating different lithology.
One sample removed from distribution due to suspected fracture in plug.
Two samples removed from distribution due to missing data.
Overburden Klinkenburg Air Vertical Permeability (mD)
Overburden Klinkenburg Air Horizontal Permeability (mD)
0.001
0.01
0.1
1
10
100
1000
10000

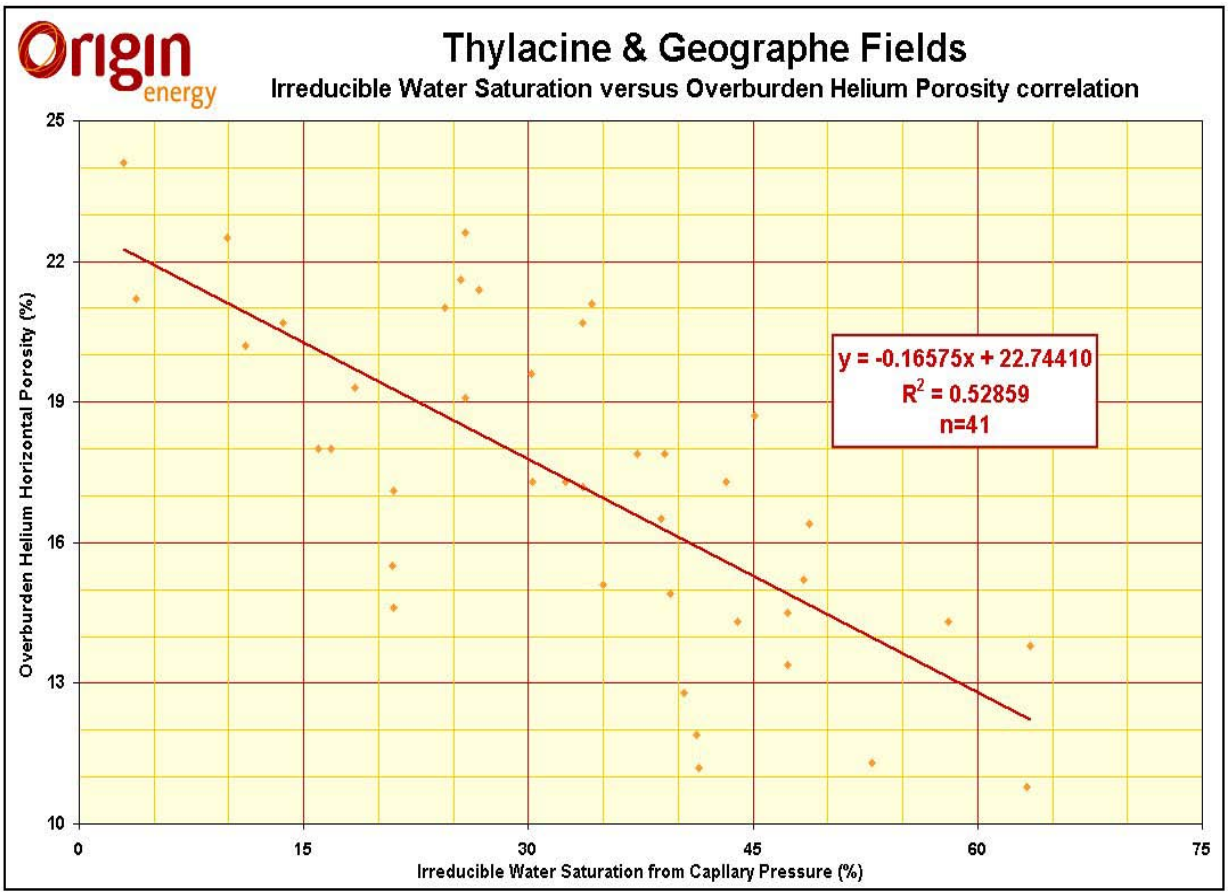

Origin energy
Thylacine & Geographe Fields
Core Plug versus Probe-permeameter Permeability correlation
y = 1.77579x^0.77516
R2 = 0.77406
n=464
Three samples removed from distribution due to fractured plugs.
Two samples removed from distribution due to missing data.
Ambient Klinkenburg PDPK Horizontal Permeability (mD)
Ambient Klinkenburg Air Horizontal Permeability (mD)
10000
1000
100
10
1
0.1
0.01
0.001
0.001
0.01
0.1
1
10
100
1000
10000

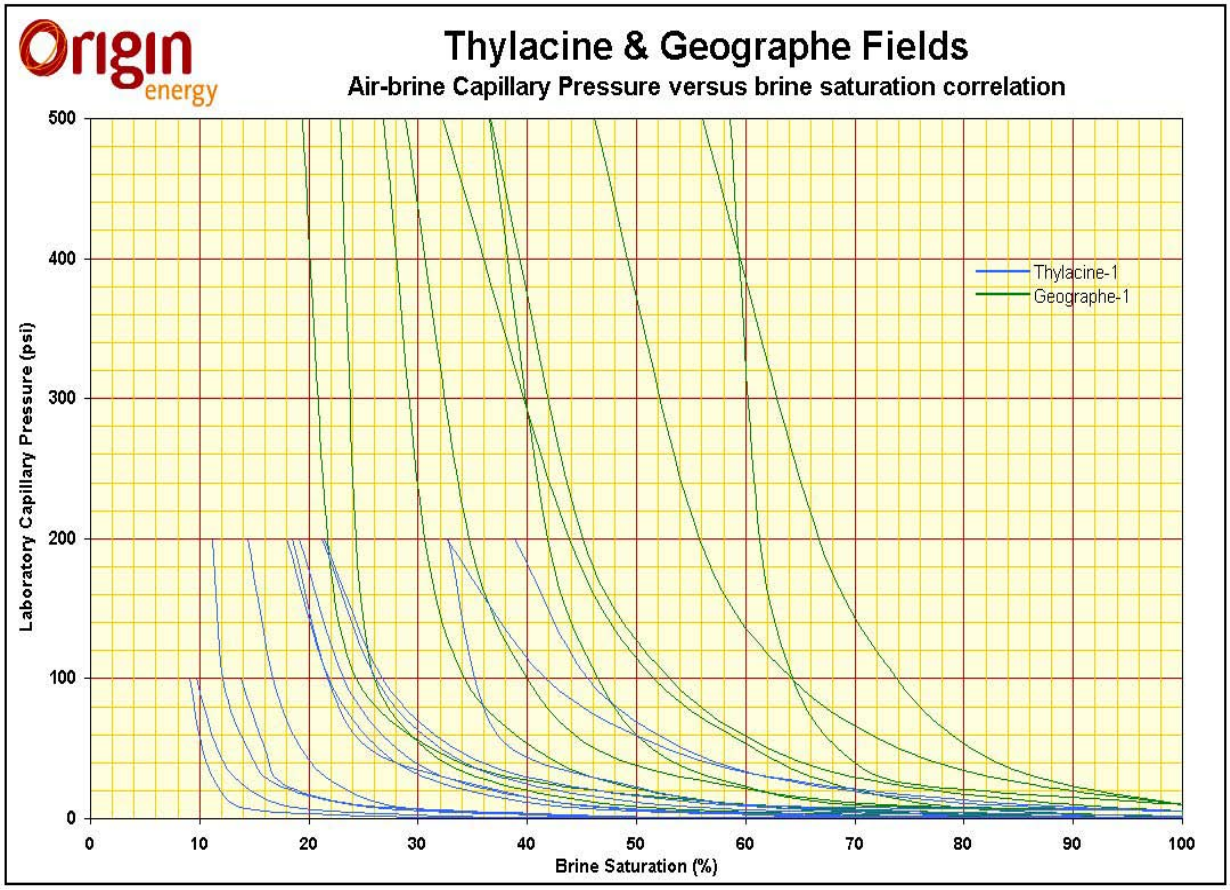

Origin energy
Thylacine & Geographe Fields
Horizontal Porosity versus Qv correlation
y = -0.06368x + 1.60398
R2 = 0.48784
n=41
Qv
Overburden Helium Horizontal Total Porosity (%)
1.000
0.800
0.600
0.400
0.200
0.000
10.0
13.0
16.0
19.0
22.0
25.0

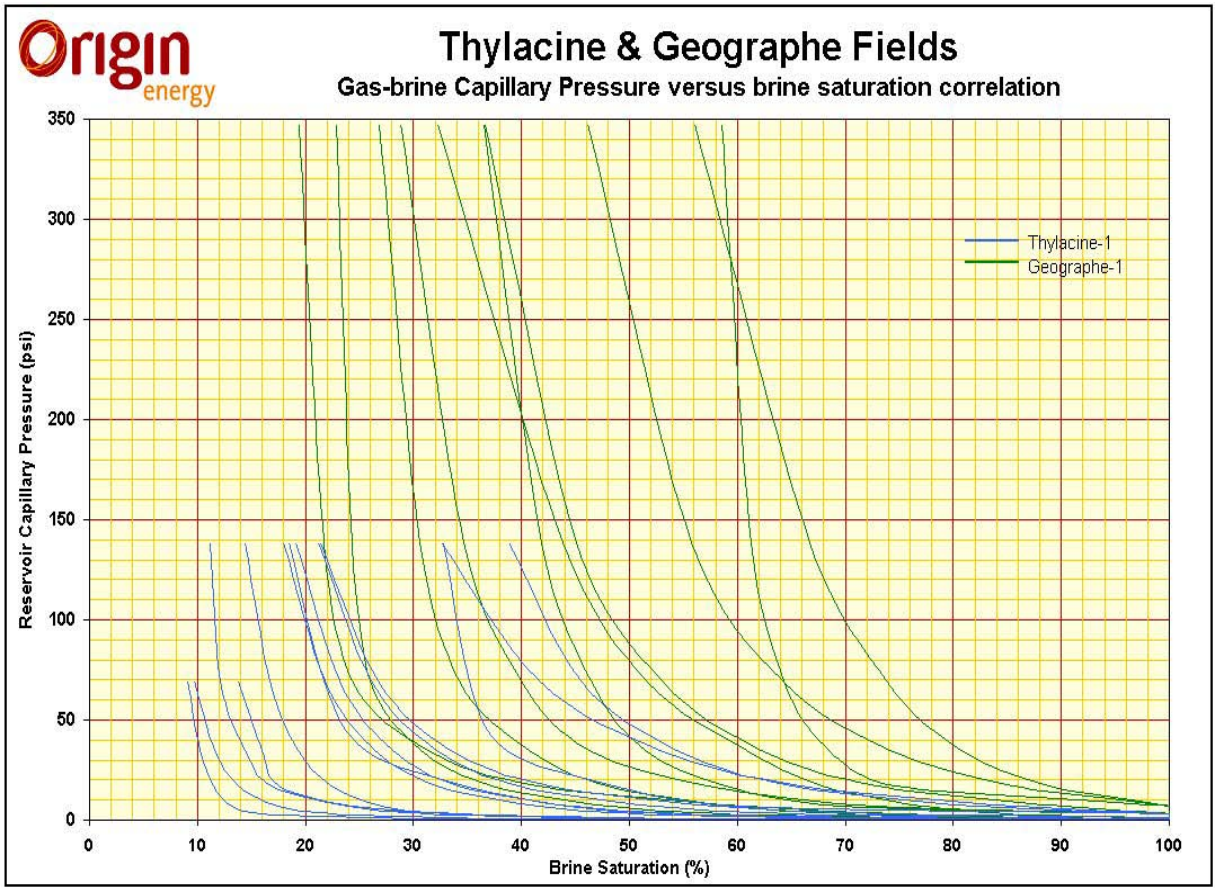

Origin energy
Thylacine & Geographe Fields
Gas versus Overburden Air Permeability correlation
Overburden Gas Permeability (mD)
Overburden Air Horizontal Permeability (mD)
10000
1000
100
10
1
0.1
0.1
1
10
100
1000
10000
y = 0.75499x^1.01924
R2 = 0.99517
n=41

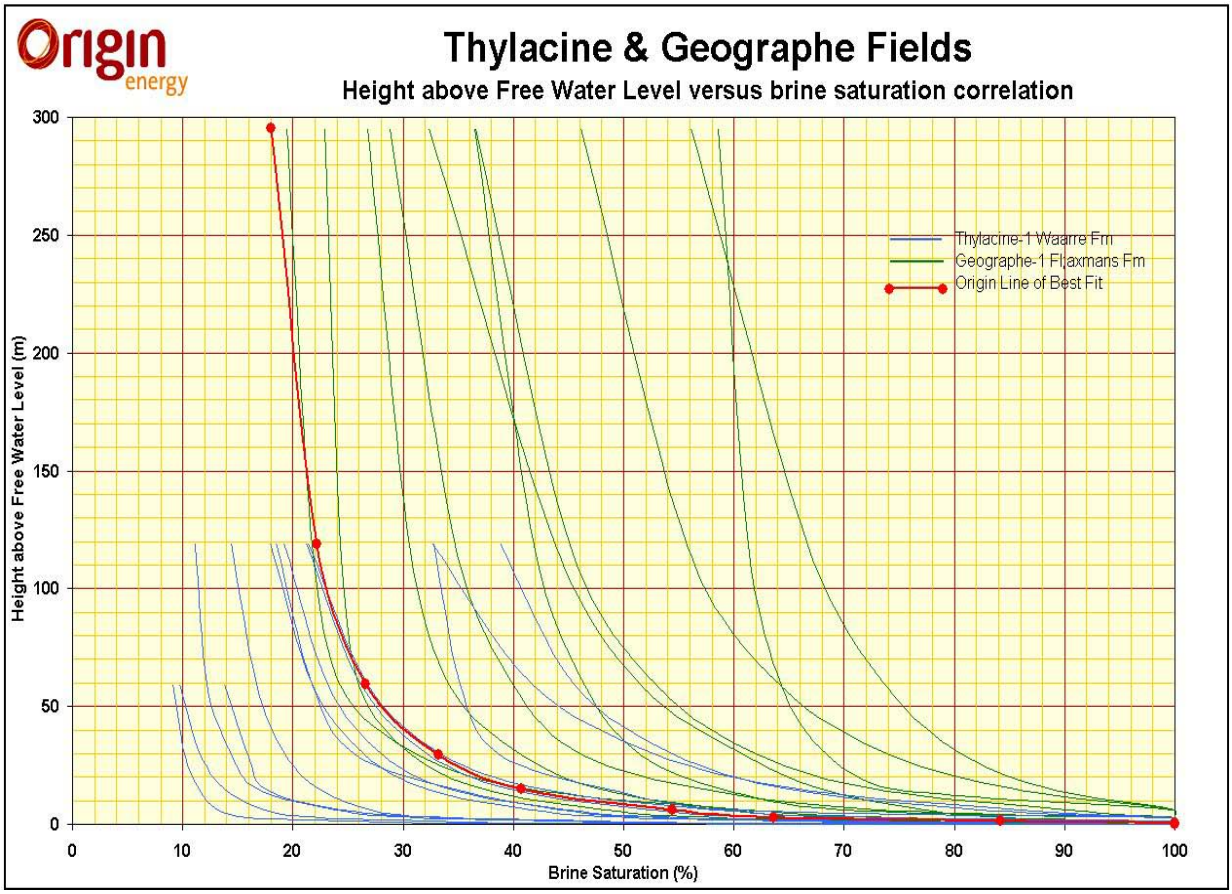

Origin energy
Thylacine & Geographe Fields
Water versus Overburden Air Permeability correlation
Overburden Water Permeability (mD)
Overburden Air Horizontal Permeability (mD)
10000
1000
100
10
1
0.1
0.1
1
10
100
1000
10000
y = 0.27116x^1.02989
R2 = 0.99169
n=41

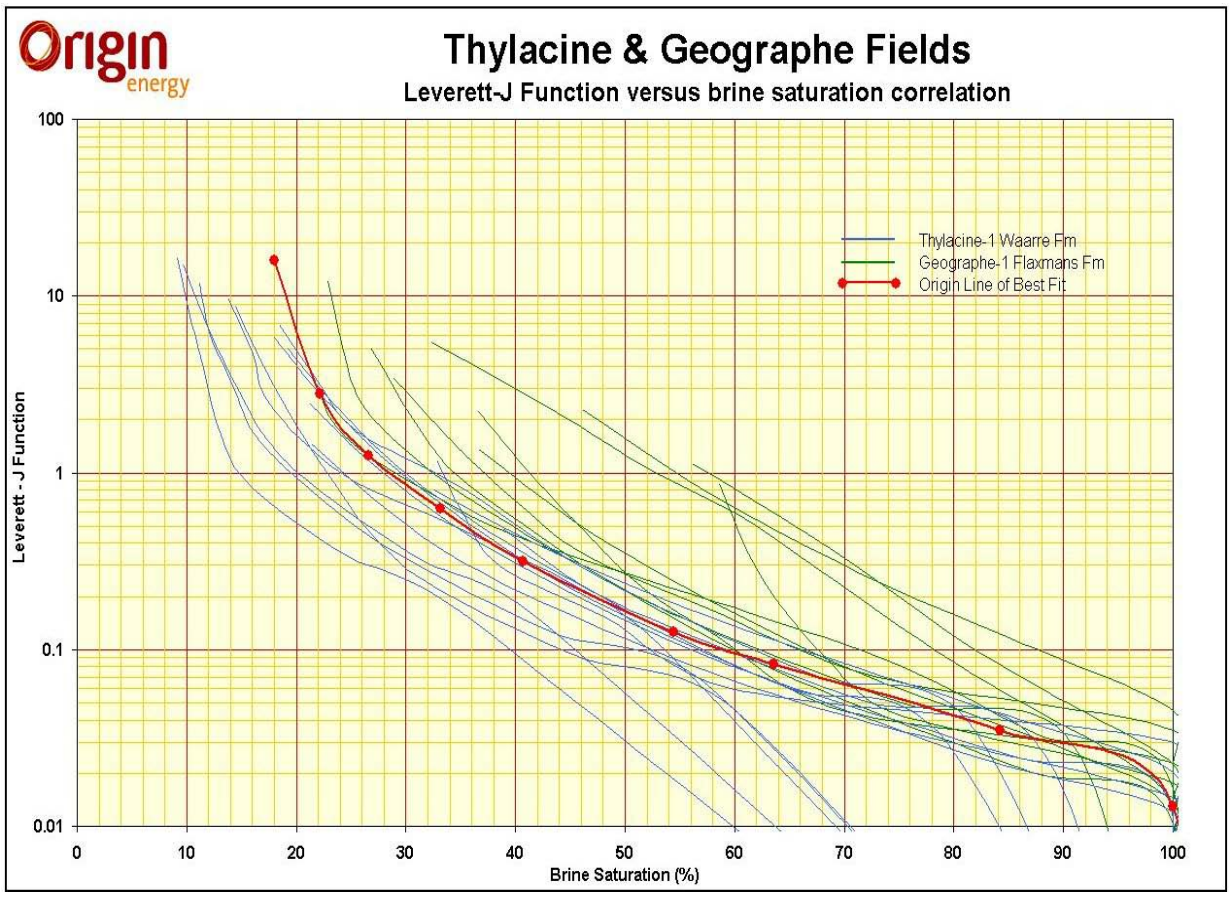

Thylacine & Geographe Fields
Irreducible Water Saturation versus Overburden Air Permeability correlation
y = 4189.3058e^-0.1796x
R2 = 0.8210
n=41
Overburden Air Air Horizontal Permeability (mD)
10000
1000
100
10
1
0.1
0
15
30
45
60
75
Irreducible Water Saturation from Capllary Pressure (%)

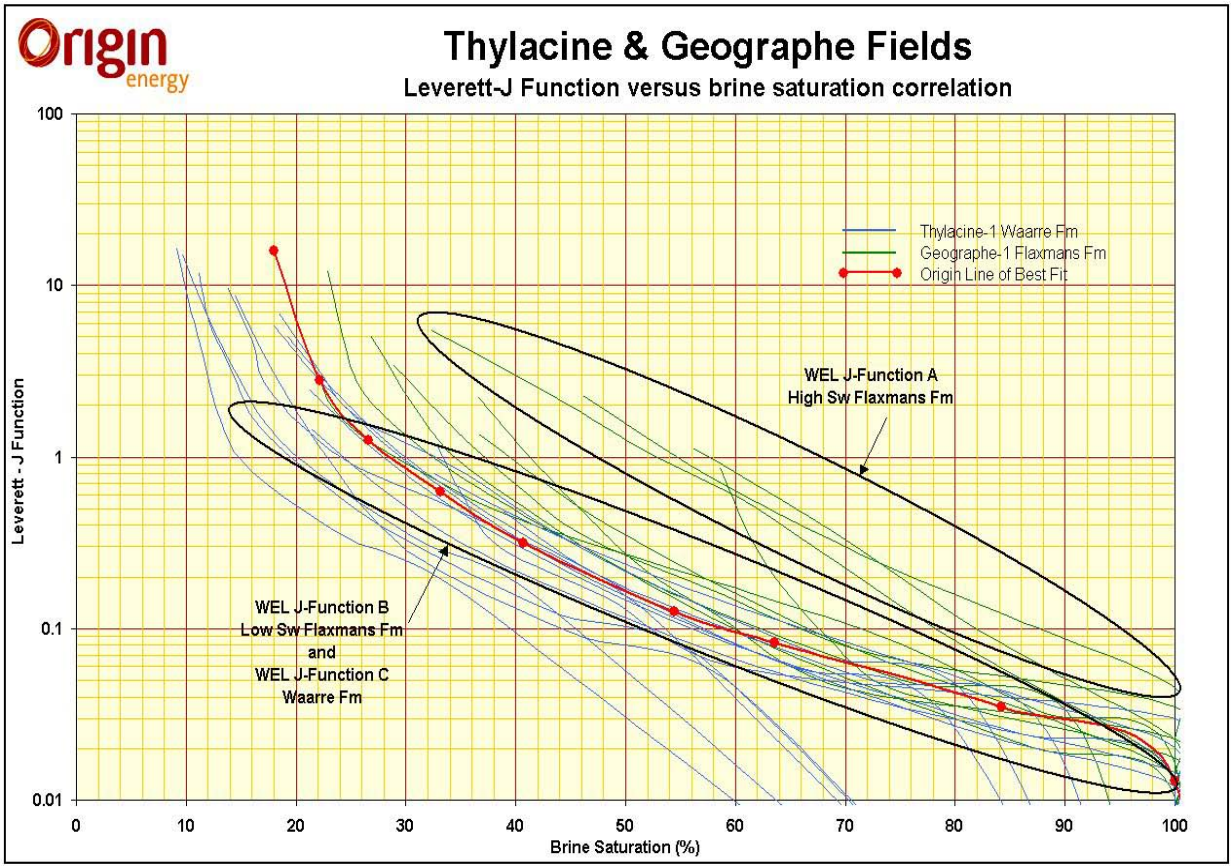

Thylacine & Geographe Fields
Irreducible Water Saturation versus Overburden Helium Porosity correlation
y = -0.16575x + 22.74410
R2 = 0.52859
n=41
Overburden Helium Horizontal Porosity (%)
25
22
19
16
13
10
0
15
30
45
60
75
Irreducible Water Saturation from Capllary Pressure (%)

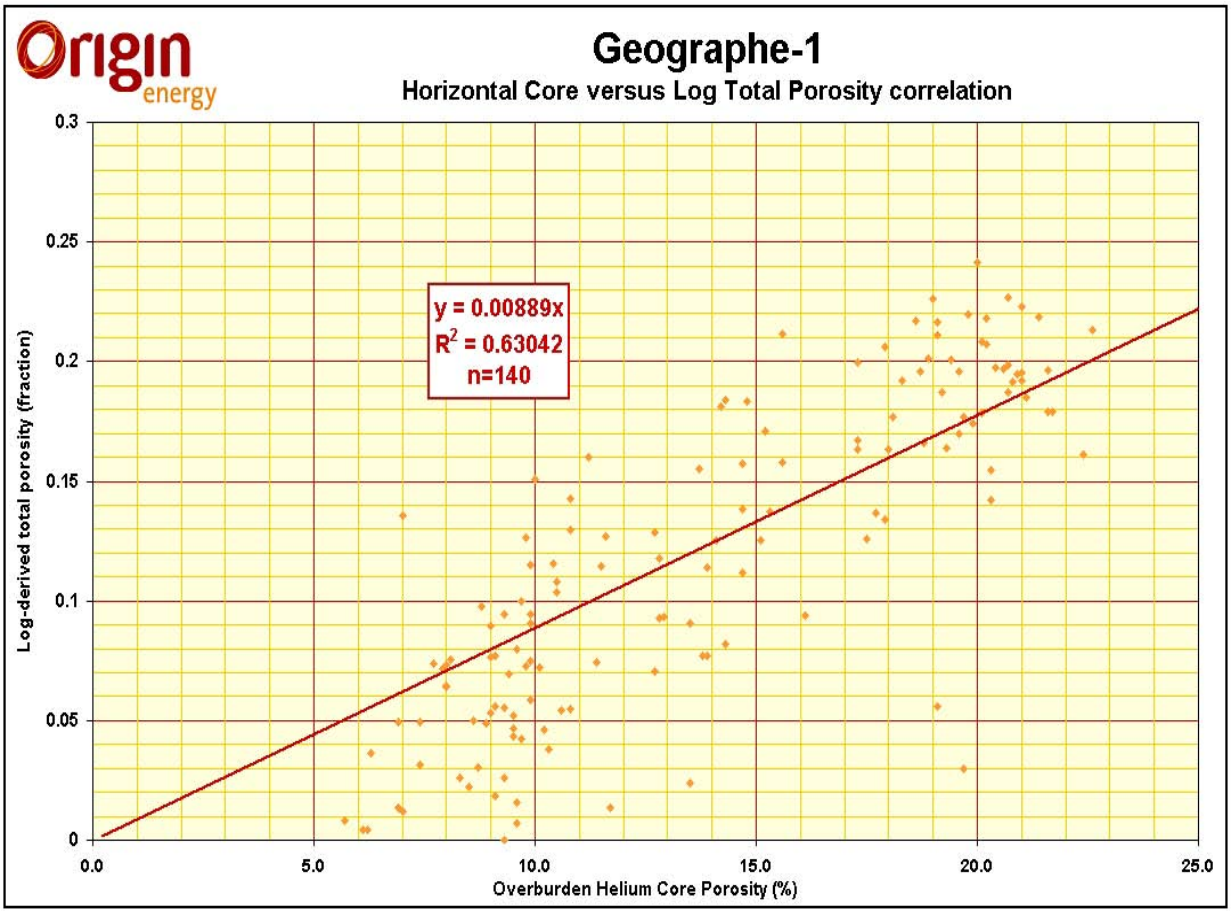

Origin energy
Thylacine & Geographe Fields
Air-brine Capillary Pressure versus brine saturation correlation
Laboratory Capillary Pressure (psi)
Brine Saturation (%)
Thylacine-1
Geographe-1
0
100
200
300
400
500
0
10
20
30
40
50
60
70
80
90
100

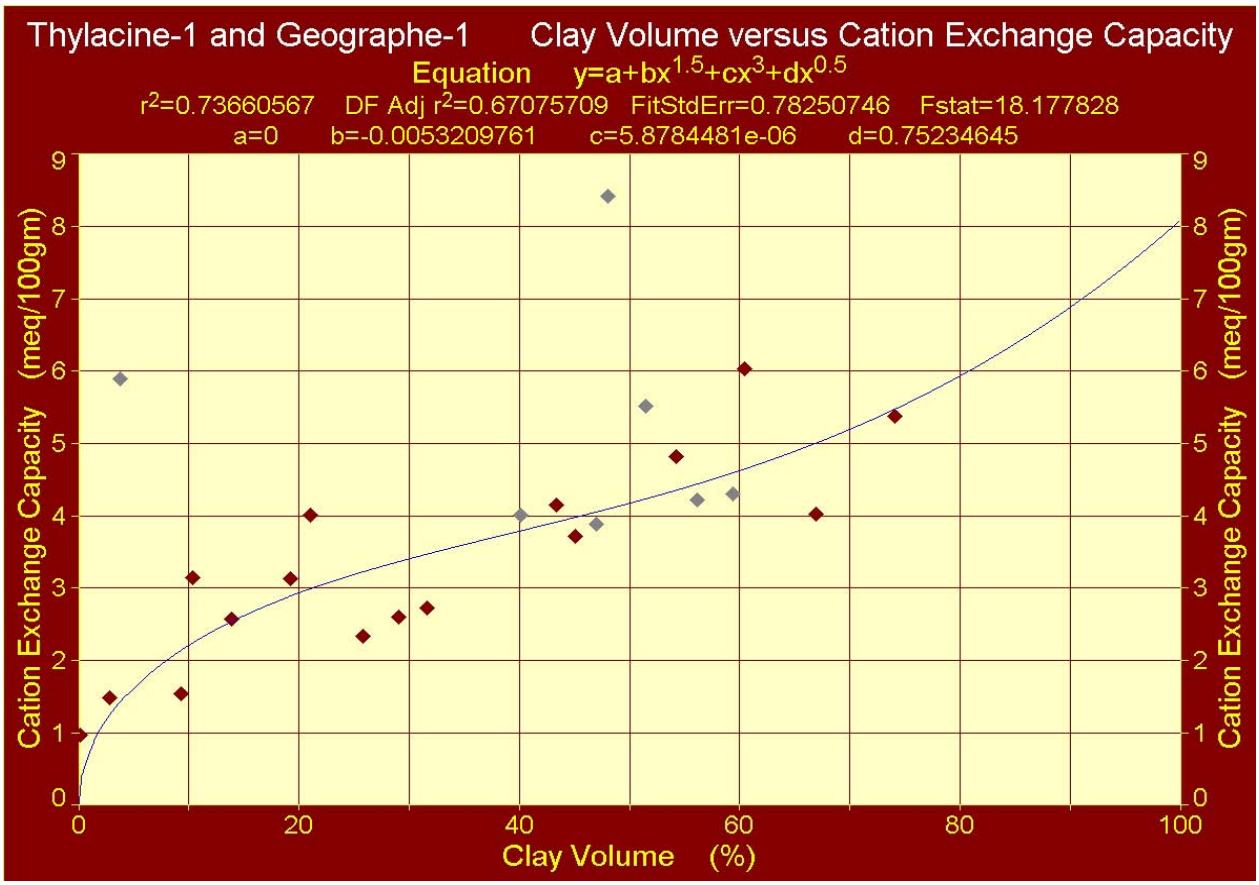

Origin energy
Thylacine & Geographe Fields
Gas-brine Capillary Pressure versus brine saturation correlation
Reservoir Capillary Pressure (psi)
Brine Saturation (%)
Thylacine-1
Geographe-1
0
50
100
150
200
250
300
350
0
10
20
30
40
50
60
70
80
90
100

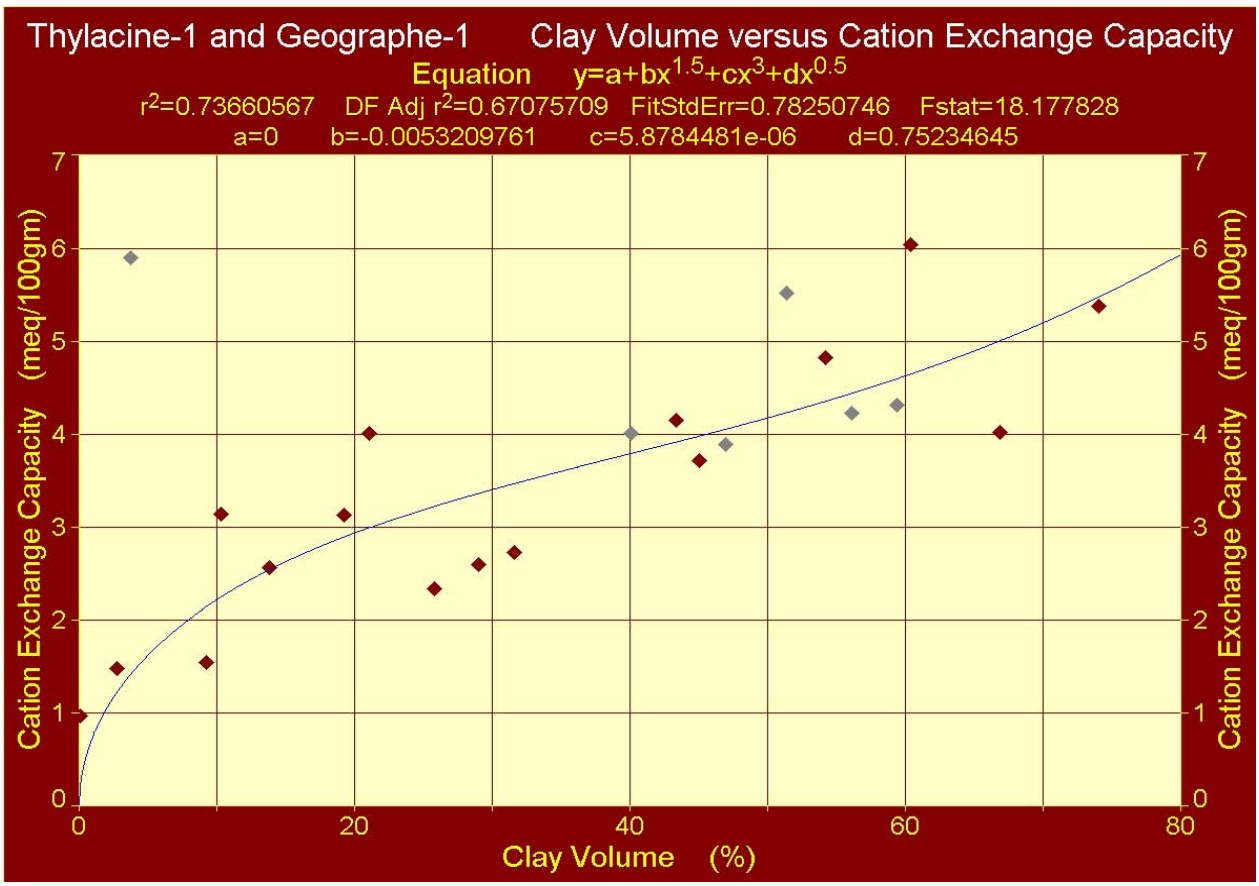

Origin energy
Thylacine & Geographe Fields
Height above Free Water Level versus brine saturation correlation
Thylacine-1 Waarre Fm
Geographe-1 Flaxmans Fm
Origin Line of Best Fit
Height above Free Water Level (m)
Brine Saturation (%)
300
250
200
150
100
50
0
0
10
20
30
40
50
60
70
80
90
100


Origin energy
Thylacine & Geographe Fields
Leverett-J Function versus brine saturation correlation
Thylacine-1 Waarre Fm
Geographe-1 Flaxmans Fm
Origin Line of Best Fit
Leverett - J Function
Brine Saturation (%)
100
10
1
0.1
0.01
0
10
20
30
40
50
60
70
80
90
100


Thylacine & Geographe Fields
Leverett-J Function versus brine saturation correlation
Thylacine-1 Waarre Fm
Geographe-1 Flaxmans Fm
Origin Line of Best Fit
WEL J-Function A
High Sw Flaxmans Fm
WEL J-Function B
Low Sw Flaxmans Fm
and
WEL J-Function C
Waarre Fm
Leverett - J Function
Brine Saturation (%)
100
10
1
0.1
0.01
0
10
20
30
40
50
60
70
80
90
100


Geographe-1
Horizontal Core versus Log Total Porosity correlation
y = 0.00889x
R2 = 0.63042
n=140
Log-derived total porosity (fraction)
Overburden Helium Core Porosity (%)
0.3
0.25
0.2
0.15
0.1
0.05
0
0.0
5.0
10.0
15.0
20.0
25.0


Thylacine-1 and Geographe-1 Clay Volume versus Cation Exchange Capacity
Equation y=a+bx^1.5+cx^3+dx^0.5
r^2=0.73660567 DF Adj r^2=0.67075709 FitStdErr=0.78250746 Fstat=18.177828
a=0 b=-0.0053209761 c=5.8784481e-06 d=0.75234645
Cation Exchange Capacity (meq/100gm)
Clay Volume (%)
0
20
40
60
80
100
1
2
3
4
5
6
7
8
9


Thylacine-1 and Geographe-1 Clay Volume versus Cation Exchange Capacity
Equation y=a+bx^1.5+cx^3+dx^0.5
r^2=0.73660567 DF Adj r^2=0.67075709 FitStdErr=0.78250746 Fstat=18.177828
a=0 b=-0.0053209761 c=5.8784481e-06 d=0.75234645
Cation Exchange Capacity (meq/100gm)
Clay Volume (%)
0
20
40
60
80
1
2
3
4
5
6
7

Appendix – E
Petrophysical Model and Constant Report

```
Company           : Woodside Energy Ltd.
Well Name         : THYLACINE-2
Field             : THYLACINE
State             : VICTORIA
Field Location    : OTWAY BASIN
Latitude          : 039 13' 42.675" S    DMS
Longitude         : 142 50' 55.000" E    DMS
Permanent Datum   : LAT
Elevation of PD   :        .00 M

Hole depth M     Temperature C     Gradient Deg C / 100 M
    2529.0          100.00          3.3389
        .0           15.56

Log data
Column     Logs       Logs
Position   Available  Used
    1      DEPT       DEPT
    2      GR
    3      SPDC       SP
    4      BS
    5      HCAL       CALI
    6      RT         ERT
    7      RXO        MSFL
    8      RLA5
    9      RLA4
   10      RLA3       LLS
   11      RLA2
   12      RLA1
   13      RXOI
   14      RXO8
   15      RXOZ
   16      RM_H
   17      DI_H
   18      HMIN
   19      HMNO
   20      RSO8
   21      RSOZ
   22      QCRX
   23      QCMC
   24      RHO8       RHOB
   25      RHOZ
   26      PEF8       PEF
   27      PEFZ
   28      HDRA       DRHO
   29      HPRA
   30      DSO8
   31      DSOZ
   32      NPHI
   33      TNPH
   34      HTNP       NPHI
   35      QCRH
   36      QCPE
   37      QCPO
   38      DTCO       DT
   39      DTSM
   40      PR
   41      VPVS
   42      HSGR
   43      HCGR       GR
   44      HTHO       THOR
   45      HURA       URAN
   46      HFK        POTA
   47      HTPR
   48      HTUR
   49      HUPR
   50      EHGR
   51      TENS
   52      CS
   53      DF
   54      SCD
   55      ROP
   56      TGAS
   57      METH
   58      ETH
   59      PRP
   60      iC4
   61      nC4
   62      iC5
   63      nC5
   64      CO2
   65      WOB
   66      RPM
   67      SPP
   68      FLOW
```

69	TQA
70	CALC
71	DOLO
72	TVD
73	RCA
74	CPOR
75	CKHA
76	CKVA
77	CPOO
78	CKHO
79	CKVO
80	GDEN
81	SNUM
82	Prob
83	CKHP
84	SNUM
85	Core
86	COGR
87	COGR
88	COGR
89	COGR
90	Faci
91	RCA-
92	CPOR
93	CKHA
94	CKVA
95	CPOO
96	CKHO
97	CKVO
98	GDEN
99	SNUM
100	PROB
101	CKHP
102	SNUM
103	CORE
104	COGR
105	COGR
106	COGR
107	FLAG
108	RCA_
109	CPOR
110	CKHA
111	CPOO
112	CKVA
113	CKHO
114	CKVO
115	GDEN
116	SNUM
117	CKHP
118	SNUM
119	COGR
120	CPOR
121	CKHA
122	CKVA
123	CPOO
124	CKHO
125	CKVO
126	GDEN
127	SNUM
128	CKHP
129	SNUM

```
                        Caliper recorded in : Inches
                        Mud weight units    : g/cc
                        Density log units   : g/cc
                        DRHO    log units   : g/cc
                        Sonic   log units   : Us/ft
                        Neutron log units   : LS POR
                        Density tool type   : LDT
                        RHO (H,MA,f)  units : g/cc
                        Dens. X-plots units : g/cc
                        GRV units           : Mbbl
```

Log scaling data

Log Mnemonic	Scaling Option	Coeff. A	Coeff. B
POTA	1	.00000	100.00000
PEF	1	-.55000	1.00000

Mineral table

Zone no.		1	2	3	4	5	6	7	8	9	10
Formation Name		Belfast Gr	Thylacin	Thylacin	Thylacin	Thylacin	Flaxman	Flaxman	Flaxman	Flaxman	UpperWaa
Top depth		2115.000	2141.530	2141.530	2141.530	2141.530	2237.160	2237.160	2237.160	2237.160	2347.480
Bottom depth		2141.530	2237.150	2237.150	2237.150	2237.150	2347.470	2347.470	2347.470	2347.470	2490.000
USER Log type											
Coal	RHOB min	-INF	-INF	-INF	-INF	-INF	-INF	-INF	-INF	-INF	-INF
Coal	RHOB max	2.000	2.000	2.000	2.000	2.000	2.000	2.000	2.000	2.000	2.000
Coal	PHIN min	.500	.500	.500	.500	.500	.500	.500	.500	.500	.500
Coal	PHIN max	+INF	+INF	+INF	+INF	+INF	+INF	+INF	+INF	+INF	+INF
Coal	GR min	-INF	-INF	-INF	-INF	-INF	-INF	-INF	-INF	-INF	-INF
Coal	GR max	+INF	+INF	+INF	+INF	+INF	+INF	+INF	+INF	+INF	+INF
Coal	t min	100.000	100.000	100.000	100.000	100.000	100.000	100.000	100.000	100.000	100.000

```
      Coal   t    max        +INF      +INF      +INF      +INF      +INF      +INF      +INF      +INF      +INF      +INF
      Coal   RT   min       20.000    20.000    20.000    20.000    20.000    20.000    20.000    20.000    20.000    20.000
      Coal   RT   max         +INF      +INF      +INF      +INF      +INF      +INF      +INF      +INF      +INF      +INF
      Coal   USER min     -999.250  -999.250  -999.250  -999.250  -999.250  -999.250  -999.250  -999.250  -999.250  -999.250
      Coal   USER max     -999.000  -999.000  -999.000  -999.000  -999.000  -999.000  -999.000  -999.000  -999.000  -999.000
          Zone no.           11        12        13
      Formation Name    UpperWaa  UpperWaa  UpperWaa
      Top depth          2347.480  2347.480  2347.480
      Bottom depth       2490.000  2490.000  2490.000
     USER Log type
      Coal   RHOB min         -INF      -INF      -INF
      Coal   RHOB max        2.000     2.000     2.000
      Coal   PHIN min         .500      .500      .500
      Coal   PHIN max         +INF      +INF      +INF
      Coal   GR   min         -INF      -INF      -INF
      Coal   GR   max         +INF      +INF      +INF
      Coal   t    min      100.000   100.000   100.000
      Coal   t    max         +INF      +INF      +INF
      Coal   RT   min       20.000    20.000    20.000
      Coal   RT   max         +INF      +INF      +INF
      Coal   USER min     -999.250  -999.250  -999.250
      Coal   USER max     -999.000  -999.000  -999.000

Lithology models
    1.   Sand-Dolomite               2.64 to     2.89
    2.   Sand-Limestone              2.64 to     2.75
    3.   Sand                        2.64 to     2.69
    4.   Limestone                   2.67 to     2.75
    5.   Dolomite                    2.75 to     2.89
    6.   Limestone-Dolomite          2.68 to     2.89

 CPX flag values
    1.  VCL greater than 0.95
    2.  VN  greater than 0.75
    3.  VS  greater than 0.75
    4.  Bad hole condition
    5.  Matrix density greater than Lithological model
    6.  Matrix density less than Lithological model
    7.  Porosity derived from Sonic Log
    8.  Porosity derived from or limited by PHIMAX
    9.  Porosity derived from Density Log
    $.  Pay zone

Water saturation equations
    1.  Indonesia
    2.  Simandoux
    3.  Fertl & Hammock
    4.  Laminar
    5.  Bussian
    6.  Charlebois
    7.  Single Sonic

 VGRTYPE :Vclay from GR Equations used
    0.  Not Used
                          IGR=(GR-GRmin)/(GRmax-GRmin)
    1.  Linear            VGR=IGR
    2.  Asymmetric (S shaped)
            Defined by 2 sets of intermediate points
            through which the S bend passes through.
            GR1, VGR1 and GR2, VGR2.
        Steiber equation:  VGR= IGR/(A + (A-1.0)*IGR)
    3.  Steiber 1  A = 2.0
    4.  Steiber 2  A = 3.0
    5.  Steiber 3  A = 4.0
    6.  Steiber 50%
         A is computed to give VGR= 0.5 when GR = GR50%)
    7.  Larinov Old Rocks: VGR= (2**(2*IGR)-1.0)/3.0
    8.  Larinov Tertiary : VGR= 0.083*(2.0*(3.7058*IGR)-1.0)
    9.  Clavier          : VGR= 1.7-SQRT(3.38-(IGR+0.7)**2.0)

 Cementation factor m
    1.  Linear        m = m
    2.  Shell formula m = 1.87 + 0.019/PHI
    3.  Borai formula m = 2.2 -0.035/(PHI+0.042)

              THYLACINE-2                        Complex Lithology Results
              Woodside Energy Ltd.               04-02-2004
                                Neutron           RT Determination
 Logging Company   Mud type     log type          Flags by priority
 0. Schlumberger   0. NaCl      0. CNL CORR       23. ERT (external RT)
 1. HLS            1. KCl %     1. TNPH            1. Dual Laterolog - RXO
 2. Dresser        2. Oil-base  2. SNP            20. PHASOR-SFL
 3. BPB/Reeves     3. Barite    3. N              21. PHASOR-RXO
 4. Sperry MWD                  4. HLS DSN2        2. Dual Induction - LL8
 5. Baker MWD                   5. CNL PRE 86      3. ILD-SFL-RXO
 6. Anadril MWD                 6. APLU           10. DIL-SFL
 7. Computalog                  7. FPLU           11. DIL-LL3
 8. Probe                       8. CDN 6.5"        8. ILD & 16 inch Normal
 9. Tucker                      9. CDN 8.0"       17. LLD-LLS
 Formation                     10. ADN 6.75       18. ID PHASOR
 Water                         11. ATLAS 2435 CN   4. ILD
 0=NaCl                        12. ATLAS 2420 CN   5. LLD
 1=NaHCO3                      13. ATLAS SNP       6. LL3 or LL7
```

14. BPB/Reeves
15. HLS G
16. Tucker_SNP
17. Tucker_CNL

7. Dual Laterolog
13. LLS
19. IM PHASOR
14. ILM
15. LL8
9. 64 inch Normal Log
12. SFL
22. N16
16. RXO
0. No RT logs

Zone no.	1	2	3	4	5	6	7	8	9	10
Formation Name	Belfast Gr	Thylacin	Thylacin	Thylacin	Thylacin	Flaxman	Flaxman	Flaxman	Flaxman	UpperWaa
Top depth	2115.000	2141.530	2141.530	2141.530	2141.530	2237.160	2237.160	2237.160	2237.160	2347.480
Bottom depth	2141.530	2237.150	2237.150	2237.150	2237.150	2347.470	2347.470	2347.470	2347.470	2490.000
Logging Company	0	0	0	0	0	0	0	0	0	0
Mud type	4	4	4	4	4	4	4	4	4	4
Formation Water Type	0	0	0	0	0	0	0	0	0	0
Neutron Log Type	1	1	1	1	1	1	1	1	1	1

Zone no.	11	12	13
Formation Name	UpperWaa	UpperWaa	UpperWaa
Top depth	2347.480	2347.480	2347.480
Bottom depth	2490.000	2490.000	2490.000
Logging Company	0	0	0
Mud type	4	4	4
Formation Water Type	0	0	0
Neutron Log Type	1	1	1

Zone no.	1	2	3	4	5	6	7	8	9	10
Formation	Belfast Gr	Thylacin	Thylacin	Thylacin	Thylacin	Flaxman	Flaxman	Flaxman	Flaxman	UpperWaa
1. Top depth	2115.000	2141.530	2141.530	2141.530	2141.530	2237.160	2237.160	2237.160	2237.160	2347.480
2. Bottom depth	2141.530	2237.150	2237.150	2237.150	2237.150	2347.470	2347.470	2347.470	2347.470	2490.000
3. No logs										
4. No logs	.000	.000	.000	.000	.000	.000	.000	.000	.000	.000
5. RM	.103	.103	.103	.103	.103	.103	.103	.103	.103	.103
6. Temp. RM	15.000	15.000	15.000	15.000	15.000	15.000	15.000	15.000	15.000	15.000
7. RMF	.0903000	.0903000	.0903000	.0903000	.0903000	.0903000	.0903000	.0903000	.0903000	.0903000
8. Temp. RMF	15.000	15.000	15.000	15.000	15.000	15.000	15.000	15.000	15.000	15.000
9. RMC	.236	.236	.236	.236	.236	.236	.236	.236	.236	.236
10. Temp. RMC	14.000	14.000	14.000	14.000	14.000	14.000	14.000	14.000	14.000	14.000
11. Bit size	8.500	8.500	8.500	8.500	8.500	8.500	8.500	8.500	8.500	8.500
12. Mud wt	1.160	1.160	1.160	1.160	1.160	1.160	1.160	1.160	1.160	1.160
13. SSP	.000	.000	.000	.000	.000	.000	.000	.000	.000	.000
14. RW (SP)	.0305057	.0299412	.0299412	.0299412	.0299412	.0290353	.0290353	.0290353	.0290353	.0279954
15. Temperature	86.620	88.659	88.659	88.659	88.659	92.097	92.097	92.097	92.097	96.318
16. RW @ FT	.191	.188	.188	.188	.188	.182	.182	.182	.182	.175
17. RW@75F(23.9C	.455	.455	.455	.455	.455	.455	.455	.455	.455	.455
18. RW salinity	13000.000	13000.010	13000.010	13000.010	13000.010	13000.000	13000.000	13000.000	13000.000	13000.000
19. RMF @ FT	.0305057	.0299412	.0299412	.0299412	.0299412	.0290353	.0290353	.0290353	.0290353	.0279954
20. RMF salinity	.105	.105	.105	.105	.105	.105	.105	.105	.105	.105
21. RM @ FT	.0346947	.0340527	.0340527	.0340527	.0340527	.0330224	.0330224	.0330224	.0330224	.0318397
22. RHO H	.510	.510	.510	.510	.510	.510	.510	.510	.510	.510
23. Gas Flag	1.000	1.000	1.000	1.000	1.000	1.000	1.000	1.000	1.000	1.000
24. RHO F	1.062	1.062	1.062	1.062	1.062	1.061	1.061	1.061	1.061	1.060
25. t F	188.972	188.972	188.972	188.972	188.972	188.972	188.972	188.972	188.972	188.972
26. RHOMA	2.670	2.670	2.670	2.670	2.670	2.670	2.670	2.670	2.670	2.670
27. PHIN min	-.0350000	-.0350000	-.0350000	-.0350000	-.0350000	-.0350000	-.0350000	-.0350000	-.0350000	-.0350000
28. t MA	55.500	55.500	55.500	55.500	55.500	55.500	55.500	55.500	55.500	55.500
29. t MA min	48.000	48.000	48.000	48.000	48.000	48.000	48.000	48.000	48.000	48.000
30. Sonic option	.000	.000	.000	.000	.000	.000	.000	.000	.000	.000
31. Compact/Ovrt	1.000	1.000	1.000	1.000	1.000	1.000	1.000	1.000	1.000	1.000
32. CAL cut off	16.000	16.000	16.000	16.000	16.000	16.000	16.000	16.000	16.000	16.000
33. RUGO.cut off	1.000	1.000	1.000	1.000	1.000	1.000	1.000	1.000	1.000	1.000
34. DRHO cut off	.150	.150	.150	.150	.150	.150	.150	.150	.150	.150
35. Bad Hole	.000	.000	.000	.000	.000	.000	.000	.000	.000	.000
36. No clay	SP RT N MN SN	SP RT N MN SN	SP RT N MN SN	SP RT N MN SN	SP RT N MN SN	SP RT N MN SN	SP RT N MN SN	SP RT N MN SN	SP RT N MN SN	SP RT N MN SN
37. Vclay Flag	.000	.000	.000	.000	.000	.000	.000	.000	.000	.000
38. Vclay type	.000	.000	.000	.000	.000	.000	.000	.000	.000	.000
39. Vclay inp1	.200	.200	.200	.200	.200	.200	.200	.200	.200	.200
40. Vclay out1	.150	.150	.150	.150	.150	.150	.150	.150	.150	.150
41. Vclay inp2	.800	.800	.800	.800	.800	.800	.800	.800	.800	.800
42. Vclay out2	.800	.800	.800	.800	.800	.800	.800	.800	.800	.800
43. Vclay 50%	.500	.500	.500	.500	.500	.500	.500	.500	.500	.500
44. VclayGR type	1.000	1.000	1.000	1.000	1.000	1.000	1.000	1.000	1.000	1.000
45. GR clean	17.027	16.768	16.818	16.818	16.818	16.898	16.818	16.818	16.818	16.638
46. GR clay	82.326	82.239	82.326	82.326	82.326	82.239	82.326	82.326	82.326	82.326
47. GR1	36.000	36.000	36.000	36.000	36.000	36.000	36.000	36.000	36.000	36.000
48. VGR1	.100	.100	.100	.100	.100	.100	.100	.100	.100	.100
49. GR2	81.326	84.000	81.326	84.000	84.000	84.000	84.000	81.326	84.000	84.000
50. VGR2	.800	.800	.800	.800	.800	.800	.800	.800	.800	.800
51. GR50%	70.000	70.000	70.000	70.000	70.000	70.000	70.000	70.000	70.000	70.000
52. R clay	20.000	50.000	50.000	50.000	50.000	50.000	50.000	50.000	50.000	50.000
53. R limit	1000.000	1000.000	1000.000	1000.000	1000.000	1000.000	1000.000	1000.000	1000.000	1000.000
54. Rclay1 flag	.000	.000	.000	.000	.000	.000	.000	.000	.000	.000
55. Rclay1	1.000	1.000	1.000	1.000	1.000	1.000	1.000	1.000	1.000	1.000
56. Vcl @ Rclay1	.150	.150	.150	.150	.150	.150	.150	.150	.150	.150
57. RHOB sand	2.169	2.169	2.169	2.169	2.169	2.169	2.169	2.169	2.169	2.169
58. RHOB silt	2.680	2.680	2.680	2.680	2.680	2.680	2.680	2.680	2.680	2.680

59.	RHOB clay	2.685	2.685	2.685	2.685	2.685	2.685	2.685	2.685	2.685	2.685
60.	RHO Dry Clay	2.725	2.400	2.400	2.400	2.400	2.540	2.540	2.540	2.540	2.725
61.	Rhob Calcite	2.800	2.800	2.800	2.800	2.800	2.800	2.800	2.800	2.800	2.800
62.	PHIN Sand	.265	.265	.265	.265	.265	.265	.265	.265	.265	.265
63.	PHIN silt	.100	.100	.100	.100	.100	.100	.100	.100	.100	.100
64.	PHIN clay	.321	.321	.321	.321	.321	.321	.321	.321	.321	.321
65.	Phin Calcite	.100	.100	.100	.100	.100	.100	.100	.100	.100	.100
66.	PHISILT	.100	.100	.100	.100	.100	.100	.100	.100	.100	.100
67.	Calcite Flag	.000	.000	.000	.000	.000	.000	.000	.000	.000	.000
68.	t clay	77.519	77.519	77.519	77.519	77.519	77.519	77.519	77.519	77.519	77.519
69.	M clay	.687	.687	.687	.687	.687	.686	.686	.686	.686	.686
70.	N clay	.418	.418	.418	.418	.418	.418	.418	.418	.418	.418
71.	PHIN 2.2	.0550000	.0550000	.0550000	.0550000	.0550000	.0550000	.0550000	.0550000	.0550000	.208
72.	t 2.2	83.000	83.000	83.000	83.000	83.000	83.697	83.000	83.000	83.000	86.700
73.	a	1.000	1.000	1.000	1.000	1.000	1.000	1.000	1.000	1.000	1.000
74.	A1	1.000	1.000	1.000	1.000	1.000	1.000	1.000	1.000	1.000	1.000
75.	m	2.200	2.000	1.800	2.000	2.350	2.000	1.800	2.000	2.350	2.000
76.	m1	2.500	2.150	1.950	2.150	2.500	2.150	1.950	2.150	2.500	2.150
77.	m Function	1.000	1.000	1.000	1.000	1.000	1.000	1.000	1.000	1.000	1.000
78.	n	2.000	2.000	1.750	1.950	2.150	2.000	1.750	1.950	2.150	2.000
79.	n1	2.450	2.200	2.050	2.250	2.450	2.200	2.050	2.250	2.450	2.200
80.	B from BQV	10.286	10.492	10.492	10.492	10.492	10.835	10.835	10.835	10.835	11.249
81.	A(QV)	.0003050	.0003050	.0003050	.0003050	.0003050	.0003050	.0003050	.0003050	.0003050	.0003050
82.	B(QV)	-3.450	-3.450	-3.450	-3.450	-3.450	-3.450	-3.450	-3.450	-3.450	-3.450
83.	Lithomod	1.000	1.000	1.000	1.000	1.000	1.000	1.000	1.000	1.000	1.000
84.	SXO limit	.200	.200	.200	.200	.200	.200	.200	.200	.200	.200
85.	PHI max	.298	.226	.226	.226	.226	.216	.218	.199	.199	.220
86.	PHI min c.o.	.0010000	.0010000	.0010000	.0010000	.0010000	.0010000	.0010000	.0010000	.0010000	.0010000
87.	EXPX	1.500	1.500	1.500	1.500	1.500	1.500	1.500	1.500	1.500	1.500
88.	Pay Flag typ	.000	.000	.000	.000	.000	.000	.000	.000	.000	.000
89.	Clay cut off	.400	.400	.400	.400	.400	.400	.400	.400	.400	.400
90.	PHIe cut off	.0100000	.0100000	.0100000	.0100000	.0100000	.0100000	.0100000	.0100000	.0100000	.0100000
91.	PHIt cut off	.100	.100	.100	.100	.100	.100	.100	.100	.100	.100
92.	SWe cut off	.650	.650	.650	.650	.650	.650	.650	.650	.650	.650
93.	SWt cut off	.600	.600	.600	.600	.600	.600	.600	.600	.600	.600
94.	GrossRockVol	.000	.000	.000	.000	.000	.000	.000	.000	.000	.000
95.	Oil Exp.Fact	1.200	1.200	1.200	1.200	1.200	1.200	1.200	1.200	1.200	1.200
96.	FormGeom.Fac	1.000	1.000	1.000	1.000	1.000	1.000	1.000	1.000	1.000	1.000
97.	RecoveryFact	.200	.200	.200	.200	.200	.200	.200	.200	.200	.200
98.	SWB max	1.000	1.000	1.000	1.000	1.000	1.000	1.000	1.000	1.000	1.000
99.	RWB	.419	.146	.262	.146	.0525395	.621	.964	.621	.288	1.488
100.	SWB cut off	.300	.300	.300	.300	.300	.300	.300	.300	.300	.300
101.	RWF	.191	.188	.188	.188	.188	.182	.182	.182	.182	.175
102.	RMFF	.0305057	.0299412	.0299412	.0299412	.0299412	.0290353	.0290353	.0290353	.0290353	.0279954
103.	Sw Eq. CPX	1.000	1.000	1.000	1.000	1.000	1.000	1.000	1.000	1.000	1.000
104.	Sw Eq. SSS	1.000	1.000	1.000	1.000	1.000	1.000	1.000	1.000	1.000	1.000
105.	Glauconite	.000	.000	.000	.000	.000	.000	.000	.000	.000	.000
106.	SWirr.cutoff	.300	.300	.300	.300	.300	.300	.300	.300	.300	.300
107.	Perm Expon.	6.000	6.000	6.000	6.000	6.000	6.000	6.000	6.000	6.000	6.000
108.	PERM K coef	62500.000	62500.000	62500.000	62500.000	62500.000	62500.000	62500.000	62500.000	62500.000	62500.000
109.	RHOMA 1	2.670	2.670	2.670	2.670	2.670	2.670	2.670	2.670	2.670	2.670
110.	RHOMA 2	2.710	2.710	2.710	2.710	2.710	2.710	2.710	2.710	2.710	2.710
111.	RHOMA 3	3.000	3.000	3.000	3.000	3.000	3.000	3.000	3.000	3.000	3.000
112.	UMA 1	4.800	4.800	4.800	4.800	4.800	4.800	4.800	4.800	4.800	4.800
113.	UMA 2	27.950	27.950	27.950	27.950	27.950	27.950	27.950	27.950	27.950	27.950
114.	UMA 3	10.867	10.867	10.867	10.867	10.867	10.867	10.867	10.867	10.867	10.867
115.	UF	.400	.400	.400	.400	.400	.400	.400	.400	.400	.400
116.	UMACL	10.889	10.889	10.889	10.889	10.889	10.889	10.889	10.889	10.889	10.889
117.	GR Dispersed	60.000	60.000	60.000	60.000	60.000	60.000	60.000	60.000	60.000	60.000
118.	PHIT Dispers	.0400000	.0400000	.0400000	.0400000	.0400000	.0400000	.0400000	.0400000	.0400000	.0400000
119.	PHIT Laminat	.0250000	.0250000	.0250000	.0250000	.0250000	.0250000	.0250000	.0250000	.0250000	.0250000
120.	PHIT Sand	.275	.275	.275	.275	.275	.275	.275	.275	.275	.275
121.	Vp/Vs Sand	1.500	1.500	1.500	1.500	1.500	1.500	1.500	1.500	1.500	1.500
122.	Vp/Vs LS	1.900	1.900	1.900	1.900	1.900	1.900	1.900	1.900	1.900	1.900
123.	Vp/Vs DOL	1.800	1.800	1.800	1.800	1.800	1.800	1.800	1.800	1.800	1.800
124.	Vp/Vs VCL	1.700	1.700	1.700	1.700	1.700	1.700	1.700	1.700	1.700	1.700
125.	Vp/Vs Salt	2.150	2.150	2.150	2.150	2.150	2.150	2.150	2.150	2.150	2.150
126.	Vp/Vs Trona	2.250	2.250	2.250	2.250	2.250	2.250	2.250	2.250	2.250	2.250
127.	Vp/Vs Anhyd	2.450	2.450	2.450	2.450	2.450	2.450	2.450	2.450	2.450	2.450
128.	Vp/Vs Gypsum	2.350	2.350	2.350	2.350	2.350	2.350	2.350	2.350	2.350	2.350
129.	Vp/Vs Coal	2.000	2.000	2.000	2.000	2.000	2.000	2.000	2.000	2.000	2.000
93.	PHINmat1	.200	.200	.200	.200	.200	.200	.200	.200	.200	.200
94.	PHIDmat1	.240	.240	.240	.240	.240	.240	.240	.240	.240	.240
95.	PHINmat2	.350	.350	.350	.350	.350	.350	.350	.350	.350	.350
96.	PHIDmat2	.200	.200	.200	.200	.200	.200	.200	.200	.200	.200
97.	PHINmat3	.050	.050	.050	.050	.050	.050	.050	.050	.050	.050
98.	PHIDmat3	.000	.000	.000	.000	.000	.000	.000	.000	.000	.000
99.	PHINmat4	.200	.200	.200	.200	.200	.200	.200	.200	.200	.200
100.	PHIDmat4	-.100	-.100	-.100	-.100	-.100	-.100	-.100	-.100	-.100	-.100

	Zone no.	11	12	13
	Formation	UpperWaa	UpperWaa	UpperWaa
1.	Top depth	2347.480	2347.480	2347.480
2.	Bottom depth	2490.000	2490.000	2490.000
3.	No logs			
4.	No logs	.000	.000	.000
5.	RM	.103	.103	.103
6.	Temp. RM	15.000	15.000	15.000
7.	RMF	.0903000	.0903000	.0903000
8.	Temp. RMF	15.000	15.000	15.000
9.	RMC	.236	.236	.236
10.	Temp. RMC	14.000	14.000	14.000
11.	Bit size	8.500	8.500	8.500

12.	Mud wt	1.160	1.160	1.160
13.	SSP	.000	.000	.000
14.	RW (SP)	.0279954	.0279954	.0279954
15.	Temperature	96.318	96.318	96.318
16.	RW @ FT	.175	.175	.175
17.	RW@75F(23.9C	.455	.455	.455
18.	RW salinity	13000.000	13000.000	13000.000
19.	RMF @ FT	.0279954	.0279954	.0279954
20.	RMF salinity	.105	.105	.105
21.	RM @ FT	.0318397	.0318397	.0318397
22.	RHO H	.510	.510	.510
23.	Gas Flag	1.000	1.000	1.000
24.	RHO F	1.060	1.060	1.060
25.	t F	188.972	188.972	188.972
26.	RHOMA	2.670	2.670	2.670
27.	PHIN min	-.0350000	-.0350000	-.0350000
28.	t MA	55.500	55.500	55.500
29.	t MA min	48.000	48.000	48.000
30.	Sonic option	.000	.000	.000
31.	Compact/Ovrt	1.000	1.000	1.000
32.	CAL cut off	16.000	16.000	16.000
33.	RUGO.cut off	1.000	1.000	1.000
34.	DRHO cut off	.150	.150	.150
35.	Bad Hole	.000	.000	.000
36.	No clay	SP RT N MN SN	SP RT N MN SN	SP RT N MN SN
37.	Vclay Flag	.000	.000	.000
38.	Vclay type	.000	.000	.000
39.	Vclay inp1	.200	.200	.200
40.	Vclay out1	.150	.150	.150
41.	Vclay inp2	.800	.800	.800
42.	Vclay out2	.800	.800	.800
43.	Vclay 50%	.500	.500	.500
44.	VclayGR type	1.000	1.000	1.000
45.	GR clean	16.818	16.818	16.818
46.	GR clay	82.326	82.326	82.368
47.	GR1	36.000	36.000	36.000
48.	VGR1	.100	.100	.100
49.	GR2	84.000	84.000	84.000
50.	VGR2	.800	.800	.800
51.	GR50%	70.000	70.000	70.000
52.	R clay	50.000	50.000	50.000
53.	R limit	1000.000	1000.000	1000.000
54.	Rclay1 flag	.000	.000	.000
55.	Rclay1	1.000	1.000	1.000
56.	Vcl @ Rclay1	.150	.150	.150
57.	RHOB sand	2.169	2.169	2.169
58.	RHOB silt	2.680	2.680	2.680
59.	RHOB clay	2.685	2.685	2.685
60.	RHO Dry Clay	2.725	2.725	2.725
61.	Rhob Calcite	2.800	2.800	2.800
62.	PHIN Sand	.265	.265	.265
63.	PHIN silt	.100	.100	.100
64.	PHIN clay	.321	.321	.321
65.	Phin Calcite	.100	.100	.100
66.	PHISILT	.100	.100	.100
67.	Calcite Flag	.000	.000	.000
68.	t clay	77.519	77.519	77.519
69.	M clay	.686	.686	.686
70.	N clay	.418	.418	.418
71.	PHIN 2.2	.208	.208	.208
72.	t 2.2	86.700	86.700	86.700
73.	a	1.000	1.000	1.000
74.	A1	1.000	1.000	1.000
75.	m	1.800	2.000	2.350
76.	m1	1.950	2.150	2.500
77.	m Function	1.000	1.000	1.000
78.	n	1.750	1.950	2.150
79.	n1	2.050	2.250	2.450
80.	B from BQV	11.249	11.249	11.249
81.	A(QV)	.0003050	.0003050	.0003050
82.	B(QV)	-3.450	-3.450	-3.450
83.	Lithomod	1.000	1.000	1.000
84.	SXO limit	.200	.200	.200
85.	PHI max	.220	.220	.220
86.	PHI min c.o.	.0010000	.0010000	.0010000
87.	EXPX	1.500	1.500	1.500
88.	Pay Flag typ	.000	.000	.000
89.	Clay cut off	.400	.400	.400
90.	PHIe cut off	.0100000	.0100000	.0100000
91.	PHIt cut off	.100	.100	.100
92.	SWe cut off	.650	.650	.650
93.	SWt cut off	.600	.600	.600
94.	GrossRockVol	.000	.000	.000
95.	Oil Exp.Fact	1.200	1.200	1.200
96.	FormGeom.Fac	1.000	1.000	1.000
97.	RecoveryFact	.200	.200	.200
98.	SWB max	1.000	1.000	1.000
99.	RWB	2.115	1.488	.804
100.	SWB cut off	.300	.300	.300

101.	RWF	.175	.175	.175
102.	RMFF	.0279954	.0279954	.0279954
103.	Sw Eq. CPX	1.000	1.000	1.000
104.	Sw Eq. SSS	1.000	1.000	1.000
105.	Glauconite	.000	.000	.000
106.	SWirr.cutoff	.300	.300	.300
107.	Perm Expon.	6.000	6.000	6.000
108.	PERM K coef	62500.000	62500.000	62500.000
109.	RHOMA 1	2.670	2.670	2.670
110.	RHOMA 2	2.710	2.710	2.710
111.	RHOMA 3	3.000	3.000	3.000
112.	UMA 1	4.800	4.800	4.800
113.	UMA 2	27.950	27.950	27.950
114.	UMA 3	10.867	10.867	10.867
115.	UF	.400	.400	.400
116.	UMACL	10.889	10.889	10.889
117.	GR Dispersed	60.000	60.000	60.000
118.	PHIT Dispers	.0400000	.0400000	.0400000
119.	PHIT Laminat	.0250000	.0250000	.0250000
120.	PHIT Sand	.275	.275	.275
121.	Vp/Vs Sand	1.500	1.500	1.500
122.	Vp/Vs LS	1.900	1.900	1.900
123.	Vp/Vs DOL	1.800	1.800	1.800
124.	Vp/Vs VCL	1.700	1.700	1.700
125.	Vp/Vs Salt	2.150	2.150	2.150
126.	Vp/Vs Trona	2.250	2.250	2.250
127.	Vp/Vs Anhyd	2.450	2.450	2.450
128.	Vp/Vs Gypsum	2.350	2.350	2.350
129.	Vp/Vs Coal	2.000	2.000	2.000
93.	PHINmat1	.200	.200	.200
94.	PHIDmat1	.240	.240	.240
95.	PHINmat2	.350	.350	.350
96.	PHIDmat2	.200	.200	.200
97.	PHINmat3	.050	.050	.050
98.	PHIDmat3	.000	.000	.000
99.	PHINmat4	.200	.200	.200
100.	PHIDmat4	-.100	-.100	-.100

ENCLOSURE-1
Petrophysical and Composite Plot
2113-2542mMDRT (1:500)

THYLACINE-2

COMPOSITE AND PETROPHYSICAL SUMMARY

Company	Woodside Energy Ltd.
Well Name	THYLACINE-2
Field	THYLACINE
Location	OFFSHORE VICTORIA
State	VICTORIA
County or Rig name	Ocean Bounty
Field Location	OTWAY BASIN
Field Loca. Line 1	LAT(DG) -43.9364 2 SS
Field Loca. Line 2	LONG(DG) 146.9 0 0 E 0 0 SS
Latitude	038 12' 42.670" S DMS
Longitude	142 59' 53.000" E DMS
Permanent Datum	LAT
Elevation of PD	-98 M
Elevation KB	114.20 M
Elevation Ground/ft	101.20 M
Elevation Log Zero	21.00 M
Above Perm. Datum	21.00 M
Log measured from	RT
Drilling measured	RT
Other Services 1-3	HNGS GR
Other Services 1a 2	EMI GR
Other Services 1a 3	VSP GR
Other Services 1a 4	CST GR
Log date	8-Sep-2001
Date computed	12-05-03
Run number	ONE/TWO
Time plotted	11:24:27

PETROLOG SOFTWARE Revision: 9.10

CROCK 8.8.0.

RUN INFORMATION

Run number	Un
Log date	8-Sep-2001
Depth-Driller	2325.00 M
Depth-Logger	2329.00 M
Casing-Driller	2101.00 M
Casing Diameter	9.6250 inch
Casing-Logger	2101.00 M
Casing Depth	2101.00 M
Bit Size	8.5000 inch
Hole Fluid type	KCl/POLYGLYCOL
Fluid Density	1.1600 gm/cc
Fluid Viscosity	0.0000
Fluid PH	9.00000
Fluid Loss	2.7000 CC
Mud Sample Source	FLOWLINE
RM @ Surface	.1027 Ohmm
Mud Filtrate @	.0855 Ohmm
RMF @ Surface	.0982 Ohmm
ME temp Surface	11.00 degC
RMC @ Surface	.2355 Ohmm
MC Temp Surface	14.00 degC
Source of RMF/RMC	PRESSED
Mud Sample Temp	11.00 degC
Mud Filt Sample Temp	11.00 degC
Mud Cake/sample Source	PRESSED
Time circ. stopped	13:15
Date circ. stopped	8-Sep-2001
Inst. logged Date	8-Sep-2001
Max rec. surface temp	20.00 degC
Bottom hole temp	100.00 degC
Surface temperature	15.56 degC
Max recorded temp	100.00 degC
Logging unit No	3476
Logging truck no	VIC/P(3476)
Logging Company ID	440
Recorded by	F. Marcano / M. Vu
Witness	M. Bilek / G. Wren
Program Version	SC2.303
Well Status	WDFW
Avg Angular Deviat	.000000
General Temp Select	TEMP
Maximum Hole Deviat	1.9200 deg
Total depth	2325.00 M
Temp Com. Ware/Samp	37.78 degC

FIELD REMARKS

1. First run in hole. Schlumberger depth procedures observed.
2. Borehole correction applied to logs.
3. Neutron porosity corrected for the presentation of neutron porosity.
4. Bottom hole temperature - degC at 0000h on 00-Sep-01.
5. Data acquired in high resolution mode for the entire interval as per client request.
6. Well sketch shows driller's depth.
7. Caliper check in casing reading 00.00 in. ID expected 00.00 in.
8. Tools run as per tool sketch.
9. Circulation time 1.93 hrs stopped at 1136 l on 08-Sep-01.

Thank you for using Schlumberger

Mud Properties:
Barite conc = 5.74%, CI(Kcl) conc. = 43 000ppm, Potassium conc. = 29500ppm
Solids corrected = 95.0%, Solids content = 8.0%, Corr. Solids content = 5.65%
Effectif conc. = 3%, Calcium conc. = 540 mg/l

COMPUTATION PARAMETERS

DEPTH INTERVAL	RW PPM	RW 1000MM	TEMP DEGC	GR MIN	GR MAX	R CLAY	RHOB CLAY	PHIN CLAY	I CLAY	RHOB	a	m
2110.0 - 2141.5	13000	191	86.6	17	82	20	2.68	321	70	51	1.00	2.20
2141.5 - 2227.5	13000	188	89.7	17	82	50	2.68	321	70	51	1.00	2.00
2141.5 - 2227.5	13000	188	89.7	17	82	50	2.68	321	70	51	1.00	1.80
2141.5 - 2227.5	13000	188	89.7	17	82	50	2.68	321	70	51	1.00	2.00
2141.5 - 2227.5	13000	188	89.7	17	82	50	2.68	321	70	51	1.00	2.15
2227.2 - 2347.5	13000	182	92.1	17	82	50	2.68	321	70	51	1.00	2.00
2227.2 - 2347.5	13000	182	92.1	17	82	50	2.68	321	70	51	1.00	1.80
2227.2 - 2347.5	13000	182	92.1	17	82	50	2.68	321	70	51	1.00	2.00
2227.2 - 2347.5	13000	182	92.1	17	82	50	2.68	321	70	51	1.00	2.15
2347.5 - 2490.0	13000	175	96.5	17	82	50	2.68	321	70	51	1.00	2.00
2347.5 - 2490.0	13000	175	96.5	17	82	50	2.68	321	70	51	1.00	1.80
2347.5 - 2490.0	13000	175	96.5	17	82	50	2.68	321	70	51	1.00	2.00
2347.5 - 2490.0	13000	175	96.5	17	82	50	2.68	321	70	51	1.00	2.15

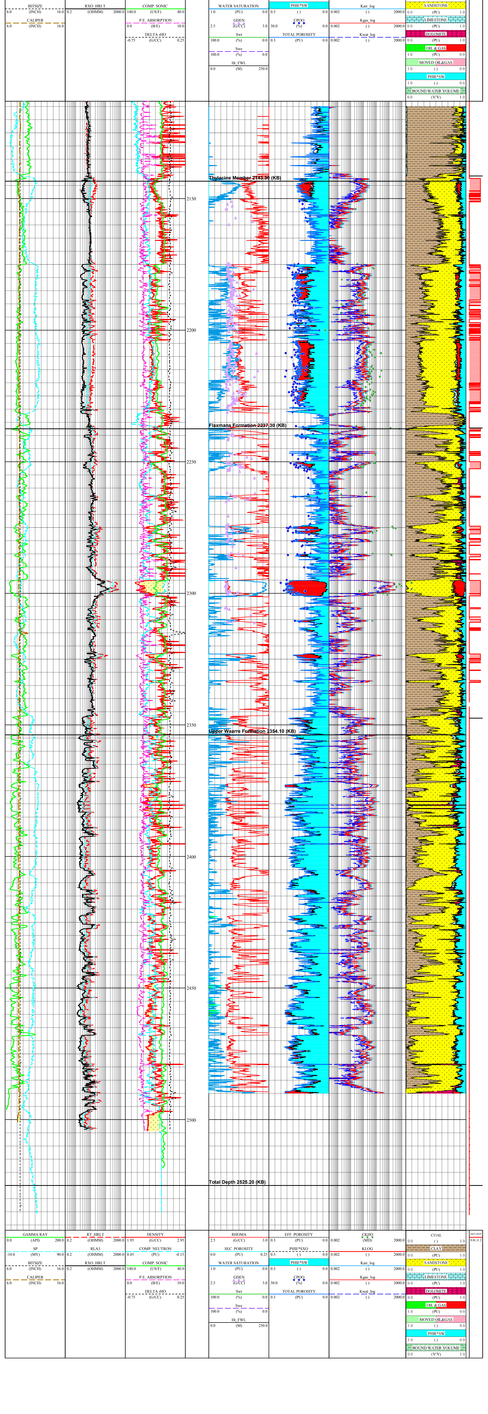
LITHOLOGIES

Clay
Sandstone
Bound Water
OIL
GAS
MOVED OIL
MOVED GAS
Sandstone
Limestone
Dolomite

LOG DESCRIPTION

RSWA-CPS	Apparent Matrix Density (Complex Litho Model)
RHOM-CPS	Matrix Density (Complex Litho Model) (Complex Litho Model)
SW -CPS	Formation Water Saturation (=1-I/Complex Litho Model)
PHIE-CPS	Effective Porosity (Complex Litho Model)
PHINAVCPS	Product (PHIF * SAVG/Complex Litho Model)
PHIW-CPS	Product (PHIF * SW) (Complex Litho Model)
PHIWX-CPS	Product (PHIF * SXO/Complex Litho Model)(Hydrocarbon Corrected)
VCL -CPS	Volume of clay (Complex Litho Model)
VSND-CPS	Volume of Sand (Complex Litho Model)
VLS -CPS	Volume of Limestone (Complex Litho Model)
VDOL-CPS	Volume of Dolomite (Complex Litho Model)
VANH-CPS	Volume of Anhydrite (Complex Litho Model)
PHINAVCPS	Product (PHIF * SAVG/Complex Litho Model)
PHIW-CPS	Product (PHIF * SW) (Complex Litho Model)
VHW -CPS	Volume of bound water (Complex Litho Model)
SUGR	SNGS Computed Gamma Ray
HTNP	Hilt Thermal
HFK	Hilt Kaliber
HCAL	HRGC Cal. Caliper
RHOB	HRDD High Resolution Formation Density
HTNP	Hilt Thermal Neutron Porosity
DTCO	Delta T Compressional
PEFA	HRDD High Resolution Formation Photoelectric Factor
DRHO	HRDD Density Correction
CPOO	
CKHO	
PHIT-CPS	Total porosity from CPS model after hydrocarbon correction (Complex Litho Model)
RT	True formation resistivity
RXO	Flushed zone resistivity (Invaded Resistivity 1
RXO	Invaded zone resistivity
GDEN	
SET-PAY	

Kair_log
Kpm_log
Kvar_log



ENCLOSURE-2
Petrophysical and Composite Plot
2128-2382mMDRT (1:200)

Origin
Energy

THYLACINE-2

COMPOSITE AND PETROPHYSICAL SUMMARY

Company	Woodside Energy Ltd
Well Name	THYLACINE 2
Field	THYLACINE
Location	VIC/P44(V)
State	VICTORIA
County or Reg name	Ocean Beauty
Field Conv Line 1	EASTING: 595564.5 M
Field Conv Line 2	NORTHING: 5836256.5 M
Latitude	-38° 15' 49.8" S - DMS
Longitude	141° 35' 09.85" E - DMS
Permanent Datum	LAT
Elevation of RT	20.50
Elevation of KB	20.50
Elevation Ground/S	101.20 M
Above Perm Datum	20.50 M
Above Perm Datum	20.50 M
Log Measured from	RT
Drilling Measured	RT
Other Services Ln 1	MSFL/GR
Other Services Ln 2	FBI/GR
Other Services Ln 3	DSI/GR
Other Services Ln 4	UTI/GR
Log Date	6-Sep-2001
Run number	ONE/ONE
Depth datum	4910.2 DMF
Time printed	11:33:05

PETROPHYSICIST: Michael Hill

RUN INFORMATION

Run number	1A
Log date	6-Sep-2001
Depth Driller	2535.00 M
Depth Logger	2535.00 M
Casing Driller	2441.00 M
Casing Logger	2441.00 M
Casing Weight	47.0000 lb/ft
Casing Depth	2441.00 M
Bit Size	311.1 MM
Hole Fluid type	KCL/PHPA/LCM/GEL
Fluid Density	1.1600 gm/cc
Fluid Viscosity	0.0000 s/l
Fluid PH	9.0000
Fluid Loss	3.7000 CC
Source of Rmf and Rmc	MEASURED
Rmf at BHT	0.0000 ohmm
Rmc at BHT	0.0000 ohmm
Source of RMF/RMC	PRESSED
Mud Sample Temp	15.00 degC
Rmf at Measured Temp	0.0000 ohmm
Rmf at Formation Temp	PRESSED
Time circ. stopped	11:15
Logger on bottom	6-Sep-2001
Time logger at Btm	6-Sep-2001
Surface hole temp	20.00 degC
Bottom hole temp	100.00 degC
Surface temperature	15.56 degC
Max. recorded temp	100.00 degC
Equipment No.	
Logging unit Loc	VLA-4(W)
Logging Company ID	Baker
Recorded By	Hamilton / M Tie
Witness	M. Mraz / G. Ward
Program Version	WL2.3/5
Probe Model/Type	HNGS
Frq Angular/Vertical	4000000
General Temp Sched	TEMP
Max Recorded Deviat	2.00 @ 0deg
Total depth	2535.00 M
Temp Comb Rotor/Stator	37.78 degC

FIELD REMARKS

1. First run in hole. Schlumberger depth procedures observed.
2. Borehole corrections applied on logs.
3. Limestone matrix model used in computation of neutron porosity.
4. Bottom hole temperature degC at 0000m on the log.
5. Caliper check in casing reading 40.00 in. ID expected 40.00 in.
6. Well drilled 3m deep to rathole.
7. Caliper check in casing reading 40.00 in. ID expected 40.00 in.
8. Well drilled 3m deep to rathole.
9. Circulation time 3.45 hrs stopped at 1561 on the log bell.

Thank you for using Schlumberger

Mud Properties:
Mud cake = 1.5mm, Chloride conc. = 43 000ppm, Potassium conc. = 29500ppm
Water content = 60.0%, Solids content = 8.4%, Core Solids content = 5.64%
Oil/syn conc. = 3%, Calcium conc. = 340 mg/l

COMPUTATION PARAMETERS

DEPTH INTERVAL	RW PPM	RW OHMM	TEMP C	GR MIN	GR MAX	K CLAY	RHOB CLAY	PHIN CLAY	t CLAY	RHOE	a	m
2110.0 - 2161.5	13000	.101	86.6	17	82	50	2.60	0.53	76	1.11	1.00	2.20
2161.5 - 2237.1	13000	.100	88.7	17	82	50	2.60	0.53	76	1.11	1.00	2.00
2237.1 - 2314.0	13000	.100	90.8	17	82	50	2.60	0.53	76	1.11	1.00	2.00
2314.0 - 2317.1	13000	.100	88.7	17	82	50	2.60	0.53	76	1.11	1.00	2.00
2317.1 - 2337.1	13000	.100	88.7	17	82	50	2.60	0.53	76	1.11	1.00	2.33
2337.1 - 2347.1	13000	.100	88.7	17	82	50	2.60	0.53	76	1.11	1.00	2.00
2347.1 - 2357.1	13000	.102	92.1	17	82	50	2.60	0.53	76	1.11	1.00	2.00
2357.1 - 2367.1	13000	.102	92.1	17	82	50	2.60	0.53	76	1.11	1.00	2.00
2367.1 - 2377.1	13000	.102	92.1	17	82	50	2.60	0.53	76	1.11	1.00	2.00
2377.1 - 2387.1	13000	.102	92.1	17	82	50	2.60	0.53	76	1.11	1.00	2.00
2387.1 - 2400.0	13000	.101	96.3	17	82	50	2.60	0.53	76	1.11	1.00	2.00
2400.0 - 2447.1	13000	.101	96.3	17	82	50	2.60	0.53	76	1.11	1.00	2.00
2447.1 - 2490.0	13000	.101	96.3	17	82	50	2.60	0.53	76	1.11	1.00	2.00
2490.0 - 2535.0	13000	.101	96.3	17	82	50	2.60	0.53	76	1.11	1.00	2.33

LITHOLOGIES

Clay
Sandstone
Bound Water
OIL
GAS
MOVED OIL
MOVED GAS
Sandstone
Limestone
Dolomite

LOG DESCRIPTION

BDHA CPE	Apparent Mean Density (Complex Lobo Model)
SW_CPL	Saturation Porosity Indicator = PHIT-PHIE = f (Complex Lobo Model)
SW_CPL	Formation Water Saturation = f (Complex Lobo Model)
PHIA CPE	Porosity (PHIE * (1-Vcl)) (Archie)
PHIAQ CPE	Product (PHIE * (1-Vcl) (Complex Lobo Model)
PHIW CPE	Product (PHIE * (1-Vcl) (Complex Lobo Model)
VCL_CPL	Volume of Clay (Complex Lobo Model) - Same as Schlumb (Expanded Cad)
VCL_CPL	Volume of Clay (Complex Lobo Model)
VDOA CPE	Volume of Sand (Complex Lobo Model)
VDOA CPE	Volume of Dolomite (Complex Lobo Model)
VMA CPE	Volume of Matrix (Complex Lobo Model)
PHE CPE	Effective Porosity (Complex Lobo Model)
PHIT CPE	Total Porosity (Complex Lobo Model)
PHIW CPE	Product (PHIE * (1-Vcl) (Complex Lobo Model)
VBW CPE	Volume of bound water (Complex Lobo Model)
VDW	Volume of Dolomite and Gamma Ray
MDC	SP Shaled
IK	Bit Size
HCAL	Hole Size - Caliper
RHOB	HRDD/High Resolution Formation Density
DTMP	Hilbe Thermal Neutron Porosity
DTCO	Delta-T Compressional
PEFZ	HRDD/High Resolution Formation Photoelectric Factor
HDRA	HRDD Density Correction
CALI	
CGRD	
PHIT CPA	Total porosity from CPL model after hydrocarbon correction (Complex Lobo Model)
RT	Deep Resistivity
RLA5	HRLA Resistivity Corrected Borehole 5
RXO	Invaded zone resistivity
SP	
VCLAVG	

Xaxis_Tag
Xaxis_Tag
X-axis_Tag

APPENDIX 2
MDT REPORT

Thylacine 2 MDT Report

Origin Energy Resources Ltd

September 2003

Thylacine 2 MDT Report

Contents

1 Summary 3
2 Background 3
3 Pre-Test Interpretation 4
3.1 Pressure Data 4
3.2 Temperature 4
3.3 Pre Test Derived Fluid Gradients and Contacts 4
3.4 Pre Test Derived Mobility 5
3.5 Regional Pressure Comparison 5
4 Sampling 5
4.1 Summary 5
4.2 Sample Derived Fluid Gradients and Fluid Contacts 6
5 Integration with Thylacine 1 Pressure Data 6

List of Figures

1. Thylacine 2 Hydrostatic Pressure Before and After Pre-test
2. Thylacine 2 Pressure Data Schematic
3. Thylacine 2 MDT Temperature Data
4. Thylacine 2 Raw Formation Pressure Data
5. Thylacine 2 Formation Pressure Data, Fluid Gradient and Free Water Level
6. Thylacine 2 Drawdown Mobility
7. Thylacine 2 Pressure and Regional Pressure
8. Thylacine 2 Pressure and Sample Derived Gas Gradients
9. Thylacine Field Pressure
10. Thylacine Field Aquifer Pressure

List of Tables

1. Thylacine 2 : Compositional Data

1 Summary

The Thylacine 2 MDT survey showed the presence additional complexity in the Thylacine field, compared to the simple system interpreted for Thylacine 1.

At least 4 individual hydraulic systems were encountered with significant pressure offsets between the Thylacine Member and individual Flaxman sands evident.

The Flaxman sands encountered in Thylacine 2 do not appear to be connected to the equivalent Flaxman sequence at Thylacine 1 and have significantly deeper interpreted Free Water Levels.

The Thylacine Member Unit 1 (Upper Sand) at Thylacine 2 is a separate system to both the Flaxman sands in Thylacine 2 and the equivalent Thylacine Member sequence at Thylacine 1.

Insufficient valid pressure data was obtained from the Thylacine Member Unit 2 (Lower Sands) to make any conclusions about this reservoir at Thylacine 2.

The gas composition measured from Thylacine 2 samples contains a slightly lower CO_2 content (8 - 9 %) than samples from Thylacine 1. Average liquids content is similar to Thylacine 1 although a large variation in LPG content (10 – 20 bbl/MMscf) was observed between the two Thylacine 2 samples.

2 Background

The Thylacine 2 well was drilled in permit T/30P in the Otway Basin, offshore Victoria to appraise the earlier Thylacine 1 discovery. Thylacine 2 was located approximate 4 km WNW of the discovery well. The well intersected a similar gas column in the Santonian Thylacine Member (Belfast Formation) and Turonian Flaxman Formation to that encountered in the discovery well. An extensive MDT survey was conducted to further evaluate the Thylacine gas discovery.

The objectives of the survey included:

1. The establishment of reservoir fluid gradients and fluid contacts to identify pressure discontinuities between Thylacine 2 and Thylacine 1.
2. Recovery of representative formation fluid samples for compositional and PVT analysis

The survey was conducted on September 9 – 10, 2001 and included 80 pre-test attempts and the collection of four samples at two sample depths.

3 Pre-Test Interpretation

3.1 Pressure Data

Formation pressures were measured with a quartz gauge and strain gauge. The quartz gauge functioned correctly throughout the survey, and showed excellent stability and repeatability in the measurement of hydrostatic pressures before and after each pre-test (Figure 1). Consequently, pressures from the quartz gauge were used for all interpretation due to their inherently greater accuracy and resolution.

The complete pressure dataset can be found in the Basic Data volume. A filtered and sorted dataset used for the analysis presented in this document can be found in Figure 2

3.2 Temperature

Figure 3 shows the temperatures measured in the Thylacine 1 and 2 wells versus depth.

3.3 Pre Test Derived Fluid Gradients and Contacts

Figure 4 shows the raw pre-test derived formation pressures measured in the Thylacine 2 well versus depth. Initial inspection of this plot shows a significantly more complicated pressure regime than that observed on the nearby Thylacine 1 well with multiple hydraulic systems evident.

The approach taken in interpreting this data has been to group pre-test pressures by individual sands and fit a known gas gradient through sands that appear to fall on a common hydraulic system. The gas gradient initially used for this analysis was nominally 0.247 psi/m, which is the Thylacine 1 gradient measured from pre-test pressures. Results of this analysis can be found in Figures 5a and 5b. At least 4 and probably five different pressure systems are apparent as summarised below:

- Thylacine Member Unit 1 (Upper) Sands
- Upper Flaxman sand at 2239 m MD
- Mid Flaxman sand package from 2251m MD to 2260 m MD
- Lower Flaxman sand package below 2275 m MD

The Thylacine Member Unit 2 (Lower) sands also probably form a fifth pressure system however a large amount of scatter is evident from pre-test pressures over this interval. It is tempting to conclude that this reservoir forms a common system with the equivalent reservoir intersected at Thylacine 1 as shown on Figure 5b where the Thylacine 1 gas gradient passes through the cloud of Thylacine 2 Unit 2 pre-test pressures. However, when the Thylacine 2 Unit 2 pre-tests are examined in detail it does not appear that any reservoir pressures can be determined over this interval with any confidence. All the pre-tests over this interval are referred to as either being affected by

supercharging, or being unstable and aborted due to lack of sufficient permeability.

Free Water Levels corresponding to each pressure system are summarised below. It should be noted that these assume a common aquifer pressure throughout which may not be the case. No aquifer pressures have been obtained for the Flaxman although the Thylacine 1 result previously suggested a simple, common system. The complexity encountered at Thylacine 2 questions this assumption:

- Thylacine Member Unit 1 FWL : 2260 mSS
- Upper Flaxman FWL : 2325 mSS
- Mid Flaxman FWL : 2339 mSS
- Lower Flaxman FWL : 2346 mSS

3.4 Pre Test Derived Mobility

Figure 6 shows the pre-test derived formation mobility as measured in the Thylacine 2 well versus depth. The contrast between the high quality Flaxman reservoir and overlying Thylacine Member is evident.

3.5 Regional Pressure Comparison

Figure 7 shows the Thylacine 2 formation pressure plotted against the pressures reported in the nearby wells Thylacine 1, Geographe 1, Minerva-1, Minerva-2, Eric The Red-1 and La Bella-1. Significant pressure discontinuities in the aquifer are evident with Thylacine 1 and 2 aquifer pressures approximately 50 psi greater than the pressure observed at Minerva and Geographe and 100 psi under pressured relative to La Bella.

4 Sampling

4.1 Summary

Four reservoir gas samples were collected with the MDT. Two samples were obtained at each of the following depths:

Thylacine Member:	2144.0 m MD (2118.8 m SS)
	Chamber No's SN-157, SN-186
Flaxman Fm:	2296.8 m MD (2271.6 m SS)
	Chamber No's SN-187, SN-193

These samples were retained for later compositional and PVT analysis.

Full results of analysis of these samples can be found in the relevant report and a summary of the compositional analysis can be found in Table 1.

The Thylacine 2 gas composition is slightly different to that measured at Thylacine 1. The CO_2 content (8 - 9%) is slightly lower while nitrogen content is similar (approximately 1.5%) to give a total inerts content around 10%. The LPG

content measured at Thylacine 2 varies significantly between the Thylacine Member and Flaxman Formation samples (1.5 - 3%). In terms of bbl/MMscf this gives a range from 10 – 20 bbl/MMscf.

The condensate content ($C5_+$ basis) is in the range 0.9 – 1.2% or 11–14 bbl/MMscf.

4.2 Sample Derived Fluid Gradients and Fluid Contacts

Using the results of the compositional analysis, an estimate of reservoir fluid density and reservoir conditions has been made for the two samples taken over the Thylacine 2 gas column. Results of this analysis are summarised below:

Thylacine Member Unit 1:	2144.0 m MD (2118.8 mSS) Chamber No SN-157 0.237 psi/m
Lower Flaxman:	2296.8 m MD (2271.6 mSS) Chamber No SN-187 0.221 psi/m

In the absence of samples, the Lower Flaxman sample derived gradient has been used throughout the Flaxman Formation to give a revised estimate of Free Water Levels for each system as shown in Figure 8. These are slightly different to those quote in Section 3.2 and are summarised below:

- Thylacine Member Unit 1 FWL : 2261 mSS
- Upper Flaxman FWL : 2323 mSS
- Mid Flaxman FWL : 2338 mSS
- Lower Flaxman FWL : 2345 mSS

5 Integration with Thylacine 1 Pressure Data

Figure 9 incorporates Thylacine 1 and Thylacine 2 formations pressures and sample derived gas gradients to summarise the multiple hydraulic systems and contacts determined from the MDT surveys in both wells.

Aquifer pressures in the two wells has also been integrated to define the common aquifer gradient of 1.384 psi/m as shown in Figure 10.

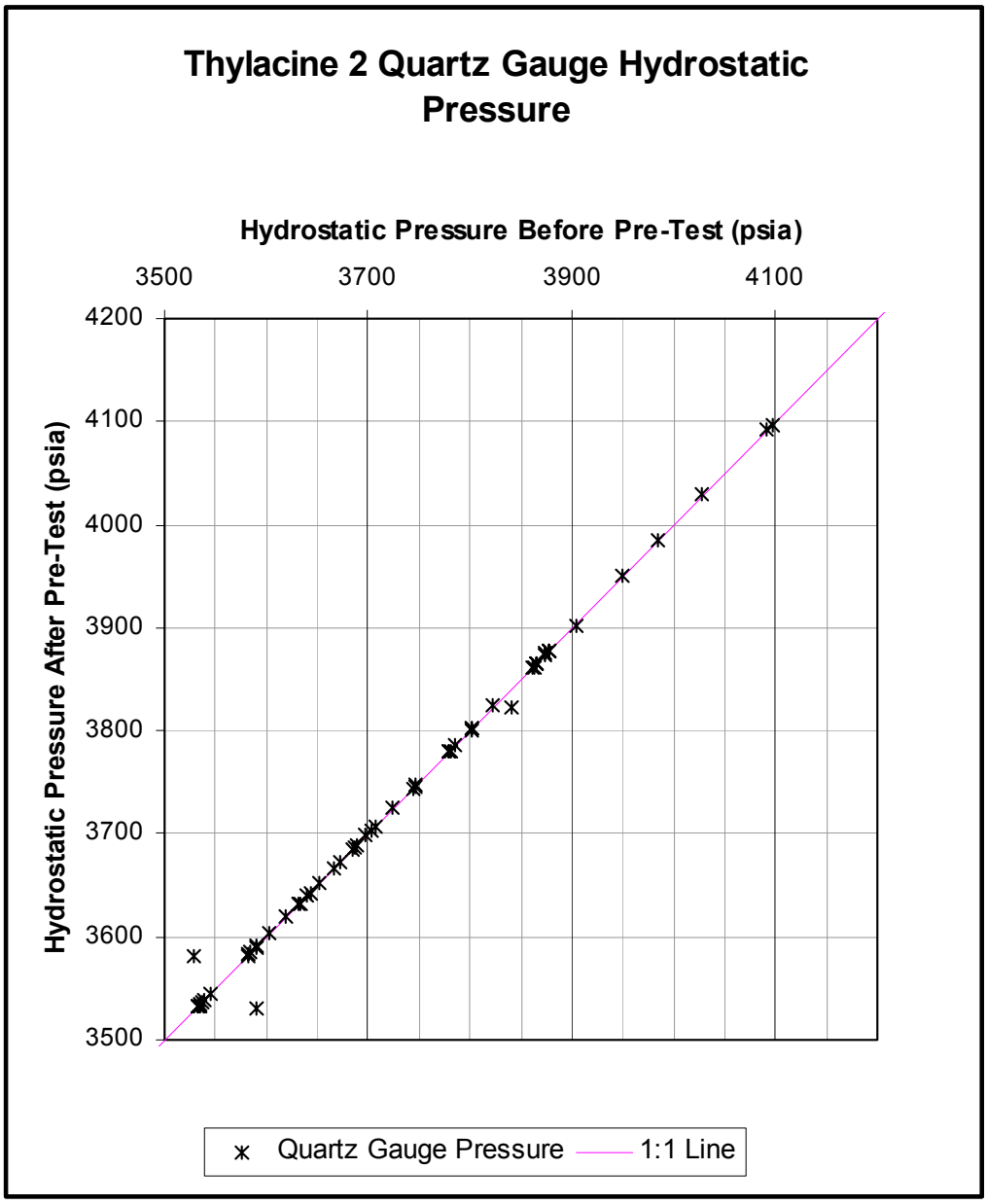

Thylacine 2 Quartz Gauge Hydrostatic Pressure
Hydrostatic Pressure Before Pre-Test (psia)
3500
3700
3900
4100
Hydrostatic Pressure After Pre-Test (psia)
4200
4100
4000
3900
3800
3700
3600
3500
Quartz Gauge Pressure
1:1 Line

Figure 1

Thylacine-2

KB Elevation **25.0** m ASL

Depth mKB	Depth mSS	Pressure psia	Mobility mD/cP				Comment
2143.8	2118.77	3265.70	2.10		THYLACINE MBR	Unit 1	
2143.8	2118.77	3264.42	53.10				*good 53 md/cP
2143.8	2118.80	3265.88	9.50				
2143.8	2118.80	3264.53					
2144.9	2119.87	3266.45	8.30				
2145.8	2120.77	3267.26	5.20				
2145.8	2120.77	3267.65	2.10				
2148.1	2123.07	3271.15	0.80				
2148.2	2123.17	3269.40	2.20				
2151.8	2126.77	3280.96					*supercharged
2176.4	2151.36	3295.52	1.00			Unit 2	*unstable ?
2180.2	2155.16	3314.20	0.80				*unstable
2180.3	2155.26	3316.39	0.80				*unstable
2180.3	2155.27	3317.30	0.80				*poor stablisation
2198.2	2173.17	3317.92	0.60				*slow to stabilise
2205.4	2180.36	3309.69	3.00				*poss unstable
2205.4	2180.40	3302.93	3.30				*tight
2206.3	2181.27	3321.38	2.40				*possibly tight ??, slow stabilisation
2206.3	2181.30	3304.30	1.70				*tight
2211.1	2186.07	3327.01	1.60				*possibly tight ??, slow stabilisation
2212.8	2187.75	3334.80	0.60				*unstable
2219.2	2194.20	3318.33	2.60				*tight
2227.2	2202.20	3322.29	1.30				*tight test
2231.8	2206.80	3295.71	2.10			2232m Sand	*tight test
2238.5	2213.50	3359.83	17.60		FLAXMAN FM	2239m Sand	
2251.2	2226.20	3381.07	1.80			2251m Sand	
2259.9	2234.90	3381.42	6.40			2260m Sand	
2275.6	2250.60	3393.12	13.10			2275m Sand	
2277.0	2252.00	3394.46	27.90				
2286.1	2261.10	3395.44	10.60			2286m Sand	
2296.5	2271.54	3398.09	258.50			2300m Sand	
2296.6	2271.60	3398.78	1.20				
2296.6	2271.60	3398.49	788.80				
2297.2	2272.24	3398.17	442.00				
2298.3	2273.34	3398.26	65.90				
2299.3	2274.30	3399.03	2428.90				
2301.4	2276.44	3398.99	44.60				
2324.1	2299.14	3403.52	74.00			2324m Sand	
2334.1	2309.14	3407.64	4.40			2334m Sand	
2348.2	2323.24	3385.56	13.30		UPPER WAARRE FM		
2348.2	2323.24	3385.45					
2348.3	2323.30	3385.61	11.60				
2350.3	2325.30	3393.14	19.50				
2350.5	2325.49	3394.07	6.10				
2350.5	2325.49	3393.90	3.00				
2355.0	2330.00	3394.17	405.50				
2355.8	2330.80	3395.33	77.70				
2357.8	2332.80	3399.00	3.50				
2373.9	2348.90	3420.42	215.50				
2402.7	2377.70	3460.46	194.40				
2423.5	2398.50	3488.61	179.40				
2450.7	2425.70	3525.80	183.50				
2489.1	2464.10	3578.91	69.00				
2492.9	2467.90	3584.05	142.80				

Figure 2

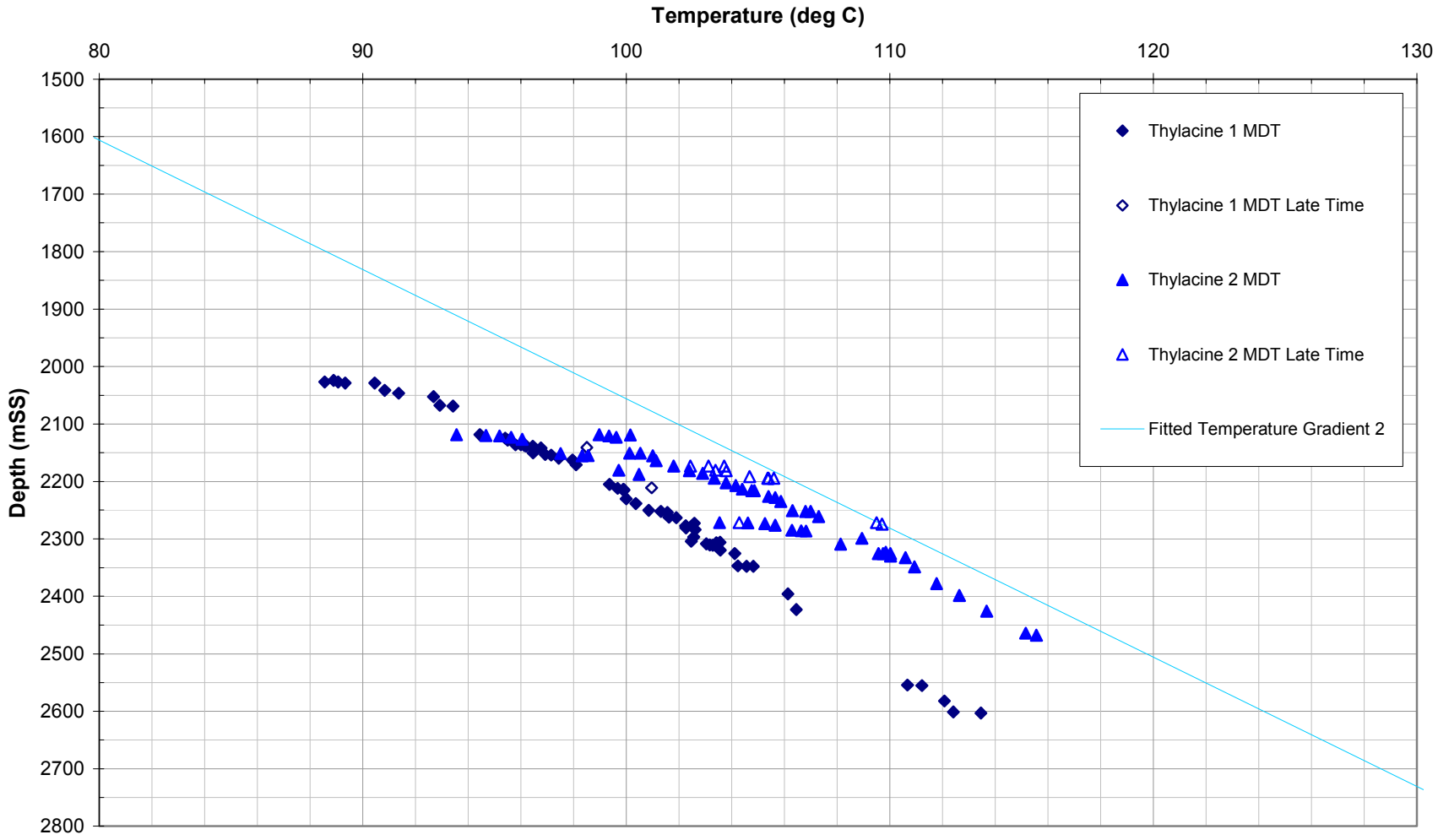

Offshore Otway Temperature Data : Thylacine 1 and Thylacine 2
Temperature (deg C)
80
90
100
110
120
130
Depth (mSS)
1500
1600
1700
1800
1900
2000
2100
2200
2300
2400
2500
2600
2700
2800
Thylacine 1 MDT
Thylacine 1 MDT Late Time
Thylacine 2 MDT
Thylacine 2 MDT Late Time
Fitted Temperature Gradient 2

Figure 3

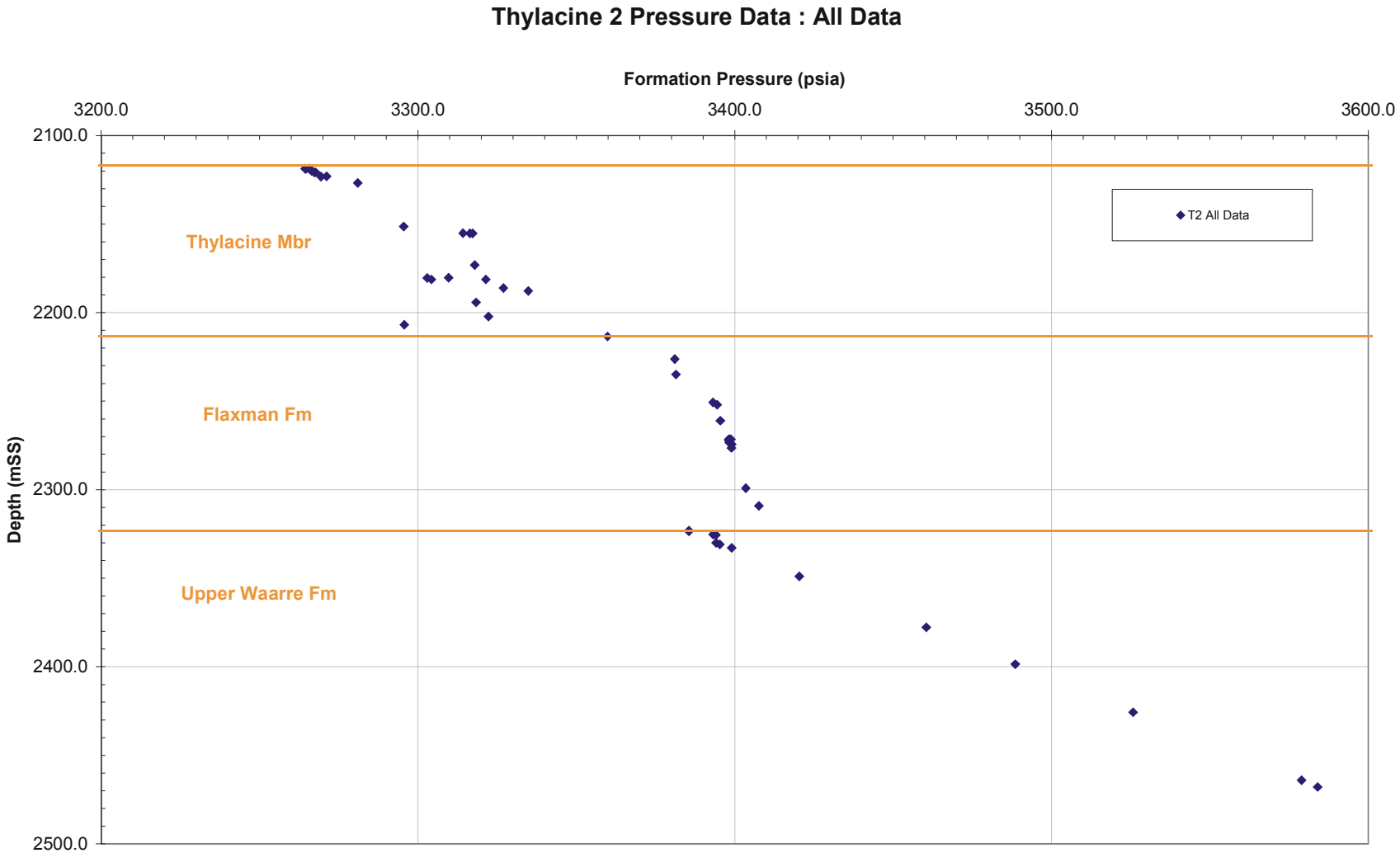

Thylacine 2 Pressure Data : All Data
Formation Pressure (psia)
3200.0
3300.0
3400.0
3500.0
3600.0
2100.0
2200.0
2300.0
2400.0
2500.0
Depth (mSS)
Thylacine Mbr
Flaxman Fm
Upper Waarre Fm
T2 All Data

Figure 4

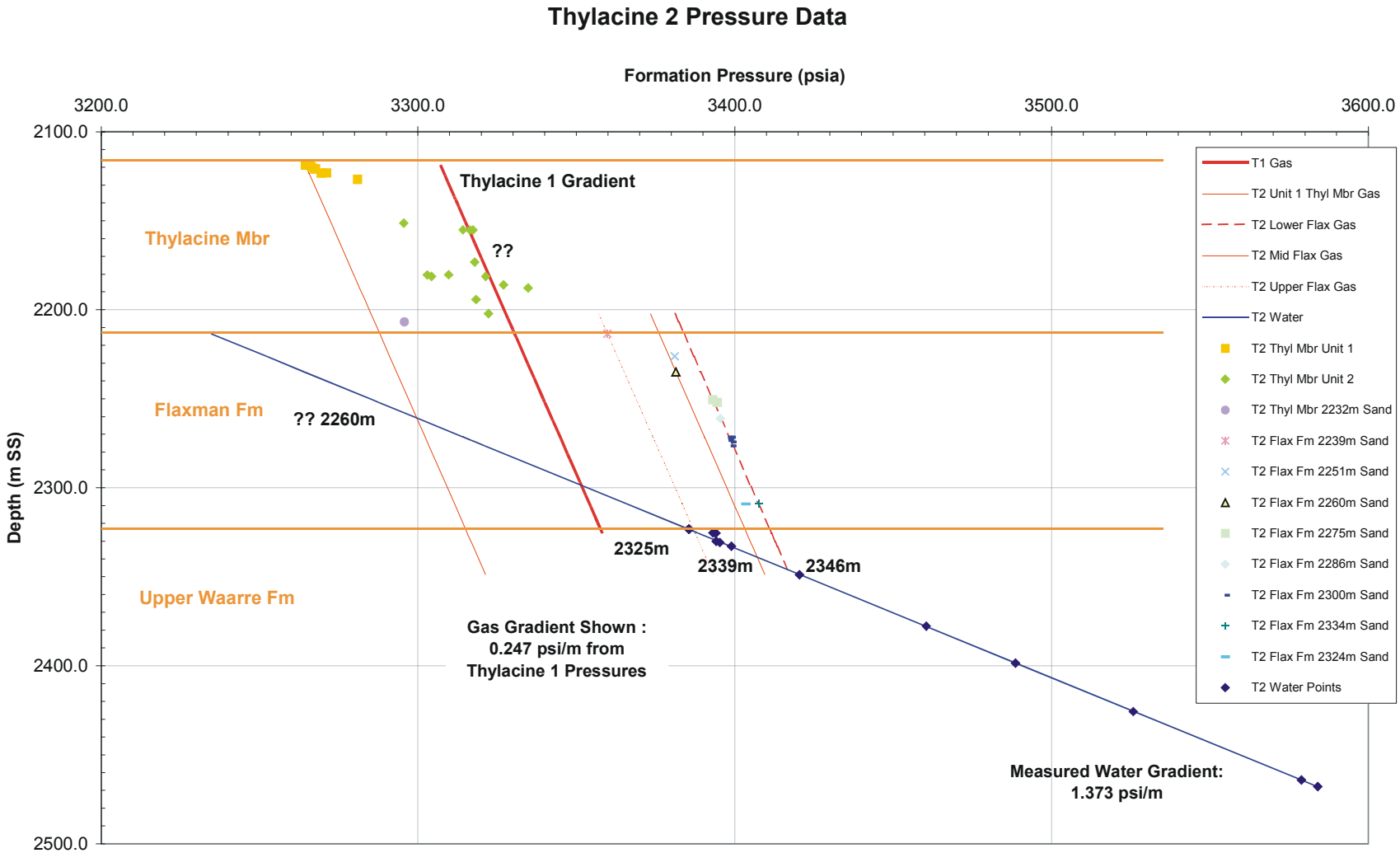

Thylacine 2 Pressure Data
Formation Pressure (psia)
3200.0
3300.0
3400.0
3500.0
3600.0
2100.0
2200.0
2300.0
2400.0
2500.0
Depth (m SS)
Thylacine Mbr
Flaxman Fm
Upper Waarre Fm
Thylacine 1 Gradient
??
?? 2260m
2325m
2339m
2346m
Gas Gradient Shown :
0.247 psi/m from
Thylacine 1 Pressures
Measured Water Gradient:
1.373 psi/m
T1 Gas
T2 Unit 1 Thyl Mbr Gas
T2 Lower Flax Gas
T2 Mid Flax Gas
T2 Upper Flax Gas
T2 Water
T2 Thyl Mbr Unit 1
T2 Thyl Mbr Unit 2
T2 Thyl Mbr 2232m Sand
T2 Flax Fm 2239m Sand
T2 Flax Fm 2251m Sand
T2 Flax Fm 2260m Sand
T2 Flax Fm 2275m Sand
T2 Flax Fm 2286m Sand
T2 Flax Fm 2300m Sand
T2 Flax Fm 2334m Sand
T2 Flax Fm 2324m Sand
T2 Water Points

Figure 5a

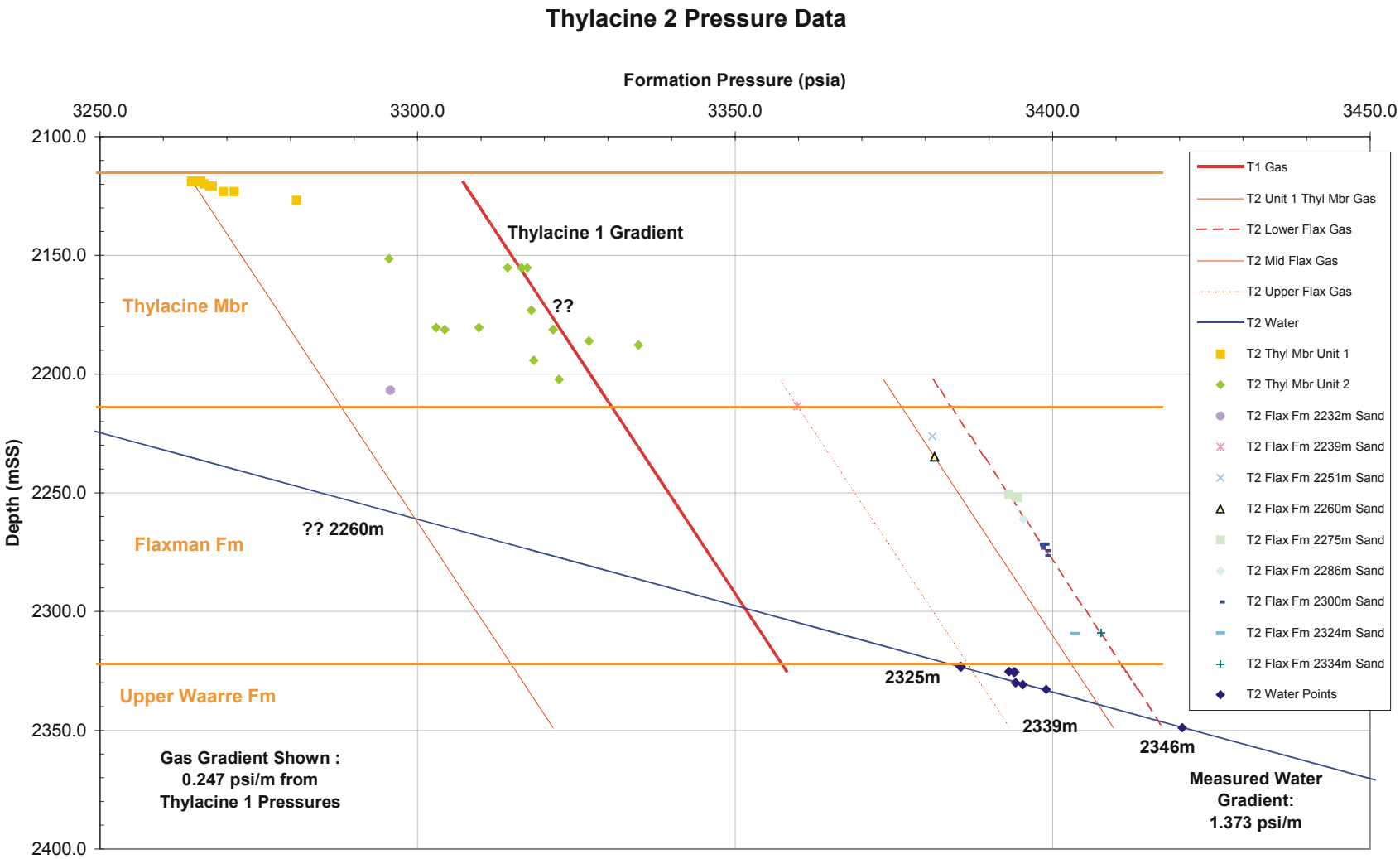

Thylacine 2 Pressure Data
Formation Pressure (psia)
3250.0
3300.0
3350.0
3400.0
3450.0
2100.0
2150.0
2200.0
2250.0
2300.0
2350.0
2400.0
Depth (mSS)
Thylacine Mbr
Flaxman Fm
Upper Waarre Fm
Thylacine 1 Gradient
??
?? 2260m
2325m
2339m
2346m
Gas Gradient Shown :
0.247 psi/m from
Thylacine 1 Pressures
Measured Water
Gradient:
1.373 psi/m
T1 Gas
T2 Unit 1 Thyl Mbr Gas
T2 Lower Flax Gas
T2 Mid Flax Gas
T2 Upper Flax Gas
T2 Water
T2 Thyl Mbr Unit 1
T2 Thyl Mbr Unit 2
T2 Flax Fm 2232m Sand
T2 Flax Fm 2239m Sand
T2 Flax Fm 2251m Sand
T2 Flax Fm 2260m Sand
T2 Flax Fm 2275m Sand
T2 Flax Fm 2286m Sand
T2 Flax Fm 2300m Sand
T2 Flax Fm 2324m Sand
T2 Flax Fm 2334m Sand
T2 Water Points

Figure 5b

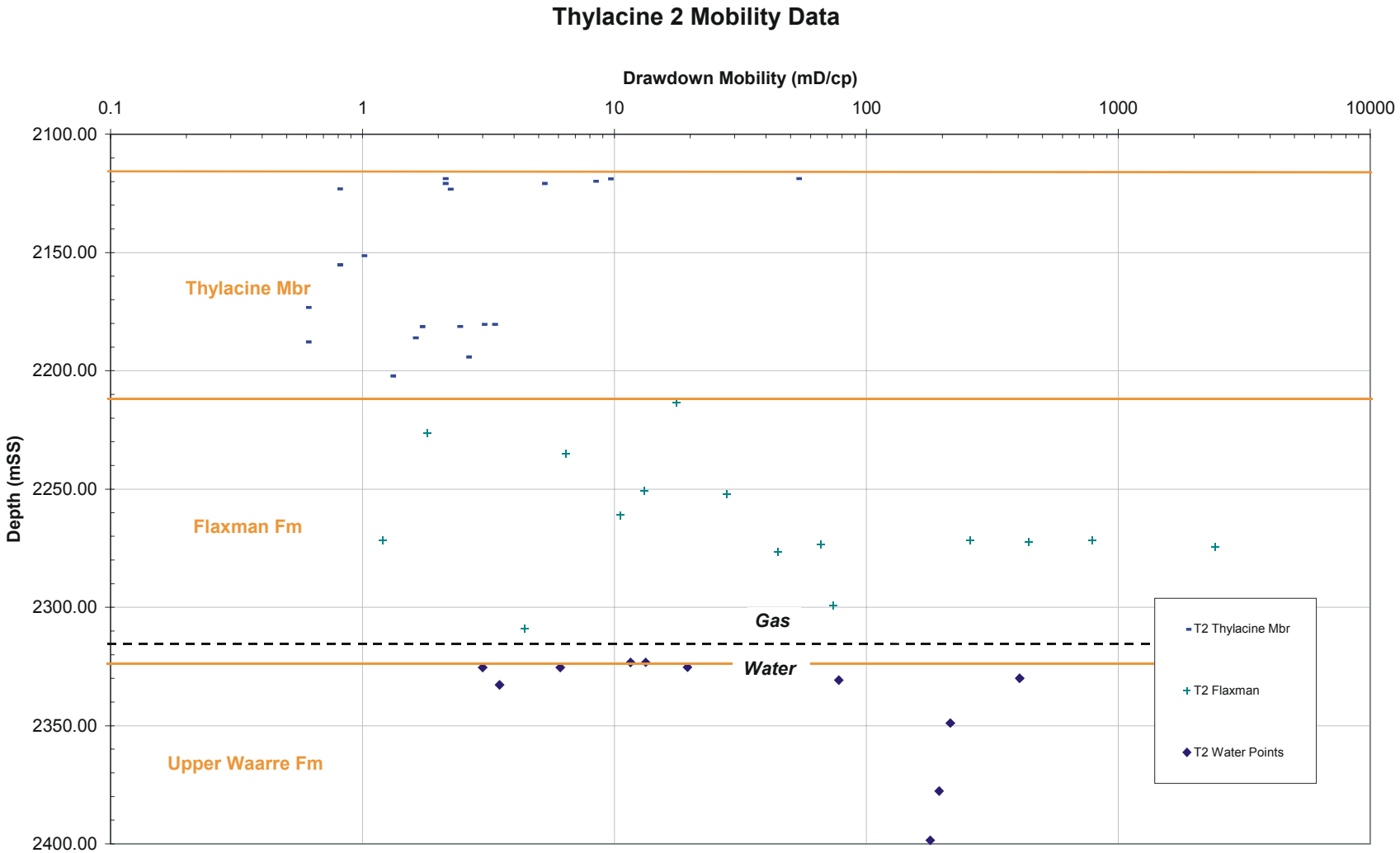

Thylacine 2 Mobility Data
Drawdown Mobility (mD/cp)
0.1
1
10
100
1000
10000
2100.00
2150.00
2200.00
2250.00
2300.00
2350.00
2400.00
Depth (mSS)
Thylacine Mbr
Flaxman Fm
Upper Waarre Fm
Gas
Water
T2 Thylacine Mbr
T2 Flaxman
T2 Water Points

Figure 6

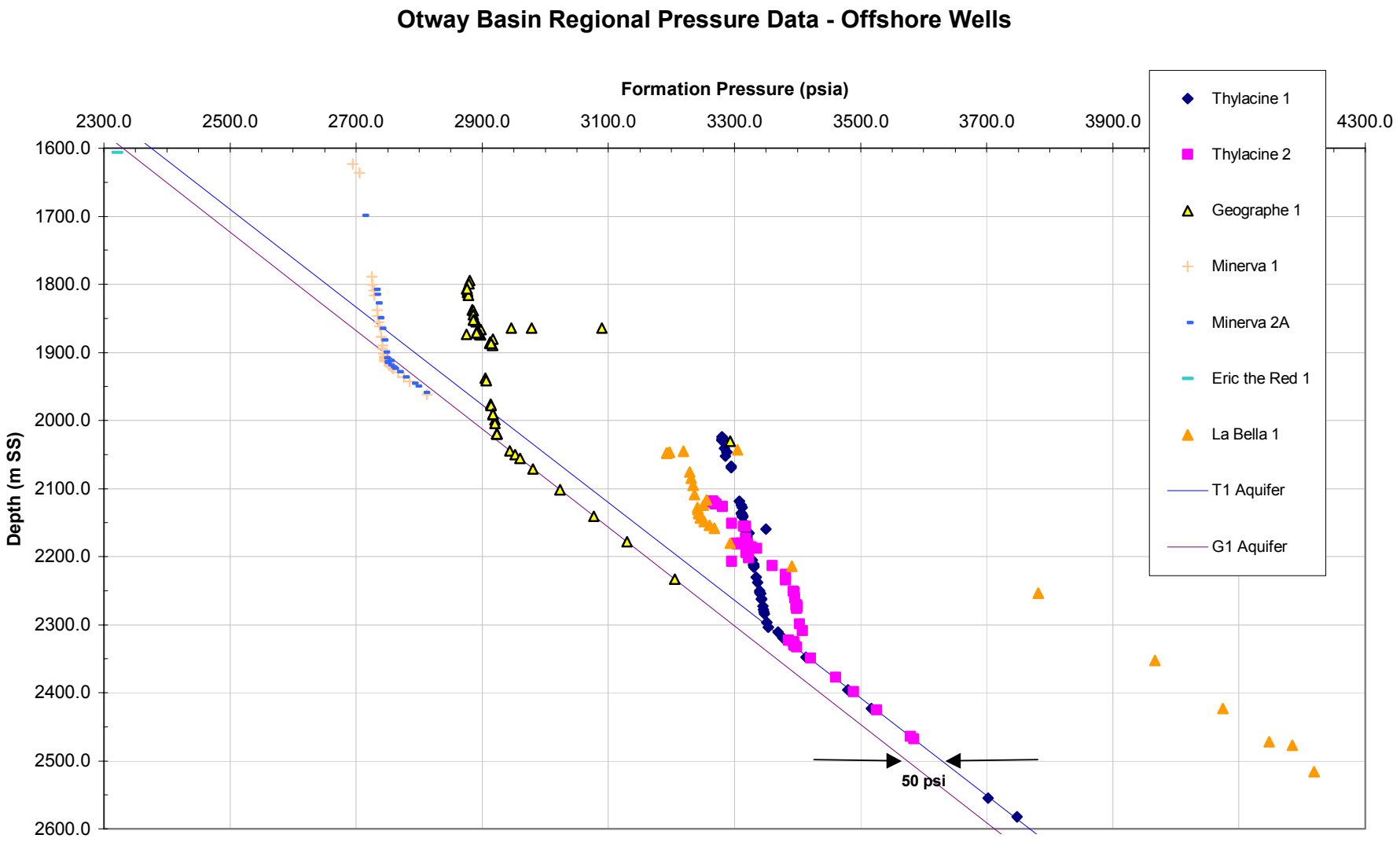

Otway Basin Regional Pressure Data - Offshore Wells
Formation Pressure (psia)
2300.0
2500.0
2700.0
2900.0
3100.0
3300.0
3500.0
3700.0
3900.0
4300.0
Depth (m SS)
1600.0
1700.0
1800.0
1900.0
2000.0
2100.0
2200.0
2300.0
2400.0
2500.0
2600.0
Thylacine 1
Thylacine 2
Geographe 1
Minerva 1
Minerva 2A
Eric the Red 1
La Bella 1
T1 Aquifer
G1 Aquifer
50 psi

Figure 7

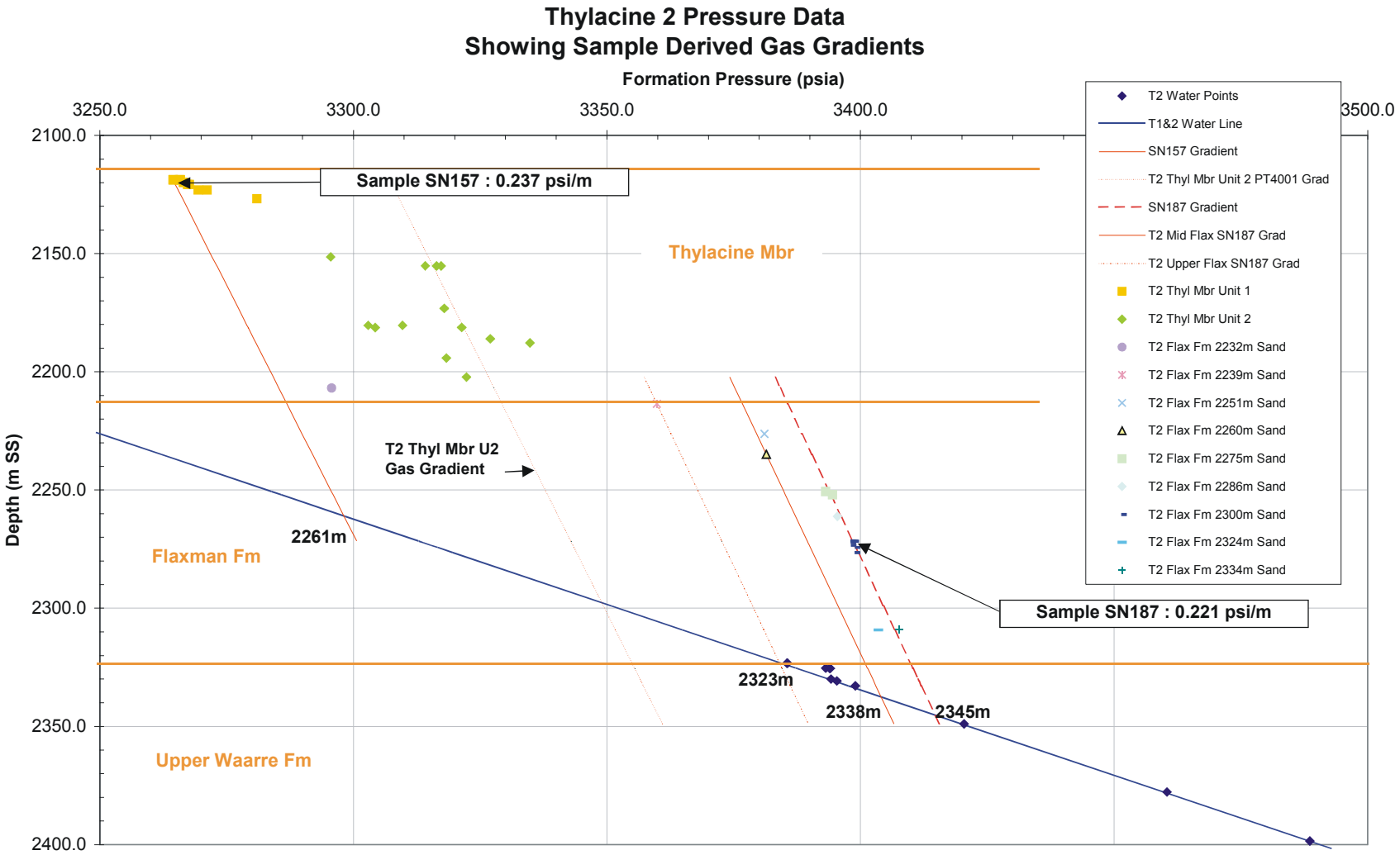

Thylacine 2 Pressure Data
Showing Sample Derived Gas Gradients
Formation Pressure (psia)
3250.0
3300.0
3350.0
3400.0
3500.0
Depth (m SS)
2100.0
2150.0
2200.0
2250.0
2300.0
2350.0
2400.0
Sample SN157 : 0.237 psi/m
Thylacine Mbr
T2 Thyl Mbr U2
Gas Gradient
2261m
Flaxman Fm
Sample SN187 : 0.221 psi/m
2323m
2338m
2345m
Upper Waarre Fm
T2 Water Points
T1&2 Water Line
SN157 Gradient
T2 Thyl Mbr Unit 2 PT4001 Grad
SN187 Gradient
T2 Mid Flax SN187 Grad
T2 Upper Flax SN187 Grad
T2 Thyl Mbr Unit 1
T2 Thyl Mbr Unit 2
T2 Flax Fm 2232m Sand
T2 Flax Fm 2239m Sand
T2 Flax Fm 2251m Sand
T2 Flax Fm 2260m Sand
T2 Flax Fm 2275m Sand
T2 Flax Fm 2286m Sand
T2 Flax Fm 2300m Sand
T2 Flax Fm 2324m Sand
T2 Flax Fm 2334m Sand

Figure 8

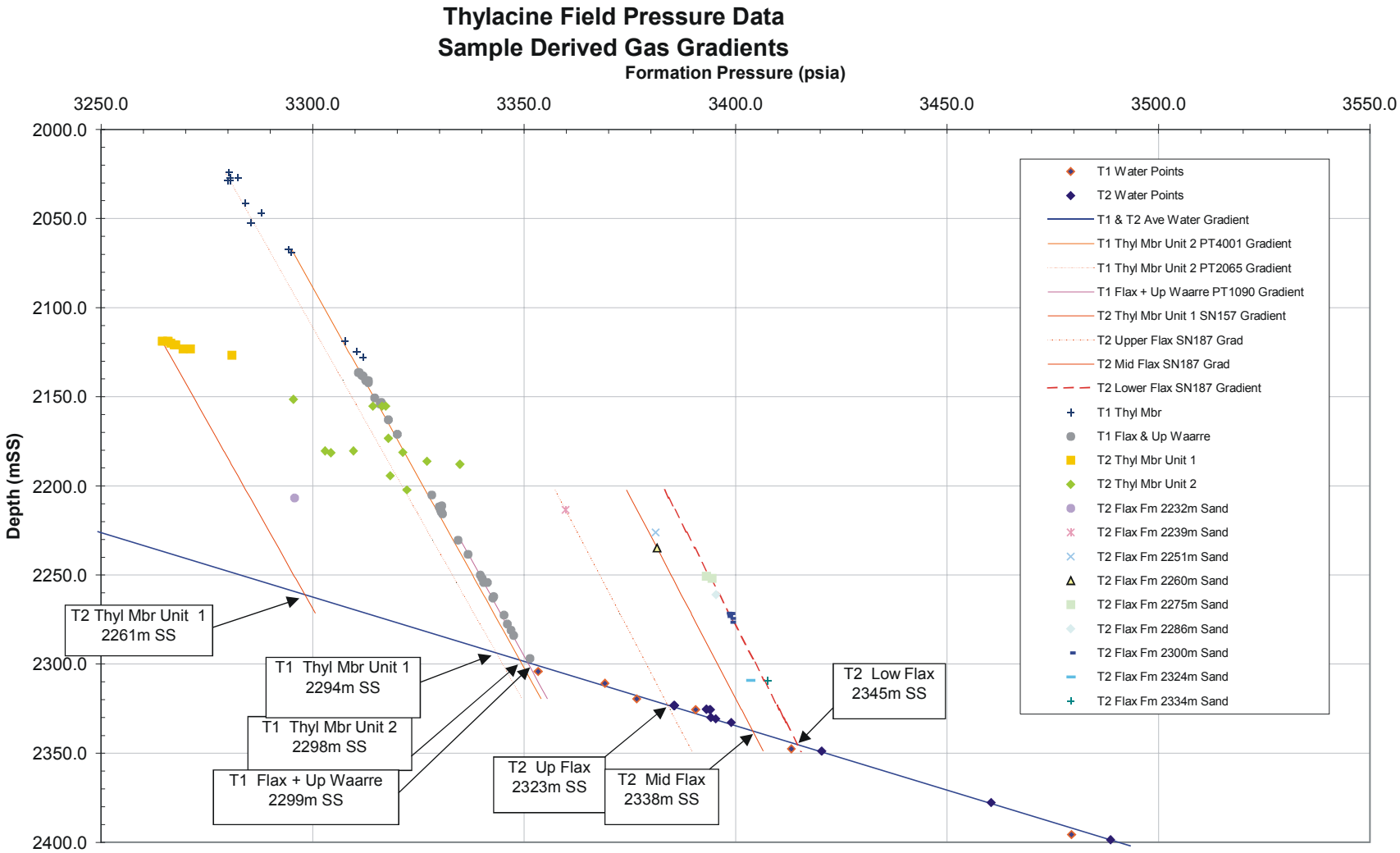

Thylacine Field Pressure Data
Sample Derived Gas Gradients
Formation Pressure (psia)
3250.0
3300.0
3350.0
3400.0
3450.0
3500.0
3550.0
Depth (mSS)
2000.0
2050.0
2100.0
2150.0
2200.0
2250.0
2300.0
2350.0
2400.0
T1 Water Points
T2 Water Points
T1 & T2 Ave Water Gradient
T1 Thyl Mbr Unit 2 PT4001 Gradient
T1 Thyl Mbr Unit 2 PT2065 Gradient
T1 Flax + Up Waarre PT1090 Gradient
T2 Thyl Mbr Unit 1 SN157 Gradient
T2 Upper Flax SN187 Grad
T2 Mid Flax SN187 Grad
T2 Lower Flax SN187 Gradient
T1 Thyl Mbr
T1 Flax & Up Waarre
T2 Thyl Mbr Unit 1
T2 Thyl Mbr Unit 2
T2 Flax Fm 2232m Sand
T2 Flax Fm 2239m Sand
T2 Flax Fm 2251m Sand
T2 Flax Fm 2260m Sand
T2 Flax Fm 2275m Sand
T2 Flax Fm 2286m Sand
T2 Flax Fm 2300m Sand
T2 Flax Fm 2324m Sand
T2 Flax Fm 2334m Sand
T2 Thyl Mbr Unit 1
2261m SS
T1 Thyl Mbr Unit 1
2294m SS
T1 Thyl Mbr Unit 2
2298m SS
T1 Flax + Up Waarre
2299m SS
T2 Up Flax
2323m SS
T2 Mid Flax
2338m SS
T2 Low Flax
2345m SS

Figure 9

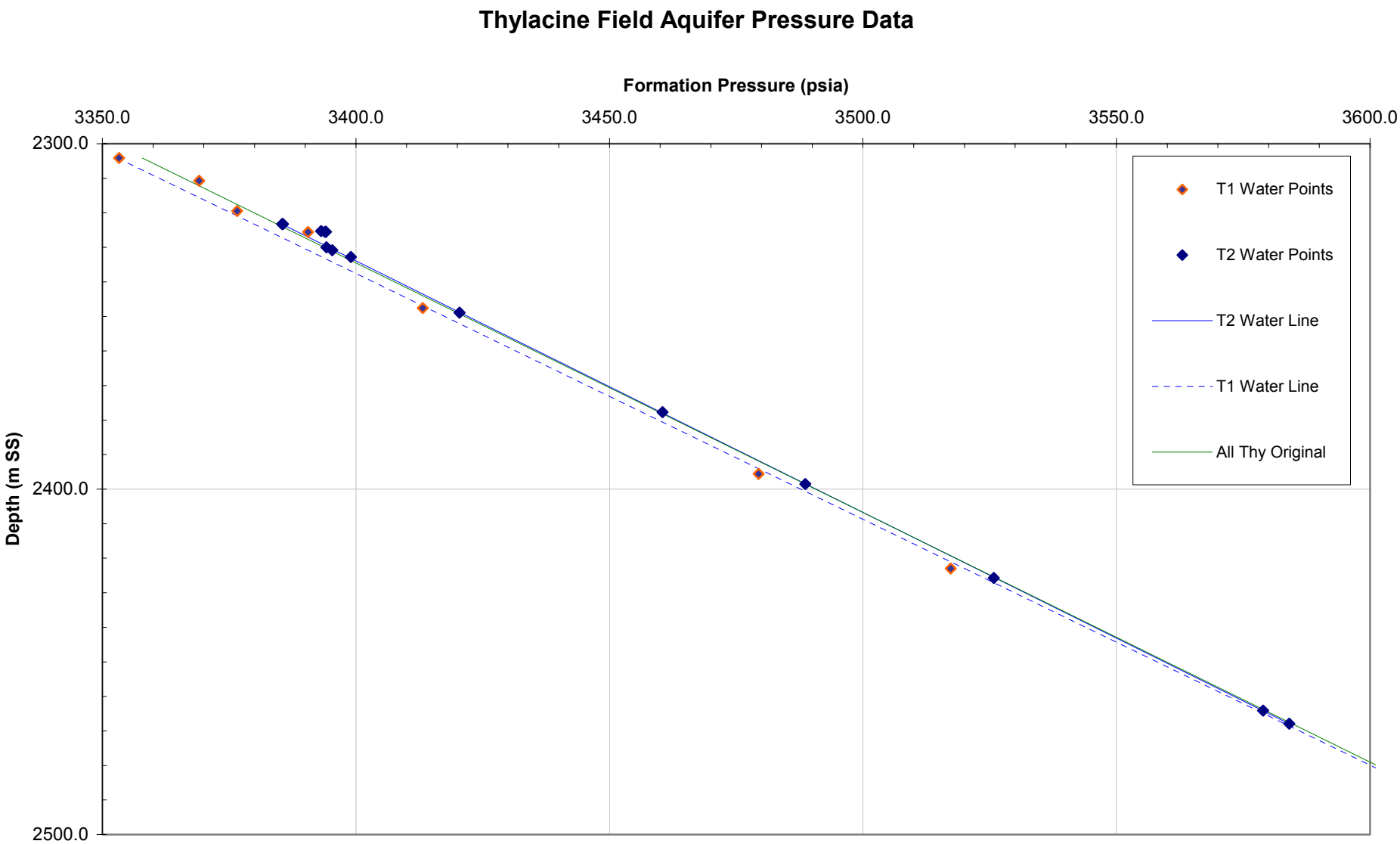

Thylacine Field Aquifer Pressure Data
Formation Pressure (psia)
3350.0
3400.0
3450.0
3500.0
3550.0
3600.0
2300.0
2400.0
2500.0
Depth (m SS)
T1 Water Points
T2 Water Points
T2 Water Line
T1 Water Line
All Thy Original

Figure 10

Table 1: Compositional Data

Well	Formation	Depth	Sample ID	N2	CO2	C1	C2	C3	iC4	nC4	iC5	nC5	nC6	C7	C8	C9	C10	C11	C12+	Inerts	LPG's	C5+	C8+
		mMDKB		mol%	mol%	mol%	mol%	mol%	mol%	mol%	mol%	mol%	mol%	mol%	mol%	mol%	mol%	mol%	mol%	mol%	mol%	mol%	mol%
Thylacine-2	Thylacine Mbr	2144.0	SN157	1.39	8.22	80.60	5.56	2.09	0.41	0.51	0.21	0.15	0.19	0.26	0.22	0.06	0.03	0.02	0.08	9.61	3.01	1.22	0.41
Thylacine-2	Thylacine Mbr	2144.0	SN186	1.38	8.21	80.47	5.63	2.17	0.42	0.51	0.21	0.15	0.19	0.25	0.21	0.06	0.04	0.02	0.08	9.59	3.10	1.21	0.41
			Mean	**1.39**	**8.22**	**80.54**	**5.60**	**2.13**	**0.42**	**0.51**	**0.21**	**0.15**	**0.19**	**0.26**	**0.22**	**0.06**	**0.04**	**0.02**	**0.08**	**9.60**	**3.06**	**1.22**	**0.41**
Thylacine-2	Flaxman Fm	2296.8	SN187	1.29	8.54	84.24	3.58	1.01	0.17	0.26	0.10	0.07	0.10	0.19	0.21	0.08	0.04	0.03	0.09	9.83	1.44	0.91	0.45
Thylacine-2	Flaxman Fm	2296.8	SN193	1.25	8.80	83.90	3.64	1.07	0.18	0.26	0.10	0.07	0.11	0.19	0.21	0.08	0.03	0.02	0.09	10.05	1.51	0.90	0.43
			Mean	**1.27**	**8.67**	**84.07**	**3.61**	**1.04**	**0.18**	**0.26**	**0.10**	**0.07**	**0.11**	**0.19**	**0.21**	**0.08**	**0.04**	**0.03**	**0.09**	**9.94**	**1.48**	**0.91**	**0.44**

APPENDIX 3
DST INTERPRETATION REPORT

8/01/02
WJR
FINAL Copy

Woodside Energy Ltd.
Thylacine-2
DST #1 and DST#2
September 2001

Well Test Report

Pressure Build-Up Interpretation

Final Report

Joop de Wit
KAPPA
January 2002

Thylacine-2, DST#1 and DST#2 Well Test Analysis

Table of Contents

TABLE OF CONTENTS 2

SUMMARY 3

CONCLUSION 3

PRE-FLOW DATA 4

DETAILED DISCUSSION 4

RESERVOIR DATA 4
PRODUCTION RATES 5
GAUGE DATA QUALITY 5
TEMPERATURES 5

DST#1 6

MAIN BUILD UP ANALYSIS 6
Analysis, Most likely model 6
Remarks on the Match 7
Drawdown 7
Pre-Test Flow and Build-Up 7
Initial Pressures 7
Analysis, Alternative Model: Leaky Fault 8
Expected Production from Slanted Well. 8
NUMERICAL SIMULATION 8

DST#2 9

BUILD UP ANALYSIS 9
Analysis, Most likely model: 2> faults @ 90° 9
Alternative model: 60° Fault Angle. 10
Initial Pressures 10
NUMERICAL SIMULATION 11
Depletion 11
COMPARISON OF THE RESULTS 11

REMARK ON PERMEABILITY 12

REMARKS ON THE TEST 13

LIST OF FIGURES 14

DST#1 14
DST#2 14

Summary

Company	Woodside Energy Ltd.
Well	Thylacine-2
Test	DST #1 and DST#2
Test Objectives	Estimation of in-situ Permeability and Heterogeneity
Formations	DST#1 : Flaxmans('B' sand)
	DST#2 : added Waarre ('D' sand)
Perforations	DST#1 : 2176 - 2226 mRT
	DST#2 : 2176 - 2226 mRT + 2296 - 2302 mRT
Type of Test	Standard gas test
Date of Test	18th - 22nd September 2001
Interpreted by	Joop de Wit, KAPPA (Perth) using Saphir 3.01.08
Main data source	Working papers and Field Report (Slb spreadsheet)
Remarks	Depths are in meters below RT, pressures in psi (absolute) at lower gauge depth 2,148 mbRT unless stated otherwise.
	SS depths are 25 meter below RT (vertical well).

Note: a boundary or sealing fault in Well Test Analysis is a border at which there is a strong reduction in mobility, caused by the presence of a fault, sand pinch-out, boundary of a channel sand, area with a much lower permeability, high contrast in viscosity or any other feature which can reflect a pressure wave.

Conclusion

The well was tested twice: DST#1 tested the upper zone, Flaxmans 'B' sand. For DST#2 the underlying zone Waarre 'D' sand was additionally perforated and the two zones were tested simultaneously, albeit with a very short build-up period (< 25 minutes).

The Flaxmans had a low productivity with a maximum rate of less than 8 MMscf/d; the Waarre sand was much better where the well was producing around 28 MMscf/d with less drawdown.

The following reservoir parameters were derived from the analysis:

Parameter	DST#1: Flaxmans	DST#2: + Waarre
well	storage and skin	Id.
reservoir	homogenous	Id.
boundary	none	2 faults @ 90° (60°)
kh	30	1140
k	1.7	193

skin	1.9	2.8
P_i @ gauge depth	3,246	3,294 (3,342)
last recorded BU pressure	3,187	3,190
Pressures at 2,175 mSS		
P_i [1]	3,260	3,310 (3,358)
MDT	3,309	3,374
Max. press. from pre-flow	3,230 - 3,300	
Quality Indicator	High	Medium-High

2126 2115.4

Gauge depth is 2,123 mss for DST#1 (lower gauge) and 2,112 mss for DST#2 (upper gauge).

The build-up in DST#2 is very short, therefore there is no certainty about the extend of the faulting, and the presence of boundaries further form the wellbore than, say 50 meters.

The angle between the two faults in the Waarre reservoir is not certain. A proper comparison with quality controlled MDT pressure data might resolve the question.

The measured pressures from the tests are around 50 psi lower than expected from the MDT data, from both zones. Cause of this difference is not known.

Pre-Flow Data

Before the DST#1 there was a 15-minute pre-flow period followed by a shut-in. This period was too short to clean-up the volume between the gauges and the perforations. The maximum pressure during this shut-in period is 3,215 psi @ 2,133 mss (lower gauge). The gradient of the fluid between the gauges and the perforations is not known. The extrapolated pressures at 2,175 mSS can therefore vary between around 3,230 psi and 3,300 psi.

Detailed Discussion

The reservoir and well data used for the interpretation are detailed in Figure 1. The operational and production data is from the Well Test Data (spreadsheet) as generated during the test.

Reservoir Data

The geological reservoir data is from the analysis as supplied by Woodside. The sandstone is considered to be one layer, as there was no indication of a dual layer effect during the build-up. The net sand thickness used in the evaluation is 18 meter (compared to 56.3 m gross thickness), porosity 15.7%. The gas properties are from the MDT sample #3. This sample is taken to enable to use common gas properties between DST#1 and DST#2 (Figures 1a and 1b).

[1] Gradient used is 0.26 psi/m (based on MDT data of reservoir pressures)



The MDT pressure data used in this report are derived from the plot made supplied by Woodside, Figure 21, and the calculations are in Figure 22. Figure 23 was supplied later and has the results of the analysis added in the plot.

The completion diagram is in Figure 24.

Production Rates

The production rates are imported directly from the Schlumberger Test Report and are tabulated in Figure 2.

Gauge Data Quality

Data from five pressure gauges was received. The measurements are plotted in Figure 3 and the details of the gauges are in the following table:

Gauge	Type	Sampling [sec]	Remarks	Carrier
#776	WTQR	10	BU 30s early in DST#1. data used in DST#2	Upper
#1837	WTQR	5	60s interv. DST#2	
#1917	WCQR	5	Interpolated data	
#1846	WTQR	5	60s interv. DST#2. data used in DST#1	Lower
#2855	WCQR	5	interpolated data	

The pressure data is of good quality, only the sampling frequencies are lower than expected for most of the survey time. Although the gauges were programmed for a sampling frequency of 5 seconds, most gauges switched to approximately 1-minute intervals rather early in the test sequence. Gauges #1917 and #2855 have an apparent density of 5 seconds, but the software has made a linear interpolation between measured data points, which are 1 minute apart.

The difference channel shows that the gauges are stable and no apparent drift is observed in any of the gauges.

Temperatures

The temperature data is of good quality, all gauges show very similar temperature responses, see Figure 3. No anomalies can be found during the tests. The minimum temperature is 93°C during the drawdown of DST#1. The well stabilises to 109°C.

In DST#2 a warmer (lower) zone is added, but the temperature of the total mixture only drops with approximately 1°C, due to the low drawdown, therefore a low cooling effect. After the shut-in the temperature at the gauges stabilises at 114°C, due to the hotter fluids from the lower perforations rising in the tubing.

DST#1

Main Build Up Analysis

The build-up analysis is done on the main closed-in period of around 10 hours. The total closed-in period is longer, but during that time the well was being worked over for the additional perforations of the lower zone, disturbing the build-up pressures.

Analysis, Most likely model

Figure 4 shows the log-log plot of the main build-up, with a match using a homogeneous reservoir model and no boundary. This model matches the observed pressure trend well. The analysis parameters are as follows:

Reservoir Model	homogeneous
Boundary	none
Well	Storage and skin
kh	29.7 mD.m
k	1.7 mD
Skin	1.9
P_i	3,246 psi at 2,148 mTV, (2,123 mSS), lower gauge depth, from the PBU analysis
Last recorded BU pressure	3,187 psi at gauge depth
Pressures at Datum (2,175 mSS)	
P_i	3,260 psi (0.26 psi/m)
Last recorded BU pressure	3,201 psi
MDT	3,309 psi

The match just before the IARF period, is not perfect. This might be an indication of dual layer effect, but this can also be caused by the large pressure difference between the drawdown and the build-up (see 'remarks' in the next section).

After around 14 hours into the build-up, the pressures are distorted by well intervention activities by wireline (additional perforations). But the model seems to continue to match the pressures after the initial pressure 'jolts'.

The linear match on the superposition plot (IARF, Figure 5) gives very similar results, only the initial reservoir pressure is about 7 psi higher than from the model with the fault. Figure 6 is the history match.

The early time can be matched better by using a dual layer model, but 99.7% is from one layer with a very high connectivity factor (λ), so the overall production will be as from one layer, see Figure 7.

The pressure at end of the build-up is approximately 60 psi below the extrapolated reservoir pressure. This is due to the low permeability and therefore relatively slow



build-up. To achieve the initial pressure from the MDT requires an additional 114 psi.

Remarks on the Match

The derivative is calculated using a pseudo time function to correct for the change in compressibility during the early time of the build-up, but this method is not perfect: the model assumes ideal gas (e.g., no deviation due to condensate) and the temperature is constant during the test. In reality the exact pressure performance can be somewhat different, causing deviations of the prefect pressure response especially in high drawdown gas-well tests.

Drawdown

The drawdown pressures are depicted on a larger scale in Figure 8. The continuous increase in bottom hole pressures shows that the well was still cleaning up during this flow period.

Pre-Test Flow and Build-Up

At the start of the test, the well was flowed for 10 minutes and shut-in. Figure 9 shows the pressure response during this period. This period cannot be analysed with any degree of accuracy due to:

a) there is no flow rate available from this period

b) the rate will have been varying and

c) the flow rate was too short and too low to lift all liquids to surface, so the pressures are distorted by liquids falling back towards the perforations. This can be seen in the pressure fluctuations in the early part of the build-up pressures (Figure 9).

d) the gradient of the fluid between the gauges and perforations is unknown. The pressure differential between the upper and lower gauges shows that it is lighter than the original fluid wellbore fluid (brine: 1.64 psi/m), but heavier than gas (0.26 psi/m). The maximum recorded pressure at the close-in during this period is 3,215 psi. The pressures at 2,175 mss can therefore between around 3,230 psi and 3,300 psi.

Initial Pressures

The initial reservoir pressure from the analysis is 3,260 psi at datum depth, compared with 3,309 psi from the MDT pressure data. This is a much larger difference than is to be expected with modern gauges. No unique explanation for this difference can be given at this moment. NB: all gauges have similar pressures, therefore it is not due to measurement/calculation errors of a particular gauge.

The straight line from the superposition plot gives very similar values for the kh and skin, and a slightly higher initial pressure: 3,253 against 3,246 from the homogenous model and 3,254 from the dual layer model.



The pressures from the initial flow period do not help either: Pressures before the test were 3,569 psi (too high) and after the 10 minute flow period the pressure came to 3,215 psi, approximately 30 psi below the value derived from the test analysis, probably caused by the presence of liquid between the gauges and the perforations.

Analysis, Alternative Model: Leaky Fault

Figure 10 shows the match with a leaky fault. The leakage factor is 99.9%; i.e. there is hardly any faulting at all, just a line with a very slight reduction in permeability. All parameters are however the same. This model is only shown to indicate that the reservoir is rather homogeneous, and that any heterogeneity will be very small in the area around the well.

Expected Production from Slanted Well.

To assess the potential of the Flaxmans reservoir, a model is made using a slanted well. The well model assumes a deviation of 80°, effective drained well length is 104 meters (this assumes 18 meters of net pay, the total well length is 324 meters) and a very low kv/kh of 0.01 as the reservoir will have limited vertical connectivity. This model has a much higher productivity than the vertical well (see Figure 11) and the expected forecast with a minimum bottom hole pressure of 1,000 psi is in Figure 12. This shows that after the initial 'spurt' production, the well stabilises around 10 MMscf/d in the first year. Of course the productivity will go down after that as the reservoir depletes over time (this forecast assumes infinite reservoir).

Numerical Simulation

The analytical model is sufficient to describe the observed pressure response and numerical modelling will not add substantially to the reservoir description.



DST#2

After the test of the 'B' sand the underlying 'D' sand was perforated. This zone has a much higher productivity: the well increased production from less than 8 MMscf/d from a 18 meter net pay interval to 28 MMscf/d by adding 6 meters of reservoir sand.

Build Up Analysis

The build-up is very short: around 25 minutes. The pressures after that time are affected by wellbore intervention.

The interpretation is done using a dual layer model, whereby layer 1 is the lower newly perforated 'D' sand, and layer 2 is the 'B' sand from DST#1 with the same properties as found in DST#1. The productivity of the 'D' sand is much higher than of the 'B' sand, so the drawdown and build-up are governed by the newly perforated layer.

Analysis, Most likely model: 2> faults @ 90°

Figure 13 shows the log-log plot of the main build-up, Figures 14 and 15 are the Superposition and History plots respectively. The main feature on the log-log plot is the sharp increase in the derivative curve, indicative of the presence of boundaries. The model to match this pressure performance is:

layer 1, 'D' sand, homogenous reservoir, 2 intersecting faults at 90°. P_i = 3,294 psi

layer 2, 'B' sand, homogenous reservoir, no boundaries, P_i = 3,243 psi. The upper gauge has a 3 psi lower pressure than the lower gauge. See Figure 21 for the pressure calculations of the MDT at gauge depth).

The reservoir parameters are:

Parameter	Flaxmans'B' sand layer 1 (from DST#1)	Waarre 'D' sand layer 2
Well	storage and skin	storage and skin
Reservoir	homogenous	homogenous
Boundary	none	2 < faults @ 90° @ 24m-24m
kh [mD.m]	29.7	1140
k [mD]	1.7	193

Skin	1.9	2.8
P_i @ Upper gauge[2]	3,243	3,294
Last BU pressure		3,190
Pressures @ 2,175 mSS		
P_i	3,260	3,310
Last BU pressure		3,206
P_{MDT}		3,374

The match is good, even for such a short close-in period. The confidence level in the derived parameters is Medium-High, apart from the angle between the 2 boundaries. This is due to the short close-in period, whereby the pressure response only describes the status close to the wellbore (say within 50 meters).

The pressure match on the drawdown is in Figure 16. Drawdowns are notoriously noisy and unreliable, but the overall pressure match is not bad, e.g. the shape of the derivative matches. One of the problems in the first drawdown is the variation of the skin due to the clean-up.

The skin value is 2.8, which is low for a well, which produces such a high rate. Assuming a non-Darcy skin component of 0.1per MMscf/d, the skin for Q = 0 is around zero, indicating a very clean completion. But even with no dS/dQ, the skin is still a low 2.8.

Alternative model: 60° Fault Angle.

The confidence factor of the boundaries is high, but not the exact angle between the boundaries as the derivative has stabilised. Also the lengths of the boundaries are uncertain due to the short close-in period, and their existence might be limited to the immediate region around the well. A second model using an intersection angle of 60° for the Waarre reservoir was created and the match is depicted in Figure 17. As can be seen, the match is very similar, there is just a slight difference in the shape of the pressure derivative, as the one from the 60° model stabilises at a value which is 5 times that of the IARF, while with the 90° model the stabilisation is at 4 times that value.

Initial Pressures

The reservoir pressure of the underlying Waarre reservoir is around 50 psi higher than the pressure from the Flaxmans. This is in-line with the difference as found from the MDT log. However, the pressures from the DST's are approximately 60 psi below the values from the MDT. The reason for this (systematic) difference is not known.

The initial pressure in the Waarre reservoir can be increased by decreasing the angle between the faults; i.e. a smaller angle means a higher initial reservoir

[2] Upper gauge is at 2,137 mTV, e.g. 2,112 mSS. Gradient is 0.26 psi/m



pressure. But this increases the pressure differences between the two reservoirs, and the top reservoir does not have 2 intersecting faults in the reservoir model, which could increase the P_i. However, the MDT pressure points in the Flaxmans show considerable spread, so the average reservoir pressure is not well known.

The pressures of the gauges used during the test all show very similar values, so the difference with the MDT log is not caused by an offset in one gauge.

It might be prudent to do a quality check of the MDT pressures, like calibration data, temperature stability etc. and to do a thorough quality check of the individual build-up pressures to check for proper seals, super-charging etc.

Numerical Simulation

An analytical model was made to see if the build-up could be simulated with a simple reservoir model. The model, depicted in Figure 18, is 2D, e.g. the Waarre reservoir only, but as one layer is the dominant producer, the impact of a second layer will be limited. The model has two faults close to the well, Figures 19 and 20 show the match on the log-log and History plots respectively. Please note that the faults are limited in size, so the presence of the faults is no guarantee that the reservoir is limited in its extension.

Depletion

The analytical reservoir models are all infinite, e.g. they have two boundaries but are open at the side where there are no faults. The Voronoi model is bounded, but the borders of the reservoir have not been observed. This as the build-up is too short to see any considerable distance into the reservoir. Also on the drawdown there is no indication of any closed boundary.

No depletion is expected using the reservoir as drawn on the map. The total amount of gas withdrawn during DST#2 is 9 MMscf. A quick check using the material balance option in the Voronoi modelling indicates that the expected pressure drop would be in the order of 0.1 psi, which is too low to measure.

Therefore, there is no indication of depletion.

Comparison of the Results

The three models for the DST#2 have the following parameters:

	2 faults 90°	2 faults 60°	Voronoi 90°
kh [mD.m]	1140	1140	1100
P_i [psi] ('B'- 'D')	3,246 - 3,294	3,246 - 3,342	3,306
Distance to faults [m]	24 - 24	24 - 24	13 - 13



All parameters are very similar; the only one, which can show a difference, is the initial reservoir pressure. That depends on the angle between the faults: smaller angle means a higher initial reservoir pressure.

As stated in the section on the initial reservoir pressures, the MDT pressure have to be quality controlled to determine the proper initial reservoir pressures, so that the corresponding model (e.g. angle between the boundaries) can be established.

Remark on Permeability

The permeability from the test for the Upper zone, the Flaxmans, is 1.7 mD. This compares qualitatively well with the values from the mini-permeameter as plotted on the composite log. The k-phi transform shows consistent lower values.

The permeability value of 193 mD for the Upper zone, the Waarre, is lower than form the composite log, where values up to 5 Darcy are shown. There are however also values below the 10mD.

To get a qualitative comparison of the average permeabilities of the different methods, one should look at the sum of the kh values of the mini-permeameter measurements, as that is the parameter which is calculated by the transient analysis and which is divided by the drained thickness to obtain the (effective) permeability.

Another reason for differences in the permeabilities might be that the mini-permeameter is done on a core[3] and the pressure transient analysis looks at the average value of the rock in a cylindrical volume around the well bore.

Disclaimer. This interpretation has been carried out on a best effort basis, but no responsibility can be accepted for any consequence of errors in the derived parameters. The use of the results of this analysis is the responsibility of the client.

[3] Core measurements are done on one vertical section (line) in the reservoir, and is subjected to changes in stress, pressure and temperature.



Remarks on the Test

Following is a small list of observations on this specific test. This list is focussed on obtaining reservoir parameters only, so no other test objectives like PVT sampling is taken into account.

1. The value of the 10 minute pre-test flow and shut-in period is very limited. The time is too short for a proper clean-up and the presence of liquids prohibit establishing the initial reservoir pressure with any certainty. Also the kh cannot be measured, as there is no reliable measurement of the flow rate. The interval between the gauges and top perforations is filled with fluids of different densities, causing phase effects. The pressure difference between the gauges during the tests during shut-in is around 4 psi (gas). Before the 15 minute flow this difference is more than 19 psi, after close-in it is 15 psi, indicating a mixture of fluids.
2. The long interval in DST#1 could have been considered for a production log during the flow period. This could have shown how homogenous the interval produces or which interval flows preferentially.
3. It could have been considered to change the flow sequence in DST#2: first a high flow rate to clean-up the well and to ensure that the whole interval is producing, followed by a stabilising period where the well is producing lees, followed by the build-up. This minimizes skin and assures a stable flow before the close-in.
4. The main Build-Up period of 25 minutes is too short for a high-confidence analysis. In general a couple of hours is recommended.
5. Sampling frequencies needs to be determined and agreed upon in advance. The gauges, which were set to a sampling frequency of every 5 seconds, were automatically adjusted to 60 second intervals when the memory was getting full. This is a too long interval to be of use in the early time of a build-up analysis.
6. Pressure data from the gauges #1917 and #2855 were interpolated to look like 5 second intervals, from the measured 60 seconds. This is to be avoided as is creates data, which is not measured and can create confusion in the analysis.
7. Surface Read-Out can assist in maximising the information from a production test. It enables the engineer to do an initial analysis so the test can be adjusted based on the measurements so far and the objectives of the test (e.g. observations of faults, depletion etc.). Also the memory of the gauges can be read and re-set, so they can continue sampling with the required (high) density mode without running out of memory.

Joop de Wit
10 January 2001



List of Figures

Figure 1a Basic interpretation/reservoir data for analysis for DST#1

Figure 1b Basic interpretation/reservoir data for analysis for DST#2

Figure 2 Production data

Figure 3 Pressure and Temperature plot of all gauges

DST#1

Figure 4 Log-Log plot of main build-up: homogenous model

Figure 5 Superposition plot of main build-up

Figure 6 Match of the historical pressure data: homogeneous model

Figure 7 Log-log plot of the dual layer model

Figure 8 Zoom-in on the Drawdown pressures.

Figure 9 Initial 10 minute flow and shut-in

Figure 10 Log-Log plot of a leaky fault.

Figure 11 Pressure response of 80° Slanted Well

Figure 12 1 year forecast of slanted well in infinite 'B' reservoir

DST#2

Figure 13 Log-Log plot of dual layer, Waarre with 2 intersecting faults under 90°, Flaxmans: no boundaries

Figure 14 Superposition plot

Figure 15 Historical pressures and match

Figure 16 Log-log plot of the draw-down period

Figure 17 Log-log plot of dual layer, Waarre with 2 intersecting faults under 60°, Flaxmans no boundaries

Figure 18 Voronoi model with 2 90° intersecting faults

Figure 19 Log-log plot of the build-up of Voronoi

Figure 20 History plot Voronoi model

Figure 21 Pressure plot of MDT data used for the comparisons

Figure 22 MDT Pressure calculations as function of Depths

Figure 23 Pressure plot of MDT and test results.

Figure 24 Completion string diagram.

Main Results	Figure 1
Company Woodside	Field Thylacine
Well Thylacine-2	Test Name / # DST#1

Test date / time	18 Sept 2001
Formation interval	Flaxman
Perforated interval	2176 - 2226 mRT
Gauge type / #	WTQR/CQR
Gauge depth	Upper: 2137.4mRT
TEST TYPE	Standard
Porosity Phi (%)	15.7
Well Radius rw	0.10795 m
Pay Zone h	18 m
Connate Water (%)	0
Water Salt (ppm)	10000
Rock compr.	3E-6 psi-1
Reservoir T	110 °C
Reservoir P	3200 psia
FLUID TYPE	Gas
Gas Gravity	0.702043
Pseudo-Critical P	703.824 psia
Pseudo-Critical T	373.433 °R
Sour gas composition	
Hydrogen sulphide	0
Carbon dioxide	0.088
Nitrogen	0.0125
Hydrocabon fraction(s)	
Methane	0.839
Ethane	0.0364
Propane	0.0107
Iso-butane	0.0018
N-butane	0.0026
Iso-pentane	1E-3
N-pentane	7E-4
N-hexane	0.0011
N-heptane	0.0062
Reservoir T	110 °C
Reservoir P	3200 psia
Properties	@ Reservoir T&P
Z	0.918577
Mug	0.0205409 cp
Bg	0.00559764 cf/scf
Cg	2.84335E-4 psi-1
Rhog	0.15361 g/cc
Total Compr. ct	2.87335E-4 psi-1
Selected Model	
Model Option	Standard Model
Well	Storage + Skin
Reservoir	Homogeneous
Boundary	Infinite

Results	
TMatch	607 [hr]**-1
PMatch	1.31E-8 [psi2/cp]**-1
C	0.00231 STB/psi
skin	1.93
Delta P Skin	446.95 psi
Pi	3245.99 psia
k.h	29.7 md.m
k	1.65 md
Rinv	90.4 m
Test. Vol.	4.5643E+5 Barrels



History Listings | Figure 2

Company Woodside | Field Thylacine

Well Thylacine-2 | Test Name / # DST#1



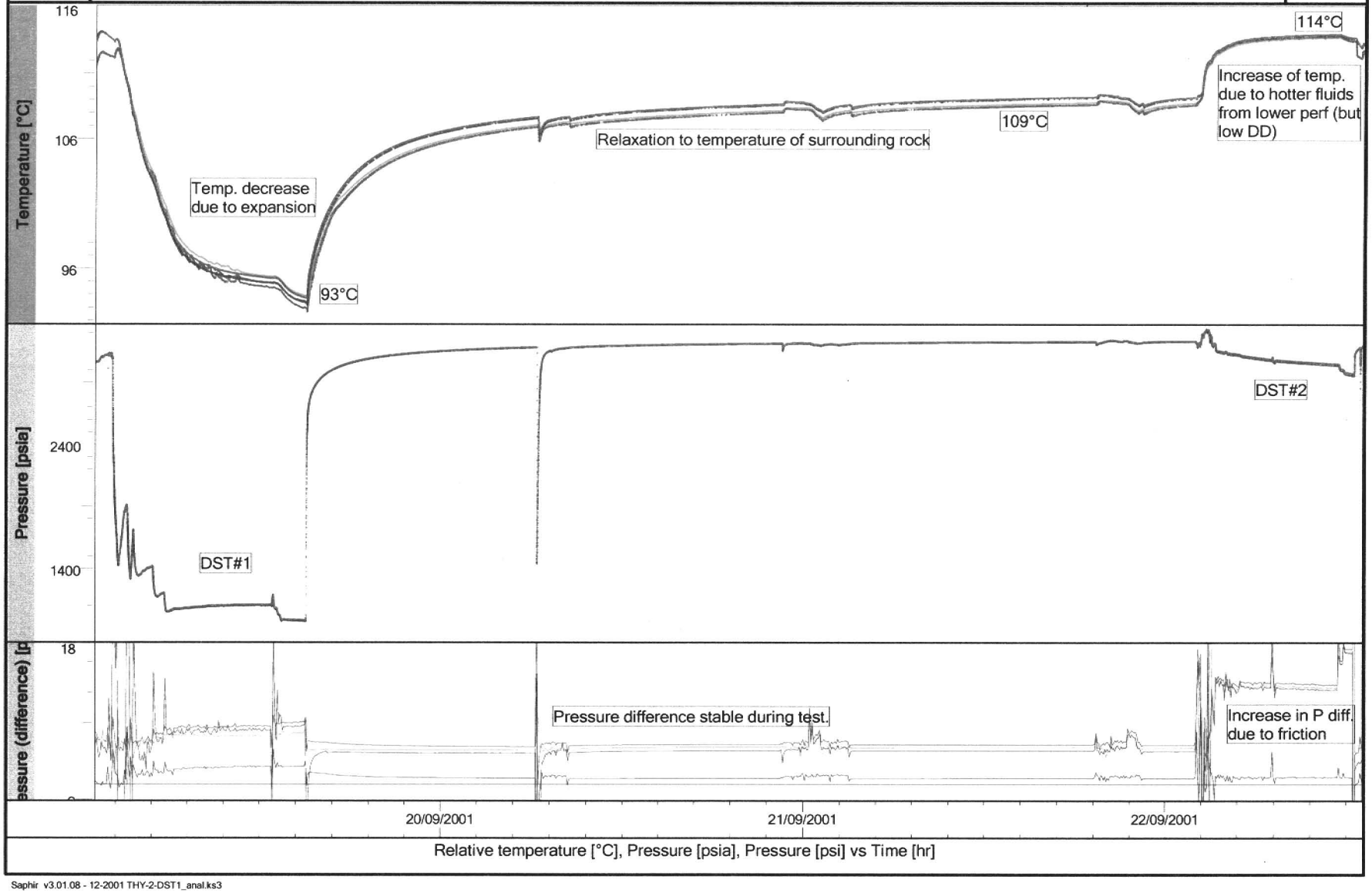
Date	ToD	FP #	Gas Rate MMscf/D	Duration hr
19/09/2001	00:00:00	1	0	2.59028
19/09/2001	02:35:25	2	4.64429	2.29306
19/09/2001	04:53:00	3	5.8	0.8
19/09/2001	05:41:00	4	6.8	1.23333
19/09/2001	06:55:00	5	7	5.88333
19/09/2001	12:48:00	6	7.6	2.27692
19/09/2001	15:04:37	7	0	59.8611
22/09/2001	02:56:17	8	23	8.55556
22/09/2001	11:29:37	9	25.9	0.294444
22/09/2001	11:47:17	10	27.83	0.378611
22/09/2001	12:10:00	11	28.06	0.0833333
22/09/2001	12:15:00	12	28.03	0.0833333
22/09/2001	12:20:00	13	27.76	0.0833333
22/09/2001	12:25:00	14	27.38	0.05
22/09/2001	12:28:00	15	27.06	0.0463889
22/09/2001	12:30:47	16	0	0.386944

QA / QC

Figure 3

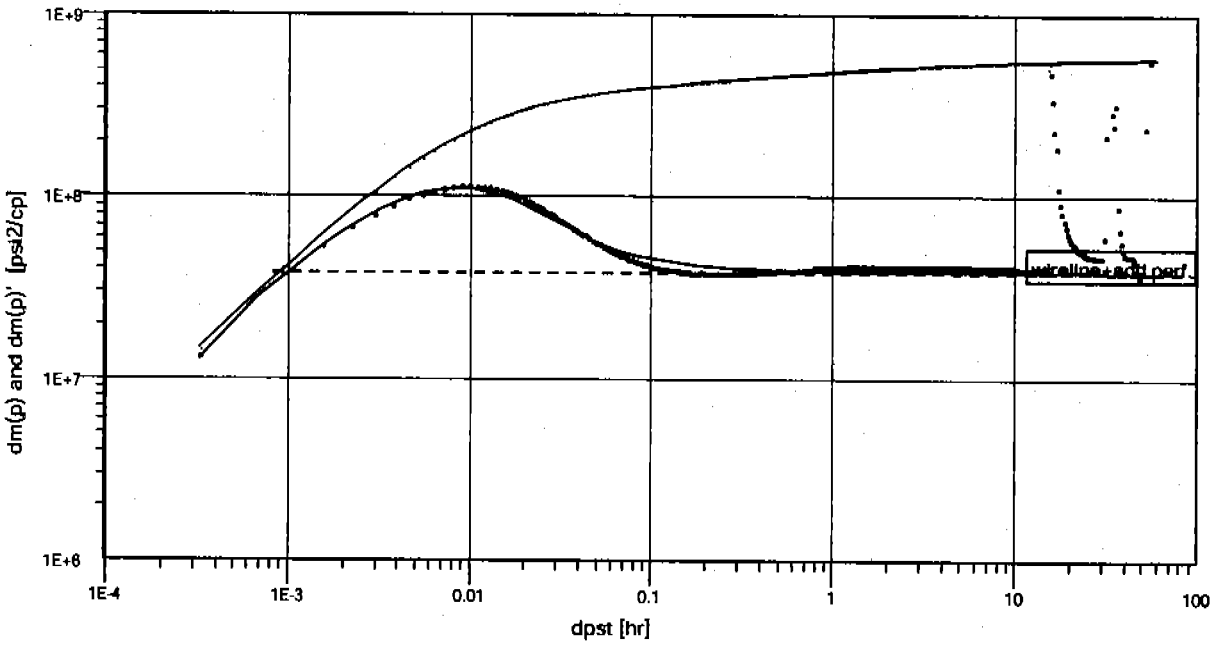
Company Woodside
Well Thylacine-2

Field Thylacine
Test Name / # DST#1



Saphir v3.01.08 - 12-2001 THY-2-DST1_anal.ks3

Log-Log plot	Figure 4
Company Woodside Well Thylacine-2	Field Thylacine Test Name / # DST#1



1846L build-up #1

Rate	0 MMscf/D
Rate Change	7.6 MMscf/D
P@dt=0	980.408 psia
Pi	3245.99 psia
PseudoTime used	
Smoothing	0

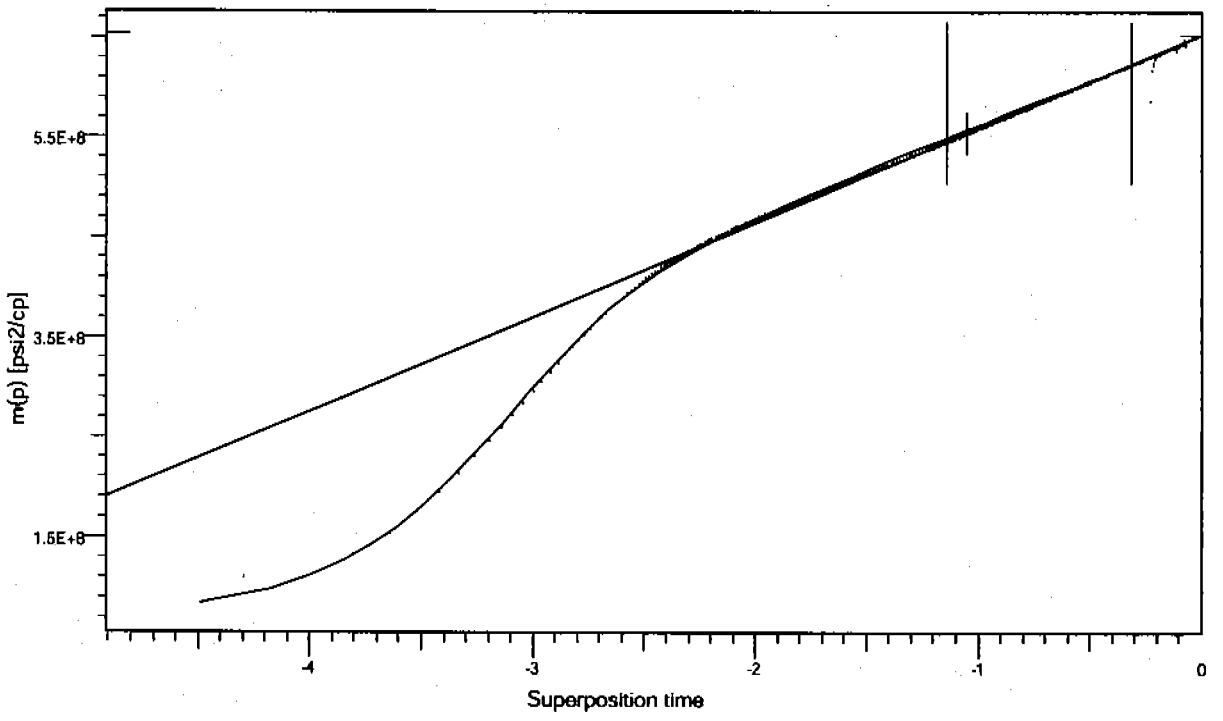
Selected Model

Model Option	Standard Model
Well	Storage + Skin
Reservoir	Homogeneous
Boundary	Infinite

Results

TMatch	607 [hr]**-1
PMatch	1.31E-8 [psi2/cp]**-1
C	0.00231 STB/psi
skin	1.93
Delta P Skin	446.95 psi
Pi	3245.99 psia
k.h	29.7 md.m
k	1.65 md
Rinv	90.4 m
Test. Vol.	4.5643E+5 Barrels

Semi-Log plot	Figure 5
Company Woodside Well Thylacine-2	Field Thylacine Test Name / # DST#1



1846L build-up #1

Rate	0 MMscf/D
Rate Change	7.6 MMscf/D
P@dt=0	980.408 psia
Pi	3245.99 psia
PseudoTime used	
Smoothing	0

Selected Model

Model Option	Standard Model
Well	Storage + Skin
Reservoir	Homogeneous
Boundary	Infinite

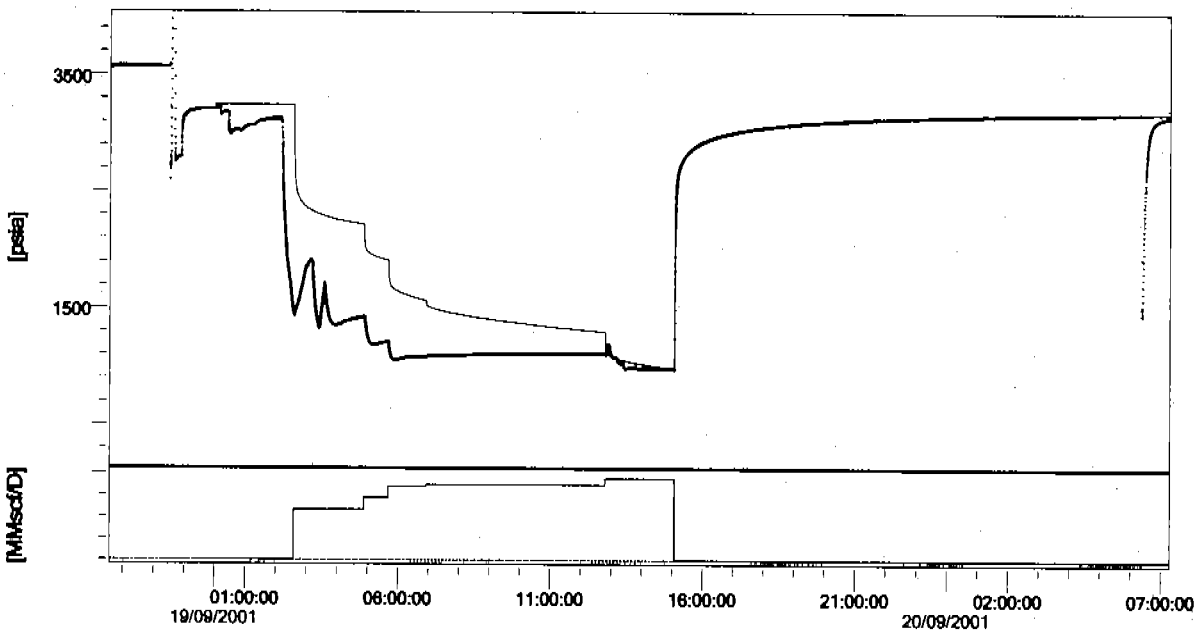
Results

TMatch	607 [hr]**-1
PMatch	1.31E-8 [psi2/cp]**-1
C	0.00231 STB/psi
skin	1.93
Delta P Skin	446.95 psi
Pi	3245.99 psia
k.h	29.7 md.m
k	1.65 md
Rinv	90.4 m
Test. Vol.	4.5643E+5 Barrels

Semilog Line (1846L build-up #1)

From	39.9681 hr
To	49.3917 hr
Slope	9.44401E+7 psi2/cp
Intercept	6.52979E+8 psi2/cp
M(p)@1hr	5.53838E+8 psi2/cp
PMatch	1.22E-8 [psi2/cp]**-1
k.h	27.7 md.m
k	1.54 md
p*	3253.15 psia
Skin	1.49
Delta P Skin	366.298 psi

History plot	hom Figure 6
Company Woodside Well Thylacine-2	Field Thylacine Test Name / # DST#1



Pressure [psia], Gas Rate [MMscf/D] vs Time [hr]

1846L build-up #1

Rate	0 MMscf/D
Rate Change	7.6 MMscf/D
P@dt=0	980.408 psia
Pi	3245.99 psia
PseudoTime used	
Smoothing	0
Prod. Index	0.00335454 MMscf/D/psia

Selected Model

Model Option	Standard Model
Well	Storage + Skin
Reservoir	Homogeneous
Boundary	Infinite

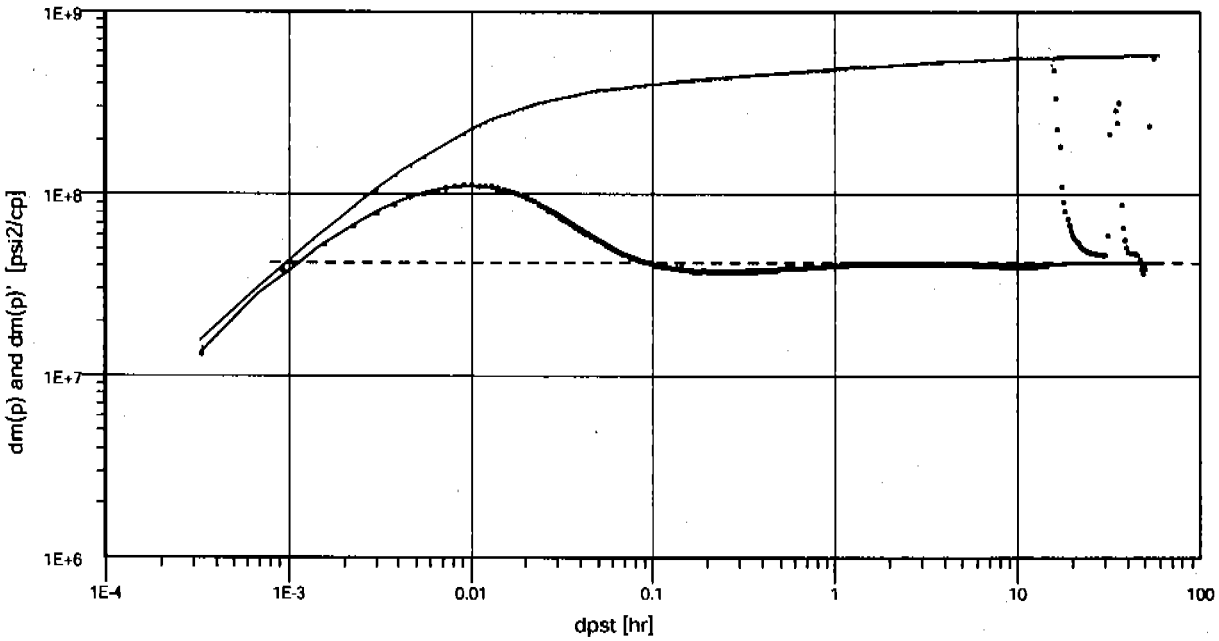
Results

TMatch	607 [hr]**-1
PMatch	1.31E-8 [psi2/cp]**-1
Prod. Index	0.00335454 MMscf/D/psia
C	0.00231 STB/psi
skin	1.93
Delta P Skin	446.95 psi
Pi	3245.99 psia
k.h	29.7 md.m
k	1.65 md
Rinv	90.4 m
Test. Vol.	4.5643E+5 Barrels

Semilog Line (1846L build-up #1)

From	39.9681 hr
To	49.3917 hr
Slope	9.44401E+7 psi2/cp
Intercept	6.52979E+8 psi2/cp
M(p)@1hr	5.53838E+8 psi2/cp
PMatch	1.22E-8 [psi2/cp]**-1
k.h	27.7 md.m
k	1.54 md
p*	3253.15 psia
Skin	1.49
Delta P Skin	366.298 psi

Log-Log plot	Figure 7
Company Woodside Well Thylacine-2	Field Thylacine Test Name / # DST#1



1846L build-up #1

Rate	0 MMscf/D
Rate Change	7.6 MMscf/D
P@dt=0	980.408 psia
Pi	3253.91 psia
PseudoTime used	
Smoothing	0

Selected Model

Model Option	Standard Model
Well	Storage + Skin
Reservoir	Two Layers
Boundary	Infinite

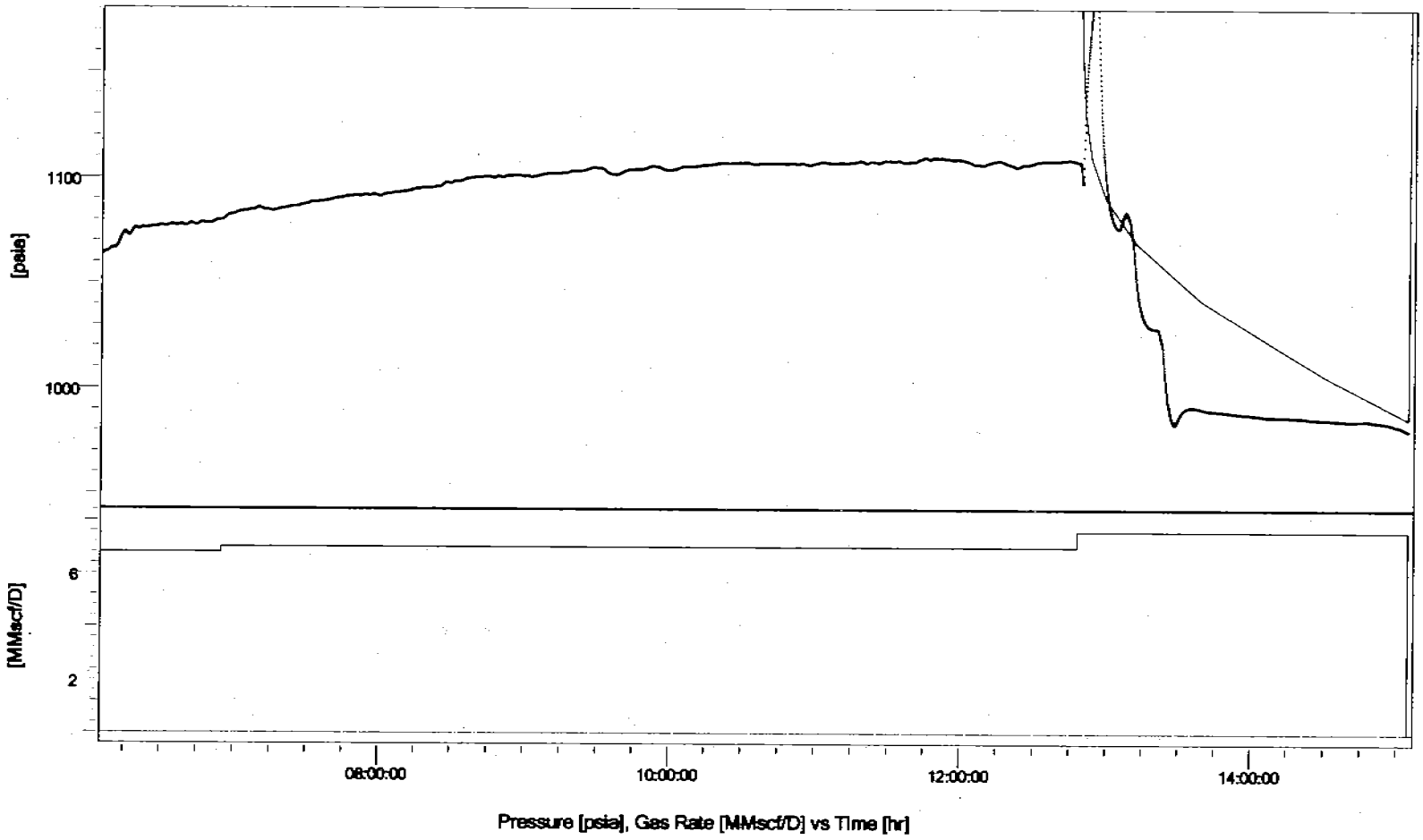
Results

TMatch	633 [hr]**-1
PMatch	1.2E-8 [psi2/cp]**-1
C	0.00203 STB/psi
skin1	2.01
skin2	-2.41
Pi	3253.91 psia
k.h	27.2 md.m
k	1.51 md
Omega	0.247
Lambda	0.00299
Kappa	0.997

History plot | Figure 8

Company Woodside
Well Thylacine-2

Field Thylacine
Test Name / # DST#1

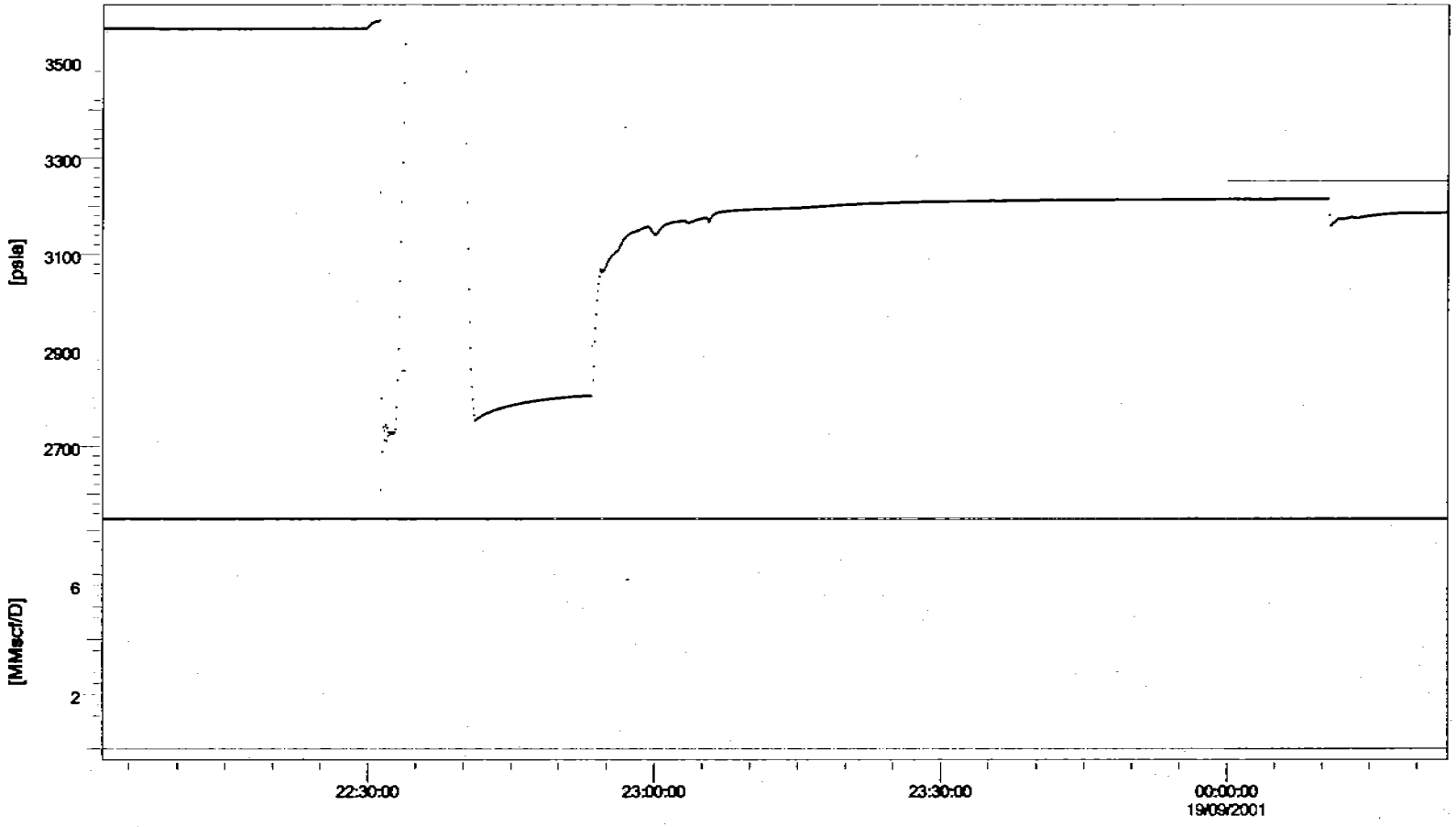


Pressure [psia], Gas Rate [MMscf/D] vs Time [hr]

History plot | Figure 9

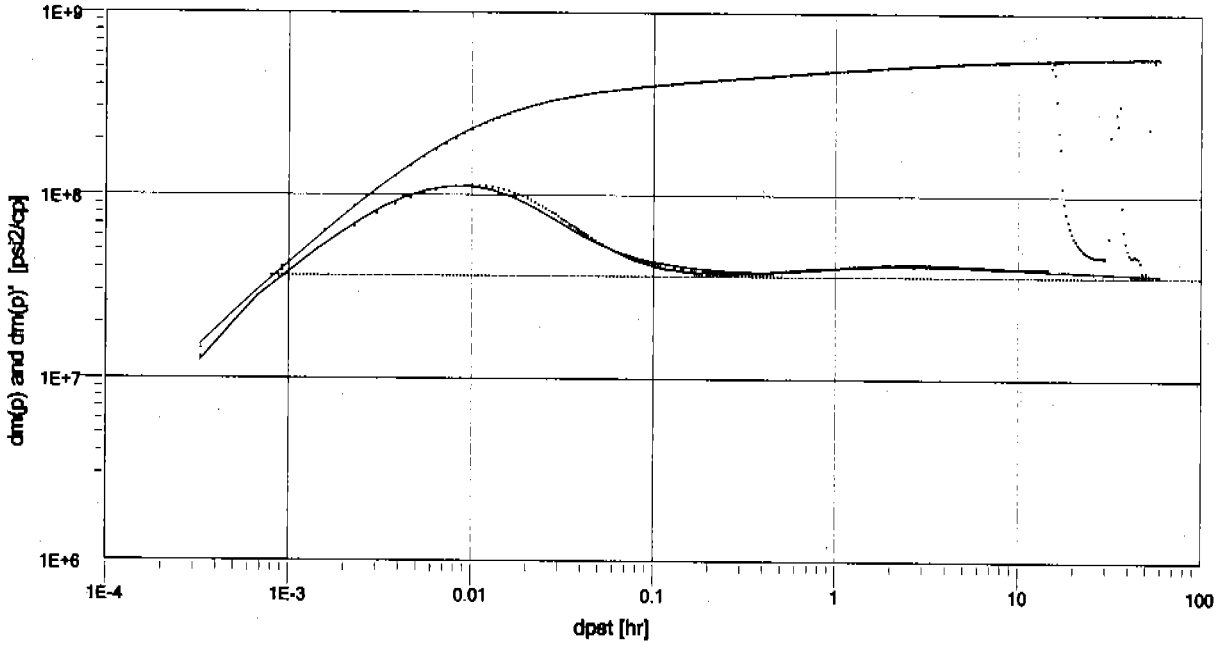
Company Woodside
Well Thylacine-2

Field Thylacine
Test Name / # DST#1



Company Woodside
Well Thylacine-2

Field Thylacine
Test Name / # DST#1



1846L build-up #1

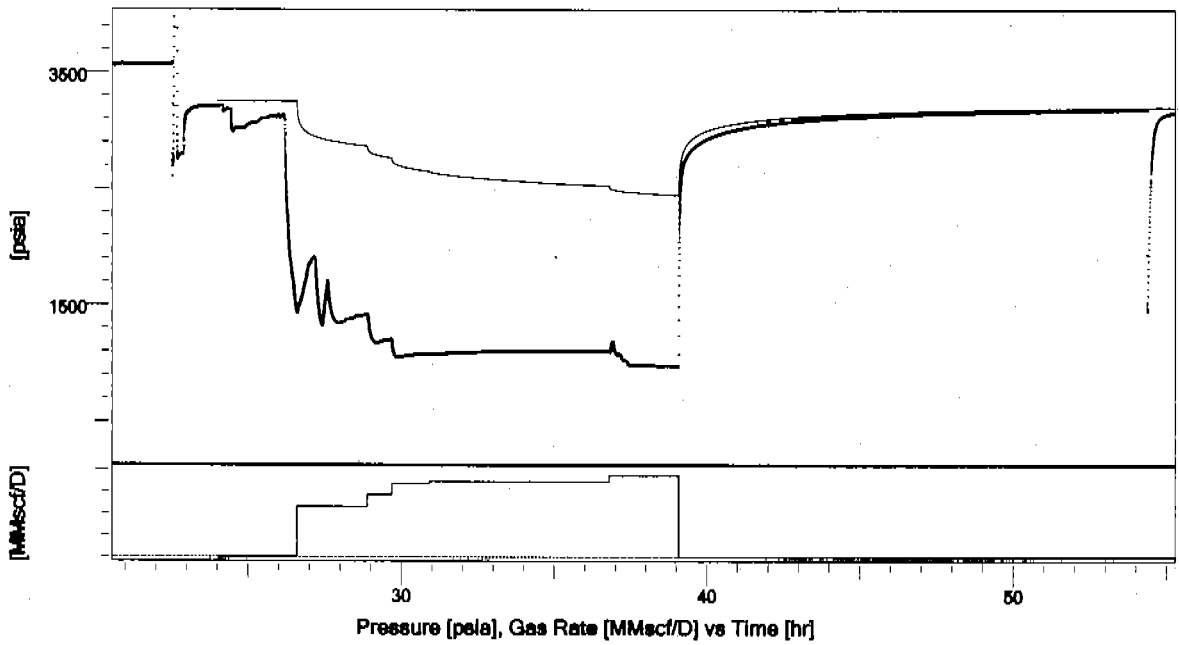
Rate	0 MMscf/D
Rate Change	7.6 MMscf/D
P@dt=0	980.408 psia
PI	3252.47 psia
PseudoTime used	
Smoothing	0
Prod. Index	0.00334498 MMscf/D/psia

Selected Model

Model Option	Standard Model
Well	Storage + Skin
Reservoir	Homogeneous
Boundary	Leaky Fault

Results

TMatch	631 [hr]**-1
PMatch	1.38E-8 [psi2/cp]**-1
Prod. Index	0.00334498 MMscf/D/psia
C	0.00235 STB/psi
skin	2.2
Delta P Skin	483.332 psi
PI	3252.47 psia
k.h	31.4 md.m
k	1.74 md
L	8.7 m
Leakage Factor	0.999



1846L build-up #1

Rate	0 MMscf/D
Rate Change	7.6 MMscf/D
P@dt=0	980.408 psia
PI	3252.47 psia
PseudoTime used	
Smoothing	0
Prod. Index	0.00334498 MMscf/D/psia

Selected Model

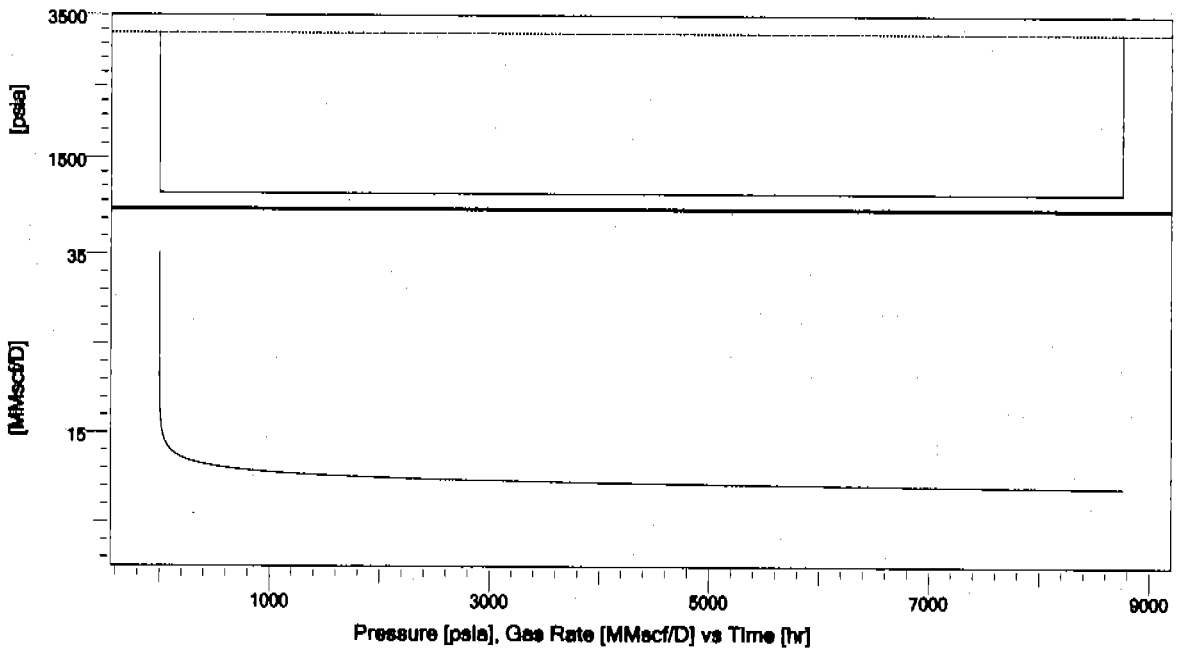
Model Option	External Model
Reservoir	Fully penetrating slanted well, infinite reservoir

Results

TMatch	631 [hr]**-1
PMatch	1.38E-8 [psi2/cp]**-1
Prod. Index	0.00334498 MMscf/D/psia
C	0.00235 STB/psi
PI	3252.47 psia
k.h	31.4 md.m
k	1.74 md
Skin	0
Well Length, hw	104 m
kz/kr	0.01

Company Woodside
Well Thylacine-2

Field Thylacine
Test Name / # DST#1



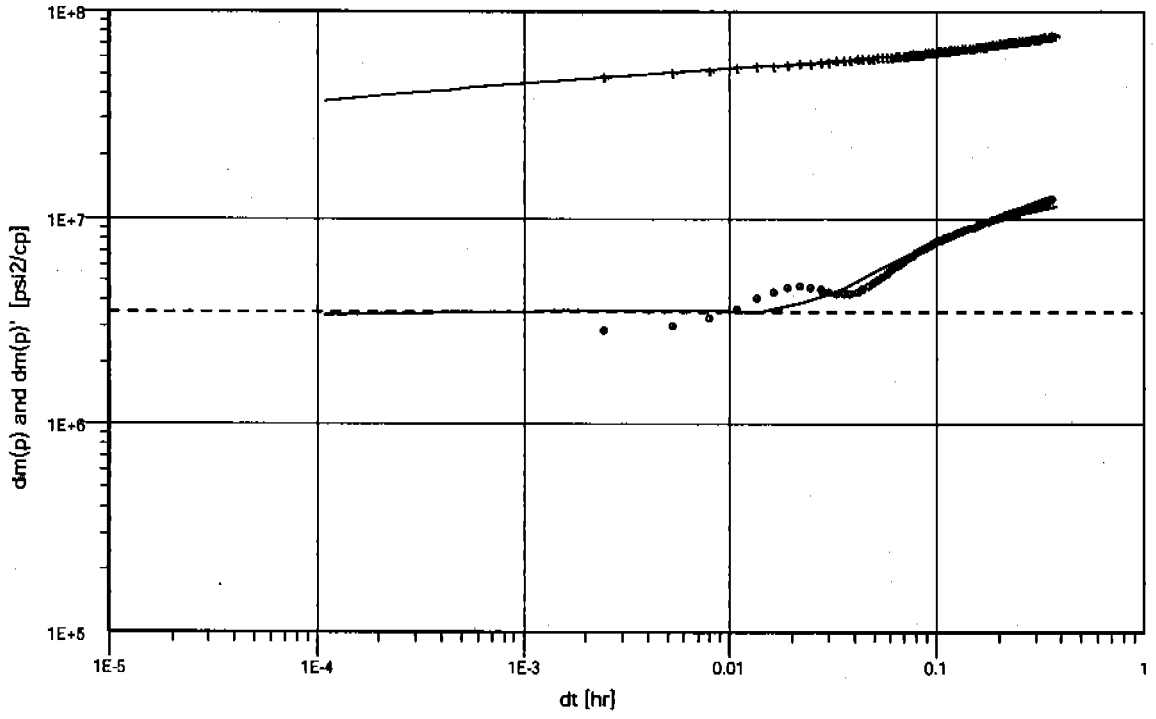
Selected Model

Model Option	External Model
Reservoir	Fully penetrating slanted well, infinite reservoir

Results

TMatch	631 [hr]**-1
PMatch	1.38E-8 [psi2/cp]**-1
Prod. Index	0.00334498 MMscf/D/psia
C	0.00235 STB/psi
PI	3252.47 psia
k.h	31.4 md.m
k	1.74 md
Skin	0
Well Length, hw	104 m
kz/kr	0.01

Log-Log plot	2L-Diff-P-2<-90d Figure 13
Company Woodside Well Thylacine-2	Field Thylacine Test Name / # DST#2



776U build-up #1

Rate	0 MMscf/D
Rate Change	27.61 MMscf/D
P@dt=0	2958.89 psia
Pi	3293.06 psia
Smoothing	0.1

Selected Model

Model Option	Multi-Layer Model
Nb Layers	2

Results

TMatch	2.29E+7 [hr]**-1
PMatch	1.42E-7 [psi2/cp]**-1

Layer parameters, layer # 1

Storage + Skin - Homogeneous - Intersecting Faults

skin	2.8
Delta P Skin	57.6791 psi
Pi	3294.28 psia
k.h	1140 md.m
k	193 md
L1 - No Flow	23.5 m
L2 - No Flow	23.8 m
N	2

Layer parameters, layer # 2

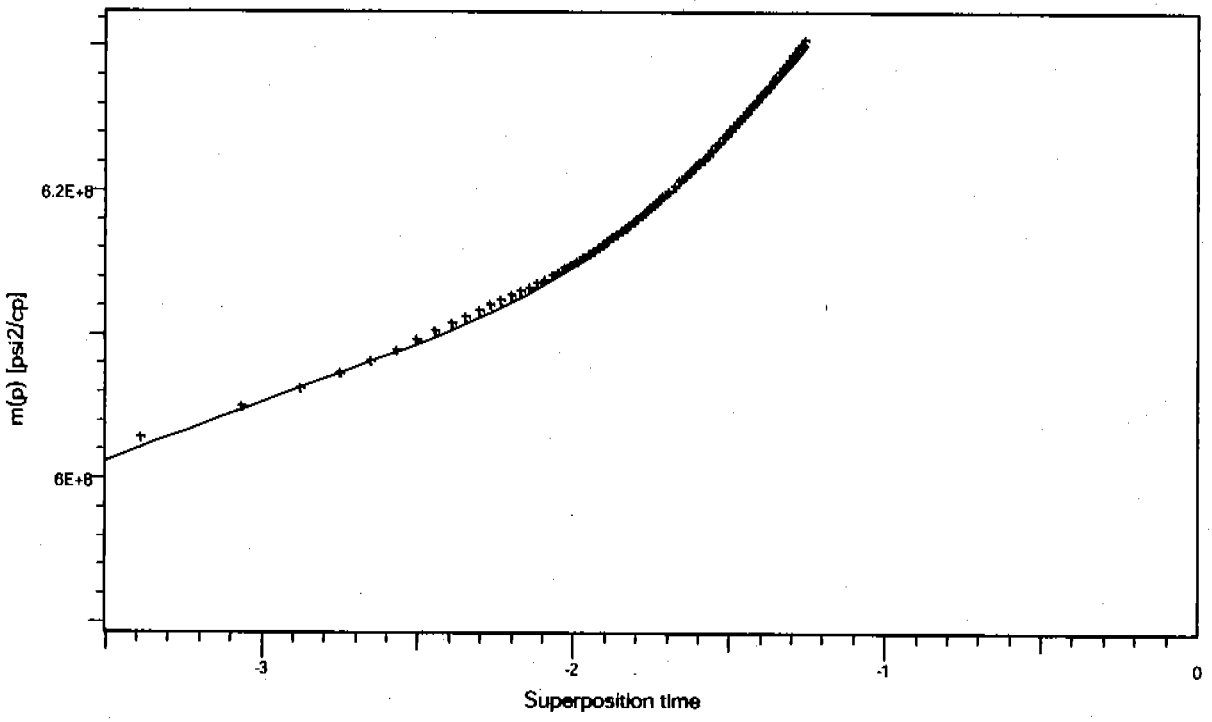
Storage + Skin - Homogeneous - Infinite

skin	1.94
Delta P Skin	39.9539 psi
Pi	3246 psia
k.h	29.7 md.m
k	1.65 md

Wellbore & other reservoir parameters

C	1.86E-6 STB/psi

Semi-Log plot	2L-Diff-P-2< 90d Figure 14
Company Woodside Well Thylacine-2	Field Thylacine Test Name / # DST#2



776U build-up #1

Rate	0 MMscf/D
Rate Change	27.61 MMscf/D
P@dt=0	2958.89 psia
Pi	3293.06 psia
Smoothing	0.1

Selected Model

Model Option	Multi-Layer Model
Nb Layers	2

Results

TMatch	2.29E+7 [hr]**-1
PMatch	1.42E-7 [psi2/cp]**-1

Layer parameters, layer # 1

Storage + Skin - Homogeneous - Intersecting Faults

skin	2.8
Delta P Skin	57.6791 psi
Pi	3294.28 psia
k.h	1140 md.m
k	193 md
L1 - No Flow	23.5 m
L2 - No Flow	23.8 m
N	2

Layer parameters, layer # 2

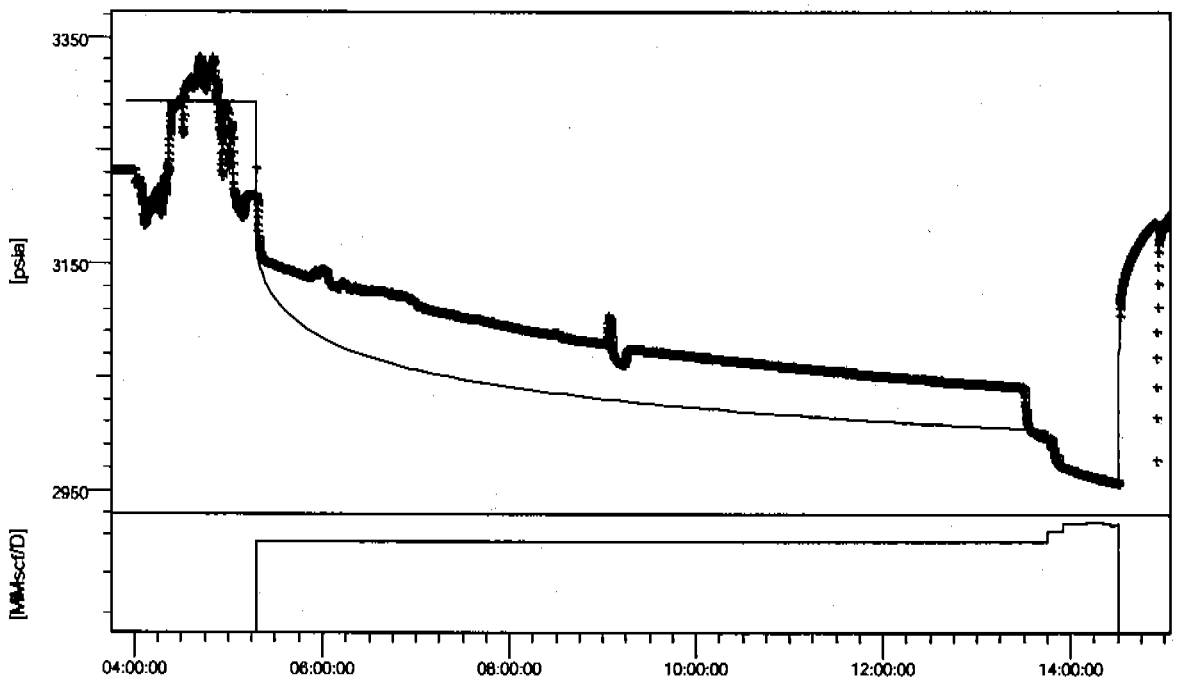
Storage + Skin - Homogeneous - Infinite

skin	1.94
Delta P Skin	39.9539 psi
Pi	3246 psia
k.h	29.7 md.m
k	1.65 md

Wellbore & other reservoir parameters

C	1.86E-6 STB/psi

History plot	2L-Diff-P-2< 90D Figure 15
Company Woodside Well Thylacine-2	Field Thylacine Test Name / # DST#2



Pressure [psia], Gas Rate [MMscf/D] vs Time [hr]

776U build-up #1

Rate	0 MMscf/D
Rate Change	27.61 MMscf/D
P@dt=0	2958.89 psia
Pi	3293.06 psia
Smoothing	0.1

Selected Model

Model Option	Multi-Layer Model
Nb Layers	2

Results

TMatch	2.29E+7 [hr]**-1
PMatch	1.42E-7 [psi2/cp]**-1

Layer parameters, layer # 1

Storage + Skin - Homogeneous - Intersecting Faults

skin	2.8
Delta P Skin	57.6791 psi
Pi	3294.28 psia
k.h	1140 md.m
k	193 md
L1 - No Flow	23.5 m
L2 - No Flow	23.8 m
N	2

Layer parameters, layer # 2

Storage + Skin - Homogeneous - Infinite

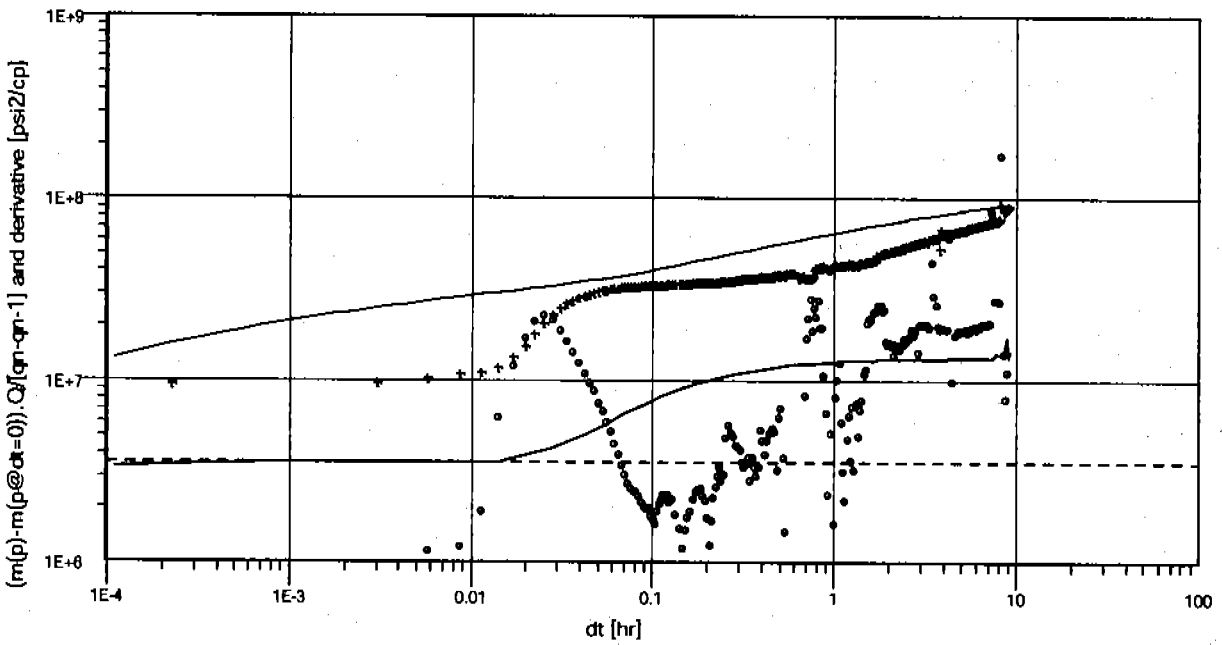
skin	1.94
Delta P Skin	39.9539 psi
Pi	3246 psia
k.h	29.7 md.m
k	1.65 md

Wellbore & other reservoir parameters

C	1.86E-6 STB/psi

Company Woodside
Well Thylacine-2

Field Thylacine
Test Name / # DST#2



776U production #1

Rate	27.61 MMscf/D
Rate Change	27.61 MMscf/D
P@dt=0	3234.42 psia
PI	3293.06 psia
Smoothing	0.1

Selected Model

Model Option	Multi-Layer Model
Nb Layers	2

Results

TMatch	2.29E+7 [hr]**-1
PMatch	1.42E-7 [psi2/cp]**-1

Layer parameters, layer # 1
Storage + Skin - Homogeneous - Intersecting Faults

skin	2.8
Delta P Skin	57.6791 psi
PI	3294.28 psia
k.h	1140 md.m
k	193 md
L1 - No Flow	23.5 m
L2 - No Flow	23.8 m
N	2

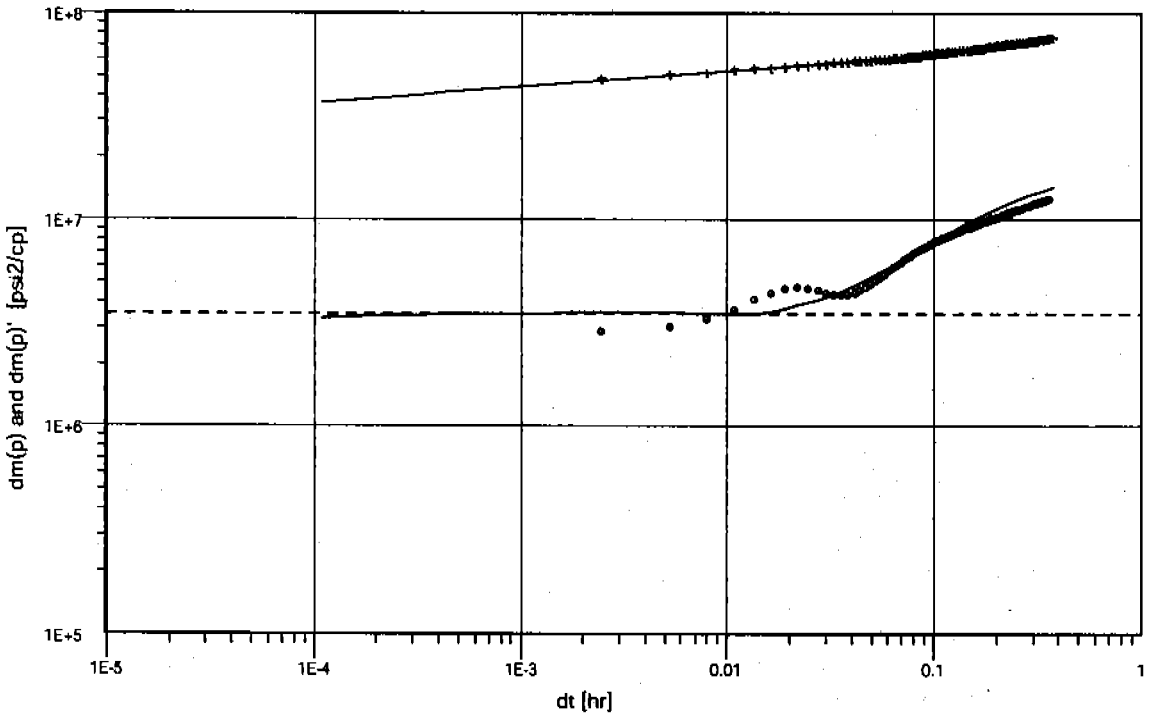
Layer parameters, layer # 2
Storage + Skin - Homogeneous - Infinite

skin	1.94
Delta P Skin	39.9539 psi
PI	3246 psia
k.h	29.7 md.m
k	1.65 md

Wellbore & other reservoir parameters

C	1.86E-6 STB/psi

Log-Log plot	2l-dP-60d Figure 17
Company Woodside Well Thylacine-2	Field Thylacine Test Name / # DST#2



776U build-up #1

Rate	0 MMscf/D
Rate Change	27.61 MMscf/D
P@dt=0	2958.89 psia
PI	3339.52 psia
Smoothing	0.1

Selected Model

Model Option	Multi-Layer Model
Nb Layers	2

Results

TMatch	2.29E+8 [hr]**-1
PMatch	1.42E-7 [psi2/cp]**-1

Layer parameters, layer # 1

Storage + Skin - Homogeneous - Intersecting Faults

skin	2.78
Delta P Skin	57.0979 psi
PI	3341.96 psia
k.h	1140 md.m
k	193 md
L1 - No Flow	23.5 m
L2 - No Flow	23.8 m
N	3

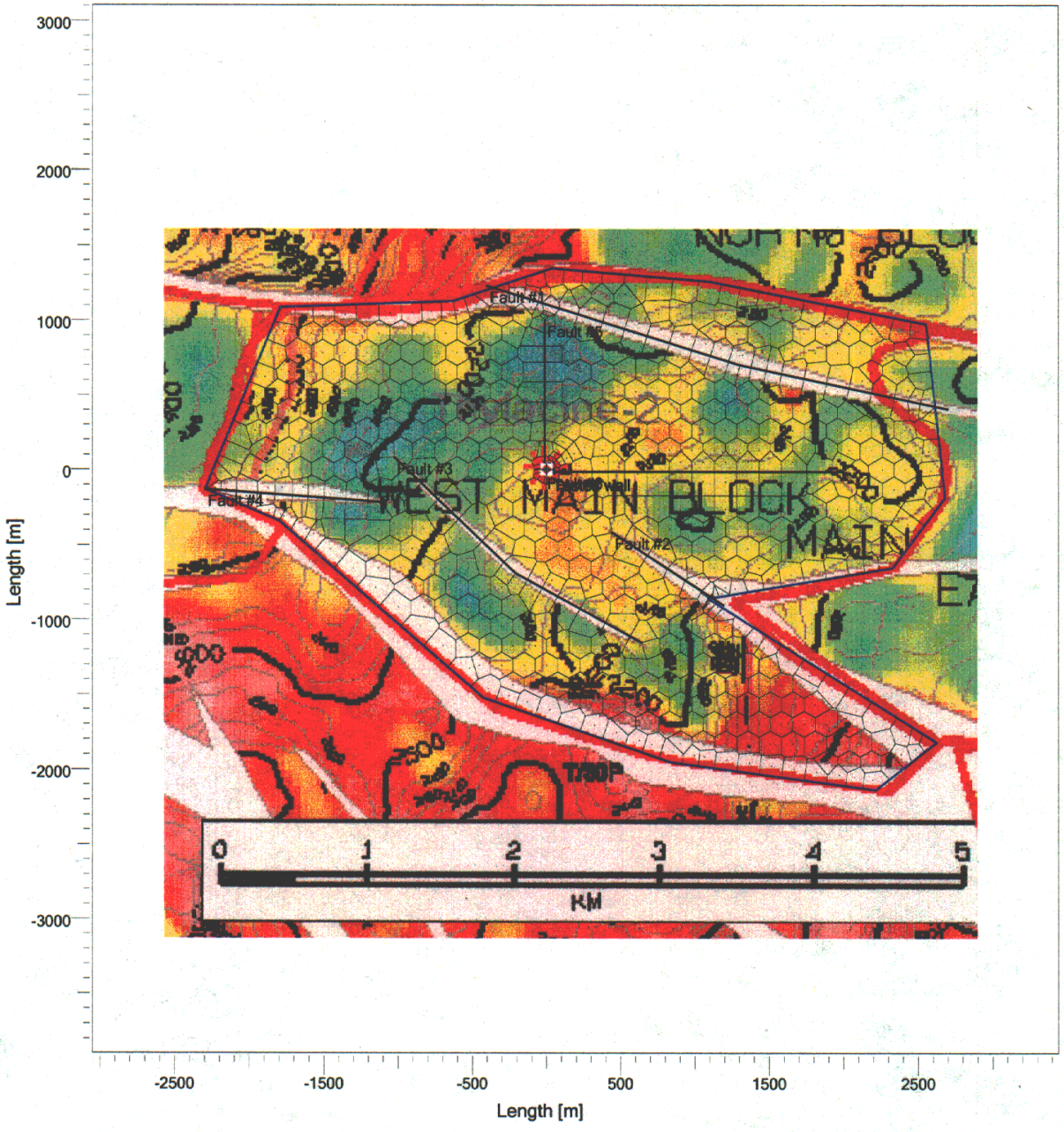
Layer parameters, layer # 2

Storage + Skin - Homogeneous - Infinite

skin	1.94
Delta P Skin	39.7296 psi
PI	3246 psia
k.h	29.7 md.m
k	1.65 md

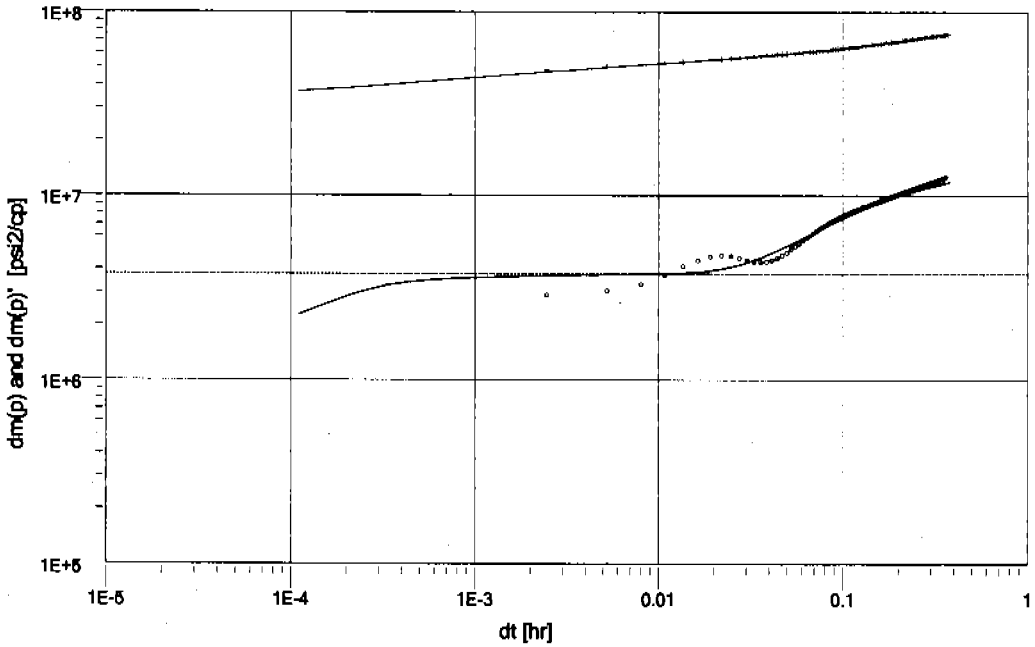
Wellbore & other reservoir parameters

C	1.86E-7 STB/psi


3000
2000
1000
0
-1000
-2000
-3000
Length [m]
-2500
-1500
-500
500
1500
2500
Length [m]
Fault #1
Fault #2
Fault #3
Fault #4
WEST MAIN BLOCK
MAIN
T/SOP
0
1
2
3
4
5
KM

Company Woodside
Well Thylacine-2

Field Thylacine
Test Name / # DST#2



776U build-up #1

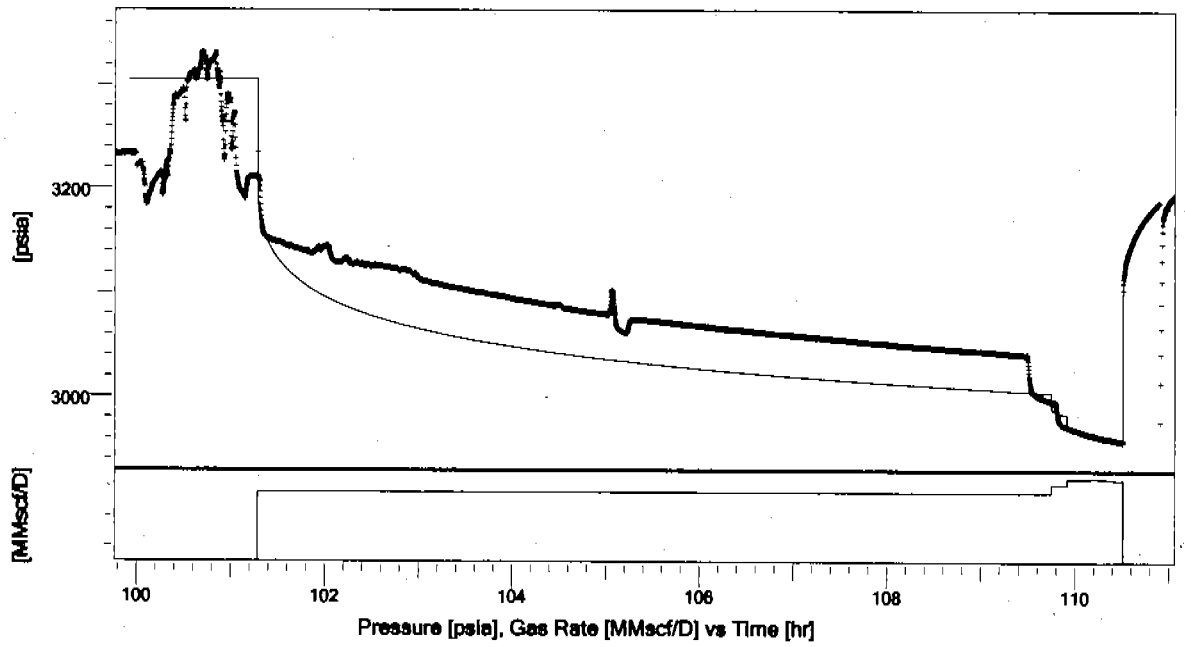
Rate	0 MMscf/D
Rate Change	27.61 MMscf/D
P@dt=0	2958.89 psia
PI	3305.63 psia
Smoothing	0.1

Selected Model

Model Option	Voronoi Model

Results

TMatch	2.29E+7 [hr]**-1
PMatch	1.33E-7 [psi2/cp]**-1
C	1.75E-6 STB/psi
skin	2.83
Delta P Skin	61.9335 psi
PI	3305.63 psia
k.h	1100 md.m
k	46.1 md
Test. Vol.	2.62652E+8 Barrels



776U build-up #1

Rate	0 MMscf/D
Rate Change	27.61 MMscf/D
P@dt=0	2958.89 psia
PI	3305.63 psia
Smoothing	0.1

Selected Model

Model Option	Voronoi Model

Results

TMatch	2.29E+7 [hr]**-1
PMatch	1.33E-7 [psi2/cp]**-1
C	1.75E-6 STB/psi
skin	2.83
Delta P Skin	61.9335 psi
PI	3305.63 psia
k.h	1100 md.m
k	46.1 md
Test. Vol.	2.62652E+8 Barrels

Figure 21

Thylacine-2: DST#1 and #2 September 2002
MDT pressures at the gauge depths.

TVD - ss=	25	m	
Gas density	0.260	psi/m (MDT plot)	

	mTV	mss	RFT plot mTV	RFT plot psi
Upper gauge	2,137	2,112	2,100	3,302
Lower gauge	2,148	2,123	2,400	3,380

Flaxmans (B)	mTV		mss	RFT press	
Perfs	2,176		2,151	3,315	from plot
	2,226		2,201		
dP with gauge	10.0	psi		3,305	Upper gauge
	7.3	psi		3,308	Lower gauge

Waarre (D)					
Perfs	2,296		2,271	3,399	from plot
	2,302		2,277		
dP with gauge	41.2	psi		3,358	Upper gauge
	38.5	psi		3,360	Lower gauge

APPENDIX 4
GEOCHEMISTRY REPORT

THYLACINE-2
GEOCHEMISTRY REPORT
OTWAY BASIN



Document Control No. xx
CONFIDENTIAL

Revision: 1
Date: 21/11/02
David Cliff

THYLACINE-2 GEOCHEMISTRY REPORT

1 Introduction

Following the completion of the Thylacine-2 well, a limited program was undertaken to evaluate the source rock character of the drilled sequence and the fluids recovered from it.

This report provides a compilation of the petroleum geochemistry data from Thylacine-2 well, together with an interpretation of these data.

The evaluation consisted of the following analyses:

DESCRIPTION	TYPE	QUANTITY
Bulk Volatile Chemistry from Fluid Inclusions (FIS analysis)	SED	180
Lithological description	SED	5
Total organic carbon (TOC)	SED	5
Rock-Eval pyrolysis	SED	5
Wax determination by high temperature gas chromatography (HTGC)	COND	1

Table 1 : Analytical program

Geotechnical Services Pty in Perth performed the source rock analyses, Fluid Inclusion Technologies (FIT) in Oklahoma, the fluid inclusion screening, and Shell Global Solutions (SGS) in Houston, the wax determination.

2 Fluid Inclusion Screening (FIS)

- Fluid Inclusion Screening is a rapid and relatively cheap tool used to:
  - Check for the presence of paleocolumns and migration zones
  - Assess seal effectiveness
  - Detect the presence of live hydrocarbons near a dry well bore (proximity to pay or PTP signal)
- It is unaffected by drilling mud contamination and can be applied to all cuttings samples
- It needs to be calibrated for each basin

180 cuttings samples from Thylacine-2 were selected for Fluid Inclusion screening from 560 mMDRT to 2525 mMDRT.

The results of FIS analysis are displayed in Figure 1. There is a strong gas inclusion signal in the present day gas-bearing zone, demonstrating effective inclusion formation after charging.

The lack of gas in the inclusions through the seal section above and in the upper section of the well indicate the Belfast Formation is an effective seal.

In the gas-bearing zone there is only a minor liquids signal which is consistent with the low CGR of gas currently reservoired in the Thylacine Field (Figure 2). There is no indication of an early oil migration/trapping phase, which is consistent with our understanding of the poor capacity of coaly terrigenous source rocks in the Lower Waarre and the Eumeralla Formations to source liquids.

The Fluid Inclusion gas signal continues into the water leg and down to TD with no indication of a palaeo-gas water contact.

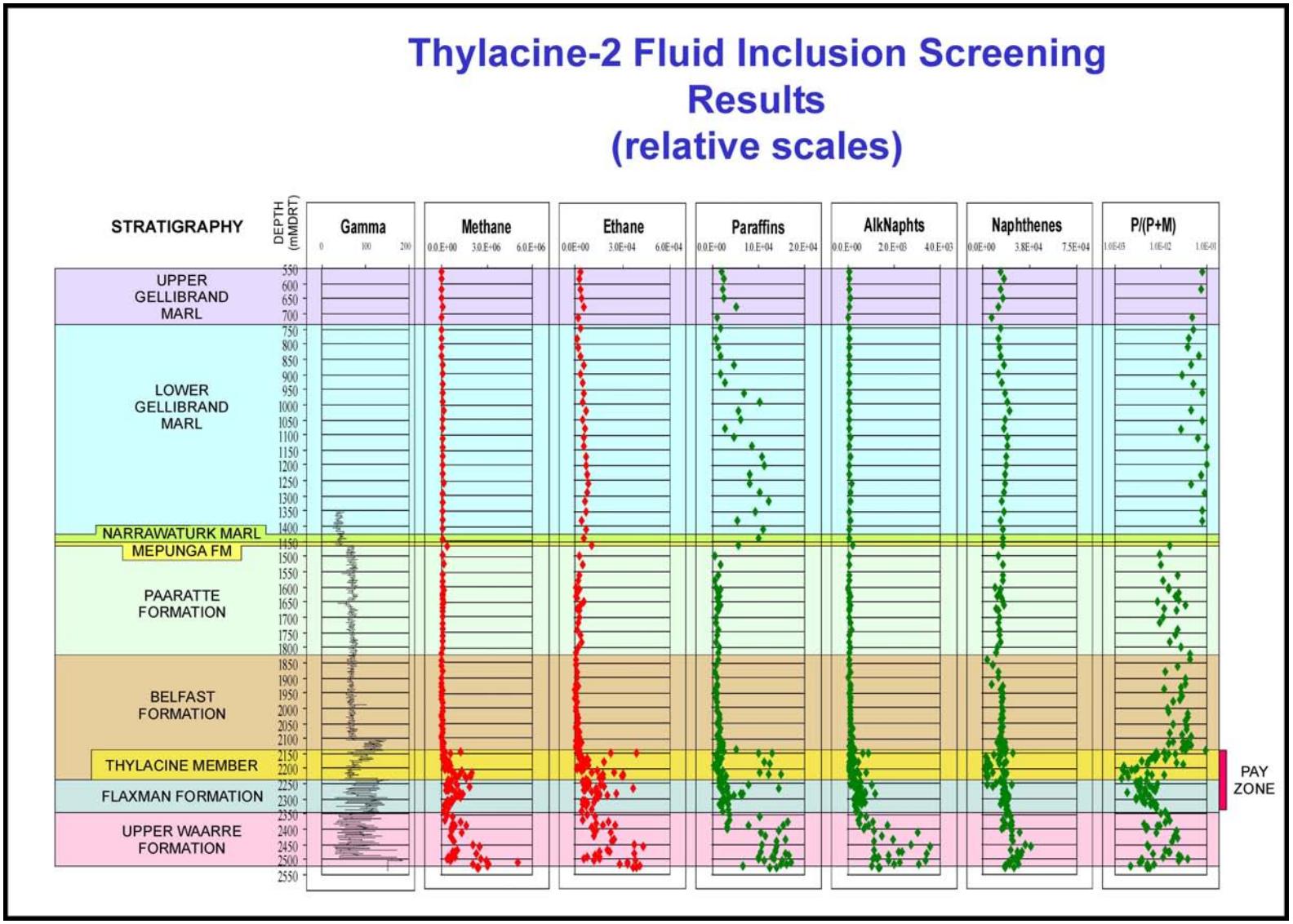


Figure 1: Fluid inclusion screening data

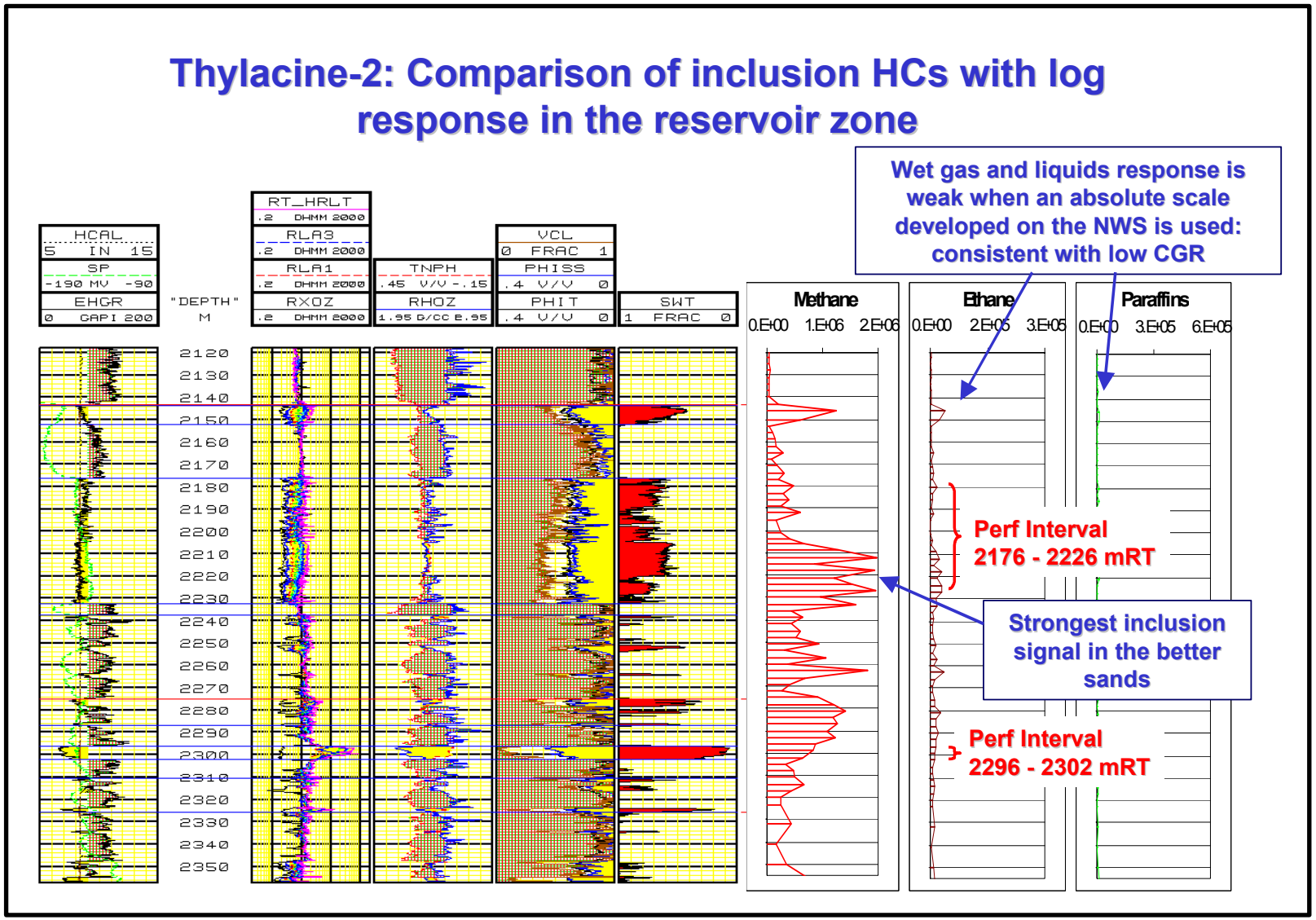


Figure 2: Comparison of inclusion hydrocarbons with log response in reservoir zone

3 Source Rock Potential

After a fairly comprehensive source rock study in Thylacine-1, only one high gamma ray Santonian aged shale was sampled (core plugs from 2232-2235m) for TOC and Rock Eval Pyrolysis in Thylacine 2. The results are summarised in Table 2. A graph of Hydrogen index vs TOC (Figure 3) shows that the source rock potential of the Santonian shale is fair, but strongly gas-prone. TOC ranges from 1.8 to 2.0%, while HI's are significantly less than 100. In general the kerogen appears to be oxidised Type III/IV, though oxygen indices remain low.

ANALYSIS OF ORGANIC MATTER BY ROCK-EVAL PYROLYSIS

THYLACINE-2

GEOTECH

Depth (m)		*Tmax*	*S1*	*S2*	*S3*	*S1+S2*	*S2/S3*	*PI*	*TOC*	*HI*	OI
2232.1	swc	432	0.29	0.95	0.19	1.24	5.00	0.23	1.97	48	10
2233.5	swc	437	0.24	0.68	0.23	0.92	2.96	0.26	1.80	38	13
2234.5	swc	434	0.30	1.26	0.16	1.56	7.88	0.19	1.79	70	9
2235.0	swc	436	0.33	1.30	0.44	1.63	2.95	0.20	1.88	69	23
2235.4	swc	433	0.30	1.30	0.23	1.60	5.65	0.19	1.78	73	13

A TMAX value is not reported if the S2 is <0.2mg/g

TMAX = Max. temperature S2 | S1 = Volatile hydrocarbons (HC) | S2 = HC generating potential

S1+S2 = Potential yield | S3 = Organic carbon dioxide | PI = Production index

OI = Oxygen Index | TOC = Total organic carbon | HI = Hydrogen index

nd = no data | GEOTECHNICAL SERVICES PTY LTD

Table 2: TOC and Rock-Eval data

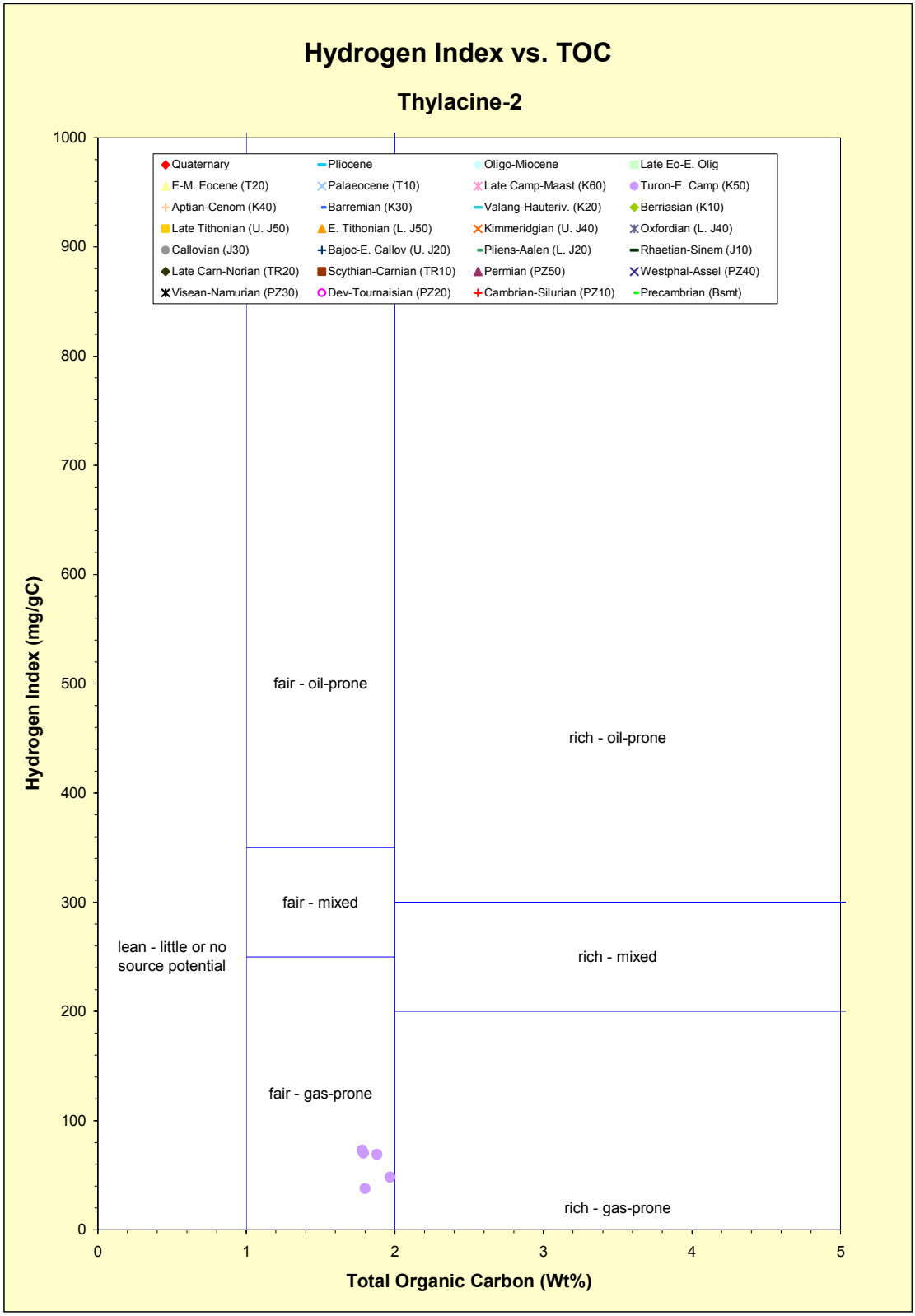


Figure 3: TOC vs. Hydrogen Index

4 Thylacine HTGC Wax Study

Two condensate samples (combined reservoir fluid from Thylacine-1 MDT samples 6, TS5702 and 7, TS5601 (2236.8 mRT), and a separator sample (dead condensate) from Thylacine-2 DST-2, (2296-2302 mRT)) were subjected to wax analysis by High Temperature Gas Chromatography (HTGC). Basic fluid properties (%water, API, %S, specific gravity and density) were also determined for the separator sample (Table 3). These results were used to evaluate whether the Thylacine gas discovery has potential wax precipitation problems.

The dead condensate from Thylacine-2 displayed a rapid decrease in higher n-paraffin content above n-C_{20}. The derived cloud point was -3°C and the derived pour point was <-17°C. The distribution of the light normal paraffins (n-C_{25} to n-C_{35}) in the Thylacine-1 combined reservoir fluid was almost identical to that of the Thylacine-2 separator sample, which validated the quality of the latter.

Both fluids exhibited a rapid decline in the concentration of normal alkanes above nC_{20}. In the separator sample, heavier normal alkanes are present in very low quantities (Figure 4). Assuming that all fluids in the reservoir have the same wax properties as the ones investigated in this study, the low calculated cloud point and pour point temperatures indicate that under normal operating conditions (lowest pipeline T~ 4°C) there is no risk for wax precipitation from the Thylacine fluid during production.

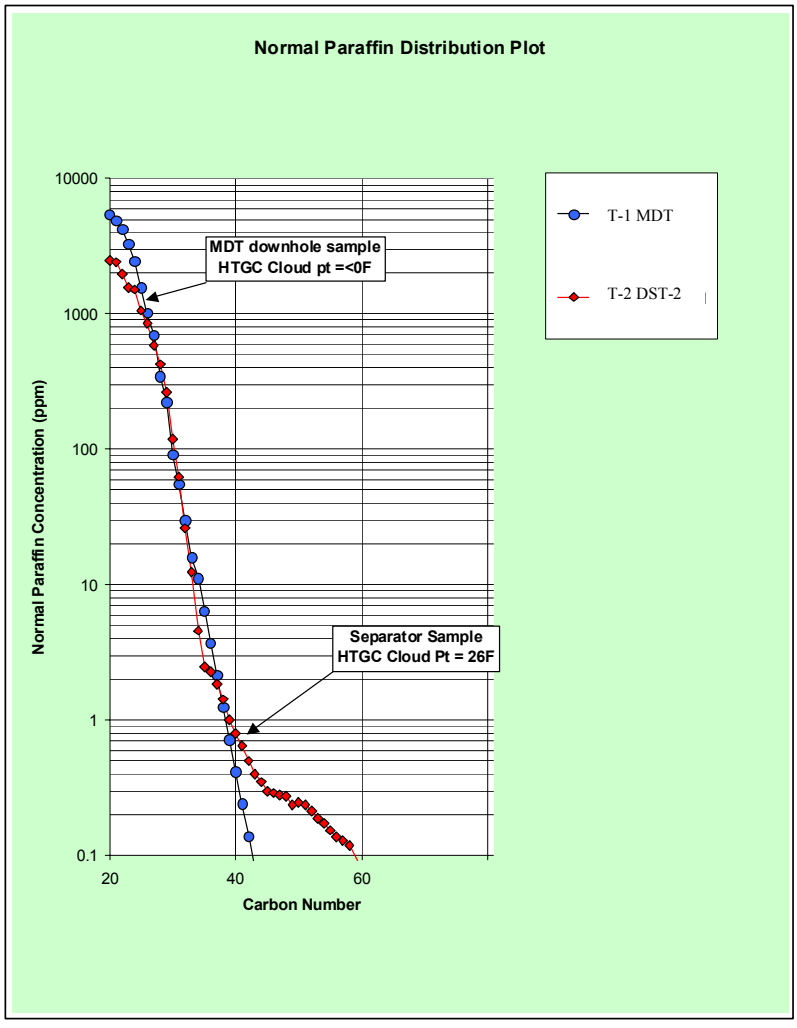


Figure 4: Paraffin distribution plot from HTGC analysis

SAM #	Well #	Type	T_{res} (°C)	P_{res} (psi)	API	%water	%S	Spec. Gravity	Density (g cm^{-3})
AUS-O-32	Thylacine-2	separator	89	3280	44	0.03	0.0092	0.8072	0.8064
AUS-O-33	Thylacine-1	reservoir	insufficient sample						

Table 3: Thylacine-2 condensate bulk properties

APPENDIX 5
PALYNOLOGICAL REPORT

PALYNOLOGY OF

THYLACINE-2

OFFSHORE OTWAY BASIN, AUSTRALIA

BY

ROGER MORGAN

for **WOODSIDE ENERGY LTD** **FEBRUARY 2002**

REF: OTW.THYLACINE-2 REPORT

PALYNOLOGY OF

THYLACINE-2

OFFSHORE OTWAY BASIN, AUSTRALIA

CONTENTS **PAGE**

1	SUMMARY	3
2	INTRODUCTION	4
3	PALYNOSTRATIGRAPHY	10
4	REFERENCES	19
5	UNPUBLISHED NAMES	20

Table 1	Individual Sample Summary – Thylacine-2
Table 2	Summary of sample lithologies – Thylacine-2
Figure 1	Tertiary Zonation Scheme (Partridge 1976, pers. comm)
Figure 2	Cretaceous Zonation used herein (from Morgan, 2001)
Figure 3	Comparison of Zonations of Morgan etc.
Figure 4	Maturity Profile : Thylacine-2

APPENDIX 1 PALYNOLOGICAL DATA CHARTS

1 SUMMARY

1410/20 m (cutts) : ***D. heterophlycta* Zone** : Middle Eocene : offshore marine : immature

1450/60 m (cutts) : ***P. asperopolus* Zone** : Early Eocene : ?shelfal marine : immature

1470/75 m (cutts) : ***M. diversus* (lower) Zone – *P. asperpolous* Zone** : Early Eocene : very nearshore marine : immature

1505/10 m (cutts) – 1535/40 m (cutts) : ***X. australis* (upper) Zone**, *N. senectus* (upper) Zone : Campanian : ?marginal marine : immature

2060/65 m (cutts) : ***N. aceras* (middle) Zone**, *N. senectus* Zone : Campanian : nearshore marine : immature

2080/85 m (cutts) – 2105/10 m (cutts) : ***N. aceras* (lower) Zone**, *N. senectus* Zone : Campanian : shelfal marine : immature

2113/16 m (cutts) – 2134/37 m (cutts) : ***I. cretaceum* (upper b) Zone**, *T. apoxyexinus* (upper) Zone : Santonian : shelfal marine : marginally mature

2140/43 m : mixed ***I. cretaceum* (lower b) Zone with *O. porifera* (upper) Zone**, *T. apoxyexinus* (middle) Zone : Santonian : shelfal marine : marginally mature

2152.31 m (core) – 2236.77 m (core) : ***O. porifera* (upper) Zone**, *T. apoxyexinus* (?middle) Zone : Santonian : nearshore to very nearshore marine : marginally mature

2242.96 m (core) – 2350/56 m (cutts) : ***P. infusorioides* (upper) Zone**, *T. apoxyexinus* (lower) Zone : Turonian : very nearshore to shelfal marine : marginally mature

2 INTRODUCTION

A total of 45 samples (29 cores, 16 cutts) have been studied from **Thylacine-2** for Woodside Energy Ltd. The zonation used for the Tertiary is that of Alan Partridge (1976 and pers. comm) as shown on Figure 1. The zonation used for the Cretaceous is based on the scheme of Helby, Morgan and Partridge (1987), revised and refined using Otway Basin cuttings by Morgan (1992, 1994, 2001), and summarised in Figure 2. Alan Partridge has also revised this zonation in unpublished studies and published it as an outline table in Partridge (1997) and Partridge (2001). The two schemes are easily reconciled as in Figure 3. The main difference being in the definition of the base of the *T. apoxyexinus* Zone and his belief that the Cenomanian is entirely missing in the Otway Basin. A summary of the palynological details for each sample is presented on Table 1. Throughout, core depths are corrected to log depth as on Table 1.

All informal species names are shown in quotation marks and listed in Section 5 with informal authorship. Names are given in full when first mentioned in the text, but only the genus initial and full species name is given when subsequently mentioned.

Maturity data were generated in the form of Spore Colour Index, and are plotted on Figure 4 Maturity Profile: Thylacine-2. The oil and gas windows on Figure 4 follow the general consensus of geochemical literature. The oil window corresponds to spore colours of light-mid brown (Staplin Spore Colour Index of 2.7) to dark brown (3.6), equivalent to vitrinite reflectance values of 0.6% to 1.3%. Geochemists argue variations on kerogen type, basin type and basin history. The maturity interpretation is thus open to reinterpretation using the basic colour observations as raw data. However, the range of interpretation philosophies is not great, and probably would not move the oil window by more than 200 m.

Raw palynological data are included in Appendix 1. The data are based on a 250+ specimen count in swcs and core from which an indication of marine microplankton to terrestrial palynomorph proportions can be derived. The microplankton percentages are listed in Table 1, which also summarizes other palynological details. Environmental assessments are derived from the palynomorph counts using content and diversity of saline taxa (dinoflagellates and spiny acritarchs), other microplankton (mostly freshwater algae), and terrestrial spores and pollen. The criteria for these assessments are defined in Table 1. However, dinoflagellate content and diversity in the Otway Basin are lower than might be expected from other data sources, especially sedimentology in the offshore marine shales. It may be

that dinoflagellate productivity is suppressed by lowered salinity or restricted oceanic circulation caused by the enclosed nature of a long narrow marine gulf. Environments interpreted here may therefore underestimate marine influence in this section with environments really being more marine than interpreted here. In running text, frequency of taxa is discussed in the following intervals: Very rare = <1%, Rare = 1-3%, Frequent = 4-10%, Common = 11-29%, Abundant = 30-49%, Super-abundant = 50-100%.

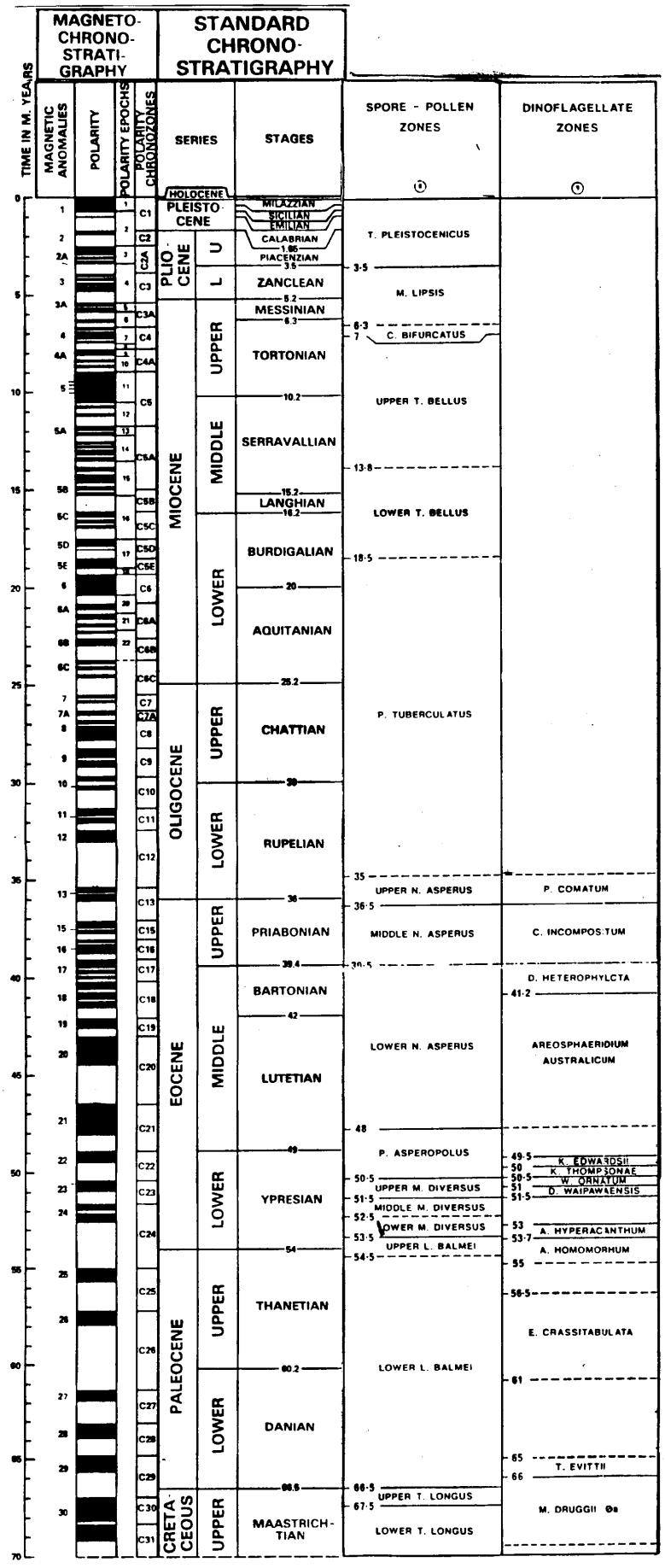


FIGURE 1 **TERTIARY ZONATION SCHEME (Partridge 1976 and pers. comm. using time scale of Haq et al)**

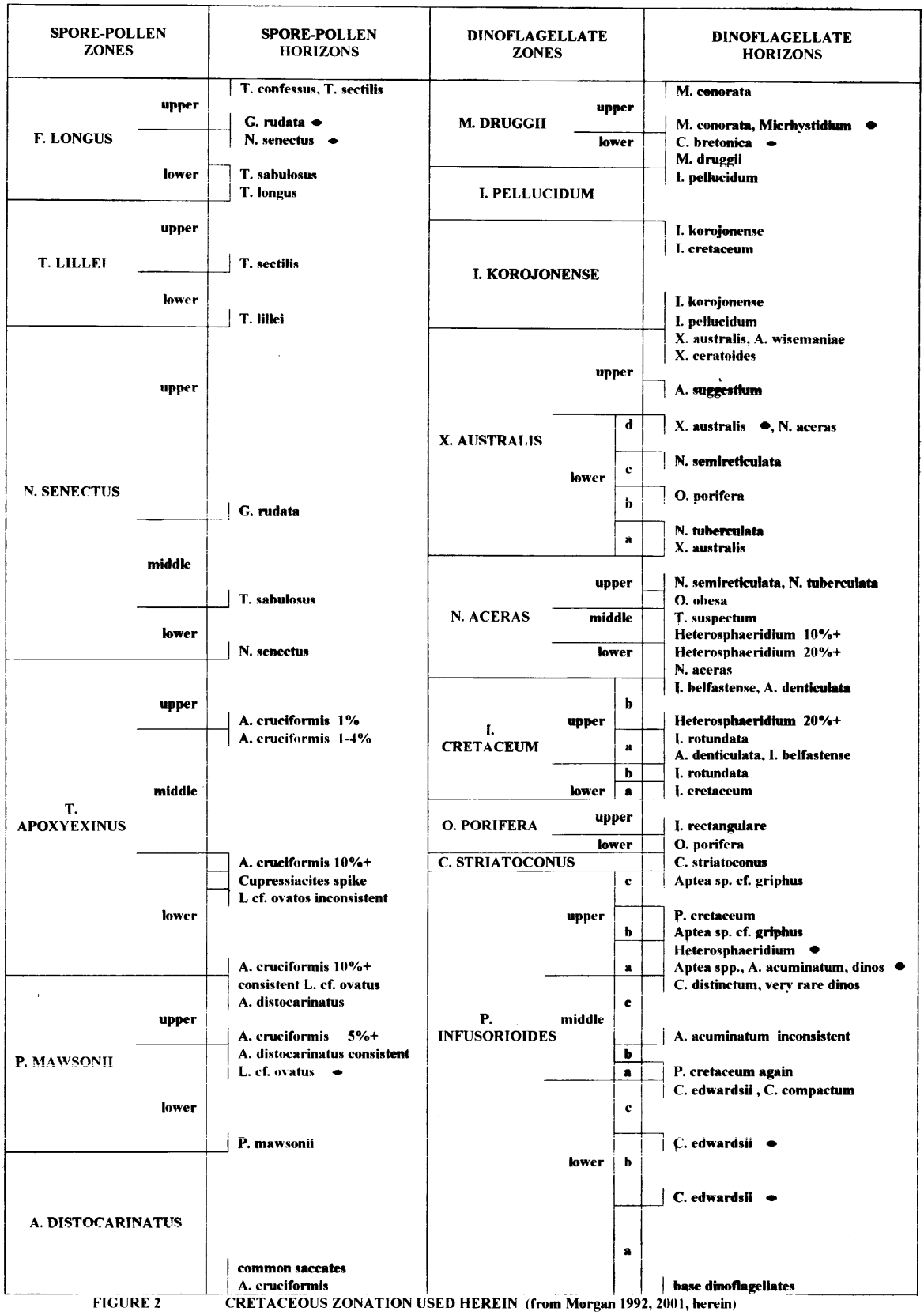


FIGURE 2 CRETACEOUS ZONATION USED HEREIN (from Morgan 1992, 2001, herein)

● = frequent (4-10%) ● = common (11-30%)

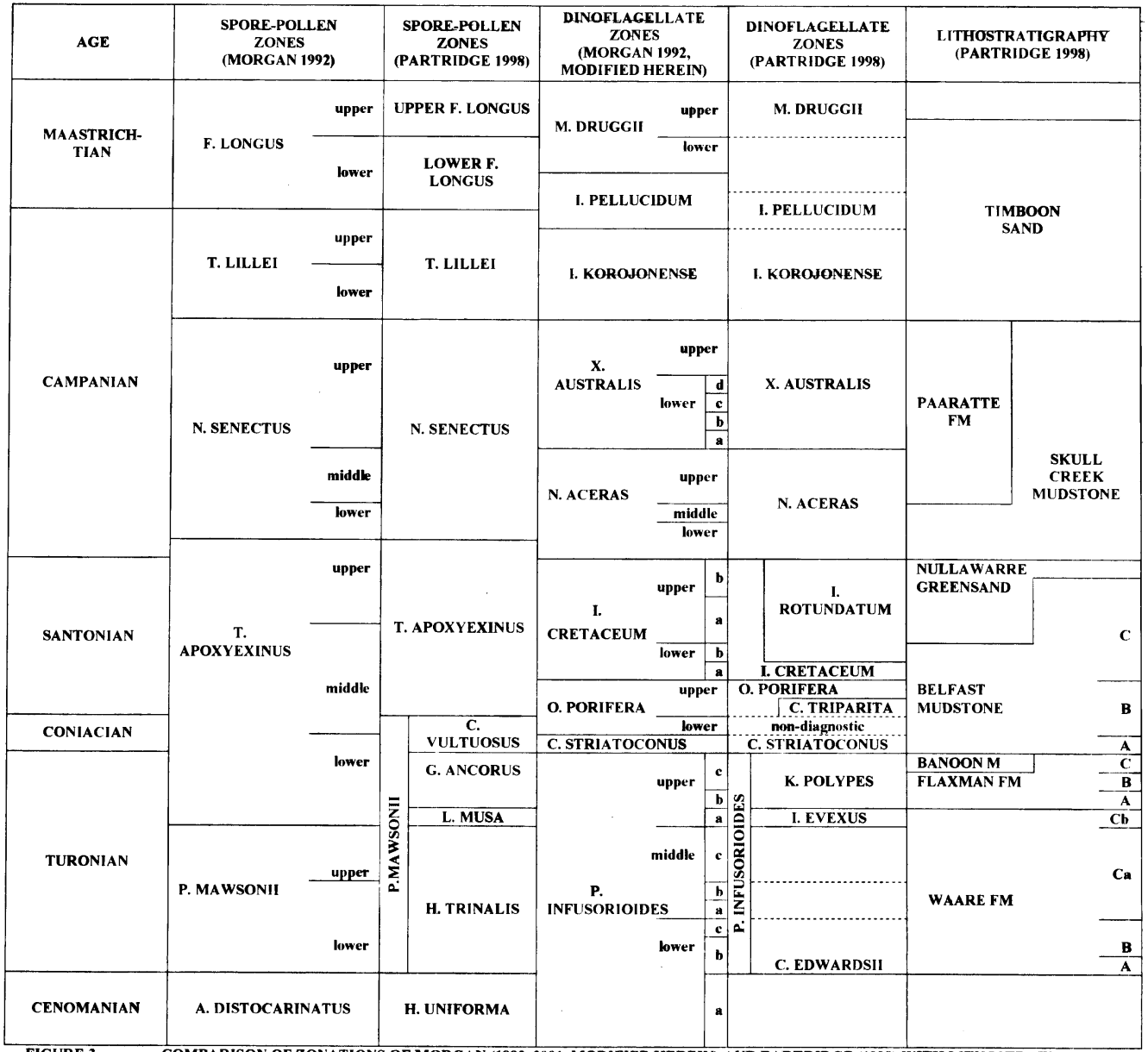
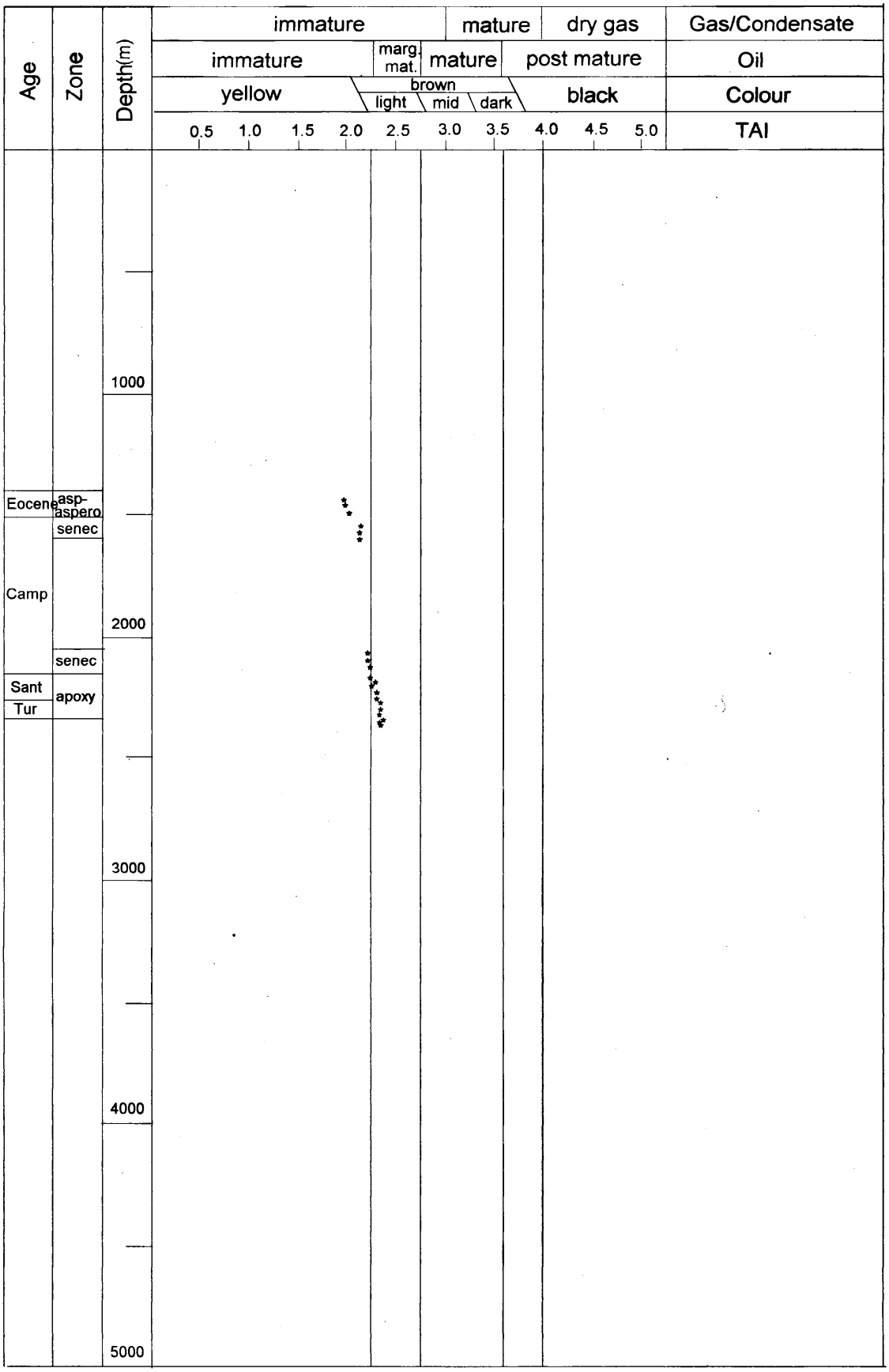


FIGURE 3 COMPARISON OF ZONATIONS OF MORGAN (1992, 2001, MODIFIED HEREIN) AND PARTRIDGE (1998) WITH LITHOSTRATIGRAPHY FROM PARTRIDGE (1998)

FIGURE 4 MATURITY PROFILE : THYLACINE-2



3 PALYNOSTRATIGRAPHY

3.1 1410/20 m (cutts) : *D. heterophlycta* Zone, offshore marine

Assignment is indicated by the presence of *Deflandrea heterophlycta* and *Tritonites inaequalis*. Other taxa supporting the assignment include *Areosphaeridium multispinosum, Deflandrea phosphoritica* and frequent *Systematophora placacantha*. Amongst the microplankton, *Spiniferites ramosus* is super-abundant with common *Operculodinium centrocarpum* and frequent *S. placacantha*. Rare elements include *A. multispinosum, D. heterophlycta, Thalassphora pelagica, Heteraulacysta paxilla* and *T. inaequalis.*

Spores and pollen are minor with frequent *Nothofagidites* spp. including *N. deminutus* and *N. falcata* indicating the *N. asperus* spore-pollen Zone. Subzonal assignment is not possible with so few spores and pollen present, but the associated dinoflagellate zone indicates that the *N. asperus*, (lower) zone would be expected.

Offshore marine environments are indicated by the totally dominant dinoflagellates and minor spore-pollen.

Yellow spore colours indicate immaturity for hydrocarbons.

3.2 1450/60 m (cutts) *: P. asperopolus* Zone, ?shelfal marine

Assignment is indicated by the downhole influx of *Holoragacidites harrisii* at the top, marking the "harrisii reversal" of Stover and Partridge (1973), and at the base by oldest *Proteacidites asperopolus*. Common are *H. harrisii* and *Proteacidites* spp. with frequent *Nothofagidites emarcidus.* Rare elements include *Cupanieidites orthoteichus, Malvacipollis subtilis, N. falcata* (considered caved), *P. asperopolus, Proteacidites clarus, Proteacidites kopiensis* and *Proteacidites pachypolus*.

The dinoflagellates suggest the *D. heterophlycta* Zone (*D. heterophlycta*, *Areosphaeridium arcuatum, Achilleodinium biformoides, Tritonites tricornus*) but are considered caved.

Very common is *S. ramosus* with frequent *S. placacantha* and *O. centrocarpum*, but all are considered caved. Taxa first seen downhole and considered in place include *Cassidium fragile, Diphes colligerum* and *Alisocysta circumtabulata*.

Shelfal marine environments are suggested by subequal proportions of marine dinoflagellates and terrestrial spores and pollen, but the dinoflagellate content may have been enhanced by caving, with more nearshore environments likely.

Yellow spore colours indicate immaturity for hydrocarbons.

3.3 1470/75 m (cutts) : *M. diversus* (lower) Zone – *P. asperopolus* Zone, nearshore marine

Zonal assignment is not possible on the assemblages seen, but assignment somewhere in the interval *M. diversus* (lower) zone to *P. asperopolus* Zone is indicated by youngest *Malvacipolis diversus, Proteacidites grandis* and *Proteacidites tuberculiformis* (the last species seen at 1505/10 m in the sample beneath). Very common are *Proteacidites* spp. with common *Cyathidites* spp., *Dilwynites granulatus* and *Falcisporites similis*. Rare elements include *C. orthoteichus, M. diversus, Periporopollenites demarcatus, P. clarus* and *P. grandis*.

Dinoflagellates are rare and not zone diagnostic, but the presence of *Deflandrea truncata* in this sample and *Deflandrea obliquipes* caved at 1505/10 m beneath, is consistent with the Early Eocene. Frequent is *S. ramosus* with all other elements very rare.

Very nearshore marine environments are suggested by the very few low diversity microplankton and the dominant and diverse spore-pollen.

Yellow spore colours indicate immaturity for hydrocarbons.

3.4 1505/10 m (cutts) – 1535/40 m (cutts) : *X. australis*, (upper) Zone, *N. senectus* (upper) Zone, nearshore marine

Inertinite is dominant. Assignment is indicated by youngest *Xenikoon australis* and *Xenascus ceratoides* without older markers (especially *Nelsoniella aceras*). Microplankton are minor with *Botryococcus* spp. and *Micrhystridium* spp. frequent only at 1505/10 m. Minor caving from the Early Eocene includes *D. obliquipes*.

Spores and pollen are totally dominant and assignment to the *N. senectus* (upper) Zone is indicated by *Gambierina rudata* and *Forcipites sabulosus* without younger

markers. Common are *C. minor, D. granulatus, F. similis* and *Proteacidites* spp. Rare to frequent are *Nothofagidites senectus* and *Nothofagidites endurus*. Rare elements include *G. rudata, Tricolpites confessus, Forcipites stiplatus, F. sabulosus, Peninsulapollis gillii* and at 1505/10 m, *Tricolporites apoxyexinus*. Eocene caving is also present including *P. tuberculiformis* and *P. grandis*.

Marginal marine environments are suggested by the minor low diversity microplankton and the dominant and diverse spores and pollen, but these seem likely to be an underestimate of marine influence. Nearshore marine environments seem more likely.

Yellow to light brown spore colours indicate immaturity for hydrocarbons.

3.5 2060/65 m (cutts) : *N. aceras* (middle) Zone, *N. senectus* Zone, shelfal marine

Inertinite is dominant. Assignment is indicated at the top by youngest *Heterosphaeridium* spp. >10% and youngest *Odontochitinia "obesa"* and at the base by the absence of older markers. Common is *Heterosphaeridium "solida"* with frequent *O. "obesa"* and *Trthryrodinium "marshallii"*. Rare elements include *N. aceras, Odontochitina porifera, Odontochitina cribropoda* and *Spinidinium echinoidea.* Rare *X. australis* is considered caved.

Spores and pollen are dominant but lack angiosperm diversity. Assignment to the *N. senectus* Zone is indicated by the presence of *F. stiplatus,* but subzonal assignment is not possible. Common are *C. minor* and *F. similis* with frequent *D. granulatus, Microcachryidites antarcticus* and *Proteacidites* spp. Rare elements include *Australopollis obscurus, Phyllocladidites mawsonii* and *F. stiplatus*.

Nearshore marine environments are suggested by the subordinate marine dinoflagellates and dominant terrestrial spores and pollen.

Yellow to light brown spore colours indicate immaturity for hydrocarbons.

3.6 2080/85 m (cutts) – 2105/10 m (cutts) : *N. aceras* (lower) Zone, *N. senectus* Zone, shelfal marine

Assignment is indicated at the top by youngest *Heterosphaeridium* spp. >20% coincident with youngest *Eucladinium madurense* and *Trithyrodinium "thick reticulate"*. Assignment is indicated at the base by the absence of older markers. Common is *H. "solida"* with *Palaeohystrichophora infusorioides* frequent only at 2080/85 m. Consistent to rare are *Canningia "scabrata", E. madurense, Heterosphaeridium* cf. *laterobrachius, Maduradinium pentagonum, N. aceras, O. cribropoda, O. porifera* and *T. "thick reticulate"*.

Spores and pollen are common but lack angiosperm diversity. Assignment to the *N. senectus* Zone is indicated by the presence of *F. stiplatus*, but subzonal assignment is not possible. Common are *C. minor* and *F. similis* with frequent *D. granulatus* and *Proteacidites* spp. Rare elements include *Amosopollis cruciformis, P. mawsonii* and *F. stiplatus*.

Shelfal marine environments are suggested by subequal proportions of marine dinoflagellates and terrestrial spores and pollen, but the dinoflagellate content may have been enhanced by caving, with more nearshore environments likely.

Yellow to light brown spore colours indicate immaturity for hydrocarbons.

3.7 2113/16 m (cutts) – 2134/37 m (cutts) : *I. cretaceum* (upper b) Zone, *T. apoxyexinus* (upper) Zone, shelfal marine

Assignment is indicated at the top by youngest *Amphidiadema denticulata* and *Isabelidinium belfastense "belfastense"* and at the base by the absence of older markers (especially *Isabelidinium belfastense"rotundata")*. Common is *H. "solida"* with consistent to frequent *Odontochitina costata, O. porifera, P. infusorioides, T. "marshallii"* and *T. "thick reticulate"*. Possibly caved are rare *N. aceras* and *E. madurense*. Rare elements include *A. denticulata, Chatangiella victoriensis, H.* cf. *laterobrachius* and *I. belfastense "belfastense"*. At 2113/16 m, *A. denticulata* is frequent, a feature seen in nearby wells throughout the subzone. This suggests that the lower part (2122/25 m – 2134/37 m) of the current interval is not seen elsewhere, and is new or expanded.

In a complete section, within the *I. cretaceum* (upper) Zone, the following subzones can be recognised.

upper a subzone = *A. denticulata* and *I. belfastense "befastense"* above youngest *I. belfastense "rotundata"* (2113/15 m – 2134/37 m)
lower a subzone = *I. belfastense "rotundata"* above oldest *A. denticulata* and *I. belfastense "belfastense"* (interval not seen here)

Spores and pollen are common with *A. cruciformis* about 1%, consistent with assignment to the *T. apoxyexinus* (upper) Zone. Common are *C. minor* and *F. similis* with frequent *Dilwynites "pusillum", M. antarcticus, Proteacidites* spp. and *V. pallidus*. *Proteacidites* are near 5% in this interval and 1% or less beneath. Rare elements include *A. cruciformis, A. obscurus* and *P. mawsonii*.

Shelfal marine environments are suggested by subequal proportions of marine dinoflagellates and terrestrial spores and pollen, but the dinoflagellate content may have been enhanced by caving, with more nearshore environments likely.

Light brown spore colours indicate marginal maturity for oil but immaturity for gas/condensate.

3.8 2140/43 m : mixed *I. cretaceum* (lower b) Zone with *O. porifera* (upper) Zone, shelfal marine

Inertinite is dominant. This assemblage is mixed showing two clear elements. Youngest *Isabelidinium rectangulare "rectangulare"* and *I. rectangulare "contractum"* indicate penetration of the *O. porifera* (upper) Zone. However, also present is youngest *I. belfastense "rotundata"* without *A. denticulata* or *I. belfastense "belfastense"*, indicating the *I. cretaceum* (lower b) Zone. This is presumably either present in the upper part of the cuttings interval, or caved from the sample gap 2137 m – 2140 m. It is possible that the *I. cretaceum* (upper a) Zone and the *I. cretaceum* (lower a) Zone intervals are present but undetected. In a complete section, within the *I. cretaceum* (lower) Zone, the following subzones are recognised.

lower a subzone =*I. belfastense "rotundata"* beneath oldest *A. denticulata* and *I. belfastense "belfastense"* (2140/43 m)
lower a subzone = *I. cretaceum* beneath younger markers (interval not seen here)

Common is *H. "solida"* with frequent *Trithyrodinium glabra,* typical of the *I. cretaceum* Zone, not the *O. porifera* Zone. Consistent elements include *Batiacasphaera kekerengensis, C. victoriensis, Odontochitina operculata* and *T.*

"thick reticulate". Rare elements include *I. cretaceum, I. belfastense "rotundata", I. rectangulare "rectangulare"* and *I. rectangulare "contractum"*.

Spores and pollen are common with *A. cruciformis* 5%, within the 1-10% range for the *T. apoxyexinus* (middle) Zone and consistent with the dinoflagellate assignment. Common are *C. minor* and *F. similis* with frequent *A. cruciformis, Osmundacidites wellmanii* and *V. pallidus*. Rare elements include *A. obscurus* and *P. mawsonii*.

Shelfal marine environments are suggested by subequal proportions of marine dinoflagellates and terrestrial spores and pollen, but the dinoflagellate content may have been enhanced by caving, with more nearshore environments likely.

Light brown spore colours indicate marginal maturity for oil but immaturity for gas/condensate.

3.9 2152.31 m (core) – 2236.77 m (core) : *O. porifera* (upper) Zone, *T. apoxyexinus* (?middle) Zone, nearshore to very nearshore marine

Inertinite and cuticle are dominant. Assignment is indicated at the top by *youngest I. rectangulare "rectangulare"* and *I. rectangulare "contractum"* and at the base by oldest occurences of these two, coincident here with oldest *C. victoriensis* and *T. "marshallii"*. Frequent to common is *H. "solida"*. Consistent to frequent are *I. rectangulare "rectangulare", Spiniferites ramosus* and *T. "marshallii"*. Very rare elements include *Aptea "gigantis", C. victoriensis, Hystrichodinium furcatum, O. porifera, Prolixosphaeridium "pandora"* and *Gillinia hymenophora*. Dinoflagellates are richer near the top (2152.31 m – 2157.79 m) and base (2189.50 m – 2236.77 m) and less common in the middle interval (2162.97 m – 2178.34 m). The following events have potential for event stratigraphy and detailed intra-reservoir correlation. Those marked with an asterisk are most likely to provide new subzones in closely sampled sections.

2140/43 m (cutts) : top *I. rectangulare "rectangulare, I. rectangulare "contractum",* top richer dinos
2152.31 m (core) : top *A. "gigantis", H. furcatum*
2157.79 m (core) : base richer dinos, top *P. "pandora"*
2162.97 m (core) : top leaner dinos, influx *A. cruciformis*
2165.97 m (core) : top very consistent *A. "gigantis"*
2175.68 m (core) : minor acme *I. rectangulare*
2178.34 m (core) : base leaner dinos

2189.50 m (core) : top richer dinos*, minor acme *A. "gigantis"*
2222.51 m (core) : top *Chatangiella tripartita**
2229.86 m (core) : renewed top *C. victoriensis*
2232.62 m (core) : renewed top *P. "pandora"*
2234.77 m (core) : minor acme *P. "pandora",* base *O. porifera*
2236.77 m (core) : top *I. rectangulare "diversum"**
: base *C. victoriensis, I. rectangulare "rectangulare", P. "pandora", T. "marshallii"*

Spore pollen assignment is unclear. The dinoflagellate zone suggests correlation with the middle *T. apoxyexinus* Zone, but *A. cruciformis* content varies between 5-10% (suggesting the middle *T. apoxyexinus* Zone) and 10-20% (suggesting the lower *T. apoxyexinus* Zone). In other nearby wells, these features have been seen and are anomolous with the inshore pattern close to the previously BHP acreage. They are being evaluated here, and the dinoflagelle zones are considered a much better basis for correlation. *Proteacidites* spp. are extremely rare in contrast to the overlying section, and this is consistent with the middle *T. apoxyexinus* Zone. Common are *C. minor, F. simils* and *M. antarticus* with intermittently frequent *D. "pusillum", D. granulatus* and *V. pallidus*. Rare elements include *P. mawsonii* and *Ornamentifera sentosa* to the interval base.

Nearshore to very nearshore marine environments are indicated by the subordinate moderate to low diversity dinoflagellates amongst the dominant and diverse spores and pollen.

Light brown spore colours indicate marginal maturity for oil but immaturity for gas/condensate.

3.10 2242.96 m (core) – 2350/56 m (cutts) : *P. infusorioides* (upper) Zone, *T. apoxyexinus* (lower) Zone, nearshore to marginal marine

Dinoflagellate zonal assignment is indicated at the top by youngest consistent/frequent *Aptea* sp. (cf. *gryphus*) coincident with youngest *Kiokansium polypes* and slightly above youngest *Chlamydophorella nyei* (2246.51 m) and at the base by oldest *Aptea* spp., consistent *A. acuminatum* and common dinoflagellates (20%+) The upper part (2242.96 m – 2279.44 m) is dominated by plant debris with minor dinoflagellates. *K. polypes, Circulodinium "solida", Aptea* sp. (cf. *gryphus*) and *Heterosphaeridium* spp. are frequent to consistent. The lower part (2285.62 m – 2350/56.0 m) is dominated by plant debris and is more marine, with common to very

common *H. heteracanthum* and frequent *Botryococcus* sp. and *C. "solida"*. Consistent are *Aptea* spp., *Cribroperidinium* sp., *K. polypes, O. operculata* and *O. complex*. The following dinoflagellate subdivisions can be recognised.

upper c subzone = consistent *Aptea* sp. (cf. *gryphus*) above youngest *P. cretaceum* (2242.96 m – 2259.27 m swc)

upper b subzone = *P. cretaceum* above *Heterosphaeridium* spp. acme (2266.83 m – 2279.44 m)

upper a subzone = *Heterosphaeridium* spp. acme above base *Aptea* spp. (2285.62 m – 2350/56 m)

Within the interval, the following events have further potential for event stratigraphy and detailed local intra-reservoir correlation.

2242.96 m (core) : top consistent *Aptea* sp. (cf. *gryphus*), *K. polypes*
: *Cupressiacites* acme (12%)
2246.51 m (swc) : acme *Aptea* sp. (cf. *gryphus*) (8%), top *C. nyei*
2250.55 m (core) : top inconsistent *L.* cf. *ovatus*
2255.82 m (core) : repeat acme *Aptea* sp. (cf. *gryphus*) (7%)
: base part range consistent *A. acuminatum*
: base frequent *H. "solida"*
2259.27 m (core) : less dinoflagellates
: top *D." pusillum"* acme (40%+)
: *Dilwynites* acme (45%)
2266.83 m (core) : top *P. cretaceum*
2269.03 m (core) : repeat acme *Aptea* sp. (cf. *gryphus*) (10%)
2285.62 m (core) : base *Aptea* sp. (cf. *gryphus*), top *H. heteracanthum* acme (20%)
: top *Aptea* sp. (spiny)
2290.83 m (core) : *A. cruciformis* acme (20%)
: base consistent *P. cretaceum*
2332/41 m (cutts): repeat top *A. acuminatum,*top *Spinidinium* sp.
2350/56 m (cutts): base common dinoflagellates (20%+), base *Aptea* spp.
: base *Spinidinium* sp.

Assignment to the spore-pollen zone is indicated by near 10%+ content of *A. cruciformis*. At the top (2242.96 m) , a *Cupressiacites* spp. spike (12%) is seen and is normally associated with the Banoon Member at the top of the Flaxmans Formation, in the sense of Partridge (1998). Frequent to common at the top (2242.96 m – 2255.82 m) are *Cupressiacites* spp., *C. minor, D. granulatus, D. "pusillum", F. similis* and *M. antarcticus*. In the middle (2259.27 m – 2285.62 m), *D. "pusillum"*

becomes abundant and has been seen in other wells nearby. At the bottom (2290.83 m – 2350/56 m), *A. cruciformis* and *M. antarcticus* become common to abundant. Rare elements throughout include inconsistent *Laevigatosporites* cf. sp. *L. ovatus* (=*L. musa* of Partridge). Occasional specimens of *Appendicisporites distocarinatus* are considered reworked but may be just inconsistent. Permian and occasionally Triassic reworking are mostly minor, but persistent.

Environments are marine throughout, but are mostly nearshore to very nearshore towards the top, and nearshore to shelfal towards the bottom. Overall, transgressian is suggested to a marine maximum at 2303.46 m, then overall regressian above (by the changing dinoflagellate contents).

Light brown spore colours indicate marginal maturity for oil but immaturity for gas/condensate.

4 REFERENCES

Helby, R., Morgan, R., & Partridge, A.D., (1987) A palynological zonation of the Australian Mesozoic. Mem. Assoc. Aust. Palaeontol. 4, 1-94.

Marshall, N.G., (1984) Late Cretaceous dinoflagellates from the Perth Basin, Western Australia. Unpubl. Ph.D. thesis, U.W.A.

McMinn, A., (1986) Dinoflagellate palynostratigraphy of the Late Cretaceous of northwestern Australia Unpubl. Ph.D. thesis, Macquarie University

Morgan, R.P., (1992) Overview of new cuttings based Late Cretaceous correlations, Otway Basin, Australia. Unpubl. rept. for BHPP

Morgan, R.P., (1994) Palynology of BHPP Minerva-2A, Offshore Otway Basin, Victoria, Australia. Unpubl. rept. for BHPP

Morgan, R.P., (2001) Palynology of Thylacine-1, offshore Otway Basin, Australia, Unpubl. rept. for Woodside

Partridge, A.D., (1976) The geological expression of eustacy in the Early Tertiary of the Gippsland Basin APEA Journal 16 (1), 73-79

Partridge, A.D., (1997) New Upper Cretaceous palynology of the Sherbrook Group, Otway Basin In Victoria Supplement PESA News April/May, 9

Partridge, A.D., (2001) Revised stratigraphy of the Sherbrook Group, Otway Basin In Hill K.C. and Bernecker T. (Eds) Eastern Australasian Basin Symposium, a refocussed energy perspective for the future PESA spec. Publ. 455-464

Stover, L.E., and Partridge, A.D., (1973) Tertiary and Late Cretaceous spores and pollen from the Gippsland Basin, southeastern Australia Proc. Roy. Soc. Vic. 85, 237-286

5 UNPUBLISHED NAMES

Dinoflagellates

Aptea "gigantis"	Morgan
Aptea sp. (cf. *gryphus*)	Morgan (=*V. gryphus* sensu Partridge)
Aptea "spiny"	Morgan
Aptea "loopy"	Morgan, herein
Aptea polymorpha cf.	Morgan, herein
Canningia "scabrata"	Morgan
Circulodinium "solida"	Morgan
Cribroperidinium sp.	Morgan
Heterosphaeridium cf. *laterobrachius*	Morgan
Heterosphaeridium "hidesi"	Morgan
Heterosphaeridium "minutum"	Morgan
Heterosphaeridium "solida"	Morgan
Isabelidinium belfastense "belfastense"	Marshall (1984)
Isabelidinium belfastense "rotundata"	Marshall (1984)
Isabelidinium rectangulare "contractum"	Marshall (1984)
Isabelidinium rectangulare "diversum"	Marshall (1984)
Isabelidinium rectangulare "rectangulare"	Marshall (1984)
Occisucysta "septata"	Marshall (1984)
Odontochitina "obesa"	Morgan
Odontochitina "stubby"	Morgan
Odontochitina "triangulata"	Marshall (1984)
Prolixosphaeridium "pandora"	Morgan
Spinidinium cf. *sverdrupiana*	Morgan
Spinidinium sp.	Morgan
Trithyrodinium "thick reticulate"	Morgan
Trithyrodinium "marshallii"	Morgan

Spores and Pollen

Dilwynites "pusillum"	Partridge
Gleicheniidites sp. "(thick)"	Morgan (?=*G. "ancorus"* Partridge)
Laevigatosporites cf. *ovatus*	Morgan (=*L. musa* Partridge)
Perotriletes "baldii"	Morgan

TABLE 1: SUMMARY PALYNOLOGICAL DATA, THYLACINE-2

RT= 25 m

LOG DEPTH [mbRT]	CORE DEPTH [mbRT]	SAMPLE TYPE	ORGANIC YIELD *1	MICROFOSSIL YIELD	PRESERVATION *2	PERCENTAGE				DIVERSITY *3		DINOFLAGELLATE ZONE	SPORE-POLLEN ZONE	ENVIRONMENT *4
						MICROPLANKTON			SPORE-POLLEN	MICROPLANKTON	SPORE-POLLEN			
						DINOFLAG.	SPINY AC.	OTHER						
1410/20		CUTTS	0.129	HIGH	EXCELLENT	93	1	0	6	HIGH	MODERATE	D. HETEROPHLYCTA	N. ASPERUS	OFFSHORE
1450/60		CUTTS	0.033	MODERATE	EXCELLENT	34	5	5	56	HIGH	HIGH		P. ASPEROPOLUS	?SHELFAL
1470/75		CUTTS	0.198	MODERATE	EXCELLENT	5	3	0	92	LOW	VERY HIGH		M. DIVERS-P. ASPERO	VERY NEARSHORE
1505/10		CUTTS	0.06	MODERATE	GOOD	3	3	4	90	MODERATE	VERY HIGH	X. AUSTRALIS, UPPER	N. SENECTUS (UPPER)	?MARGINAL
1535/40		CUTTS	0.065	MODERATE	GOOD	1	0	3	96	LOW	VERY HIGH	X. AUSTRALIS, UPPER	N. SENECTUS (UPPER)	?MARGINAL
2060/65		CUTTS	0.067	MODERATE	GOOD	30	0	1	69	MODERATE	HIGH	N. ACERAS, MIDDLE	N. SENECTUS	NEARSHORE
2080/85		CUTTS	0.053	MODERATE	GOOD	41	0	5	54	HIGH	HIGH	N. ACERAS, LOWER	N. SENECTUS	SHELFAL
2105/10		CUTTS	0.025	MODERATE	GOOD	37	0	3	60	MODERATE	HIGH	N. ACERAS, LOWER	N. SENECTUS	SHELFAL
2113/16		CUTTS	0.053	MODERATE	GOOD	43	0	0	57	HIGH	HIGH	I. CRETACEUM, UPPER b	T. APOXYEXINUS (UPPER)	SHELFAL
2122/25		CUTTS	0.071	MODERATE	GOOD	48	<1	2	48	HIGH	HIGH	I. CRETACEUM, UPPER b	T. APOXYEXINUS (UPPER)	SHELFAL
2134/37		CUTTS	0.065	MODERATE	GOOD	49	0	1	50	HIGH	HIGH	I. CRETACEUM, UPPER b	T. APOXYEXINUS (UPPER)	SHELFAL
2140 / 43		CUTTS	0.031	LOW	GOOD	43	2	4	51	HIGH	HIGH	O. POR, UP & I. CRET, LOW b	T. APOXYEXINUS (MIDDLE)	SHELFAL
2152.31	2150.34	CORE	0.033	LOW	GOOD	10	1	9	80	MODERATE	VERY HIGH	O. PORIFERA (UPPER)	T. APOXYEXINUS (?MIDDLE)	VERY NEARSHORE
2157.79	2155.82	CORE	0.093	LOW	GOOD	12	2	5	81	MODERATE	HIGH	O. PORIFERA (UPPER)	T. APOXYEXINUS (?MIDDLE)	NEARSHORE
2162.97	2161.00	CORE	0.085	LOW	GOOD	8	0	11	81	MODERATE	HIGH	O. PORIFERA (UPPER)	T. APOXYEXINUS (?MIDDLE)	VERY NEARSHORE
2165.97	2164.00	CORE	0.070	LOW	GOOD	15	0	12	73	HIGH	HIGH	O. PORIFERA (UPPER)	T. APOXYEXINUS (?MIDDLE)	NEARSHORE
2173.97	2172.00	CORE	0.060	LOW	GOOD	9	1	11	79	MODERATE	HIGH	O. PORIFERA (UPPER)	T. APOXYEXINUS (?MIDDLE)	VERY NEARSHORE
2175.68	2173.71	CORE	0.031	LOW	GOOD	14	0	12	74	MODERATE	HIGH	O. PORIFERA (UPPER)	T. APOXYEXINUS (?MIDDLE)	NEARSHORE
2178.34	2176.37	CORE	0.100	LOW	GOOD	4	0	7	89	LOW	HIGH	O. PORIFERA (UPPER)	T. APOXYEXINUS (?MIDDLE)	MARGINAL
2189.50	2187.53	CORE	0.038	LOW	GOOD	15	0	14	71	MODERATE	HIGH	O. PORIFERA (UPPER)	T. APOXYEXINUS (?MIDDLE)	NEARSHORE
2197.15	2195.95	CORE	0.028	LOW	GOOD	10	0	12	78	MODERATE	HIGH	O. PORIFERA (UPPER)	T. APOXYEXINUS (?MIDDLE)	VERY NEARSHORE
2222.51	2220.95	CORE	0.042	LOW	GOOD	14	0	12	74	HIGH	HIGH	O. PORIFERA (UPPER)	T. APOXYEXINUS (?MIDDLE)	NEARSHORE
2229.86	2228.30	CORE	0.118	LOW	GOOD	17	0	10	73	MODERATE	HIGH	O. PORIFERA (UPPER)	T. APOXYEXINUS (?MIDDLE)	NEARSHORE
2232.62	2231.06	CORE	0.165	LOW	GOOD	14	0	9	77	MODERATE	HIGH	O. PORIFERA (UPPER)	T. APOXYEXINUS (?MIDDLE)	NEARSHORE
2234.77	2233.00	CORE	0.157	LOW	GOOD	27	<1	11	62	HIGH	HIGH	O. PORIFERA (UPPER)	T. APOXYEXINUS (?MIDDLE)	NEARSHORE
2236.77	2235.00	CORE	0.130	LOW	GOOD	25	0	9	66	MODERATE	HIGH	O. PORIFERA (UPPER)	T. APOXYEXINUS (?MIDDLE)	NEARSHORE
2242.98	2241.47	CORE	0.097	MODERATE	GOOD	4	0	1	95	LOW	MODERATE	P. INFUSORIOIDES (UPPER c)	T. APOXYEXINUS (LOWER)	MARGINAL
2246.51	2245.00	CORE	0.069	MODERATE	GOOD	28	0	4	68	MODERATE	MODERATE	P. INFUSORIOIDES (UPPER c)	T. APOXYEXINUS (LOWER)	NEARSHORE
2250.55	2248.73	CORE	0.094	MODERATE	GOOD	9	2	0	89	MODERATE	HIGH	P. INFUSORIOIDES (UPPER c)	T. APOXYEXINUS (LOWER)	VERY NEARSHORE
2255.82	2254.00	CORE	0.073	MODERATE	GOOD	41	0	8	51	MODERATE	MODERATE	P. INFUSORIOIDES (UPPER c)	T. APOXYEXINUS (LOWER)	SHELFAL
2259.27	2257.45	CORE	0.100	MODERATE	GOOD	6	0	4	90	MODERATE	HIGH	P. INFUSORIOIDES (UPPER c)	T. APOXYEXINUS (LOWER)	VERY NEARSHORE
2266.83	2266.00	CORE	0.063	MODERATE	GOOD	13	0	7	80	HIGH	HIGH	P. INFUSORIOIDES (UPPER b)	T. APOXYEXINUS (LOWER)	NEARSHORE
2269.03	2268.20	CORE	0.045	MODERATE	GOOD	19	1	10	70	HIGH	MODERATE	P. INFUSORIOIDES (UPPER b)	T. APOXYEXINUS (LOWER)	NEARSHORE
2272.83	2272.00	CORE	0.061	MODERATE	GOOD	16	<1	13	71	HIGH	HIGH	P. INFUSORIOIDES (UPPER b)	T. APOXYEXINUS (LOWER)	NEARSHORE
2279.44	2278.61	CORE	0.059	MODERATE	GOOD	21	0	7	72	MODERATE	HIGH	P. INFUSORIOIDES (UPPER b)	T. APOXYEXINUS (LOWER)	NEARSHORE
2285.62	2284.79	CORE	0.050	MODERATE	GOOD	34	0	15	51	MODERATE	MODERATE	P. INFUSORIOIDES (UPPER b)	T. APOXYEXINUS (LOWER)	SHELFAL
2290.83	2290.00	CORE	0.093	HIGH	GOOD	31	2	20	47	HIGH	HIGH	P. INFUSORIOIDES (UPPER a)	T. APOXYEXINUS (LOWER)	NEARSHORE
2294.83	2294.00	CORE	0.092	HIGH	GOOD	41	0	9	50	MODERATE	HIGH	P. INFUSORIOIDES (UPPER a)	T. APOXYEXINUS (LOWER)	SHELFAL
2303.46	2302.63	CORE	0.197	HIGH	GOOD	43	0	11	46	MODERATE	HIGH	P. INFUSORIOIDES (UPPER a)	T. APOXYEXINUS (LOWER)	SHELFAL
2308.71	2307.88	CORE	0.060	HIGH	GOOD	33	0	13	54	MODERATE	HIGH	P. INFUSORIOIDES (UPPER a)	T. APOXYEXINUS (LOWER)	NEARSHORE
2314.18	2313.35	CORE	0.062	HIGH	GOOD	28	0	12	60	MODERATE	HIGH	P. INFUSORIOIDES (UPPER a)	T. APOXYEXINUS (LOWER)	NEARSHORE
2323/32		CUTTS	0.03	HIGH	EXCELLENT	45	0	22	33	MODERATE	MODERATE	P. INFUSORIOIDES (UPPER a)	T. APOXYEXINUS (LOWER)	SHELFAL
2332/41		CUTTS	0.064	HIGH	EXCELLENT	43	0	12	45	MODERATE	HIGH	P. INFUSORIOIDES (UPPER a)	T. APOXYEXINUS (LOWER)	SHELFAL
2341/50		CUTTS	0.068	HIGH	EXCELLENT	23	0	13	64	MODERATE	HIGH	P. INFUSORIOIDES (UPPER a)	T. APOXYEXINUS (LOWER)	NEARSHORE
2350/56		CUTTS	0.046	HIGH	EXCELLENT	21	0	14	65	MODERATE	HIGH	P. INFUSORIOIDES (UPPER a)	T. APOXYEXINUS (LOWER)	NEARSHORE

*1 ORGANIC YLD=VOL(cc)/WGHT(g)
<0.01 : EXTREMELY LOW
0.01 - 0.10 : LOW
0.1 - 0.5 : MODERATE
>0.5 : HIGH

*2 NOTE:PRESERVATION
(FRAGMENTATION INDEX)
1 = SUPERB
2 = EXCELLENT
3 = GOOD
4 = FAIR
5 = POOR

*3 DIVERSITY	
V HIGH	30+ SPECIES
HIGH	20-29 SPECIES
MOD	10-19 SPECIES
LOW	5-9 SPECIES
EX LOW	1-4 SPECIES

*4 ENVIRONMENTS	DINOFLAGELLATE CONTENT %	DINOFLAGELLATE DIVERSITY	FRESHWATER ALGAE CONTENT%
OFFSHORE MARINE	67 to 100	VERY HIGH	LOW
SHELFAL MARINE	34 to 66	HIGH	"
NEARSHORE MARINE	11 to 33	MODERATE	"
VERY NEARSHORE MARINE	5 to 10	MODERATE-LOW	"
MARGINAL MARINE	<1 to 4	LOW-VERY LOW	"
BRACKISH	0, SPINY ACRITARCHS ONLY	EXTREMELY LOW	"
NON-MARINE (UNDIFF)	0, NO SPINY ACRITARCHS	NIL	LOW <3
NON-MARINE (LACUSTRINE)	0, NO SPINY ACRITARCHS	NIL	MODERATE 3-10+

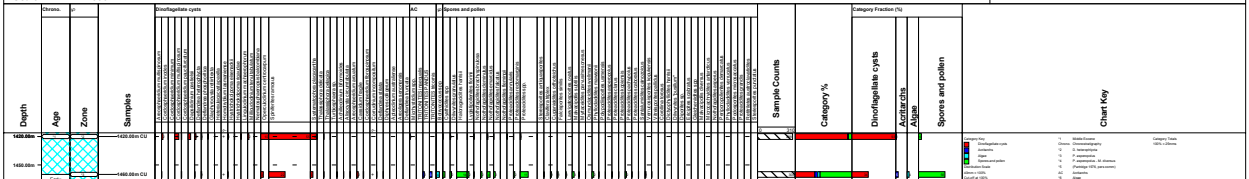
TABLE 2: SUMMARY OF SAMPLE LITHOLOGIES, THYLACINE-2
RT= 25 m

LOG DEPTH [mbRT]	CORE DEPTH [mbRT]	SAMPLE TYPE	LITHOLOGY
1410/20		CUTTS	MED GY SLTST
1450/60		CUTTS	MED GY SLTST/SST
1470/75		CUTTS	DK GY SLTST
1505/10		CUTTS	MED GY SLTST
1535/40		CUTTS	MED GY SLTST
2040/43		CUTTS	MED GY SLTST
2060/65		CUTTS	MED GY SLTST
2080/85		CUTTS	MED GY SLTST [above casing]
2105/10		CUTTS	MED GY SLTST [below casing]
2113/16		CUTTS	MED DK GY SLTST
2122/25		CUTTS	MED DK GY SLTST
2134/37		CUTTS	MED DK GY SLTST
2152.31	2150.34	CORE	LT GY SILT SST., COARSELY BIOTURB.
2157.79	2155.82	CORE	MED GY SLTST., LAMINATED, BIOTURB.
2162.97	2161.00	CORE	MED GY SLTST., LAMINATED, BIOTURB.
2165.97	2164.00	CORE	MED GY SLTST., LAMINATED, BIOTURB.
2173.97	2172.00	CORE	MED GY SLTST., LAMINATED, BIOTURB.
2175.68	2173.71	CORE	MED GY SANDY SLTST., LAMINATED, BIOTURB.
2178.34	2176.37	CORE	DK GY SLTST., LAMINATED, 5 CM BAND
2189.50	2187.53	CORE	DK GY SILTY SST., LAMINATED, 30 CM BAND
2197.15	2195.95	CORE	DK GY SILTY SST., LAMINATED, 30 CM BAND
2222.51	2220.95	CORE	DK GY SILTY SST., LAMINATED, 10 CM BAND
2229.86	2228.30	CORE	DK GY SLTST., LAMINATED,10 CM BAND
2232.62	2231.06	CORE	DK GY SLTST., TOP OF MASSIVE INTERVAL
2234.77	2233.00	CORE	DK GY CLYST; MASSIVE
2236.77	2235.00	CORE	DK GY CLYST; MASSIVE
2242.98	2241.47	CORE	DK GY SLTST, F. LAM.
2246.51	2245.00	CORE	DK GY CLYST; MASSIVE
2250.55	2248.73	CORE	DK GY SLTST, COARSELY BIOTURB.
2255.82	2254.00	CORE	DK GY SLTST, COARSELY BIOTURB.
2259.27	2257.45	CORE	DK GY SLTST, FINELY BIOTURB.
2266.83	2266.00	CORE	DK GY SLTST, LAMINATED
2269.03	2268.20	CORE	DK GY SLTST, COARSELY BIOTURB.
2272.83	2272.00	CORE	DK GY SLTST
2279.44	2278.61	CORE	DK GY SLTST, FINELY BIOTURB.
2285.62	2284.79	CORE	DK GY SLTST, COARSELY BIOTURB.
2290.83	2290.00	CORE	DK GY SLTST, FINELY BIOTURB.
2294.83	2294.00	CORE	DK GY SLTST, FINELY BIOTURB.
2303.46	2302.63	CORE	DK GY SLTST, COARSELY BIOTURB., LAM.
2308.71	2307.88	CORE	DK GY SLTST, COARSELY BIOTURB.
2314.18	2313.35	CORE	DK GY SLTST, COARSELY BIOTURB., LAM.
2323/32		CUTTS	MED GY SLTST
2332/41		CUTTS	MED DK GY SLTST
2341/50		CUTTS	MED DK GY SLTST/SST
2350/56		CUTTS	MED DK GY SLTST/SST

Well Name : THYLACINE-2 TERTIARY
Operator :
Interval : 1420.00m - 1475.00m
Scale : 1:2000

THYLACINE-2 Tertiary Interpretive Data
Style : % Abundance Histogram
Author : Roger Morgan
Date : 28-February-2002
Palynology Distribution Chart

Morgan Palaeo Associates
South Australia



Well Name : THYLACINE-2 CRETACEOUS
Operator : WOODSIDE ENERGY LTD
Interval : 1510.00m - 2356.00m
Scale : 1:2000

THYLACINE-2 Cretaceous Interpretive Data
Style : % Abundance Histogram
Author : Roger Morgan
Date : 28-February-2022
Palynology Distribution Chart

Morgan Palaeo Associates
South Australia

Depth | Chrono. | Age | Zone | Sub Zone | Samples | Dinoflagellate cysts | Ac | Algae | Spores and pollen | Sample Counts | Category % | Category Fraction (%) | Dinoflagellate cysts | Acritarchs | Foram test linings | Algae | Spores and pollen | ChartKey

Cenomanian | Turonian | Santonian | Campanian

P. striatoconus | C.? pellucida | N. acuta | H. stellata

upper A | upper B | upper C | upper D | upper E | upper F | upper G | upper H | upper I | upper J | upper K | upper L | upper M | upper N | upper O | upper P | upper Q | upper R | upper S | upper T | upper U | upper V | upper W | upper X | upper Y | upper Z

1510.00m CU
1540.00m CU
2065.00m CU
2068.00m CU
2110.00m CU
2116.00m CU
2120.00m CU
2127.00m CU
2143.00m CU
2152.31m CO
2157.79m CO
2162.97m CO
2165.97m CO
2170.97m CO
2175.66m CO
2178.34m CO
2189.09m CO
2197.15m CO
2202.91m CO
2228.86m CO
2232.82m CO
2240.77m CO
2242.86m CO
2246.51m CO
2250.59m CO
2255.93m CO
2258.27m CO
2266.83m CO
2270.83m CO
2273.83m CO
2278.44m CO
2286.83m CO
2290.83m CO
2294.83m CO
2303.46m CO
2306.71m CO
2314.15m CO
2318.15m CO
2322.15m CO
2350.00m CU
2356.00m CU

Category Key
Dinoflagellate cysts
Acritarchs
Foram test linings
Algae
Spores and pollen
Distribution Scale
Above = 50%
Cut-off at 100%
Chrono. Chronostratigraphy
C. = Cretaceous, P. = Paleo
U. = Upper, L. = Lower
L. (AMP, GSE, modified)
AC = Acritarchs
FT = Foram test linings
Category Totals
100% = 20mms

APPENDIX 6
PETROLOGY REPORT

RESERVOIR SOLUTIONS PTY LTD
LEVEL 2, 2 PARK RD, MILTON, 4064, QLD
PO BOX 2098, MILTON, 4064, QLD
ABN 27 088 995 073

PETROLOGY, DIAGENESIS AND RESERVOIR QUALITY OF SAMPLES FROM THYLACINE-2 (T/30P) AND GEOGRAPHE-1 (VIC/P43)

Julian C. Baker PhD

A report to:

Woodside Energy Ltd.
1 Adelaide Terrace
Perth WA 6000

31 July, 2002

C O N T E N T S

Page

EXECUTIVE SUMMARY **1**

1. INTRODUCTION **2**

2. ANALYTICAL PROGRAM

2.1 THIN-SECTION ANALYSIS **2**

2.2 X-RAY DIFFRACTION ANALYSIS **2**

2.3 SCANNING ELECTRON MICROSCOPY **2**

3. TEXTURE **4**

4. THIN-SECTION COMPOSITION **4**

5. X-RAY DIFFRACTION ANALYSES **11**

6. DIAGENESIS **13**

7. RESERVOIR QUALITY

7.1 GENERAL **15**

7.2 SAMPLES **23**

8. SUMMARY AND CONCLUSIONS **25**

REFERENCES **26**

KEY TO PLATES IN APPENDIX 4 ..... **27**

C O N T E N T S cont.

Page

FIGURES

FIGURE 1. GRAIN SIZE/SORTING CROSS-PLOT 6
FIGURE 2. QFR COMPOSITIONS 9
FIGURE 3. DIAGENETIC PARAGENESIS 14
FIGURE 4. POROSITY/PERMEABILITY CROSS-PLOT 16
FIGURE 5. VISIBLE POROSITY/PERMEABILITY CROSS-PLOT 18
FIGURE 6. MEAN GRAIN SIZE/PERMEABILITY CROSS-PLOT 19
FIGURE 7. CLAY + MRF/PERMEABILITY CROSS-PLOT - T-2 20
FIGURE 8. KAOLIN/PERMEABILITY CROSS-PLOT (T-1 & -2) 21
FIGURE 9. CLAY + SIDERITE/PERMEABILITY CROSS-PLOT - G-1 22
FIGURE 10. FERROAN CARBONATE/GRAIN DENSITY CROSS-PLOT .. 24

TABLES

TABLE 1. ANALYSES PERFORMED 3
TABLE 2. TEXTURE 5
TABLE 3. THIN-SECTION COMPOSITION AND QFR RATIOS 7
TABLE 4. BULK-ROCK XRD ANALYSES 12

APPENDICES

APPENDIX 1. GRAIN SIZE COMPARISON TABLE
APPENDIX 2. GRAIN SIZE FREQUENCY CURVES
APPENDIX 3. X-RAY DIFFRACTOGRAMS
APPENDIX 4. PHOTOMICROGRAPHS

EXECUTIVE SUMMARY

A petrological study was carried out on thirteen core samples from Thylacine-2 (2153.10-2300.80m) and Geographe-1 (1832.47m). Analytical techniques used were thin-section analysis, quantitative bulk-rock X-ray diffraction analysis and scanning electron microscopy.

Samples from 2153.10-2300.80m in Thylacine-2 are very fine to lower medium grained sublitharenites and litharenites and upper medium to very coarse grained quartzarenites. Geographe-1 (1832.47m) is a lower medium grained litharenite. Framework grains are mainly quartz and also include K-feldspar (absent in samples from below 2218.40m in Thylacine-2), metamorphic rock fragments, sedimentary rock fragments, mica, glauconite, organics and accessory heavy minerals. Compositional maturity increases below 2218.40m in Thylacine-2.

Some of the finer sandstones contain minor detrital clay that is concentrated within scattered burrow infills and along fine, discontinuous laminae. Authigenic clay ranges up to 26.1% and is mainly kaolin (kaolinite, dickite) that occurs where labile grains have altered. Illitic remnants of micaceous precursor grains are locally associated with authigenic kaolin, and minor authigenic illite is associated with partly altered and compactionally deformed micaceous/argillaceous metamorphic rock fragments.

Diagenetic effects besides authigenic clay formation include ductile grain/authigenic clay compaction, grain contact dissolution, labile grain dissolution, cementation by quartz overgrowths, and cementation/replacement by siderite and ankerite.

Porosity reduction is mainly the result of authigenic clay formation, ductile grain/clay compaction, grain contact dissolution, quartz overgrowth cementation and localised ankerite cementation. Unlike the finer sandstones, upper medium to very coarse grained sandstones were quartzose at the time of accumulation and thus were not susceptible to significant authigenic clay formation and physical compaction.

In the very fine to lower medium grained sandstones, visible porosity ranges up to 3.8% and is accounted for mostly by scattered secondary mouldic/intragranular grain dissolution pores and subordinate primary intergranular pores. Upper medium to very coarse grained sandstones contain 10.2-19.8% visible porosity, nearly all of which is accounted for by primary intergranular pores and subordinate secondary intergranular grain dissolution pores.

Reservoir quality in Thylacine-2 is controlled mainly by grain size and authigenic kaolin + metamorphic rock fragment content. Permeability increases with increasing grain size partly because clay + metamorphic rock fragment content decreases with increasing grain size. Earlier work has shown that permeability variation in Geographe-1 (1814.10-1908.90m) largely reflects differences in detrital clay and siderite content.

Most very fine to lower medium grained sandstones from Thylacine-2 and Geographe-1 have less than 30mD permeability, whereas upper medium to very coarse grained sandstones from Thylacine-2 have 199-5960mD permeability.

1. INTRODUCTION

A petrological study was carried out on twelve core samples from 2153.10-2300.80m in Thylacine-2 (T/30P) and one core sample from 1832.47m in Geographe-1 (VIC/P43) in order to provide information on texture, mineralogy, diagenesis and controls on reservoir quality. A list of sample depths, analyses performed and routine core analyses carried out by Core Laboratories Australia Pty Ltd is given in Table 1. Complementary petrological and geochemical data on the same sections in Thylacine-1 and -2 and Geographe-1 are given in Baker (2001, 2002a,b,c).

2. ANALYTICAL PROGRAM

2.1 THIN-SECTION ANALYSIS

Polished thin-sections were cut in kerosene and impregnated with blue dyed epoxy resin to assist in porosity recognition. Mineral composition and visible porosity were determined by a count of 400 points in all thin-sections, and grain size and sorting of all thin-sections were determined by measuring the long dimension of 100 point-counted quartz grains. From the grain size measurements, mean grain size and sorting (ϕ standard deviation, Trask) were calculated. Photomicrographs were taken of each thin-section to illustrate texture, composition, clay distribution, diagenetic effects and porosity.

2.2 X-RAY DIFFRACTION ANALYSIS

Bulk-rock X-ray diffraction (XRD) analysis was carried out on all samples in order to quantify mineral abundance. The XRD analysis used a finely ground whole rock powder sample and the SIROQUANT processing technique was used to calculate mineral abundance. Fine-fraction XRD analyses were not carried out.

2.3 SCANNING ELECTRON MICROSCOPY

Scanning electron microscopy (SEM) was carried out on freshly broken surfaces of ten samples to provide information on clay distribution, paragenetic relationships and porosity characteristics. An energy dispersive spectrometer (EDS) attached to the SEM provided qualitative elemental data on clays and carbonate cements.

TABLE 1. ANALYSES PERFORMED

Well	Sample #	Depth (mRT)	PETROLOGICAL ANALYSES					CORE ANALYSES		
			MA	GSA	XRD	SEM	PM	Por (%)*	Perm (mD)* †	GD (g/cc)
Thylacine-2	5	2153.10	X	X	X	X	X	13.8	0.409	2.64
"	44	2185.55	X	X	X	-	X	15.4	0.728	2.70
"	97	2207.84	X	X	X	X	X	22.1	25.1	2.90
"	128	2218.40	X	X	X	X	X	11.8	0.445	2.66
"	181	2249.85	X	X	X	X	X	19.7	9.21	2.66
"	186	2251.20	X	X	X	-	X	14.7	0.692	2.76
"	187	2251.59	X	X	X	X	X	17.1	1.16	2.79
"	205	2275.17	X	X	X	X	X	19.8	199	2.65
"	234	2296.94	X	X	X	-	X	24.8	5260	2.65
"	241	2299.40	X	X	X	X	X	21.9	5960	2.65
"	244	2300.20	X	X	X	X	X	12.4	0.840	2.67
"	246	2300.80	X	X	X	X	X	16.0	9.64	2.74
Geographe-1	57H	1832.47	X	X	X	X	X	18.7	15.7	2.67

MA = modal analysis GSA = grain size analysis XRD = quantitative bulk-rock X-ray diffraction analysis SEM = scanning electron microscopy PM = photomicroscopy

* ambient † air

3. TEXTURE

Texture is given in Table 2, a grain size comparison table is included in Appendix 1, and grain size frequency curves are given in Appendix 2.

All samples except #234 and #241 are moderately-well to well sorted, very fine to medium grained sandstones with a mean grain size between 0.12mm and 0.40mm. Sample #234 is a well sorted, coarse grained sandstone, and #241 is a poorly sorted, very coarse grained sandstone.

Although #241 is poorly sorted and very coarse grained according to the grain size analysis, it actually consists of ?interbedded well sorted coarse grained sandstone (with widely scattered pebbles) and moderately-well sorted granule conglomerate, which together produce two distinct grain size modes.

Samples #5 and #181 contain sporadic, argillaceous burrow infills and fine argillaceous laminae, #186 includes a single, fine, argillaceous/carbonaceous/sideritic lamination, #187 contains scattered argillaceous/sandy burrow infills, and #244 and #246 include sporadic thin sideritic laminae.

Samples #44, #97, #128, #205, #234 and #57H are massive, grain supported sandstones that contain little (<0.4%) or no detrital clay.

Grain size and sorting are weakly (R^2 = -0.471) negatively correlated. The correlation is even weaker (R^2 = -0.260) if all available grain size and sorting data for Thylacine-2 and Geographe-1 (from Baker 2002a,b) are combined (Fig. 1). Figure 1 shows that most fine to lower medium grained sandstones are moderately-well to well sorted, whereas most upper medium to very coarse grained sandstones are moderately to moderately-well sorted.

Ignoring quartz overgrowths and the effects of grain contact dissolution, most quartz grains are subangular to subrounded, although angular and rounded quartz grains are also common in the finest and coarsest sandstones, respectively.

4. THIN-SECTION COMPOSITION

Thin-section composition and QFR ratios are shown in Table 3, and QFR ratios are plotted in Figure 2. Data summary sheets, thin-section descriptions and annotated photomicrographs for each sample are presented in Appendix 4. A key to plates in Appendix 4 is given on p. 27.

Sandstones from Thylacine-2 (2153.10-2218.40m) are lithic-rich sublitharenites and litharenites with a mean QFR ratio of 76:1:23, whereas sandstones from Thylacine-2 (2249.85-2300.80m) are quartz-rich sublitharenites and quartzarenites with a mean QFR ratio of 95:0:5 (Fig. 2). Accordingly, compositional maturity increases below 2218.40m in Thylacine-2. Geographe-1 (1832.47m) (#57H) is a litharenite with a QFR ratio of 74:6:20. The section in Geographe-1 (1814.10-1908.90m) is generally slightly more feldspathic than the equivalent section in Thylacine-2 (based on data in Baker, 2002a,b and this study). Framework grains are mainly quartz and also include K-feldspar, metamorphic rock fragments, sedimentary rock fragments, mica, organics and accessory heavy minerals.

TABLE 2. TEXTURE

Well	Sample #	Depth (mRT)	GRAIN SIZE			SORTING		
			ϕ	mm	Class	Trask	ϕSD	Class
Thylacine-2	5	2153.10	2.38	0.19	fine	1.18	0.37	well
"	44	2185.55	2.07	0.24	fine	1.25	0.46	well
"	97	2207.84	1.78	0.29	medium	1.26	0.50	mod-well
"	128	2218.40	1.93	0.26	medium	1.21	0.43	well
"	181	2249.85	2.60	0.16	fine	1.21	0.43	well
"	186	2251.20	2.97	0.13	fine	1.19	0.44	well
"	187	2251.59	3.03	0.12	very fine	1.20	0.39	well
"	205	2275.17	1.32	0.40	medium	1.35	0.61	mod-well
"	234	2296.94	0.73	0.60	coarse	1.23	0.44	well
"	241	2299.40	-0.03	1.02	very coarse	1.84	1.03	poor
"	244	2300.20	2.92	0.13	fine	1.31	0.59	mod-well
"	246	2300.80	2.23	0.21	fine	1.26	0.48	well
Geographe-1	57H	1832.47	1.94	0.26	medium	1.20	0.43	well

GRAIN SIZE (ϕ)

Class	*ϕ*
very coarse sand	-1.0-0.0
coarse sand	0.0-1.0
medium sand	1.0-2.0
fine sand	2.0-3.0
very fine sand	3.0-4.0
silt	<4.0

SORTING (ϕSD)

Class	*ϕ Standard Deviation*
very-well sorted	<0.35
well sorted	0.35-<0.50
moderately-well sorted	0.50-<0.71
moderately sorted	0.71-1.00
poorly sorted	>1.00+

FIGURE 1. MEAN GRAIN SIZE/SORTING CROSS-PLOT

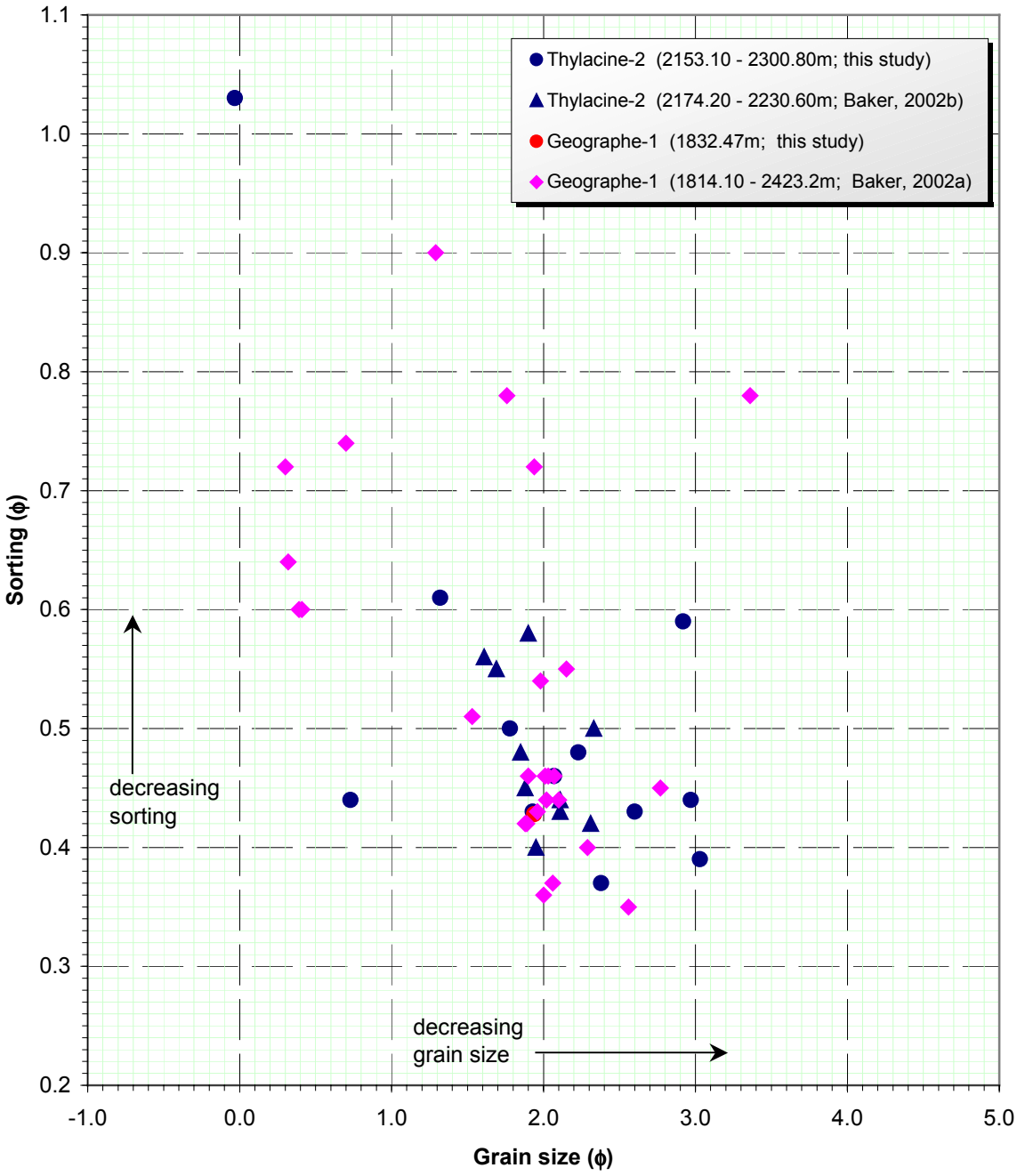


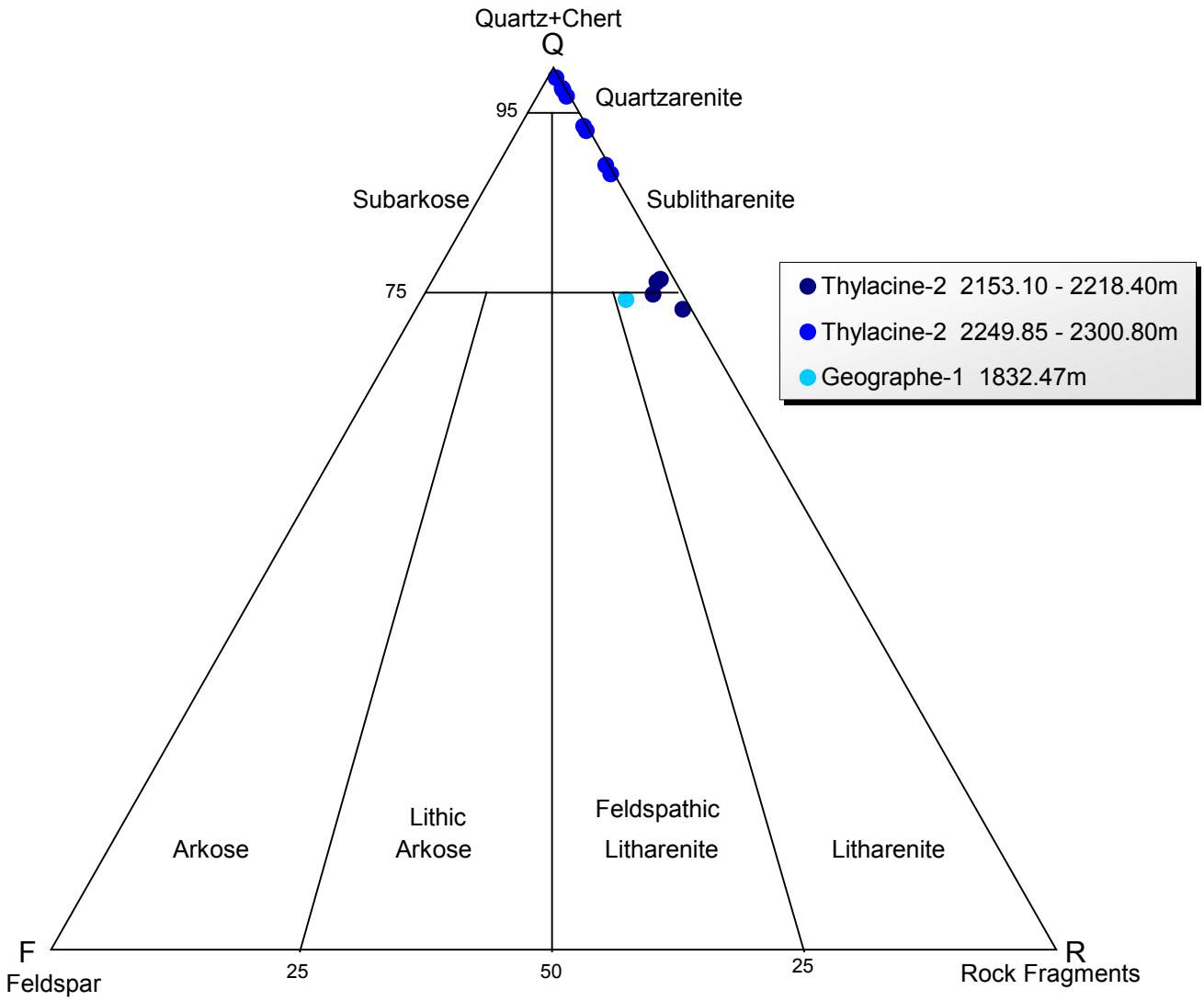
TABLE 3. THIN-SECTION COMPOSITION AND QFR RATIOS

Well	T-2	T-2	T-2	T-2	T-2	T-2	T-2	T-2	T-2	T-2
Sample #	5	44	97	128	181	186	187	205	234	241
Depth (mRT)	2153.10	2185.55	2207.84	2218.40	2249.85	2251.20	2251.59	2275.17	2296.94	2299.40
Quartz (monocrystalline)	42.3	44.4	32.3	46.9	63.1	47.1	46.3	67.4	65.5	67.8
Quartz (polycrystalline)	4.0	4.9	6.0	5.7	2.0	2.9	2.6	0.9	1.8	6.1
Quartz overgrowths	1.1	1.4	3.0	2.0	5.5	3.4	3.1	6.9	5.4	4.9
Chert	1.4	1.1	1.1	1.1	0.3	0.7	-	0.3	-	0.7
K-feldspar	1.7	0.7	0.7	1.1	-	-	-	-	-	-
Plagioclase	-	-	-	-	-	-	-	-	-	-
Volcanic rock fragments	0.7	0.7	0.6	-	0.3	-	0.3	-	-	-
Granitic rock fragments	-	-	-	-	-	-	-	-	-	-
Metamorphic rock fragments	11.5	12.9	11.7	13.7	8.4	3.4	5.4	1.4	1.2	0.3
Sedimentary rock fragments	2.3	1.4	2.9	2.3	0.3	-	0.3	-	-	-
Mica	-	-	0.3	-	-	0.7	0.3	-	-	-
Heavy minerals	-	0.3	-	0.3	0.3	0.7	0.3	-	-	-
Organics	0.7	-	-	0.7	-	0.4	0.3	-	0.3	-
Pyrite	0.7	-	0.3	-	0.7	0.9	2.2	-	-	0.3
Leucoxene	-	-	-	-	0.3	0.3	0.3	-	-	-
Siderite (pore filling)	-	-	15.5	-	-	-	-	-	-	-
Siderite (replacement)	-	8.4	4.0	0.9	0.3	3.1	3.7	-	0.3	-
Ankerite (pore filling)	-	-	-	-	-	12.0	11.2	-	-	-
Ankerite (replacement)	-	0.9	-	0.7	-	7.4	6.0	-	-	-
Calcite (pore filling)	-	-	-	-	-	-	-	-	-	-
Calcite (replacement)	-	-	-	-	-	-	-	-	-	-
Glauconite	-	0.3	0.3	0.3	0.3	0.3	-	-	-	-
Authigenic kaolin (pore filling)	5.8	5.2	3.0	5.8	2.8	2.0	2.4	2.3	1.6	0.6
Authigenic kaolin (replacement)	17.3	15.1	12.8	15.6	10.3	11.4	11.7	10.0	3.8	2.3
Authigenic illite (pore filling)	-	-	-	-	-	-	-	-	-	-
Authigenic illite (replacement)	3.0	2.0	1.7	2.9	3.1	1.9	2.7	0.6	-	-
Detrital clay	7.5	-	-	-	1.1	0.7	0.3	-	0.3	-
Primary porosity (intergranular)	-	-	2.1	-	0.3	0.3	0.3	7.4	13.0	12.7
Secondary porosity (intergranular)	-	-	0.7	-	-	-	-	2.1	6.1	4.3
Secondary porosity (mouldic)	-	-	0.3	-	0.3	0.4	0.3	-	-	-
Secondary porosity (intragranular)	-	0.3	0.7	-	0.3	-	-	0.7	0.7	-
Q (quartz + chert)	75.1	76.8	73.4	76.5	88.7	94.1	89.7	98.2	98.4	99.6
F (feldspar)	2.6	1.0	0.5	1.5	0.0	0.0	0.0	0.0	0.0	0.0
R (rock fragments)	22.3	22.2	26.1	22.0	11.3	5.9	10.3	1.8	1.6	0.4

TABLE 3. THIN-SECTION COMPOSITION AND QFR RATIOS cont.

Well	T-2	T-2	G-1
Sample #	244	246	57H
Depth (mRT)	2300.20	2300.80	1832.47
Quartz (monocrystalline)	61.3	60.6	44.9
Quartz (polycrystalline)	1.7	1.4	4.8
Quartz overgrowths	4.0	4.8	2.0
Chert	-	0.6	1.4
K-feldspar	-	-	4.0
Plagioclase	-	-	-
Volcanic rock fragments	-	-	0.6
Granitic rock fragments	-	0.3	-
Metamorphic rock fragments	4.3	1.1	11.6
Sedimentary rock fragments	0.3	0.3	2.0
Mica	0.9	0.6	0.6
Heavy minerals	0.3	-	-
Organics	1.7	0.3	-
Pyrite	0.3	-	-
Leucoxene	0.3	-	-
Siderite (pore filling)	0.7	3.7	1.3
Siderite (replacement)	5.2	3.5	5.0
Ankerite (pore filling)	-	-	-
Ankerite (replacement)	-	-	-
Calcite (pore filling)	-	-	-
Calcite (replacement)	-	-	-
Glauconite	-	-	0.3
Authigenic kaolin (pore filling)	2.3	5.4	4.3
Authigenic kaolin (replacement)	13.0	15.5	12.3
Authigenic illite (pore filling)	-	-	-
Authigenic illite (replacement)	3.7	0.9	2.6
Detrital clay	-	-	-
Primary porosity (intergranular)	-	0.7	0.9
Secondary porosity (intergranular)	-	-	-
Secondary porosity (mouldic)	-	0.3	0.7
Secondary porosity (intragranular)	-	-	0.7
Q (quartz + chert)	93.6	97.5	74.5
F (feldspar)	0.0	0.0	5.6
R (rock fragments)	6.4	2.5	19.9

FIGURE 2. QFR COMPOSITIONS



Detrital quartz content ranges from 38.3% to 73.9% and varies mainly according to metamorphic rock fragments + clay + carbonate content. Data from Baker (2002a,b) and this study show that there is a weak positive correlation between detrital quartz content and grain size for Thylacine-2 and Geographe-1. Most quartz is monocrystalline, even in the coarse to very coarse grained sandstones. Quartz types include recrystallised metamorphic quartz, metaquartzite and plutonic quartz. Metamorphic quartz locally includes oriented phyllosilicates, and granitic quartz rarely contains K-feldspar intergrowths. Quartz grains are locally enveloped by thin syntaxial quartz overgrowths and have welded (including microstylolitic) grain contacts that result from grain contact dissolution. Quartz overgrowth content ranges from less than 2% in the clay/lithic-rich sands to 6.9% in a clean, quartzose sandstone (#205).

The section at 2153.10-2218.40m in Thylacine-2 contains very minor (<2%) feldspar, and Geographe-1 (#57H) contains 4.0% feldspar. Feldspar disappears below 2225.12m in Thylacine-2 and below 1908.90m in Geographe-1 (Baker, 2002a,b). Feldspar is fresh to slightly altered granitic K-feldspar (orthoclase, microcline, microperthite) that is commonly etched or partly dissolved. Plagioclase is absent.

Rock fragment content is 14.5-16.0% above 2249.85m and 0.3-9.0% below 2218.40m in Thylacine-2. Geographe-1 (#57H) contains 14.2% rock fragments. Most lithic grains are low grade metasedimentary rock fragments that include quartz/mica schist, illitic meta-argillite, phyllite, and mica/illite-bearing quartzite. Mica/illite-rich metamorphic rock fragments, which dominate over mica/illite-poor metamorphic rock fragments, are commonly compactionally deformed between adjacent rigid grains and partly altered to illite and kaolin. Other lithic grains include sedimentary rock fragments (mudrock, argillaceous siltstone), felsic volcanic rock fragments (composed mainly of cherty/microcrystalline quartz and chalcedony) and rare granitic rock fragments (intergrown quartz and K-feldspar). Chert content does not exceed 1.4%.

Other framework grains include muscovite, terrestrial organic fragments, reworked glauconite peloids and accessory heavy minerals (tourmaline, zircon, garnet, monazite, leucoxene). Biotite has altered to kaolin and been replaced by siderite. Organic fragments are concentrated with detrital clay and microcrystalline siderite along laminae in #186 and #244. Monazite is rimmed by radiogenically-immobilised bitumen in #97.

Authigenic clay content is 12.9-26.1% in the very fine to medium grained sandstones and is less than 6% in the coarse and very coarse grained sandstones (#234, #241) from Thylacine-2. Geographe-1 (#57H) contains 19.2% authigenic clay. Authigenic clay is mainly kaolin (kaolinite, dickite) that occurs where micaceous/argillaceous rock fragments, mica and, less commonly, feldspar have altered. Muscovite and micaceous/argillaceous rock fragments are locally partly altered to kaolin, and mica-like kaolin grains occur where biotite has altered. Illitic remnants of micaceous precursor grains are locally associated with authigenic kaolin, and minor authigenic illite is associated with partly altered and compactionally deformed micaceous/argillaceous metamorphic rock fragments.

Detrital clay does not exceed 1.1%, except in #5, which contains 7.5% detrital clay that is concentrated within scattered burrow infills and along fine, discontinuous laminae. Argillaceous burrow infills and fine argillaceous laminae also occur in some of the other finer samples (#181, #186, #187).

Data from Baker (2002a,b) and this study show that there is a weak positive correlation between between clay + metamorphic rock fragment content and grain size in Thylacine-2 and Geographe-1.

Except in #186 and #187, carbonate is mainly siderite, the content of which ranges up to 19.5% in #97, where siderite mainly forms uniformly disseminated, 50-100µm rhombic/scalenohedral crystals that fill intergranular spaces and replace altered biotite. In the other samples, all of which contain less than 8.5% siderite, siderite occurs as a microcrystalline/finely-crystalline replacement of micaceous/argillaceous grains (especially altered biotite) and clay and also forms disseminated fine rhombic crystals. Microcrystalline siderite is concentrated along thin laminae in #186, #244 and #246.

Samples #186 and #187 contain 19.4% and 17.2% ankerite, respectively, which forms a patchy, coarsely-crystalline cement that replaces framework grains and clay and occupies intergranular pores. The other samples contain little (<1%) or no ankerite. Geographe-1 (#57H) contains rare, coarsely-crystalline calcite patches.

Pyrite content does not exceed 2.3%. In #187, pyrite forms an isolated cement patch made up of fine aggregated euhedra. In the other samples, fine pyrite euhedra and framboids are locally associated with organic fragments and detrital clay.

Excluding the upper medium to very coarse grained samples (#205, #234, #241), total visible porosity ranges up to 3.8%, is mainly below 1.1%, and is accounted for mostly by scattered secondary mouldic/intragranular grain dissolution pores and subordinate primary intergranular pores. Samples #205, #234 and #241 contain 10.2-19.8% visible porosity, nearly all of which is accounted for by primary intergranular pores and subordinate secondary intergranular grain dissolution pores.

5. X-RAY DIFFRACTION ANALYSES

Quantitative bulk-rock XRD analyses were carried out on all thirteen samples. XRD analyses are given in Table 4, and annotated XRD traces are given in Appendix 3.

Quantitative XRD analyses complement the thin-section analyses but cannot be compared directly. This is because thin-section clay and siderite components include microporosity, and therefore total thin-section clay and siderite are elevated relative to other grain types. In addition, the thin-section rock fragment component includes quartz, K-feldspar, kaolin, mica and illite that are recorded as these phases by XRD. Finally, XRD analyses do not include visible porosity. Therefore, in the case of the macroporous sandstones, component abundances as determined by XRD analysis will be higher than those determined by thin-section analysis.

Quantitative XRD analyses show that all samples are dominated by quartz (59.7-95.1%), the amount of which varies according to clay + carbonate content.

Detected clays are kaolin (4.6-24.4%) and illite/mica (0.1-11.4%). The three coarsest sandstones (#205, #234, #241) contain the least kaolin and illite/mica. Kaolin polytypes are kaolinite and, below 2218.40m in Thylacine-2, kaolinite and dickite.

Samples from Thylacine-2 (2153.10-2218.40m) contain 1.2-2.8% K-feldspar, and Geographe-1 (1832.47m) (#57H) contains 4.7% K-feldspar. Feldspar was not detected in the other samples.

Other detected minerals are siderite and ankerite, which exceed 10% in #97 (siderite), #186 and #187 (ankerite), and trace to very minor (<1%) pyrite and, in Geographe-1 (#57H), calcite.

Fine-fraction XRD analyses indicate that clay minerals in Thylacine-1 (2166.81-2193.59m) are kaolinite (dominant) and discrete illite (Baker, 2001). Fine-fraction XRD analyses were not carried out for the current study.

TABLE 4. BULK-ROCK XRD ANALYSES

Well	Sample #	Depth (mRT)	Qtz	KF	Ka	I/M	Sid	Ank	Cal	Pyr
Thylacine-2	5	2153.10	61.0	2.8	24.4	11.4	-	-	-	0.4
"	44	2185.55	67.9	2.5	19.3	4.3	5.6	0.4	-	-
"	97	2207.84	59.7	1.2	17.9	5.0	16.2	-	-	-
"	128	2218.40	71.0	1.3	22.5	4.4	-	0.8	-	-
"	181	2249.85	81.1	-	13.0	5.0	0.7	-	-	0.2
"	186	2251.20	62.9	-	15.8	4.4	1.5	15.3	-	0.1
"	187	2251.59	64.6	-	19.0	4.7	0.7	10.5	-	0.5
"	205	2275.17	90.0	-	9.5	0.5	-	-	-	-
"	234	2296.94	89.6	-	10.2	0.1	0.1	-	-	-
"	241	2299.40	95.1	-	4.6	0.1	-	-	-	0.2
"	244	2300.20	74.0	-	19.3	6.1	0.6	-	-	-
"	246	2300.80	79.1	-	17.6	1.4	1.9	-	-	-
Geographe-1	57H	1832.47	71.8	4.7	12.5	8.3	2.3	0.3	0.1	-

Qtz = quartz KF = K-feldspar Ka = kaolin I/M = illite/mica Sid = siderite Ank = ankerite Cal = calcite Pyr = pyrite

6. DIAGENESIS

The main diagenetic processes are authigenic clay formation, ductile grain/authigenic clay compaction, grain contact dissolution, labile grain dissolution, quartz overgrowth cementation and carbonate cementation/replacement.

Authigenic clay is mainly kaolin that forms common, compacted, highly microporous grain-sized patches and patchy pseudomatrix that occur where micaceous/argillaceous rock fragments, mica and feldspar have altered (Plates 1, 2, 3, 6, 7, 8, 9, 12, 16, 18; Plate 20, Fig. 2; Plates 21, 22, 23, 25, 26). Muscovite and micaceous/argillaceous rock fragments are locally partly altered to kaolin, and mica-like kaolin grains occur where biotite has altered. The other authigenic clay is illite, which is mainly associated with partly altered and compactionally deformed micaceous/argillaceous metamorphic rock fragments (Plate 9, Fig. 2; Plate 11; Plate 19, Fig. 2). In the Thylacine-2 samples, authigenic clay content ranges from 2.9% to 26.1% and is moderately (R^2 = -0.622) negatively correlated with grain size.

Micaceous/illitic metamorphic rock fragments, argillaceous sedimentary rock fragments, mica and authigenic clay are commonly compactionally deformed, locally to form pseudomatrix (Plates 6, 21). The very fine to lower medium grained sandstones in particular were susceptible to physical compaction and authigenic clay formation on account of their high micaceous/argillaceous grain content at the time of accumulation. Organic fragments and glauconite peloids are also compactionally deformed.

Grain contact dissolution has increased framework grain packing density by producing long, embayed and rare sutured grain contacts between juxtaposed quartz grains, quartzose/illitic rock fragments and feldspar grains (Plates 6, 8, 13, 15, 17, 21). Grain suturing and microstylolitisation have occurred where grain contact dissolution was promoted by the presence of thin illitic clay films between grains.

Above 2249.85m in Thylacine-2 and at Geographe-1 (1832.47m), a few feldspar grains and labile rock fragments have partly to completely dissolved to form widely scattered secondary mouldic pores and intragranular pores (Plate 2, Fig. 2; Plate 3; Plate 5, Fig. 1; Plate 26, Fig. 1). In some of the other samples, particularly the upper medium to very coarse grained sandstones (#205, #234, #241), labile rock fragments have partly to completely dissolved to form common secondary intergranular macropores (Plates 15, 16, 17; Plate 19, Fig. 2).

Quartz overgrowth cement content ranges from 1.1% to 6.6%. In the very fine to lower medium grained sandstones, quartz overgrowths, despite being thinly developed, largely or completely fill all available intergranular space between juxtaposed quartz grains (Plates 1, 3, 7, 8, 12, 22, 23, 25, 26). In contrast, in the upper medium to very coarse grained sandstones, most intergranular pores are only partly occluded by quartz overgrowths (Plates 13, 14, 15, 18, 19; Plate 20, Fig. 1). In the very fine to medium grained sandstones, quartz overgrowth development was inhibited by the presence of abundant compacted ductile grains and authigenic clay (Plate 2, Fig. 1; Plate 24).

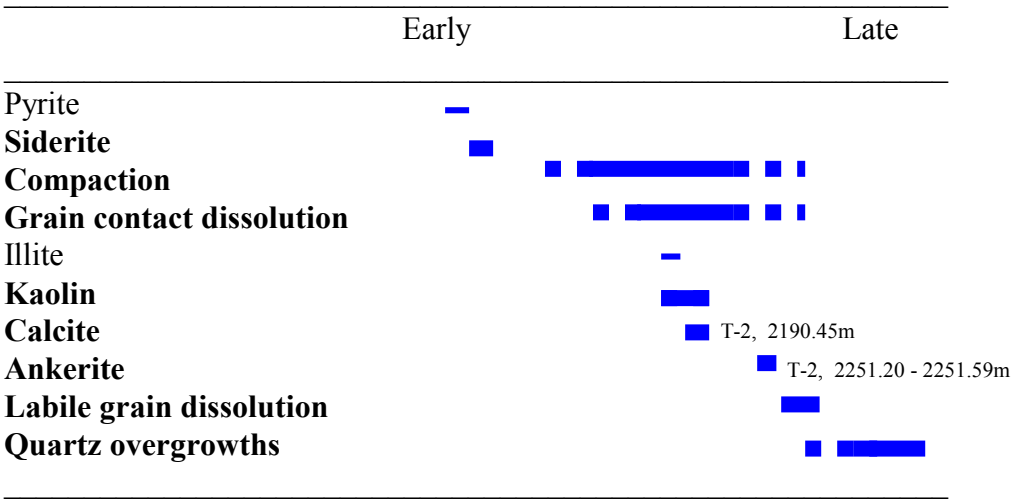
Except in #186 and #187, carbonate is mainly siderite that forms microcrystalline patches that replace coarse mica flakes (Plates 3, 11), argillaceous grains and detrital clay and, particularly in #97, also forms disseminated, fine rhombic/scalenohedral crystals that occur along grain contacts and within intergranular spaces and authigenic kaolin (Plates 4, 5, 23). In #186 and #187, carbonate is mainly patchy, coarsely-crystalline ankerite that replaces framework grains and clay and occupies intergranular pores (Plates 10, 11; Plate 12, Fig. 1). Some of the other

samples contain sporadic patches of coarsely-crystalline ankerite (Plate 6) and, in the case of Geographe-1 (#57H), calcite.

Sample #187 contains a 1cm pyrite cement patch made up of aggregated fine euhedra. Some of the other samples contain disseminated and concentrated fine pyrite euhedra/framboids that are locally associated with organic fragments and detrital clay.

The interpreted paragenetic history is shown in Figure 3, and is essentially the same as the one given by Baker (2002b) for Thylacine-2 (2174.20-2230.60m). All textural relationships observed in the current study are consistent with this paragenetic history. Textural relationships used to interpret the diagenetic paragenesis are described in Baker (2002b). The isotopic composition of siderite in Geographe-1 (1838.00m) and Thylacine-2 (2208.00m) is consistent with siderite formation during shallow burial (<50˚C) (Baker, 2002c).

FIGURE 3. DIAGENETIC PARAGENESIS*



* main diagenetic effects in bold

7. RESERVOIR QUALITY

7.1 GENERAL

Routine core analyses for the thirteen samples are given in Table 1 and plotted in Figure 4. Figure 4 also includes core analyses for samples from Thylacine-2 (cores #1, #2, #3) and Geographe-1 (cores #1, #2) that were not petrologically analysed. Figure 4A shows that the twelve petrologically-analysed Thylacine-2 samples cover most of the porosity and permeability range above 11% porosity and 0.40mD permeability. Figure 4B shows that Geographe-1 (#57H) is representative of moderately permeable sandstone within the cored section.

Figure 5 shows that a strong (R^2 = 0.807) positive correlation between visible macroporosity and permeability emerges if all available visible porosity/permeability data for Thylacine-2 and Geographe-1 are plotted together (excluding a strongly calcite-cemented sample from Thylacine-2, 2190.45m; #58). A strong correlation is expected given that visible macroporosity is conducive to permeability.

Figure 6 shows that there is a moderate (R^2 = 0.568) positive correlation (excluding Thylacine-2; #58) between grain size and permeability, indicating that permeability variation is largely due to grain size differences. Thylacine-2 (#58) has anomalously low permeability for its grain size on account of being tightly cemented by calcite, whereas Thylacine-2 (#241) has anomalously low permeability for its grain size on account of poor sorting arising from the inclusion of two ?interbedded lithologies – coarse grained sandstone and granule conglomerate.

Figure 7 shows that there is a strong (R^2 = -0.807) negative correlation between clay + metamorphic rock fragments and permeability (excluding Thylacine-2; #58, #186, #187) in Thylacine-2, indicating, given that clay + metamorphic rock fragment content generally increases with decreasing grain size in Thylacine-2, that permeability increases with increasing grain size largely because clay + metamorphic rock fragment content decreases with increasing grain size. Metamorphic rock fragments influence permeability on account of being largely micaceous/argillaceous and thus prone to compactional deformation and dispersion, commonly to form pseudomatrix. Thylacine-2 (#58, #186, #187) have anomalously low permeability for their clay + metamorphic rock fragment content on account of being strongly cemented by calcite (#58) and ankerite (#186, #187).

Authigenic kaolin alone is a major control on permeability in both Thylacine-2 and Thylacine-1 as shown by the moderately strong (R^2 = -0.688) negative correlation between authigenic kaolin and permeability for these two wells (excluding Thylacine-1, 2076.50m; M5 and Thylacine-2, 2190.45m; #58) (Fig. 8). Thylacine-1 (M5) and Thylacine-2 (#58) have anomalously low permeability for their authigenic kaolin content on account of being strongly cemented by siderite (M5) and calcite (#58).

In summary, permeability variation in Thylacine-2 mainly reflects differences in grain size and clay (particularly authigenic kaolin) + metamorphic rock fragment content. Permeability increases with increasing grain size in Thylacine-2 partly because clay + metamorphic rock fragment content decreases with increasing grain size.

FIGURE 4A. POROSITY/PERMEABILITY CROSS-PLOT
THYLACINE-2

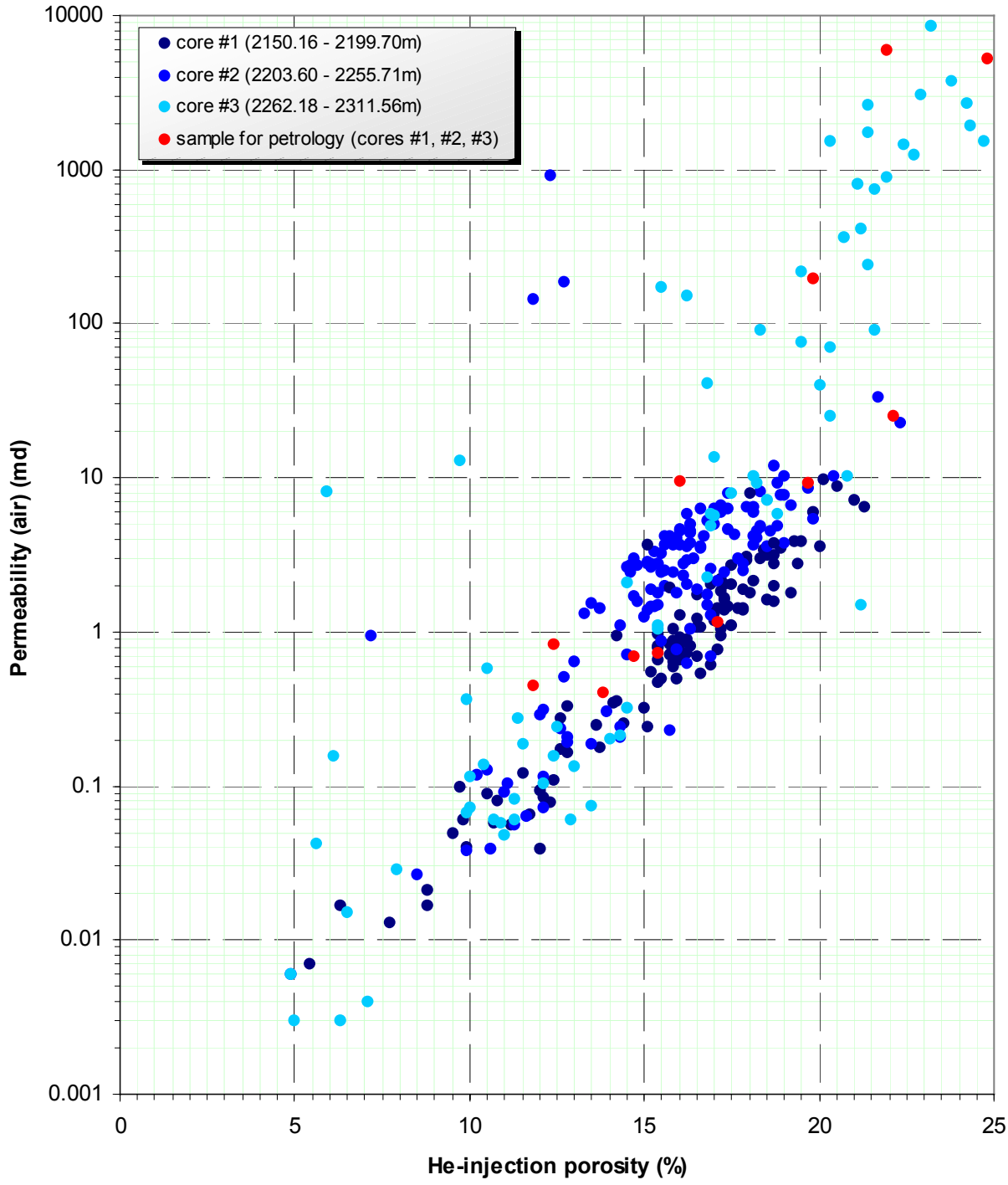


FIGURE 4B. POROSITY/PERMEABILITY CROSS-PLOT GEOGRAPHE-1

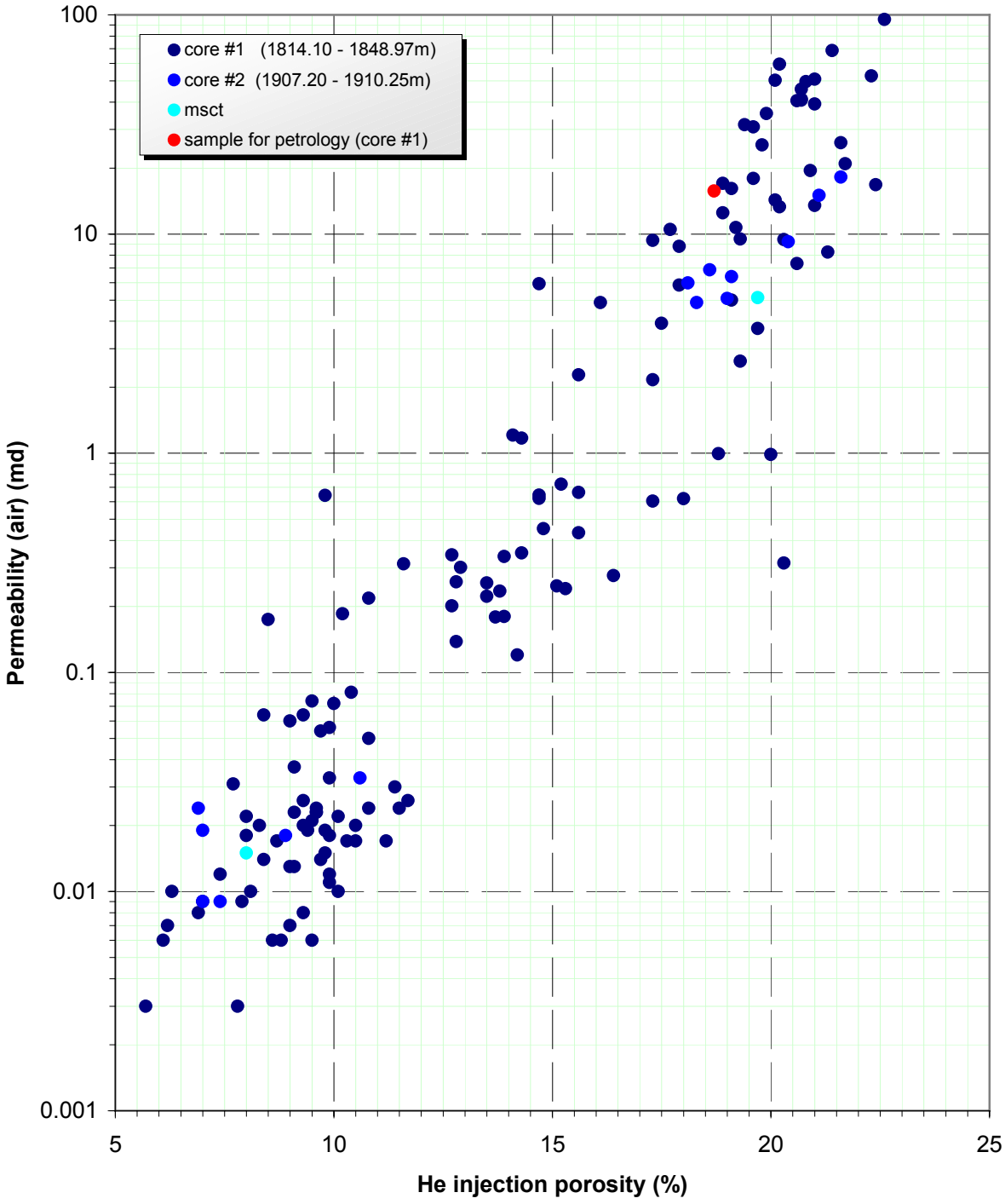


FIGURE 5. VISIBLE POROSITY/PERMEABILITY CROSS-PLOT

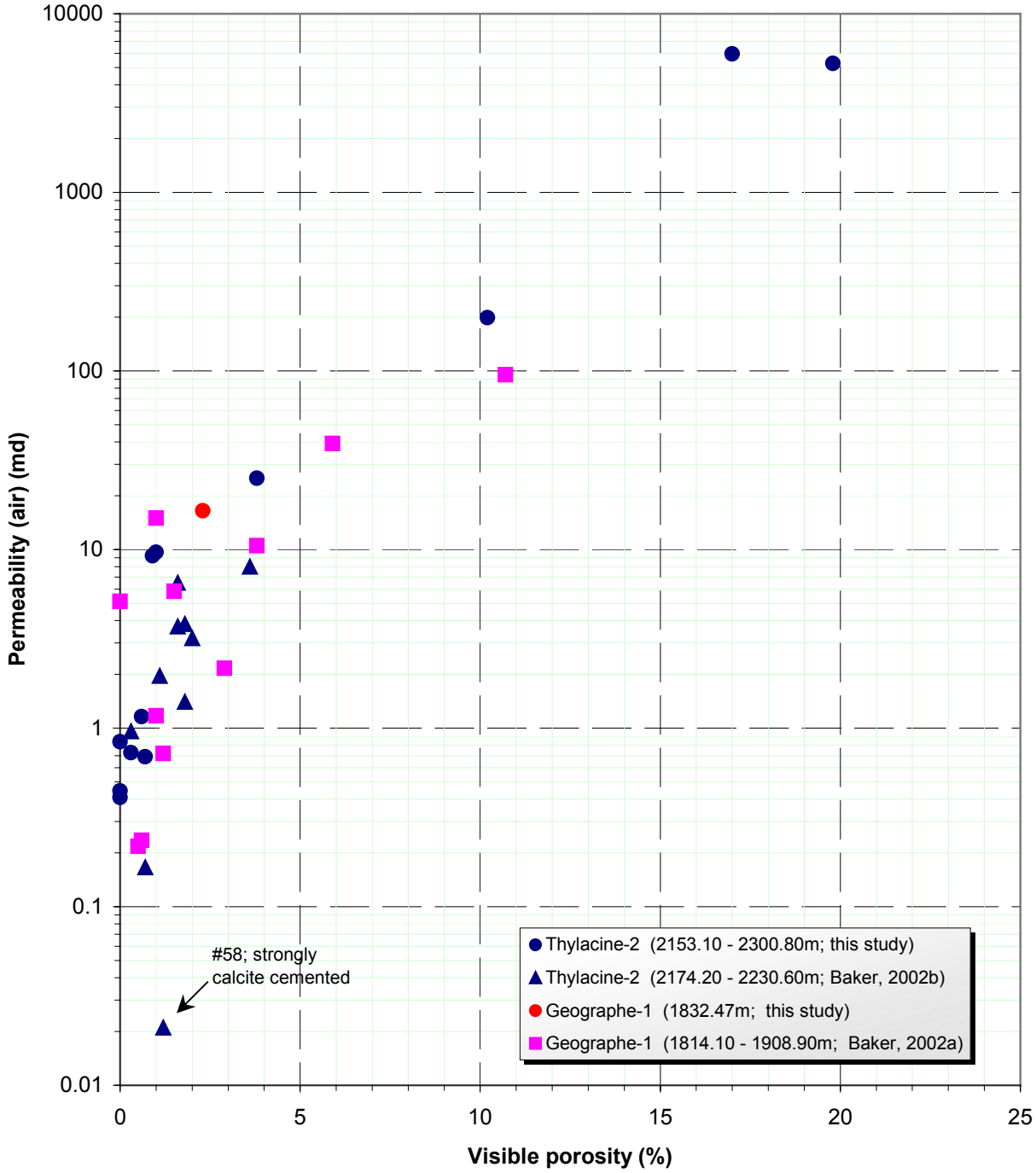


FIGURE 6. MEAN GRAIN SIZE/PERMEABILITY CROSS-PLOT

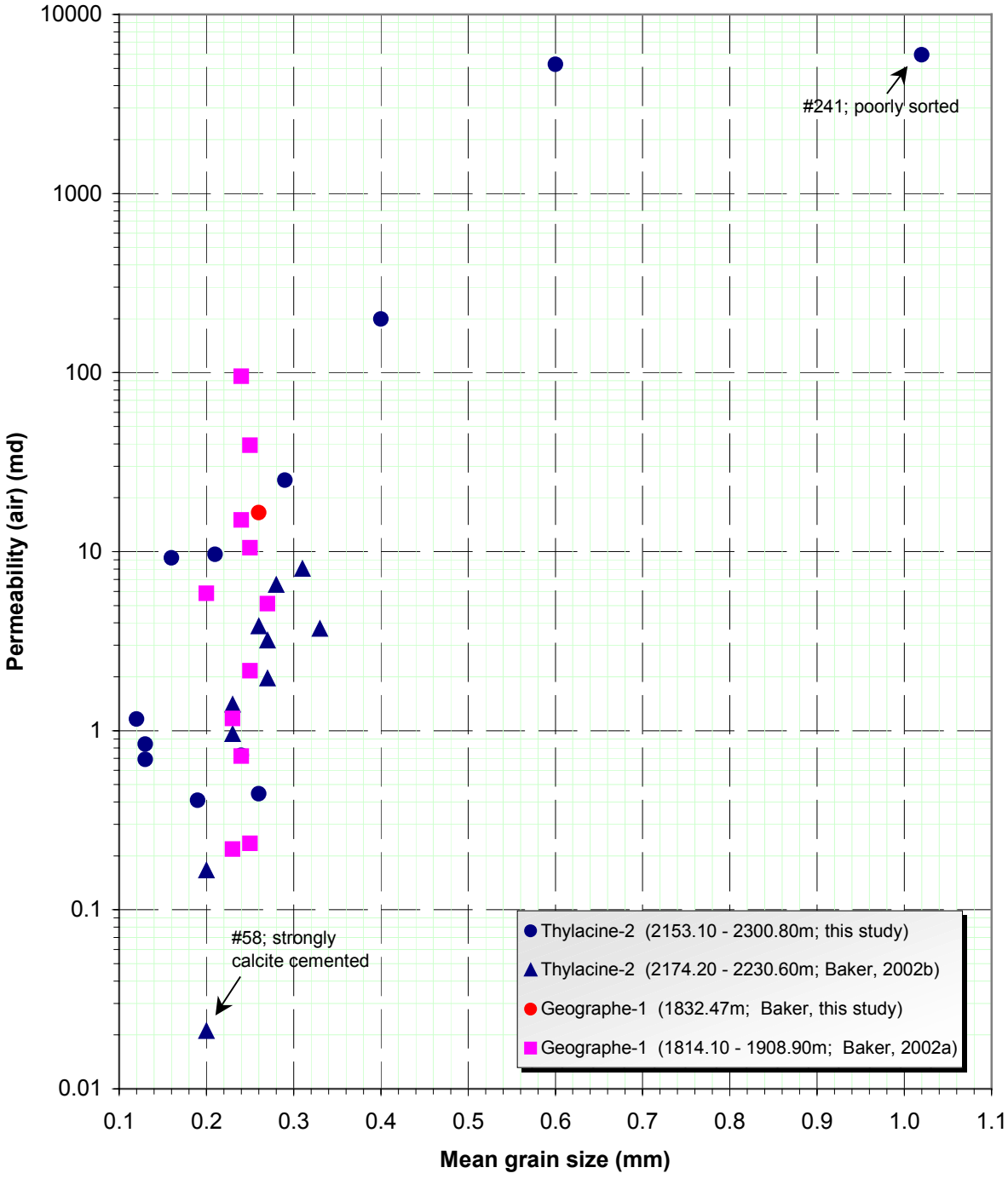


FIGURE 7. CLAY + METAMORPHIC ROCK FRAGMENTS/PERMEABILITY CROSS-PLOT - THYLACINE-2

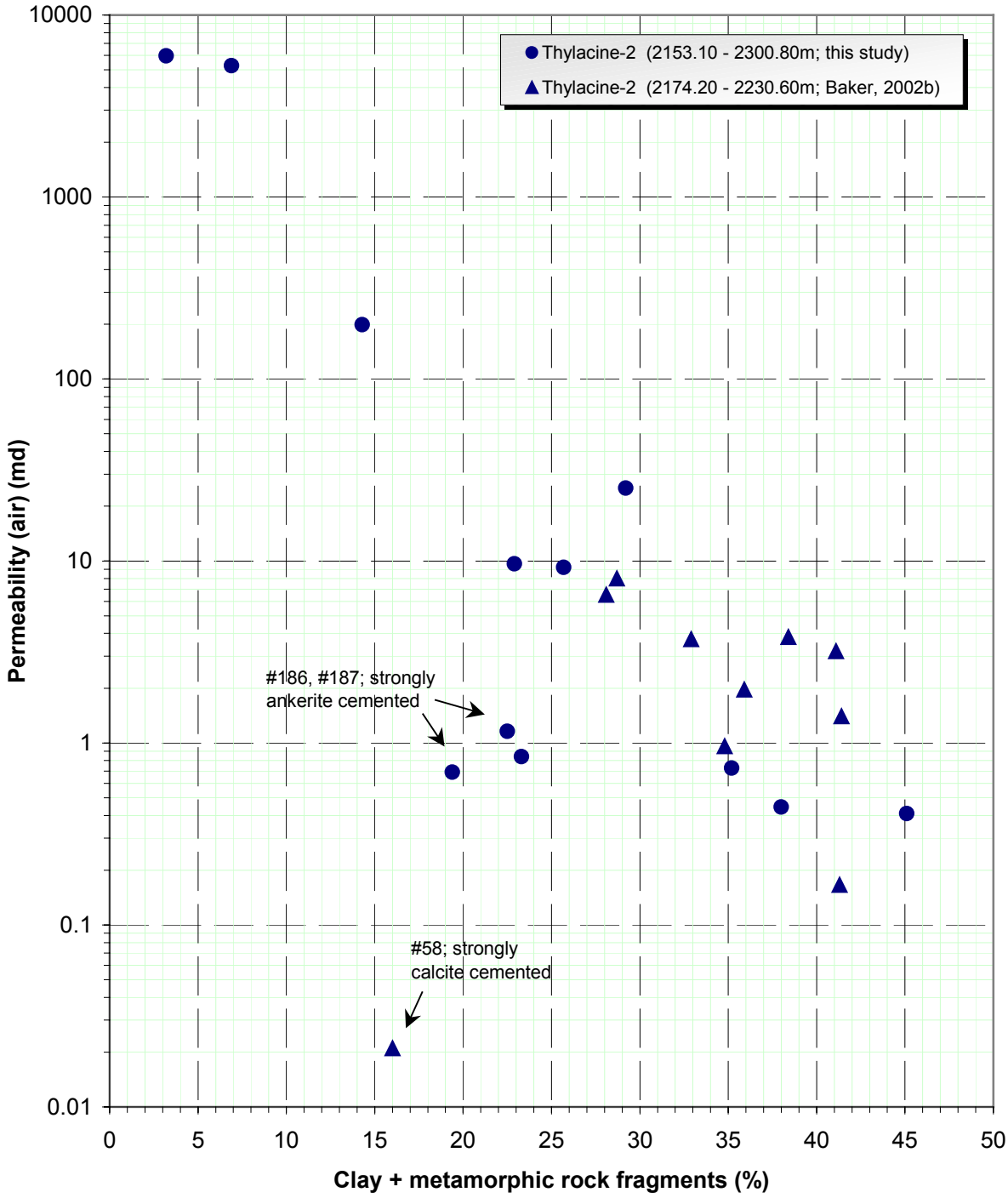


FIGURE 8. AUTHIGENIC KAOLIN/PERMEABILITY CROSS-PLOT (THYLACINE-1 & -2)

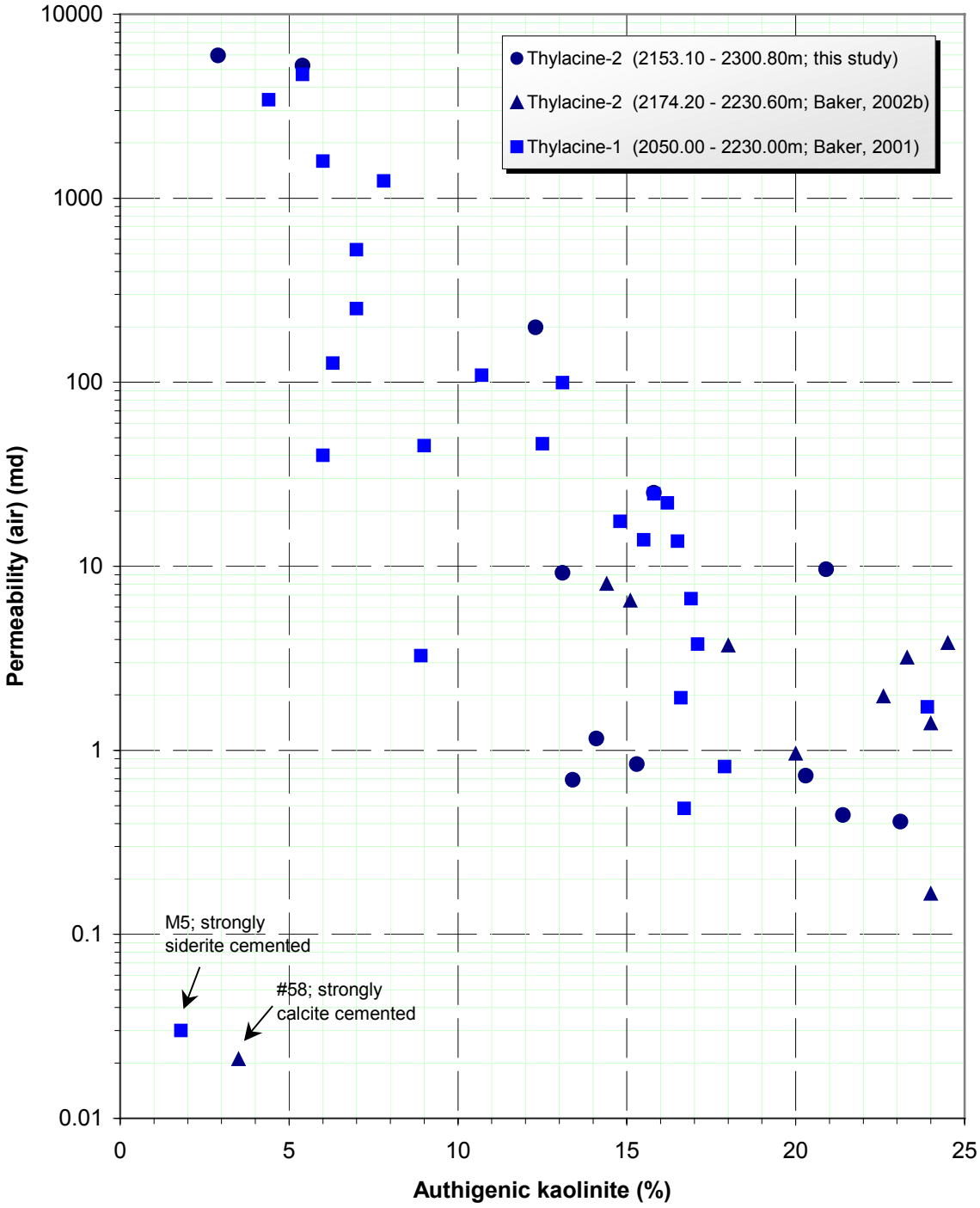


FIGURE 9. DETRITAL CLAY + SIDERITE/ PERMEABILITY CROSS-PLOT - GEOGRAPHE-1

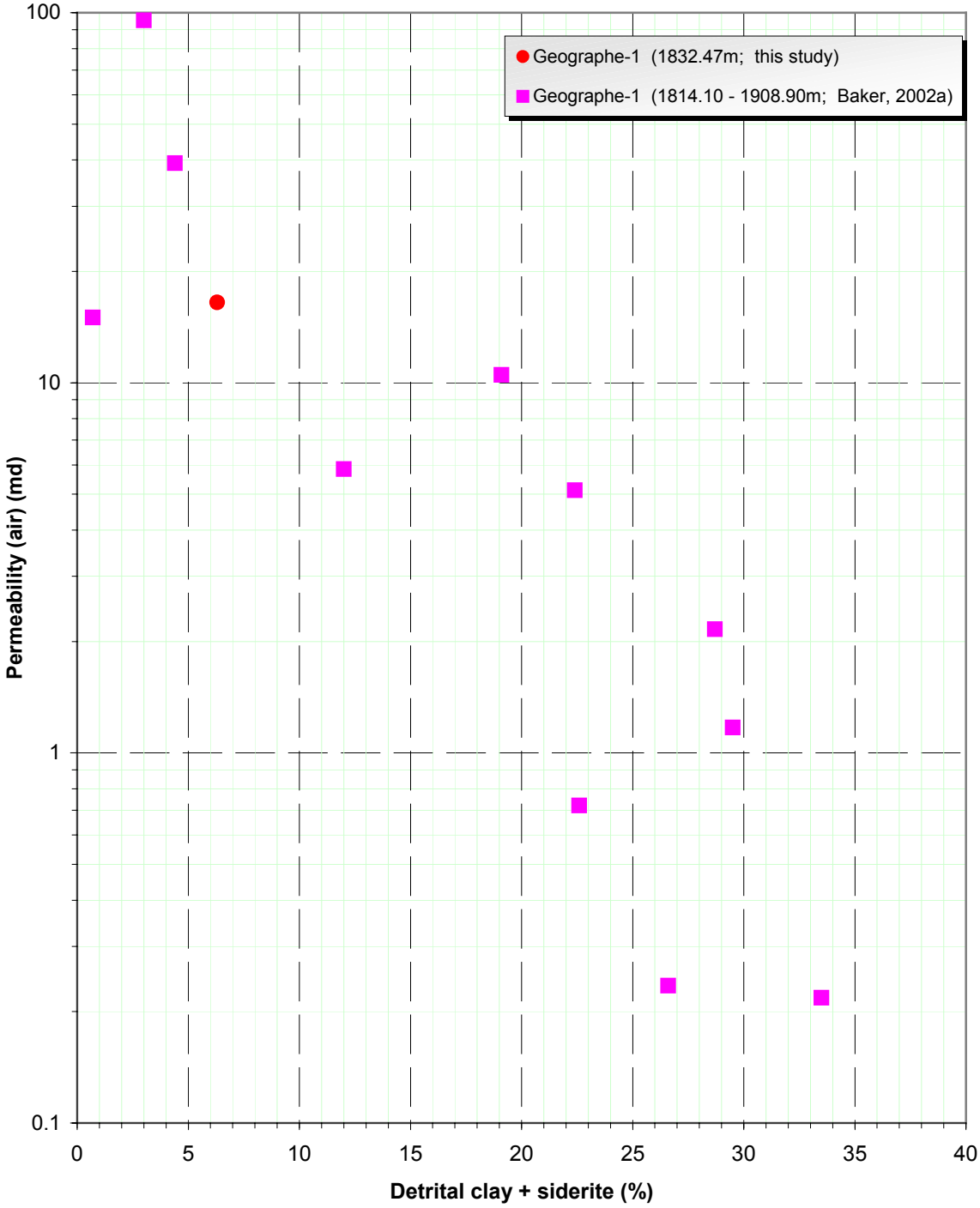


Figure 9 shows that there is a strong (R^2 = -0.795) negative correlation between detrital clay + siderite content and permeability for Geographe-1 (1814.10-1908.90m), indicating that permeability variation within this interval is largely controlled by detrital clay + siderite content. The correlation is not improved by including authigenic clay or metamorphic rock fragments with detrital clay + siderite. Unlike in Thylacine-1 and Thylacine-2, authigenic kaolin does not significantly control permeability in Geographe-1 due to the presence of abundant detrital clay and siderite. A more detailed account of reservoir quality in Geographe-1 is given in Baker (2002a).

7.2 SAMPLES

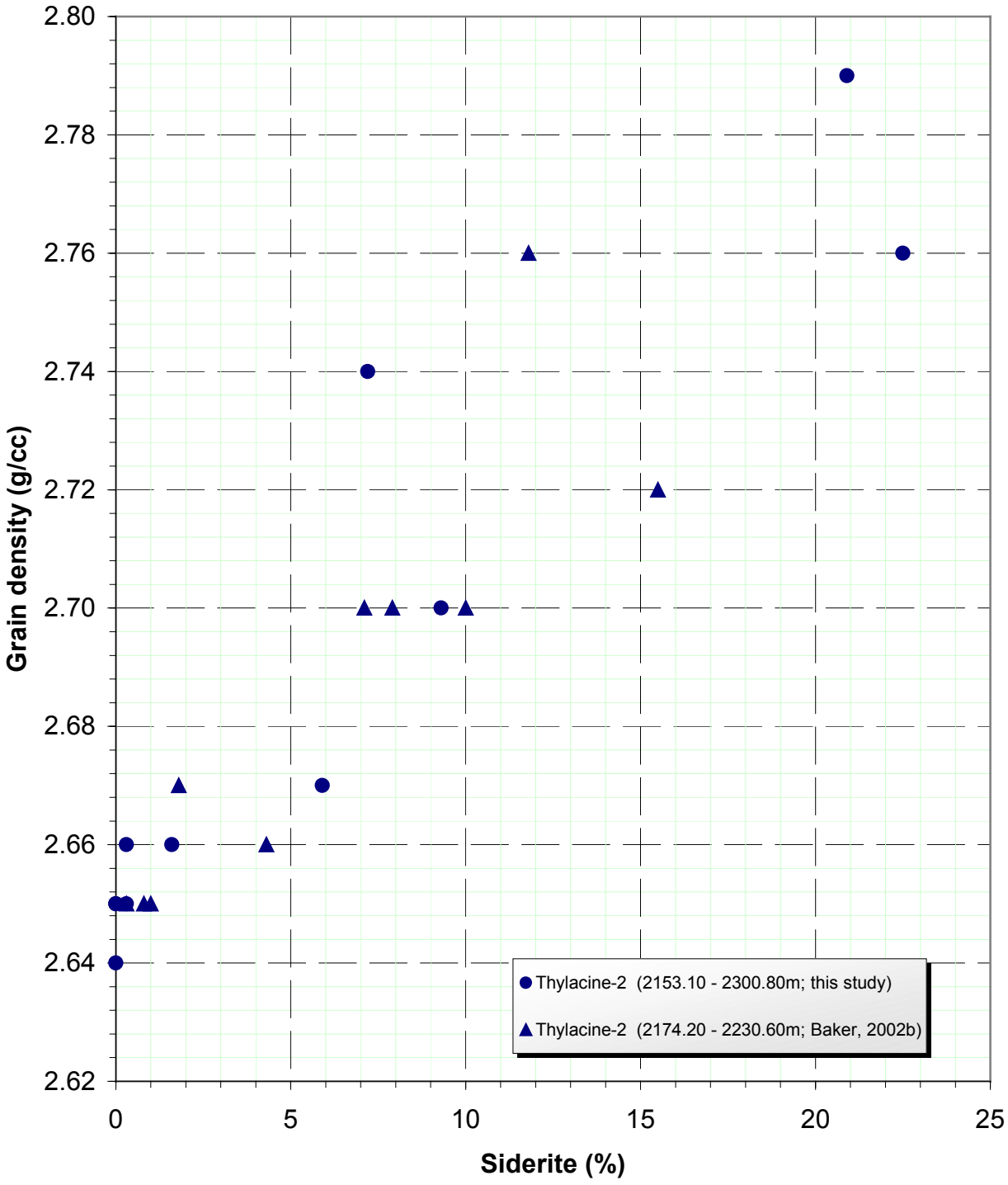
Visible porosity in the very fine to lower medium grained samples (i.e., all samples except #205, #234, #241) does not exceed 3.8%, and is accounted for mostly by scattered secondary mouldic/intragranular labile grain dissolution pores and subordinate primary intergranular pores. In these finer samples, intergranular porosity has been largely (#97) or almost completely eliminated by the combined effects of authigenic kaolin formation, ductile grain/authigenic clay compaction, grain contact dissolution, quartz overgrowth cementation and, in #186 and #187, ankerite cementation. The sands were susceptible to authigenic clay formation and physical compaction on account of containing common labile micaceous/argillaceous rock fragments at the time of accumulation. Relatively low permeability (<25.2mD) for high He-injection porosity (Fig. 4) reflects high microporous clay contents, low (<2.2%) primary intergranular porosity and generally fine (0.12-0.29mm) grain size.

In contrast to the very fine to lower medium grained sandstones, the upper medium to very coarse grained samples (#205, #234, #241) contain 10.2-19.8% visible porosity, nearly all of which is accounted for by primary intergranular pores and subordinate secondary intergranular grain dissolution pores. The sandstones are macroporous, despite porosity reduction by quartz overgrowth cementation, grain contact dissolution and pore filling by patchy authigenic kaolin (dickite). The sandstones were quartzose at the time of accumulation and thus, unlike the finer sandstones, were not susceptible to significant authigenic clay formation and physical compaction. Containing good clean intergranular porosity and being upper medium to very coarse grained, the three samples are moderately (199mD) and highly (5260mD, 5960mD) permeable.

Figure 10 shows the relationship between ferroan carbonate (siderite, ankerite) content and grain density for Thylacine-2.

Reservoir quality is briefly described for each sample in Appendix 4.

FIGURE 10. FERROAN CARBONATE/GRAIN DENSITY CROSS-PLOT



8. SUMMARY AND CONCLUSIONS

- Samples from Thylacine-2 (2153.10-2300.80m) are very fine to lower medium grained sublitharenites and litharenites and upper medium to very coarse grained quartzarenites. A sample from Geographe-1 (1832.47m) is a lower medium grained litharenite that is slightly more feldspathic than the Thylacine-2 samples. Framework grains are mainly quartz and also include K-feldspar (absent in samples from below 2218.40m in Thylacine-2), metamorphic rock fragments, sedimentary rock fragments, mica, reworked glauconite, organics and accessory heavy minerals. Compositional maturity increases below 2218.40m in Thylacine-2.

- Some of the finer sandstones contain minor detrital clay that is concentrated within scattered burrow infills and along fine, discontinuous laminae.

- Authigenic clay content is 12.9-26.1% in the very fine to medium grained sandstones and is less than 6% in the coarse and very coarse grained sandstones. Authigenic clay is mainly kaolinite and, below 2218.40m in Thylacine-2, kaolinite and dickite that occur where labile grains have altered. Illitic remnants of micaceous precursor grains are locally associated with authigenic kaolin, and minor authigenic illite is associated with partly altered and compactionally deformed micaceous/argillaceous metamorphic rock fragments.

- Diagenetic effects besides authigenic clay formation include ductile grain/authigenic clay compaction, grain contact dissolution, labile grain dissolution, cementation by quartz overgrowths, and cementation/replacement by siderite and ankerite. Siderite formed during shallow burial, whereas ankerite, secondary porosity and quartz overgrowths formed after compaction.

- Porosity reduction is mainly the result of authigenic clay formation, ductile grain/clay compaction, grain contact dissolution, quartz overgrowth cementation and, in Thylacine-2 (2251.20-2251.59m), ankerite cementation. Unlike the finer sandstones, upper medium to very coarse grained sandstones were quartzose at the time of accumulation and thus were not susceptible to significant authigenic clay formation and physical compaction.

- In the very fine to lower medium grained sandstones, visible porosity ranges up to 3.8%, is mainly below 1.1%, and is accounted for mostly by scattered secondary mouldic/intragranular labile grain dissolution pores and subordinate primary intergranular pores. Upper medium to very coarse grained sandstones contain 10.2-19.8% visible porosity, nearly all of which is accounted for by primary intergranular pores and subordinate secondary intergranular grain dissolution pores.

- Reservoir quality in Thylacine-2 is controlled mainly by grain size and authigenic kaolin + metamorphic rock fragment content. Permeability increases with increasing grain size partly because clay + metamorphic rock fragment content decreases with increasing grain size. Permeability variation in Geographe-1 (1814.10-1908.90m) largely reflects differences in detrital clay and siderite content (Baker, 2002a).

- Most very fine to lower medium grained sandstones from Thylacine-2 and Geographe-1 have less than 30mD permeability, whereas upper medium to very coarse grained sandstones from Thylacine-2 have 199-5960mD permeability.

REFERENCES

Baker, J.C., 2001, Petrology, diagenesis and reservoir quality of samples from Thylacine-1, T/30P. Report to Woodside Energy Ltd.

Baker, J.C., 2002a, Petrology, diagenesis and reservoir quality of samples from Geographe-1, VIC/P43. Report to Woodside Energy Ltd.

Baker, J.C., 2002b, Petrology, diagenesis and reservoir quality of samples from Thylacine-2, T/30P. Report to Woodside Energy Ltd.

Baker, J.C., 2002c, Petrology and geochemistry of siderite in faults in Geographe-1 and Thylacine-2. Report to Woodside Energy Ltd.

KEY TO PLATES IN APPENDIX 4

Well	Sample #	Depth (m)	Plate #
Thylacine-2	5	2153.10	1, 2*
"	44	2185.55	3
"	97	2207.84	4, 5*
"	128	2218.40	6, 7*
"	181	2249.85	8, 9*
"	186	2251.20	10
"	187	2251.59	11, 12*
"	205	2275.17	13, 14*
"	234	2296.94	15, 16
"	241	2299.40	17, 18, 19*, 20*
"	244	2300.20	21, 22*
"	246	2300.80	23, 24*
Geographe-1	57H	1832.47	25, 26*

* SEM micrographs

APPENDIX 1. GRAIN SIZE COMPARISON TABLE

	Millimetres	Microns	Phi (ϕ)	Wentworth Size Class
	4096		- 12	
	1024		- 10	Boulder (- 8 to – 12)
	256		--8	
	64		- 6	Cobble (- 6 to – 8)
	16		- 4	Pebble (- 2 to – 6)
	4		- 2	
	3.36		- 1.75	
	2.83		- 1.5	Granule
	2.38		- 1.25	
	2.00		- 1.0	
	1.68		- 0.75	
	1.41		- 0.5	Very Coarse Sand
	1.19		- 0.25	
	1.00		0.00	
	0.84		0.25	
	0.71		0.5	Coarse Sand
	0.59		0.75	
1/2	0.50	500	1.0	
	0.42	420	1.25	
	0.35	350	1.5	Medium Sand
	0.30	300	1.75	
1/4	0.25	250	2.0	
	0.210	210	2.25	
	0.177	177	2.5	Fine Sand
	0.149	149	2.75	
1/8	0.125	125	3.0	
	0.105	105	3.25	
	0.088	88	3.5	Very Fine Sand
	0.074	74	3.75	
1/16	0.0625	62.5	4.0	
	0.053	53	4.25	
	0.044	44	4.5	Coarse Silt
	0.037	37	4.75	
1/32	0.031	31	5.0	
1/64	0.0156	15.6	6.0	Medium Silt
1/128	0.0078	7.8	7.0	Fine Silt
1/256	0.0039	3.9	8.0	Very Fine Silt
	0.0020	2.0	9.0	
	0.00098	0.98	10.0	Clay
	0.00049	0.49	11.0	

APPENDIX 2.

GRAIN SIZE FREQUENCY CURVES

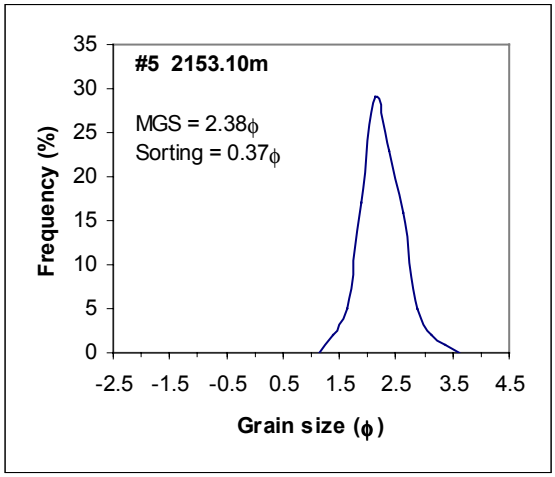
MGS = mean grain size

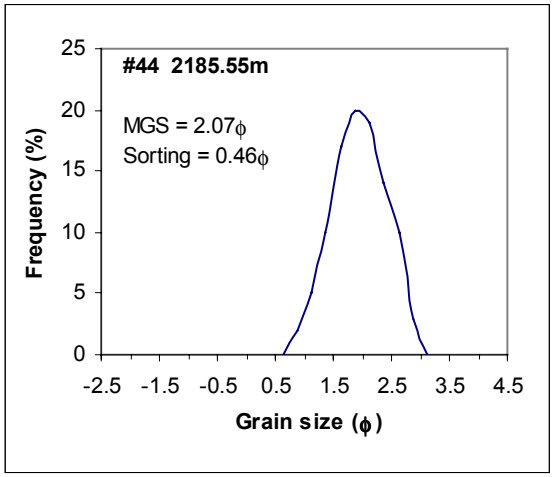
-1-0ϕ = very coarse sand; 0-1ϕ = coarse sand
1-2ϕ = medium sand; 2-3ϕ = fine sand; 3-4ϕ = very fine sand

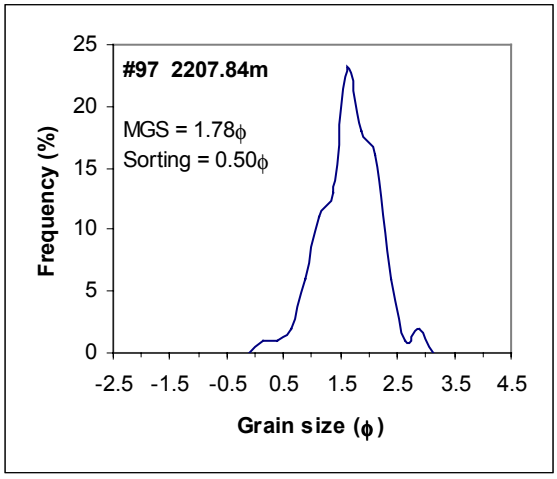
Sorting (ϕSD)

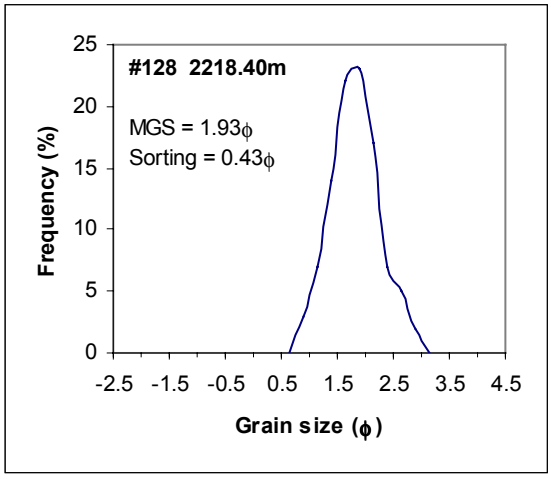
Class	*ϕ Standard Deviation*
very well sorted	<0.35
well sorted	0.35-<0.50
moderately well sorted	0.50-<0.71
moderately sorted	0.71-1.00
poorly sorted	>1.00+

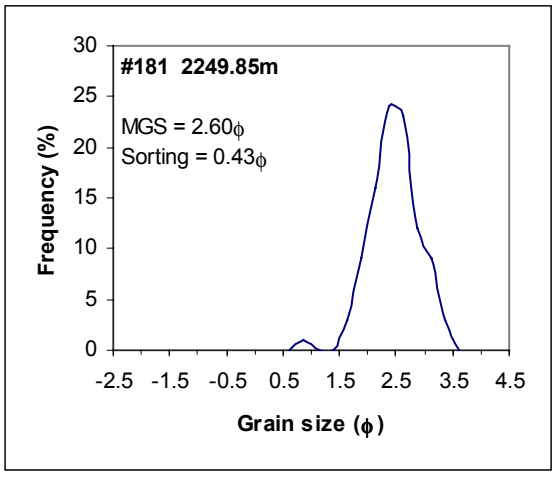
THYLACINE-2 2153.10 – 2251.20m

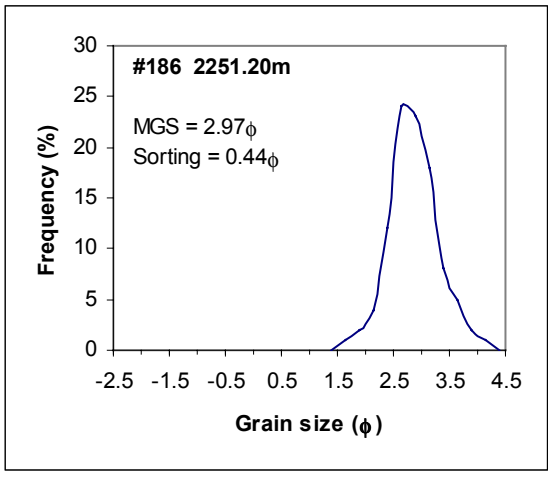




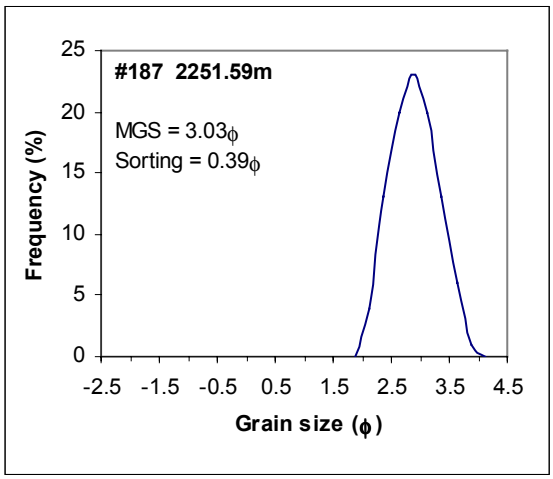


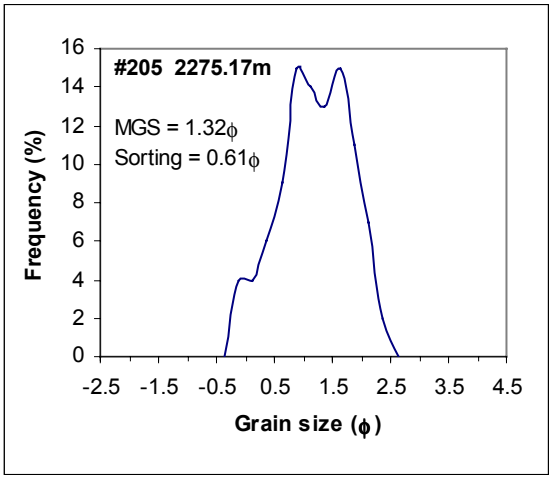


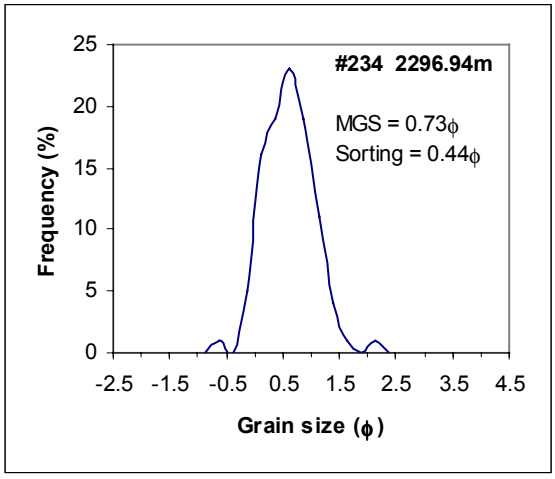


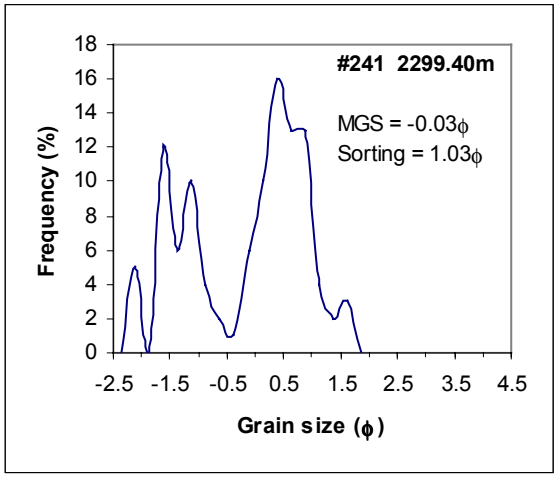


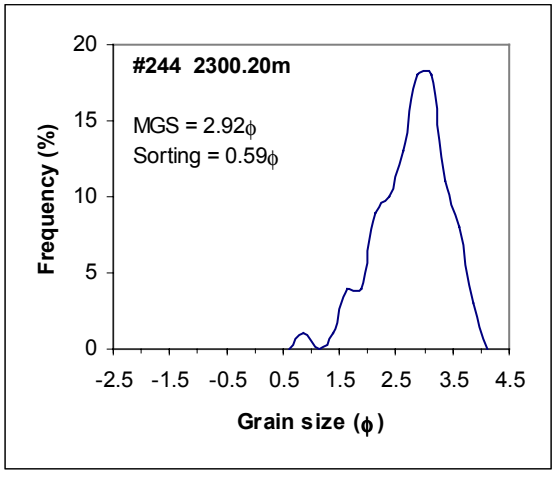
THYLACINE-2 2251.59 – 2300.80m

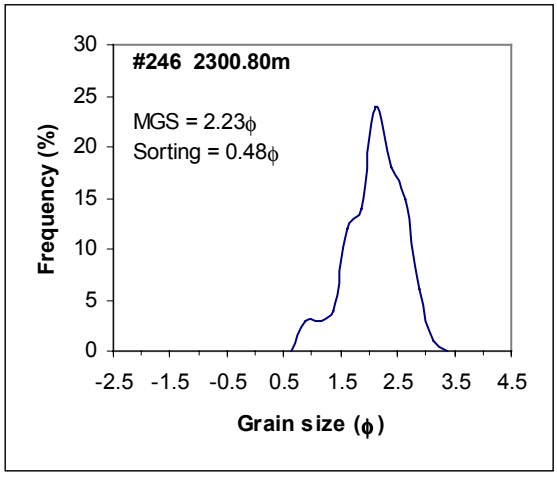




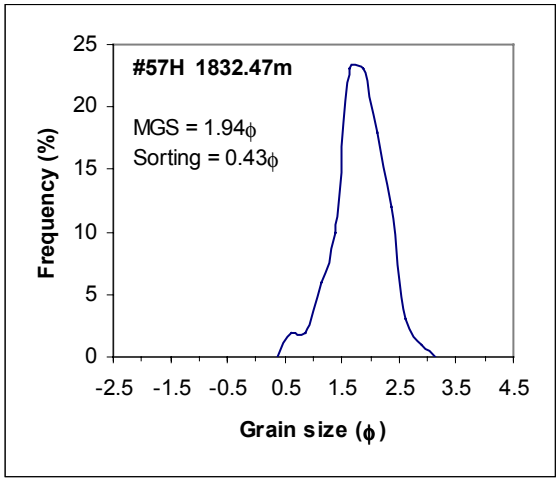








GEOGRAPHE-1 2251.59 – 2300.80m



APPENDIX 3.

X-RAY DIFFRACTOGRAMS

Key to abbreviations:

An = ankerite

Co = corundum (internal standard)

Ca = calcite

D = dickite

I = illite/mica

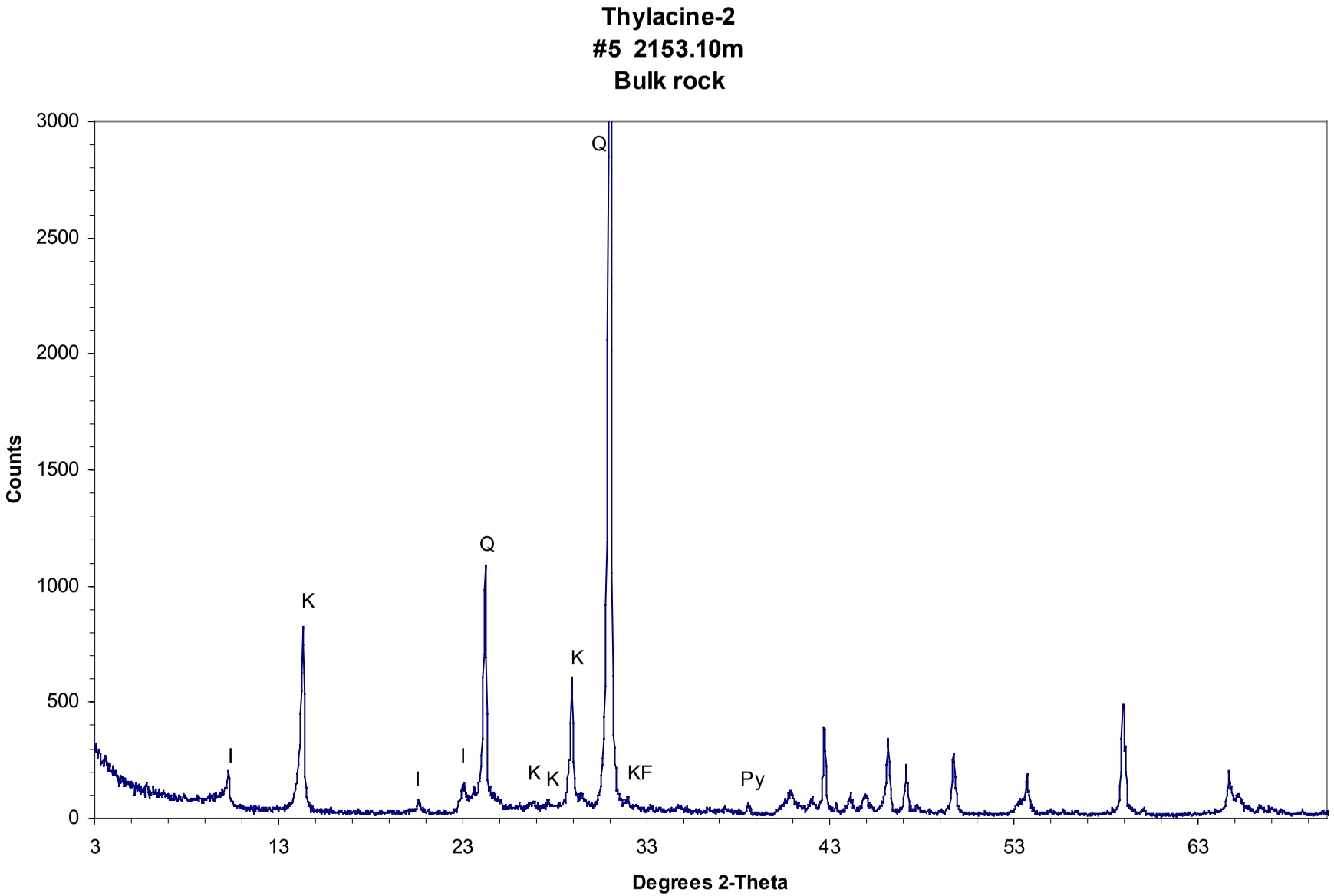
K = kaolinite

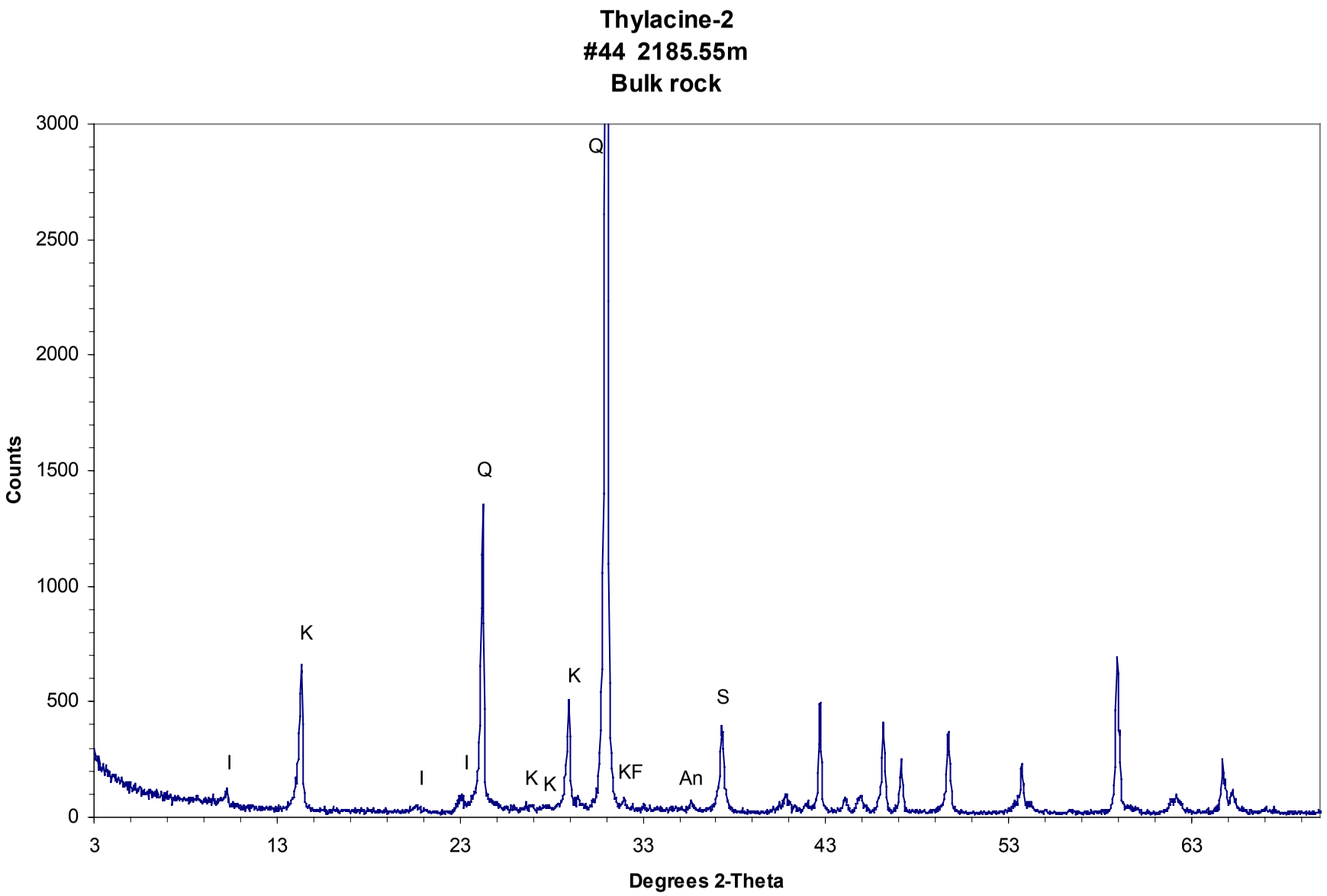
KCl = potassium chloride (contaminant)

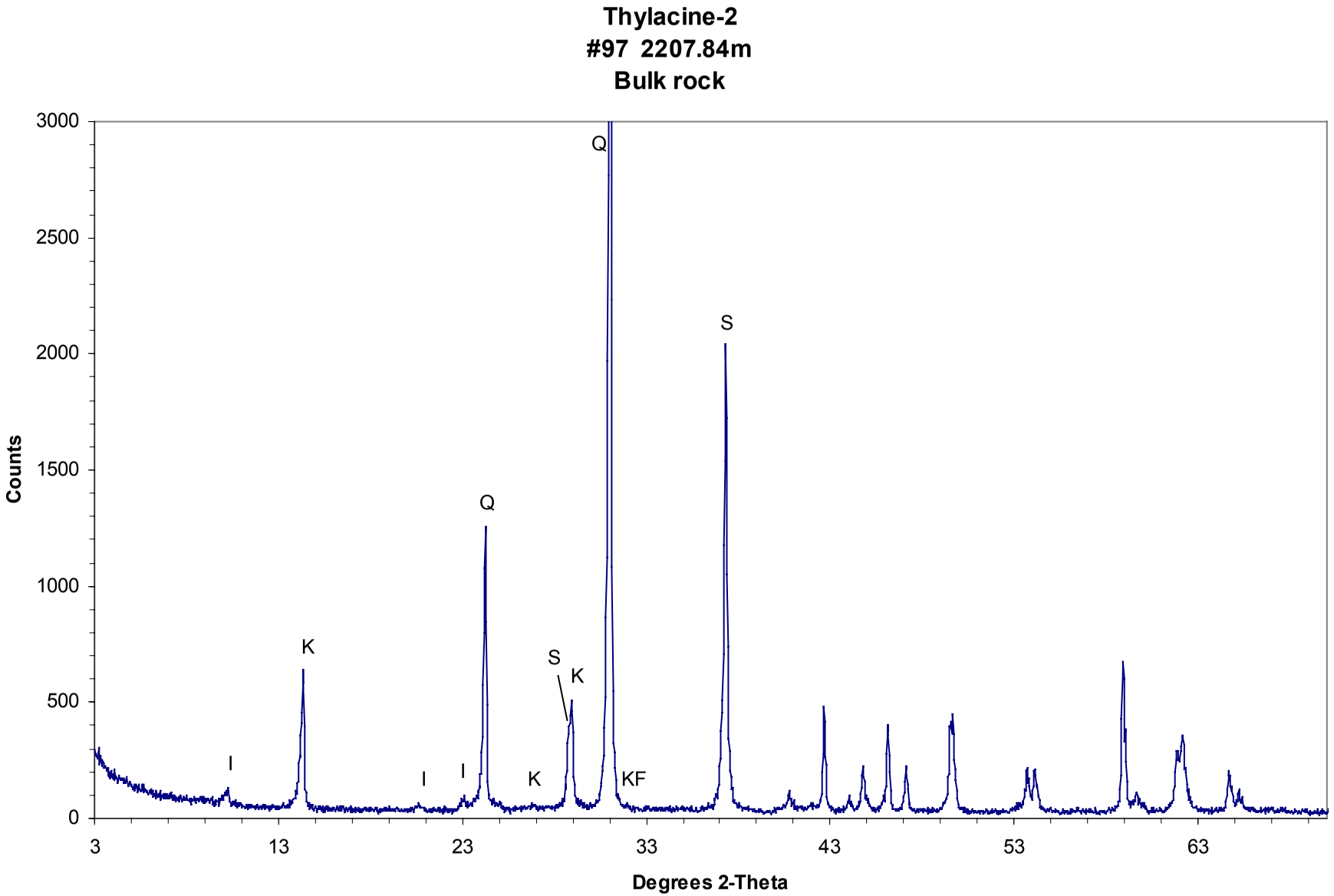
KF = K-feldspar

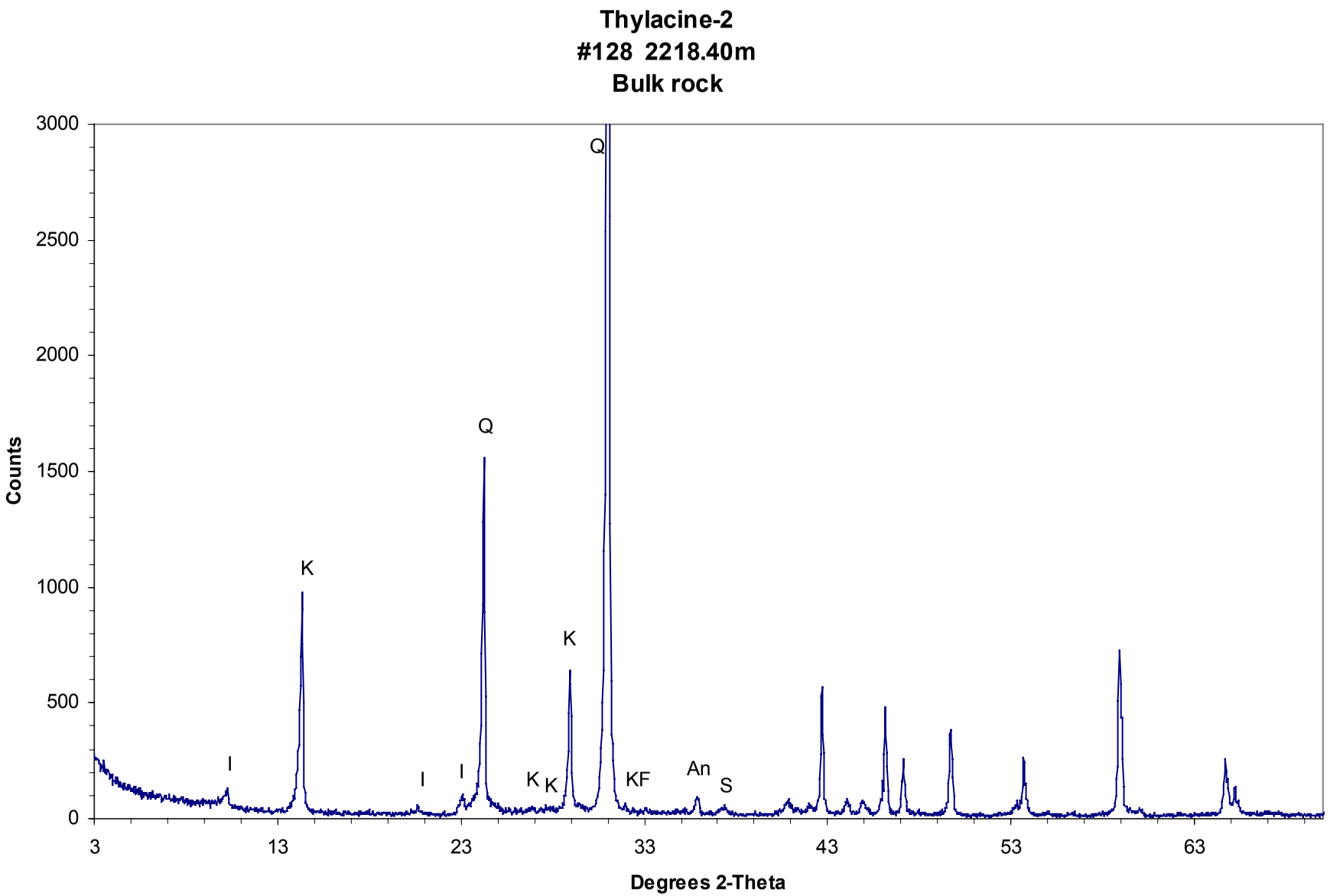
Q = quartz

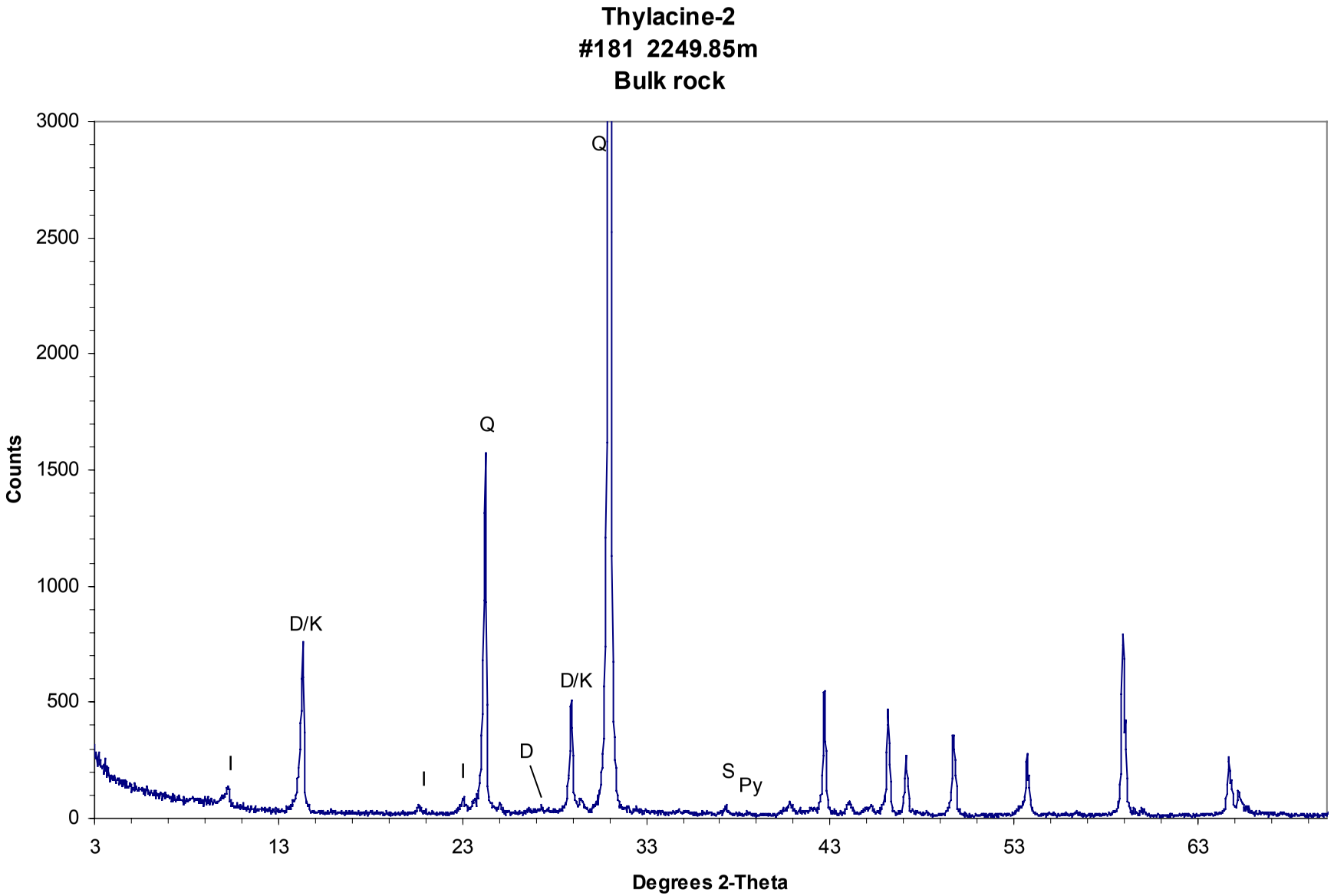
S = siderite

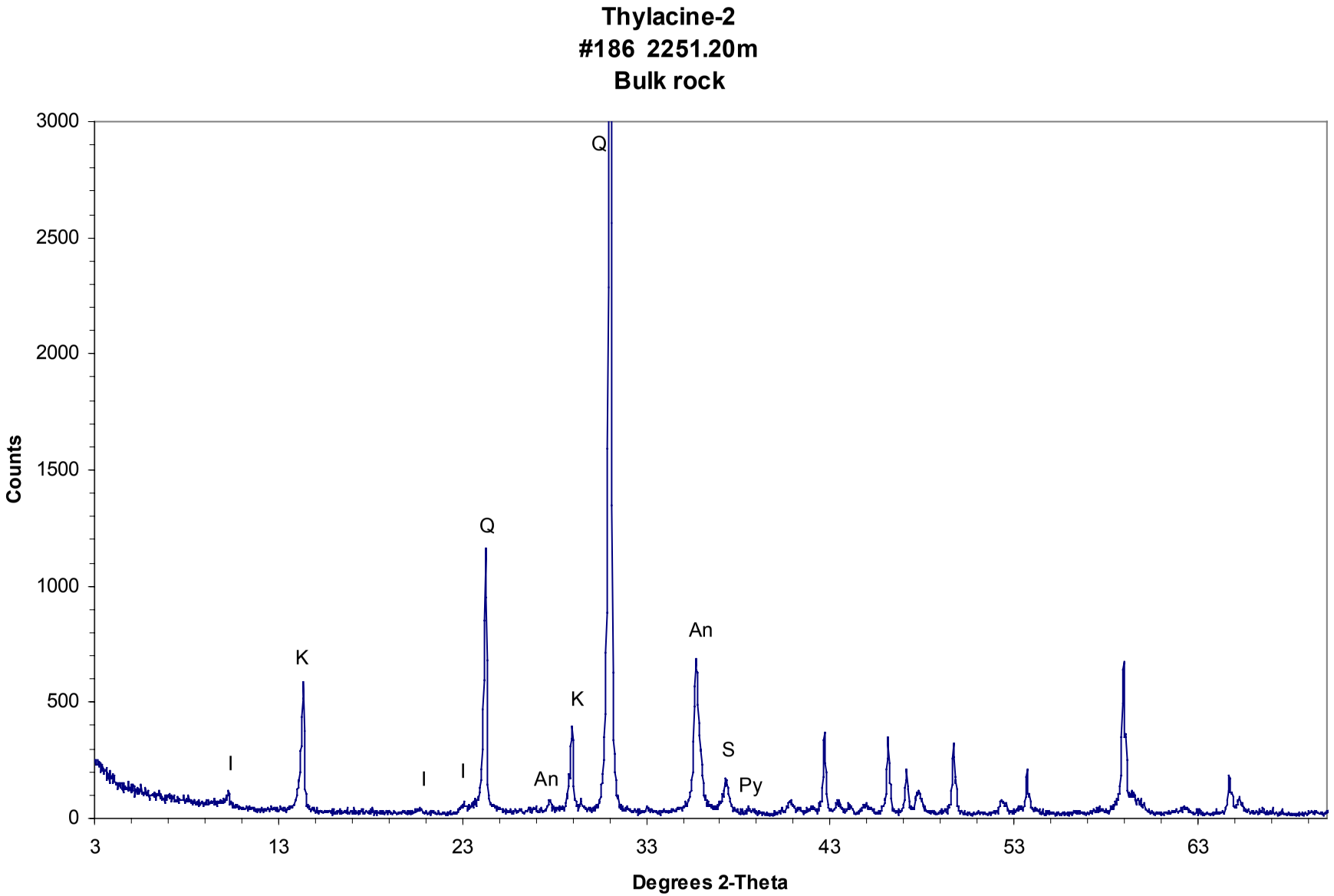

Thylacine-2
#5 2153.10m
Bulk rock
Counts
3000
2500
2000
1500
1000
500
0
3
13
23
33
43
53
63
Degrees 2-Theta
I
K
I
I
Q
K
K
K
Q
KF
Py

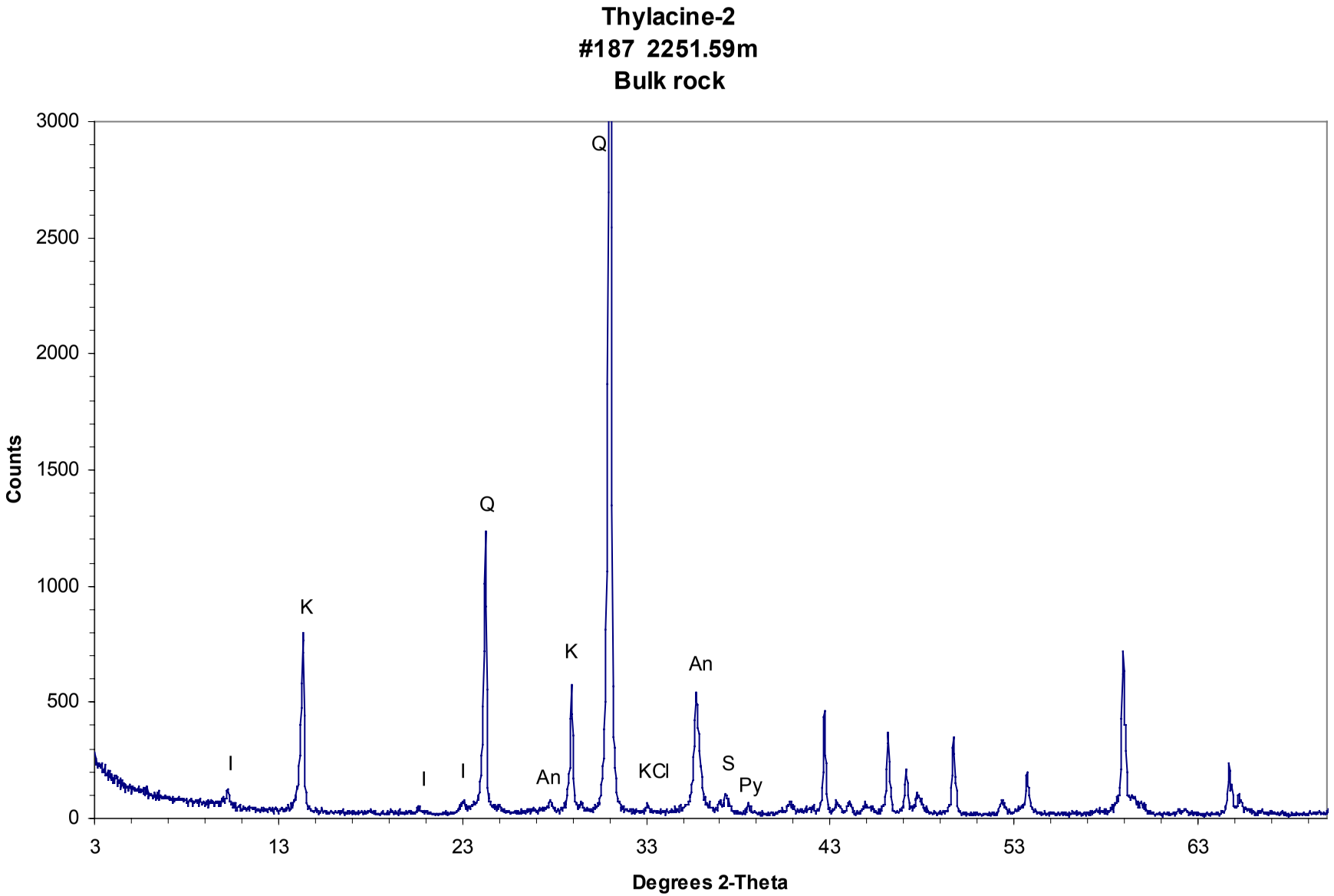

Thylacine-2
#44 2185.55m
Bulk rock
Counts
3000
2500
2000
1500
1000
500
0
3
13
23
33
43
53
63
Degrees 2-Theta
Q
Q
K
K
S
I
I
I
K
K
KF
An

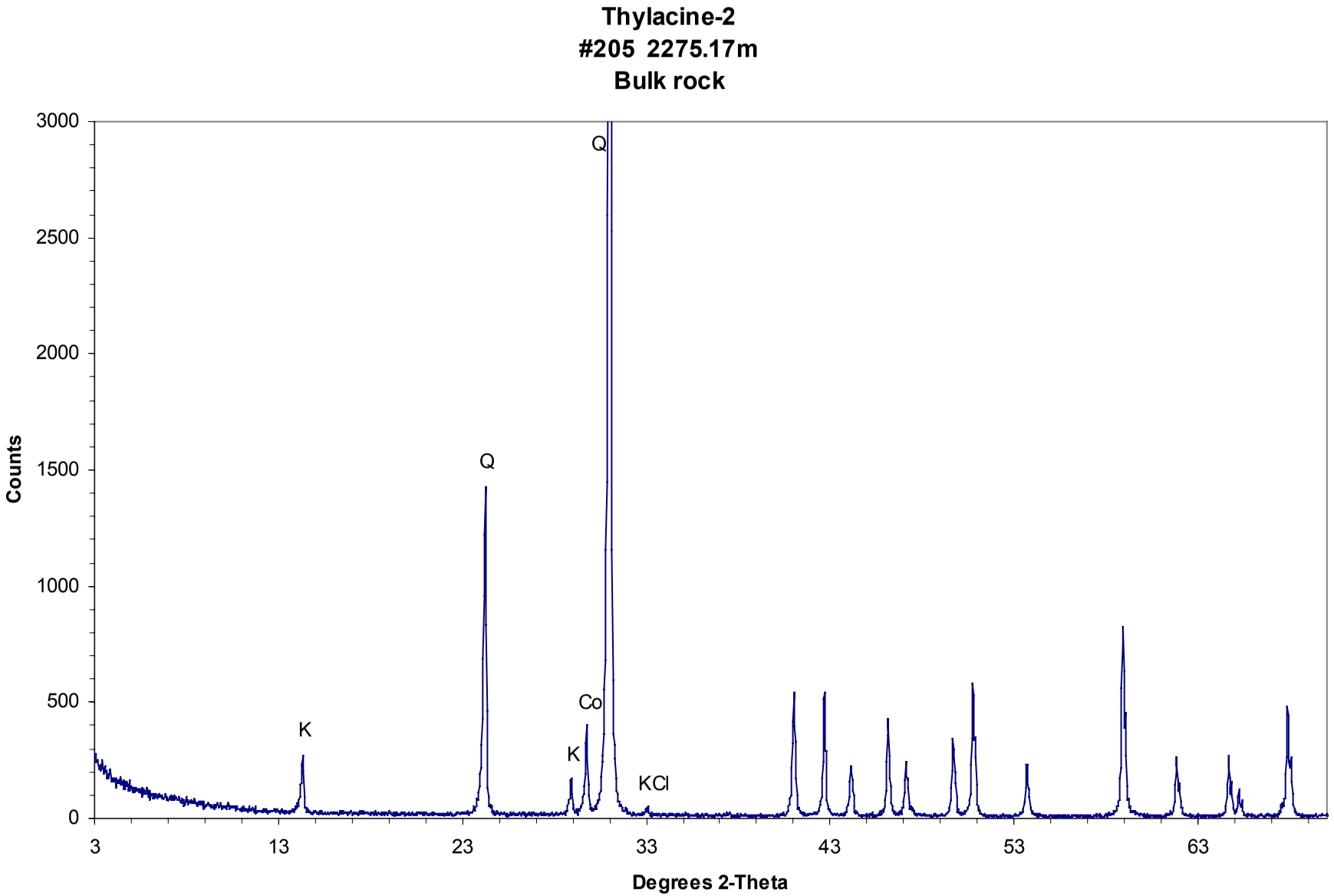

Thylacine-2
#97 2207.84m
Bulk rock
Counts
3000
2500
2000
1500
1000
500
0
3
13
23
33
43
53
63
Degrees 2-Theta
Q
S
Q
K
S
K
I
I
I
K
KF

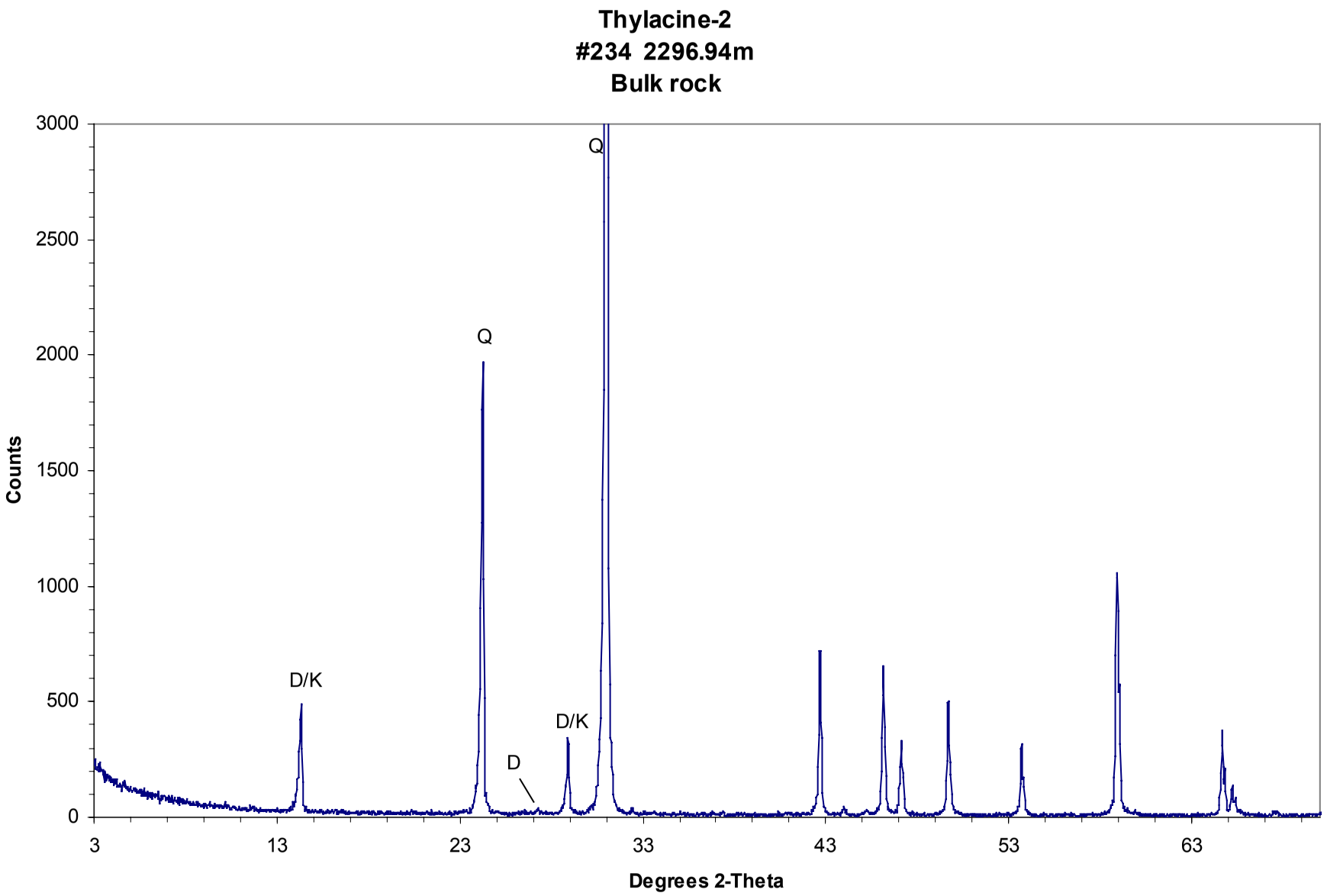

Thylacine-2
#128 2218.40m
Bulk rock
Counts
3000
2500
2000
1500
1000
500
0
3
13
23
33
43
53
63
Degrees 2-Theta
I
K
I
I
Q
K
K
K
Q
KF
An
S

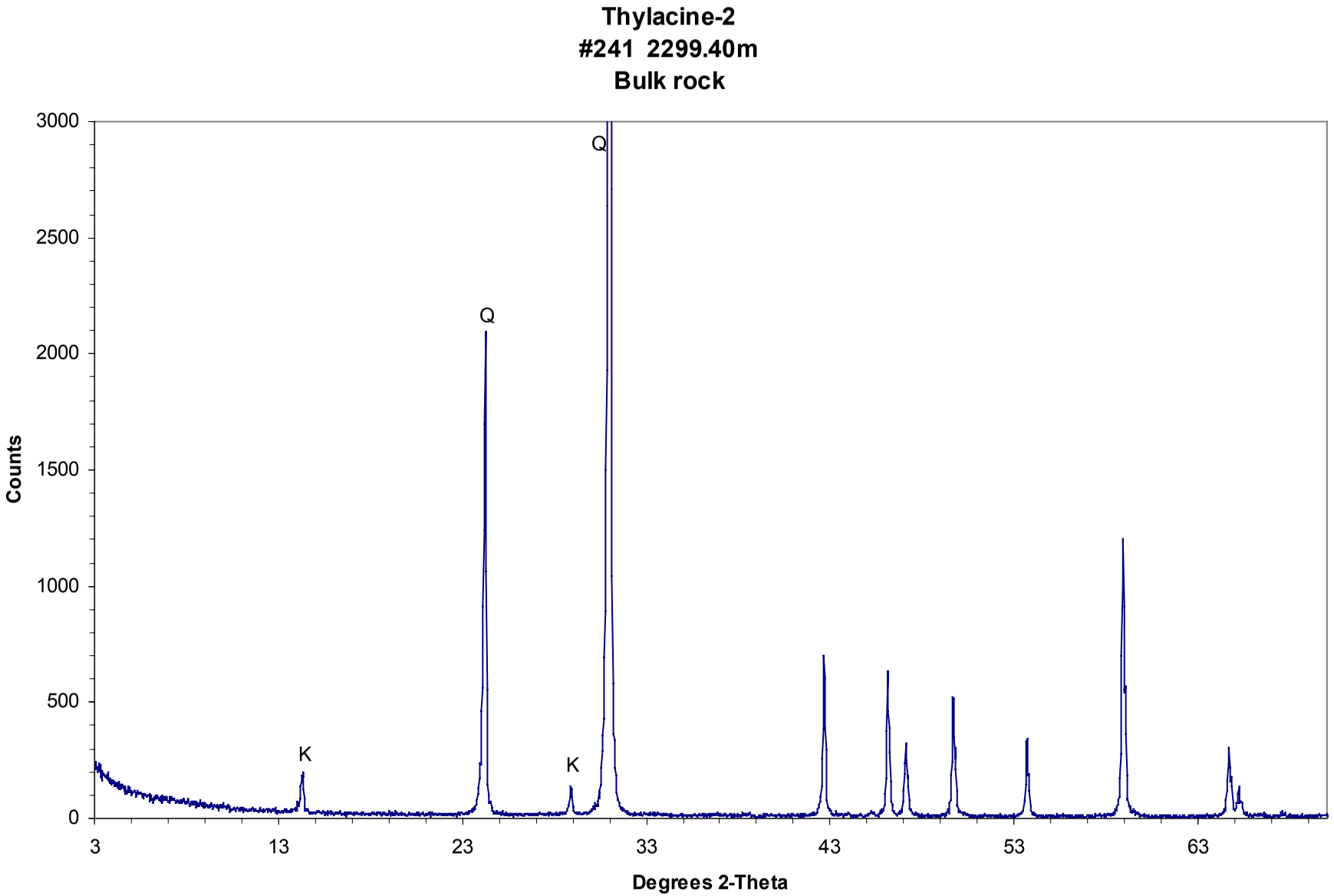

Thylacine-2
#181 2249.85m
Bulk rock
Counts
3000
2500
2000
1500
1000
500
0
3
13
23
33
43
53
63
Degrees 2-Theta
Q
Q
D/K
D/K
I
I
I
D
S
Py

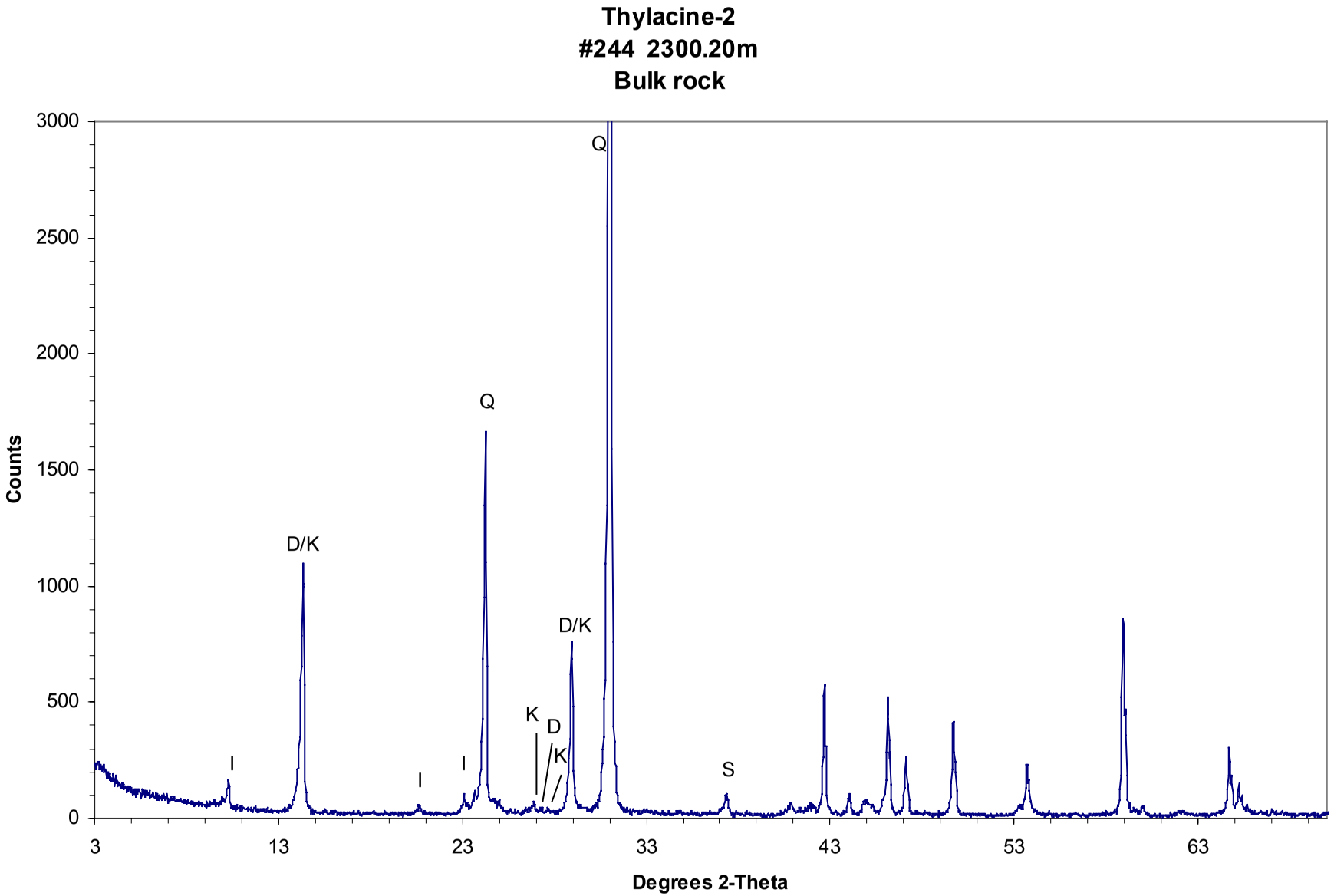

Thylacine-2
#186 2251.20m
Bulk rock
Counts
3000
2500
2000
1500
1000
500
0
3
13
23
33
43
53
63
Degrees 2-Theta
Q
Q
K
K
An
An
S
Py
I
I
I

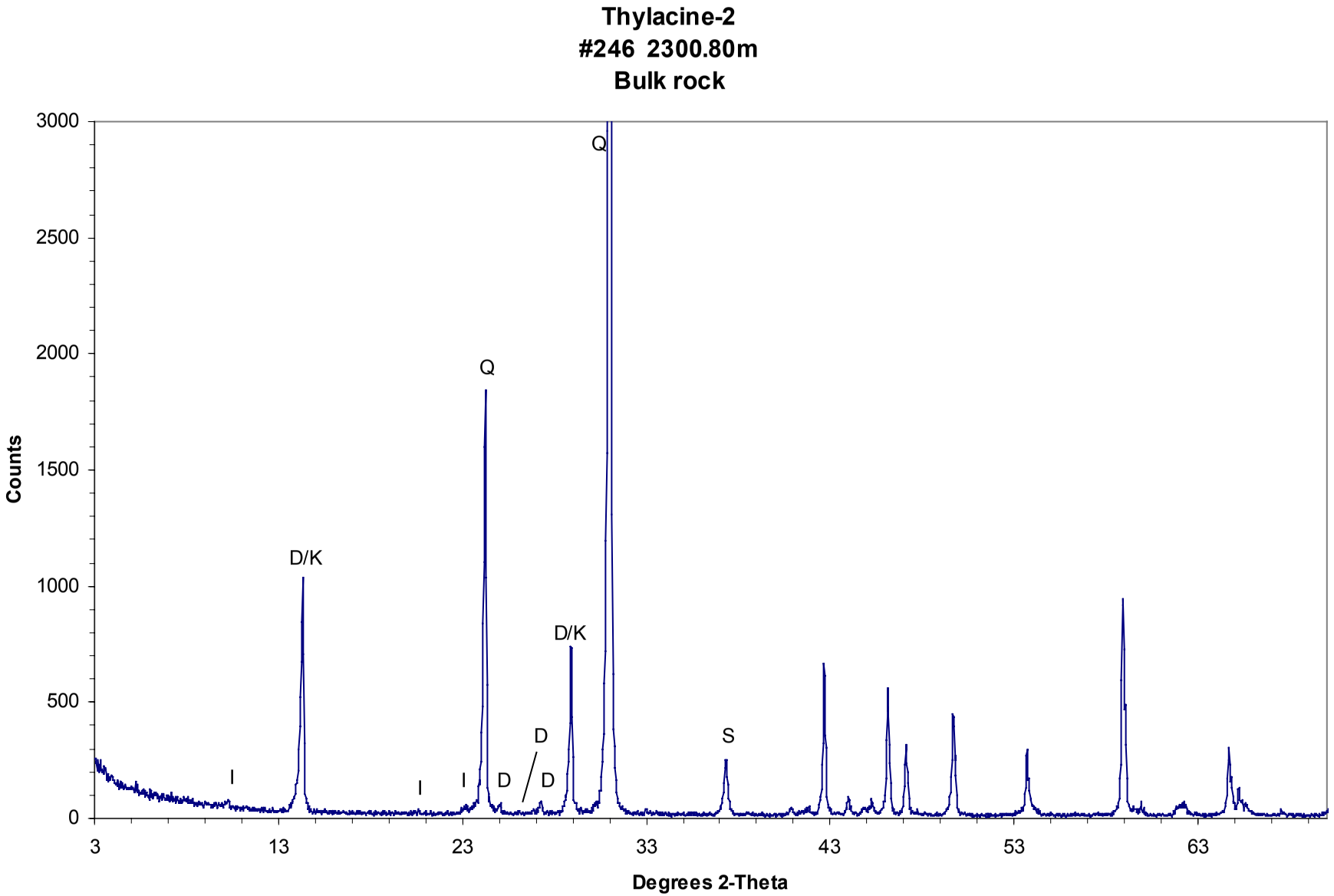

Thylacine-2
#187 2251.59m
Bulk rock
Counts
3000
2500
2000
1500
1000
500
0
3
13
23
33
43
53
63
Degrees 2-Theta
Q
Q
K
K
An
I
I
I
An
KCl
S
Py

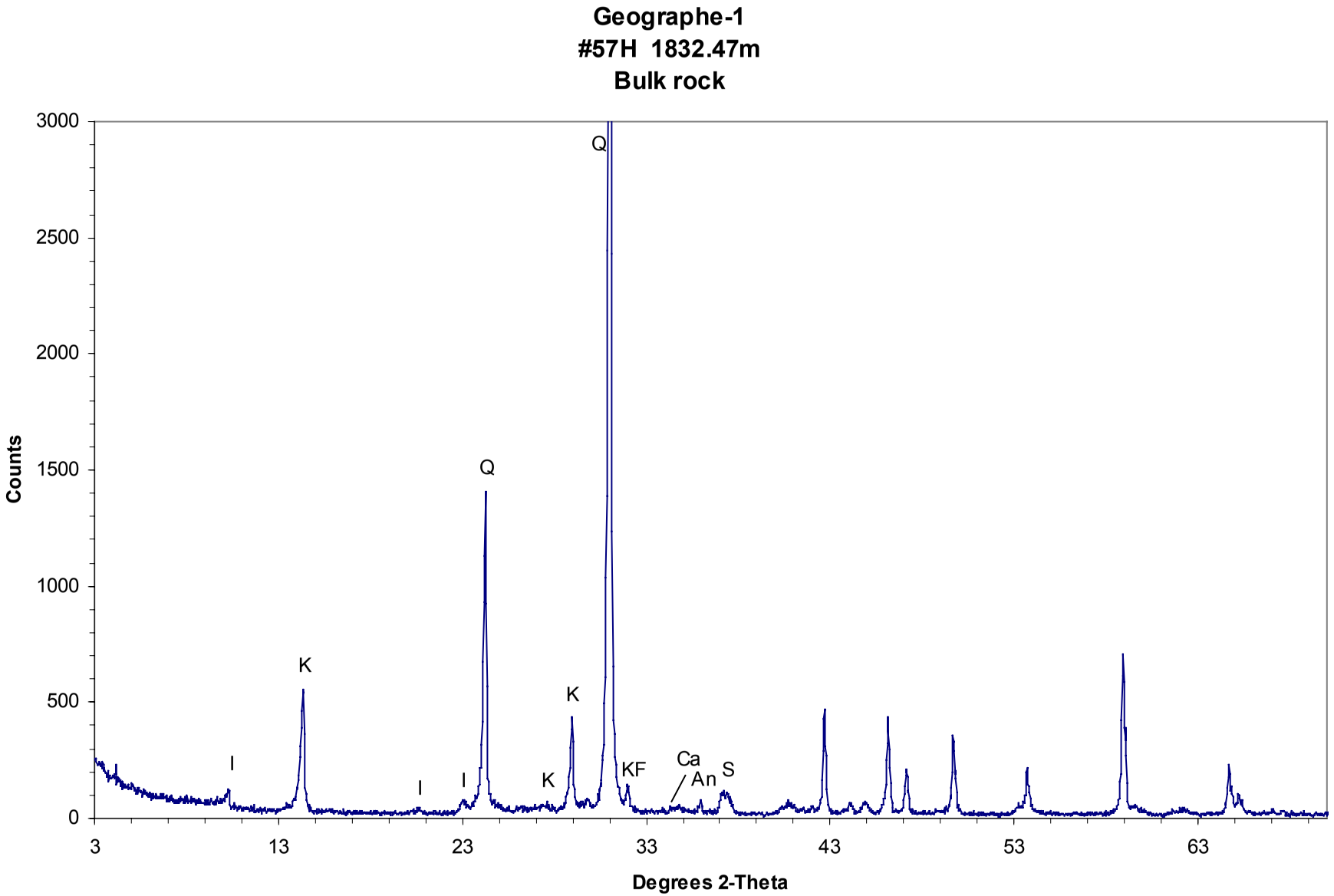

Thylacine-2
#205 2275.17m
Bulk rock
Counts
3000
2500
2000
1500
1000
500
0
3
13
23
33
43
53
63
Degrees 2-Theta
Q
Q
Q
K
K
Co
KCl


Thylacine-2
#234 2296.94m
Bulk rock
Counts
3000
2500
2000
1500
1000
500
0
Q
Q
D/K
D
D/K
3
13
23
33
43
53
63
Degrees 2-Theta


Thylacine-2
#241 2299.40m
Bulk rock
Counts
3000
2500
2000
1500
1000
500
0
Q
Q
Q
K
K
3
13
23
33
43
53
63
Degrees 2-Theta


Thylacine-2
#244 2300.20m
Bulk rock
Counts
3000
2500
2000
1500
1000
500
0
3
13
23
33
43
53
63
Degrees 2-Theta
Q
Q
D/K
D/K
I
I
I
K
D
K
S


Thylacine-2
#246 2300.80m
Bulk rock
Counts
3000
2500
2000
1500
1000
500
0
3
13
23
33
43
53
63
Degrees 2-Theta
Q
Q
D/K
D/K
I
I
I
D
D
D
S


Geographe-1
#57H 1832.47m
Bulk rock
Counts
3000
2500
2000
1500
1000
500
0
3
13
23
33
43
53
63
Degrees 2-Theta
Q
Q
K
K
K
I
I
I
KF
Ca
An
S

APPENDIX 4.

PHOTOMICROGRAPHS

PLATE 1: THYLACINE-2 #5 2153.10m

Rock classification: Sublitharenite

Texture:

Sedimentary structures:	Sporadic, argillaceous burrow infills and discontinuous, fine argillaceous laminae
Sorting:	Well
Average grain size:	0.19mm (fine sand)
Roundness:	Angular-subrounded
Texture:	Grain supported
Packing/grain contacts:	Moderate/long, embayed
Macropore types:	Rare secondary mouldic porosity
Core analyses:	Por. = 13.8%, Perm. = 0.409mD, GD = 2.64g/cc

Composition:

Quartz (monocrystalline)	42.3%	Sedimentary rock fragments	2.3%
Quartz (polycrystalline)	4.0%	Organics	0.7%
Quartz overgrowths	1.1%	Pyrite	0.7%
Chert	1.4%	Authigenic kaolin (pf)	5.8%
K-feldspar	1.7%	Authigenic kaolin (rpl)	17.3%
Volcanic rock fragments	0.7%	Authigenic illite (replacement)	3.0%
Metamorphic rock fragments	11.5%	Detrital clay	7.5%

Comments: This sublitharenite was highly susceptible to authigenic clay formation and physical compaction on account of containing abundant micaceous/argillaceous rock fragments at the time of accumulation. Primary intergranular porosity has been completely eliminated by authigenic clay (kaolin, illite) formation, ductile grain/authigenic clay compaction, grain contact dissolution and localised quartz overgrowth cementation. In addition, intergranular spaces are filled by localised detrital clay, the distribution of which has been influenced by bioturbation. Sample is almost totally microporous

PLATE 1: THYLACINE-2 #5 2153.10m

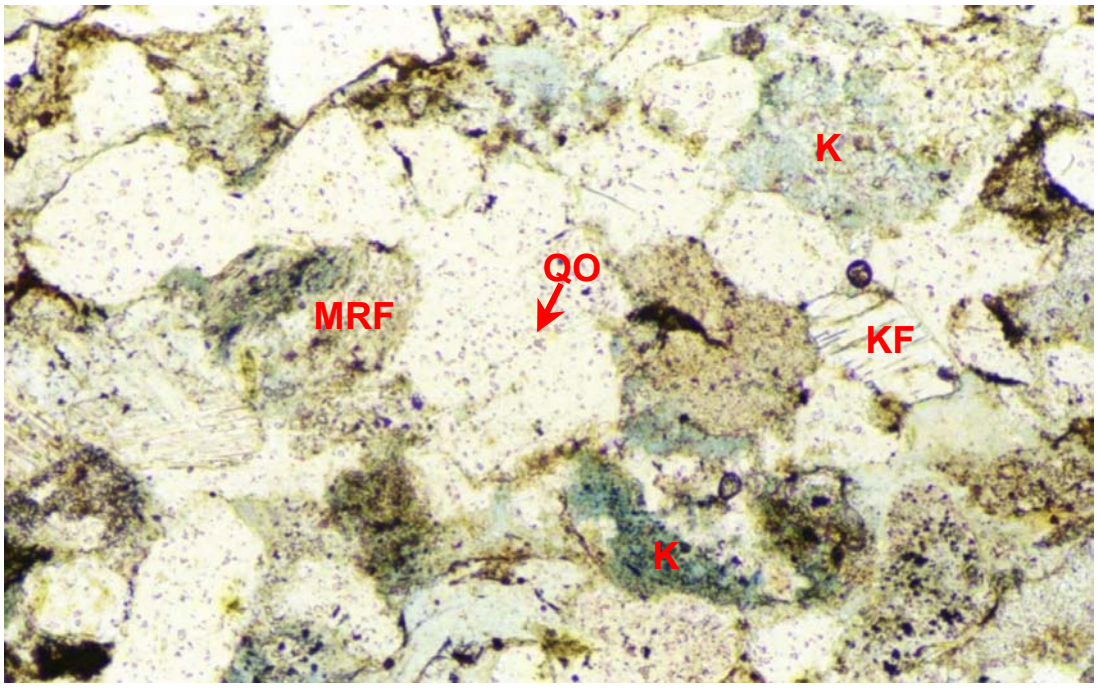
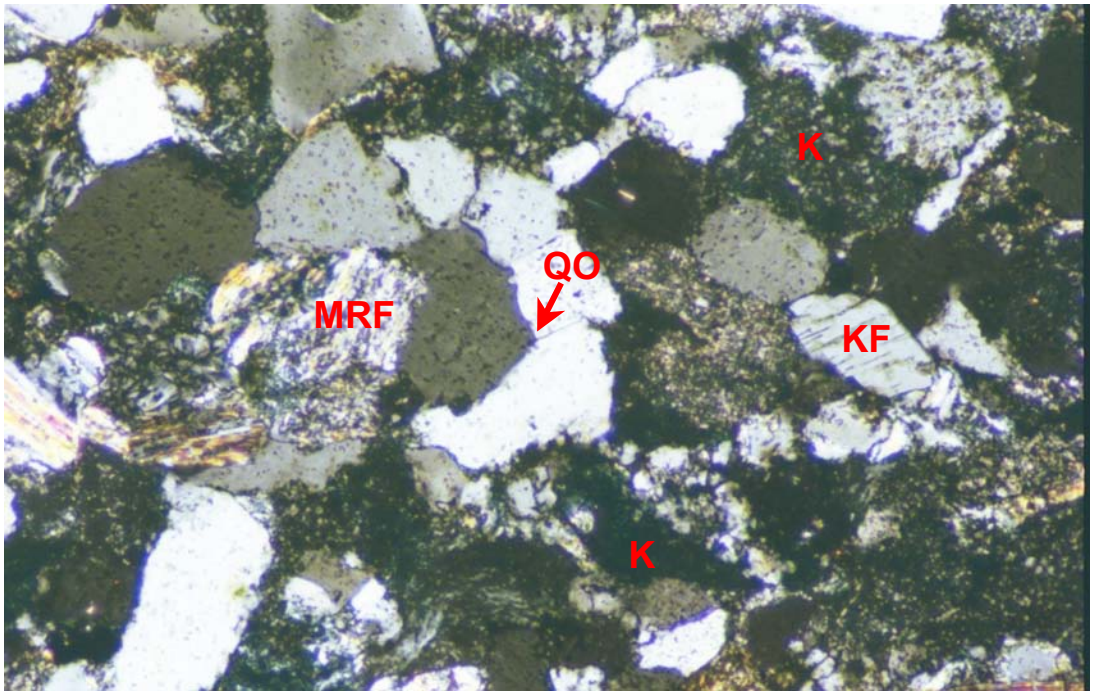


FIGURE 1 Plane polarised light

FIGURE 2 Crossed polarisers

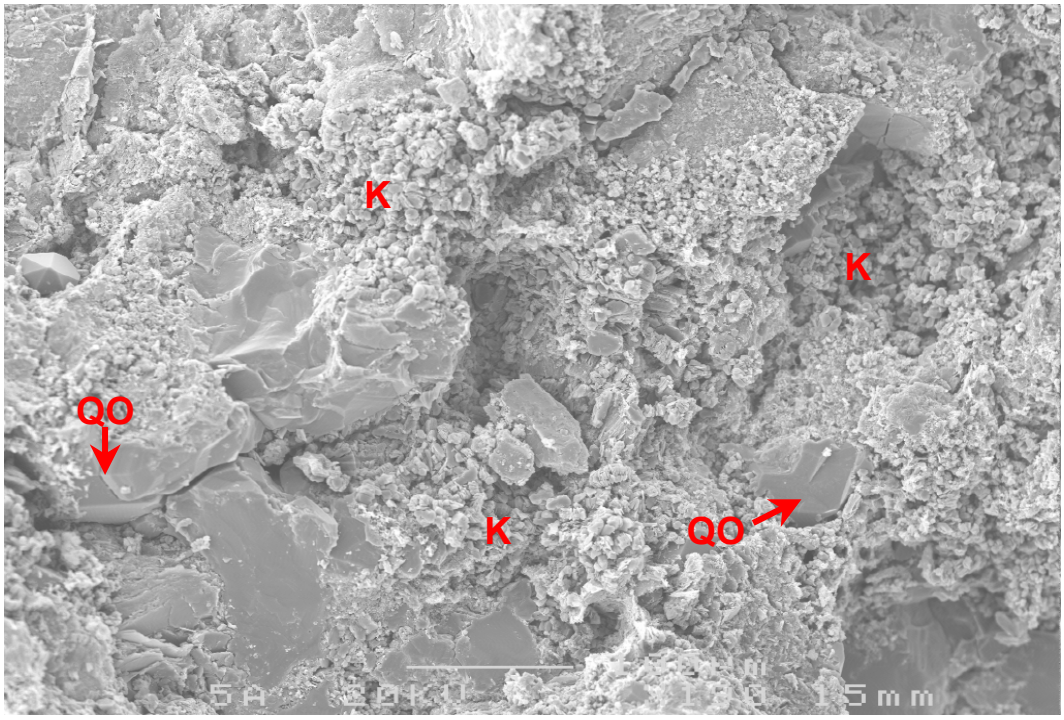
0.2mm



Intergranular porosity has been eliminated by authigenic kaolin (K) formation, physical compaction, grain contact dissolution, and, where quartz grains are juxtaposed, quartz overgrowth (QO) cementation. The marked kaolin is highly microporous as shown by its blue hue. Framework grains include micaceous metamorphic rock fragments (MRF) and K-feldspar (KF).

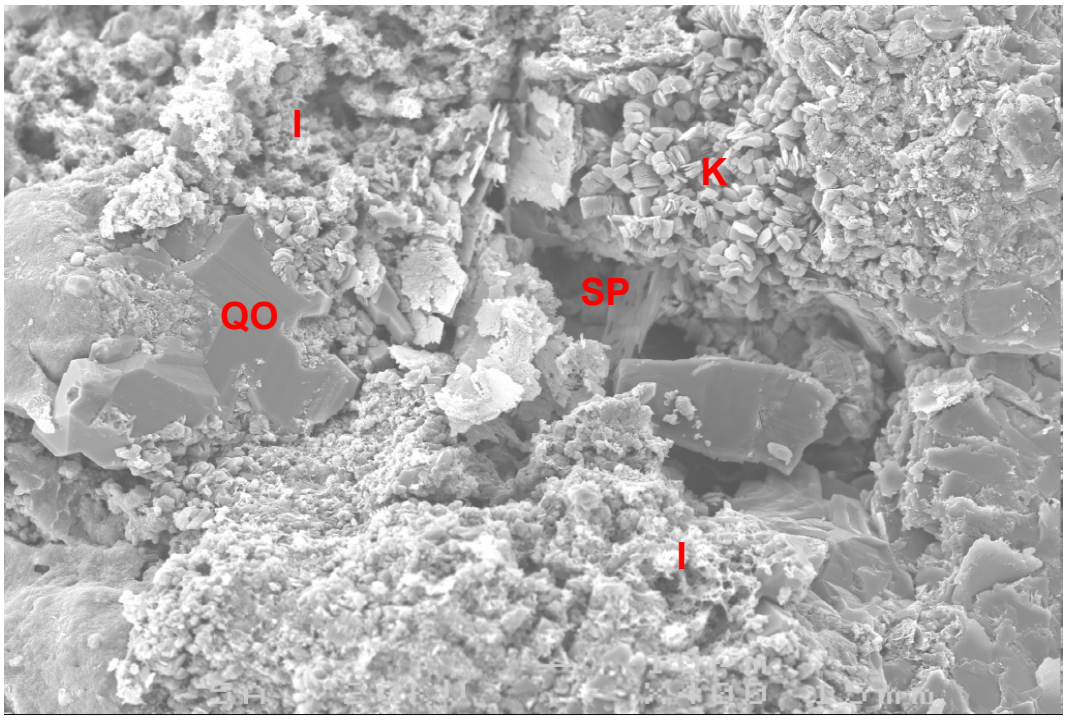
PLATE 2: THYLACINE-2 #5 2153.10m cont.

FIGURE 1



Low permeability (0.409mD) is largely explained by the high content of authigenic kaolin (K) pseudomatrix that has formed mainly by alteration of micaceous/illitic rock fragments and mica. Quartz overgrowth (QO) cementation has been inhibited by the presence of abundant authigenic kaolin and compacted ductile grains.

FIGURE 2



K-feldspar has dissolved to form a rare secondary mouldic pore (SP), the presence of which does nothing to enhance reservoir quality. The pore is largely surrounded by authigenic kaolin (K) and illite (I) that are the altered remnants of micaceous grains. Quartz grains are locally partly enveloped by quartz overgrowths (QO).

PLATE 3: THYLACINE-2 #44 2185.55m

Rock classification: Sublitharenite

Texture:

Sedimentary structures: Massive

Sorting: Well

Average grain size: 0.24mm (fine sand)

Roundness: Subangular-subrounded

Texture: Grain supported

Packing/grain contacts: Moderate/long, embayed

Macropore types: Rare secondary intragranular porosity

Core analyses: Por. = 15.4%, Perm. = 0.728mD, GD = 2.70g/cc

Composition:

Quartz (monocrystalline)	44.4%	Heavy minerals	0.3%
Quartz (polycrystalline)	4.9%	Siderite (replacement)	8.4%
Quartz overgrowths	1.4%	Ankerite (replacement)	0.9%
Chert	1.1%	Glauconite	0.3%
K-feldspar	0.7%	Authigenic kaolin (pf)	5.2%
Volcanic rock fragments	0.7%	Authigenic kaolin (rpl)	15.1%
Metamorphic rock fragments	12.9%	Authigenic illite (replacement)	2.0%
Sedimentary rock fragments	1.4%	Secondary porosity (intragran)	0.3%

Comments: Like in the previous sample, intergranular porosity has been almost completely eliminated by authigenic kaolin formation, ductile grain/authigenic clay compaction, grain contact dissolution and localised quartz overgrowth cementation. Scattered patches of microcrystalline/finely-crystalline siderite up to 0.9mm long replace biotite, and there are disseminated fine siderite rhombs and sporadic patches of coarsely-crystalline ankerite. Rare secondary intragranular porosity is the result of partial K-feldspar dissolution. Much kaolin has a blue hue that indicates that it is sufficiently microporous for impregnation by epoxy resin. Sample is almost entirely microporous.

PLATE 3: THYLACINE-2 #44 2185.55m

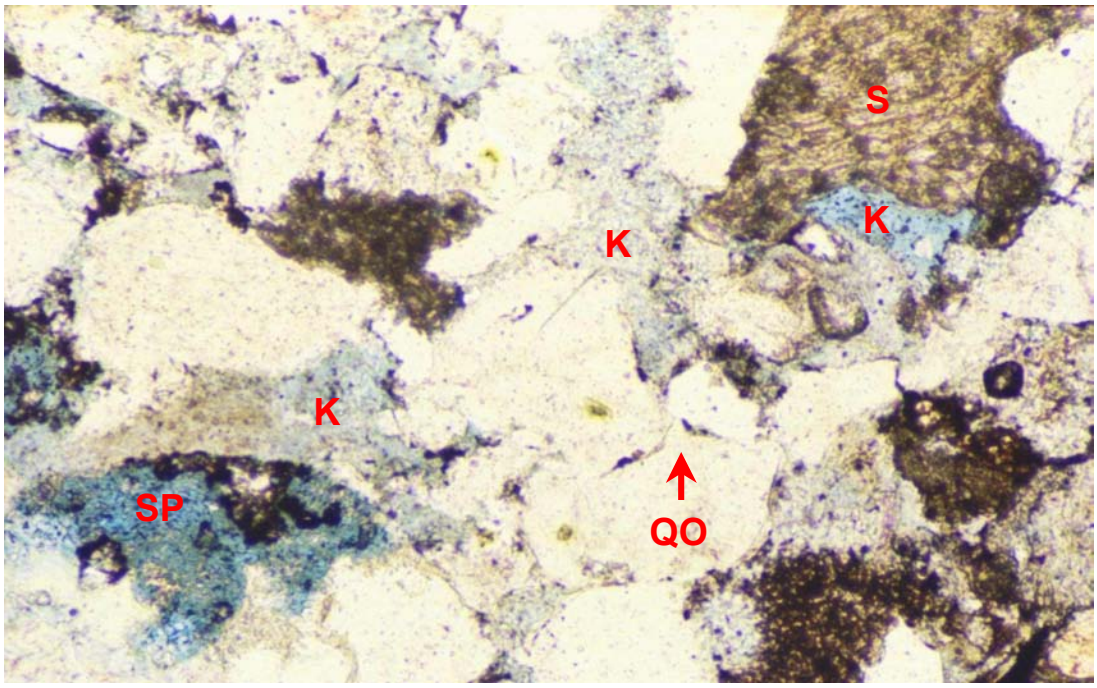
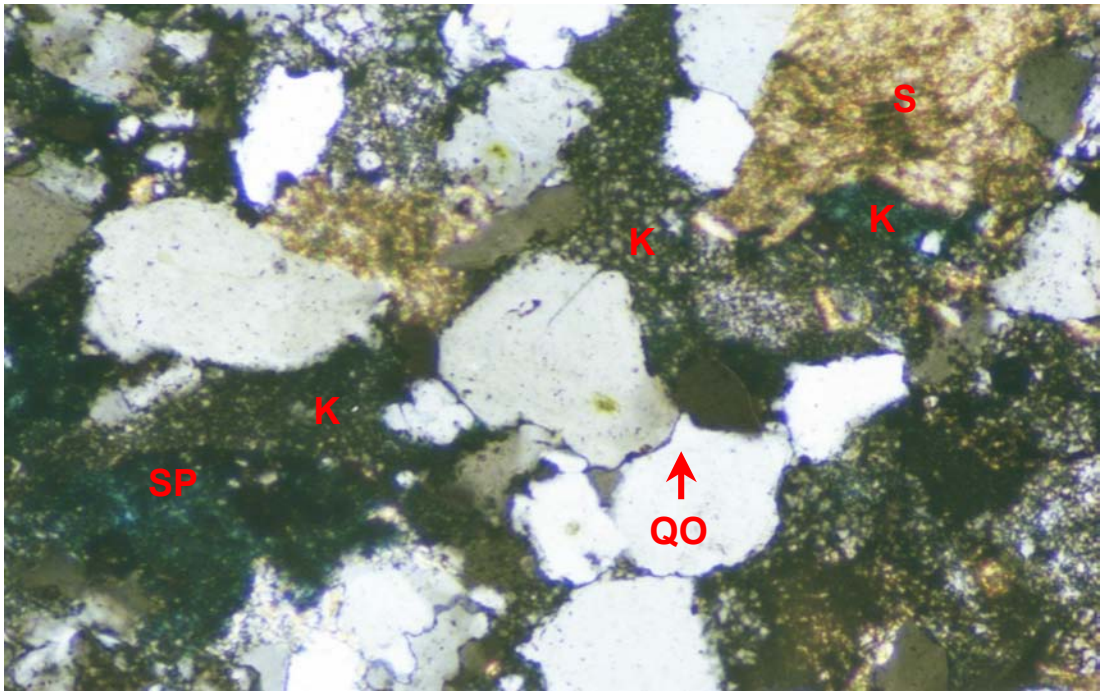


FIGURE 1 Plane polarised light
FIGURE 2 Crossed polarisers

0.2mm



Rare secondary intragranular porosity (SP) is associated with a partly dissolved K-feldspar grain. Within surrounding areas, intergranular porosity has been eliminated by authigenic kaolin (K) formation, physical compaction, grain contact dissolution and localised quartz overgrowth (QO) cementation. Biotite is replaced by finely-crystalline siderite (S). Kaolin is highly microporous as shown by its blue hue.

PLATE 4: THYLACINE-2 #97 2207.84m

Rock classification: Sideritic litharenite

Texture:

Sedimentary structures: Massive

Sorting: Moderately-well

Average grain size: 0.29mm (medium sand)

Roundness: Subangular-subrounded

Texture: Grain supported

Packing/grain contacts: Moderate/long, embayed, rarely sutured

Macropore types: Primary intergranular porosity, secondary intergranular porosity, secondary mouldic porosity, secondary intragranular porosity

Core analyses: Por. = 22.1%, Perm. = 25.1mD, GD = 2.90g/cc

Composition:

Quartz (monocrystalline)	32.3%	Siderite (pore filling)	15.5%
Quartz (polycrystalline)	6.0%	Siderite (pore filling)	4.0%
Quartz overgrowths	3.0%	Glauconite	0.3%
Chert	1.1%	Authigenic kaolin (pf)	3.0%
K-feldspar	0.7%	Authigenic kaolin (rpl)	12.8%
Volcanic rock fragments	0.6%	Authigenic illite (replacement)	1.7%
Metamorphic rock fragments	11.7%	Primary porosity (intergran)	2.1%
Sedimentary rock fragments	2.9%	Secondary porosity (intergran)	0.7%
Mica	0.3%	Secondary porosity (mouldic)	0.3%
Pyrite	0.3%	Secondary porosity (intragran)	0.7%

Comments: This sideritic litharenite contains abundant siderite that mainly forms uniformly disseminated, 50-100μm rhombic/scalenohedral crystals that occur along grain contacts and within intergranular spaces and authigenic kaolin. Siderite also occurs as a finely-crystalline replacement of biotite. In addition to siderite, intergranular areas are commonly occupied by highly microporous authigenic kaolin and localised quartz overgrowths, and there has been further porosity loss by minor grain contact dissolution and ductile grain/authigenic clay compaction. Small primary pores are preserved where quartz overgrowths and siderite do not completely fill all available intergranular space between juxtaposed quartz grains, and widely scattered secondary pores occur where K-feldspar and labile rock fragments have partly dissolved. Being invariably clogged by siderite, authigenic clay and quartz overgrowths, macropores have limited connectivity.

PLATE 4: THYLACINE-2 #97 2207.84m

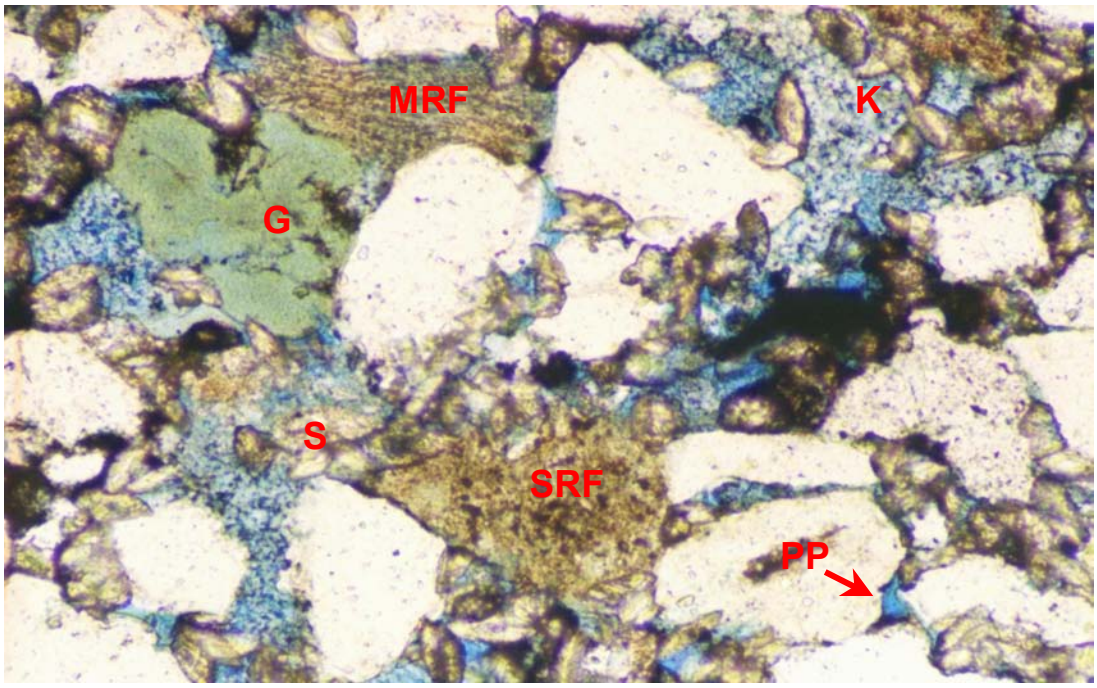
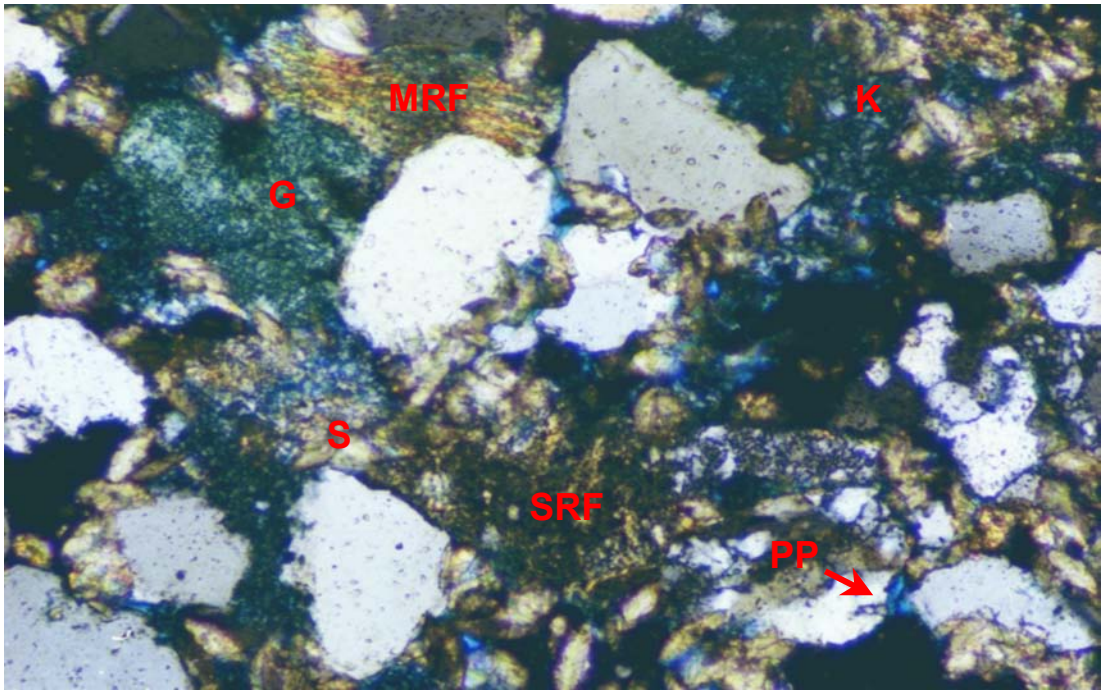


FIGURE 1 Plane polarised light
FIGURE 2 Crossed polarisers

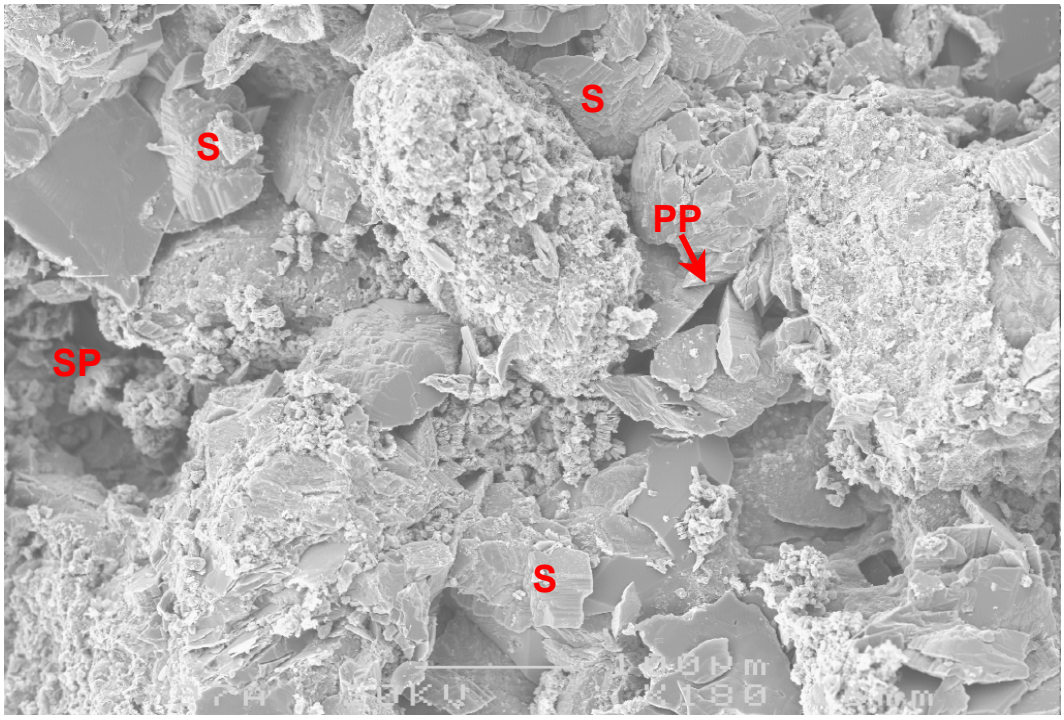
0.2mm



Connection between small primary intergranular pores (PP) is severely reduced by extensive pore filling by disseminated fine siderite crystals (S) and highly microporous authigenic kaolin (K) that has formed by labile grain alteration. Framework grains include micaceous metamorphic rock fragments (MRF), argillaceous sedimentary rock fragments (SRF) and reworked peloidal glauconite (G).

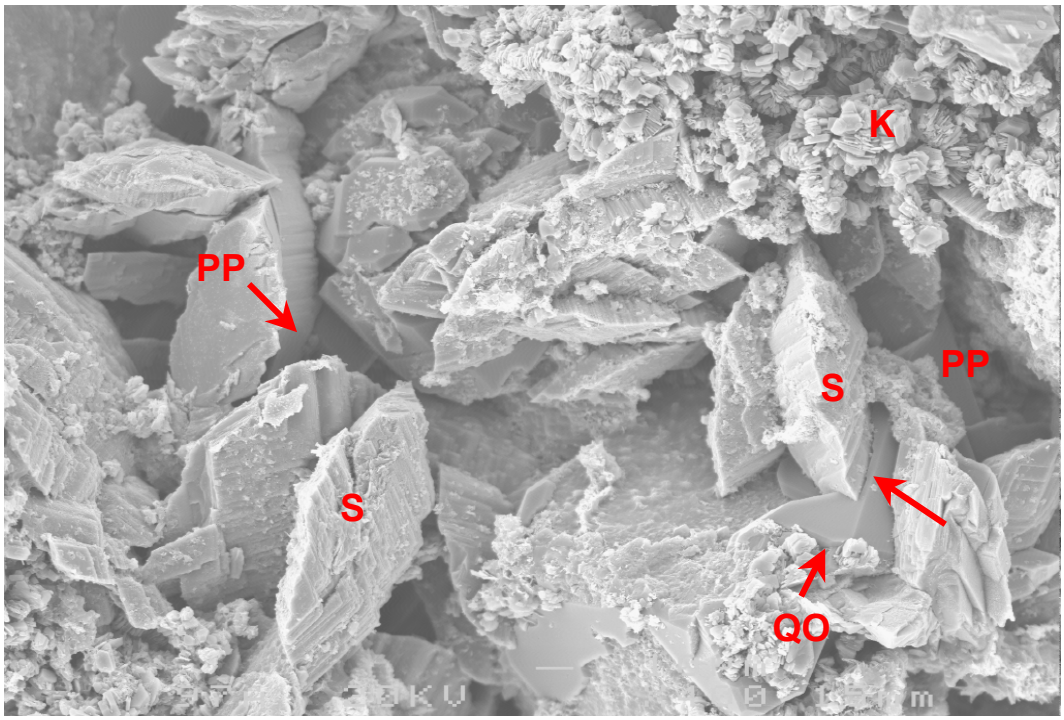
PLATE 5: THYLACINE-2 #97 2207.84m cont.

FIGURE 1



Primary porosity (PP) has been severely reduced by precipitation of fine, early-diagenetic siderite crystals (S) within all intergranular spaces. A secondary mouldic pore (SP) is the result of labile grain dissolution.

FIGURE 2



Although the presence of siderite (S) and authigenic kaolin (K) within intergranular spaces greatly reduces permeability, the sand is much more permeable than the previous two samples on account of containing minor primary porosity (PP). Siderite is enclosed (arrow) by later-formed quartz overgrowths (QO).

PLATE 6: THYLACINE-2 #128 2218.40m

Rock classification: Sublitharenite

Texture:

Sedimentary structures: Massive

Sorting: Well

Average grain size: 0.26mm (medium sand)

Roundness: Subangular-subrounded

Texture: Grain supported

Packing/grain contacts: Moderate/long, embayed, locally sutured/microstylolitic

Macropore types: Rare primary intergranular porosity

Core analyses: Por. = 11.8%, Perm. = 0.445mD, GD = 2.66g/cc

Composition:

Quartz (monocrystalline)	46.9%	Organics	0.7%
Quartz (polycrystalline)	5.7%	Siderite (replacement)	0.9%
Quartz overgrowths	2.0%	Ankerite (replacement)	0.7%
Chert	1.1%	Glauconite	0.3%
K-feldspar	1.1%	Authigenic kaolin (pf)	5.8%
Metamorphic rock fragments	13.7%	Authigenic kaolin (rpl)	15.6%
Sedimentary rock fragments	2.3%	Authigenic illite (replacement)	2.9%
Heavy minerals	0.3%		

Comments: Intergranular porosity has been almost completely eliminated by authigenic kaolin formation, ductile grain/authigenic clay compaction, grain contact dissolution (including microstylolitisation where grain contact dissolution has been promoted by illitic clay films) and localised quartz overgrowth cementation. Finely-crystalline siderite and coarsely-crystalline ankerite form scattered replacement patches. Sample is almost totally microporous.

PLATE 6: THYLACINE-2 #128 2218.40m

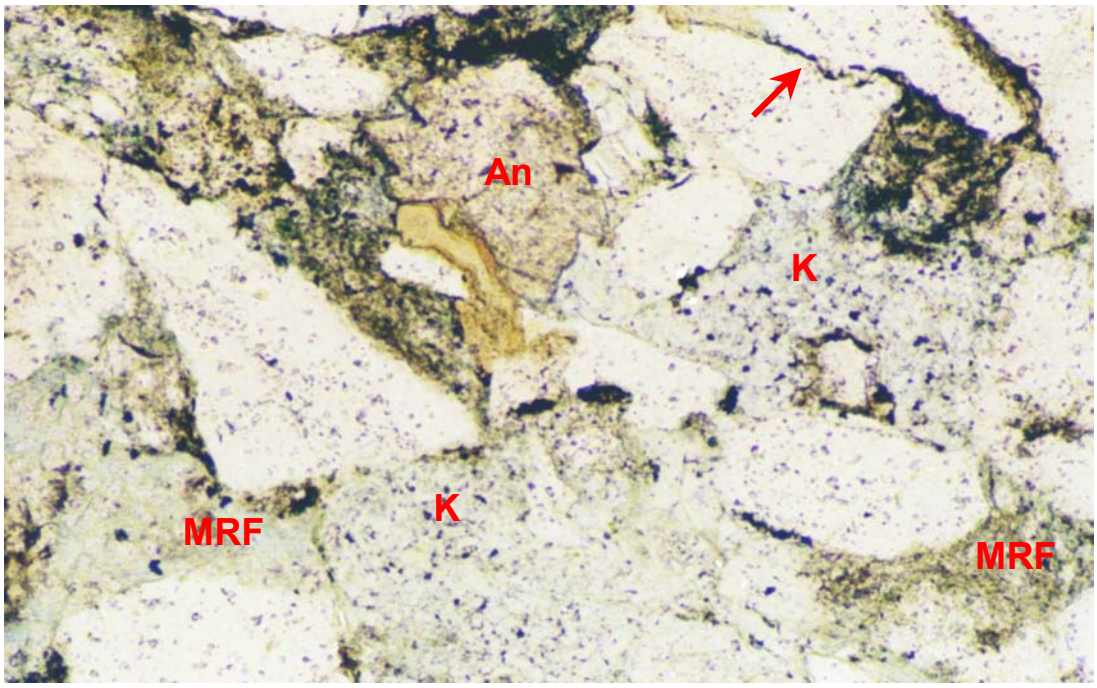
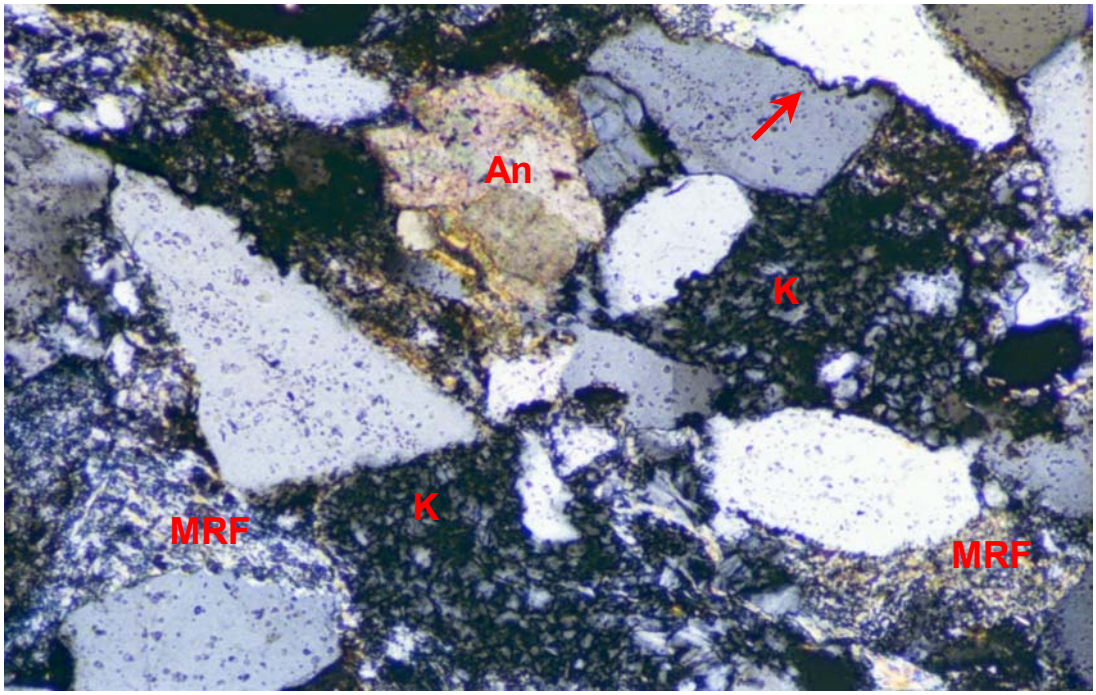


FIGURE 1 Plane polarised light
FIGURE 2 Crossed polarisers

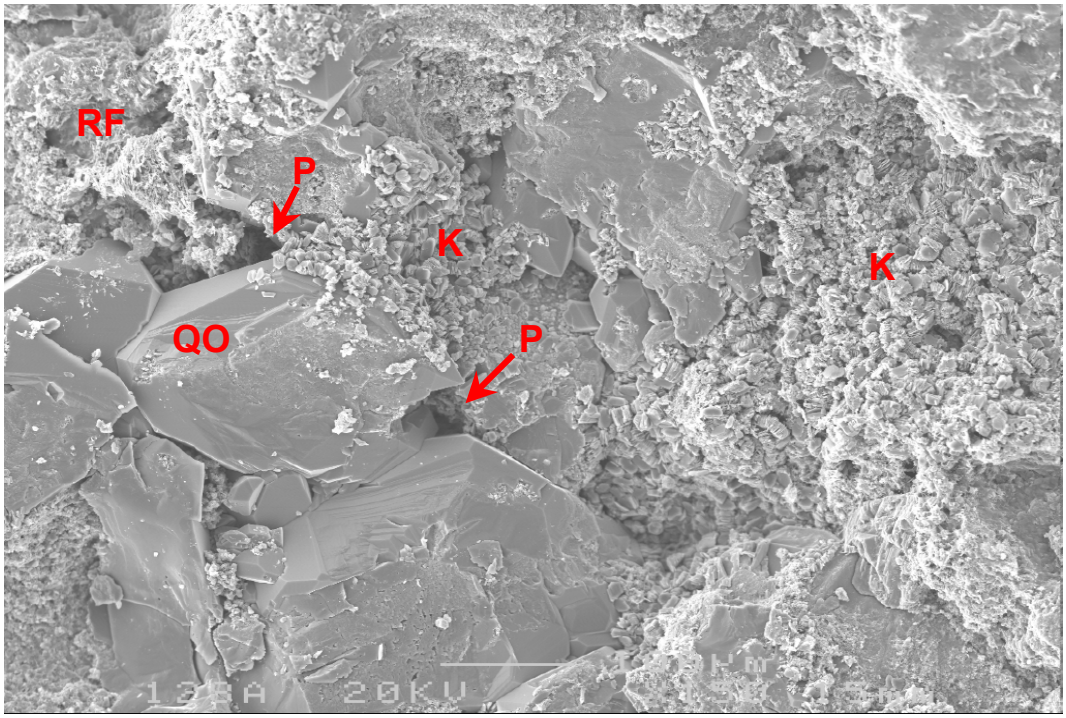
0.2mm



All intergranular areas are filled by authigenic kaolin (K) and compacted illitic metamorphic rock fragments (MRF), and there has been further porosity reduction by grain contact dissolution to form welded grain contacts (arrow). Ankerite (An) forms widely-scattered, coarsely-crystalline patches.

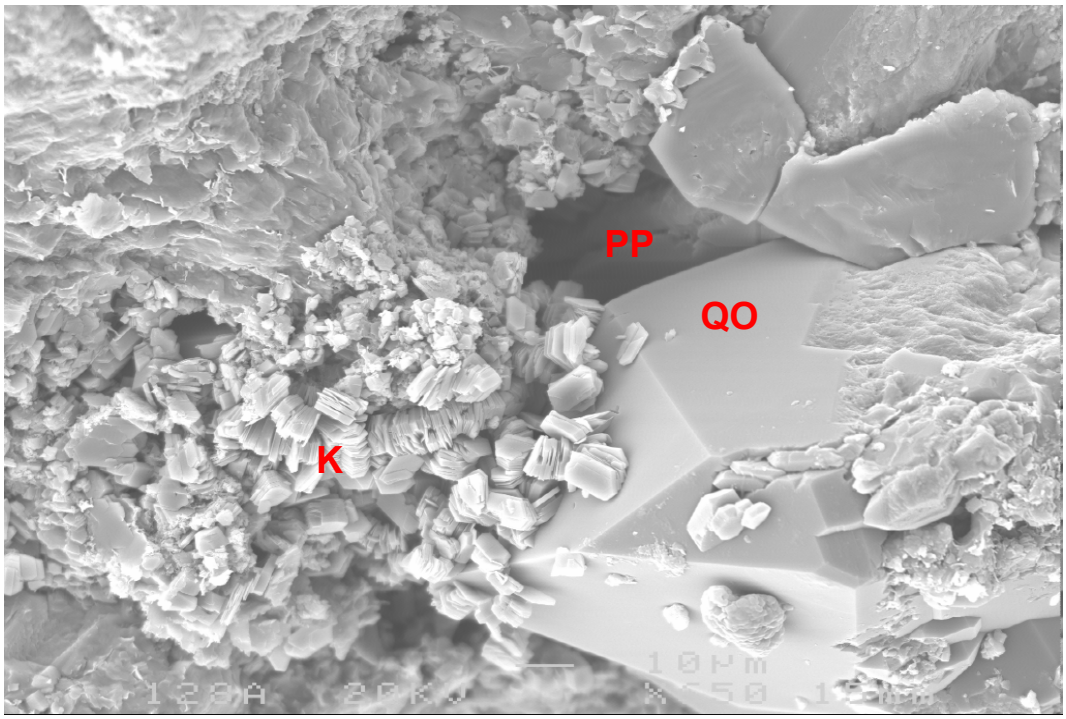
PLATE 7: THYLACINE-2 #128 2218.40m cont.

FIGURE 1



Intergranular pores (P) are preserved where quartz overgrowths (QO) do not completely fill all available space between juxtaposed quartz grains, but are not conducive to permeability due to extensive pore filling by authigenic kaolin (K) and compacted altered rock fragments (RF) in surrounding areas.

FIGURE 2



A rare primary intergranular pore (PP) is largely filled by authigenic kaolin (K) and quartz overgrowth cement (QO), the presence of which isolates the pore from any macropores in its vicinity. Throughout the sand, virtually all intergranular areas are completely filled by authigenic clay and, between juxtaposed quartz grains, quartz overgrowth cement.

PLATE 8: THYLACINE-2 #181 2249.85m

Rock classification: Sublitharenite

Texture:

Sedimentary structures:	Sporadic, argillaceous burrow fills and discontinuous, fine argillaceous laminae
Sorting:	Well
Average grain size:	0.16mm (fine sand)
Roundness:	Subangular-subrounded
Texture:	Grain supported
Packing/grain contacts:	Moderate/long, embayed
Macropore types:	Primary intergranular porosity, secondary mouldic porosity, secondary intragranular porosity
Core analyses:	Por. = 19.7%, Perm. = 9.21mD, GD = 2.66g/cc

Composition:

Quartz (monocrystalline)	63.1%	Siderite (replacement)	0.3%
Quartz (polycrystalline)	2.0%	Glauconite	0.3%
Quartz overgrowths	5.5%	Authigenic kaolin (pf)	2.8%
Chert	0.3%	Authigenic kaolin (rpl)	10.3%
Volcanic rock fragments	0.3%	Authigenic illite (replacement)	3.1%
Metamorphic rock fragments	8.4%	Detrital clay	1.1%
Sedimentary rock fragments	0.3%	Primary porosity (intergran)	0.3%
Heavy minerals	0.3%	Secondary porosity (mouldic)	0.3%
Pyrite	0.7%	Secondary porosity (intragran)	0.3%
Leucoxene	0.3%		

Comments: Little intergranular porosity is preserved on account of the combined effects of authigenic clay formation, quartz overgrowth cementation, grain contact dissolution and ductile grain/authigenic clay compaction. In addition, some intergranular spaces are filled by localised detrital clay, the distribution of which has been influenced by bioturbation. Most authigenic kaolin has a blue hue as a result of being sufficiently microporous for impregnation by epoxy resin. Primary pores are preserved where quartz overgrowths do not completely fill all available intergranular space, but are not conducive to high permeability on account of being very small and erratically distributed.

PLATE 8: THYLACINE-2 #181 2249.85m

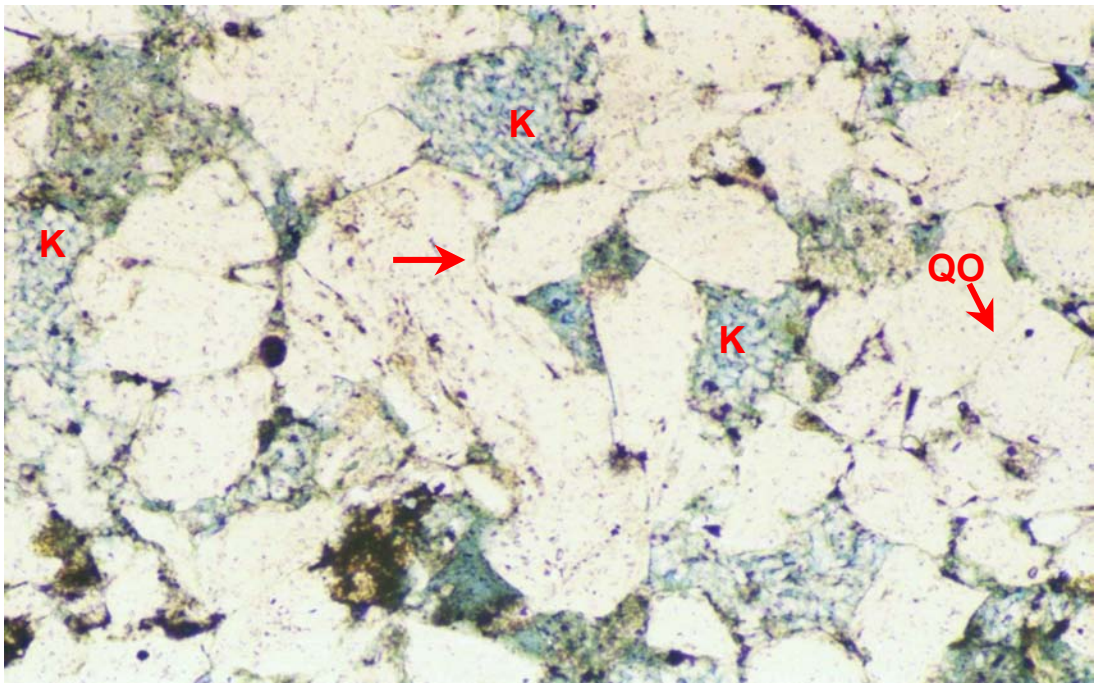
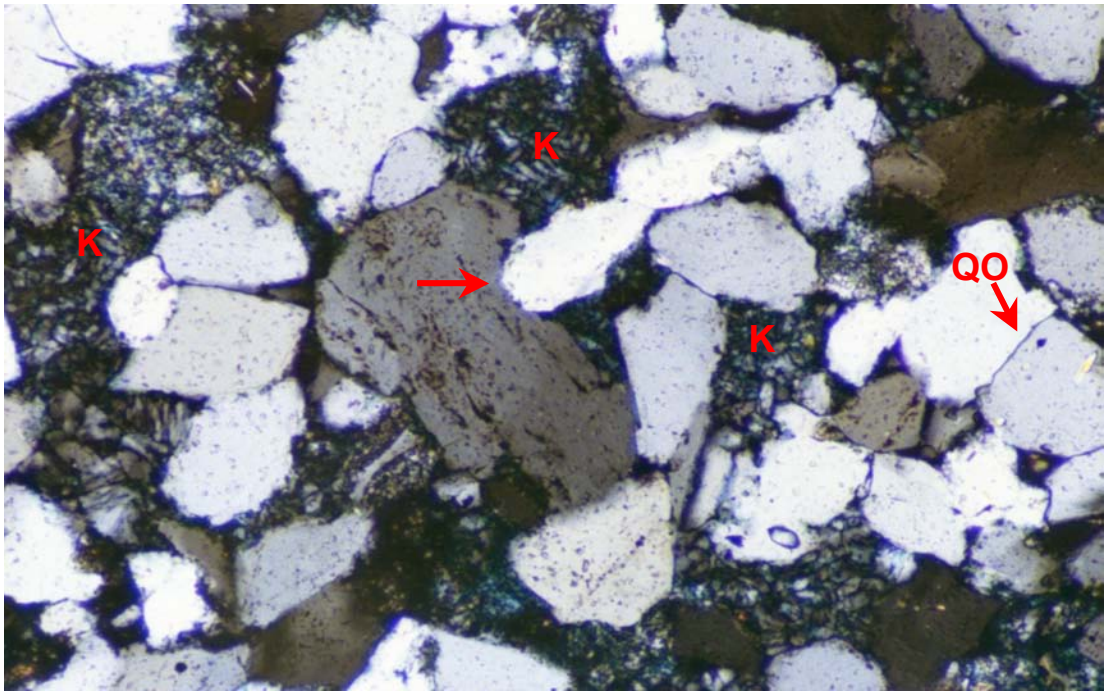


FIGURE 1 Plane polarised light
FIGURE 2 Crossed polarisers

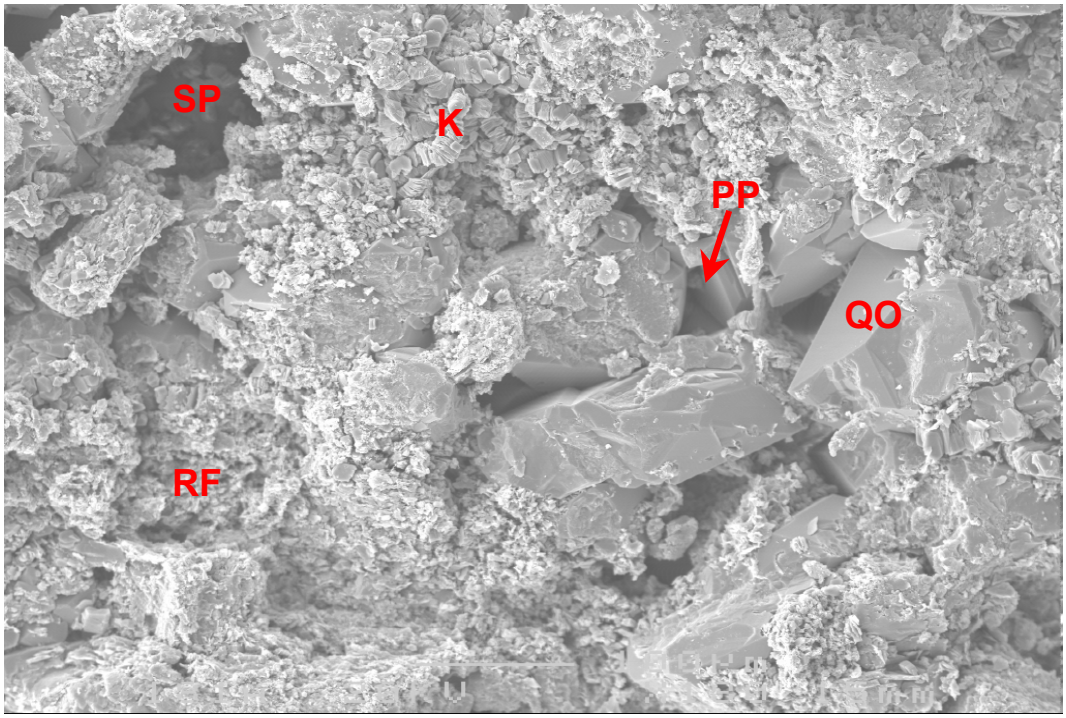
0.2mm



Common patches of highly microporous (as shown by blue hue) authigenic kaolin (K) mark the locations of labile grains that have altered. Between juxtaposed quartz grains, intergranular porosity has been almost completely eliminated by quartz overgrowth (QO) cementation and grain contact dissolution (arrow). Sample is mainly microporous.

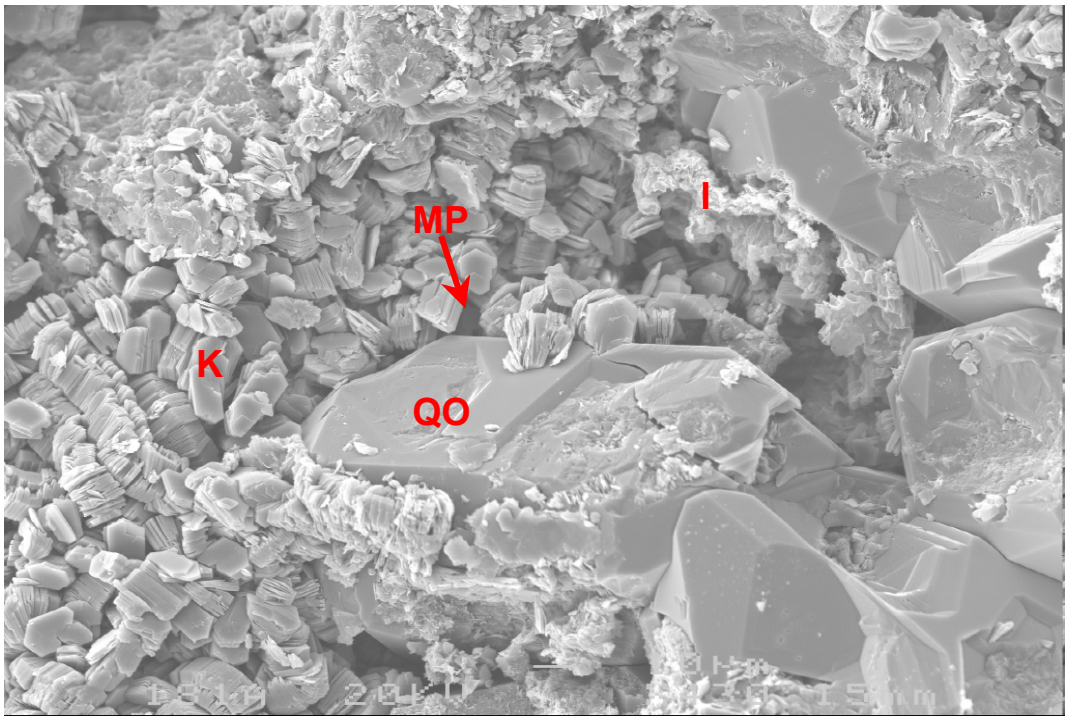
PLATE 9: THYLACINE-2 #181 2249.85m cont.

FIGURE 1



Small primary intergranular pores (PP) are preserved where quartz overgrowths (QO) are incompletely developed, and a rare secondary mouldic pore (SP) occurs where a labile grain has dissolved. Many intergranular areas are filled by authigenic kaolin (K), compacted rock fragments (RF) and quartz overgrowths, hence macropores do not have a high degree of interconnectivity through the sand.

FIGURE 2



An intergranular area is filled by authigenic kaolin (K) and later-formed quartz overgrowth cement (QO). Abundant microporosity (MP) is associated with the kaolin. The illitic remnant (I) of a labile grain that altered to kaolin is also marked.

PLATE 10: THYLACINE-2 #186 2251.20m

Rock classification: Sublitharenite

Texture:

Sedimentary structures: Single, fine, argillaceous/carbonaceous lamination; otherwise massive

Sorting: Well

Average grain size: 0.13mm (fine sand)

Roundness: Angular-subrounded

Texture: Grain supported

Packing/grain contacts: Moderate/long, embayed; microstylolitic within argillaceous lamination

Macropore types: Secondary mouldic porosity, primary intergranular porosity, numerous artifact pores

Core analyses: Por. = 14.7%, Perm. = 0.692mD, GD = 2.76g/cc

Composition:

Quartz (monocrystalline)	47.1%	Siderite (replacement)	3.1%
Quartz (polycrystalline)	2.9%	Ankerite (pore filling)	12.0%
Quartz overgrowths	3.4%	Ankerite (replacement)	7.4%
Chert	0.7%	Glauconite	0.3%
Metamorphic rock fragments	3.4%	Authigenic kaolin (pf)	2.0%
Mica	0.7%	Authigenic kaolin (rpl)	11.4%
Heavy minerals	0.7%	Authigenic illite (replacement)	1.9%
Organics	0.4%	Detrital clay	0.7%
Pyrite	0.9%	Primary porosity (intergran)	0.3%
Leucoxene	0.3%	Secondary porosity (mouldic)	0.4%

Comments: This sublitharenite contains abundant, patchy, coarsely-crystalline ankerite, which, together with authigenic clay and quartz overgrowths, completely occupies most intergranular spaces. Further porosity loss is the result of grain contact dissolution and, within a tight argillaceous lamination, microstylolitisation. Microcrystalline siderite, organic fragments and fine pyrite are concentrated along the argillaceous lamination, and pyrite also forms disseminated fine framboids that are commonly enclosed by later-formed ankerite cement. Rare primary pores are preserved where quartz overgrowths have not filled all available intergranular space between juxtaposed quartz grains, and widely scattered secondary pores are the result of labile grain dissolution. The thin-section also contains common artifact pores that resemble secondary mouldic pores. The sand is close to being very fine grained and, moreover, pore throats are choked by ankerite, authigenic clay and quartz overgrowths, hence permeability is very low.

PLATE 10: THYLACINE-2 #186 2251.20m

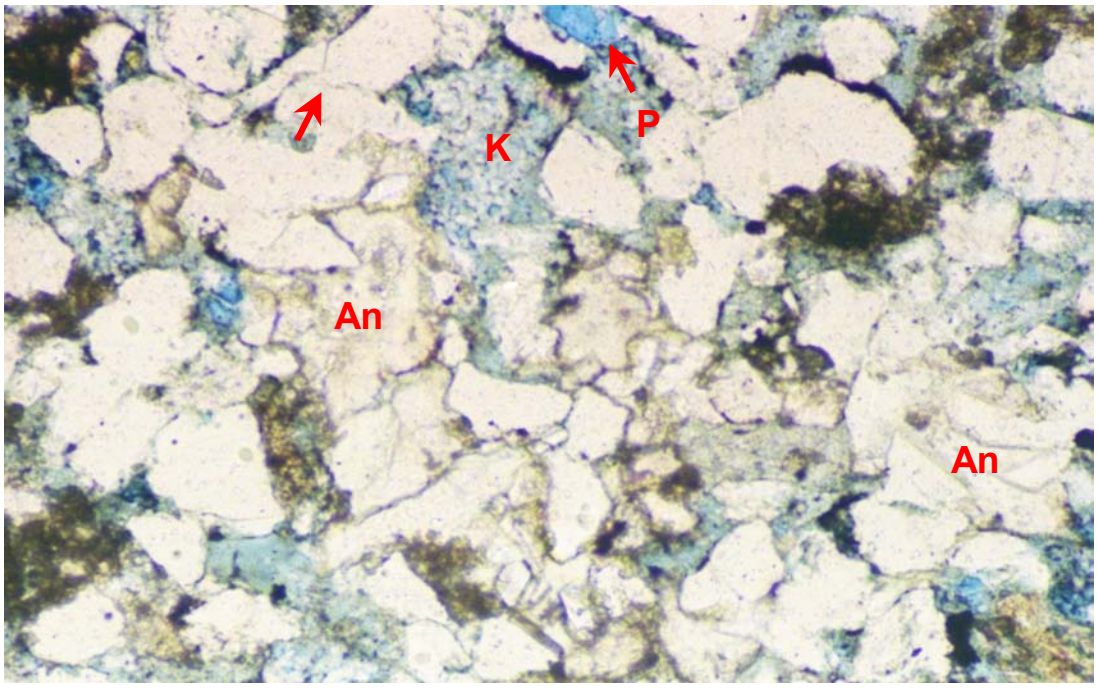
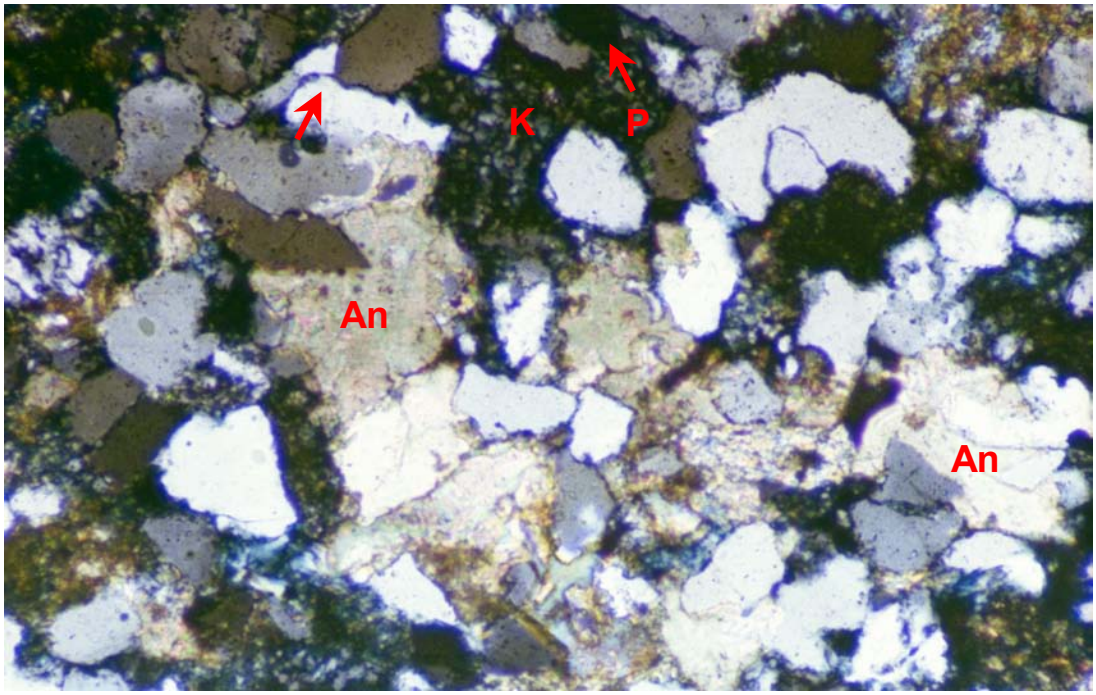


FIGURE 1 Plane polarised light

FIGURE 2 Crossed polarisers

0.2mm



Low permeability (0.692mD) is largely the result of patchy cementation by ankerite (An). Complete quartz overgrowth cementation outside ankerite-cemented areas has formed triple point grain junctions (arrow) between adjacent quartz grains. Patchy, highly microporous kaolin (K) occurs where labile grains have altered. An artifact pore (P) is also marked.

PLATE 11: THYLACINE-2 #187 2251.59m

Rock classification: Sublitharenite

Texture:

Sedimentary structures:	Scattered argillaceous/sandy burrow infills
Sorting:	Well
Average grain size:	0.12mm (very fine sand)
Roundness:	Angular-subrounded
Texture:	Grain supported
Packing/grain contacts:	Moderate/long, embayed
Macropore types:	Secondary mouldic porosity, primary intergranular porosity, numerous artifact pores
Core analyses:	Por. = 17.1%, Perm. = 1.16mD, GD = 2.79g/cc

Composition:

Quartz (monocrystalline)	46.3%	Leucoxene	0.3%
Quartz (polycrystalline)	2.6%	Siderite (replacement)	3.7%
Quartz overgrowths	3.1%	Ankerite (pore filling)	11.2%
Volcanic rock fragments	0.3%	Ankerite (replacement)	6.0%
Metamorphic rock fragments	5.4%	Authigenic kaolin (pf)	2.4%
Sedimentary rock fragments	0.3%	Authigenic kaolin (rpl)	11.7%
Mica	0.3%	Authigenic illite (replacement)	2.7%
Heavy minerals	0.3%	Detrital clay	0.3%
Organics	0.3%	Primary porosity (intergran)	0.3%
Pyrite	2.2%	Secondary porosity (mouldic)	0.3%

Comments: Like the previous sand, this sample contains abundant, patchy, coarsely-crystalline ankerite cement. Virtually all intergranular porosity has been eliminated by ankerite and quartz overgrowth cementation, authigenic clay (mainly kaolin) formation, physical compaction, grain contact dissolution and localised pyrite cementation. Scattered patches of microcrystalline siderite replace biotite flakes. Rare primary pores are preserved where quartz overgrowths have not filled all available intergranular space between juxtaposed quartz grains, and widely scattered secondary pores are the result of labile grain dissolution. The thin-section also contains common artifact pores that resemble secondary mouldic pores. The sand is very fine grained and, moreover, pore throats are choked by ankerite, authigenic clay, quartz overgrowths and pyrite, hence permeability is low.

PLATE 11: THYLACINE-2 #187 2251.59m

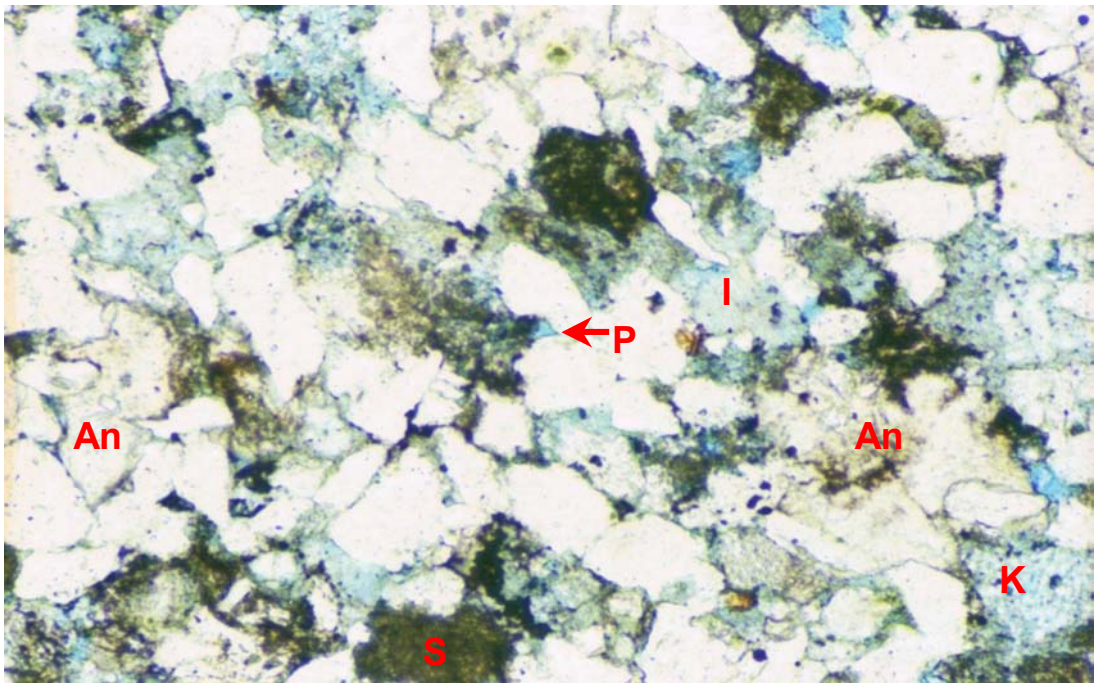
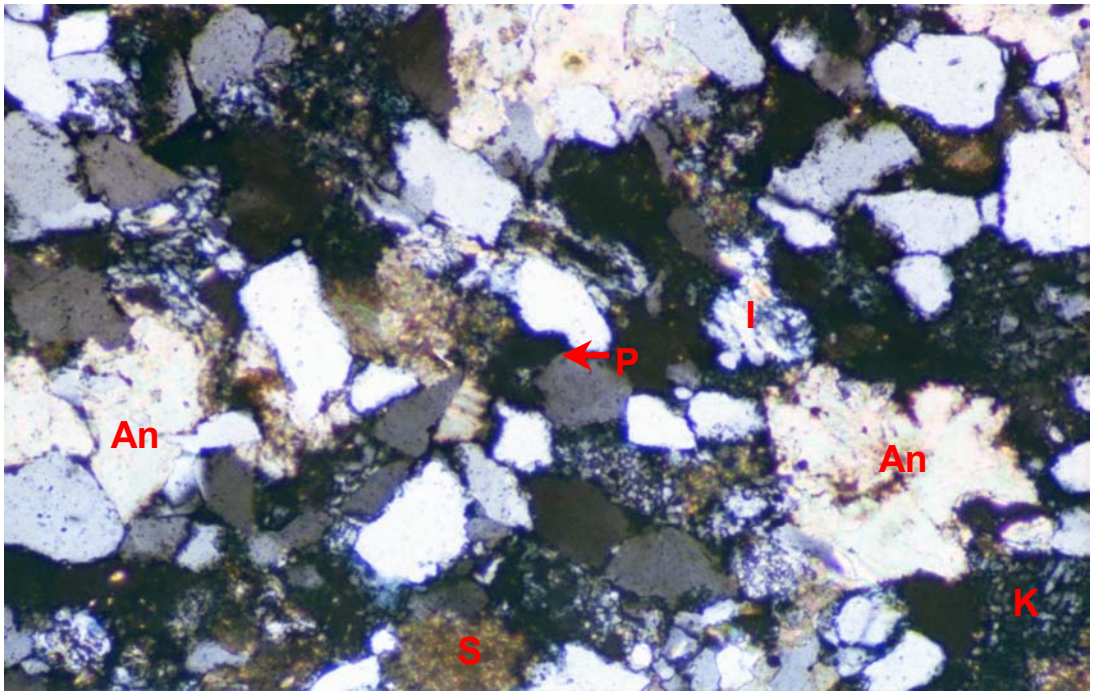


FIGURE 1 Plane polarised light

FIGURE 2 Crossed polarisers

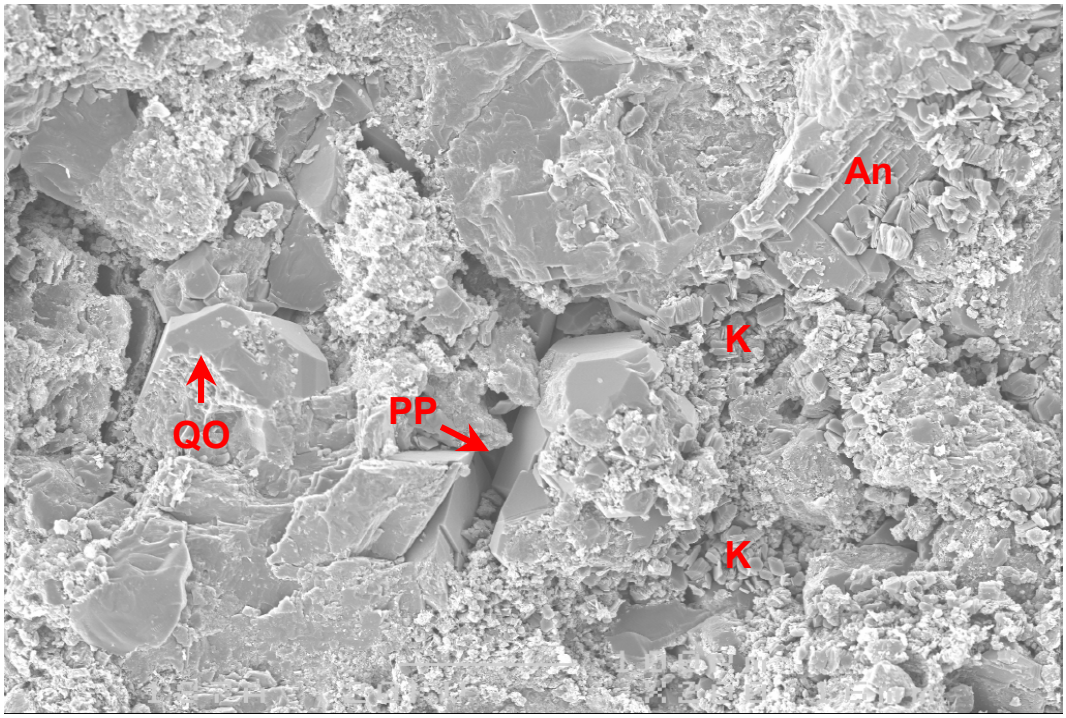
0.2mm



Very fine grained sandstone in which intergranular areas are largely filled by patchy ankerite cement (An) and highly microporous authigenic kaolin (K) and illite (I) that have formed by labile grain alteration. Intergranular pores (P) are small and isolated and thus are not conducive to permeability. Microcrystalline siderite (S) replaces biotite.

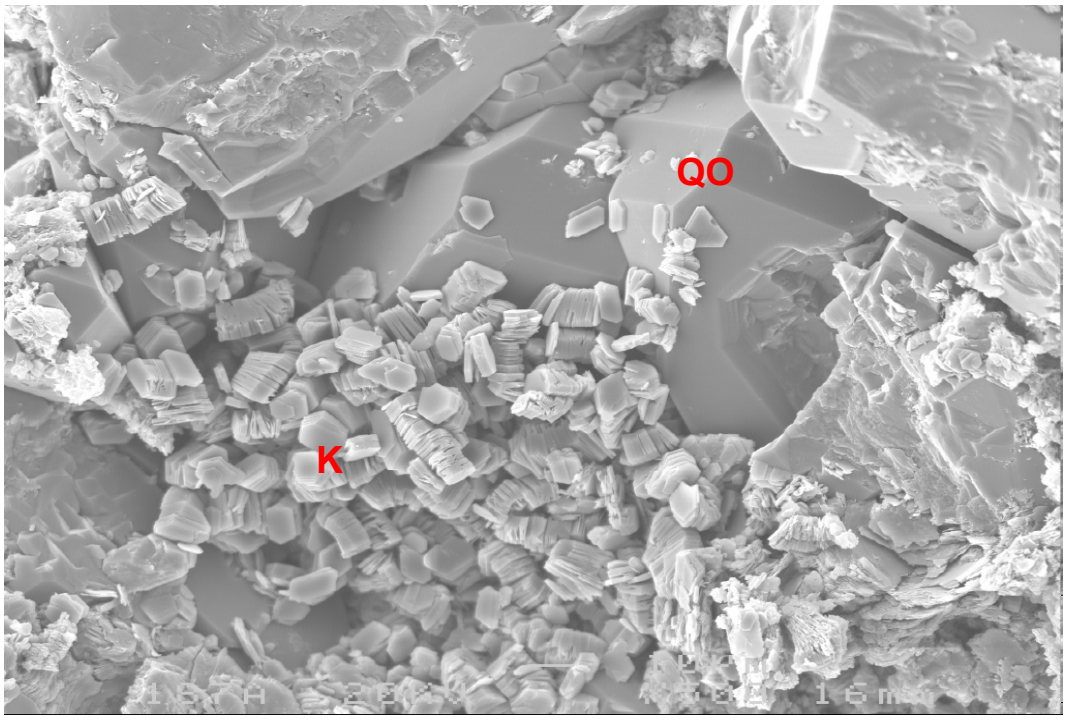
PLATE 12: THYLACINE-2 #187 2251.59m cont.

FIGURE 1



Small primary pores (PP) are preserved where quartz overgrowths (QO) have not totally filled all available intergranular space. The pores are isolated by sandstone in which intergranular porosity has been almost completely eliminated by ankerite (An) and quartz overgrowth cementation and authigenic kaolin (K) formation.

FIGURE 2



Outside ankerite-cemented areas, intergranular spaces are largely or completely filled by authigenic kaolin (K) and quartz overgrowths (QO). Quartz overgrowths are effective in occluding intergranular pores on account of the very fine grain size.

PLATE 13: THYLACINE-2 #205 2275.17m

Rock classification: Quartzarenite

Texture:

Sedimentary structures:	Massive
Sorting:	Moderately-well
Average grain size:	0.40mm (medium sand)
Roundness:	Subangular-subrounded
Texture:	Grain supported
Packing/grain contacts:	Moderate/long, embayed
Macropore types:	Primary intergranular porosity, secondary intergranular porosity, secondary intragranular porosity
Core analyses:	Por. = 19.8%, Perm. = 199mD, GD = 2.65g/cc

Composition:

Quartz (monocrystalline)	67.4%	Authigenic kaolin (rpl)	10.0%
Quartz (polycrystalline)	0.9%	Authigenic illite (replacement)	0.6%
Quartz overgrowths	6.9%	Primary porosity (intergran)	7.4%
Chert	0.3%	Secondary porosity (intergran)	2.1%
Metamorphic rock fragments	1.4%	Secondary porosity (intragran)	0.7%
Authigenic kaolin (pf)	2.3%		

Comments: This quartzose sandstone contains modest amounts of primary intergranular porosity that is supplemented by scattered secondary pores that occur where labile rock fragments have dissolved. Porosity reduction has resulted mainly from quartz overgrowth cementation, grain contact dissolution, authigenic kaolin formation and compaction of altered micaceous grains/authigenic kaolin. Authigenic kaolin, which forms scattered grain-sized patches and patchy pseudomatrix, is loosely packed and thus highly microporous. Despite the presence of the kaolin, intergranular macropores are sufficiently common to be well interconnected throughout the sand.

PLATE 13: THYLACINE-2 #205 2275.17m

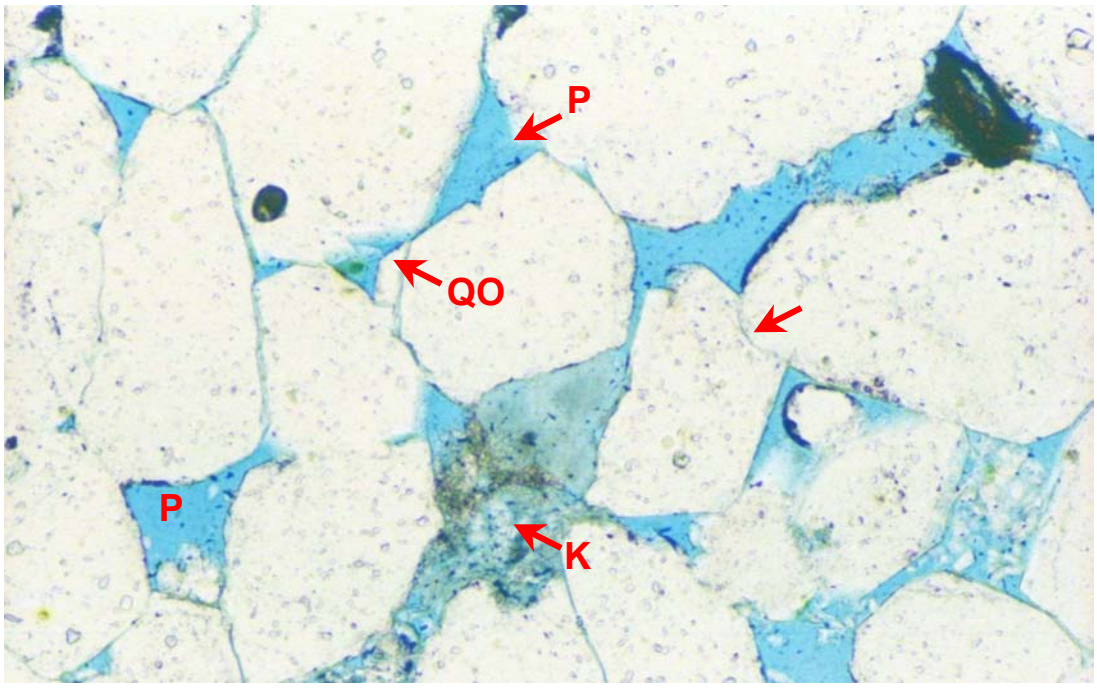
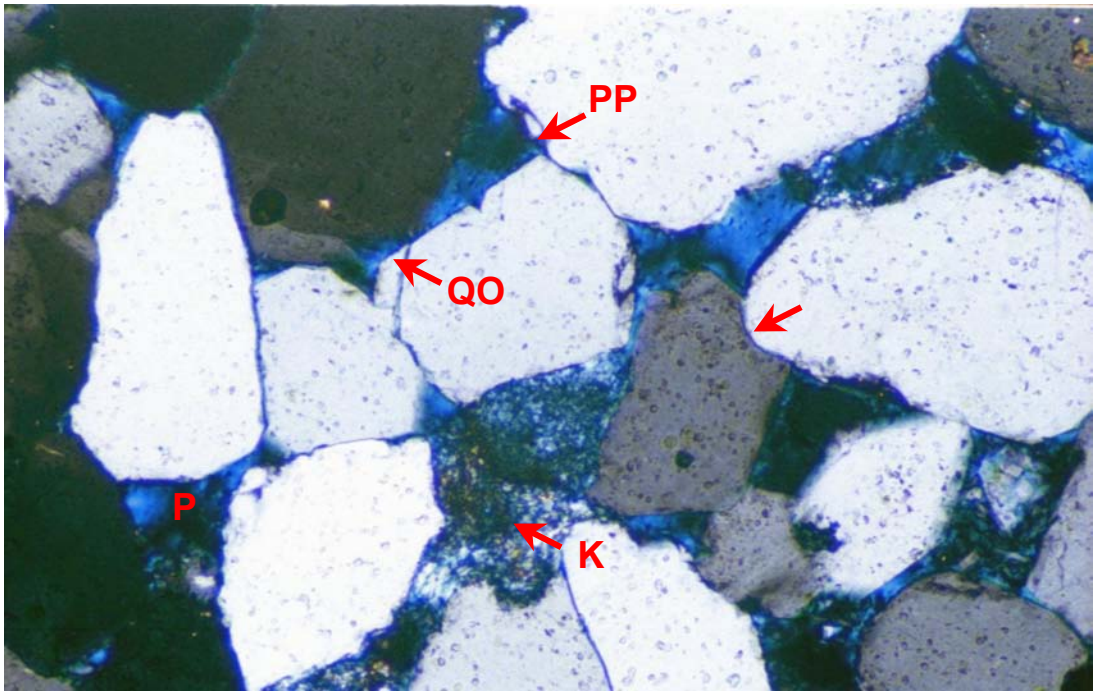


FIGURE 1 Plane polarised light

FIGURE 2 Crossed polarisers

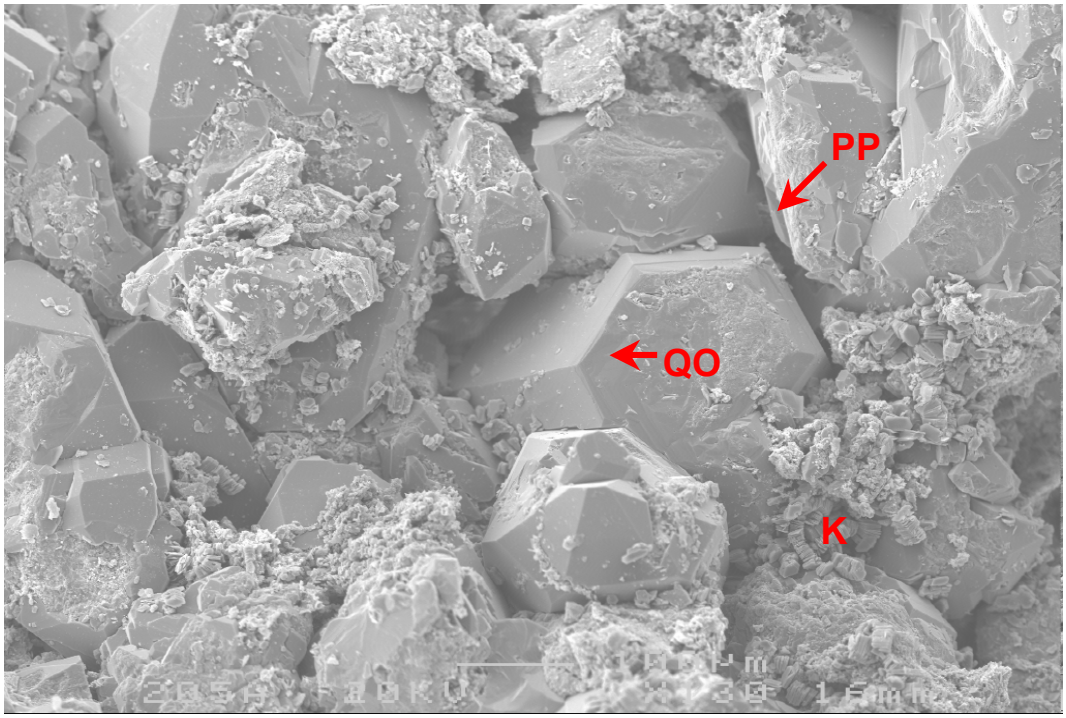
0.2mm



Good permeability (199mD) reflects the presence of common, clean, evenly distributed, hence well-interconnected intergranular pores (P) that are preserved despite porosity reduction by quartz overgrowth (QO) cementation and grain contact dissolution (arrow). Authigenic kaolin (K) is associated with a compacted, partly altered illitic grain.

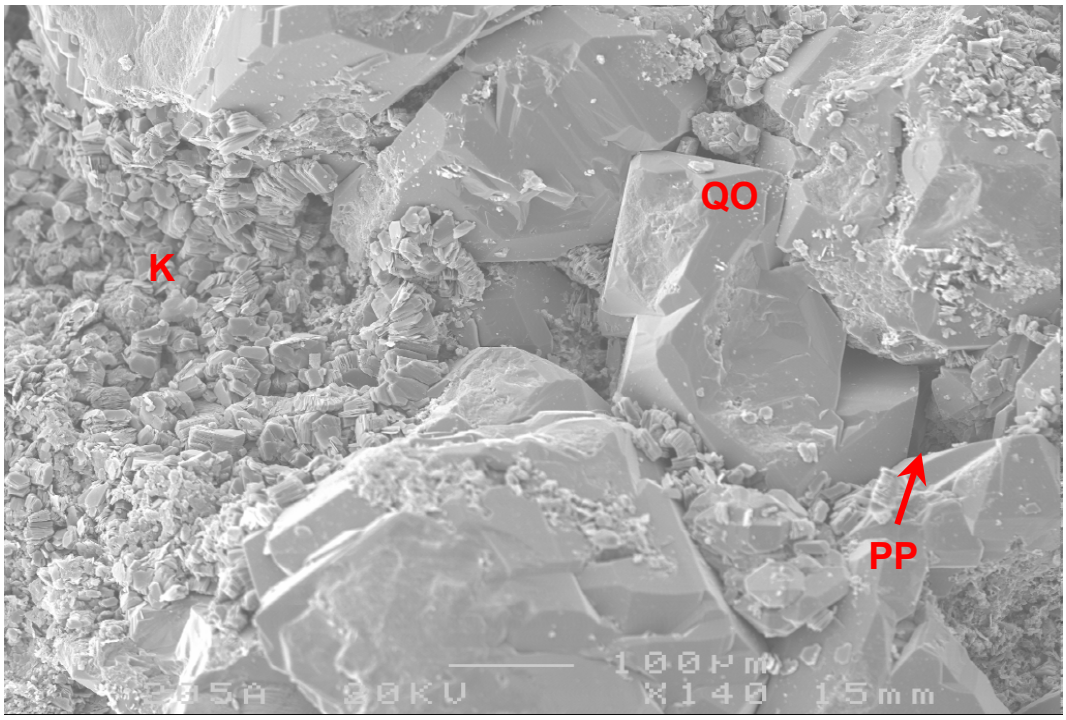
PLATE 14: THYLACINE-2 #205 2275.17m cont.

FIGURE 1



Preservation of good primary intergranular porosity (PP) reflects the quartzose and relatively coarse character of the sandstone. Quartz overgrowths (QO) are common, but only partly occlude intergranular spaces. Intergranular areas locally contain authigenic kaolin (K) that is the altered remnant of labile grains.

FIGURE 2



Authigenic kaolin (K) commonly forms large patches that are the altered remnants of compacted micaceous grains. Areas free of kaolin are cemented by quartz overgrowths (QO), but still contain common primary intergranular pores (PP).

PLATE 15: THYLACINE-2 #234 2296.94m

Rock classification: Quartzarenite

Texture:

Sedimentary structures:	Massive
Sorting:	Well
Average grain size:	0.60mm (coarse sand)
Roundness:	Subangular-subrounded
Texture:	Grain supported
Packing/grain contacts:	Moderate/long, embayed, locally sutured
Macropore types:	Primary intergranular porosity, secondary intergranular porosity, secondary intragranular porosity
Core analyses:	Por. = 24.8%, Perm. = 5260mD, GD = 2.65g/cc

Composition:

Quartz (monocrystalline)	65.5%	Authigenic kaolin (pf)	1.6%
Quartz (polycrystalline)	1.8%	Authigenic kaolin (rpl)	3.8%
Quartz overgrowths	5.4%	Detrital clay	0.3%
Metamorphic rock fragments	1.2%	Primary porosity (intergran)	13.0%
Organics	0.3%	Secondary porosity (intergran)	6.1%
Siderite (replacement)	0.3%	Secondary porosity (intragran)	0.7%

Comments: This quartzose sandstone contains abundant primary intergranular porosity that is supplemented by scattered secondary pores that occur where labile rock fragments have partly and completely dissolved. Porosity reduction has resulted mainly from quartz overgrowth cementation, grain contact dissolution, authigenic kaolin formation and compaction of altered micaceous grains/authigenic kaolin. Authigenic kaolin, which forms scattered grain-sized patches and patchy pseudomatrix, is loosely packed and thus highly microporous. Detrital clay and associated organic fragments are concentrated in one small area, where the presence of thin detrital clay films has promoted microstylolitisation. High permeability reflects the coarse grain size and the presence of a system of large, generally clean, evenly distributed (hence well interconnected) primary and secondary intergranular pores. Clay patches are not sufficiently common to significantly impact permeability.

PLATE 15: THYLACINE-2 #234 2296.94m

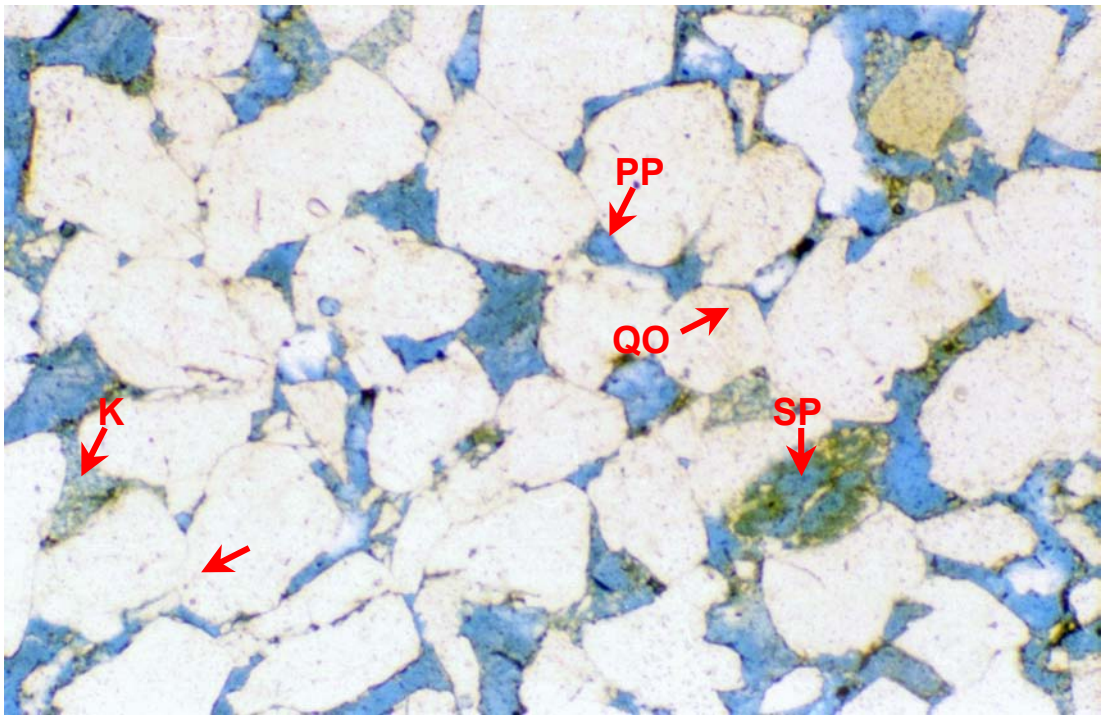
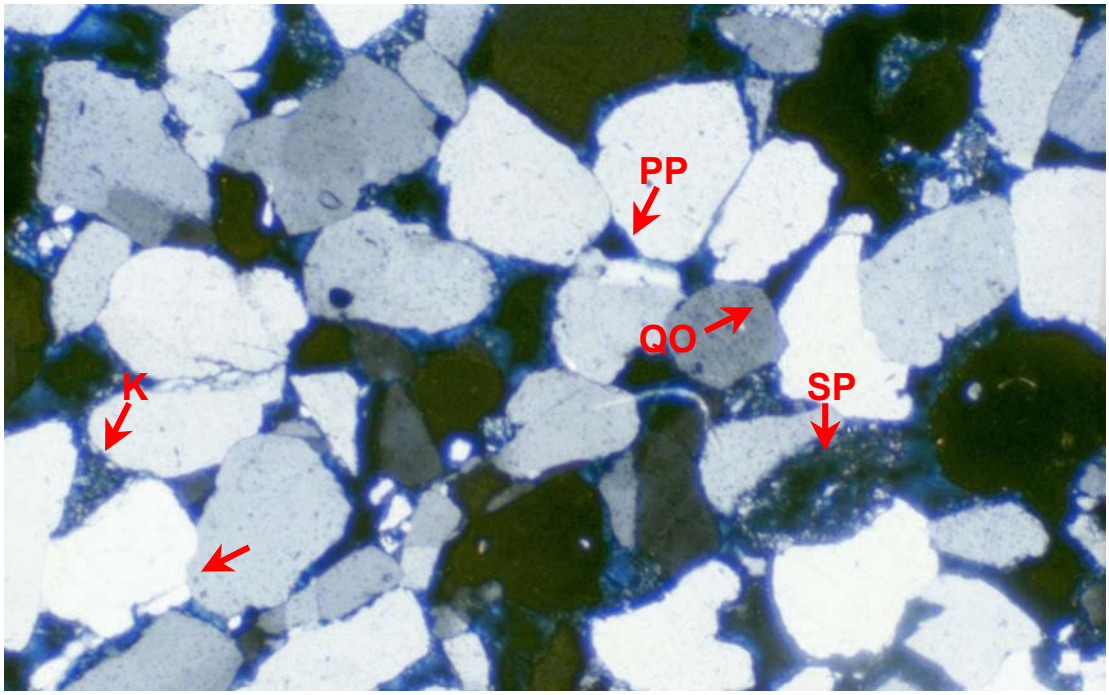


FIGURE 1 Plane polarised light
FIGURE 2 Crossed polarisers

0.4mm



Despite porosity reduction by quartz overgrowth (QO) cementation and grain contact dissolution (arrow), this quartzose sandstone contains abundant primary intergranular porosity (PP) that is supplemented by scattered secondary pores (SP) that are the result of labile grain dissolution. Patchy authigenic kaolin (K) has little impact on permeability.

PLATE 16: THYLACINE-2 #234 2296.94m cont.

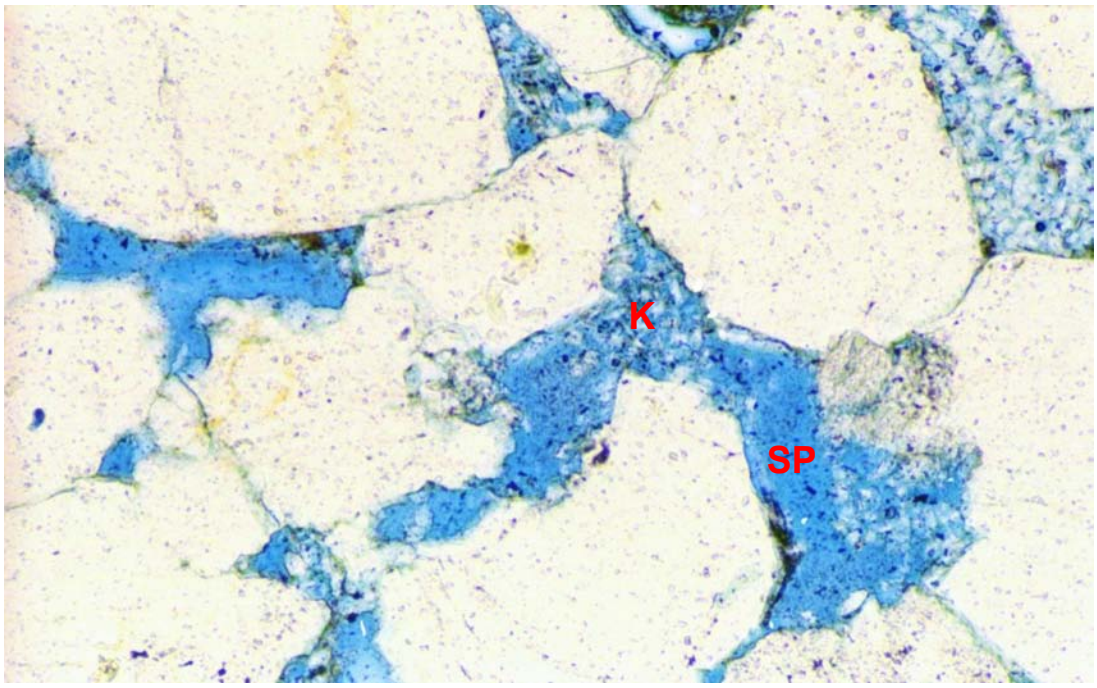
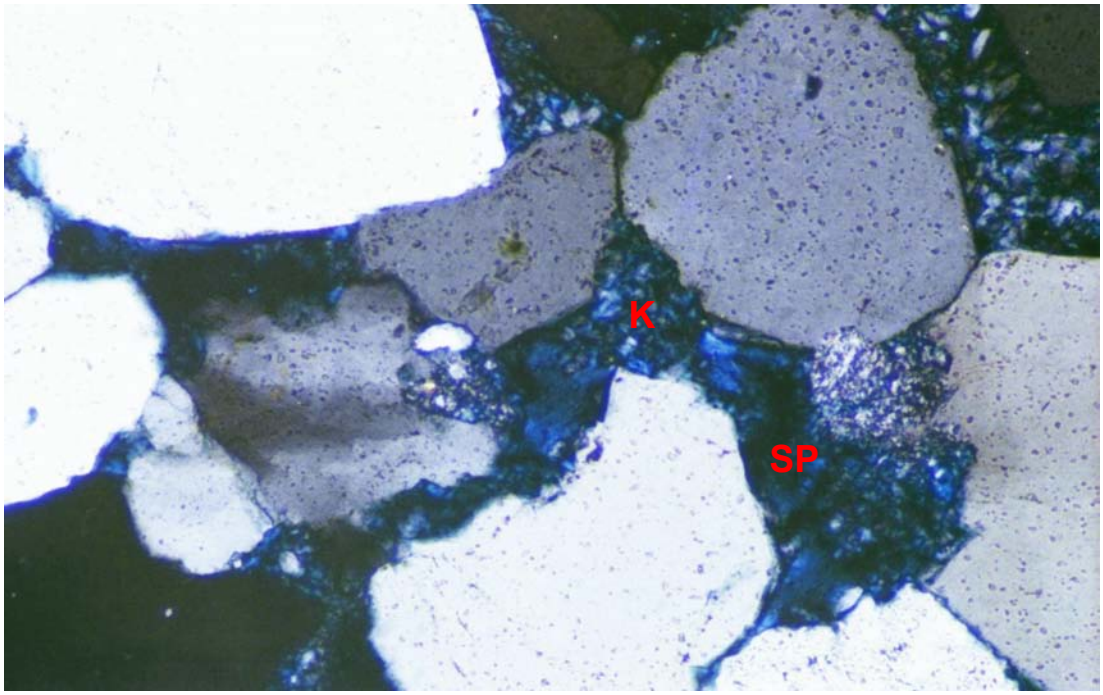


FIGURE 1 Plane polarised light

FIGURE 2 Crossed polarisers

0.2mm



A significant component of total macroporosity in the sand is secondary intergranular porosity (SP) that has formed by labile grain dissolution. The marked pore is partly filled by loosely-packed kaolin (K) that is the altered remnant of the pore-precursor grain.

PLATE 17: THYLACINE-2 #241 2299.40m

Rock classification: Quartzarenite

Texture:

Sedimentary structures:	Contact between massive coarse sandstone bed and granule conglomerate bed
Sorting:	Overall poor, but sandstone and conglomerate beds are individually well and moderately-well sorted, respectively
Average grain size:	1.02mm (very coarse sand)
Roundness:	Subangular-rounded
Texture:	Grain supported
Packing/grain contacts:	Moderate/long, embayed,
Macropore types:	Primary intergranular porosity, secondary intergranular porosity, secondary intragranular porosity
Core analyses:	Por. = 21.9%, Perm. = 5960mD, GD = 2.65g/cc

Composition:

Quartz (monocrystalline)	67.8%	Pyrite	0.3%
Quartz (polycrystalline)	6.1%	Authigenic kaolin (pf)	0.6%
Quartz overgrowths	4.9%	Authigenic kaolin (rpl)	2.3%
Chert	0.7%	Primary porosity (intergran)	12.7%
Metamorphic rock fragments	0.3%	Secondary porosity (intergran)	4.3%

Comments: This sample, which consists of coarse quartzose sandstone and granule conglomerate, is the most permeable of the sample suite. Like the previous sample, it contains abundant primary intergranular porosity that is supplemented by scattered secondary pores that occur where labile rock fragments have dissolved. Porosity reduction has resulted mainly from quartz overgrowth cementation, grain contact dissolution and, particularly within the conglomerate, authigenic kaolin formation. Within the conglomerate, authigenic kaolin fills most intergranular spaces, although it appears that some of this kaolin was mobilised during coring. Within the sandstone, kaolin forms widely scattered, highly microporous patches that mark the location of labile grains that have altered. High permeability reflects very coarse grain size and the presence of a system of large, clean, evenly distributed (hence well interconnected) primary and secondary intergranular pores.

PLATE 17: THYLACINE-2 #241 2299.40m

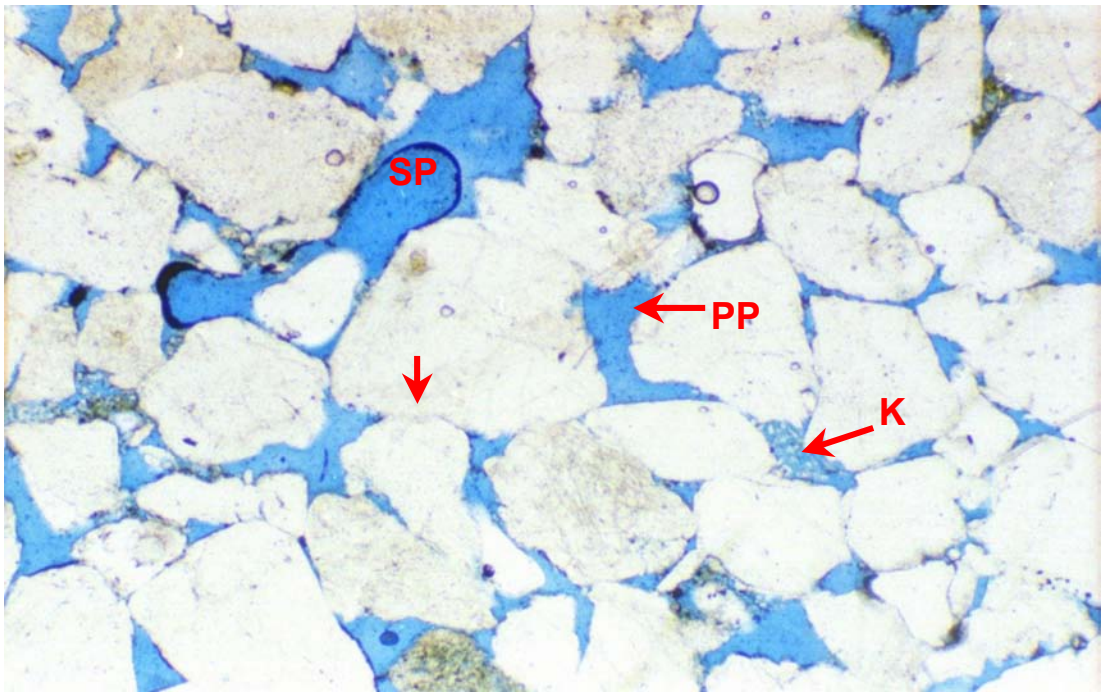
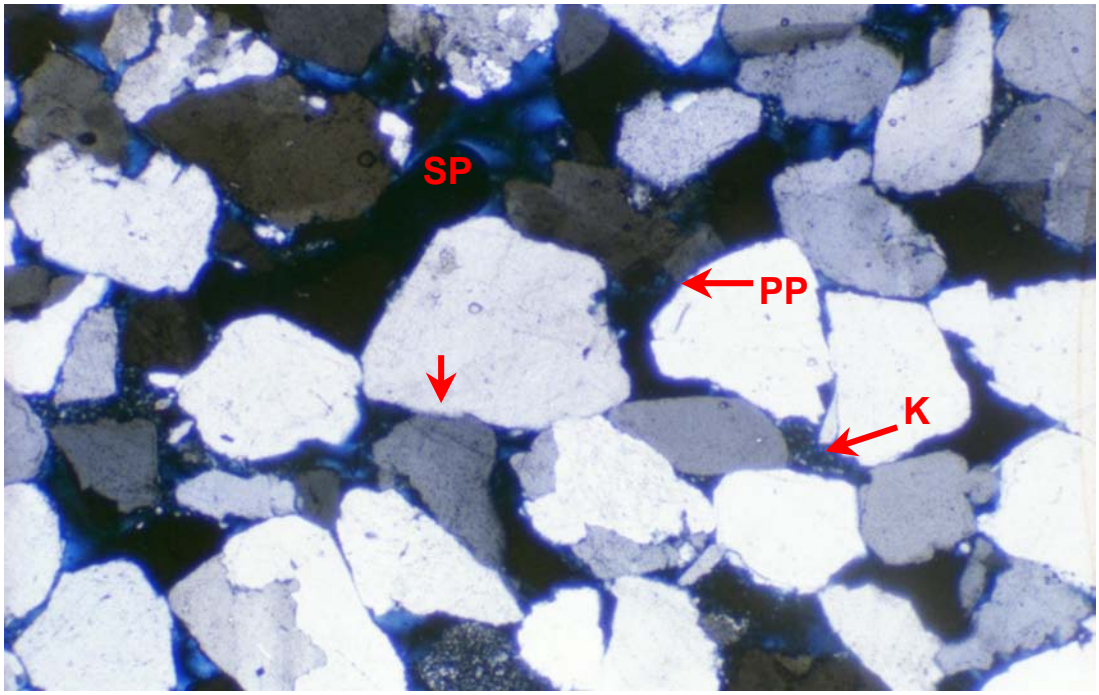


FIGURE 1 Plane polarised light

FIGURE 2 Crossed polarisers

0.4mm



Coarse sandstone in which large primary intergranular pores (PP) are preserved between most framework grains, despite porosity reduction by grain contact dissolution (arrow) and quartz overgrowth cementation. Primary porosity is supplemented by scattered secondary pores (SP) that are the result of labile rock fragment dissolution. Loosely-packed, authigenic kaolin (K) forms widely scattered patches that have no impact on permeability.

PLATE 18: THYLACINE-2 #241 2299.40m cont.

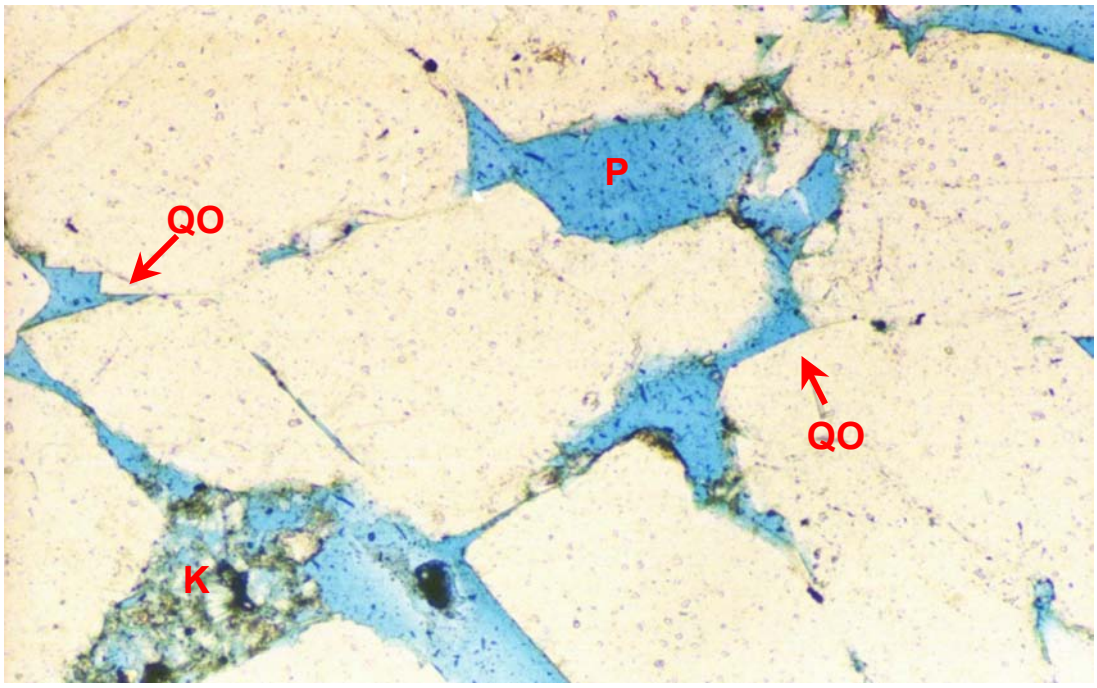
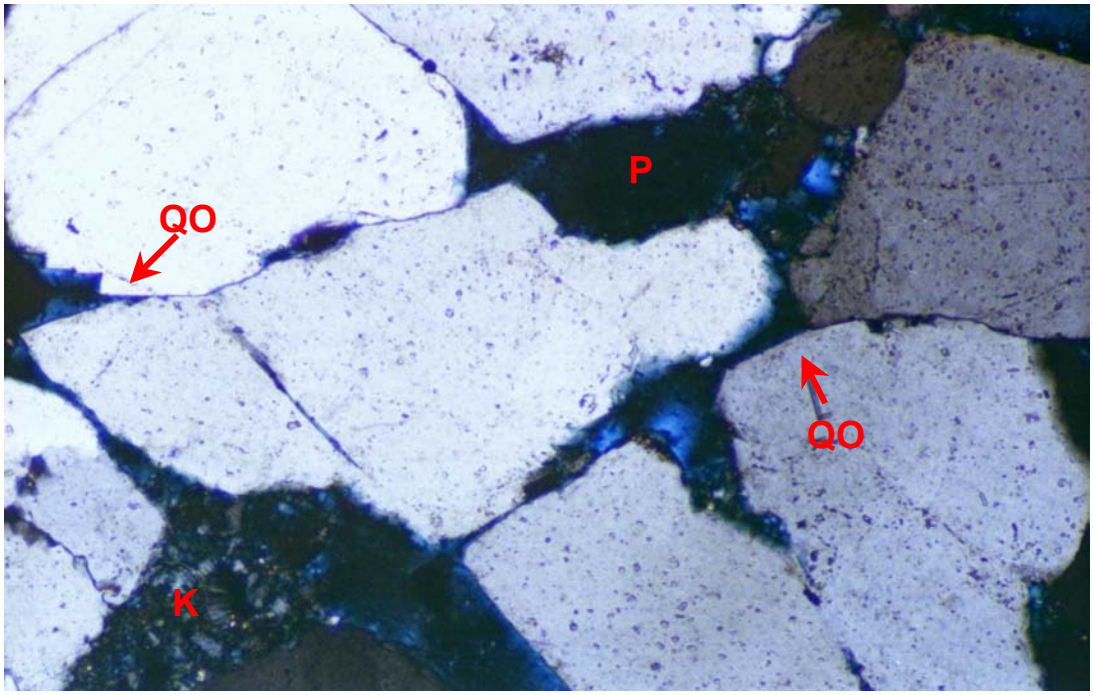


FIGURE 1 Plane polarised light
FIGURE 2 Crossed polarisers

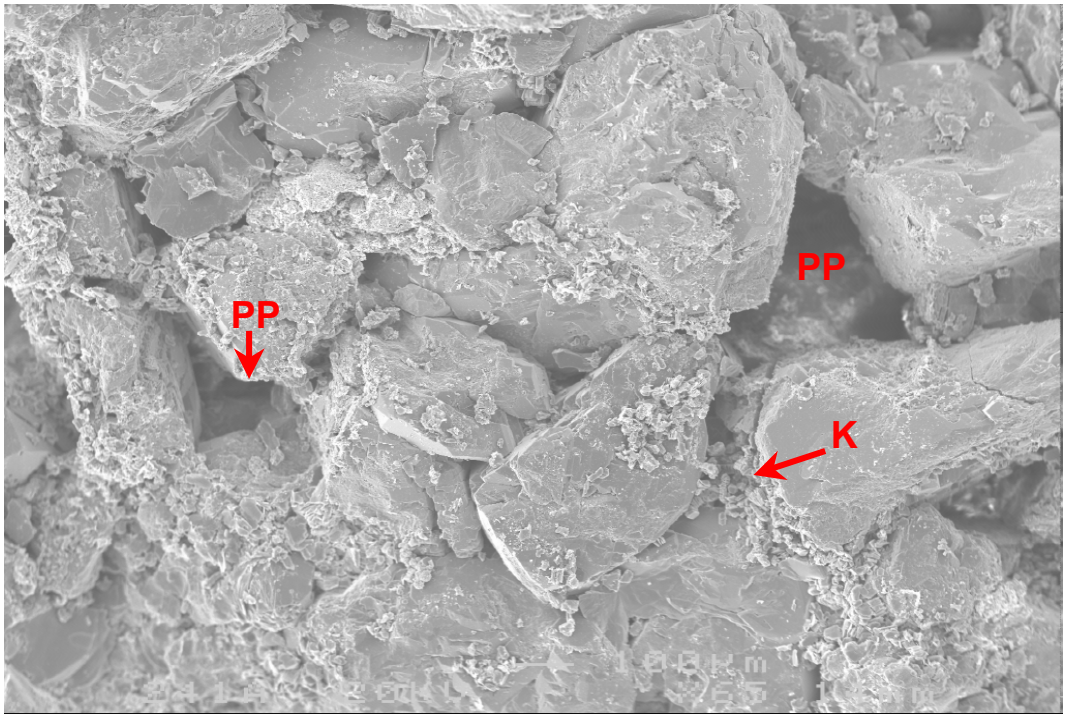
0.2mm



Quartz overgrowths (QO) are thinly developed and thus fill only a small portion of adjacent intergranular pores (P). Most clay is loosely-packed authigenic kaolin (K) that forms widely scattered patches where micaceous/argillaceous grains have altered.

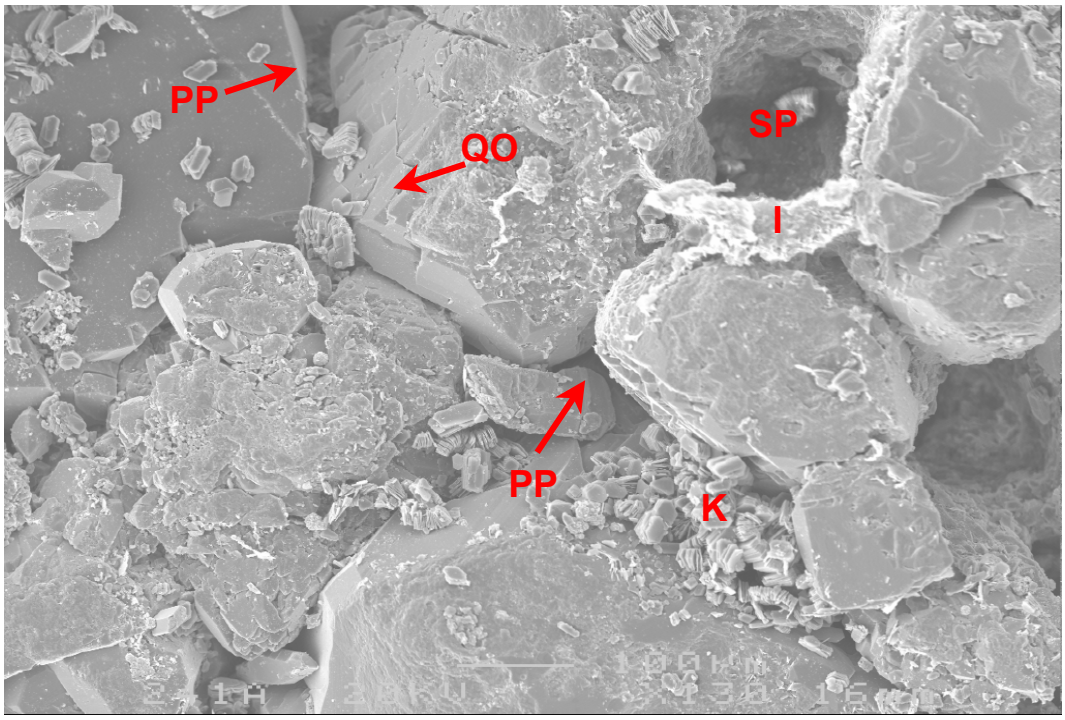
PLATE 19: THYLACINE-2 #241 2299.40m cont.

FIGURE 1



Large primary intergranular pores (PP) are preserved between poorly quartz overgrowth-cemented quartz framework grains. One intergranular space is occupied by authigenic kaolin (K).

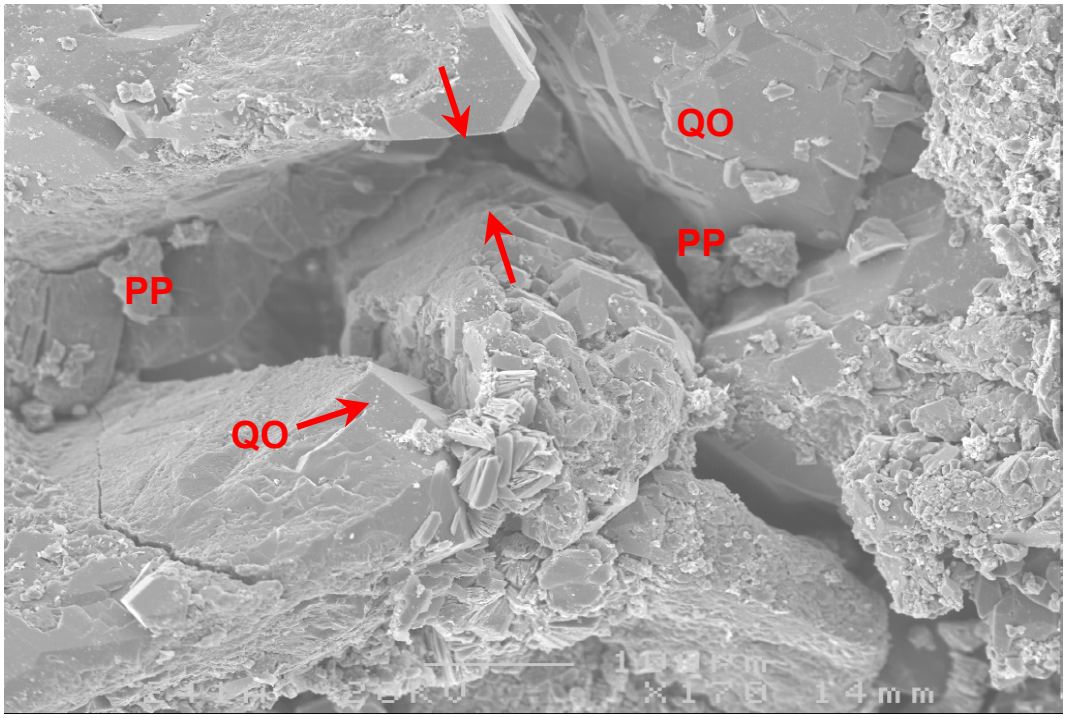
FIGURE 2



A secondary intergranular pore (SP) is partly rimmed by illitic remnants (I) of the pore-precursor grain. Elsewhere, primary intergranular pores (PP) are bounded by thinly-developed quartz overgrowths (QO). Authigenic kaolin patches (K) are insufficiently common to impact reservoir quality.

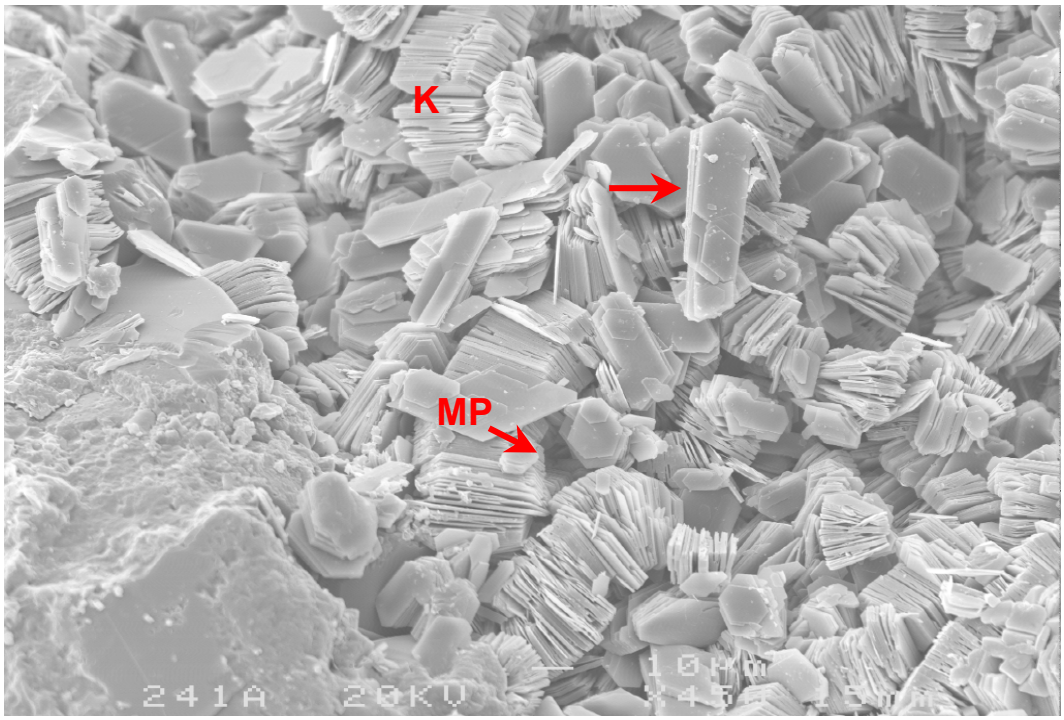
PLATE 20: THYLACINE-2 #241 2299.40m cont.

FIGURE 1



Detail of typical primary intergranular pores (PP), the volume of which has not been significantly reduced by development of quartz overgrowths (QO) on bounding grains. Most pore throats (between arrows) are large and unobstructed.

FIGURE 2



Detail of typical authigenic kaolin (K) that has formed by labile grain alteration. The kaolin is loosely packed and is thus highly microporous (MP). Kaolin plates are commonly elongated (arrow), which is consistent with the kaolin being dickite rather than kaolinite.

PLATE 21: THYLACINE-2 #244 2300.20m

Rock classification: Sublitharenite

Texture:

Sedimentary structures: Sporadic thin sideritic laminae

Sorting: Moderately-well

Average grain size: 0.13mm (fine sand)

Roundness: Angular-subrounded

Texture: Grain supported

Packing/grain contacts: Moderate/long, embayed, microstylolitic within laminae

Macropore types: None

Core analyses: Por. = 12.4%, Perm. = 0.840mD, GD = 2.67g/cc

Composition:

Quartz (monocrystalline)	61.3%	Pyrite	0.3%
Quartz (polycrystalline)	1.7%	Leucoxene	0.3%
Quartz overgrowths	4.0%	Siderite (pore filling)	0.7%
Metamorphic rock fragments	4.3%	Siderite (replacement)	5.2%
Sedimentary rock fragments	0.3%	Authigenic kaolin (pf)	2.3%
Mica	0.9%	Authigenic kaolin (rpl)	13.0%
Heavy minerals	0.3%	Authigenic illite (replacement)	3.7%
Organics	1.7%		

Comments: Primary intergranular porosity has been completely eliminated by authigenic clay (kaolin, illite) formation, ductile grain/authigenic clay compaction, grain contact dissolution and localised cementation by quartz overgrowths. In addition, the sample is cut by sporadic, tight, stylolitic laminae along which microcrystalline siderite, mica and organic fragments are concentrated. The sand was susceptible to authigenic clay formation and compaction on account of containing common micaceous/argillaceous grains at the time of accumulation. Rhombic, 10μm siderite crystals are finely disseminated throughout the sand. Low permeability reflects fine grain size and the microporous character of the sand.

PLATE 21: THYLACINE-2 #244 2300.20m

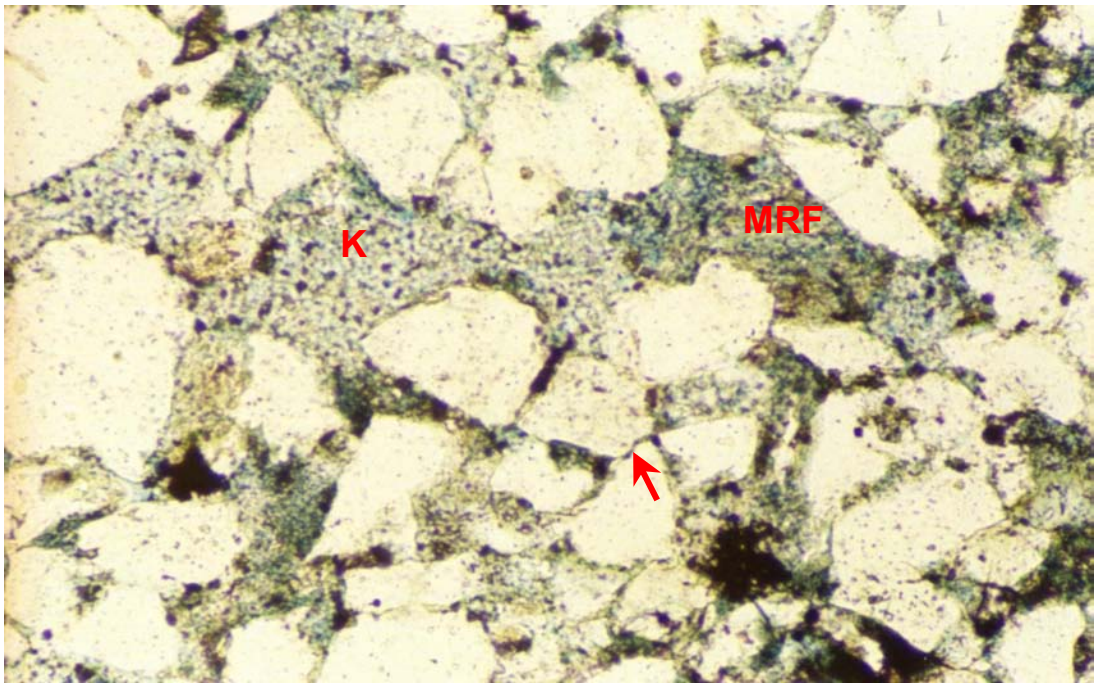
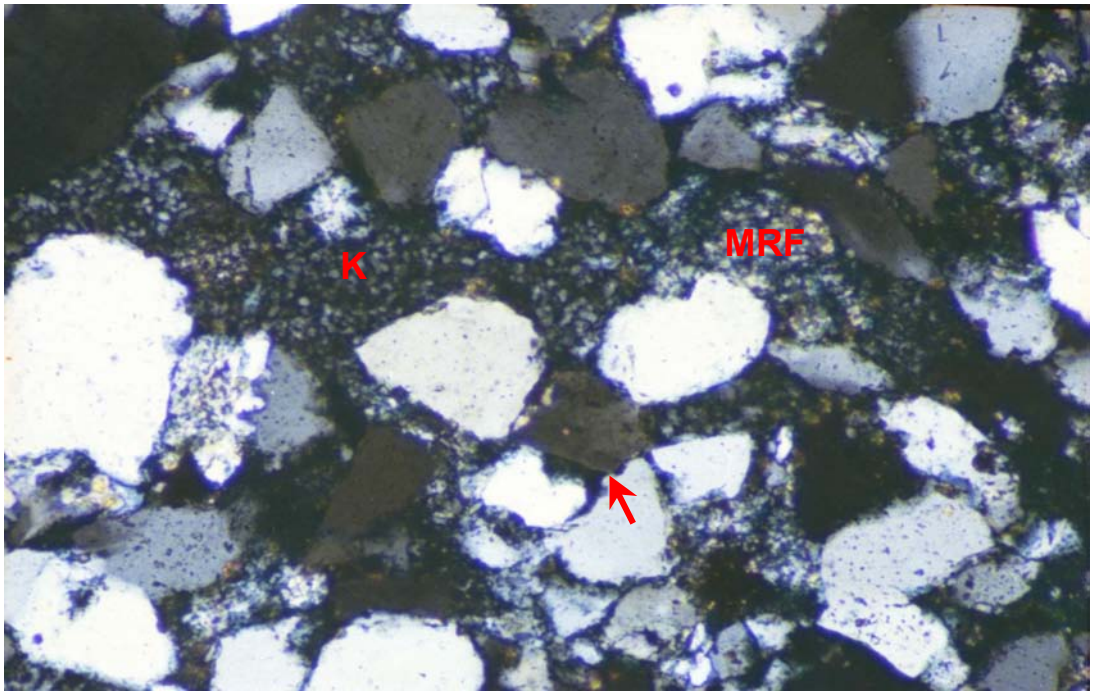


FIGURE 1 Plane polarised light

FIGURE 2 Crossed polarisers

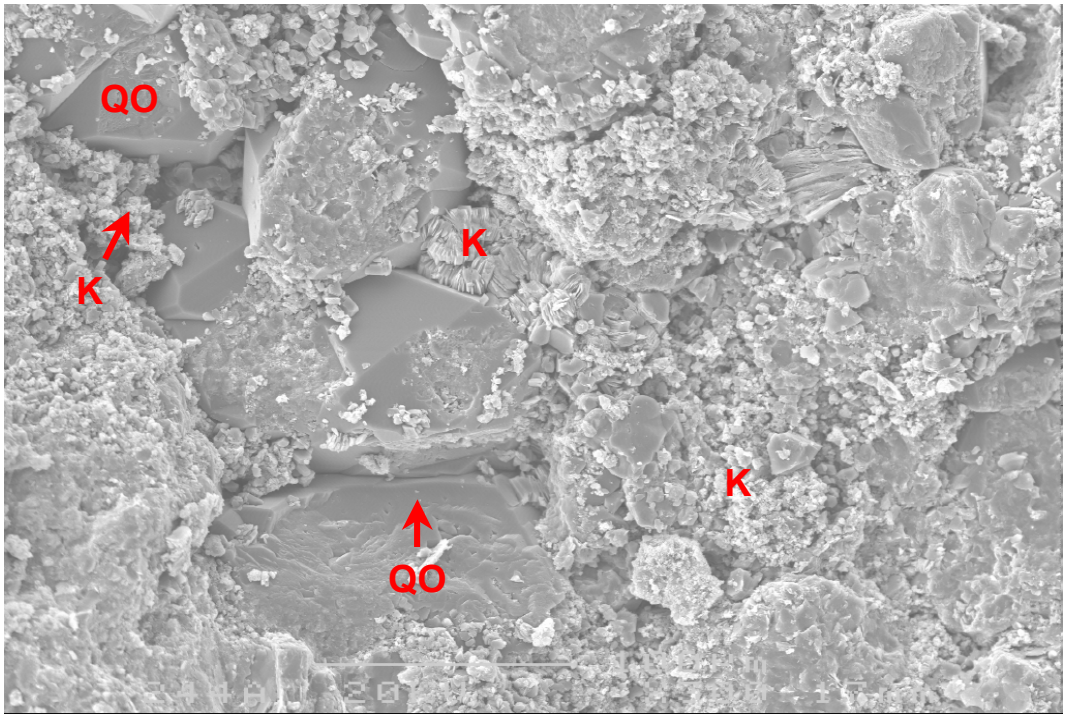
0.2mm



This fine grained sublitharenite lacks macroporosity due to authigenic kaolin (K) formation, compaction of authigenic clay and micaceous metamorphic rock fragments (MRF), grain contact dissolution (arrow) and localised quartz overgrowth cementation. Most kaolin has formed by alteration of micaceous/argillaceous grains, which were common in the sand at the time of accumulation.

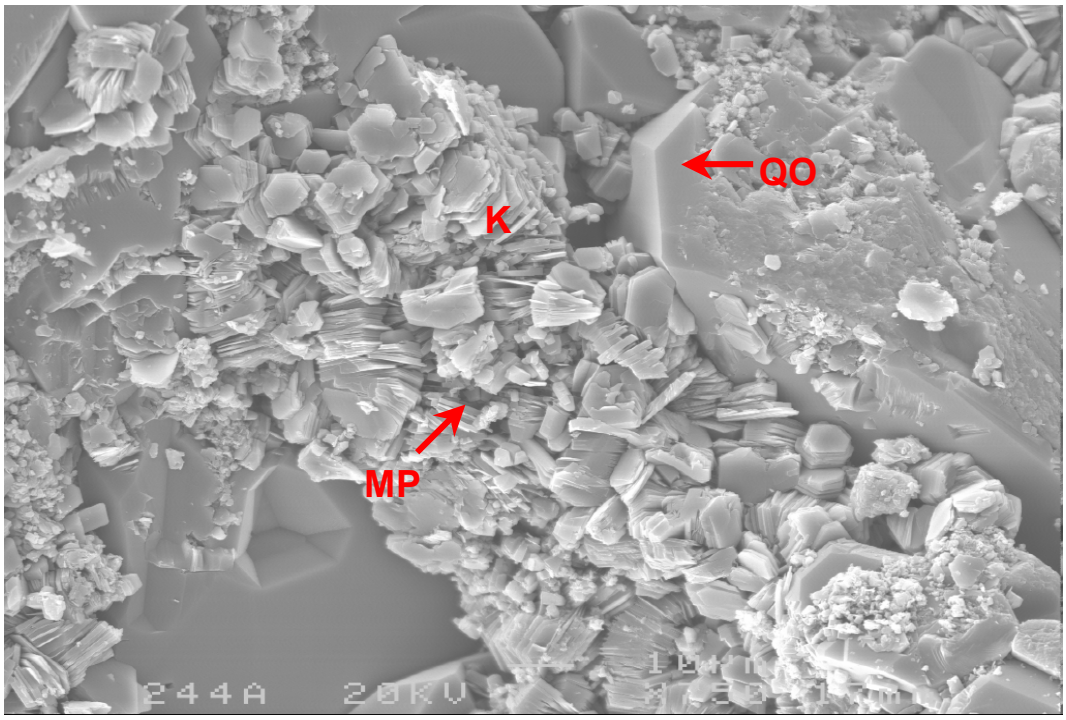
PLATE 22: THYLACINE-2 #244 2300.20m cont.

FIGURE 1



Representative area in which all intergranular areas are filled by authigenic kaolin (K) and, where quartz grains are juxtaposed, quartz overgrowth (QO) cement.

FIGURE 2



A typical intergranular area is almost completely clogged by authigenic kaolin (K) and later-formed quartz overgrowth cement (QO). Microporosity (MP) associated with authigenic kaolin would account for most porosity in the sand.

PLATE 23: THYLACINE-2 #246 2300.80m

Rock classification: Quartzarenite

Texture:

Sedimentary structures: Sporadic thin sideritic laminae

Sorting: Well

Average grain size: 0.21mm (fine sand)

Roundness: Subangular-subrounded

Texture: Grain supported

Packing/grain contacts: Moderate/long, embayed

Macropore types: Primary intergranular porosity, secondary mouldic porosity

Core analyses: Por. = 16.0%, Perm. = 9.64mD, GD = 2.74g/cc

Composition:

Quartz (monocrystalline)	60.6%	Organics	0.3%
Quartz (polycrystalline)	1.4%	Siderite (pore filling)	3.7%
Quartz overgrowths	4.8%	Siderite (replacement)	3.5%
Chert	0.6%	Authigenic kaolin (pf)	5.4%
Granitic rock fragments	0.3%	Authigenic kaolin (rpl)	15.5%
Metamorphic rock fragments	1.1%	Authigenic illite (replacement)	0.9%
Sedimentary rock fragments	0.3%	Primary porosity (intergran)	0.7%
Mica	0.6%	Secondary porosity (mouldic)	0.3%

Comments: Little intergranular porosity is preserved on account of the combined effects of authigenic kaolin formation, quartz overgrowth cementation, grain contact dissolution and ductile grain/authigenic clay compaction. Sporadic concentrations of microcrystalline and finely-crystalline siderite define fine laminae, and disseminated 10-30μm siderite crystals occur along grain contacts and within quartz overgrowths and patches of authigenic clay. Most authigenic kaolin has a blue hue as a result of being sufficiently microporous for impregnation by epoxy resin. Primary pores are preserved where quartz overgrowths do not completely fill all available intergranular space between juxtaposed quartz grains, but are not conducive to high permeability on account of being very small and erratically distributed. Sample is mainly microporous.

PLATE 23: THYLACINE-2 #246 2300.80m

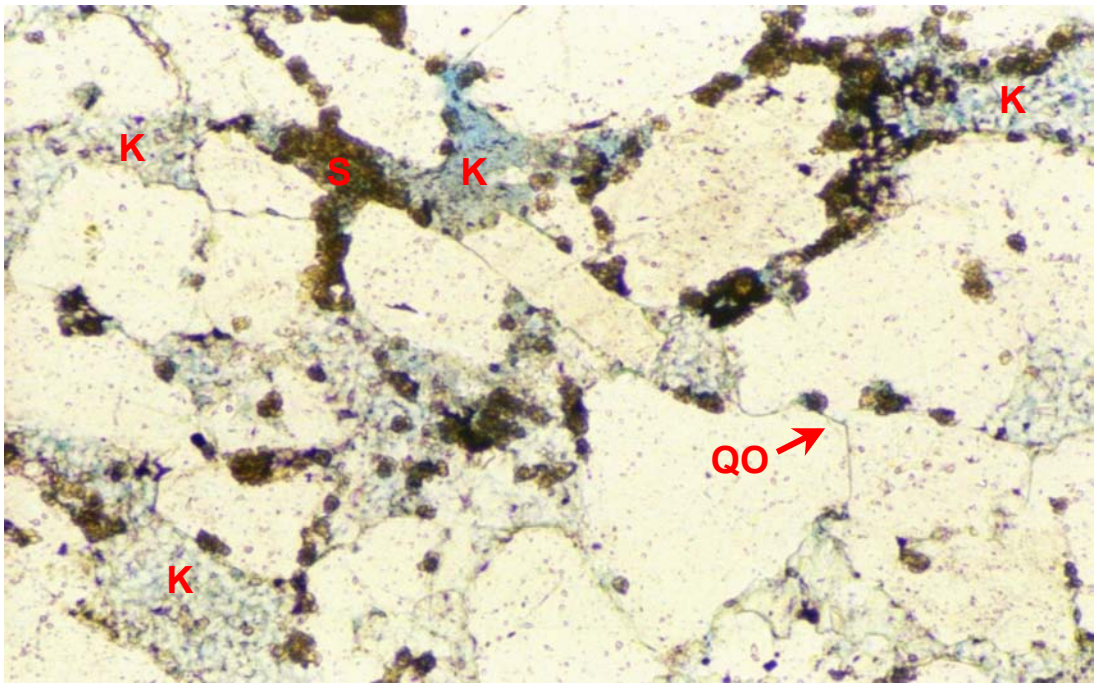
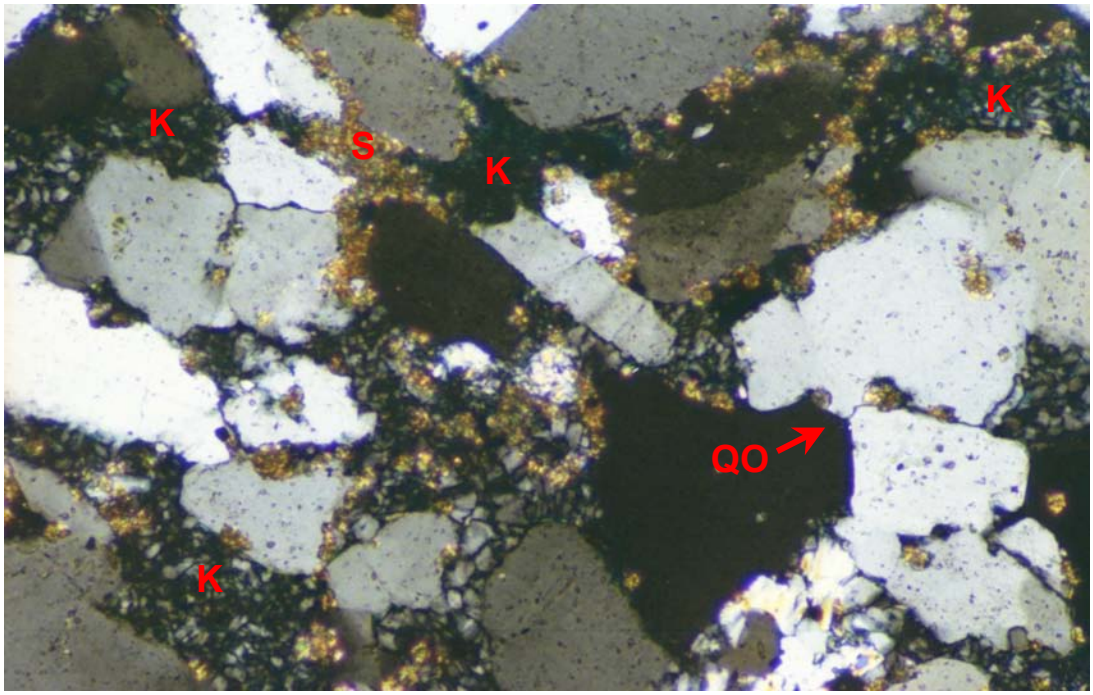


FIGURE 1 Plane polarised light

FIGURE 2 Crossed polarisers

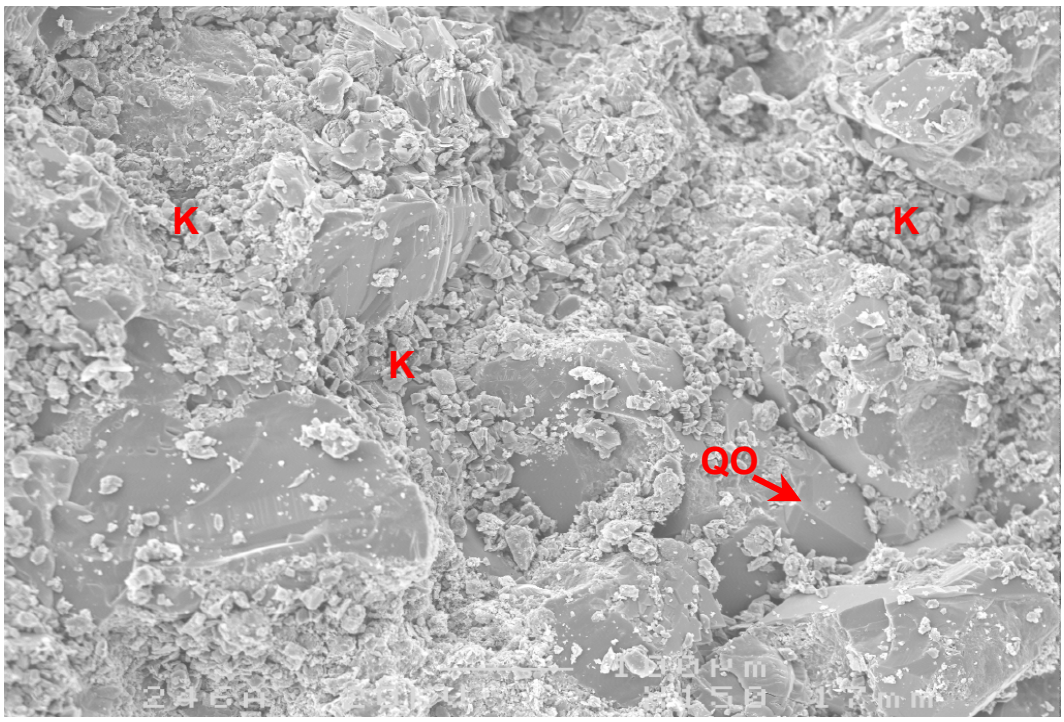
0.2mm



Intergranular spaces are filled by authigenic kaolin (K) that has formed by alteration of compacted micaceous/argillaceous grains, and there has been further porosity loss by cementation by quartz overgrowths (QO) and early-diagenetic siderite (S). Kaolin is highly microporous as shown by its blue hue.

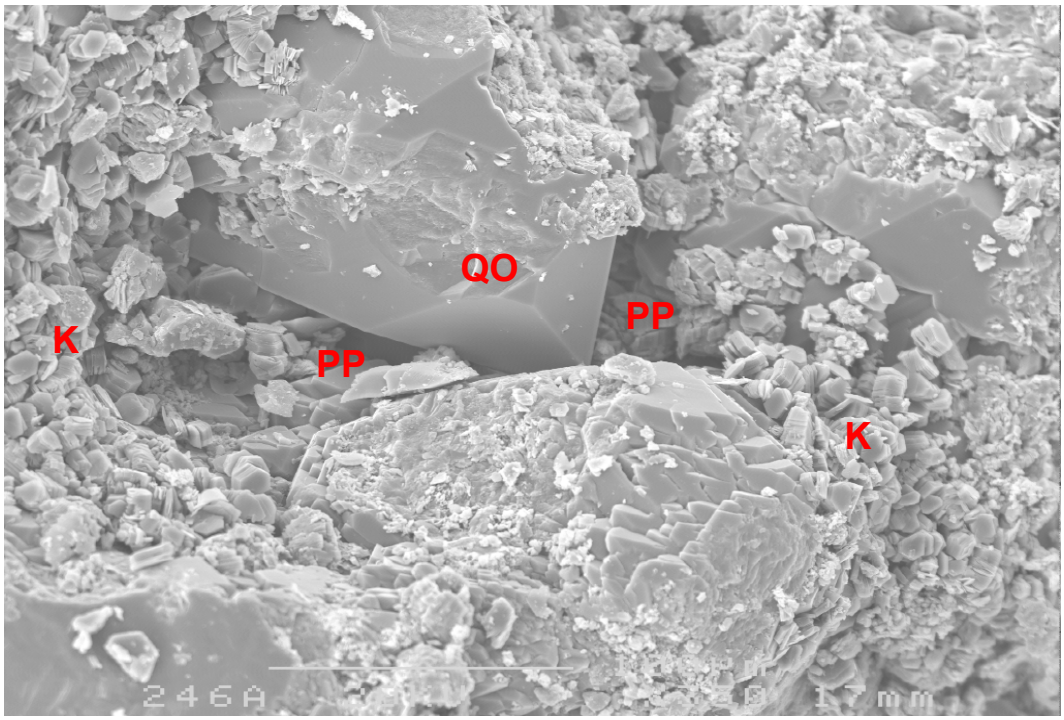
PLATE 24: THYLACINE-2 #246 2300.80m cont.

FIGURE 1



Almost complete pore filling by authigenic kaolin (K) and quartz overgrowth (QO) cement results in low permeability (9.64mD).

FIGURE 2



Small primary intergranular pores (PP) are preserved where quartz overgrowth (QO) development is incomplete. However, with adjacent intergranular spaces being filled by authigenic kaolin (K) and quartz overgrowths, the pores would have limited interconnection with any macropores in their vicinity.

PLATE 25: GE0GRAPHE-1 #57H 1832.47m

Rock classification: Litharenite

Texture:

Sedimentary structures: Massive

Sorting: Well

Average grain size: 0.26mm (medium sand)

Roundness: Subangular-subrounded

Texture: Grain supported

Packing/grain contacts: Moderate/long, embayed, rarely microstylolitic

Macropore types: Secondary mouldic pores, secondary intragranular pores, primary intergranular pores

Core analyses: Por. = 18.7%, Perm. = 15.7mD, GD = 2.67g/cc

Composition:

Quartz (monocrystalline)	44.9%	Siderite (pore filling)	1.3%
Quartz (polycrystalline)	4.8%	Siderite (replacement)	5.0%
Quartz overgrowths	2.0%	Glauconite	0.3%
Chert	1.4%	Authigenic kaolin (pf)	4.3%
K-feldspar	4.0%	Authigenic kaolin (rpl)	12.3%
Volcanic rock fragments	0.6%	Authigenic illite (replacement)	2.6%
Metamorphic rock fragments	11.6%	Primary porosity (intergran)	0.9%
Sedimentary rock fragments	2.0%	Secondary porosity (mouldic)	0.7%
Mica	0.6%	Secondary porosity (intragran)	0.7%

Comments: Intergranular porosity has been almost completely eliminated by authigenic kaolin formation, ductile grain/authigenic clay compaction, grain contact dissolution, localised quartz overgrowth cementation and pore filling by localised sideritic detrital clay and finely disseminated siderite. Rare patches of coarsely-crystalline calcite and ankerite replace framework grains and clay. Widely scattered, hence poorly interconnected secondary pores are the result of partial to complete dissolution of K-feldspar, and sporadic primary intergranular pores are preserved where quartz overgrowths have not completely filled all available intergranular space between juxtaposed quartz grains. Containing little macroporosity and abundant authigenic clay, the sand is highly microporous. Much authigenic clay has a blue hue, indicating that it is sufficiently microporous for impregnation by epoxy resin.

PLATE 25: GE0GRAPHE-1 #57H 1832.47m

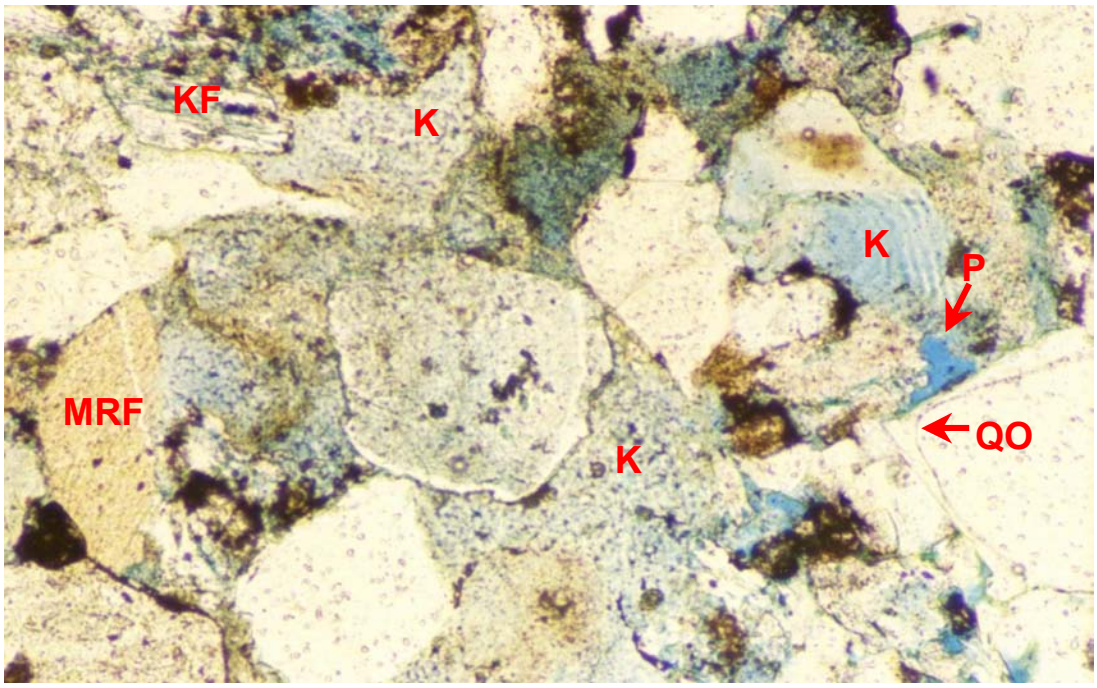
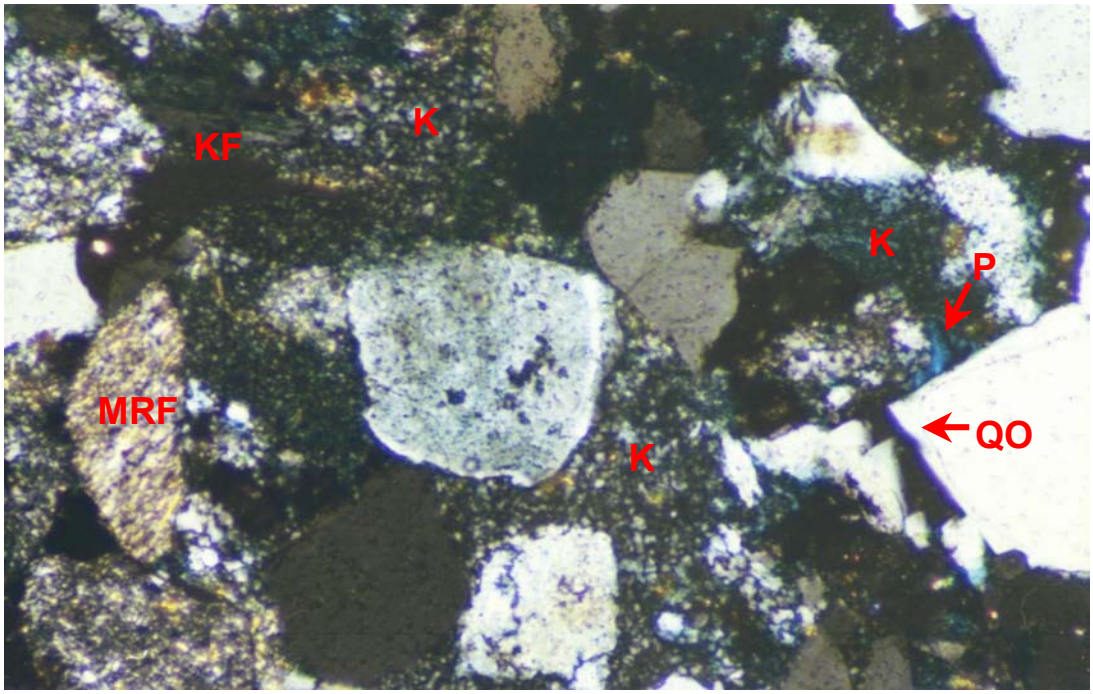


FIGURE 1 Plane polarised light
FIGURE 2 Crossed polarisers

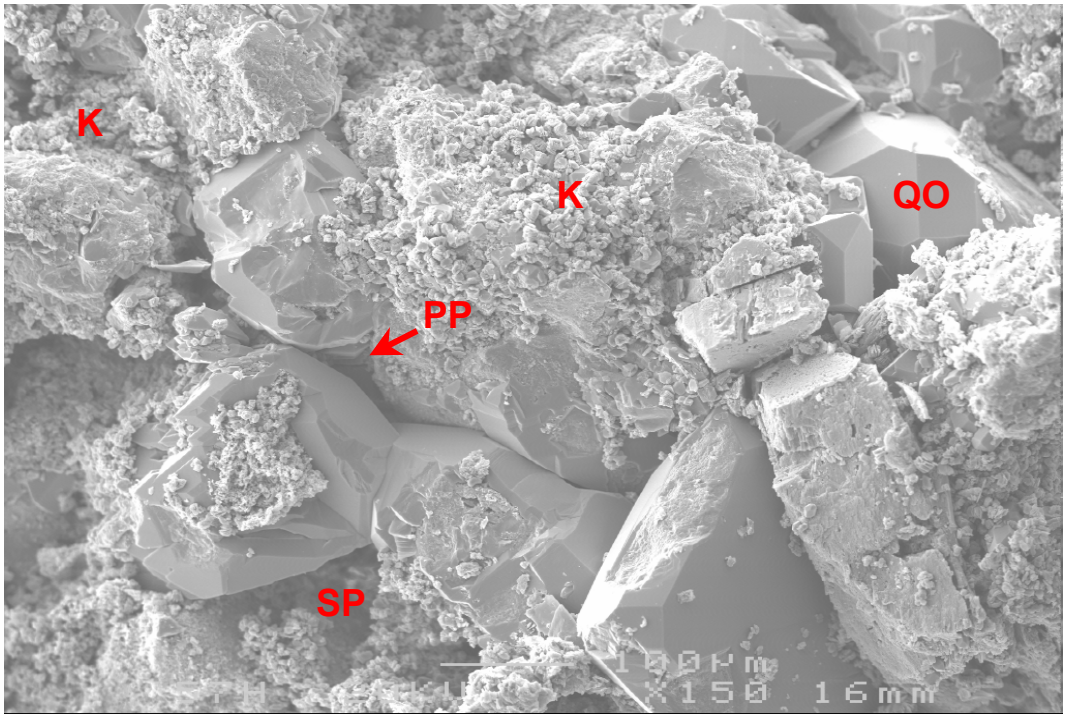
0.2mm



Connection between intergranular pores (P) is severely reduced by the presence of authigenic kaolin (K) within most intergranular areas. Further porosity loss is the result of ductile grain/authigenic clay compaction, grain contact dissolution and localised quartz overgrowth (QO) cementation. Framework grains include micaceous metamorphic rock fragments (MRF) and K-feldspar (KF). Kaolin is highly microporous as shown by its blue hue.

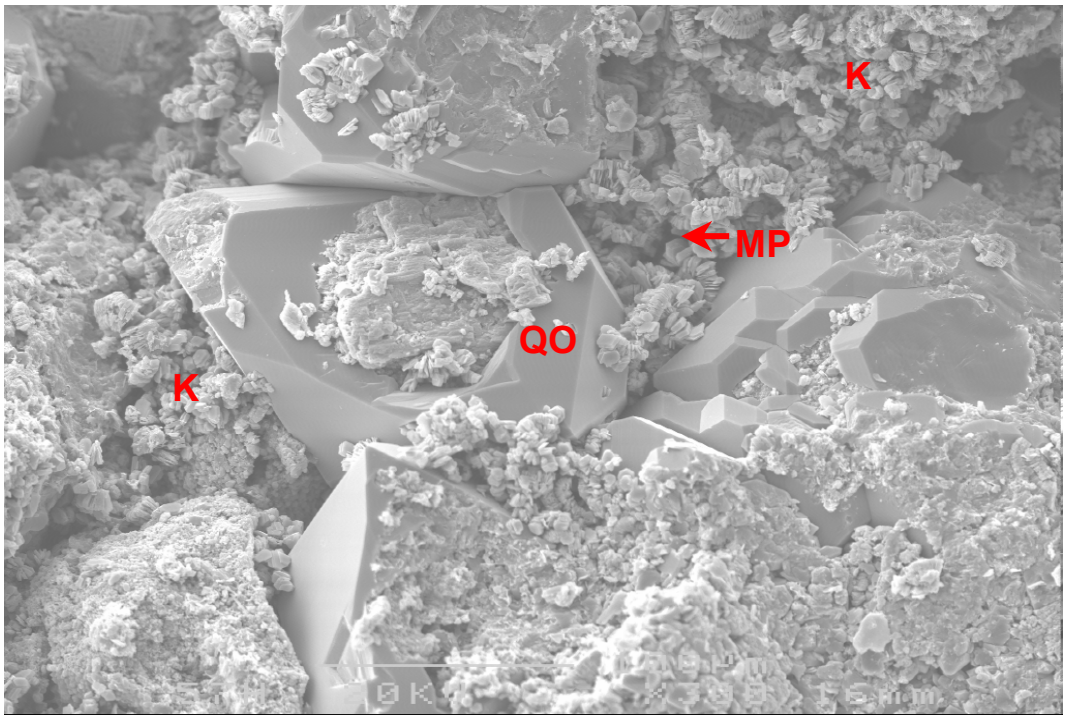
PLATE 26: GE0GRAPHE-1 #57H 1832.47m cont.

FIGURE 1



Primary intergranular pores (PP) are preserved where quartz overgrowths (QO) do not completely fill all available intergranular space between juxtaposed quartz grains, and a partly clay-filled secondary pore (SP) occurs where a labile grain has dissolved. Permeability is significant reduced by the presence of authigenic kaolin (K) within most intergranular spaces.

FIGURE 2



Intergranular spaces are typically largely to completely filled by authigenic kaolin (K). Porosity loss is also the result of localised quartz overgrowth (QO) cementation. Being loosely packed, authigenic kaolin is highly microporous (MP).

APPENDIX 7
CORE INTERPRETATION

SEDIMENTOLOGY REPORT
WELL: THYLACINE-2

Prepared For:

WOODSIDE ENERGY LTD.

By Duncan Barr

October, 2001

CONTENTS

1 SUMMARY 1

2 INTRODUCTION 3
2.1 Overview 3
2.2 Objectives 3
2.3 Cored Interval 3
2.4 Methods 3

3 SEDIMENTOLOGY 4
3.1 Overview 4
3.2 Depositional Setting 4
3.3 Sandstone Geometry And Continuity 6
3.4 Depositional Lithofacies 7
3.5 Ichnofacies 8
3.6 Depositional Sequence 8
3.6.1 Interval 1 (2314.55 – 2301.65 m) 8
3.6.2 Interval 2 (2301.65 – 2295.60 m) 10
3.6.3 Interval 3 (2295.60 – 2235.49 m) 12
3.6.4 Interval 4 (2235.49 – 2230.90 m) 16
3.6.5 Interval 5 (2230.90 – 2173.90 m) 17
3.6.6 Interval 6 (2173.90 – 2150.00 m) 20
3.7 Sequence Stratigraphy 22
3.8 Angular Bedding Contacts. 22
3.9 Reservoir Quality 23

4 REFERENCES 24

TABLE 1: Depositional Lithofacies Descriptions
TABLE 2: Ichnofacies Descriptions
TABLE 3: Main Sequence Stratigraphic Features

FIGURE 1: Examples of sand-rich slope apron and ramp settings
FIGURE 2: Wireline log display.

PLATES 1 – 30: Selected Core Photographs and Descriptions

ENCLOSURE 1: 1:40 Scale Core Description Log

ENCLOSURE 2: Data CD-ROM

1 SUMMARY

160.05 m of conventional core were described in detail from well Thylacine-2. Lithology consists mainly of interbedded argillaceous siltstones and argillaceous to clean sandstones.

Depositional environments fluctuate markedly within the cored interval and several depositional surfaces may act as important correlative markers. Based on a combination of lithofacies and ichnofacies descriptions, the cored interval can be subdivided into the following intervals:

1) ***2314.55 – 2301.65 m:*** Interbedded bioturbated argillaceous siltstones and very fine to fine, bioturbated to finely laminated sandstones. *Cruziana* ichnofacies. Environmentally restricted (possibly embayed) shallow shelf environment. Interval capped by erosive, forced-regressive surface.

2) ***2301.65 – 2295.60 m:*** Fine to coarse grained, unbioturbated, cross-bedded and ripple-laminated sandstones deposited by fluvially-dominated deltaic channels. Capped by marine flooding surface.

3) ***2295.60 – 2235.49 m:*** Series of parasequence-like cycles of siltstone to very fine and fine, bioturbated to finely laminated sandstone. *Cruziana* to *Skolithos* ichnofacies. Shallow, possibly restricted (embayed?) shelf. Minor laminated heterolithics may represent tidal deposits. Occasional granule-rich beds indicate periods of transgressive reworking. Interval capped by major flooding surface.

4) ***2235.49 – 2230.90 m:*** Dense, massive glauconitic claystones with intermittent siderite layers. *Zoophycos*/*Nereites* ichnofacies. Distal offshore muds.

5) ***2230.90 – 2173.90 m:*** Thick succession of fine to medium grained, massive sandstones. Mostly unbioturbated. Gravity deposits (probably liquefied flows) of a proximal submarine ramp or slope-apron. Common early-formed shear fractures and dewatering structures consistent with deposition on an unstable slope. Base of sequence sharp and erosional, may represent a regressive surface.

6) ***2173.90 – 2150.00 m:*** Shallow shelf siltstones and minor very fine to fine grained, bioturbated to finely laminated sandstones. *Cruziana* ichnofacies.

The marked changes in depositional environment were probably caused by tectonically-induced fluctuations in relative sea level. Tectonic movements are likely to have included syndepositional movement of faults and fault block rotation. Several depositional surfaces exhibit angular “unconformities” of up to 25 degrees, indicating some bed rotation occurred during deposition. Many of the fractures observed may have been related to this tectonic activity.

Two main intervals of reservoir sandstone are encountered: deltaic channels of 2301.7 – 2295.7 m, and gravity deposits of 2230.9 – 2173.9 m. Reservoir

quality is very good to excellent in the deltaic channels, with average profile permeability of nearly 1600 md. The gravity deposits are thicker, but contain abundant kaolinite matrix and are therefore of poor quality, exhibiting average profile permeability of only 5 md.

Irreducible water saturations are expected to be high in the gravity-deposited sandstones due to abundant kaolinite matrix. Water-free production may therefore be possible where water-cut is anticipated.

2 INTRODUCTION

2.1 Overview

160.05 metres of conventional core were described in detail from well Thylacine-2. Lithology consists of a series of alternating cycles of sandstone and argillaceous siltstone.

2.2 Objectives

The main objectives of this study are to:

1) Provide a detailed sedimentological description of the cored intervals.
2) Determine lithological facies and ichnofacies profiles.
3) Interpret depositional environments.
4) Establish the main sedimentological sequences and boundaries, and estimate their sequence stratigraphic significance.
5) Estimate likely reservoir potential.

2.3 Cored Interval

The following intervals were cored in Thylacine-2:

Core	Depth Interval
1	2150.00 – 2199.90 m
2	2203.50 – 2257.60 m
3	2258.50 – 2314.55 m

2.4 Methods

Cores were logged in digital format using AppleCore™. Colours were determined by comparing between the wet core face, and the Geological Society of America colour chart.

3 SEDIMENTOLOGY

3.1 Overview

Lithology in the cored interval of Thylacine-2 consists mainly of interbedded argillaceous siltstone and sandstone. A short interval of glauconitic claystone is also encountered approximately halfway up the cored interval. Sandstones mostly vary in grain size from very fine to coarse grained, although some localised beds of granules and rip-up clasts are also present. The siltstones are heavily bioturbated, while sandstones vary from bioturbated and argillaceous to massive and cross-bedded.

Two important successions of sandstone are encountered in the cored interval. These successions are:

1) A succession of stacked, good to excellent quality, cross-bedded fine to coarse grained sandstones between 2295.7 m and 2301.6 m.

2) A multi-story sequence of poor to locally fair quality, massive, fine to medium grained sandstones between2173.9 m and 2230.9 m.

3.2 Depositional Setting

Depositional environments in the cored interval of Thylacine-2 range from deltaic distributary channels through shallow shelfal deposits to distal offshore muds and gravity deposits. Changes in environment are often very marked and sudden, indicating they are likely to have been caused by tectonic activity at the time of deposition. Evidence from trace fossil assemblages also suggests there may have been some environmental restriction, possibly indicating deposition into a gulf or into an interdistributary bay environment. A possible palaeogeographical setting is illustrated in Figure 1.

The following six main intervals can be identified based on a combination of lithofacies and depositional environment:

1) ***2314.55 – 2301.65 m:*** This interval consists of a series of interbedded bioturbated argillaceous siltstones and bioturbated argillaceous sandstones that are thought to have been deposited on an environmentally restricted shelf, in a proximal offshore to offshore transition zone setting. The source of the restriction is thought to have been either deposition into a marine gulf, or by embayment caused by the presence of nearby deltaic channel lobes. Evidence of impending change is provided by a sudden reduction in bioturbation at 2301.85 m, just below the top of the interval.

2) ***2301.65 – 2295.60 m:*** Medium to coarse grained, cross-bedded sandstones, interpreted to represent fluvially-dominated deltaic channels, dominate this interval. These channel deposits are thought to have been tidally influenced, and consist of stacked units of medium to coarse grained sandstone with very little detrital clay present, consistent with deposition on a braided delta plain. The sharp, coarse grained base of this sandstone succession may represent a forced-regressive surface, while the top is marked by a flooding surface.

3) ***2295.60 – 2235.49 m:*** Shallow shelf siltstones and sandstones overlie the flooding surface at 2295.7 m. A number of parasequence-like cleaning-up and coarsening-up cycles are observed in these deposits, often with very coarse grained to granule-grade transgressive lags occurring at or near the top of each cycle. These cycles are believed to represent prograding shoreline successions, and represent shallowing upwards cycles that range from proximal offshore at their bases to lower or middle shoreface conditions at their tops. Trace fossil assemblages indicate some degree of environmental restriction may have occurred in some of these deposits, suggesting deposition into a marine gulf, or influence from a nearby delta. Thin, finely laminated sandstone beds that are locally encountered are interpreted

to have formed as storm sands. Localised heterolithic beds are also present, possibly representing some form of tidal flat or tidal inlet.

4) ***2235.49 – 2230.90 m:*** A major flooding surface marks the base of this short interval, which consists of dense, faintly bioturbated, glauconitic claystones that are interpreted to have formed in a very low energy, distal offshore setting.

5) ***2230.90 – 2173.90 m:*** A thin, basal lag of clay clasts and sideritic pebbles marks the base of a series of mainly massive sandstones. These sandstones are believed to have been deposited very rapidly as a series of liquefied gravitational flows, and may represent part of a sand-rich ramp or slope-apron deposit (Figure 1). As these sandstones filled up the accommodation space made available by the earlier flooding event, palaeo-water depths became gradually reduced with time. At the top of the sequence, the sandstone grades upwards into argillaceous siltstone over a distance of approximately 2 cm, suggesting a sudden reduction in sand supply. This reduction in sand supply may also have been tectonically controlled.

6) ***2173.90 – 2150.00 m:*** After gravity deposition ceased, deposition returned to shallow shelf siltstones and minor sandstones. Conditions were stable, with deposition mainly occurring in a proximal offshore environment. Towards the top of the core (above 2159 m) a series of thin, bioturbated sandstone stringers indicates a gradual increase in depositional energy. This increase in energy is thought to signify a return to gradual shoreline progradation.

3.3 Sandstone Geometry And Continuity

Sandstone geometry and continuity are influenced by a complex interplay of depositional environment, rate of creation of accommodation space, sand supply and basin morphology. However, some general inferences can be made:

1) Shoreface-related sandstone bodies are products of reworking by waves and near-shore currents, and are therefore likely to form sheet-like sandstone bodies that are elongated parallel to the palaeo-shoreline. In particular, thin finely laminated sandstone beds, which are interpreted to represent storm-generated sands, are likely to form laterally extensive thin sheets (Johnson & Baldwin, 1996).

2) The deltaic channel sandstones between 2301.7 m and 2295.5 m exhibit stacked, multi-story architecture and contain very little detrital clay. They are interpreted to have been deposited as laterally shifting bars in a tidally-influenced braided channel system. Although individual channel bars were probably aligned parallel to the axis of the main channel, reworking and shifting of these bars by fluvial and tidal processes means they are likely to intersect laterally with other bars (Orton and Reading, 1993). Given the paucity of clay in this channel succession, these sandstones may therefore be laterally continuous over quite large distances.

3) The sandstones between 2231.0 m and 2173.9 m are thought to have formed as liquefied gravity flows in a sand-rich ramp or slope-apron environment. As with the deltaic channel sandstones, individual units are likely to be elongated perpendicular to the palaeo-shoreline, but may also intersect with one another in a direction parallel to depositional strike. One of the features of a sand-rich ramp environment is a lack of channel levee development. Lateral continuity of the whole sandstone succession can therefore be quite extensive along both depositional dip and depositional strike (Stow, Reading and Collinson, 1996) .

3.4 Depositional Lithofacies

In line with the complex depositional history of the cored interval in Thylacine-2, a large number of lithofacies were encountered. These lithofacies are

annotated on the core description log (Enclosure 1) and are described in Table 1.

3.5 Ichnofacies

Several ichnofacies were encountered in the cored interval. These ichnofacies were named in accordance with Pemberton et al (1992), and include the following main types:

1. *Skolithos*
2. Distal *Skolithos*
3. Proximal *Cruziana*
4. Distal *Cruziana*
5. Restricted *Cruziana*
6. *Teichichnus*-dominated *Cruziana*
7. *Glossifungites*
8. *Zoophycos/Nereites*

Detailed descriptions of these ichnofacies types are provided in Table 2.

3.6 Depositional Sequence

The cored interval is described below, starting at the base of Core 3 and working upwards, chronologically.

3.6.1 Interval 1 (2314.55 – 2301.65 m)

Description

This interval consists of a series of interbedded argillaceous siltstones and bioturbated to faintly laminated, very fine to fine grained sandstones (Plates 1, 2, 3 and 4). Siltstone beds are heavily though faintly bioturbated (facies Mb). Trace fossil assemblages in the siltstones are moderately diverse, and include trace fossils such as *Teichichnus*, *Planolites*, *Helminthopsis/Helminthoida*, occasional *Zoophycos* and *Terebellina*; burrows that are indicative of the Distal *Cruziana* ichnofacies. However, *Teichichnus* often dominates the trace

fossil assemblage, a feature that is thought to indicate a degree of environmental restriction, possibly due to embayment. Occasional carbonaceous fragments and laminae are observed, including a large, partly pyritised wood fragment at 2306.1 m. Siderite and pyrite nodules are observed locally.

An unusual, pyrite-lined burrow (either *Ophiomorpha* or *Thalassinoides*) is observed in this interval (Plate 2). This burrow is filled with authigenic kaolinite and contains a core of carbonaceous material that may (or may not) represent the remains of a body fossil.

Sandstones are mostly heavily bioturbated and argillaceous (facies Sb and Sba), although a few, thin, faintly laminated sandstone beds (facies Sfl and Sl) are encountered. Trace fossils include *Teichichnus*, *Planolites*, *Palaeophycus*, *Thalassinoides*, *Helminthopsis/Helminthoida*, *Rhizocorallium*, *Anconichnus* and occasional *Ophiomorpha*. Ichnofacies is mainly Proximal *Cruziana*, locally grading into Distal *Skolithos* and *Teichichnus*-dominated *Cruziana*.

Towards the top of this interval, at 2304.8 m, bioturbation intensity decreases. Areas of primary silty lamination are found preserved within the argillaceous siltstones, alternating with intensely bioturbated bands and occasional thin, finely laminated sandstones. This pattern continues until 2301.8 m. A thin, sideritic band is encountered at this depth, and is overlain by approx, 15 cm of very sparsely bioturbated, laminated argillaceous siltstone (Plates 4 and 5). This laminated siltstone is in-turn overlain by a layer of coarse to very coarse grained sandstone, which marks the start of the next interval.

Interpretation

Deposition is thought to have occurred in shallow marine environment, possibly in close proximity to a deltaic source of sediment. The dominance of the trace fossil *Teichichnus* in some parts of the siltstone suggests a stressed, restricted environment. This restriction may have been due to deposition into a partially enclosed bay or gulf, or reflects deposition within a deltaic

interdistributary bay. The sandstones are interpreted to represent intermittently prograding shoreface sandstones (derived from a delta mouth sand sheet) or weak crevasse splays.

Localised zones of quartzose granules that "float" within the argillaceous sandstone facies are observed. These zones are interpreted to represent coarser grained sediment that became concentrated due to repeated reworking and winnowing of the sediment during periods of transgression.

The reduction in bioturbation intensity and partial preservation of primary bedding lamination seen in the upper part of the interval may reflect an increase in environmental restriction (possibly due to partial closing of the embayment or gulf). Whether or not the thin sideritic band observed at 2301.8 m was related to this event is unclear. However, the sudden reduction in bioturbation above this depth appears to have acted as a precursor to the fluvially-dominated sandstone deposition that followed.

Reservoir Quality

Reservoir quality is very poor to poor throughout this interval. Fine grain size and abundant detrital clay, dispersed throughout the pore network by burrowing organisms, are the main controls on reservoir quality.

Wireline Log Signature

The poorly developed, argillaceous sandstones in this interval show up as a series of broad, low to moderate gamma ray spikes (Figure 2). Separation between neutron and density curves indicates generally high clay content, while resistivity log-derived Sw in these sandstones is high.

3.6.2 Interval 2 (2301.65 – 2295.60 m)

Description

The base of this interval is marked by a sharp, undulating surface overlain by a coarse to very coarse grained sandstone lag deposit (which also includes a large sideritic pebble; Plate 5). This lag deposit is overlain by approximately

1.5 m of upper fine grained, ripple-laminated sandstone (facies Srl; Plate 6). The ripples are mainly current-formed and frequently show evidence of bimodal current direction. Thin, drape-like argillaceous laminae are common, and occasional sideritic rip-up clasts are present. Bioturbation is rare to absent.

At 2300.2 m, ripple-laminated sandstone gives way to a succession of stacked, medium to coarse grained, cross-bedded sandstone beds (facies Sx; Plate 7). Cross-bedding is mainly tabular and low-angle, and consists of alternating finer grained and coarser grained, graded laminae. Occasional bi-directional, "herring-bone" cross-stratification is observed, and angular reactivation surfaces are common (the difference between dip angles above and below these surfaces is typically between 15 and 25 degrees. Uneven carbonaceous laminae and thin concentrations of carbonaceous "coffee-grounds" are also common.

The cross-bedded sandstone sequence is almost entirely unbioturbated. Burrows are only observed in the uppermost 30 to 40 cm and consist mainly of robust *Ophiomorpha* burrows that are thought to have entered the sand from above (Plate 8). The very top of this sandstone succession is marked at 2295.6 m by a sharp, uneven bedding surface, which is overlain by granule-bearing, very argillaceous sandstone (Plate 8).

Interpretation

The coarse grained lag deposit at the base of this interval is interpreted to have formed in response to some form of regressive event. The lag's sudden appearance and sharp basal contact suggests it formed in response to a sudden reduction in sea level – brought about by tectonic forced regression.

The ripple-laminated sandstones that overlie the coarse grained lag are interpreted to represent tidal flat deposits, possibly formed by tidal reworking of channel sands within an estuarine or deltaic environment. The sudden change to overlying cross-bedded sandstones at 2300.2 m marks a landward shift in facies. This shift is thought to have been triggered by a second

regressive event. These cross-bedded sandstones are interpreted to have been deposited on a braided delta plain as fluvially-dominated distributary channel bars, with occasional herring-bone structure indicating tidal influence.

Reservoir Quality

Reservoir quality in this interval is good to excellent, with the best visible porosity observed along coarse grained, graded laminae that occur within the cross-bedded sandstones.

Wireline Log Signature

This interval stands out clearly on gamma ray, porosity and resistivity logs (Figure 2). Gamma ray is very low, and exhibits funnel-shaped profile, consistent with a progradational sandstone. Resistivity-based Sw values are very low, while a marked neutron-density cross-over indicates the presence of gas.

3.6.3 Interval 3 (2295.60 – 2235.49 m)

Description

The sharp base of this interval is overlain by granule-bearing, intensely bioturbated, argillaceous sandstone (Plate 8). This granule-bearing sandstone grades into argillaceous, sandy siltstone by 2295.0 m. The rest of the interval consists of a series of parasequence-like coarsening-up and cleaning-up cycles, starting in argillaceous, bioturbated siltstone (Plates 9 and 10), and ending in very fine to fine grained, usually bioturbated sandstone (Plate 11).

The siltstones are intensely bioturbated and mostly exhibit a moderately diverse trace fossil assemblage, with ichnofacies identified as Distal *Cruziana*. Burrows include common *Helminthopsis/Helminthoida*, *Teichichnus*, *Planolites*, *Anconichnus*, occasional *Asterosoma*, *Terebellina*, *Palaeophycus*, *Rhizocorallium* and rare *Zoophycos*.

Most of the sandstones are very fine to fine grained, and are also heavily bioturbated (facies Sb and Sba; Plates 11 and 12). Less bioturbated sandstones often exhibit fine, horizontal lamination (facies Sfl; Plate 13). Ichnofacies is mainly Proximal *Cruziana*, although a few argillaceous sandstone beds in the lower part of the interval exhibit domination by *Teichichnus* burrows. Burrow types are otherwise diverse, including *Teichichnus*, *Anconichnus*, *Helminthopsis/Helminthoida*, *Rhizocorallium*, *Planolites*, *Palaeophycus*, occasional *Ophiomorpha* and *Thalassinoides*.

Several granule-rich zones are observed in both the argillaceous sandstone and argillaceous siltstone (Plate 11), while occasional thin beds of clean granule-rich sandstone are also encountered (Plate 12). These clean granule-rich beds usually occur towards the tops of coarsening-upward cycles.

A short interval of laminated heterolithics (facies Hl) occurs between 2249.4 m and 2246.0 m (Plate 15). These heterolithic beds lie on top of a coarsening-upward succession of bioturbated sandstone (facies Sb). The bioturbated sandstone exhibits Distal *Skolithos* ichnofacies and contains common, wispy laminae of very carbonaceous clay (Plate 14). The heterolithics consist of argillaceous siltstone drapes that alternate with lenticular, very fine to fine grained sandstone. Many of these sandstone lenses contain ripples, some of which exhibit bi-directional current direction.

The heterolithic beds are intermittently bioturbated, and ichnofacies varies between Restricted *Cruziana*, Proximal *Cruziana* and Distal *Skolithos*. Trace fossils include *Planolites*, *Teichichnus*, *Palaeophycus*, *Rhizocorallium*, occasional *Ophiomorpha*, *Rosselia*, *Thalassinoides*, *Asterosoma* and possible *Diplocraterion* (Plates 15 and 16).

At the top of the heterolithics, at around 2246 m, a thin, granule-bearing horizon is underlain by a number of large, robust *Thalassinoides* burrows (Plates 17 and 18). These *Thalassinoides* burrows are filled with coarse sand

grains and quartzose granules that are very similar to those of the overlying granule horizon, indicating a *Glossifungites* ichnofacies.

The uppermost 2 m of this interval consists of a series of thinly interbedded, often intensely bioturbated sandstone layers. The grain size profile across these thin beds is highly erratic, and several very coarse grained and granule-grade layers are encountered (Plate 19).

Siderite nodules and sideritic bands are common throughout the interval, and frequently exhibit subvertical extensional fractures. Most of these fractures have been filled with authigenic kaolinite.

Interpretation

Deposition is interpreted to have occurred on a shallow marine shelf, with argillaceous siltstones representing proximal offshore muds. The coarsening-up/cleaning-up profiles are interpreted to have formed by intermittent periods of shoreface progradation and are therefore thought to represent marine parasequences. Sandstones at the top of each coarsening-up profile are interpreted to represent lower to middle shoreface deposits.

Although trace fossil assemblages are relatively diverse throughout most of the interval, some parts of the interval are dominated by *Teichichnus* burrows (*Teichichnus*-dominated *Cruziana* ichnofacies), or show reduction in both bioturbation index and trace fossil diversity (Restricted *Cruziana* ichnofacies). These reductions in trace fossil diversity imply a degree of environmental stress, possibly due to embayment, or the influence of a nearby delta, or both.

The heterolithic interval between 2249.4 m and 2246.0 m is interpreted to have formed as part of a tidal flat or tidal inlet. The underlying bioturbated sandstone (facies Sb; 2251.9 m – 2249.4 m), within its common carbonaceous claystone laminae, may have formed as a related delta-front sand sheet, formed as part of a prograding mouth bar complex. Continued progradation is presumed to have led to the formation of tidal flats.

The *Glossifungites* ichnofabric and associated quartzose granule-rich horizon observed at around 2246 m indicate a transgressive surface of erosion situated just above the heterolithic interval. The *Glossifungites* ichnofacies forms in a semi-consolidated “firmground” and is commonly associated with transgressive surfaces (Pemberton and Frey, 1985). Quartzose granules also occur within argillaceous siltstones and sandstones as zones of “floating” grains. These zones are typically heavily bioturbated and are interpreted to indicate periods of intermittent transgressive reworking.

The series of thin, often very coarse grained sandstone beds at the top of the interval is interpreted to have formed as a series of transgressive lags. These lags are believed to have formed in response to rising sea level, and probably represent coarser grained sediment that was eroded from the former shoreline and redistributed out onto the shelf as a result of transgression.

Near-vertical extensional fractures in sideritic nodules and layers are thought to have formed in response to high overburden stress during burial. Their direction is likely to be aligned perpendicular to the direction of minimum horizontal stress at the time of their formation.

Reservoir Quality

Reservoir quality in this interval is generally poor. However, fair to very good reservoir quality is locally encountered within the coarse grained transgressive lag deposits and coarser grained shoreface sandstones that occur towards the tops of coarsening-upward cycles. Unfortunately, these beds are thin, measuring less than 20 cm.

Wireline Log Signature

Wireline log signatures are similar to those of Interval 1. Sandstones show up as low to medium gamma ray spikes, while neutron and bulk density separation indicates a generally clay-rich sequence (Figure 2). Resistivity-derived Sw is moderate to high. However, the lower 20 m of this interval exhibits an overall serrated, funnel-shaped profile, indicative of progradation.

3.6.4 Interval 4 (2235.49 – 2230.90 m)

Description

This short interval consists of massive to faintly bioturbated, glauconitic, silty claystone. The contact between this claystone and the underlying sandstone is sharp and uneven, but is not thought to be erosive. Instead, the contact is believed to represent a major flooding surface (Plate 20). Several tightly siderite-replaced horizons are observed within the claystone (Plate 21).

Glauconite occurs mostly as coarse sand-sized pellets, and is unevenly distributed into thin, discontinuous lenses and what appear to be burrows (mostly faint, indistinct *Planolites*). Bioturbation intensity otherwise appears to be relatively low, and occasional, very faint detrital lamination is observed, especially towards the base of the claystone. However, burrows are difficult to both detect and identify, since there is often little difference between burrow fill and surrounding claystone. Ichnofacies is therefore difficult to determine precisely, and has been designated *Zoophycos*/*Nereites* due to the apparent low diversity and low to moderate intensity of trace fossils.

Glauconite content increases gradually upwards, and becomes mixed with quartz grains in the upper half of the interval. A few quartzose granules are also observed. Depositional lamination also becomes more evident towards the top of the claystone (mostly occurring as thin, sandy, glauconitic lenses) and culminates in two thin, very fine grained sandstone beds The first of these beds, at around 2231.5 m, exhibits thin current ripples (facies Sfl). The second bed, at 2231.3 m, is highly argillaceous and contains platy rip-up clasts that appear to “float” within a matrix of very fine grained, silty sandstone. Burrows are also more visible; a few *Teichichnus*, *Zoophycos* and *Thalassinoides* burrows are observed in addition to faint *Planolites* traces.

Interpretation

The glauconitic claystones of this interval are interpreted to have been deposited in a distal offshore setting. The sharp nature of the flooding surface at the base of the interval indicates it probably formed in response to a large

and rapid rise in sea level. Such an increase in sea level is likely to have been caused by tectonic movement.

The two thin sandstone beds encountered near the top of the interval are interpreted to represent the distal gravity deposits. The lower of the two beds is ripple-laminated and appears to be a classic Bouma-type C traction deposit. The upper bed, with its floating claystone pebbles, is more likely to represent some form of debris flow.

Reservoir Quality

The interval contains no reservoir quality beds, and could represent a significant local seal.

Wireline Log Signature

The base of this interval is marked by a sudden increase in gamma ray response (Figure 2). Gamma ray then reduces gradually upwards, reflecting a gradual increase in sand and silt content. Neutron and density logs also show this increase in sand content, with the separation between the two curves gradually decreasing upwards.

3.6.5 Interval 5 (2230.90 – 2173.90 m)

Description

This interval consists of a multi-story stack of fine to medium grained, moderately well sorted, massive to faintly laminated sandstones, locally interrupted by thin, bioturbated layers of argillaceous siltstone.

The base of the interval is sharp and scoured, and is overlain by a thin bed of claystone pebbles and sideritic clasts. Detrital lamination is absent in the bulk of the sandstone beds (Plates 22 to 27), although faint horizontal lamination is common between 2199.9 m and 2187.5 m. Grain size tends to remain constant across most beds, although the tops of many sandstone beds fine up slightly. Most sandstone beds exhibit sharp, scoured bases. Sideritic nodules and siderite-cemented lenses are locally encountered.

Clay clasts are common throughout the interval. Most are isolated, and range in size from granule grade to upper pebble sized. However, silty claystone and sideritic pebbles are very common between 2217.0 m and 2213.5 m (facies Spbl), and locally form thin, matrix-supported conglomeratic layers (facies Gms; Plate 22).

Interestingly, there are no partially sideritised claystone pebbles – claystone pebbles have either been completely siderite-replaced, or not replaced at all. This suggests that siderite replacement of these clasts occurred prior to deposition. Most silty claystone pebbles have been heavily deformed by compaction, while sideritic pebbles have retained their rounded shape (Plate 22).

The thin, argillaceous siltstones that separate several sandstone beds are intensely bioturbated (Plate 23) and in the lower part of the interval, below 2221.0 m, are glauconitic. Burrows include *Helminthopsis/Helminthoida*, *Teichichnus*, *Planolites* and *Terebellina* of the Distal *Cruziana* ichnofacies.

The tops of some sandstone beds are also bioturbated. Burrows tend to be sparse, and include weak *Palaeophycus*, *Planolites*, *Asterosoma* and occasional *Skolithos*. These burrows are thought to represent opportunistic structures and have been identified as “doomed pioneer” assemblages (Plate 26).

Fractures are commonly observed throughout the interval. Most consist of indistinct, siderite-lined fractures, or faint gouge-lined shear fractures (Plates 23, 24, 25 and 26). Dewatering sheets and flame structures are locally associated with these fractures, many of which exhibit sinuous and anastomosing shapes (Plate 27). Later-formed kaolinite-filled extensional fractures are also observed, but are confined to sideritic nodules and siderite-cemented bands.

Interpretation

The sandstones in this interval are interpreted to represent gravity deposits of a sandy ramp or slope-apron. Sand is thought to have been deposited very rapidly as a liquefied flows in a series of proximal turbidite channels. Massive to faintly laminated texture indicates that most of the sandstones are relatively disorganised deposits analogous to Bouma A to B sequences.

The moderately well sorted texture and relatively limited range of grain size seen in these sandstones indicates they were derived from a relatively well sorted source of sandy sediment. The sandstones are therefore thought to have been sourced from wave and tide-reworked near-shore sediments rather than material supplied directly by a delta.

The argillaceous siltstones that interrupt the sandstone succession become less glauconitic and more heavily bioturbated in an upward direction. These changes imply that depositional energy and palaeo-water depth were decreasing with time. This decrease in water depth suggests the basin was progressively filling up with sediment.

The top of the interval grades upwards over the space of a few centimetres into proximal offshore sandstones. This rapid return to a shallow shelf environment appears to have been caused by a sudden reduction in sand supply; there is no evidence of either flooding or forced regression at this point. As with other lithological changes observed in Thylacine-2, this reduction in sand supply may have been tectonically controlled.

Sideritic fractures and shear fractures are interpreted to have formed very early, and many may have been syndepositional. They are thought to have formed by a combination of settling and foundering of the sediment on a steep depositional gradient, a process which may have been exacerbated by syndepositional movement along nearby faults. Cross-cutting relationships between the two fracture types suggest the sideritic fractures formed first.

Reservoir Quality

Reservoir quality is mostly poor, due to the presence of common whitish clay matrix (probably authigenic kaolinite) that fills most interstices between grains.

Wireline Log Signature

The gamma ray profile exhibits a sharp-based/sharp-topped “box-car” shape often associated with proximal sandy gravity deposits (Figure 2). A slight increase in gamma ray response is observed approximately two-thirds the way up the interval. This increase reflects the more laminated, slightly more argillaceous nature of the sandstone at this point.

Most of the interval shows only slight separation between density and neutron values, and part of the interval exhibits a small degree of neutron-density cross-over. Assuming the interval is gas-saturated, the limited neutron-density separation and cross-over are likely to be due to the abundant whitish clay matrix (probably authigenic kaolinite) that is observed in the core. Much of the water saturation detected by resistivity logs (Sw is mostly over 60%) is therefore likely to be irreducible, since dispersed clay matrix has high bound water associated with it. The sandstones in this interval are therefore likely to produce without any water-cut.

3.6.6 Interval 6 (2173.90 – 2150.00 m)

Description

This interval consists predominantly of intensely bioturbated sandy, argillaceous siltstone. A few thin, very fine grained sandstones are noted, most of which occur above 2159 m.

The contact with between the argillaceous siltstone and underlying sandstones is gradational over distance of approximately 2 cm. Bioturbation intensity and trace fossil diversity are high (Plate 28). Burrows include *Helminthopsis/Helminthoida*, *Planolites*, *Teichichnus*, *Rhizocorallium*, *Anconichnus*, occasional *Terebellina*, *Thalassinoides*, *Asterosoma*,

Chondrites, *Zoophycos* and possible *Siphonichnus*. Ichnofacies is identified as Distal *Cruziana*.

Except for a few thin, very fine grained sandstone lenses just above the base of the interval, argillaceous siltstone continues almost uninterrupted until around 2159 m. Above this depth, the siltstone becomes gradually sandier and is interrupted by a series of thin, very fine to fine grained sandstone layers (Plate 29). At the very top of the core, above 2151.6 m, lithology grades upwards into very argillaceous, bioturbated sandstone (Plate 30). Ichnofacies within this sandstone is defined as Proximal *Cruziana*, with burrows becoming larger and more robust, and including common *Palaeophycus* in addition to *Planolites*, *Anconichnus* and *Rhizocorallium*.

A number of shear fractures are observed within the siltstone. Where they can be measured, displacements along these fractures mostly measure a few centimetres or less. Rare extensional fractures are observed within sideritic nodules and lenses. Sideritic nodules and lenses are common throughout the interval.

Interpretation

The argillaceous siltstones are interpreted to represent proximal offshore deposits. For most of the interval, the persistence of these siltstones indicates a stable shelfal environment. The gradual increase in grain size towards the top of the interval marks a shift towards the offshore transition zone, and indicates the onset of a cycle of shoreline progradation.

Reservoir Quality

Reservoir quality is very poor to absent.

Wireline Log Signature

The overall gamma ray profile is relatively flat over most of the siltstone, except for serrations and low gamma spikes caused by thin sandy layers. In the upper part of the interval, gamma ray values start to decrease, and the log takes on a funnel-shaped, progradational profile that leads upwards into an

overlying sandstone bed. This sandstone is situated just above the top of the cored interval and could represent either a prograding shoreface sandstone, or delta mouth bar. This progradational signature is also shown by the bulk density log, and by the calculated Vclay and PHIT curves.

3.7 Sequence Stratigraphy

Sequence stratigraphy in Thylacine-2 is characterised by sudden changes in both lithofacies and ichnofacies, most of which are thought to reflect fluctuations in relative sea level caused by tectonic subsidence and uplift.

Since the major control behind these changes was tectonic, associated depositional surfaces (e.g. flooding surfaces, forced regression surfaces) are likely to be correlatable across at least part of the basin (Emery and Myers, 1996). Table 3 summarises the main stratigraphic points of interest and highlights potentially correlative surfaces.

3.8 Angular Bedding Contacts.

Several major bedding contacts observed in Thylacine-2 exhibit marked changes in bedding dip angle and azimuth that are thought to relate to tectonic activity. These contacts are summarised below:

Major Angular Bedding Contacts, Thylacine-2

Depth	Nature of Surface	Comments
2235.49 m	Major flooding surface.	Difference in dip angle between overlying shale and underlying sandstone unclear due to heavy bioturbation at top of sandstone. However, underlying lamination suggests difference of approximately 15^{o}.
2246.80 m	Base of possible storm sand layer.	Unclear due to breakage of core at this point, but underlying shale laminae suggest change in bedding dip of 10 to 25^{o}.
2295.58 m	Flooding surface.	Contact with underlying sandstone dips at approximately 25^{o} compared to overlying shale bedding.

3.9 Reservoir Quality

Reservoir quality is best developed in the cross-bedded sandstones of Interval 2, where reservoir quality is considered to be very good to excellent. Profile permeability values in this interval commonly exceed 1000 md, and locally reach 6000 md or even higher. Arithmetic average permeability over this interval is 1590 md, while permeability-ft is 31,790 mdft.

In the thick succession of gravity-deposited sandstones of Interval 5, reservoir quality is generally poor. Profile permeability values mostly fall within the range 3 md to 8 md, while arithmetic average permeability is approximately 4.9 md. Permeability-feet over the whole of Interval 5 is therefore 900 mdft.

Elsewhere, reservoir quality ranges mostly from very poor to poor. However, fair to very good quality is observed locally in Interval 3. The better quality beds are mostly coarser grained shoreface sandstones (e.g. at around 2286.0 m), as well as coarse grained to granule grade transgressive lags (e.g. at 2281.0, 2263.4 m and 2237.3 m). Unfortunately, most of these beds are thin, mostly measuring less than 20 cm in thickness.

4 REFERENCES

Emery, D. and Myers, K.J., 1996, Sequence Stratigraphy, Blackwell Science, 297p.

Johnson, H.D., and Baldwin, C.T., 1996, Shallow clastic seas, *in* Reading, H.G. (ed.), Sedimentary Environments: Processes, Facies and Stratigraphy, Blackwell Science, p. 232-280.

Orton, G.J., and Reading, H.G., 1993, Variability of deltaic processes in terms of sediment supply, with particular emphasis on grain size, Sedimentology 40, p. 475-512.

Pemberton, S.G., and Frey, R.W., 1985, The *Glossifungites* ichnofacies: modern examples from the Georgia coast, USA, *in* Curran, H.A. (ed.), Biogenic Structures, Their Use in Interpreting Depositional Environments, SEPM Special Publication No. 35, p. 237-259

Pemberton, S.G., Van Wagoner, J.C., and Wach, G.D., 1992, Ichnofacies of a wave-dominated shoreline, *in* Pemberton, S.G. (ed.), Applications of Ichnology to Petroleum Exploration, SEPM Core Workshop No. 17.

Stow, D.A.V., Reading, H.G., Collinson, J.D., 1996, Deep seas, *in* Reading, H.G. (ed.), Sedimentary Environments: Processes, Facies and Stratigraphy, Blackwell Science, p. 395-453.

TABLE 1
DEPOSITIONAL LITHOFACIES DESCRIPTIONS

FACIES	DESCRIPTION	THICKNESS	DEPOSITIONAL ENVIRONMENT	RESERVOIR POTENTIAL
Sm	Massive, upper fine to lower medium, moderately well to well sorted sandstone. Occasional dewatering structures, scattered clay clasts, sideritic clasts, rare, faint inclined to horizontal lamination. Clay clasts often observed towards the tops of sandstone beds. Very common whitish clay matrix. Commonly cross-cut by sideritic fractures. Usually unbioturbated, rare localised *Palaeophycus*, *Asterosoma*, *Planolites* and *Skolithos* of doomed pioneer assemblages.	Individual units up to approx. 10 m.	Liquefied gravity flows formed in proximal sand-rich ramp or slope apron. Rapidly deposited.	Usually poor due to common clay matrix.
Sfl	Very fine grained, well sorted sandstone with faint, rhythmic horizontal lamination. In a few cases appears to exhibit possible swaly cross-strat. Locally siderite-cemented. Weakly to intermittently bioturbated. Opportunistic burrow assemblage.	Individual units mostly less than 30 cm.	Thin storm layers in proximal offshore to offshore transition successions	Poor to very poor due to common clay matrix, very fine grain size and localised siderite cement.
Sm/Sfl	Very fine to fine grained, well sorted sandstone with faint, often rhythmic horizontal to low-angle inclined lamination. Locally common layers of small clay rip-up clasts. Unbioturbated to weakly bioturbated. Doomed pioneer burrow assemblage.	Individual units mostly less than 40 cm.	Deceleration traction deposits in gravity-deposited beds.	Poor due to common clay matrix.
Sl	Distinctly laminated, fine grained, moderately well to well sorted sandstone. Lamination generally occurs in the form of thin, often carbonaceous clay layers. Lamination may be uneven. Occasionally bioturbated. *Planolites* commonly associated with clay layers. Common whitish clay matrix. Minor facies.	Usually less than 30 cm.	Deceleration deposits towards the tops of liquefied gravity flows. Also found as shallow shelf storm-reworked layers.	Poor. Common clay matrix.
Sx	Medium to coarse grained, moderately sorted sandstone with low angle planar cross-beds consisting of thin graded sand layers. Common reactivation surfaces, thin, uneven carbonaceous laminae, localised trough cross-bedding, occasional herringbone structure, incipient stylolites, concentrations of carbonaceous debris. Unbioturbated.	4.3 m succession of stacked units between 0.2 and 1 m each.	Tidally reworked deltaic channel, possibly formed in estuarine delta mouth environment.	Variable very good to excellent. Very high permeabilities occur within coarser grained, graded laminae.
Sd	Upper fine grained, moderately well to well sorted sandstone with prominent clay drapes. Faint cross-bedding. Moderately bioturbated, Restricted *Cruziana* to Distal *Skolithos* ichnofacies. Minor facies gradational with sandy Hl facies.	Approx. 30 cm.	Possible tidal flat or tidal inlet.	Poor to fair.

TABLE 1 (Continued)
DEPOSITIONAL LITHOFACIES DESCRIPTIONS

FACIES	DESCRIPTION	THICKNESS	DEPOSITIONAL ENVIRONMENT	RESERVOIR POTENTIAL
Srl	Ripple-laminated, fine grained, well sorted sandstone. Common thin, drape-like clay laminae, current ripples (often showing bimodal current directions), occasional horizontal lamination, possible trough cross-bedding, sideritic rip-up clasts. Lightly bioturbated to unbioturbated.	Less than 1 m.	Tidally reworked estuarine bar and/or tidal flat/inlet. In turbidite sequence represents decelerating traction deposit.	Variable, poor to good.
Sb	Intensely bioturbated, fine to medium grained, moderately to moderately well sorted sandstone. Most primary sedimentary structures destroyed by burrowing. Burrows mostly robust dwelling structures, such as *Palaeophycus* and *Ophiomorpha*. Distal *Skolithos* to Proximal *Cruziana* ichnofabric.	Usually less than 50 cm, but locally exceeds 2 m.	Thicker successions interpreted to represent lower to middle shoreface. Thinner Sb may represent bioturbated storm sands.	Poor to locally fair. Common dispersed detrital clay matrix.
Sba	Intensely bioturbated, argillaceous, fine to medium grained, moderately to moderately well sorted sandstone. Primary sedimentary structures destroyed by burrowing. Usually shows diverse trace fossil assemblage of Proximal *Cruziana* ichnofacies, including *Planolites*, *Teichichnus*, *Palaeophycus*, *Asterosoma*, *Anconichnus*, *Thalassinoides*, occasional *Ophiomorpha*, *Chondrites*, *Helminthopsis/Helminthoida*. Locally exhibits *Teichichnus*/*Planolites*-dominated *Cruziana* ichnofacies at around 2289 m.	Forms successions of up to 2 m.	Offshore transition zone to lower shoreface.	Very poor to poor due to abundant detrital clay matrix.
Sbgr	Intensely bioturbated, very argillaceous, fine to medium grained, moderately to moderately well sorted sandstone with very common quartzose granules and small pebbles. Intensely bioturbated. Usually exhibits Proximal *Cruziana* ichnofabric.	Less than 50 cm.	Usually associated with offshore transition zone. Interpreted to indicate periods of transgressive reworking.	Very poor to poor.
Sgran & Gcs	Very coarse grained, granule-rich, poorly to moderately sorted sandstone (Sgran) locally grading into clast-supported, granule-grade to lower pebble-sized conglomerate. Normally graded, massive. Little or no evidence of bioturbation. Often seen near the tops of coarsening-upward sandstone successions.	Less than 20 cm.	Transgressive lags and/or storm sand sheets. Probably related to transgressive reworking.	Good to very good. Large grain size has resulted in large, open intergranular pores.

TABLE 1 (Continued)
DEPOSITIONAL LITHOFACIES DESCRIPTIONS

FACIES	DESCRIPTION	THICKNESS	DEPOSITIONAL ENVIRONMENT	RESERVOIR POTENTIAL
Sarg	Very fine to fine grained, very argillaceous sandstone with common platy clay rip-up clasts "floating" within it. Non-bioturbated. Rare facies found towards the top of the glauconitic claystone succession (at 2230.4 m).	10 cm.	Turbidite-associated gravity deposit. Possibly some form of thin debris flow.	None.
Spbl & Gms	Massive, fine to medium grained sandstone with common claystone and siderite pebbles (Spbl), grading towards matrix-supported conglomerate (Gms). Sandstone between pebbles is moderately well sorted with very common white clay matrix. Non bioturbated.	Forms succession of approx. 3 m	Gravity flow. Liquidised flow to debris flow.	Poor to fair. Quality reduced by white clay matrix.
Hl	Laminated, heterolithically interbedded argillaceous siltstone and very fine to fine grained sandstone. Clay laminae are generally wavy and drape like. Common ripples, many showing current lamination. Occasional alternating current directions. Intermittently bioturbated, dominated by *Planolites* burrows of Restricted *Cruziana* ichnofacies.	Individual sand lenses around 1 cm, successions up to 70 cm.	Tidal flats or shallow, subtidal bay muds/sands.	Poor.
Hb	Heavily bioturbated heterolithics. *Planolites*, *Teichichnus* and *Palaeophycus* of Restricted *Cruziana* ichnofacies. Rare ichnofacies associated with facies Hl.	20 cm.	Tidal flats or shallow subtidal bay muds.	Very poor.
Ml	Laminated, argillaceous siltstone. Thin silty to sandy laminae, very sparse bioturbation, mainly isolated *Planolites* burrows. Restricted *Cruziana* ichnofacies.	10 cm.	Tidal mud flat or tidally influenced bay muds.	None.
Mb	Intensely bioturbated, argillaceous siltstone. Primary depositional fabric destroyed by bioturbation. Burrows usually diverse, including *Planolites*, *Helminthopsis/Helminthoida*, *Teichichnus*, *Thalassinoides*, *Rhizocorallium*, *Anconichnus*, *Zoophycos* of Distal to Proximal *Cruziana* ichnofacies. Locally dominated by *Teichichnus* and *Planolites* burrows. Often interrupted by facies Sfl, Sba and Sbgr. Contains common sideritic nodules and layers.	Commonly up to 2 m.	Proximal offshore to offshore transition. Open marine, although *Teichichnus*/*Planolites*-dominated zones may have suffered some environmental restriction (embayment?).	None.

TABLE 1 (Continued)

DEPOSITIONAL LITHOFACIES DESCRIPTIONS

FACIES	DESCRIPTION	THICKNESS	DEPOSITIONAL ENVIRONMENT	RESERVOIR POTENTIAL
Mb/Ml	Transitional facies between Mb and Ml. Intermittently bioturbated, alternating between sparsely bioturbated and heavily bioturbated. Commonly observed below 2302 m. Moderately diverse trace fossil assemblage similar to facies Mb.	Up to 2.5 m.	Possibly embayed proximal offshore to offshore transition zone.	None.
Mb/Mm	Very faintly but intensely bioturbated argillaceous siltstone. General lack of contrast between burrow fill and host matrix gives apparently massive appearance. Burrow types difficult to identify but appear to be moderately diverse, including *Helminthopsis/Helminthoida*, *Planolites*, *Teichichnus*, *Anconichnus*,	Up to 1 m.	Very low energy, proximal offshore. Possibly embayed.	None.
Mmgl	Glauconitic, massive to bioturbated, silty claystone. Bioturbation is faint due to lack of contrast between burrow fill and host matrix. Glauconite is very common, filling burrows (mainly *Planolites* and possible *Thalassinoides* burrows) and frequently concentrated into thin, discontinuous laminae. Located between 2231.0 m and 2235.5 m. Punctuated by thin, ripple-laminated and argillaceous sandstone beds.	4.5 m succession.	Extremely low energy, distal offshore muds.	None.

TABLE 2
ICHNOFACIES DESCRIPTIONS

ICHNOFACIES	DESCRIPTION	DEPOSITIONAL ENVIRONMENT
Skolithos & Distal *Skolithos*	Moderate bioturbation intensity with low to moderate burrow diversity, found mostly in bioturbated to faintly laminated sandstone. Burrows include mixture of dwelling and feeding structures: *Palaeophycus*, *Ophiomorpha*, *Anconichnus*, occasional *Thalassinoides*, *Teichichnus*, *Asterosoma*, *Skolithos*, possible *Chondrites*.	Shallow marine, middle to upper shoreface.
Proximal *Cruziana*	Intensely bioturbated with diverse trace fossil assemblage. Occurs in argillaceous siltstone and argillaceous sandstone. Mainly grazing traces with common dwelling traces. Grades into Distal *Skolithos* ichnofacies. Burrow types include *Planolites*, *Palaeophycus*, *Teichichnus*, *Anconichnus*, *Thalassinoides*, *Asterosoma*, *Helminthopsis/Helminthoida*, *Terebellina*, occasional *Rhizocorallium*, *Ophiomorpha*, *Chondrites*, possible *Diplocraterion* and *Zoophycos*. Many dwelling burrows occur within thin storm-reworked sandstones indicating they were formed by opportunistic burrowers.	Relatively open marine, offshore transition zone to lower shoreface.
Distal *Cruziana*	Faint but moderately intense to intense bioturbation. Occurs in argillaceous siltstone. Moderately diverse trace fossil assemblage, with common *Planolites*, *Helminthopsis/Helminthoida*, *Anconichnus*, *Teichichnus*, *Terebellina*, *Chondrites*, *Rhizocorallium*, *Zoophycos*, occasional *Asterosoma*. Lower incidence of dwelling burrows than Proximal *Cruziana* ichnofacies.	Proximal offshore to offshore transition zone.
Glossifungites	Moderate to high bioturbation intensity, characterised by robust, well preserved *Thalassinoides* burrows. Observed within argillaceous siltstone, usually beneath contact with overlying sandstone. Burrows are filled with sandstone passively infilled from overlying sandstone.	Proximal offshore to offshore transition zone. *Thalassinoides* burrows are believed to have formed within a “firmground” that was exhumed by transgressive reworking. The upper contact of this ichnofacies usually represents a transgressive surface of erosion.
Teichichnus-dominated *Cruziana*	Intensely bioturbated ichnofacies with reduced trace fossil diversity. Main traces are *Teichichnus* and *Planolites*, although *Helminthopsis/Helminthoida*, *Zoophycos*, *Rhizocorallium*, *Terebellina*, *Chondrites* and *Asterosoma* also observed. Mainly occurs within bioturbated, argillaceous siltstone and sandstone below 2286 m.	Proximal offshore to offshore transition zone with a degree of environmental restriction, possibly due to embayment. However, the persistence of other burrow types that occur in more normal *Cruziana* ichnofacies suggests at least some circulation of marine waters was maintained.

TABLE 2 (Continued)
ICHNOFACIES DESCRIPTIONS

ICHNOFACIES	DESCRIPTION	DEPOSITIONAL ENVIRONMENT
Restricted *Cruziana*	Sparsely to intermittently bioturbated ichnofacies. Mainly found within laminated heterolithics. Trace fossils assemblage is limited, mainly consisting of *Planolites* with occasional *Teichichnus*, *Helminthopsis/Helminthoida*, minor *Zoophycos*, *Rhizocorallium*, *Asterosoma*, *Palaeophycus*, *Ophiomorpha*.	Tidal flats/tidally influenced estuarine deposition. Intermittent bioturbation intensity and reduced diversity, may indicate fluctuating salinity levels, consistent with tidal deposition in an estuarine/deltaic setting.
Doomed Pioneers	Occasional, usually weak bioturbation at tops of gravity-deposited sandstone beds. Trace fossils may include *Palaeophycus*, *Skolithos*, possible *Asterosoma* and *Rhizocorallium*.	Proximal sand-rich ramp or slope apron. Burrows were formed by opportunistic organisms carried downslope by gravity flows, but were quickly wiped out by subsequent sandstone deposition, or by return of resident background assemblage of burrowers.
Zoophycos/ *Nereites*	Faint, low to high intensity bioturbation, associated with massive, glauconitic claystone. Low trace fossil diversity, mainly *Planolites* with occasional weak *Teichichnus*, *Zoophycos*, *Thalassinoides*, possible *Chondrites*.	Low energy, distal offshore muds.

TABLE 3

MAIN SEQUENCE STRATIGRAPHIC FEATURES

Interval	Nature of Contact	Depth (m)	Description
	Top of Core	2150.0	
6			Proximal offshore to offshore transition muds on stable shelf. Upper part of interval exhibits onset of shoreline progradation.
_____	Non-erosive, gradational.	2173.90	Unknown, but possibly regressive. Sudden return to proximal offshore conditions may have been caused by infilling of available accommodation space, or reduction in sand supply due to reduced fault activity, or both.
5			Sandstone: stacked gravity deposits, possibly liquefied flows of a proximal sand-rich submarine ramp environment.
_____	Erosive, sharp.	2230.90	Unknown. Deposition of overlying gravity deposits possibly caused by movement of nearby faults and destabilisation of adjacent shelf sediments.
4			Massive, glauconitic claystones of stable, distal offshore marine environment.
_____	Non-erosive, sharp.	2235.49	Major flooding surface. Possibly caused by marked tectonic subsidence.
3			Proximal offshore muds to middle shoreface sands. Repeated coarsening/cleaning-up cycles analogous of marine parasequences, capped by minor flooding surfaces. Possible environmental restriction. Coarse, transgressive lags at top of interval are precursors to major flooding event.
_____	Possibly erosive.	2295.58	Marine flooding surface.
2			Tidal sand flats overlain by fluvially-dominated, cross-bedded deltaic channel sands.
_____	Erosive, sharp.	2301.65	Forced regression surface.
1			Proximal offshore muds to lower shoreface sands. Possibly embayed. Evidence of transgressive reworking.
	Base of Core	2314.55	

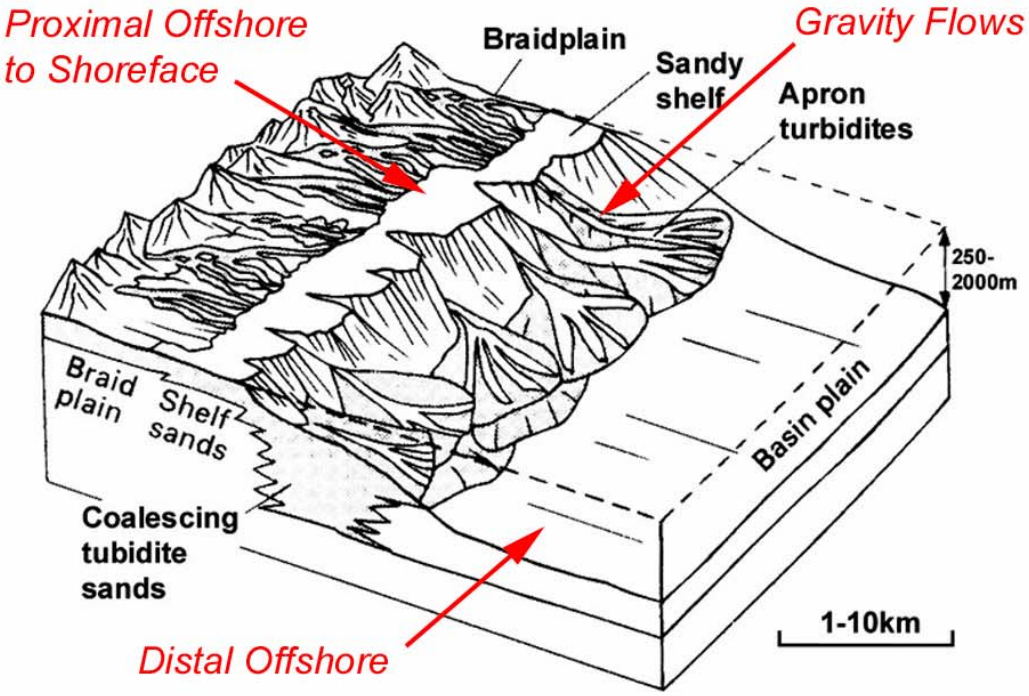


Figure 10.69 Depositional model for sand-rich slope apron (from Reading & Richards, 1994).

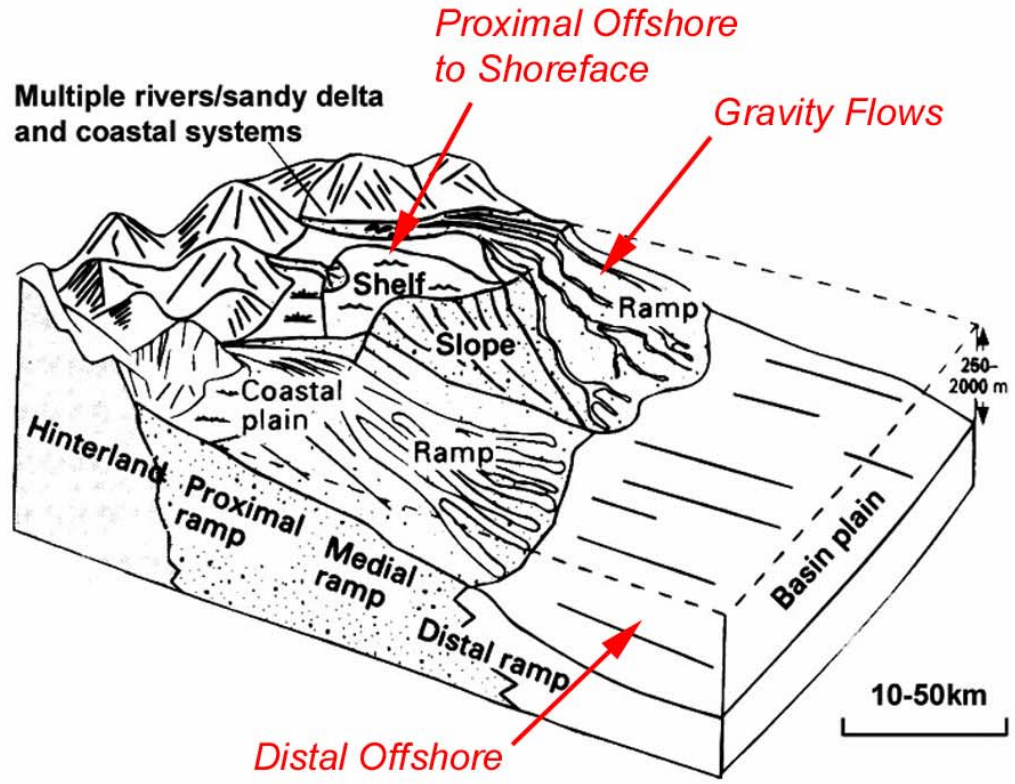


Figure 10.59 Depositional model for sand-rich ramp (from Reading & Richards, 1994).

Figure 1: Examples of sand-rich ramp and slope-apron settings. In the case of a graben or half-graben, a narrow seaway or gulf can form, resulting in restricted marine conditions. Reproduced from Stow et al, 1996. Annotations in red italics indicate approximate positions of depositional environments encountered in Thylacine-2.

Thylacine-2 Wireline Log Display

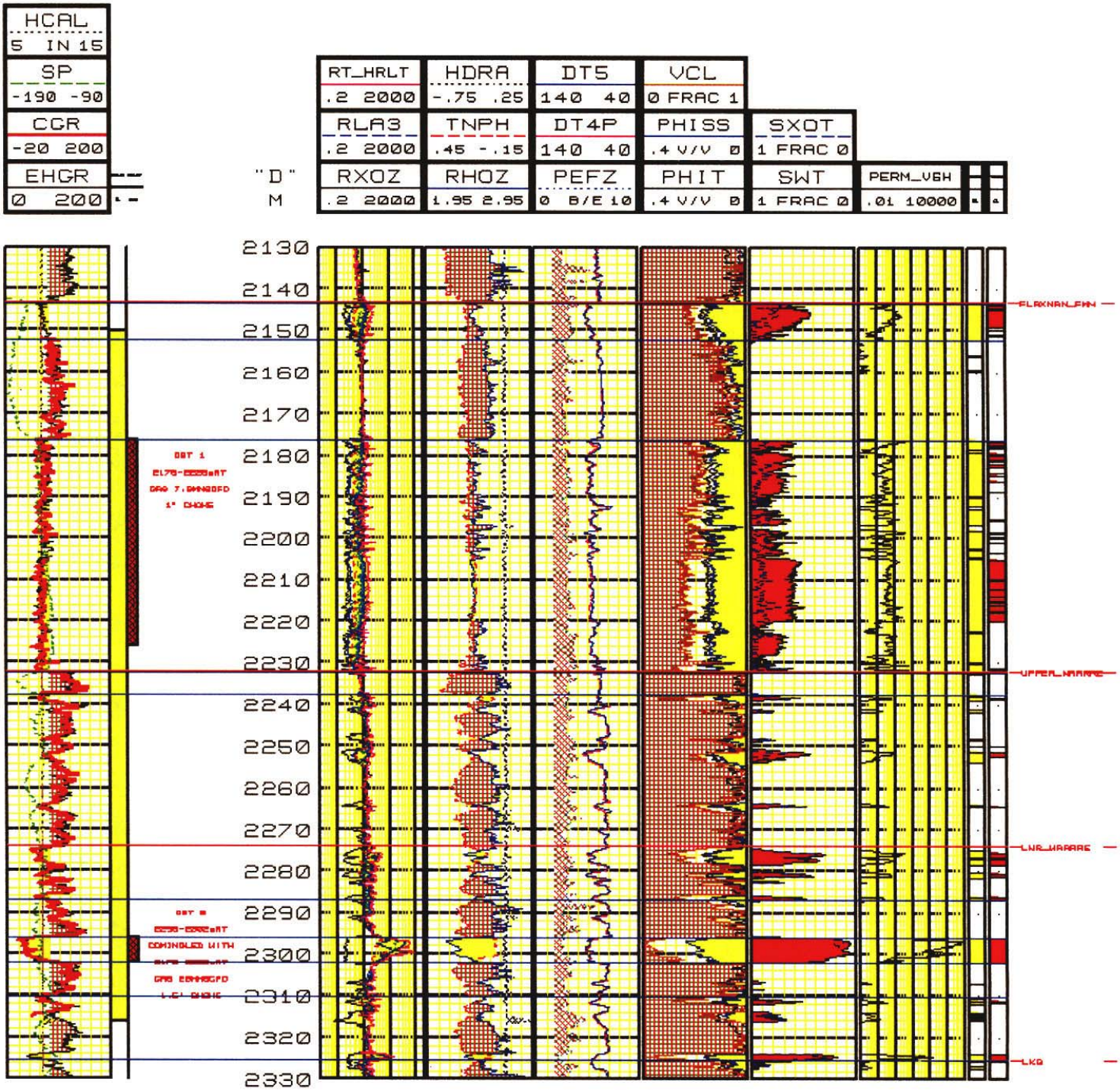


Figure 2: Wireline log display. Note that CGR is core gamma ray. All other curves are from downhole logs. Display courtesy of Woodside Energy Ltd.

SELECTED CORE PHOTOGRAPHS AND DESCRIPTIONS

PLATE 1

2310.25 – 2310.50 m

Facies Sb Grading Upwards Into Facies Sba

Less argillaceous, heavily bioturbated sandstone (facies Sb) is shown in this view grading upwards into more argillaceous, heavily bioturbated sandstone (facies Sba). This transition is thought to be mildly transgressive, marking a shift from a lower shoreface to an offshore transition environment. Although primary bedding lamination has been virtually destroyed by burrowing, parts of a few silty clay laminae (CL) have survived. Burrows include *Thalassinoides* (Th) and *Planolites* (Pl). Note also "floating" quartz granules (QG), which often accompany transgressive events. Distal *Skolithos* to Proximal *Cruziana* ichnofacies.

PLATE 2

2308.75 – 2309.00 m

Facies Sba

Silty, argillaceous, intensely bioturbated sandstone is shown in this view. Burrows include thickly-lined *Palaeophycus* (Pa), *Teichichnus* (Te), Pyritised, kaolinite-filled *Ophiomorpha* or *Thalassinoides* (Oph), possible *Zoophycos* (Z) and *Helminthopsis/Helminthoida* (H). It is thought that the dark coloured carbonaceous material may represent the remains of a body fossil (Carb). Proximal *Cruziana* ichnofacies. Note also the siderite nodule (Sid).

PLATE 3

2303.00 – 2303.25 m

Facies Mb/Ml

Moderately bioturbated, argillaceous siltstone. Some primary bedding lamination has been preserved, in the form of thinly laminated, very fine grained sandstone lenses (VfS). Bioturbation is intermittent, consisting mainly of *Planolites* (Pl), *Teichichnus* (Te), *Palaeophycus* (Pa) and undifferentiated burrows. Ichnofacies is considered to be Restricted *Cruziana*.

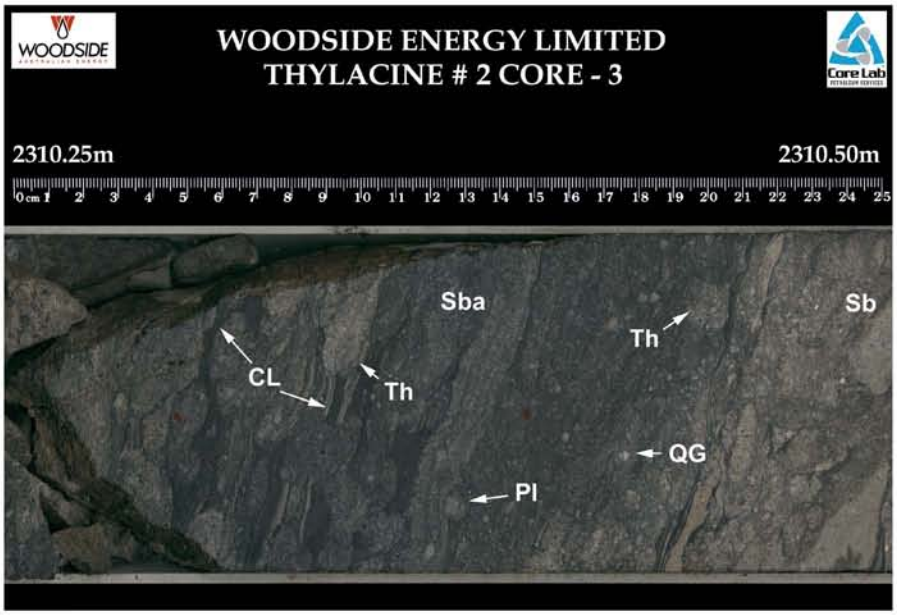


PLATE 1

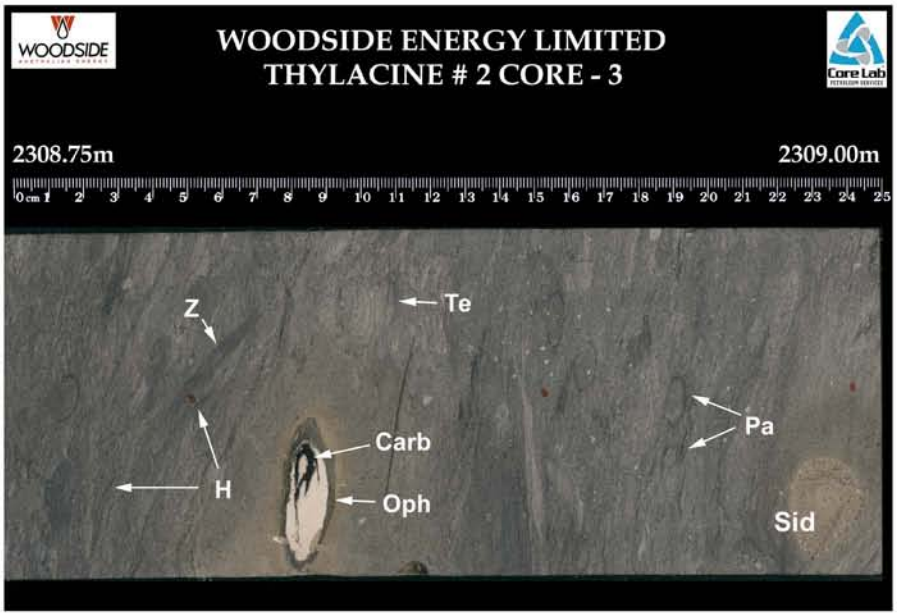


PLATE 2

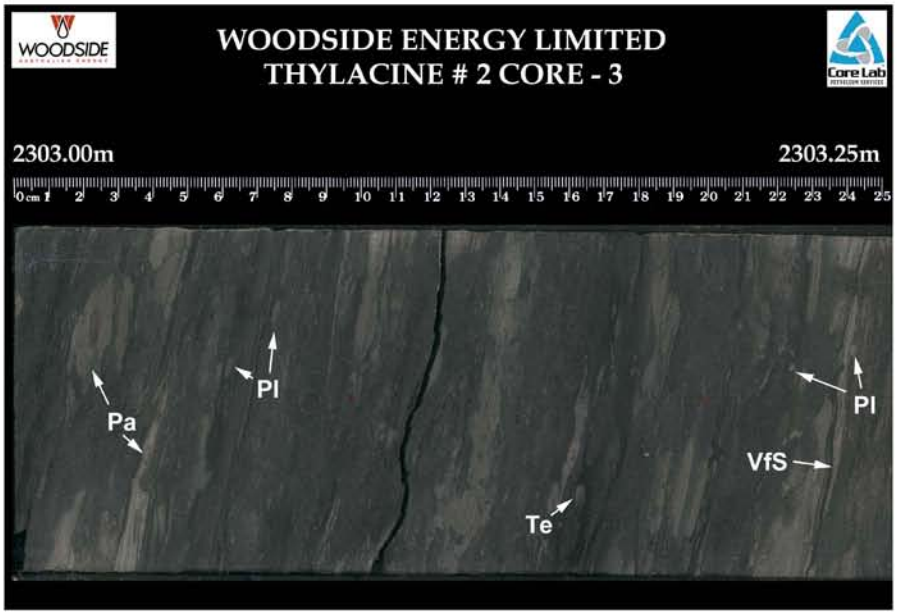


PLATE 3

PLATE 4

2301.75 – 2302.00 m

Facies Mb Overlain By Facies Ml

Intensely bioturbated argillaceous siltstone (Mb) is shown in this view overlain by sparsely bioturbated, laminated, argillaceous siltstone (Ml). The top of the bioturbated siltstone has been sideritised (Sid), and contains what appear to be mud-filled *Thalassinoides* burrows (Th; the mud fill has been sideritised along with the surrounding siltstone). Also note the very sharp contact between bioturbated and non-bioturbated siltstone. These features indicate that the sideritic layer may have formed as either a hardground, or a "firmground", and was excavated by shelfal currents prior to deposition of the laminated siltstone. Burrows within the underlying, bioturbated siltstone are indistinct, but include *Planolites* (Pl), possible *Teichichnus* (Te) and undifferentiated subhorizontal grazing traces. Note the extensional fractures in the sideritic layer (EF). These fractures probably formed in response to overburden stress during burial.

PLATE 5

2301.50 – 2301.75 m

Facies Ml Overlain By Facies Sx

An upward continuation from Plate 4 above, showing laminated, argillaceous siltstone (Ml) overlain by medium to very coarse grained, cross-bedded sandstone (Sx). The base of the sandstone is marked by a lag containing quartzose granules (QG) and a large, sideritic pebble (SP). Bioturbation is sparse in the underlying siltstone (note occasional isolated *Planolites* burrows, Pl, of a Restricted *Cruziana* ichnofacies) and is absent in the overlying sandstone.

PLATE 6

2300.75 – 2301.00 m

Facies Srl

Upper fine grained, well sorted, ripple-laminated sandstone interpreted to have been deposited as part of a bar or shoal deposited in a tidally reworked estuary or delta mouth. Note two directions of current ripples (BdR) and partially stylolitised carbonaceous laminae (Carb). Visible porosity in this facies is good to very good. Note the absence of bioturbation, possibly due to a combination of fluvial influence and rapid deposition.

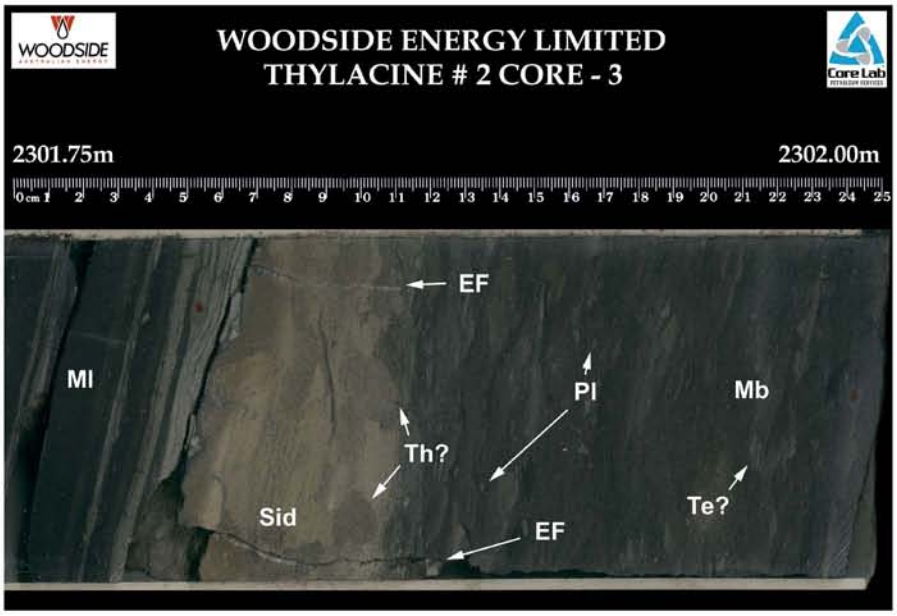


PLATE 4

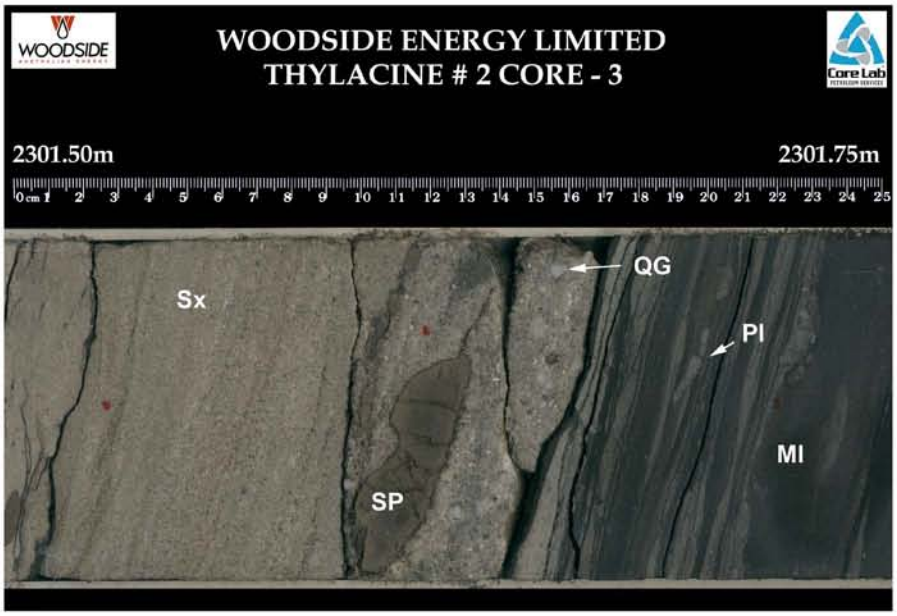


PLATE 5

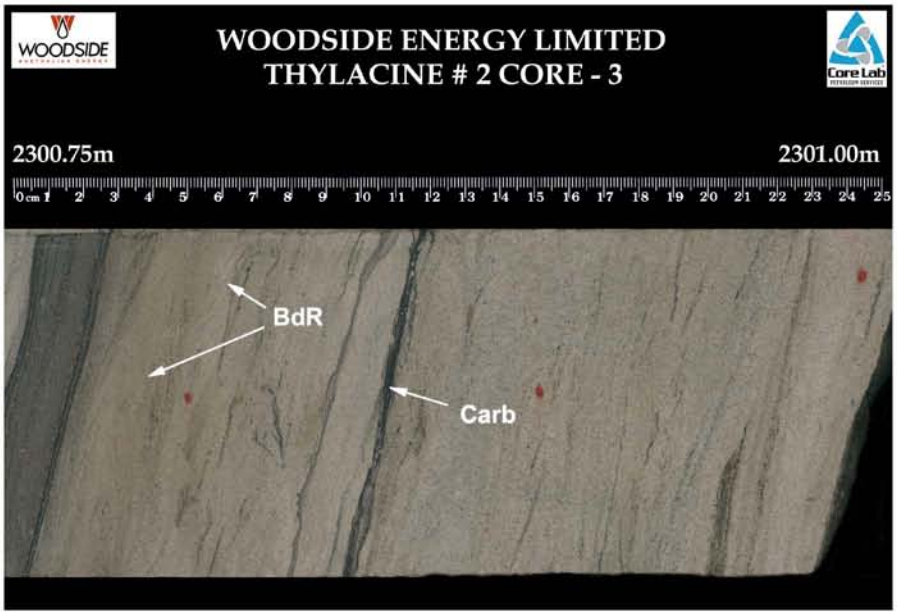


PLATE 6

PLATE 7

2297.00 – 2297.25 m

Facies Sx

Lower medium to lower coarse grained, cross-bedded sandstone. Cross-bedding laminae are very distinct, consisting of alternating coarser grained and finer grained layers. Visible porosity is excellent in the coarser grained laminae (CG). Occasional diffuse carbonaceous laminae are observed (Carb) some of which show signs of incipient stylolitisation. Note the 20 degree angle across the reactivation surface (RS) indicative of intermittent episodes of scouring and deposition within a fluvially-dominated, possibly tidally-influenced channel.

PLATE 8

2295.50 – 2295.75 m

Facies Sb Overlain By Facies Sbgr

Medium to coarse grained, poorly to moderately sorted, bioturbated sandstone (Sb) marks the top of the deltaic channel succession, and is overlain by very argillaceous, granule-bearing sandstone (Sbgr). The contact between these facies represents an important flooding surface (FS) . Burrows include robust *Ophiomorpha* (Oph), which are interpreted to have been excavated down into underlying sandstone from above. These burrows probably formed shortly after the initial flooding of the channel succession. Note the large quartzose granules (QG) “floating” within surrounding sandstone. These granules are thought to be the remnants of thin, coarse grained lag deposits that have been mostly removed by successive transgressive reworking. *Thalassinoides* burrows are visible in the overlying Sbgr facies (TH). Ichnofacies changes from *Skolithos* in the underlying sandstone to Proximal *Cruziana* above the flooding surface

PLATE 9

2290.00 – 2290.25 m

Facies Mm/Mb

Massive to faintly bioturbated, argillaceous siltstone. Bioturbation intensity is moderate to high, while trace fossil diversity is low to moderate. Burrow types are difficult to identify due to a lack of differentiation between burrow fill and host matrix. Recognisable burrow types include *Helminthopsis/Helminthoida* (H), weak *Teichichnus* (Te), occasional *Chondrites* (Ch) and *Terebellina* (Tb). Ichnofacies can be classified as Distal *Cruziana* to Proximal *Zoophycos*. Depositional environment is interpreted to have been proximal offshore.

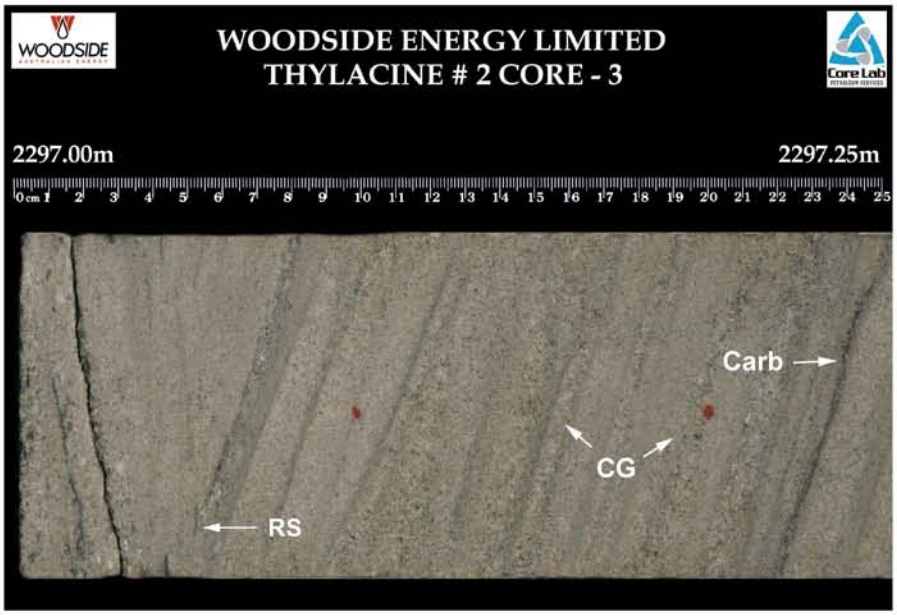


PLATE 7

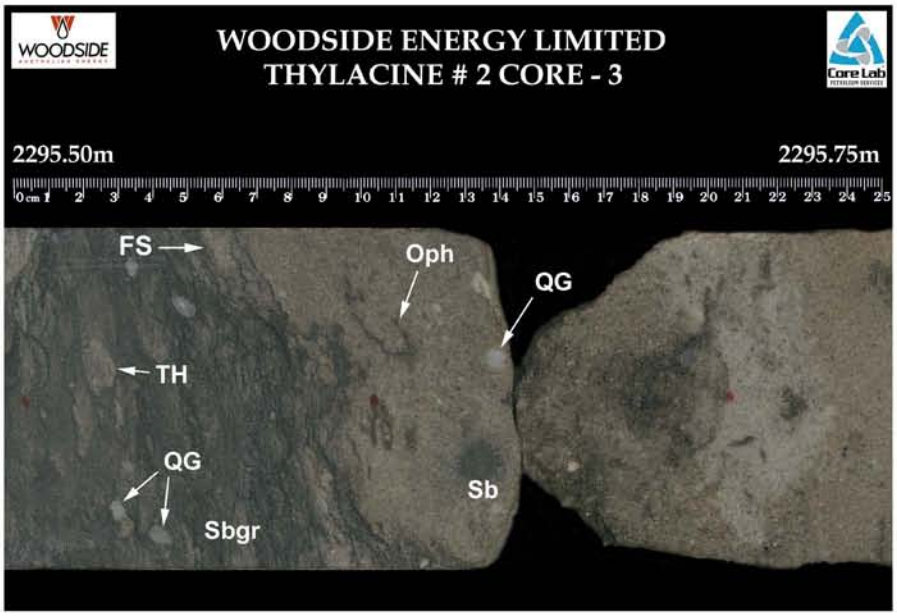


PLATE 8

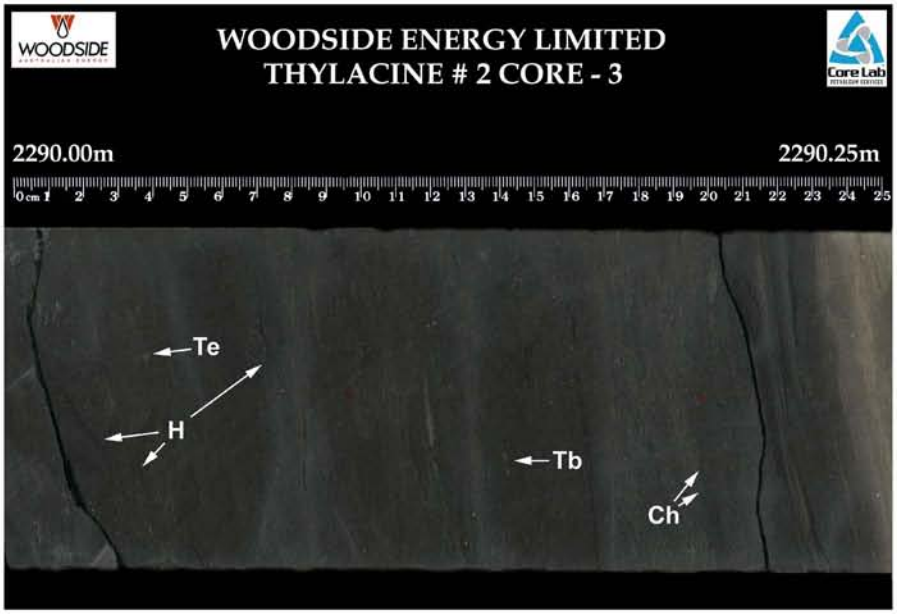


PLATE 9

PLATE 10

2289.75 – 2290.00 m

Facies Mm/Mb

Massive to faintly bioturbated, argillaceous siltstone. This view shows an upward continuation of the lithology shown in Plate 9. Visible burrows mainly consist of *Helminthopsis/Helminthoida* (H) and possible *Zoophycos* (Z). Distal *Cruziana* to Proximal *Zoophycos* ichnofacies. Proximal offshore setting, possibly slightly restricted by embayment.

PLATE 11

2281.00 – 2281.25 m

Facies Sbgr With *Glossifungites* Ichnofabric

Quartzose granules and small pebbles (QG) within this bioturbated, argillaceous, granule-bearing but otherwise fine to medium grained sandstone (Sbgr) are mainly concentrated within *Thalassinoides* burrows (Th), providing the sediment with a *Glossifungites* ichnofabric. These burrows are interpreted to have formed as dwelling burrows within a moderately firm substrate, and were later passively infilled with coarse grained sediment from above. Underlying facies is argillaceous bioturbated sandstone (Sba).

PLATE 12

2280.75 – 2281.00 m

Facies Gcs Overlain By Facies Sba

A thin layer of clast-supported conglomerate (Gcs), consisting of granule to lower pebble-sized quartzose grains is shown in this view. This layer is thought to represent a thin transgressive lag deposit. The sharp base of the deposit is interpreted to represent a transgressive surface of erosion (TSE). The view continues downwards into the area shown by Plate 11 (see above); quartzose granules that passively filled *Thalassinoides* burrows below the TSE were probably introduced from this conglomerate layer. Several sand-filled *Thalassinoides* (Th) can also be seen in the overlying bioturbated sandstone. The persistence of quartz granules (QG) above the conglomerate layer suggests continued, intermittent transgressive reworking.

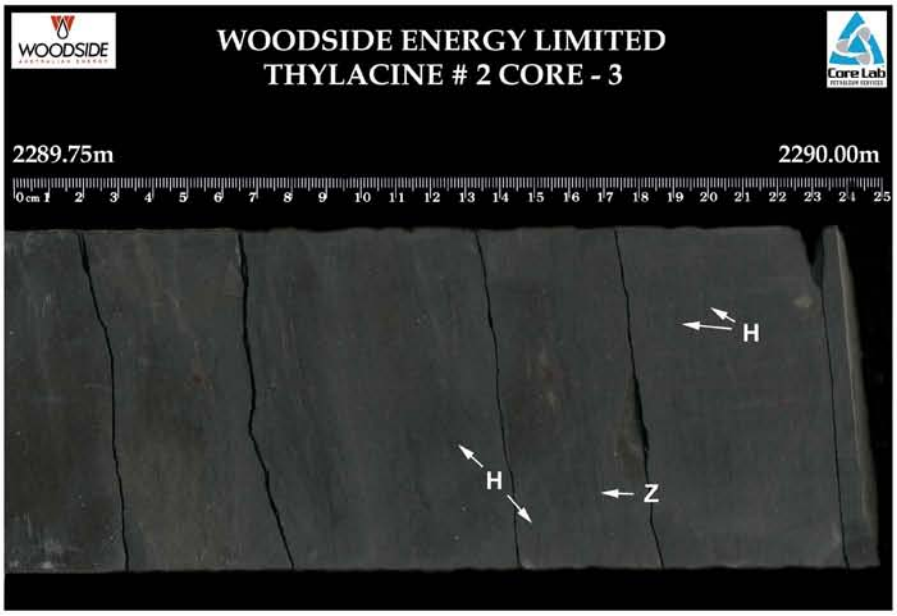


PLATE 10

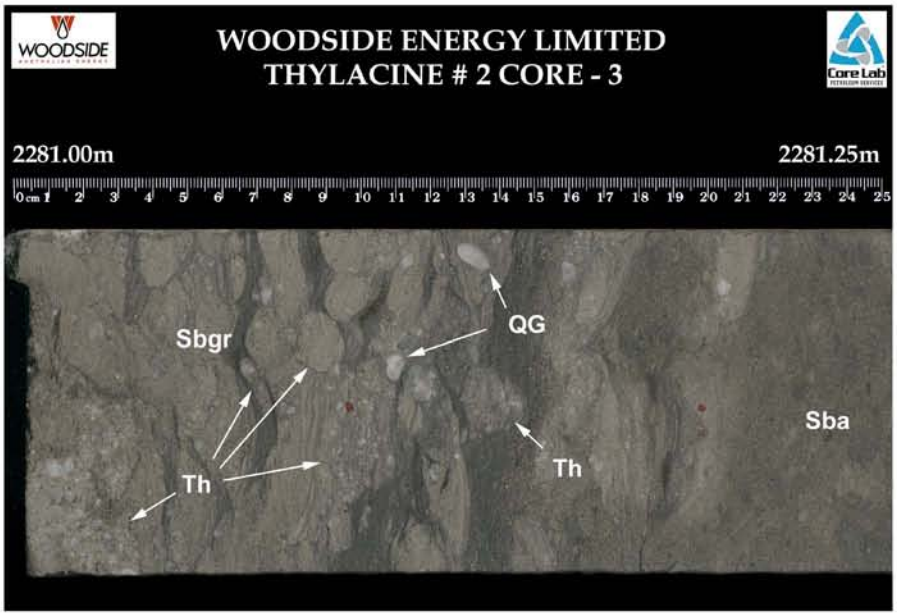


PLATE 11

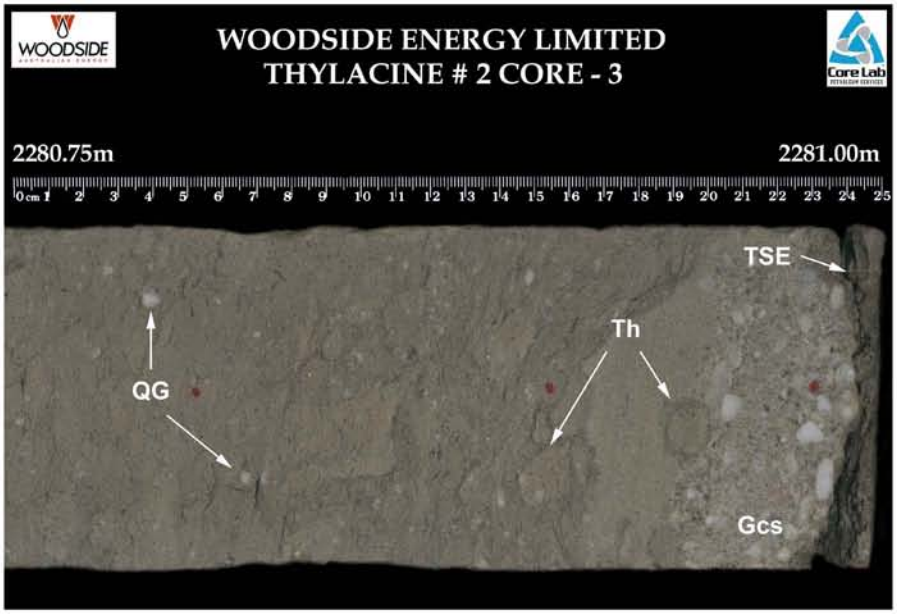


PLATE 12

PLATE 13

2265.00 – 2265.25 m

Facies Sfl

Finely laminated, very fine grained, well sorted sandstone interrupted by a dark grey, bioturbated argillaceous siltstone bed (Mb). Lamination within the sandstone is rhythmic and horizontal, and relatively free of bioturbation (except for a single, possible *Palaeophycus* burrow; Pa). Bioturbation within the siltstone layer is much heavier, and consists of a combination of *Planolites* (Pl), *Teichichnus* (Te) and *Rhizocorallium* (Rh). Most beds of finely laminated sandstone are interpreted to represent storm events, formed in a lower shoreface to offshore transition setting. In this particular case the bioturbated, argillaceous siltstone layer is thought to signify a temporary period of fair-weather conditions.

PLATE 14

2250.75 – 2251.00 m

Facies Sb

Fine grained, intensely bioturbated sandstone of an interpreted middle shoreface environment, possibly part of a prograding shoreface succession. Ichnofacies is classified as Distal *Skolithos* and includes burrow types such as common *Anconichnus* (An), possible *Chondrites* (Ch; looking superficially a bit like small rootlets), *Planolites* (Pl), *Palaeophycus* (Pa) and faint, possible *Macaronichnus* (Ma). *Ophiomorpha* are also encountered, but are not shown in this view. The dark clay making up much of the burrow fill appears to be carbonaceous.

PLATE 15

2248.25 – 2248.50 m

Facies Hl

Heterolithically interbedded very fine to fine grained sandstone and argillaceous siltstone. Argillaceous siltstone laminae are mostly drape-like (CD) while sandstone layers commonly consist of current-formed (CR) or oscillatory ripples (OR). Bioturbation is sparse, mostly consisting of a restricted *Cruziana* ichnofabric, with *Planolites* (Pl) burrows occurring within argillaceous drapes, while occasional *Palaeophycus* (Pa), *Rhizocorallium* (Rh) and possible *Ophiomorpha* (Oph) are observed in the sandstone. Depositional environment is interpreted to have been shallow subtidal to intertidal flats.

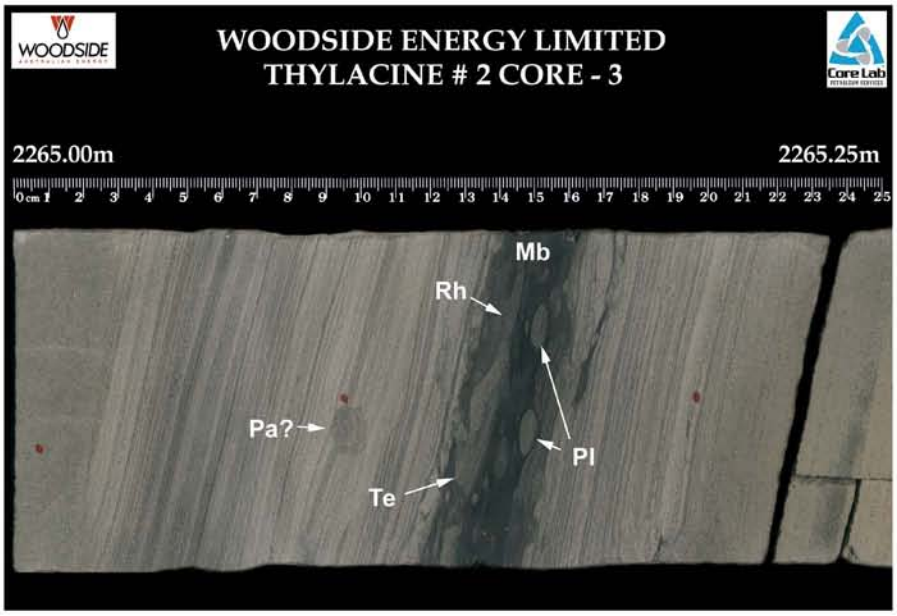


PLATE 13

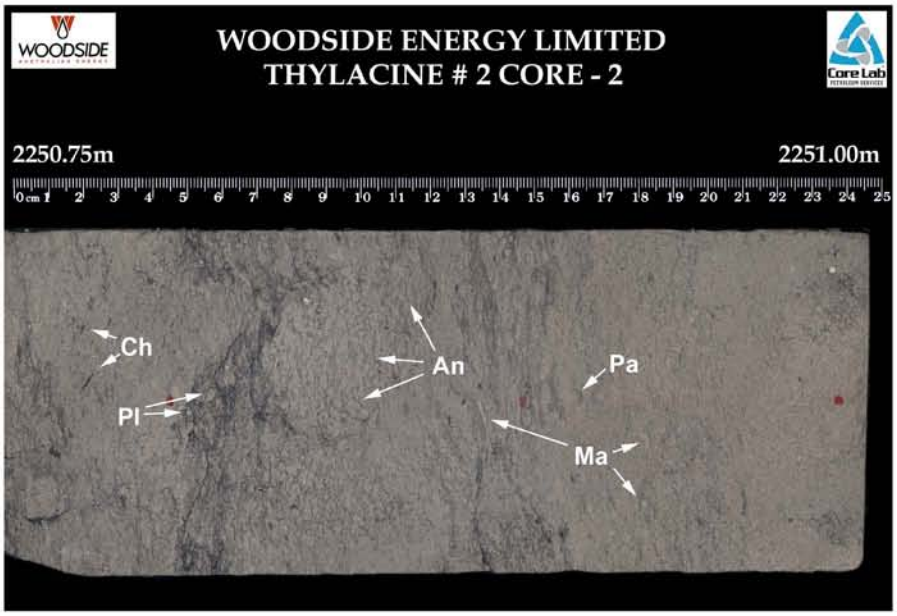


PLATE 14

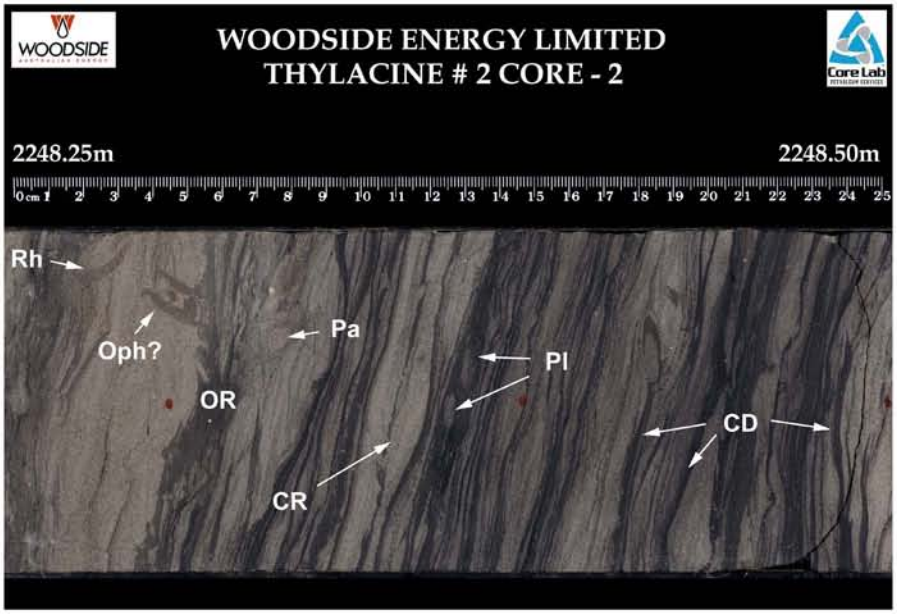


PLATE 15

PLATE 16

2247.50 – 2247.75 m

Facies Srl

Ripple-laminated, fine grained, well sorted sandstone. Ripple lamination is bi-directional (BdR) and several thin silty clay drapes are evident (CD). Bioturbation intensity is minor to moderate, although burrow diversity is high, with *Planolites* (Pl), *Palaeophycus* (Pa), *Ophiomorpha* (Oph), *Rhizocorallium* (Rh), *Asterosoma* (As) *Teichichnus* (Te) and a possible, small *Diplocraterion* present (Dp). Ichnofacies is equivalent to Distal *Skolithos*. Depositional environment appears to have been tidally influenced, with the deposit possibly formed either as part of a sand flat, or in sandy, tidal inlet. Also note the anastomosing shear fracture (SF).

PLATE 17

2245.75 – 2246.00 m

Facies Sbgr

Intensely bioturbated, argillaceous sandstone with scattered granules. Floating quartzose granules (QG) within argillaceous, bioturbated sandstone are believed to indicate successive periods of transgressive reworking combined with homogenisation of the sediment by burrowing. Note the very coarse sand grains within *Thalassinoides* burrows (Th) just below the base of the sandstone. These burrows are indicative of the *Glossifungites* ichnofacies. The base of the sandstone is interpreted to represent a transgressive surface of erosion, and marks the onset of another period of marine flooding.

PLATE 18

2245.50 – 2245.75 m

Facies Mb

Intensely bioturbated, argillaceous siltstone (Mb) overlying granule-bearing argillaceous sandstone (Sbgr). Granules are quartzose (QG) and continue to be present in the siltstone. This photo is an upward continuation from Plate 17. Note the persistence of quartz granules into the siltstone, indicating that transgressive reworking continued for some time after the initial flooding event. Burrows are difficult to identify in this view, apart from a few subhorizontal *Helminthopsis/Helminthoida* traces (H).

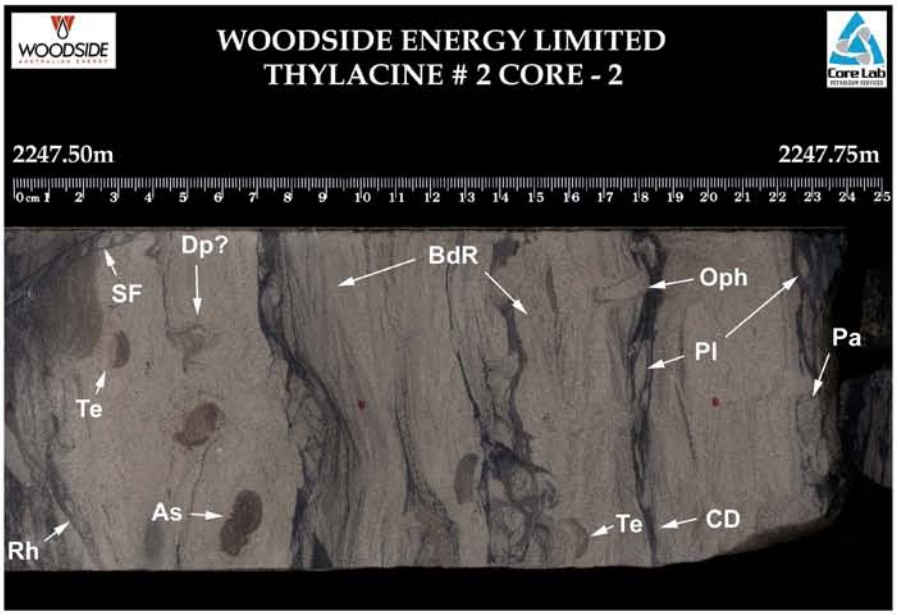


PLATE 16

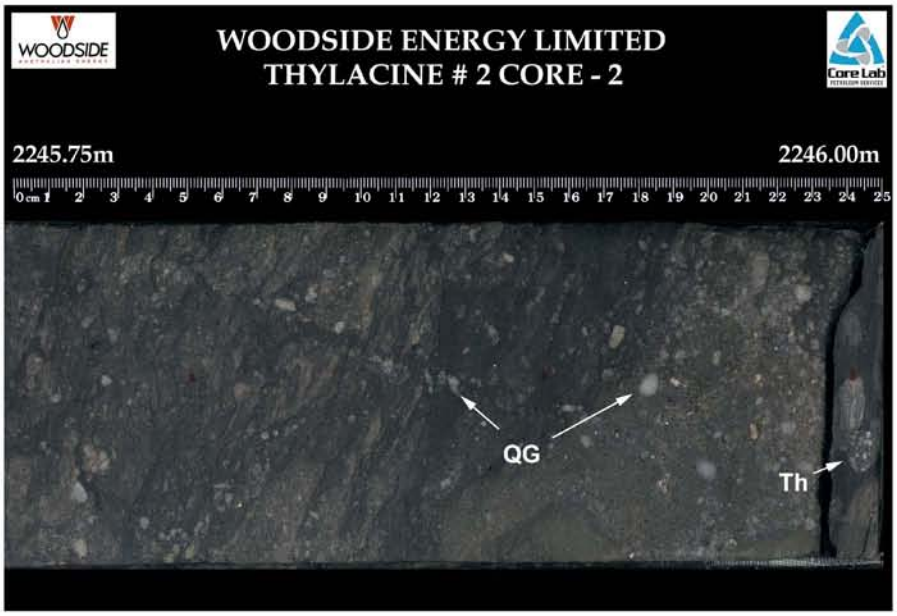


PLATE 17

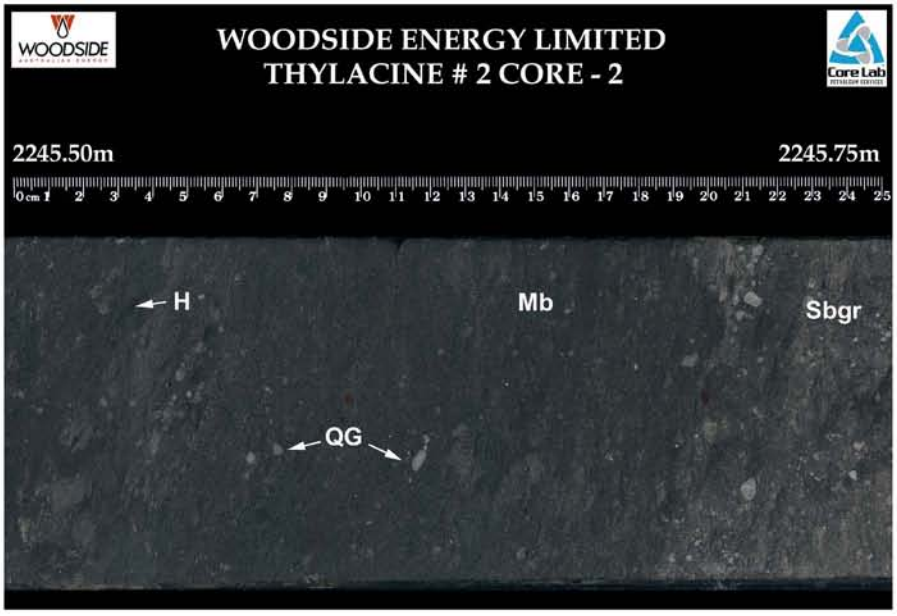


PLATE 18

PLATE 19

2237.00 – 2237.25 m

Facies Sgran Grading Upwards Into Facies Sx

Very coarse grained fining-up to coarse grained, crudely cross-bedded, poorly sorted sandstone with common quartzose granules. Punctuated by bioturbated, sideritised clay layer (Sid; note large *Thalassinoides* burrows - Th). A robust *Ophiomorpha* burrow can also be seen within the sandstone (Oph). This very coarse grained sandstone is interpreted to represent a storm deposit, possibly formed in response to transgression.

PLATE 20

2235.25 – 2235.51 m

Facies Sb Overlain By Facies Mmgl

The contact between bioturbated sandstone (Sb) and overlying massive, glauconitic claystone (Mmgl) at 2235.49 m is believed to represent a major flooding surface (FS). Depositional environment is interpreted to have changed from storm-reworked offshore transition zone for the bioturbated sandstone, to distal offshore for the glauconitic claystone. Such a sudden change was probably brought about by a rapid, tectonically-induced rise in relative sea level.

PLATE 21

2232.50 – 2232.75 m

Facies Mmgl

Massive to faintly bioturbated, glauconitic, silty claystone. Interpreted to represent a very slowly deposited, distal offshore deposit. Note prominent siderite-replaced layer (Sid) and very common glauconite (Gl) concentrated in burrows and thin, discontinuous laminae. Trace fossils are difficult to identify, although bioturbation intensity appears to have been moderate. Ichnofacies is identified as *Zoophycos/Nereites*.

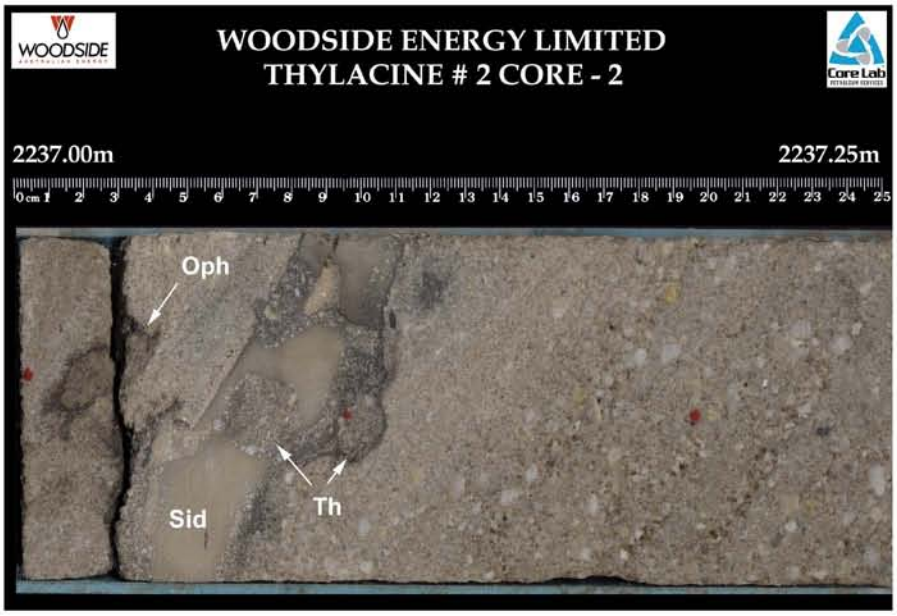


PLATE 19



PLATE 20

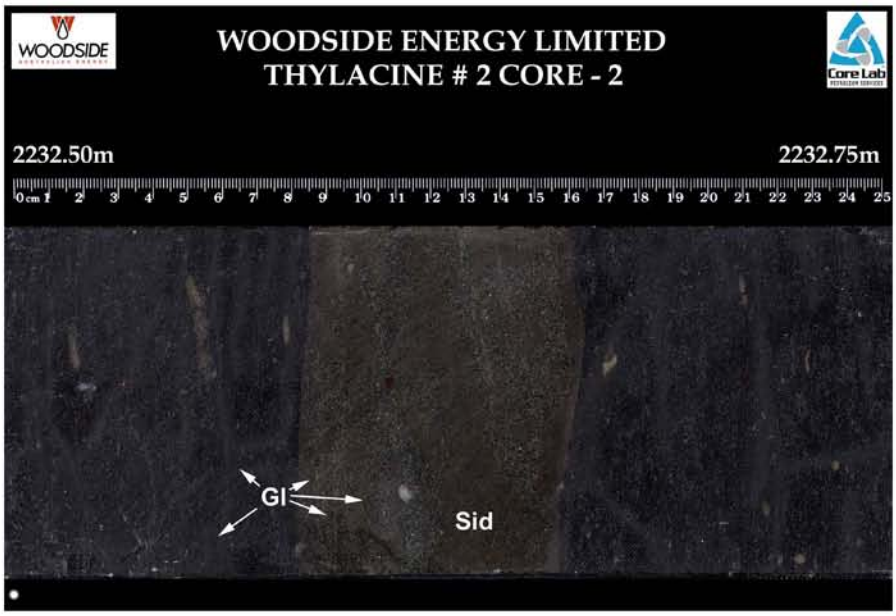


PLATE 21

PLATE 22

2215.25 – 2215.50 m

Facies Spbl And Gms Overlying Facies Sm

Massive, moderately well sorted sandstone with scattered clay and siderite pebbles (Spbl) is shown here overlying upper fine to lower medium grained, massive sandstone (Sm). Pebbles are locally concentrated into matrix-supported conglomerate (Gms). Note how clay pebbles (actually very silty claystone; CP) have been deformed by compaction, while sideritic pebbles (SP) have retained their original shape. The sideritic pebbles are believed to have been sideritised prior to transport and redeposition. These pebbly, massive sandstones are interpreted to represent mass flow deposits formed by gravitational processes on the proximal portion of a sand-rich ramp or slope apron. Note the lack of bioturbation.

PLATE 23

2195.50 – 2195.75 m

Facies Mb Overlain By Facies Sm

Massive, upper fine to lower medium grained, unbioturbated sandstone (Sm) of an interpreted liquefied gravity flow is shown in this view. The sandstone overlies intensely bioturbated argillaceous siltstone (Mb), which is believed to have been deposited in a proximal offshore marine environment. The base of the sandstone is marked by a lag deposit consisting of large sideritic pebbles (SP). Note the sandy nature of the argillaceous siltstone, and the presence of robust but indistinct burrows, probably consisting mainly of *Planolites*, *Palaeophycus* and *Teichichnus*. Also note the reverse shear fracture (SF) that offsets the basal contact of the sandstone by approximately 0.5 cm.

PLATE 24

2194.75 – 2195.00 m

Facies Sm With Small Normal Fault

Massive, unbioturbated, lower medium grained, moderately well sorted sandstone (Sm) shown in this view is cut by an early-formed, normal shear fracture (SF). Although it is impossible to determine the amount of displacement that has occurred along this fracture, fracture movement can be inferred by the deformation of the laminated beds just below the fracture plane. Note the sideritic fracture that runs just above the shear fracture (SidF). Depositional environment is interpreted to have been proximal turbidite channel. Fracturing occurred very early and may have been caused by syndepositional tectonic activity.

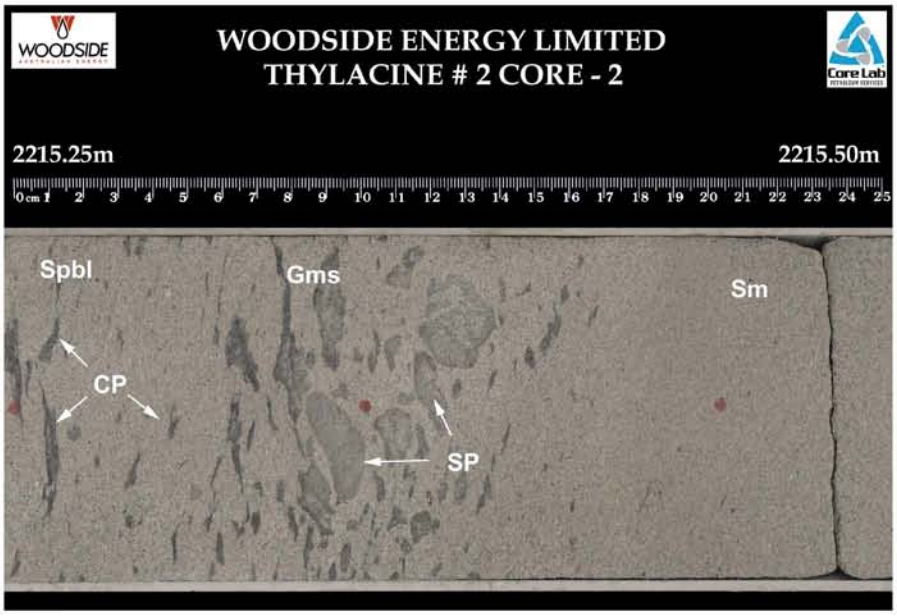


PLATE 22

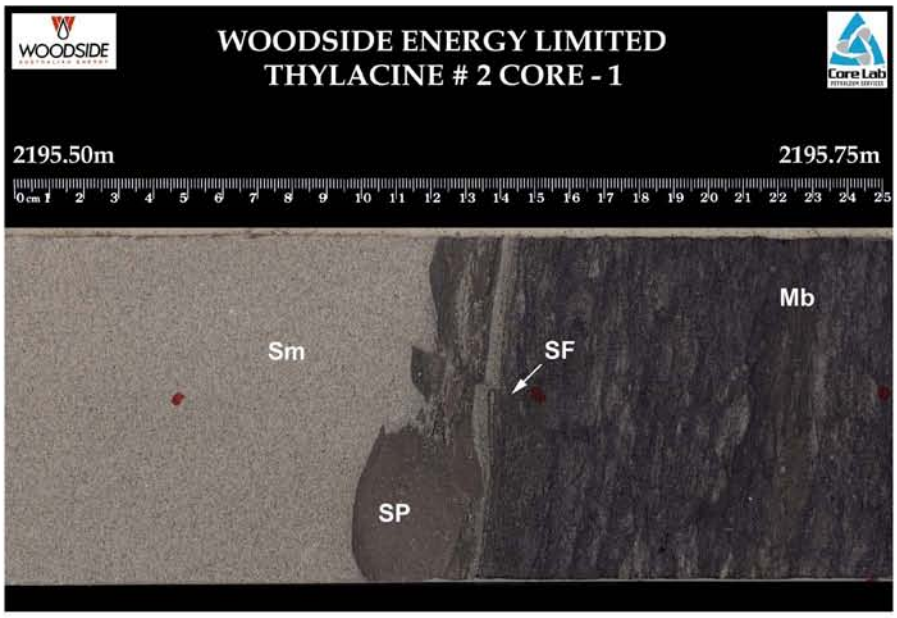


PLATE 23

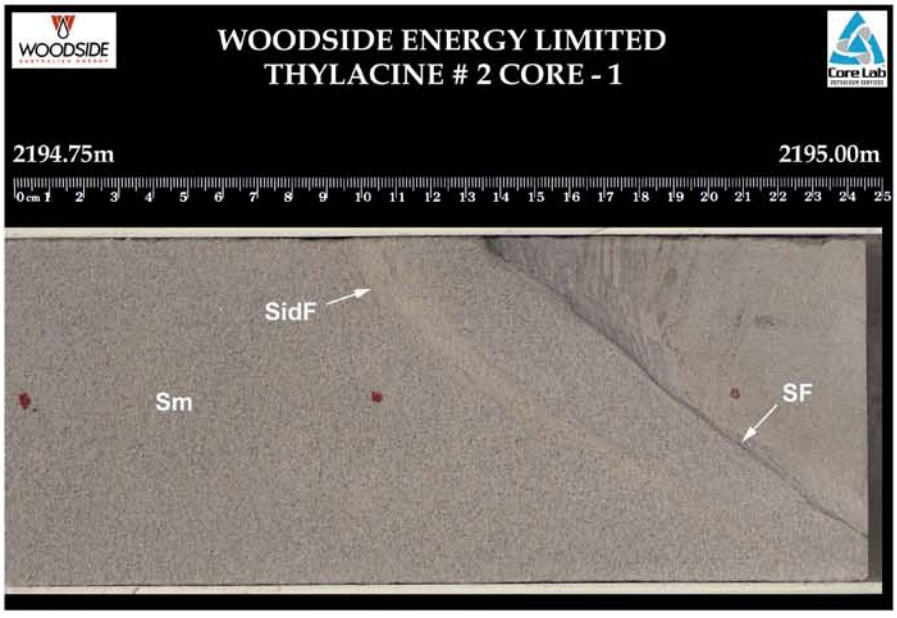


PLATE 24

PLATE 25

2183.50 – 2183.75 m

Facies Sm

Massive, upper fine grained, moderately well sorted sandstone of an interpreted proximal turbidite channel deposit. The lack of sedimentary structures indicates a degree of disorganization typical of a liquefied flow. Common small black grains give the sandstone a speckled appearance; these grains are believed to be rock fragments. Note the low-angle sideritic fractures (SiF). Red dots are profile permeability measurement points.

PLATE 26

2175.75 – 2176.00 m

Facies Sm And Mb

A thin bed of dark grey, intensely bioturbated, argillaceous siltstone (Mb) marks the top of a massive fine to medium grained sandstone bed (Sm). Bioturbation is indistinct but intense in the siltstone, and has a similar appearance to the Distal *Cruziana* ichnofacies observed lower down in the cored interval. Small *Palaeophycus* burrows (Pa) and a possible *Rhizocorallium* (Rh) at the top of the sandstone are thought to have been formed by opportunistic "doomed pioneers" that were carried downslope by gravity flows. Note the faint shear fractures (SF)

PLATE 27

2175.00 – 2175.25 m

Facies Sm And Sl, Cut By Dewatering Sheet And Shear Fractures

Carbonaceous clay-laminated, fine grained sandstone (Sl) and massive, fine to medium grained sandstone (Sm) in this view have been cut by a series of anastomosing shear fractures (SF) and a sideritic dewatering sheet (SiDW). Depositional environment is interpreted to have been a gravity flow in a proximal ramp or slope-apron environment. The often diffuse, anastomosing and sinuous character of the shear fractures, and the presence of weak gouge consisting of rotated and displaced sand grains, suggests they formed very early, while the sediment was still soft and unconsolidated. Displacement along individual fractures is normally less than a few centimetres.

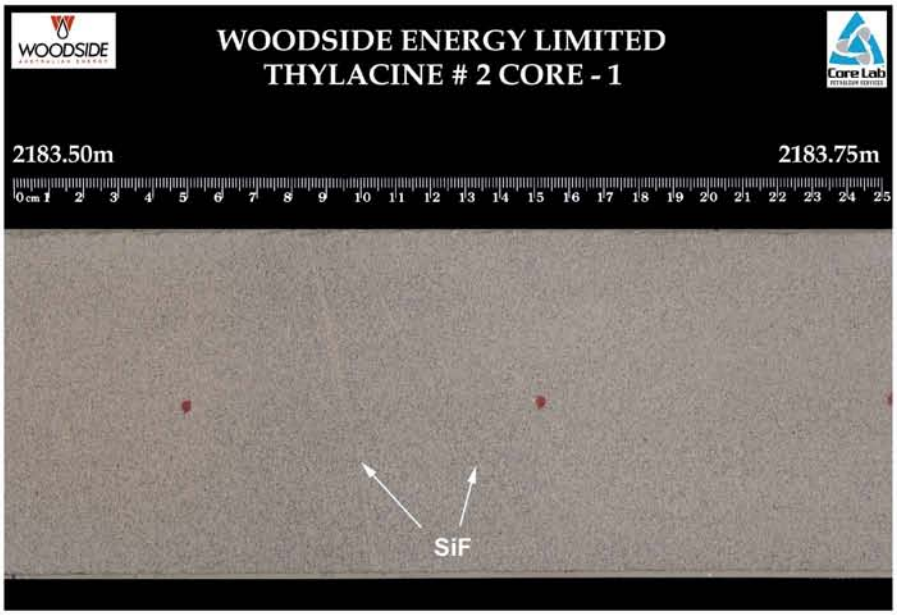


PLATE 25

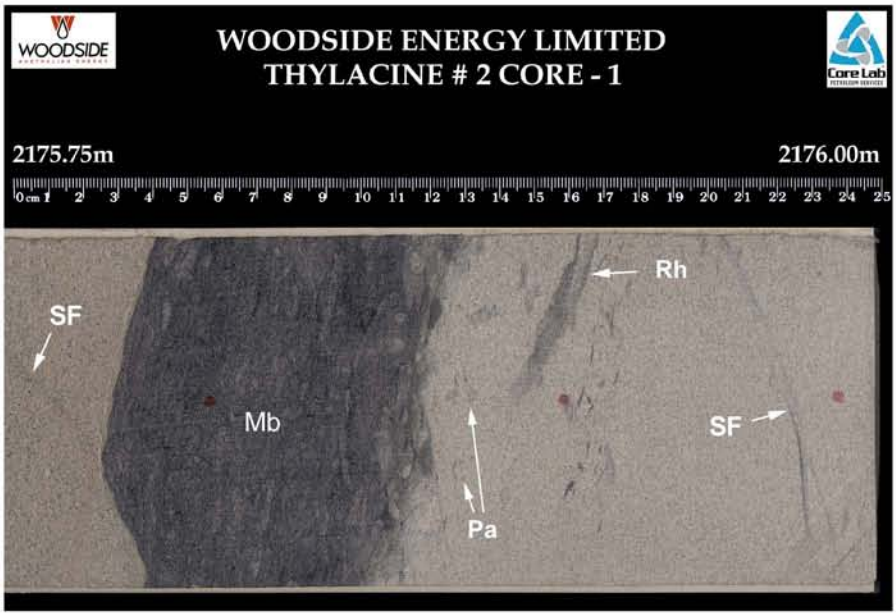


PLATE 26

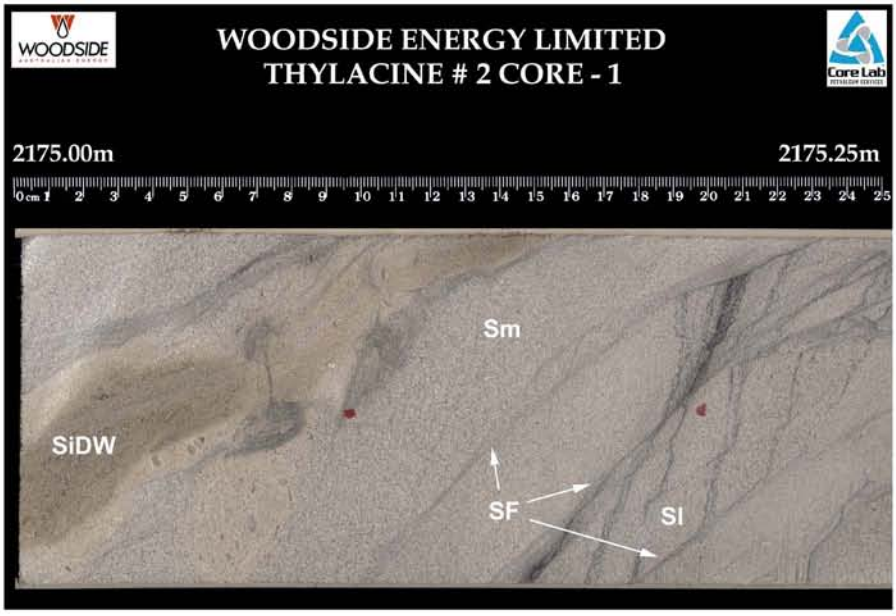


PLATE 27

PLATE 28

2173.00 – 2173.25 m

Facies Mb

Intensely bioturbated, argillaceous siltstone. Ichnofacies is considered to be Distal *Cruziana*, with faint but intense bioturbation. Burrows are often indistinct because of a lack of contrast between burrow fill and host siltstone. Recognisable types include *Planolites* (Pl), *Helminthopsis/Helminthoida* (H) and small *Terebellina* (Tb). Depositional environment was probably proximal offshore.

PLATE 29

2153.75 – 2154.00 m

Facies Sb/Sl Overlying Facies Mb

Intermittently bioturbated to faintly laminated, very fine grained sandstone (Sb/Sl) is shown in this view overlying intensely bioturbated siltstone (Mb). This sandstone layer is interpreted to represent a thin, possibly storm-reworked shoal or sheet that formed in an offshore transition to lower shoreface environment. Note occasional siderite replacement of argillaceous layers (Sid). Possible *Asterosoma* burrows (As) are visible in the sandstone.

PLATE 30

2150.75 – 2151.00 m

Facies Sba Grading Upwards Into Facies Mb

Many facies changes are extremely gradual in Thylacine-2. This view shows intensely bioturbated, argillaceous, very fine grained sandstone (Sba) grading upwards into very argillaceous, sandy siltstone (Mb). Bioturbation intensity was so high that burrow types are difficult to identify. However, the presence of a well-preserved *Rhizocorallium* (Rh; next to pyrite nodule, Pyr) small *Planolites* (Pl), occasional *Teichichnus* (Te), *Helminthopsis/Helminthoida* (H) and possible, poorly defined *Chondrites* (Ch) indicates a moderately diverse trace fossil assemblage. Ichnofacies is identified as Proximal to Distal *Cruziana*. Depositional environment is interpreted to have been offshore transition to proximal offshore. Note occasional nodular siderite (Sid).

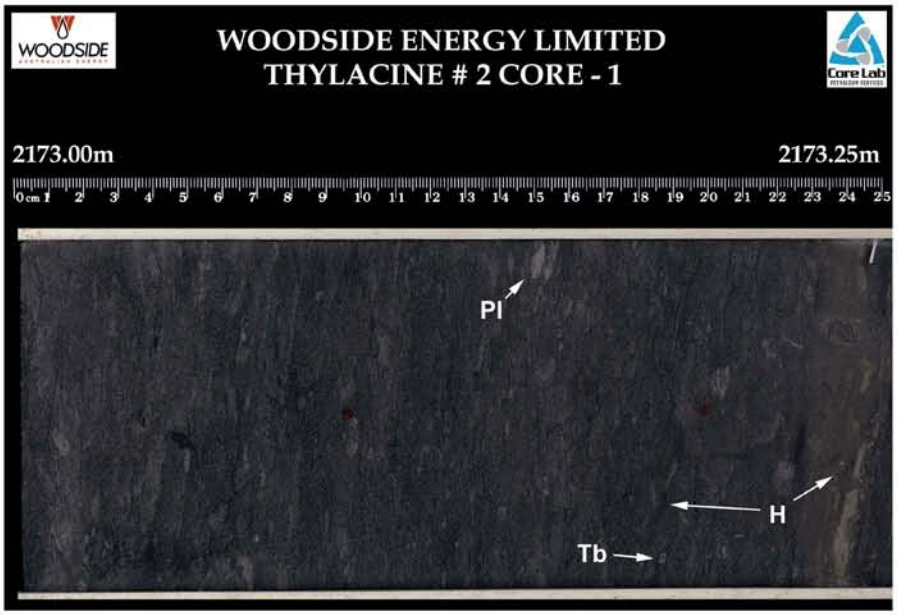


PLATE 28

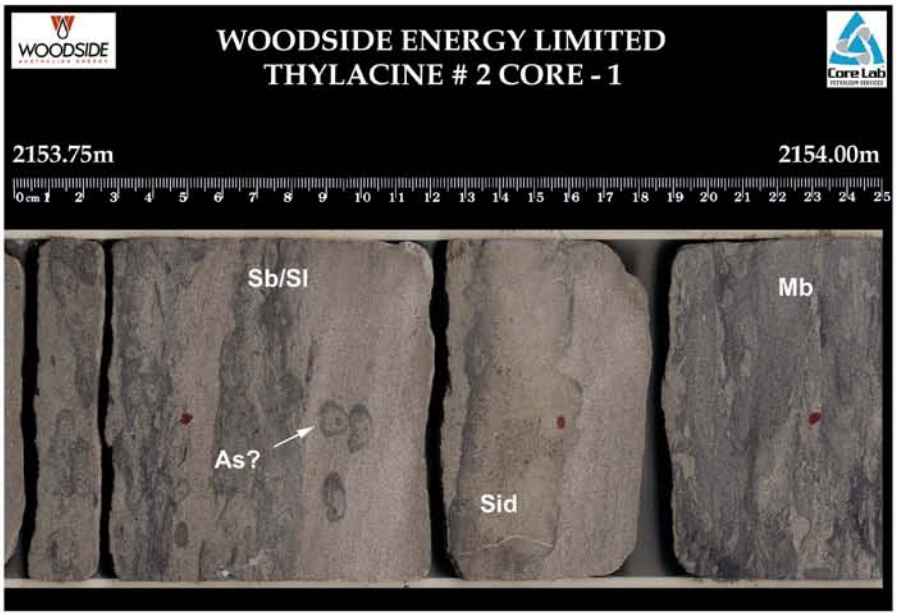


PLATE 29

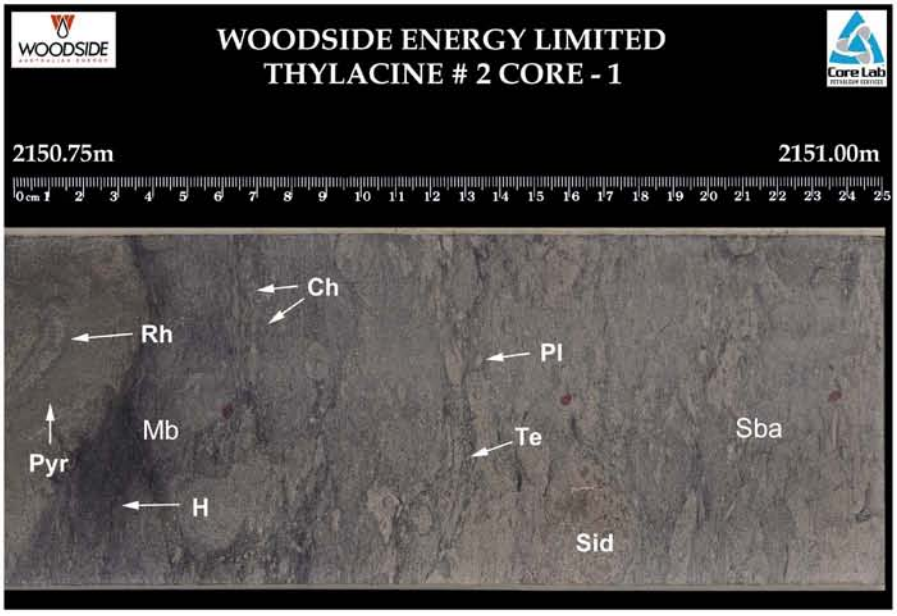
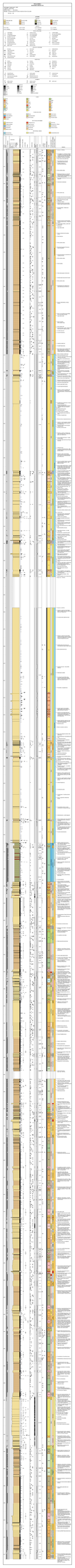


PLATE 30


Stratigraphic Column Chart - 2007
Geologic Time Scale
Modified from Gradstein et al., 2004
Geological Survey of Canada
Lithology
Sedimentary Rocks
Boundstone
Breccia
Chalk
Chert
Clastic Sediment
Coal
Conglomerate
Dolomite
Evaporite
Gypsum
Limestone
Mudstone
Phosphorite
Sandstone
Shale
Siltstone
Tillite
Igneous Rocks
Andesite
Basalt
Dacite
Diorite
Gabbro
Granite
Granodiorite
Peridotite
Rhyolite
Tuff
Volcanic Breccia
Metamorphic Rocks
Amphibolite
Gneiss
Greenschist
Hornfels
Marble
Metaconglomerate
Metasandstone
Migmatite
Quartzite
Schist
Slate
Structures
Bedding
Cross Bedding
Fault
Fossils
Ammonite
Archaeocyatha
Belemnite
Bivalve
Brachiopod
Bryozoan
Coral
Crinoid
Dinosaur
Fish
Foraminifera
Gastropod
Graptolite
Mammal
Nautiloid
Ostracod
Plant
Radiolaria
Reptile
Trace Fossil
Trilobite
Vertebrate
Other
Anhydrite
Banded Iron Formation
Barite
Bentonite
Boulders
Calcarenite
Calcilutite
Calcirudite
Carbonate
Carbonate Concretions
Cherty Limestone
Clay
Coquina
Cross Stratification
Diamictite
Dolomitic Limestone
Fossiliferous Limestone
Gravel
Halite
Ironstone
Marl
Metamorphic Rock
Nodular Limestone
Oolitic Limestone
Pebbly Sandstone
Phosphatic Limestone
Pyrite
Quartz Sandstone
Sandy Limestone
Shaly Limestone
Volcanic Rock
Wackestone
Wavy Bedding
Eras
Phanerozoic
Proterozoic
Archean
Systems
Cenozoic
Quaternary
Neogene
Paleogene
Mesozoic
Cretaceous
Jurassic
Triassic
Paleozoic
Permian
Carboniferous
Pennsylvanian
Mississippian
Devonian
Silurian
Ordovician
Cambrian
Precambrian
Neoproterozoic
Mesoproterozoic
Paleoproterozoic
Neoarchean
Mesoarchean
Paleoarchean
Eoarchean
Series
Holocene
Pleistocene
Upper
Middle
Lower
Stages
Piacenzian
Zanclean
Messinian
Tortonian
Serravallian
Langhian
Burdigalian
Aquitanian
Chattian
Rupelian
Priabonian
Bartonian
Lutetian
Ypresian
Thanetian
Selandian
Danian
Maastrichtian
Campanian
Santonian
Coniacian
Turonian
Cenomanian
Albian
Aptian
Barremian
Hauterivian
Valanginian
Berriasian
Tithonian
Kimmeridgian
Oxfordian
Callovian
Bathonian
Bajocian
Aalenian
Toarcian
Pliensbachian
Sinemurian
Hettangian
Rhaetian
Norian
Carnian
Ladinian
Anisian
Olenekian
Induan
Changhsingian
Wuchiapingian
Capitanian
Wordian
Roadian
Kungurian
Artinskian
Sakmarian
Asselian
Gzhelian
Kasimovian
Moscovian
Bashkirian
Serpukhovian
Visean
Tournaisian
Famennian
Frasnian
Givetian
Eifelian
Emsian
Pragian
Lochkovian
Pridoli
Ludlow
Wenlock
Llandovery
Hirnantian
Katian
Sandbian
Darriwilian
Dapingian
Floian
Tremadocian
Furongian
Series 3
Series 2
Terreneuvian
Stenian
Tonian
Cryogenian
Ediacaran
Orosirian
Rhyacian
Siderian
Neoarchean
Mesoarchean
Paleoarchean
Eoarchean
Ages
Ma
Lithology
Structures
Fossils
Other
Description

APPENDIX 8
SPECIAL CORE ANALYSIS

A Special Core Analysis Study Of Selected Samples From Well : THYLACINE - 2

Australia

Prepared for
WOODSIDE ENERGY LIMITED

September 2002

File: PRP-02024

Rock Properties
Core Laboratories Australia Pty. Ltd.
Perth
Australia

6th September, 2002

WOODSIDE ENERGY LIMITED.
1 Adelaide Terrace
PERTH, Western Australia, 6000

Attention : Mr. Jon Kelly

Subject: Special Core Analysis.
Well : Thylacine - 2
File : PRP-02024

Dear Jon,

Presented here are the final results of the special core analyses conducted on the selected core and sidewall samples from the well Thylacine – 2.

Thank you for the opportunity to have been of service to Woodside Energy Limited. If you have any questions regarding these results or if we can be of any further assistance please do not hesitate to contact us.

Yours sincerely,
CORE LABORATORIES

Ajit Singh
Supervisor - Rock Properties Perth

CONTENTS

SECTION 1 - INTRODUCTION AND SUMMARY

Introduction. Page 1-1
Summary of tests and results. Page 1-2
Sample identification, base data and screening results. Page 1-3

SECTION 2 - ELECTRICAL PROPERTIES

Formation resistivity factor (FRF). Page 2-1
Cation exchange capacity (CEC). Page 2-1
Formation resistivity index (RI). Page 2-6
BQv by multiple salinity (Hoyer and Spann) method. Page 2-24

SECTION 3 - CAPILLARY PRESSURE ANALYSES

Summary - air permeability (Kair) versus immobile water saturation (Swi). Page 3-1
Summary - tabular data (ambient pressure). Page 3-2
Air - brine drainage capillary pressure by centrifuge (at ambient pressure). Page 3-3

SECTION 4 - RELATIVE PERMEABILITY ANALYSIS

Summary - air permeability versus gas recovery (percent pore volume). Page 4-1
Water - gas relative permeability by centrifuge (end-point). Page 4-2

SECTION 5 - ROCK (PORE VOLUME) COMPRESSIBILITY ANALYSIS

Rock (pore volume) compressibility. Page 5-1

APPENDICES

Appendix 1 - Summary of laboratory procedures.

Appendix 2 - Rawdata from electrical properties, capillary pressure and rock compressibility tests.

SECTION 1
INTRODUCTION & SUMMARY

INTRODUCTION

This report contains the final results of the Special Core Analysis (SCAL) study performed on selected core plug samples from the well Thylacine - 2. This study was initiated by Mr Jon Kelly of Woodside.

The test programme involved :

- Selection and visual inspection of samples for the study
- CT-scanning of selected samples
- Measurement / re-measurement of porosity, permeability, and grain density values
- Formation resistivity factor (FRF) analysis
- BQv by multiple salinity
- CEC by wet chemistry
- Formation resistivity index (RI) analysis
- Air-brine drainage capillary pressure by centrifuge
- Water-gas relative permeability by centrifuge
- Rock (pore volume) compressibility

Twenty-one samples which had previously undergone routine core analysis constituted the original SCAL sample selection for electrical, capillary pressure and relative permeability analyses. Four additional duplicate samples were drilled from the core for rock (pore volume) compressibility tests (suffix “A”).

All selected samples underwent CT-scanning to screen out any samples which exhibited heterogeneity. A full list of samples which underwent SCAL analysis and also which failed initial screening are listed in SECTION 1 of this report. Sample #179 was eliminated from the SCAL selection as significant pyrite cement was noted within the sample. Please also refer to the routine core analysis report issued for this well (PRP-01042 January 2002).

A simulated formation brine of 13,500 ppm comprising 80% NaCl and 20% KCl was used during the SCAL studies conducted at Core Laboratories.

Trim ends and sample remnants for the eighteen samples which underwent electrical, capillary pressure and relative permeability tests were despatched to Julian Baker at Reservoir Solutions Limited for a petrographic study.

SUMMARY OF RESULTS

Electrical Properties

Cementation exponent “m” values, measured at net overburden pressure (NOBP), ranged between 1.70 to 1.95. The average “m” was 1.82. CEC corrected values of “m*” ranged between 1.78 and 2.24 with an average “m*” of 2.07. Resistivity index analysis yielded sample average saturation exponent “n” values ranging between 1.69 to 2.36. The average “n” was 1.93. CEC corrected values of “n*” ranged between 1.96 to 2.78 with an average “n*” of 2.36.

Cation exchange capacity (CEC) analyses were performed on all 18 sample trim-ends by the wet chemistry method on crushed sample. The recorded CEC values ranged from 0.916 to 5.57 meq/100gm. BQv values from multiple salinity tests conducted on samples #93 and #12 were 0.658 and 0.881 (1/ohm-m) respectively.

Capillary Pressure

Samples tested ranged from 0.415 md to 6680 md air permeability (Kair at ambient). At the maximum air-brine capillary pressure, the selected samples yielded immobile water saturation (Swi) values between 3.51 and 47.6 percent pore volume (% PV). For most samples the requested maximum air-brine capillary pressure of 500 psi was attained. To preserve sample integrity, samples #234 and #241 were limited to the maximum 200 psi capillary pressure. The data indicate a strong trend of immobile water saturation as a function of air permeability.

Relative permeability analyses.

Water-gas relative permeability analysis (end-point) by centrifuge were conducted on all eighteen samples following the air-brine capillary pressure analyses. Residual gas saturations from centrifuge water-gas relative permeability (representing a reservoir displacement mechanism dominated by capillary / gravity forces) ranged from 5.3% to 18.4% pore volume. Gas recoveries ranged from 77.4% to 91.4% initial gas in-place.

Rock (pore volume) compressibility.

Rock (pore volume) compressibility tests conducted on 4 samples indicated compressibility (uniaxial loading) values ranging from 1.92×10^{-6} to 2.91×10^{-6} pv/pv/psi at the maximum confining stress of 7,000 psi. As would be expected, the higher the porosity and permeability values of the samples, the larger the degree of compressibility exhibited through the range of pressure utilised in the tests.

COMPANY : WOODSIDE ENERGY LIMITED
WELL : THYLACINE - 2

POROSITY, PERMEABILITY AND GRAIN DENSITY
(Ambient & Overburden)

SAMPLE NUMBER	DEPTH (m)	Ambient			NOB PRESSURE				GRAIN DENSITY (g/cc)	Screening Pass/Fail (P/F)	
		PERMEABILITY		POROSITY (%)	NOBP (psi)	PERMEABILITY		POROSITY (%)			
		Kinf (md)	Kair (md)			Kinf (md)	Kair (md)			Visual	CT
5	2153.10	0.306	0.415	13.8	1890	0.134	0.229	13.4	2.650	P	P
5A	2153.02	2.11	2.66	16.6	1890	*	*	*	2.651	P	P
12	2174.20	0.920	1.33	17.7	1890	0.717	1.05	17.2	2.662	P	P
27	2179.50	2.35	3.11	18.4	1890	1.97	2.63	17.9	2.680	P	P
44	2185.55	0.439	0.677	15.3	1890	0.320	0.509	14.9	2.705	P	P
76	2196.75	5.15	6.44	21.1	1890	4.60	5.77	20.7	2.730	P	P
76A	2196.80	6.50	7.98	21.2	1890	*	*	*	2.740	P	P
93	2206.55	6.62	7.97	17.8	1960	5.99	7.22	17.3	2.694	P	P
97	2207.84	22.1	24.9	22.0	1960	20.8	23.4	21.6	2.898	P	F
97A	2207.90	7.03	8.31	16.8	1960	*	*	*	2.774	P	P
118	2215.15	2.79	3.60	15.0	1960	2.33	3.04	14.5	2.652	P	P
118A	2215.10	2.83	3.64	15.0	1960	*	*	*	2.653	P	P
128	2218.40	0.303	0.427	11.6	1960	0.148	0.256	11.2	2.659	P	P
146	2225.12	1.38	1.89	15.5	1960	1.18	1.62	15.1	2.701	P	P
167	2239.39	0.182	0.307	13.9	1960	0.109	0.207	13.5	2.703	P	F
179	2248.55	0.131	0.221	15.5	1960	0.102	0.176	15.2	3.028	P	P
181	2249.85	7.16	8.87	19.5	1960	6.58	8.16	19.1	2.661	P	P
186	2251.20	0.517	0.787	14.7	1960	0.422	0.650	14.3	2.760	P	P
187	2251.59	0.758	1.12	16.8	1960	0.621	0.936	16.5	2.779	P	P
205	2275.17	174	191	19.7	2030	162	179	19.3	2.652	P	P
234	2296.94	5010	5510	24.7	2030	4860	5500	24.1	2.652	P	P
241	2299.40	5750	6680	21.8	2030	4340	5640	21.2	2.646	P	P

COMPANY : WOODSIDE ENERGY LIMITED
WELL : THYLACINE - 2

POROSITY, PERMEABILITY AND GRAIN DENSITY
(Ambient & Overburden)

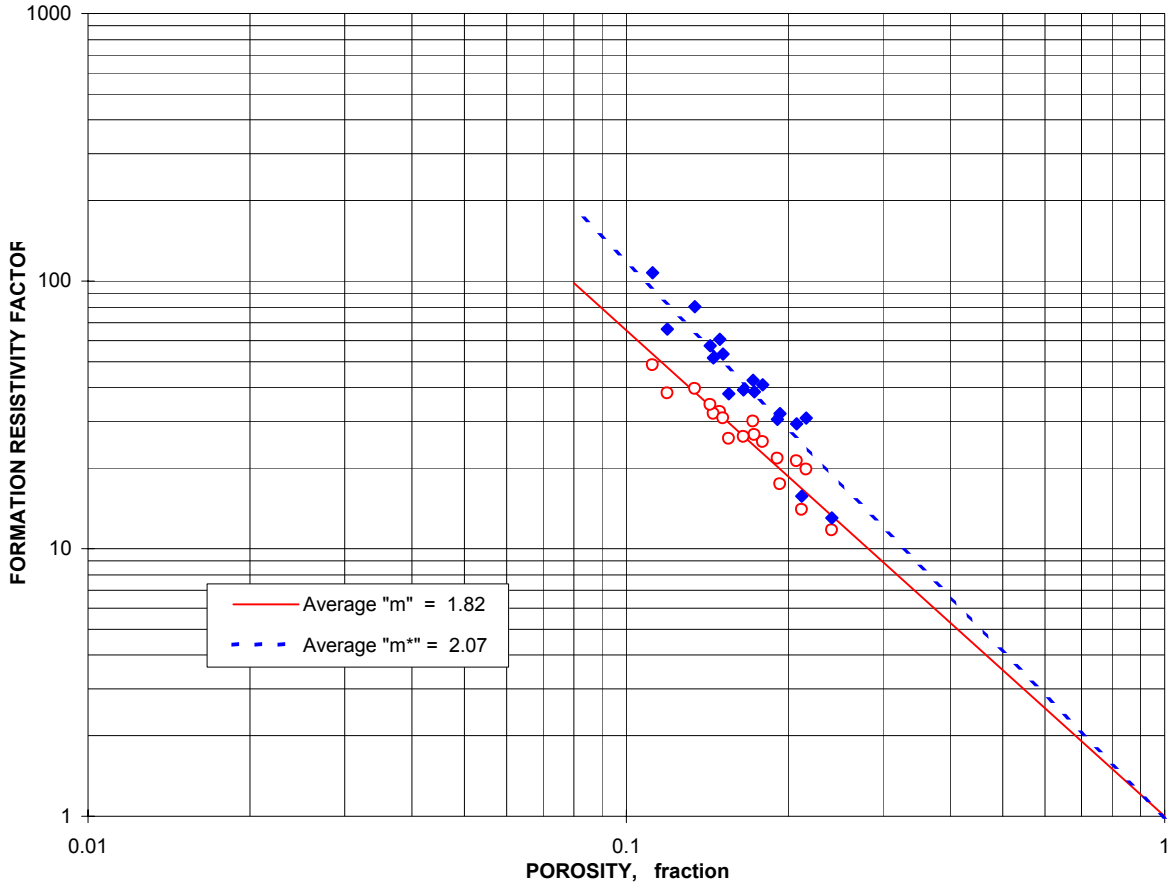
SAMPLE NUMBER	DEPTH (m)	Ambient			NOB PRESSURE				GRAIN DENSITY (g/cc)	Screening Pass/Fail (P/F)	
		PERMEABILITY		POROSITY (%)	NOBP (psi)	PERMEABILITY		POROSITY (%)			
		Kinf (md)	Kair (md)			Kinf (md)	Kair (md)			Visual	CT
244	2300.20	0.526	0.816	12.3	2030	0.450	0.704	11.9	2.680	P	P
246	2300.80	7.73	9.61	15.8	2030	7.04	8.81	15.5	2.741	P	P
254	2311.20	0.691	1.05	15.4	2030	0.533	0.838	14.9	2.658	P	P

* Permeability and porosity at NOBP not measured on samples scheduled for rock compressibility tests.

SECTION 2
ELECTRICAL PROPERTIES

Formation resistivity factor (FRF) at NOBP

Sample no.	Depth (metres)	Grain Density gm/cc	CEC meq/100gm	K air (md)	AT NOBP					
					NOBP	Porosity (%)	FRF	FRF *	m	m*
5	2153.10	2.650	4.48	0.229	1890	13.4	39.63	80.43	1.83	2.18
12	2174.20	2.662	3.25	1.05	1890	17.2	29.88	42.68	1.93	2.19
27	2179.50	2.680	3.83	2.63	1890	17.9	25.05	40.90	1.87	2.16
44	2185.55	2.705	4.17	0.509	1890	14.9	32.51	60.64	1.83	2.16
76	2196.75	2.730	2.73	5.77	1890	20.7	21.23	29.34	1.94	2.15
93	2206.55	2.694	2.61	7.22	1960	17.3	26.60	38.62	1.87	2.08
97	2207.84	2.898	3.88	23.4	1960	21.6	19.85	30.82	1.95	2.24
118	2215.15	2.652	2.96	3.04	1960	14.5	31.90	51.75	1.79	2.04
128	2218.40	2.659	4.26	0.256	1960	11.2	48.59	107.26	1.77	2.14
146	2225.12	2.701	3.64	1.62	1960	15.1	30.68	53.51	1.81	2.11
181	2249.85	2.661	2.67	8.16	1960	19.1	21.74	30.48	1.86	2.06
186	2251.20	2.760	2.81	0.650	1960	14.3	34.62	57.35	1.82	2.08
187	2251.59	2.779	2.58	0.936	1960	16.5	26.27	39.13	1.81	2.04
205	2275.17	2.652	5.57	179	2030	19.3	17.47	32.03	1.74	2.11
234	2296.94	2.652	1.00	5500	2030	24.1	11.71	13.01	1.73	1.80
241	2299.40	2.646	0.916	5640	2030	21.2	13.97	15.70	1.70	1.78
244	2300.20	2.680	2.75	0.704	2030	11.9	38.13	66.04	1.71	1.97
246	2300.80	2.741	2.34	8.81	2030	15.5	25.82	37.92	1.74	1.95
								Average Cementation Exponent	1.82	2.07



Formation resistivity factor (FRF) at net overburden pressure

Sample no.	Depth (metres)	Grain density (gm/cc)	Determined at NOBP						
			NOBP (psi)	Perm. to air (md)	Porosity (%)	Brine saturation (%pv)	Resistivity index	Sat. Exp. n	Corrected Sat. Exp. n *
5	2153.10	2.650	1890	0.229	13.4	100.0	1.00	-	-
						84.9	1.38	1.95	2.48
						72.6	1.73	1.71	2.26
						67.3	2.07	1.83	2.39
						61.9	2.21	1.65	2.22
						54.9	2.49	1.52	2.10
12	2174.20	2.662	1890	1.05	17.2	100.0	1.00	-	-
						74.6	1.88	2.15	2.53
						71.0	1.95	1.95	2.33
						62.4	2.24	1.71	2.11
						55.8	2.69	1.70	2.11
						44.2	3.82	1.64	2.09
27	2179.50	2.680	1890	2.63	17.9	100.0	1.00	-	-
						74.3	1.69	1.78	2.20
						58.3	2.47	1.67	2.13
						45.4	3.80	1.69	2.18
						40.4	4.50	1.66	2.16
						37.4	4.93	1.62	2.13
44	2185.55	2.705	1890	0.509	14.9	100.0	1.00	-	-
						82.8	1.36	1.64	2.13
						78.3	1.66	2.06	2.56
						67.0	2.14	1.90	2.41
						52.0	3.16	1.76	2.30
						43.1	3.87	1.61	2.18
76	2196.75	2.730	1890	5.77	20.7	100.0	1.00	-	-
						60.3	2.69	1.96	2.29
						56.2	3.03	1.92	2.26
						52.0	3.40	1.87	2.22
						41.4	5.01	1.83	2.20
						35.2	6.11	1.73	2.13
						31.0	7.03	1.66	2.07
93	2206.55	2.694	1960	7.22	17.3	100.0	1.00	-	-
						70.1	2.19	2.21	2.56
						60.8	2.56	1.89	2.26
						53.9	3.39	1.98	2.36
						49.0	4.21	2.01	2.41
						41.5	5.50	1.94	2.35
97	2207.84	2.898	1960	23.4	21.6	100.0	1.00	-	-
						58.5	2.70	1.86	2.27
						48.1	3.57	1.74	2.18
						41.7	4.34	1.68	2.14
						32.8	6.25	1.64	2.13
						26.8	8.73	1.65	2.16

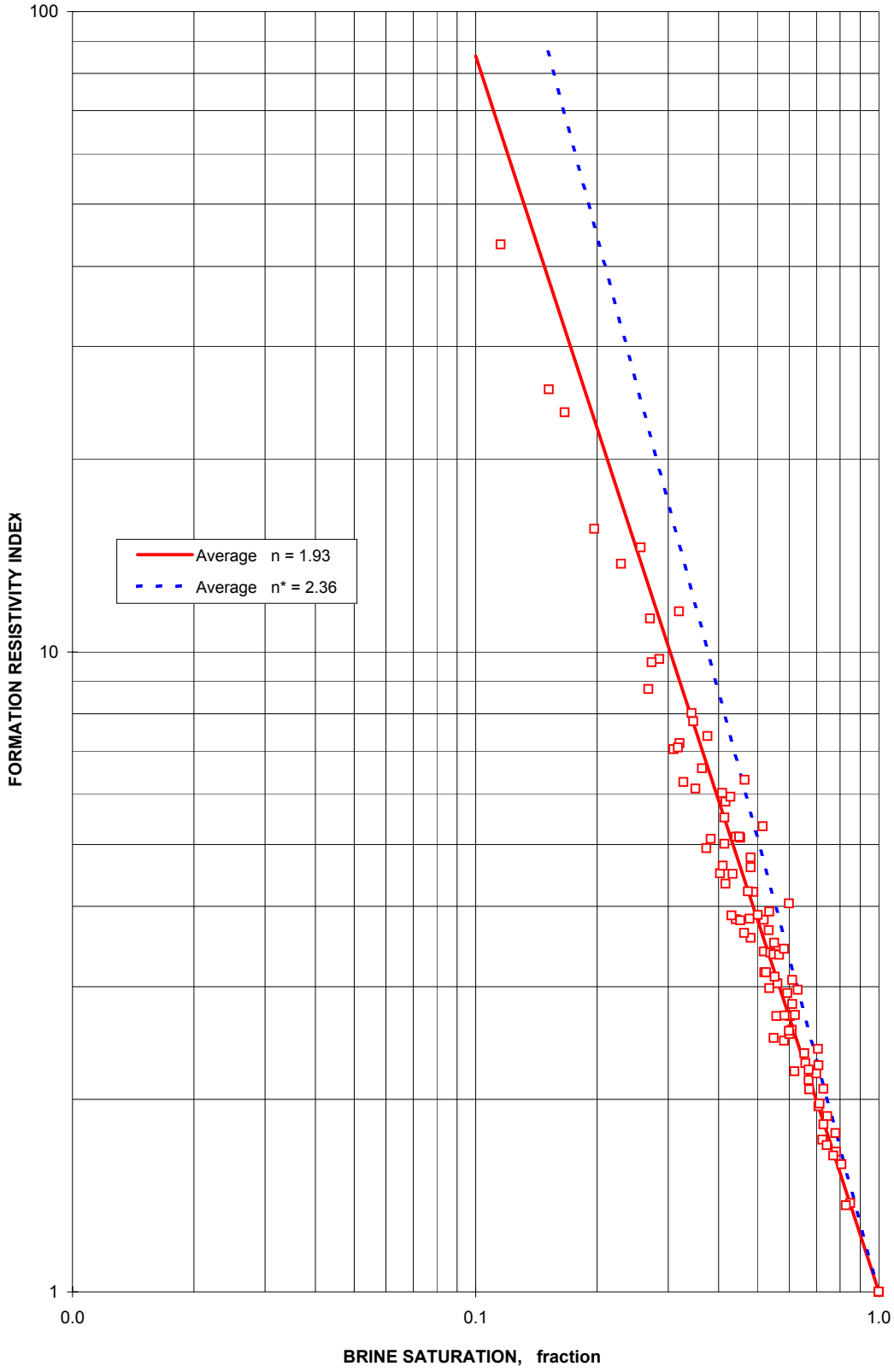
Formation resistivity factor (FRF) at net overburden pressure

Sample no.	Depth (metres)	Grain density (gm/cc)	Determined at NOBP						
			NOBP (psi)	Perm. to air (md)	Porosity (%)	Brine saturation (%pv)	Resistivity index	Sat. Exp. n	Corrected Sat. Exp. n *
118	2215.15	2.652	1960	3.04	14.5	100.0	1.00	-	-
						72.8	1.83	1.90	2.32
						55.2	3.11	1.91	2.36
						47.9	3.82	1.82	2.30
						43.5	4.50	1.81	2.29
						38.3	5.10	1.70	2.20
128	2218.40	2.659	1960	0.256	11.2	100.0	1.00	-	
						80.8	1.58	2.15	2.73
						71.4	1.97	2.01	2.60
						65.8	2.27	1.96	2.56
						60.1	2.53	1.82	2.43
						52.6	3.16	1.79	2.41
146	2225.12	2.701	1960	1.62	15.1	100.0	1.00	-	
						61.0	3.07	2.27	2.75
						51.9	3.81	2.04	2.55
						48.1	4.60	2.08	2.60
						44.2	5.14	2.00	2.53
						36.4	6.57	1.86	2.42
181	2249.85	2.661	1960	8.16	19.1	100.0	1.00	-	
						61.1	2.82	2.10	2.44
						55.0	3.51	2.10	2.46
						45.3	5.11	2.06	2.44
						41.7	5.82	2.01	2.40
						34.4	8.01	1.95	2.36
186	2251.20	2.760	1960	0.650	14.3	100.0	1.00	-	
						78.2	1.77	2.32	2.73
						72.9	2.07	2.31	2.73
						65.4	2.36	2.02	2.46
						59.4	2.93	2.06	2.51
						54.9	3.37	2.02	2.48
						47.3	4.22	1.93	2.40
187	2251.59	2.779	1960	0.936	16.5	100.0	1.00	-	
						70.6	2.39	2.51	2.88
						62.9	2.96	2.34	2.73
						56.6	3.36	2.13	2.52
						50.2	3.88	1.96	2.37
						45.1	5.14	2.05	2.48

Formation resistivity factor (FRF) at net overburden pressure

Sample no.	Depth (metres)	Grain density (gm/cc)	Determined at NOBP						
			NOBP (psi)	Perm. to air (md)	Porosity (%)	Brine saturation (%pv)	Resistivity index	Sat. Exp. n	Corrected Sat. Exp. n *
205	2275.17	2.652	2030	179	19.3	100.0	1.00	-	
						77.1	1.63	1.89	2.37
						53.4	3.67	2.07	2.61
						48.2	4.77	2.14	2.68
						42.9	5.94	2.10	2.66
						37.6	7.39	2.04	2.62
						27.1	11.27	1.85	2.46
						19.7	15.56	1.69	2.33
234	2296.94	2.652	2030	5500	24.1	100.0	1.00	-	
						67.0	2.22	2.00	2.12
						59.8	2.55	1.83	1.95
						53.6	2.98	1.75	1.88
						46.4	3.63	1.68	1.82
						32.1	7.20	1.74	1.91
						28.5	9.74	1.82	1.99
						11.5	43.30	1.74	2.01
241	2299.40	2.646	2030	5640	21.2	100.0	1.00	-	
						62.0	2.70	2.08	2.21
						41.0	4.63	1.72	1.88
						31.8	7.08	1.71	1.89
						27.4	9.62	1.75	1.94
						23.0	13.73	1.78	1.99
						16.6	23.66	1.76	2.01
						15.2	25.71	1.72	1.97
244	2300.20	2.680	2030	0.704	11.9	100.0	1.00	-	
						70.9	2.26	2.37	2.83
						58.3	3.43	2.29	2.78
						53.6	3.93	2.19	2.69
						41.0	6.01	2.01	2.54
						34.7	7.79	1.94	2.49
246	2300.80	2.741	2030	8.81	15.5	100.0	1.00	-	
						59.8	4.04	2.72	3.10
						51.6	5.33	2.53	2.93
						46.6	6.31	2.41	2.82
						32.0	11.55	2.15	2.60
						25.7	14.55	1.97	2.45
						Average Exponent		1.93	2.36

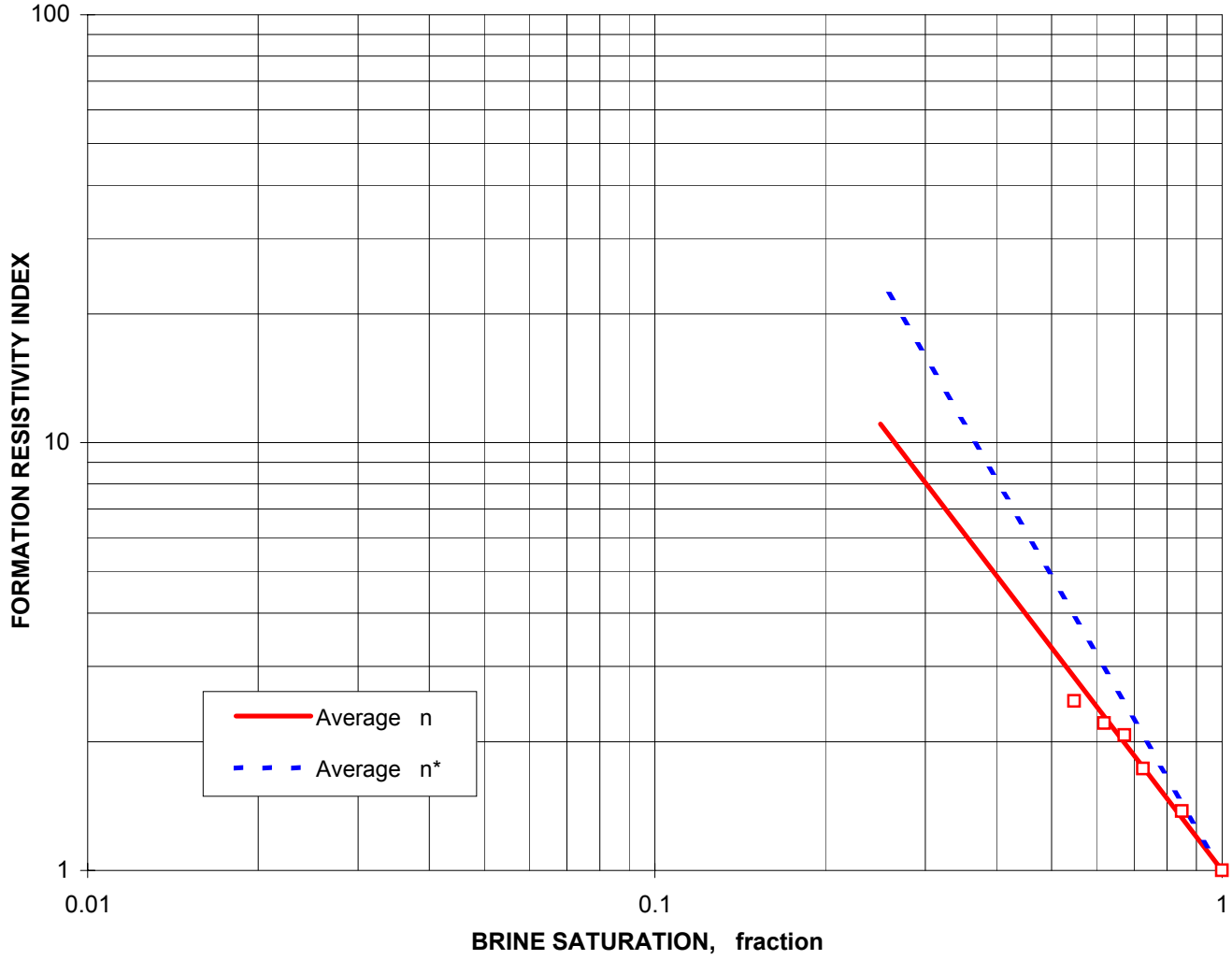
Formation resistivity factor (FRF) at net overburden pressure



Formation resistivity index at NOBP.

Sample No.	Depth (metres)	Grain density (gm/cc)	Determined at 1890 psi NOBP					
			Perm. to air (md)	Porosity (%)	Brine saturation (%pv)	Resistivity index	Sat. Exp. n	Corrected Sat. Exp. n *
5	2153.10	2.650	0.229	13.4	100.0	1.00	-	-
					84.9	1.38	1.95	2.48
					72.6	1.73	1.71	2.26
					67.3	2.07	1.83	2.39
					61.9	2.21	1.65	2.22
					54.9	2.49	1.52	2.10
						Average Exponent	1.73	2.29

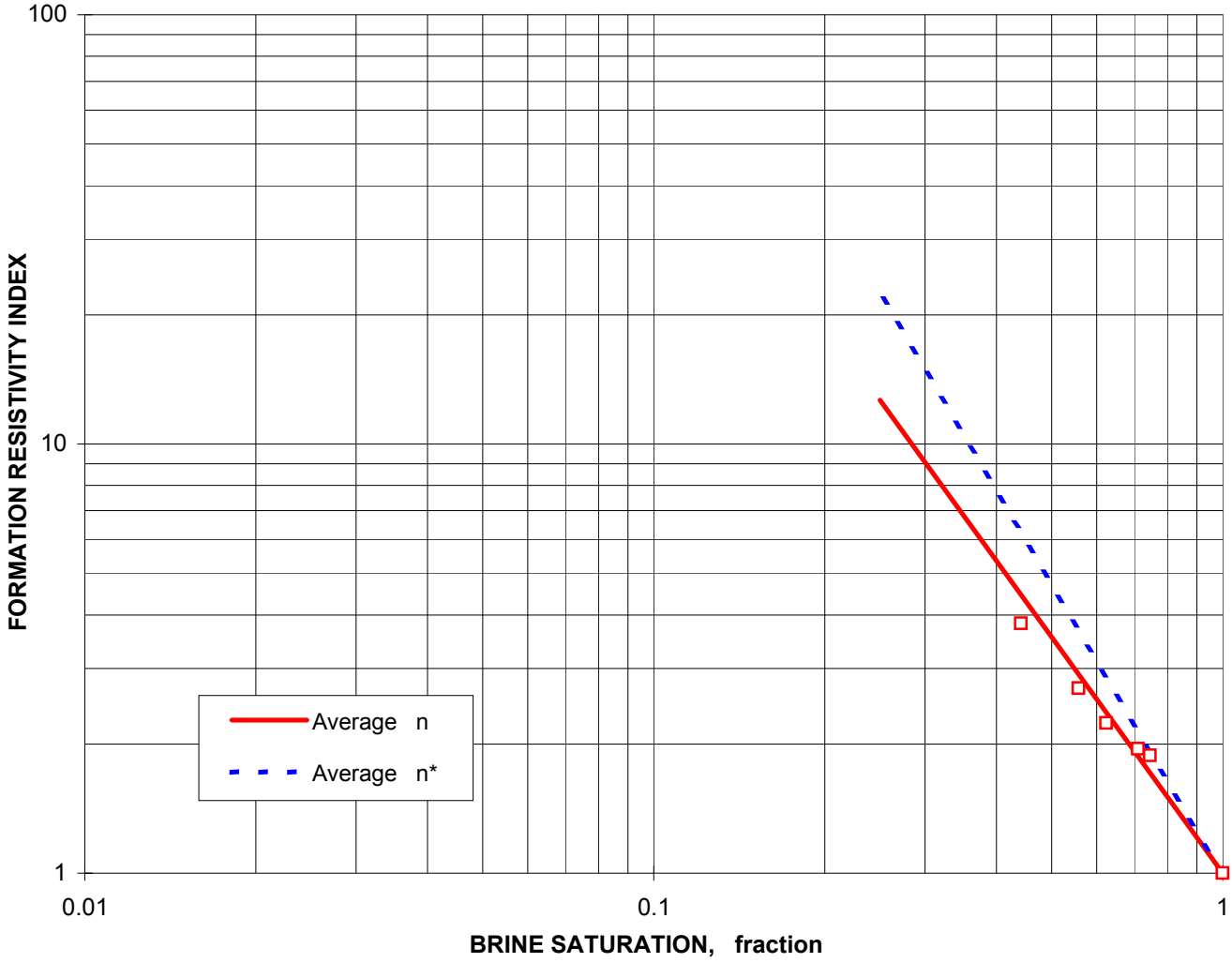
FRF at NOBP	39.63
CEC (meq / 100gm)	4.48
FRF * at NOBP	80.43
Rw at 25°C, ohm-m	0.4150



Formation resistivity index at NOBP.

Sample No.	Depth (metres)	Grain density (gm/cc)	Determined at 1890 psi NOBP					
			Perm. to air (md)	Porosity (%)	Brine saturation (%pv)	Resistivity index	Sat. Exp. n	Corrected Sat. Exp. n *
12	2174.20	2.662	1.05	17.2	100.0	1.00	-	-
					74.6	1.88	2.15	2.53
					71.0	1.95	1.95	2.33
					62.4	2.24	1.71	2.11
					55.8	2.69	1.70	2.11
					44.2	3.82	1.64	2.09
					Average Exponent		1.83	2.24

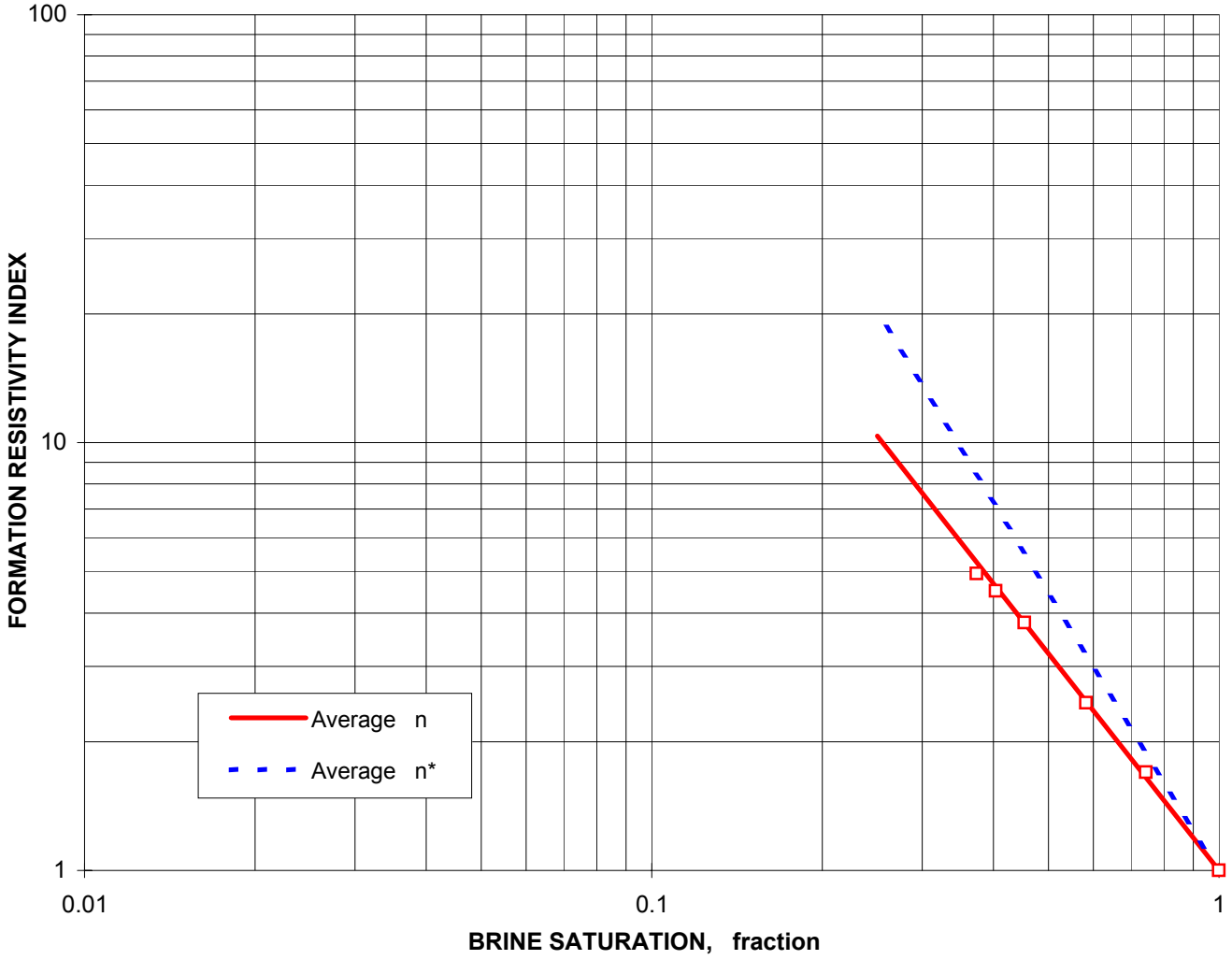
FRF at NOBP	29.88
CEC (meq / 100gm)	3.25
FRF * at NOBP	42.68
Rw at 25°C, ohm-m	0.4150



Formation resistivity index at NOBP.

Sample No.	Depth (metres)	Grain density (gm/cc)	Determined at 1890 psi NOBP					
			Perm. to air (md)	Porosity (%)	Brine saturation (%pv)	Resistivity index	Sat. Exp. n	Corrected Sat. Exp. n *
27	2179.50	2.680	2.63	17.9	100.0	1.00	-	-
					74.3	1.69	1.78	2.20
					58.3	2.47	1.67	2.13
					45.4	3.80	1.69	2.18
					40.4	4.50	1.66	2.16
					37.4	4.93	1.62	2.13
						Average Exponent	1.69	2.16

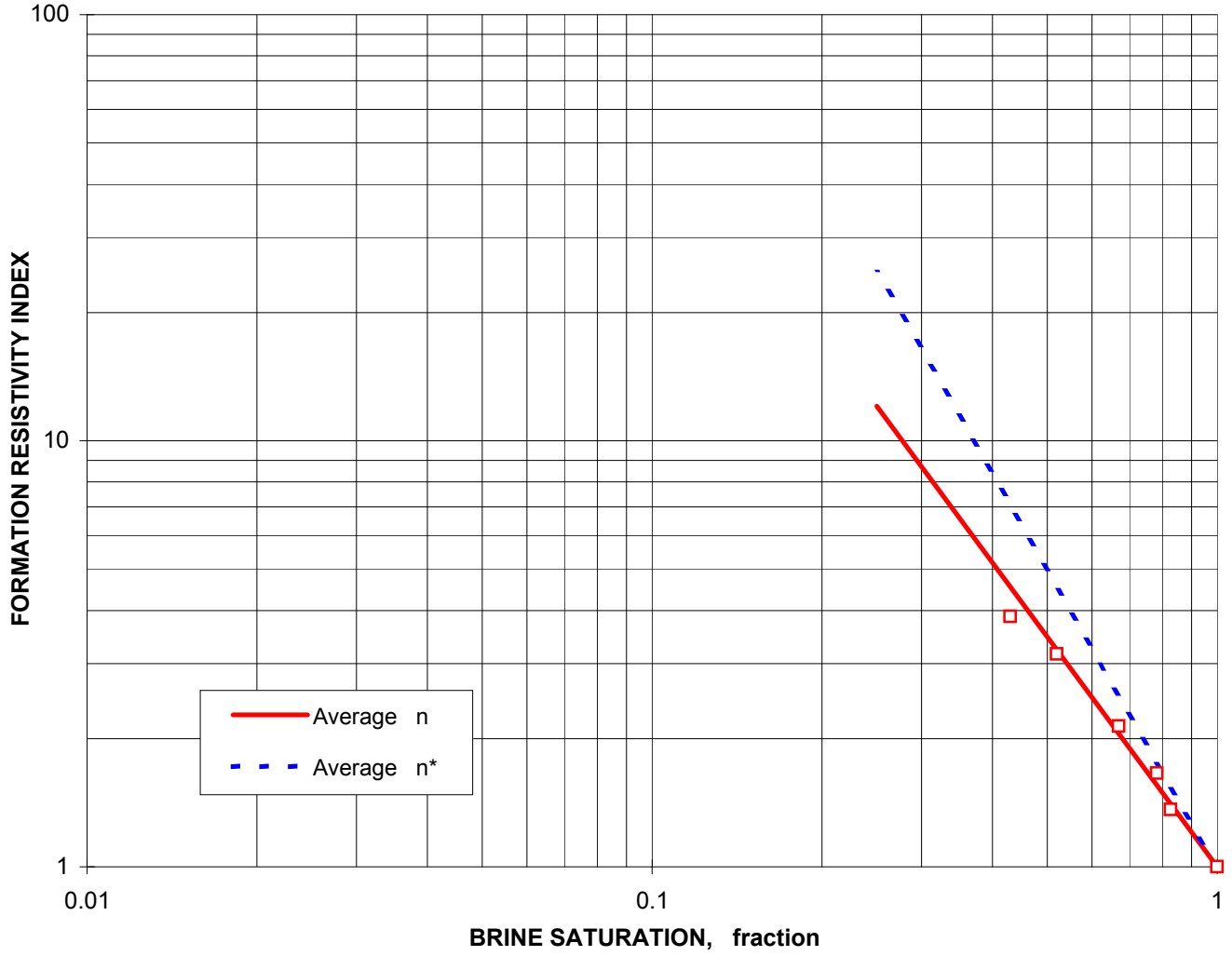
FRF at NOBP	25.05
CEC (meq / 100gm)	3.83
FRF * at NOBP	40.90
Rw at 25°C, ohm-m	0.4150



Formation resistivity index at NOBP.

Sample No.	Depth (metres)	Grain density (gm/cc)	Determined at 1890 psi NOBP					
			Perm. to air (md)	Porosity (%)	Brine saturation (%pv)	Resistivity index	Sat. Exp. n	Corrected Sat. Exp. n *
44	2185.55	2.705	0.509	14.9	100.0	1.00	-	-
					82.8	1.36	1.64	2.13
					78.3	1.66	2.06	2.56
					67.0	2.14	1.90	2.41
					52.0	3.16	1.76	2.30
					43.1	3.87	1.61	2.18
						Average Exponent	1.79	2.32

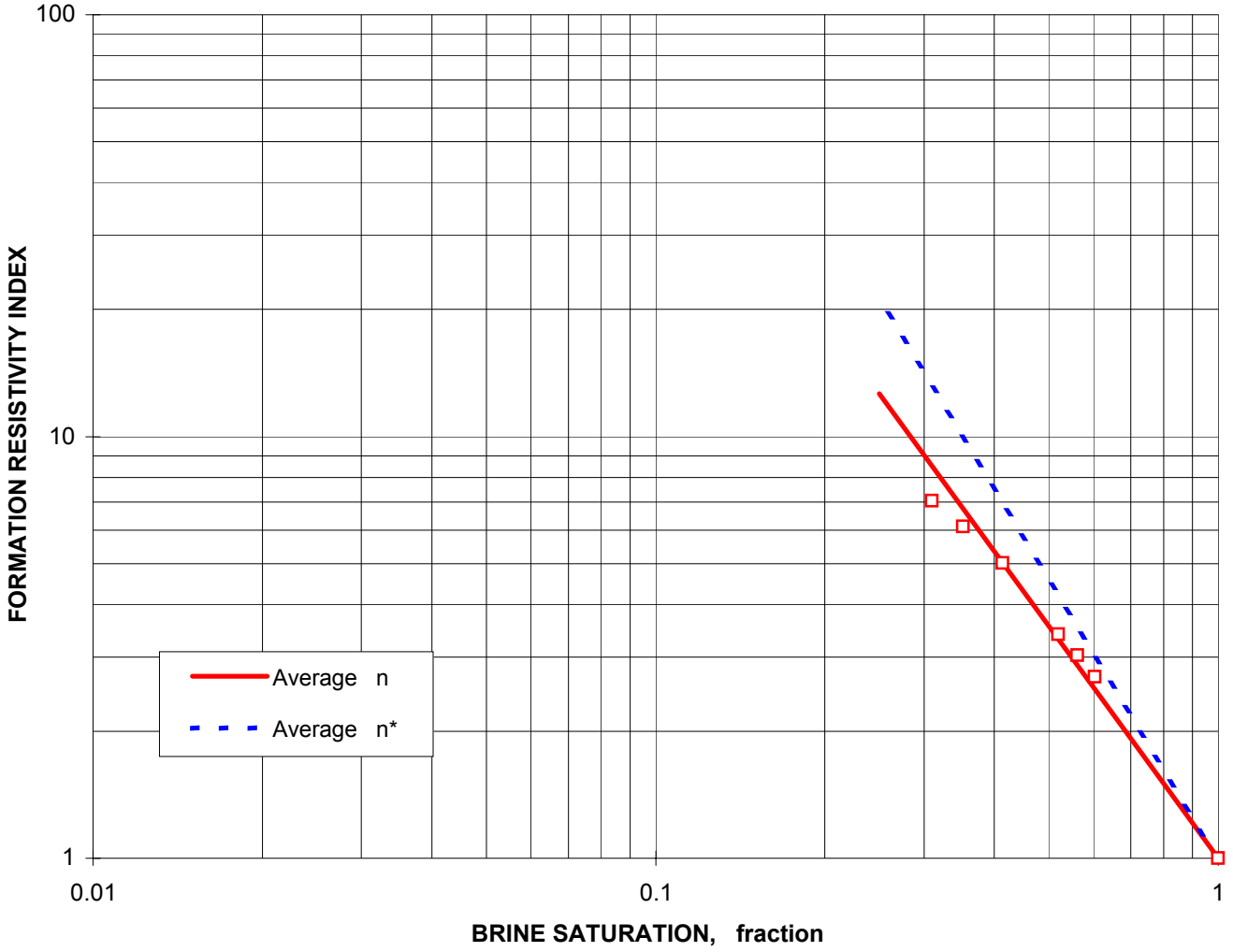
FRF at NOBP	32.51
CEC (meq / 100gm)	4.17
FRF * at NOBP	60.64
Rw at 25°C, ohm-m	0.4150



Formation resistivity index at NOBP.

Sample No.	Depth (metres)	Grain density (gm/cc)	Determined at 1890 psi NOBP					
			Perm. to air (md)	Porosity (%)	Brine saturation (%pv)	Resistivity index	Sat. Exp. n	Corrected Sat. Exp. n *
76	2196.75	2.730	5.77	20.7	100.0	1.00	-	-
					60.3	2.69	1.96	2.29
					56.2	3.03	1.92	2.26
					52.0	3.40	1.87	2.22
					41.4	5.01	1.83	2.20
					35.2	6.11	1.73	2.13
					31.0	7.03	1.66	2.07
					Average Exponent		1.83	2.20

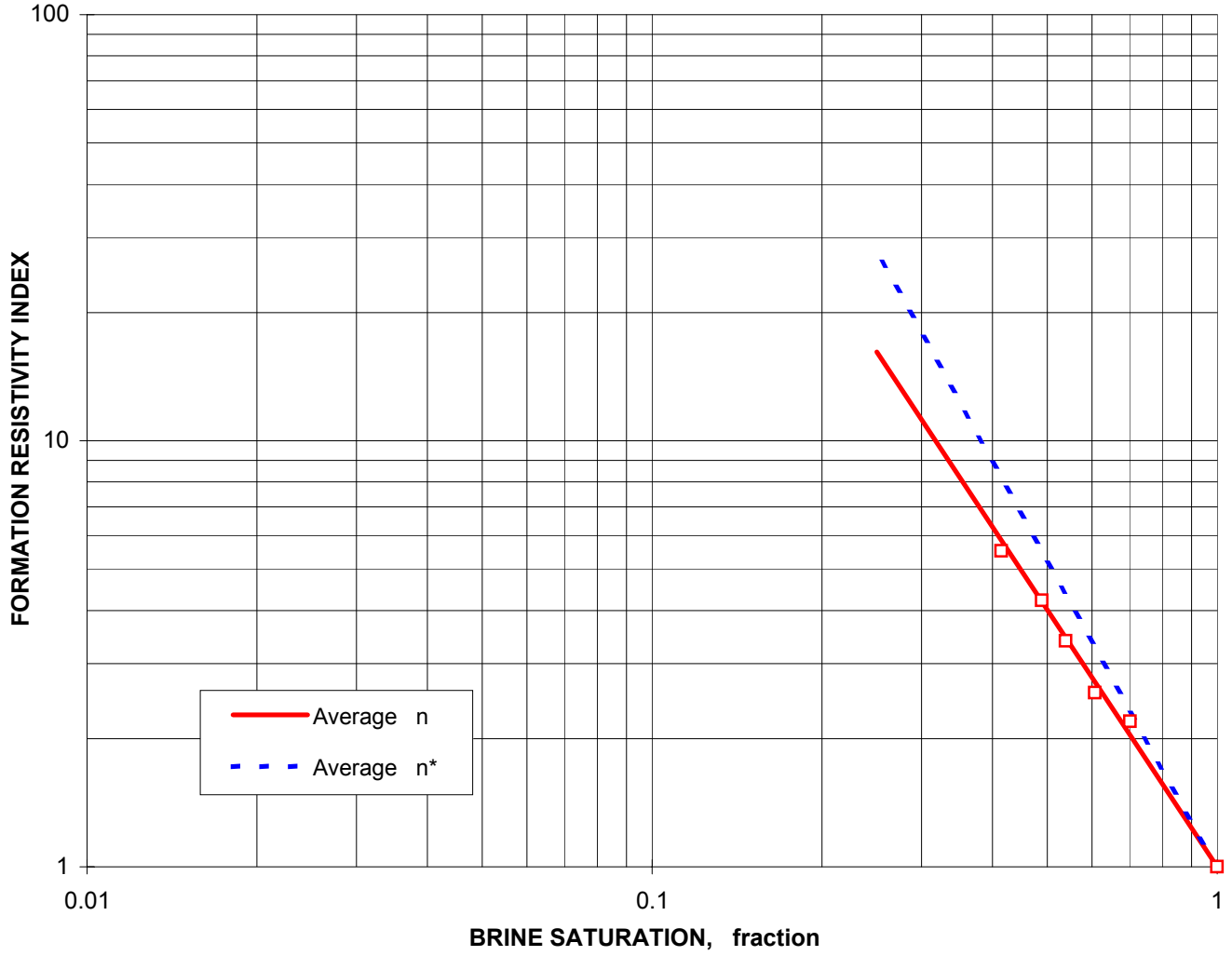
FRF at NOBP	21.23
CEC (meq / 100gm)	2.73
FRF * at NOBP	29.34
Rw at 25°C, ohm-m	0.4150



Formation resistivity index at NOBP.

Sample No.	Depth (metres)	Grain density (gm/cc)	Determined at 1960 psi NOBP					
			Perm. to air (md)	Porosity (%)	Brine saturation (%pv)	Resistivity index	Sat. Exp. n	Corrected Sat. Exp. n *
93	2206.55	2.694	7.22	17.3	100.0	1.00	-	-
					70.1	2.19	2.21	2.56
					60.8	2.56	1.89	2.26
					53.9	3.39	1.98	2.36
					49.0	4.21	2.01	2.41
					41.5	5.50	1.94	2.35
					Average Exponent		2.01	2.39

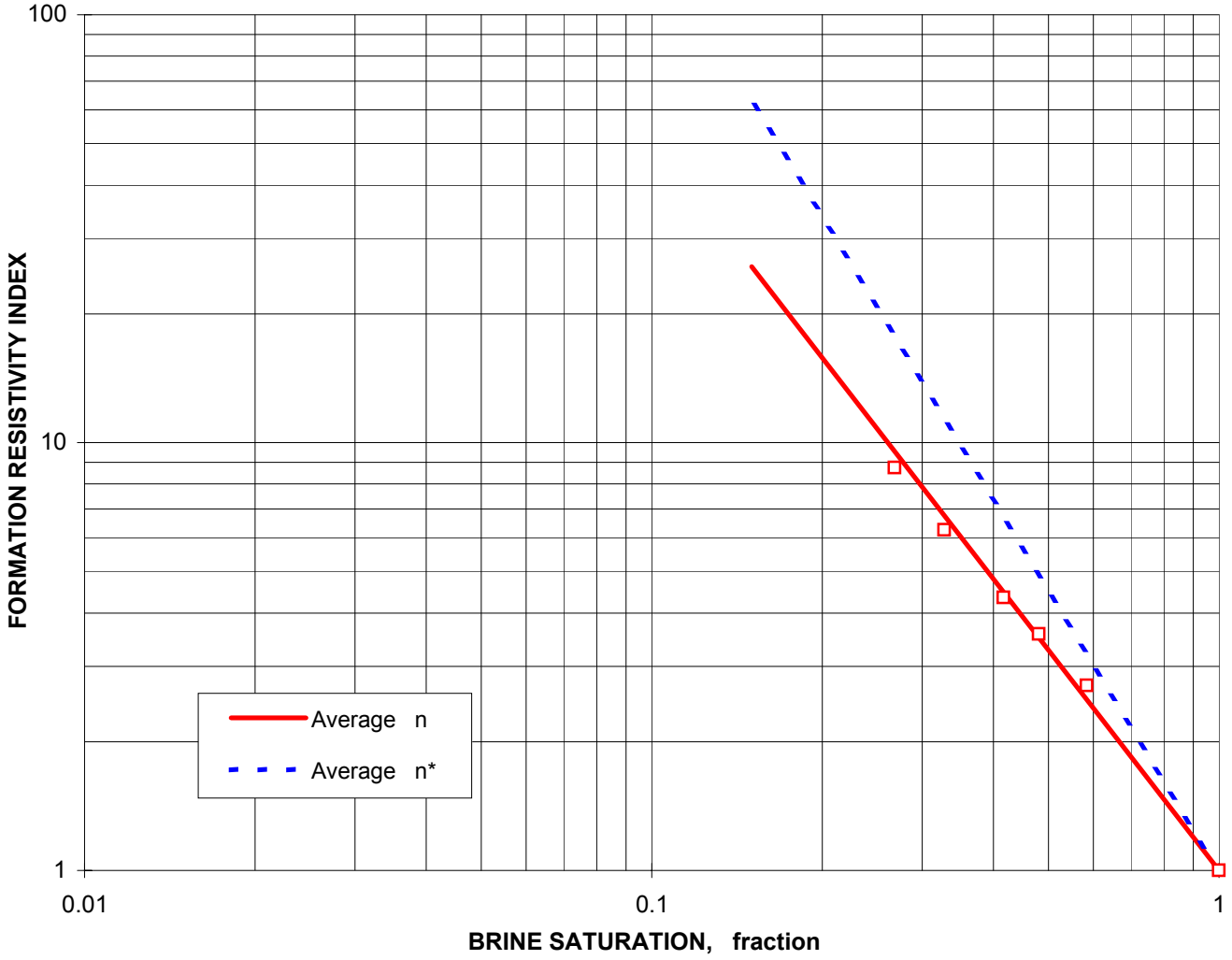
FRF at NOBP	26.60
CEC (meq / 100gm)	2.61
FRF * at NOBP	38.62
Rw at 25°C, ohm-m	0.4150



Formation resistivity index at NOBP.

Sample No.	Depth (metres)	Grain density (gm/cc)	Determined at 1960 psi NOBP					
			Perm. to air (md)	Porosity (%)	Brine saturation (%pv)	Resistivity index	Sat. Exp. n	Corrected Sat. Exp. n *
97	2207.84	2.898	23.4	21.6	100.0	1.00	-	-
					58.5	2.70	1.86	2.27
					48.1	3.57	1.74	2.18
					41.7	4.34	1.68	2.14
					32.8	6.25	1.64	2.13
					26.8	8.73	1.65	2.16
					Average Exponent		1.71	2.18

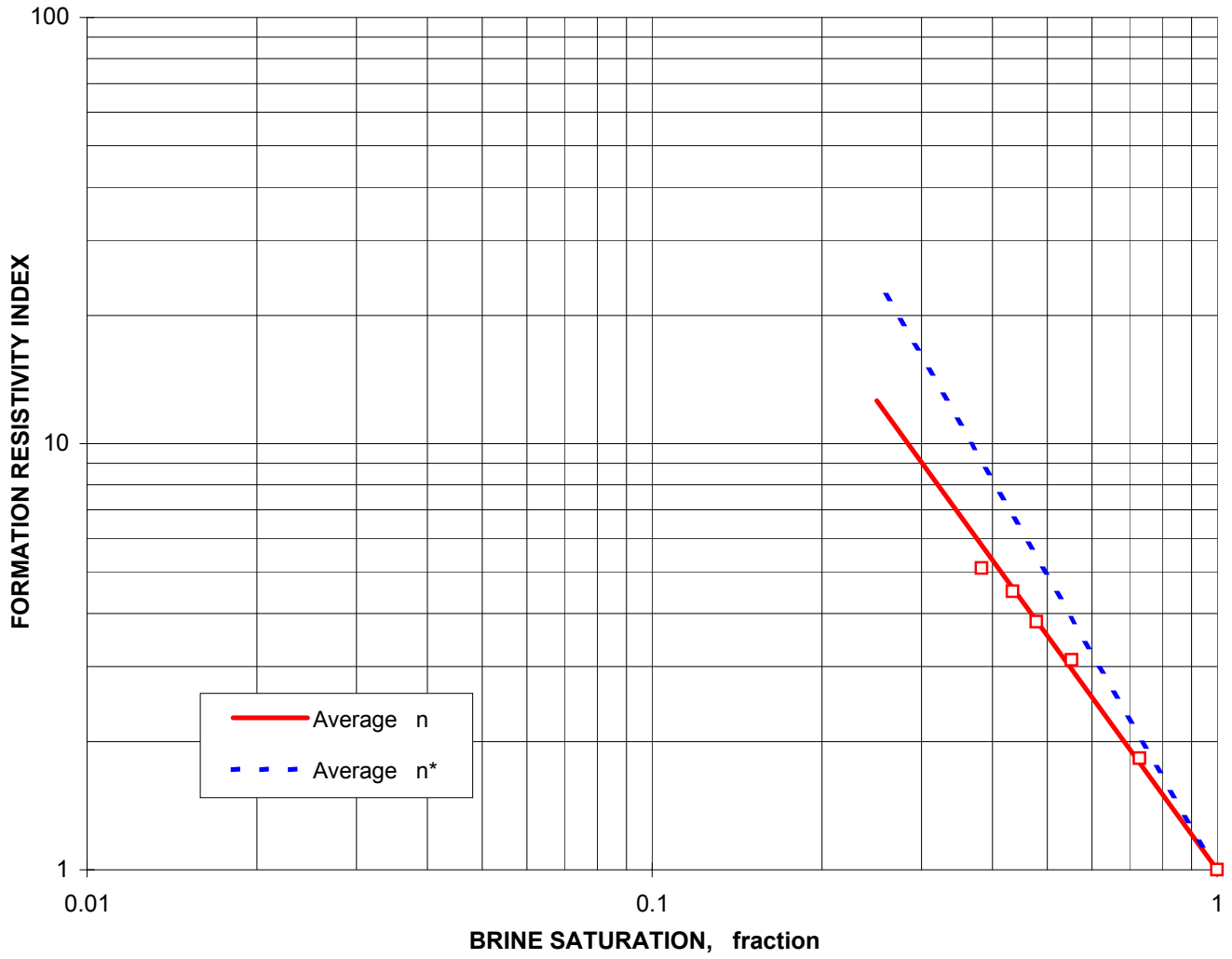
FRF at NOBP	19.85
CEC (meq / 100gm)	3.88
FRF * at NOBP	30.82
Rw at 25°C, ohm-m	0.4150



Formation resistivity index at NOBP.

Sample No.	Depth (metres)	Grain density (gm/cc)	Determined at 1960 psi NOBP					
			Perm. to air (md)	Porosity (%)	Brine saturation (%pv)	Resistivity index	Sat. Exp. n	Corrected Sat. Exp. n *
118	2215.15	2.652	3.04	14.5	100.0	1.00	-	-
					72.8	1.83	1.90	2.32
					55.2	3.11	1.91	2.36
					47.9	3.82	1.82	2.30
					43.5	4.50	1.81	2.29
					38.3	5.10	1.70	2.20
					Average Exponent		1.83	2.29

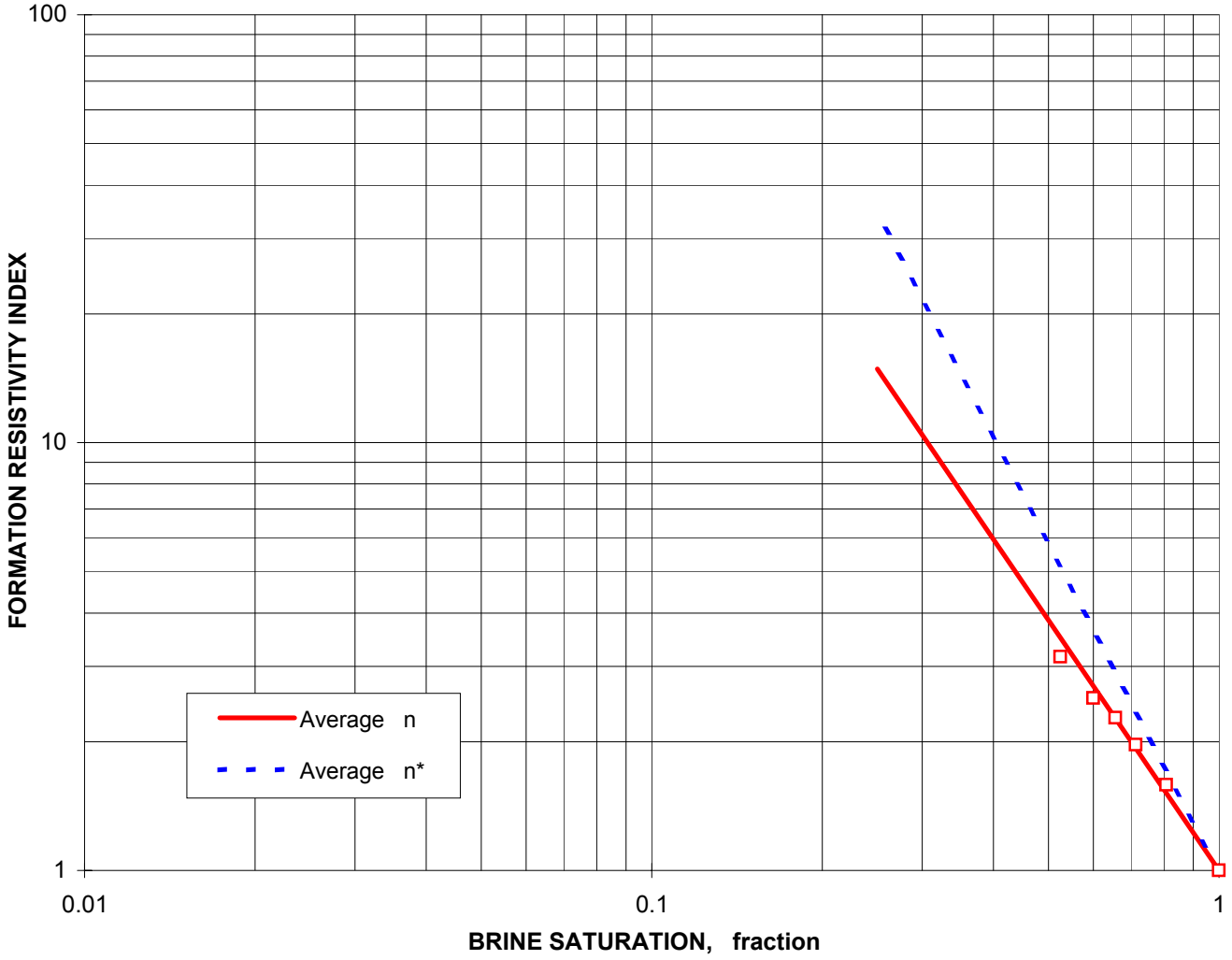
FRF at NOBP	31.90
CEC (meq / 100gm)	2.96
FRF * at NOBP	51.75
Rw at 25°C, ohm-m	0.4150



Formation resistivity index at NOBP.

Sample No.	Depth (metres)	Grain density (gm/cc)	Determined at 1960 psi NOBP					
			Perm. to air (md)	Porosity (%)	Brine saturation (%pv)	Resistivity index	Sat. Exp. n	Corrected Sat. Exp. n *
128	2218.40	2.659	0.256	11.2	100.0	1.00	-	-
					80.8	1.58	2.15	2.73
					71.4	1.97	2.01	2.60
					65.8	2.27	1.96	2.56
					60.1	2.53	1.82	2.43
					52.6	3.16	1.79	2.41
					Average Exponent		1.95	2.54

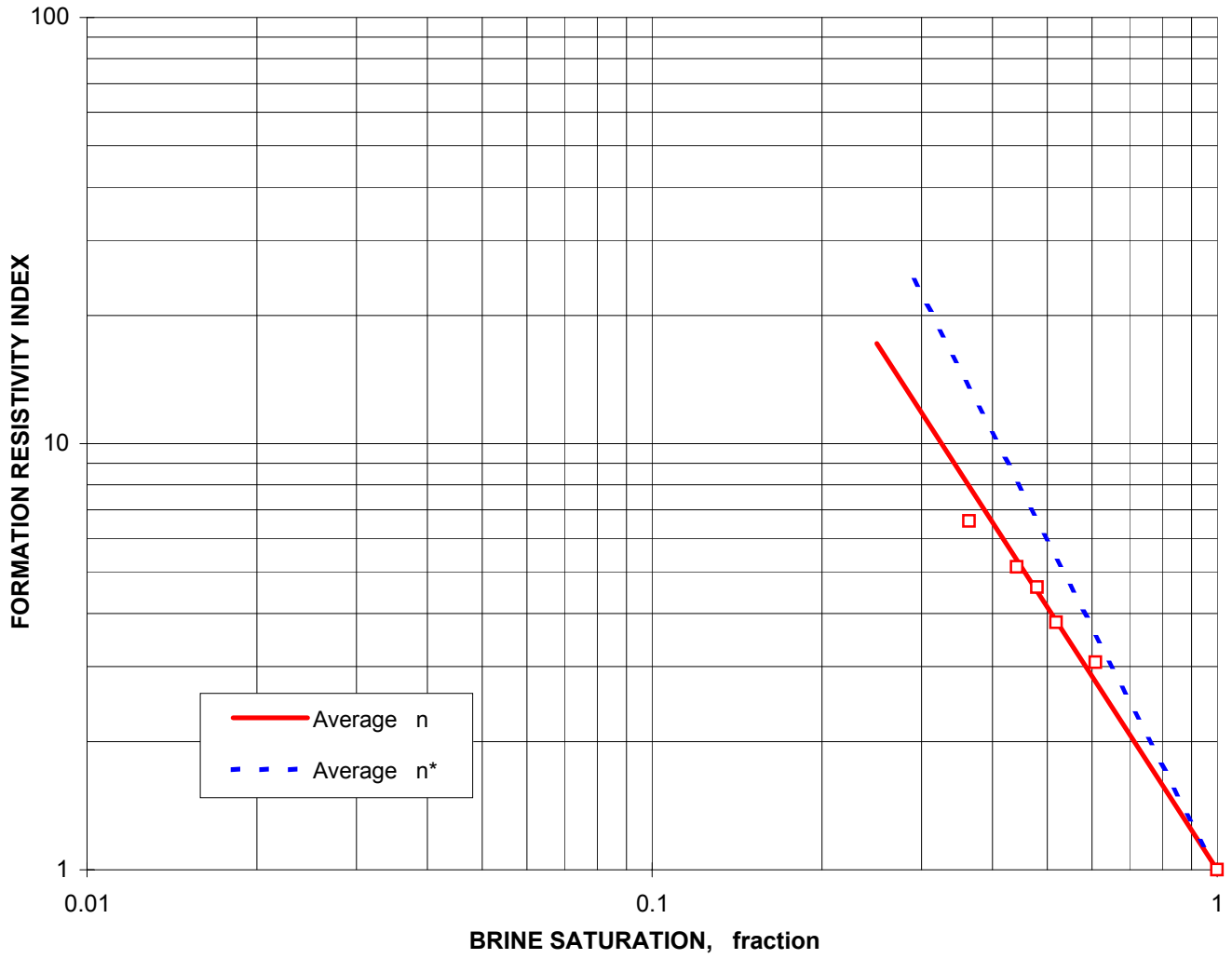
FRF at NOBP	48.59
CEC (meq / 100gm)	4.26
FRF * at NOBP	107.26
Rw at 25°C, ohm-m	0.4150



Formation resistivity index at NOBP.

Sample No.	Depth (metres)	Grain density (gm/cc)	Determined at 1960 psi NOBP					
			Perm. to air (md)	Porosity (%)	Brine saturation (%pv)	Resistivity index	Sat. Exp. n	Corrected Sat. Exp. n *
146	2225.12	2.701	1.62	15.1	100.0	1.00	-	-
					61.0	3.07	2.27	2.75
					51.9	3.81	2.04	2.55
					48.1	4.60	2.08	2.60
					44.2	5.14	2.00	2.53
					36.4	6.57	1.86	2.42
					Average Exponent		2.05	2.57

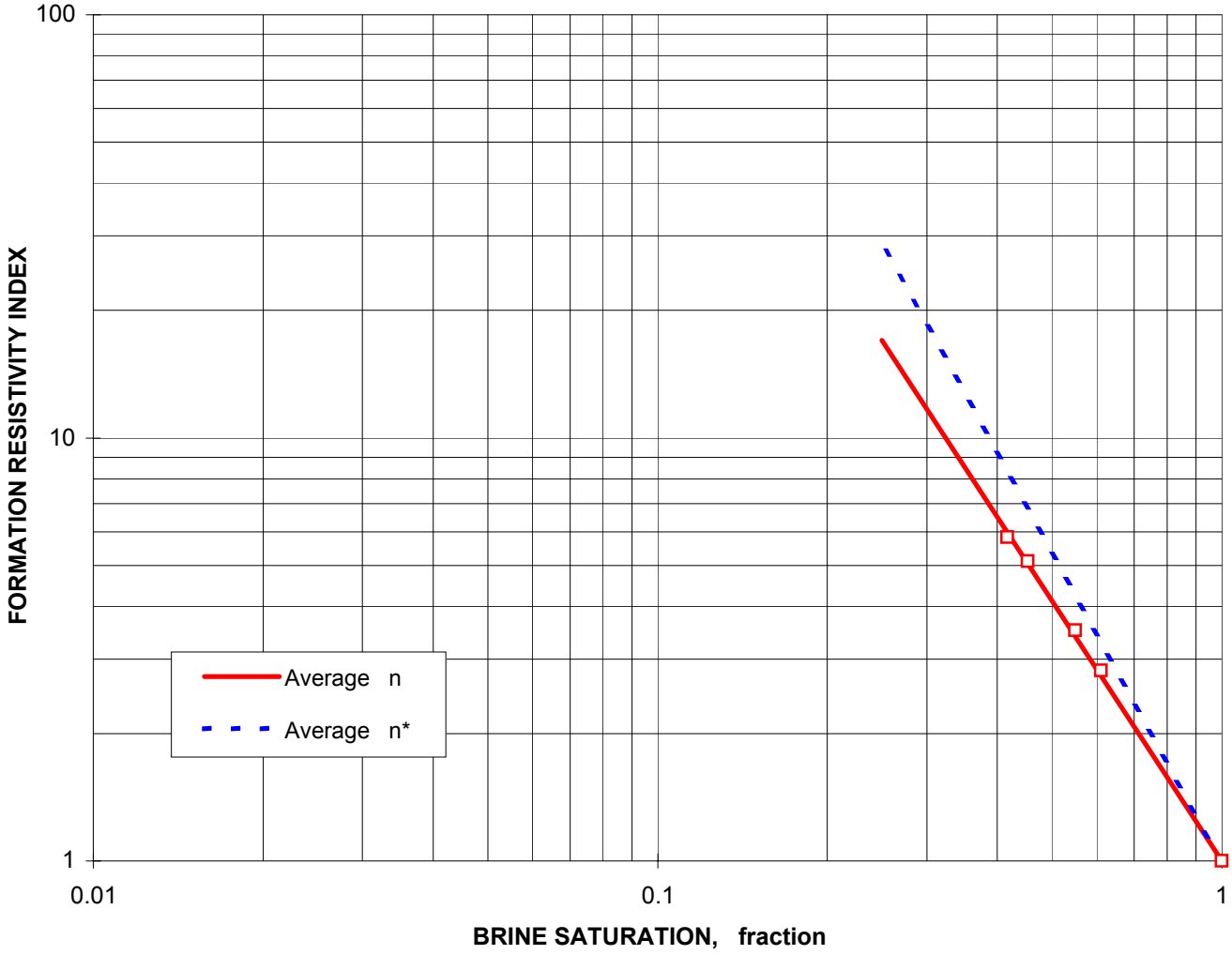
FRF at NOBP	30.68
CEC (meq / 100gm)	3.64
FRF * at NOBP	53.51
Rw at 25°C, ohm-m	0.4150



Formation resistivity index at NOBP.

Sample No.	Depth (metres)	Grain density (gm/cc)	Determined at 1960 psi NOBP					
			Perm. to air (md)	Porosity (%)	Brine saturation (%pv)	Resistivity index	Sat. Exp. n	Corrected Sat. Exp. n *
181	2249.85	2.661	8.16	19.1	100.0	1.00	-	-
					61.1	2.82	2.10	2.44
					55.0	3.51	2.10	2.46
					45.3	5.11	2.06	2.44
					41.7	5.82	2.01	2.40
					34.4	8.01	1.95	2.36
					Average Exponent		2.04	2.42

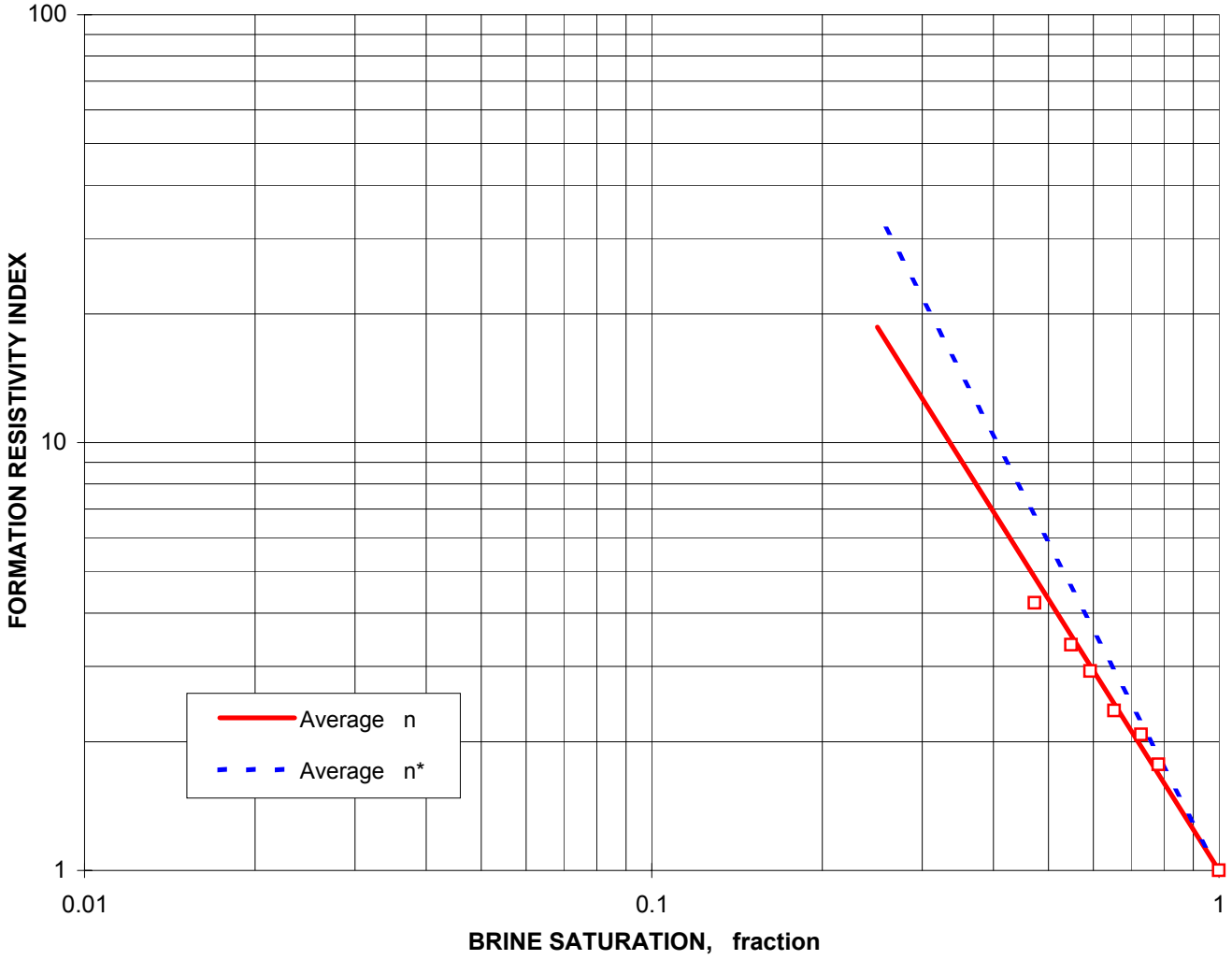
FRF at NOBP	21.74
CEC (meq / 100gm)	2.67
FRF * at NOBP	30.48
Rw at 25°C, ohm-m	0.4150



Formation resistivity index at NOBP.

Sample No.	Depth (metres)	Grain density (gm/cc)	Determined at 1960 psi NOBP					
			Perm. to air (md)	Porosity (%)	Brine saturation (%pv)	Resistivity index	Sat. Exp. n	Corrected Sat. Exp. n *
186	2251.20	2.760	0.650	14.3	100.0	1.00	-	-
					78.2	1.77	2.32	2.73
					72.9	2.07	2.31	2.73
					65.4	2.36	2.02	2.46
					59.4	2.93	2.06	2.51
					54.9	3.37	2.02	2.48
					47.3	4.22	1.93	2.40
					Average Exponent		2.11	2.55

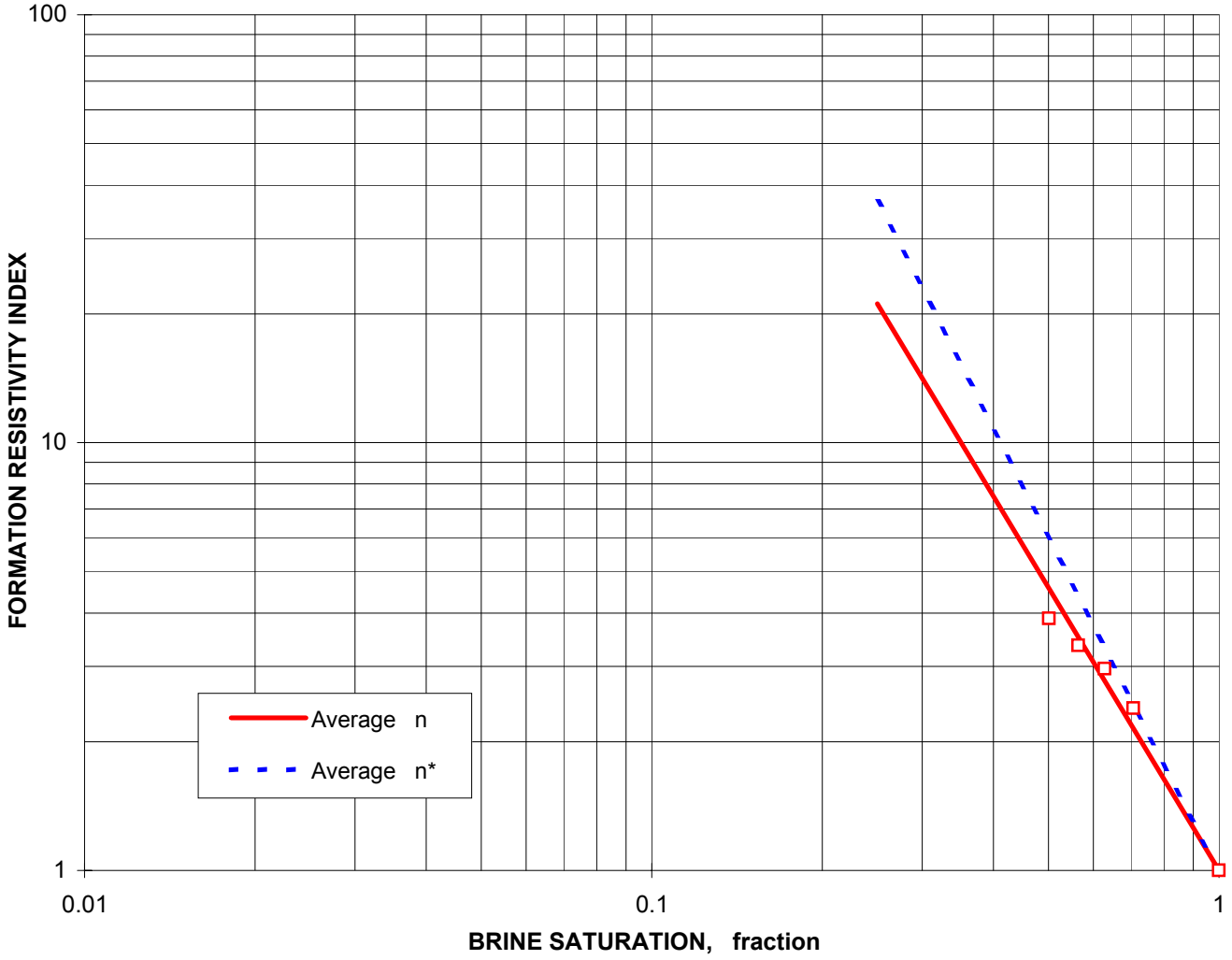
FRF at NOBP	34.62
CEC (meq / 100gm)	2.81
FRF * at NOBP	57.35
Rw at 25°C, ohm-m	0.4150



Formation resistivity index at NOBP.

Sample No.	Depth (metres)	Grain density (gm/cc)	Determined at 1960 psi NOBP					
			Perm. to air (md)	Porosity (%)	Brine saturation (%pv)	Resistivity index	Sat. Exp. n	Corrected Sat. Exp. n *
187	2251.59	2.779	0.936	16.5	100.0	1.00	-	-
					70.6	2.39	2.51	2.88
					62.9	2.96	2.34	2.73
					56.6	3.36	2.13	2.52
					50.2	3.88	1.96	2.37
					45.1	5.14	2.05	2.48
					Average Exponent		2.20	2.59

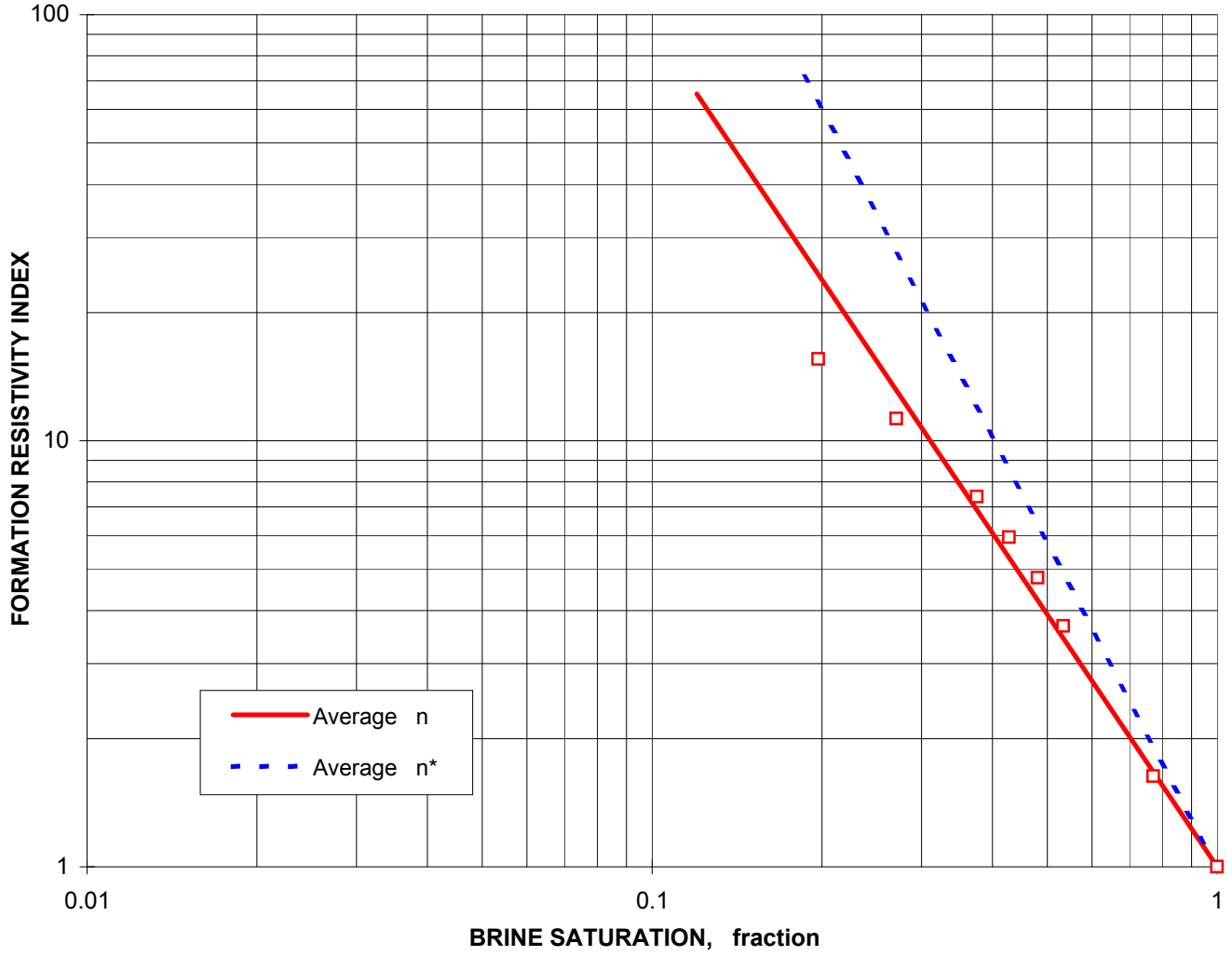
FRF at NOBP	26.27
CEC (meq / 100gm)	2.58
FRF * at NOBP	39.13
Rw at 25°C, ohm-m	0.4150



Formation resistivity index at NOBP.

Sample No.	Depth (metres)	Grain density (gm/cc)	Determined at 2030 psi NOBP					
			Perm. to air (md)	Porosity (%)	Brine saturation (%pv)	Resistivity index	Sat. Exp. n	Corrected Sat. Exp. n *
205	2275.17	2.652	179	19.3	100.0	1.00	-	-
					77.1	1.63	1.89	2.37
					53.4	3.67	2.07	2.61
					48.2	4.77	2.14	2.68
					42.9	5.94	2.10	2.66
					37.6	7.39	2.04	2.62
					27.1	11.27	1.85	2.46
					19.7	15.56	1.69	2.33
					Average Exponent		1.97	2.53

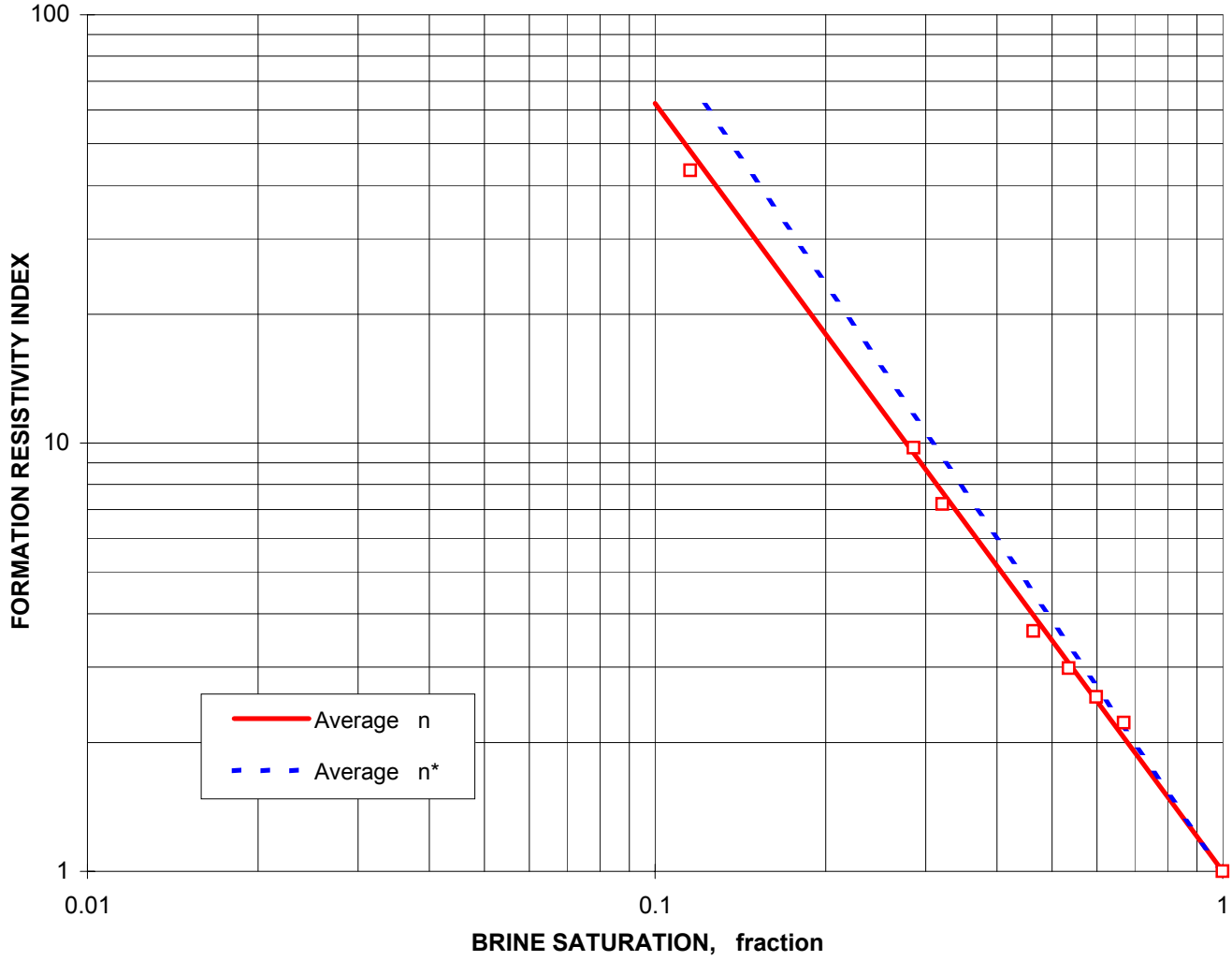
FRF at NOBP	17.47
CEC (meq / 100gm)	5.57
FRF * at NOBP	32.03
Rw at 25°C, ohm-m	0.4150



Formation resistivity index at NOBP.

Sample No.	Depth (metres)	Grain density (gm/cc)	Determined at 2030 psi NOBP					
			Perm. to air (md)	Porosity (%)	Brine saturation (%pv)	Resistivity index	Sat. Exp. n	Corrected Sat. Exp. n *
234	2296.94	2.652	5500	24.1	100.0	1.00	-	-
					67.0	2.22	2.00	2.12
					59.8	2.55	1.83	1.95
					53.6	2.98	1.75	1.88
					46.4	3.63	1.68	1.82
					32.1	7.20	1.74	1.91
					28.5	9.74	1.82	1.99
					11.5	43.30	1.74	2.01
					Average Exponent		1.79	1.96

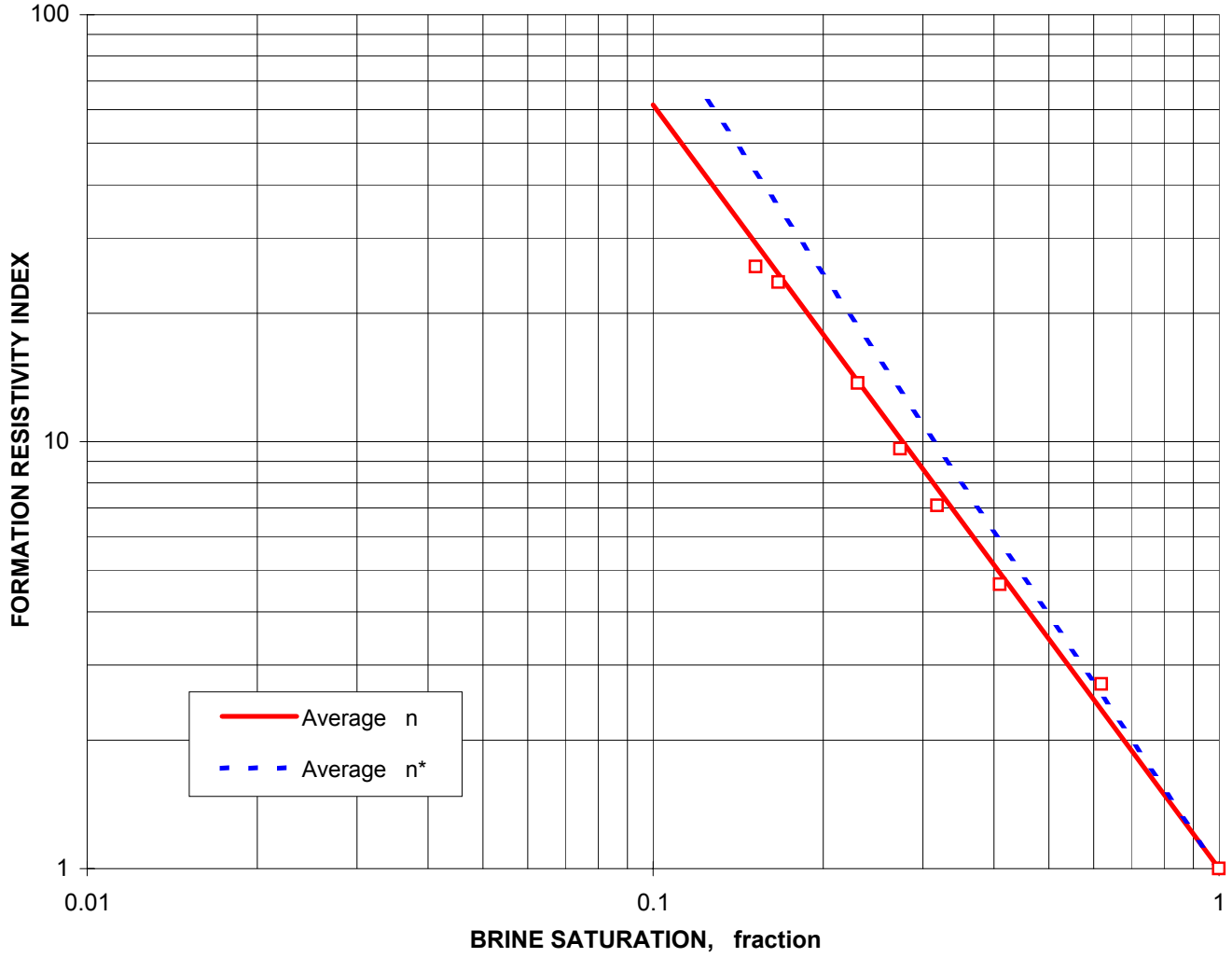
FRF at NOBP	11.71
CEC (meq / 100gm)	1.00
FRF * at NOBP	13.01
Rw at 25°C, ohm-m	0.4150



Formation resistivity index at NOBP.

Sample No.	Depth (metres)	Grain density (gm/cc)	Determined at 2030 psi NOBP					
			Perm. to air (md)	Porosity (%)	Brine saturation (%pv)	Resistivity index	Sat. Exp. n	Corrected Sat. Exp. n *
241	2299.40	2.646	5640	21.2	100.0	1.00	-	-
					62.0	2.70	2.08	2.21
					41.0	4.63	1.72	1.88
					31.8	7.08	1.71	1.89
					27.4	9.62	1.75	1.94
					23.0	13.73	1.78	1.99
					16.6	23.66	1.76	2.01
					15.2	25.71	1.72	1.97
					Average Exponent		1.79	1.99

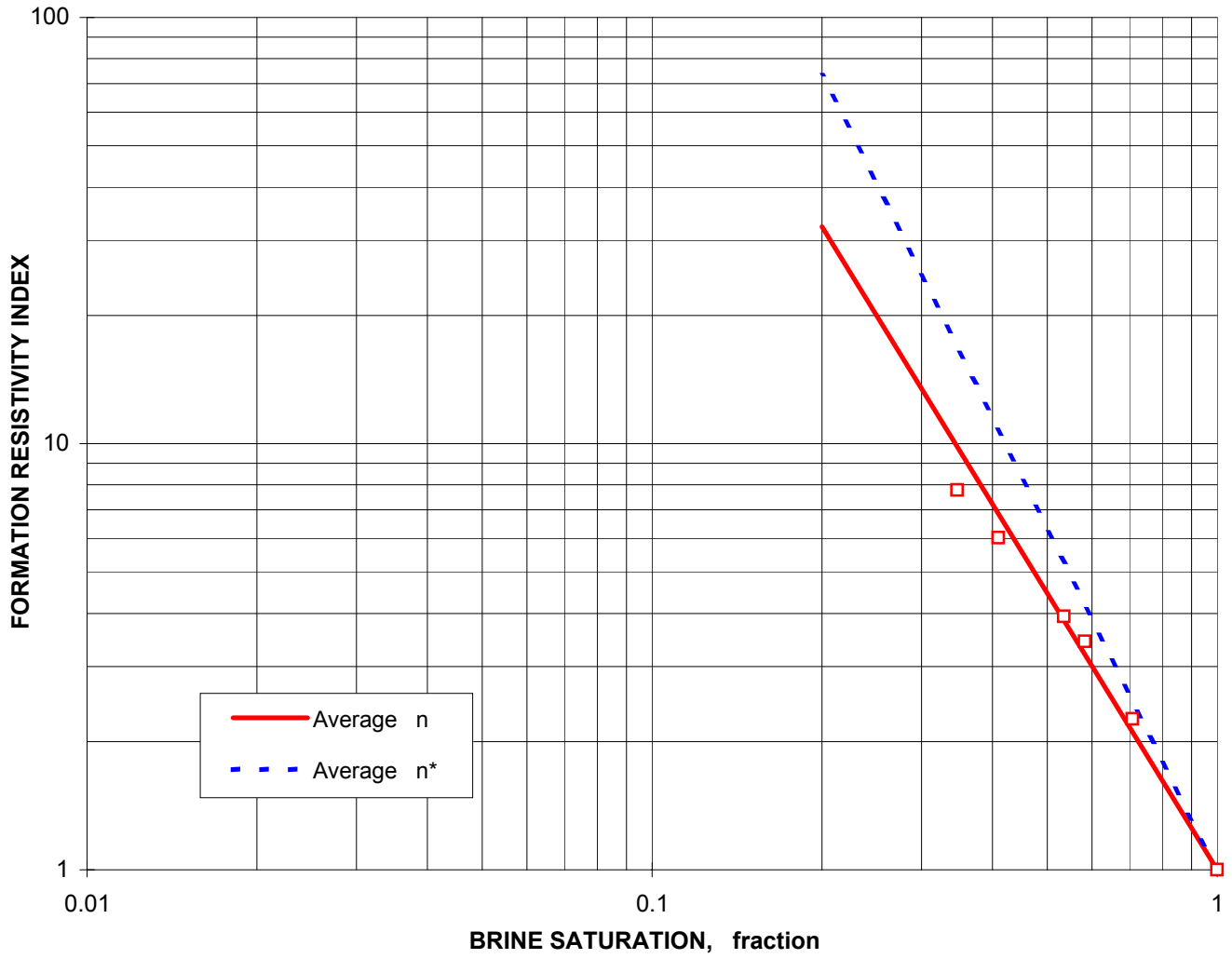
FRF at NOBP	13.97
CEC (meq / 100gm)	0.916
FRF * at NOBP	15.70
Rw at 25°C, ohm-m	0.4150



Formation resistivity index at NOBP.

Sample No.	Depth (metres)	Grain density (gm/cc)	Determined at 2030 psi NOBP					
			Perm. to air (md)	Porosity (%)	Brine saturation (%pv)	Resistivity index	Sat. Exp. n	Corrected Sat. Exp. n *
244	2300.20	2.680	0.704	11.9	100.0	1.00	-	-
					70.9	2.26	2.37	2.83
					58.3	3.43	2.29	2.78
					53.6	3.93	2.19	2.69
					41.0	6.01	2.01	2.54
					34.7	7.79	1.94	2.49
					Average Exponent		2.16	2.67

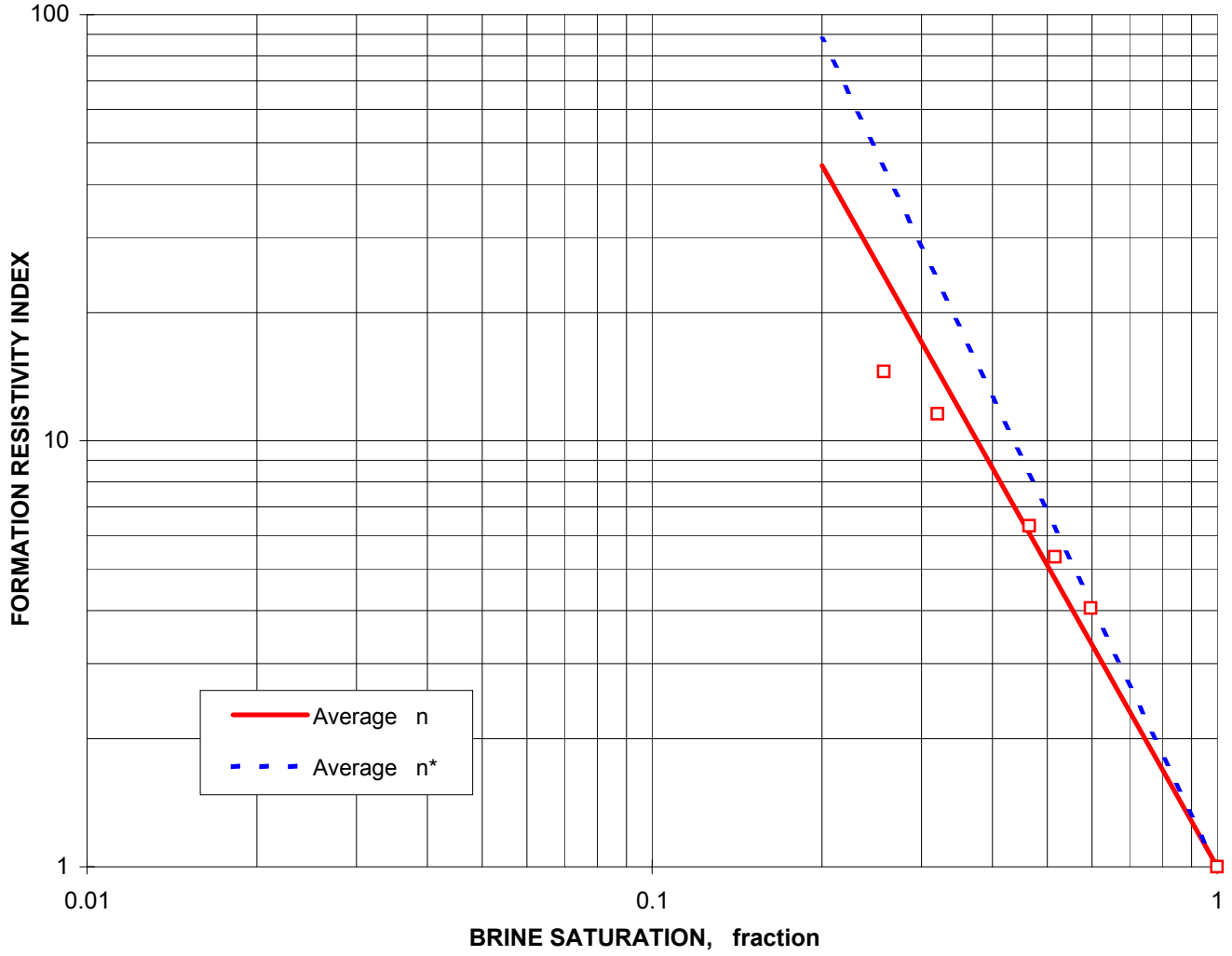
FRF at NOBP	38.13
CEC (meq / 100gm)	2.75
FRF * at NOBP	66.04
Rw at 25°C, ohm-m	0.4150



Formation resistivity index at NOBP.

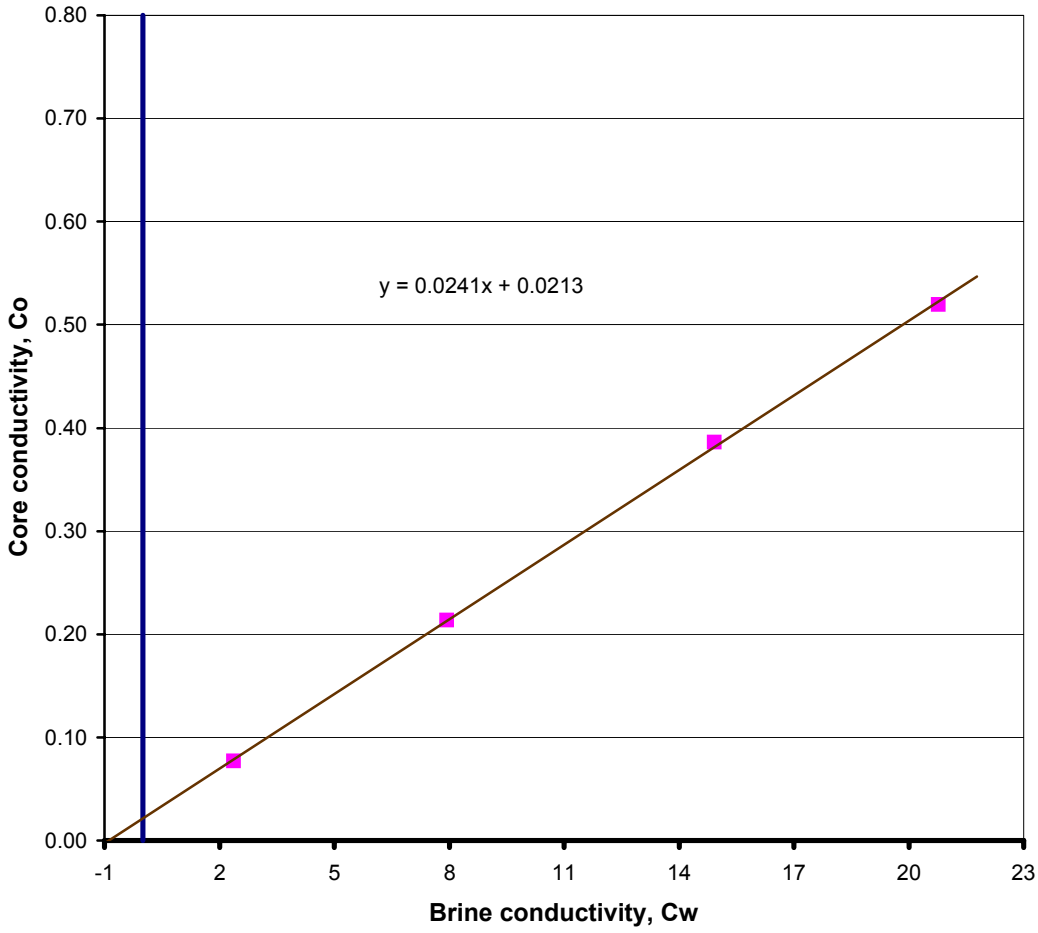
Sample No.	Depth (metres)	Grain density (gm/cc)	Determined at 2030 psi NOBP					
			Perm. to air (md)	Porosity (%)	Brine saturation (%pv)	Resistivity index	Sat. Exp. n	Corrected Sat. Exp. n *
246	2300.80	2.741	8.81	15.5	100.0	1.00	-	-
					59.8	4.04	2.72	3.10
					51.6	5.33	2.53	2.93
					46.6	6.31	2.41	2.82
					32.0	11.55	2.15	2.60
					25.7	14.55	1.97	2.45
					Average Exponent		2.36	2.78

FRF at NOBP	25.82
CEC (meq / 100gm)	2.34
FRF * at NOBP	37.92
Rw at 25°C, ohm-m	0.4150



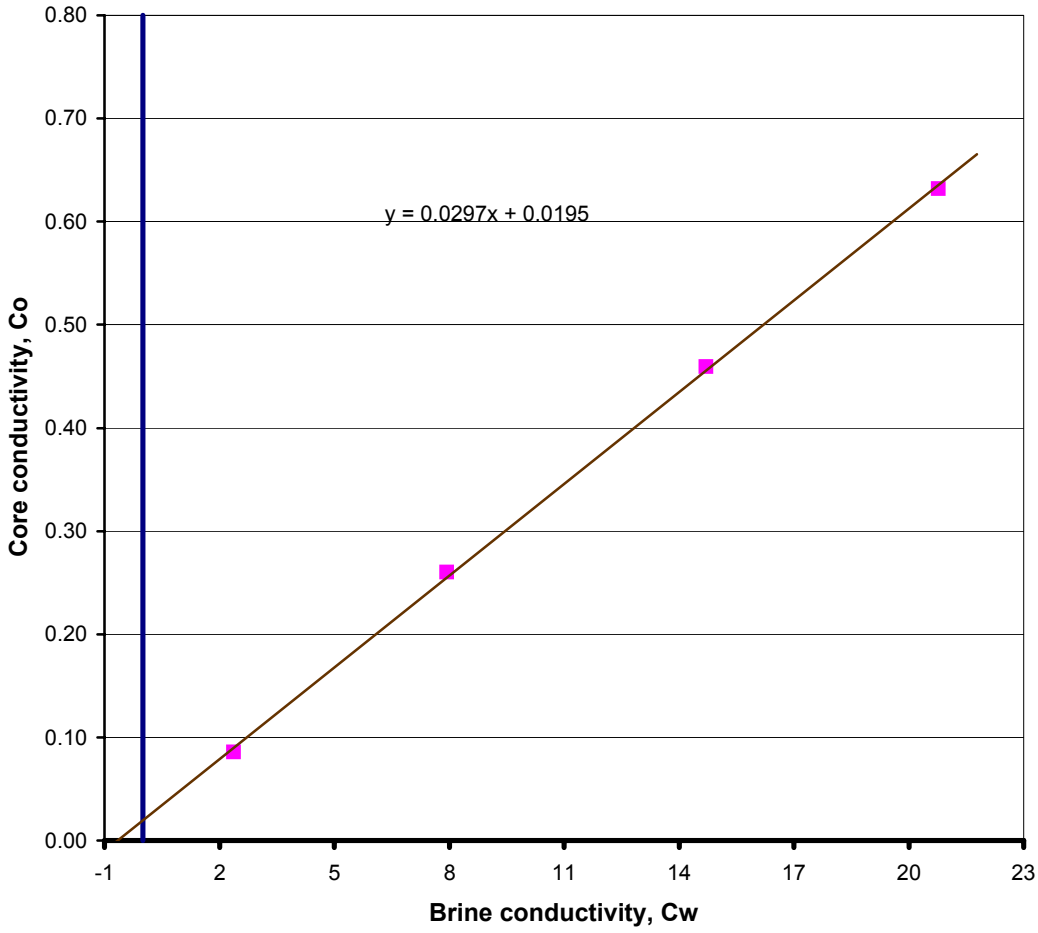
Determination of BQv by multiple salinity (Hoyer and Spann) method.

Sample no.	Depth (m)	At 1890 psi NOB		Grain density (gm/cc)	Brine salinity (ppm)	Conductivity (mho-m)	
		K inf (md)	Porosity (%)			Brine Cw	Core Co
12	2174.20	1.05	17.2	2.662	13.5 K	2.38	0.08
					50 K	7.94	0.21
					110 K	14.93	0.39
					200 K	20.77	0.52
					BQv , (1/ohm-m)		0.881



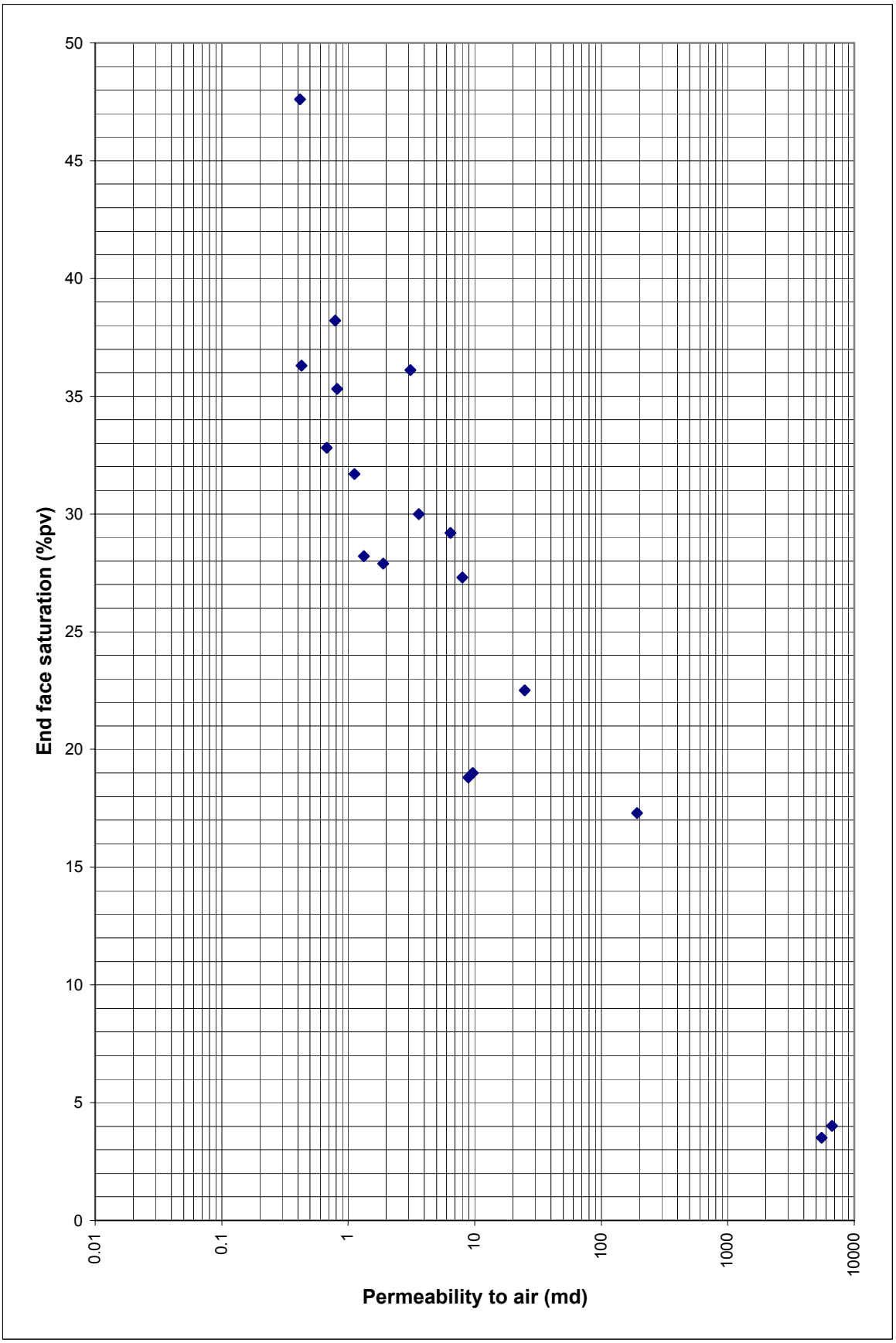
Determination of BQv by multiple salinity (Hoyer and Spann) method.

Sample no.	Depth (m)	At 1960psi NOB		Grain density (gm/cc)	Brine salinity (ppm)	Conductivity (mho-m)	
		K inf (md)	Porosity (%)			Brine Cw	Core Co
93	2206.55	7.22	17.3	2.694	13.5 K	2.38	0.09
					50 K	7.94	0.26
					110 K	14.71	0.46
					200 K	20.77	0.63
					BQv , (1/ohm-m)		0.658



SECTION 3
CAPILLARY PRESSURE

End face saturation (Swi) vs permeability to air



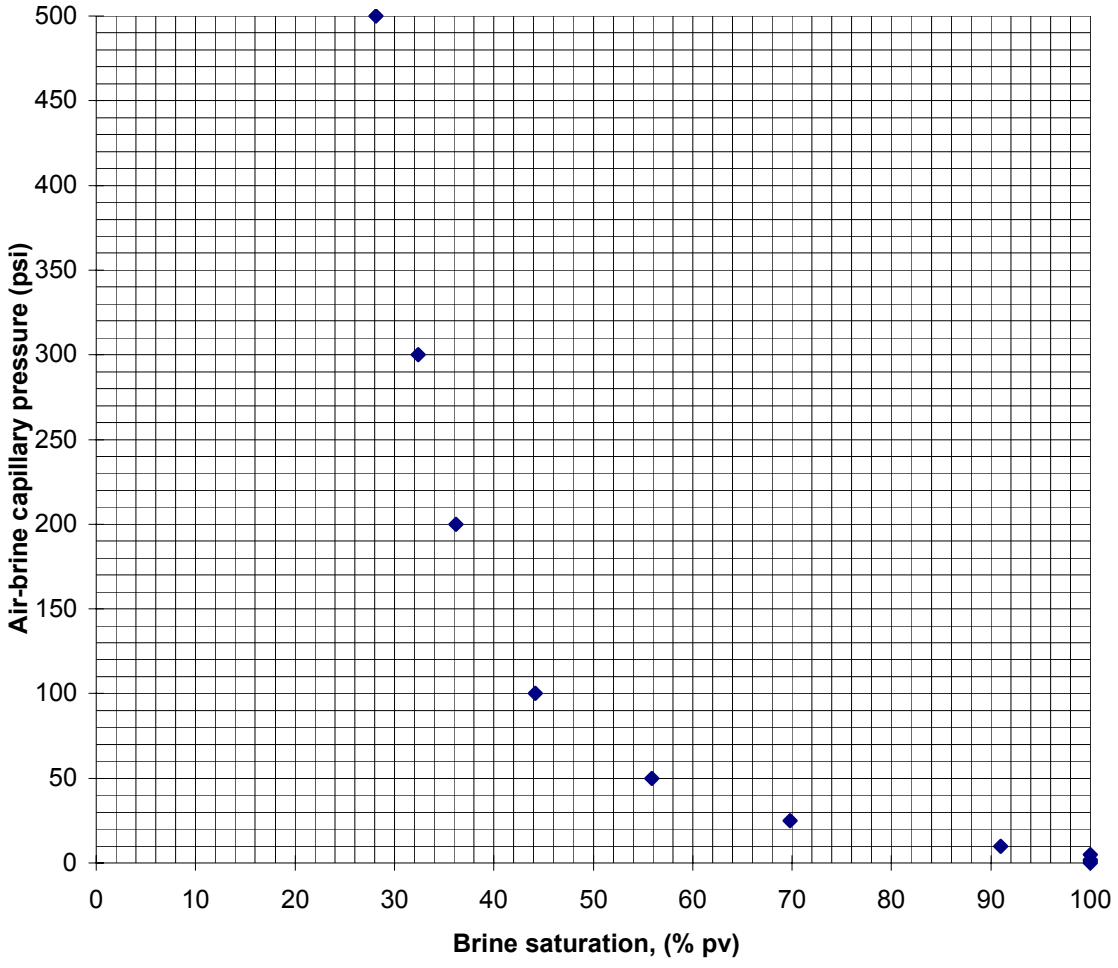
Summary of air-brine capillary pressure at ambient conditions by centrifuge

Sample No.	Depth (m)	Kair (md)	Porosity (%)	AIR - BRINE CAPILLARY PRESSURE (psi)										
				0	1	2	5	10	25	50	100	200	300	500
				END FACE SATURATION Sw (%pv)										
5	2153.10	0.415	13.8	100.0	100.0	100.0	100.0	91.0	69.8	55.9	44.2	36.2	32.4	28.2
12	2174.20	1.33	17.7	100.0	100.0	100.0	100.0	100.0	83.0	72.2	62.9	54.8	50.5	47.6
27	2179.50	3.11	18.4	100.0	100.0	85.2	69.3	58.4	48.9	44.0	40.6	38.2	37.2	36.1
44	2185.55	0.677	15.3	100.0	100.0	100.0	100.0	69.2	56.3	48.2	41.2	37.2	35.1	32.8
76	2196.75	6.44	21.1	100.0	100.0	100.0	81.6	65.4	48.9	39.2	34.0	31.5	30.4	29.2
93	2206.55	7.97	17.8	100.0	100.0	100.0	70.4	60.2	49.0	42.0	35.9	31.0	29.3	27.3
97	2207.84	24.9	22.0	100.0	100.0	73.3	57.8	48.4	38.2	31.9	26.7	24.1	23.3	22.5
118	2215.15	3.60	15.0	100.0	100.0	100.0	100.0	79.1	60.7	48.6	38.4	34.0	32.1	30.0
128	2218.40	0.427	11.6	100.0	100.0	100.0	100.0	85.8	68.2	57.3	48.2	41.2	38.9	36.3
146	2225.12	1.89	15.5	100.0	100.0	100.0	100.0	69.0	55.3	46.7	39.5	33.4	30.3	27.9
181	2249.85	8.87	19.5	100.0	100.0	100.0	76.3	59.2	42.4	34.2	28.6	23.8	21.4	18.8
186	2251.20	0.787	14.7	100.0	100.0	100.0	100.0	82.4	68.8	60.1	52.4	45.7	42.2	38.2
187	2251.59	1.12	16.8	100.0	100.0	100.0	100.0	87.4	68.8	53.8	44.1	36.1	33.4	31.7
205	2275.17	191	19.7	100.0	81.0	64.8	48.2	38.6	28.7	22.2	19.5	18.3	17.8	17.3
234	2296.94	5510	24.7	100.0	43.5	28.9	13.4	7.42	4.59	3.99	3.74	3.51	*	*
241	2299.40	6680	21.8	100.0	38.6	20.3	8.77	5.94	4.54	4.36	4.19	4.02	*	*
244	2300.20	0.816	12.3	100.0	100.0	100.0	100.0	91.7	70.4	56.4	44.5	38.5	36.9	35.3
246	2300.80	9.61	15.8	100.0	100.0	100.0	62.4	42.2	25.2	22.6	21.0	20.0	19.5	19.0

* To preserve sample integrity, maximum capillary pressure limited to 200 psi.

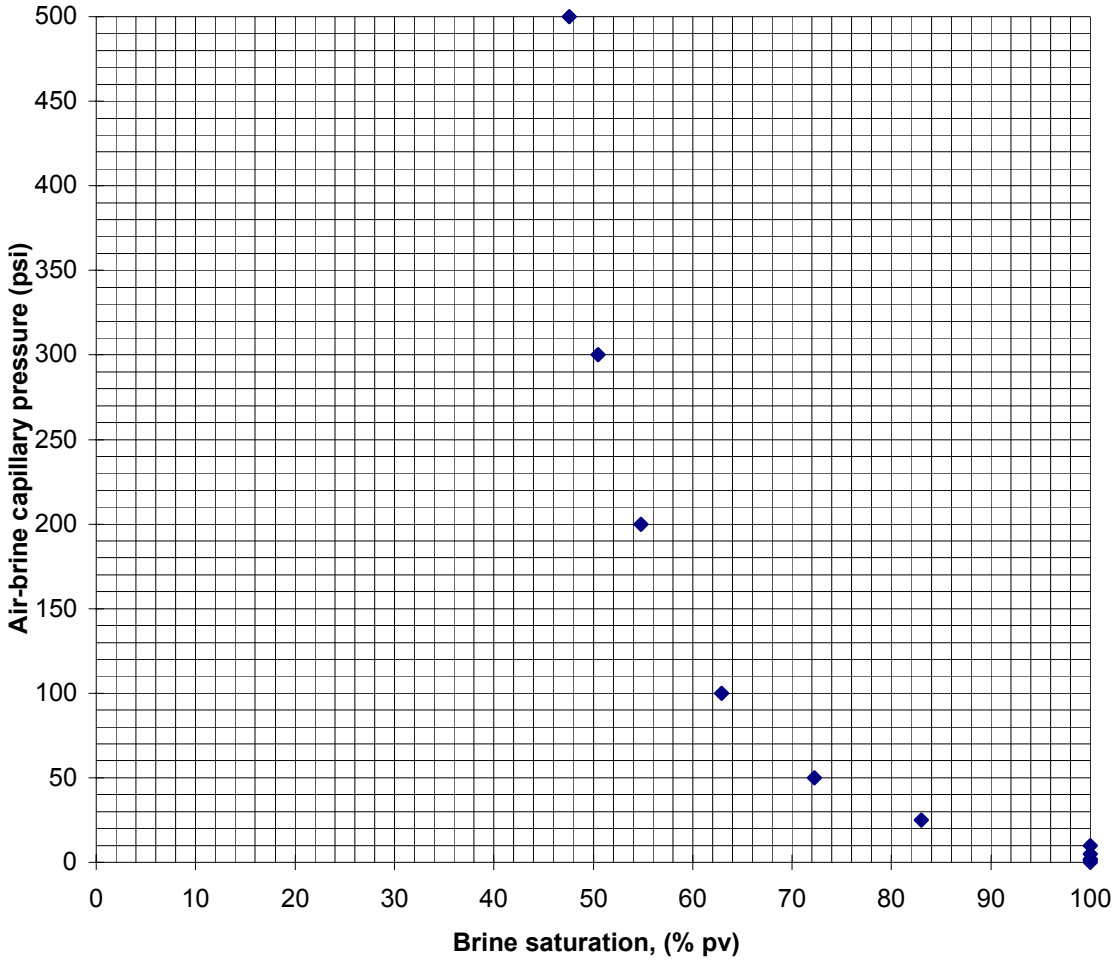
Air-brine capillary pressure by centrifuge at ambient conditions

Sample No.	Depth (m)	Kinf (md)	Kair (md)	Porosity (%)	Capillary pressure (psi)	Brine saturation (%pv)
5	2153.10	0.306	0.415	13.8	0	100.0
					1	100.0
					2	100.0
					5	100.0
					10	91.0
					25	69.8
					50	55.9
					100	44.2
					200	36.2
					300	32.4
					500	28.2



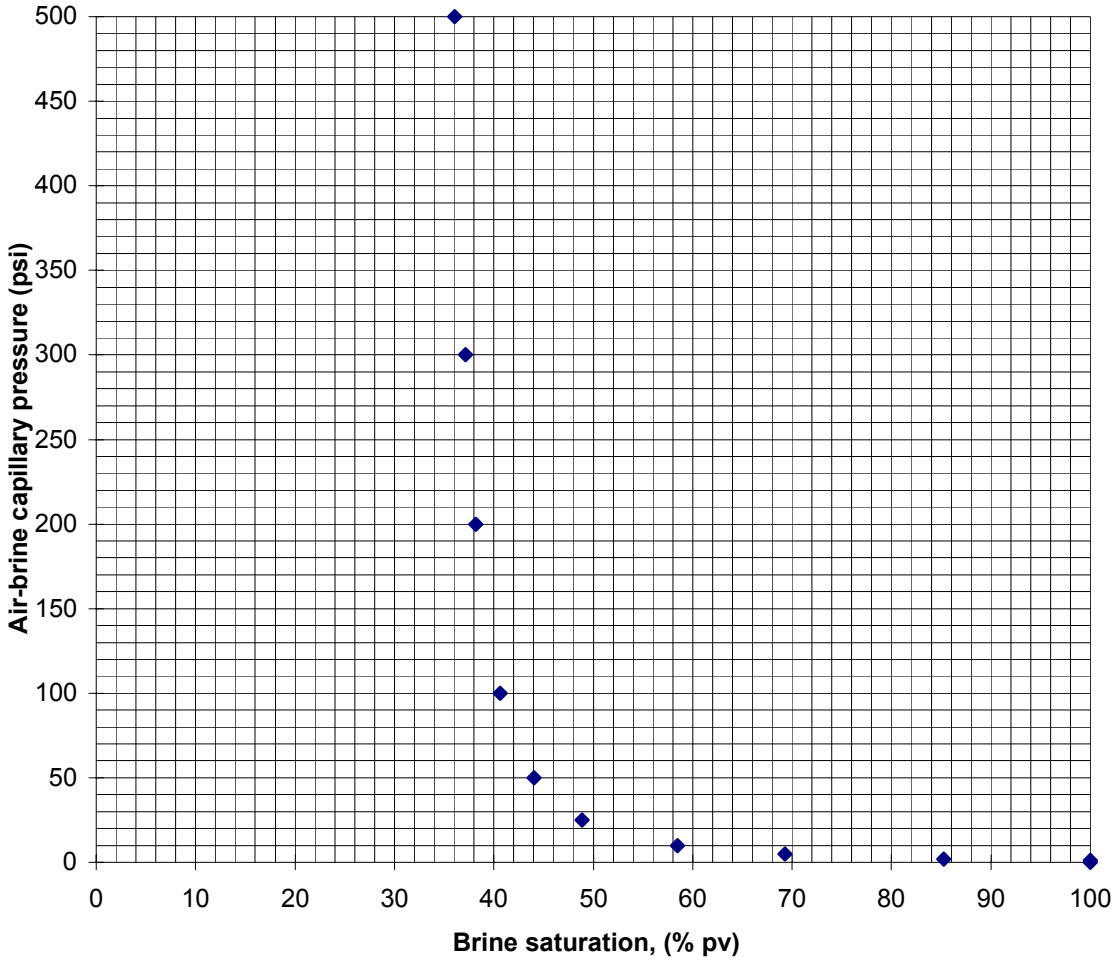
Air-brine capillary pressure by centrifuge at ambient conditions

Sample No.	Depth (m)	Kinf (md)	Kair (md)	Porosity (%)	Capillary pressure (psi)	Brine saturation (%pv)
12	2174.20	0.920	1.330	17.7	0	100.0
					1	100.0
					2	100.0
					5	100.0
					10	100.0
					25	83.0
					50	72.2
					100	62.9
					200	54.8
					300	50.5
					500	47.6



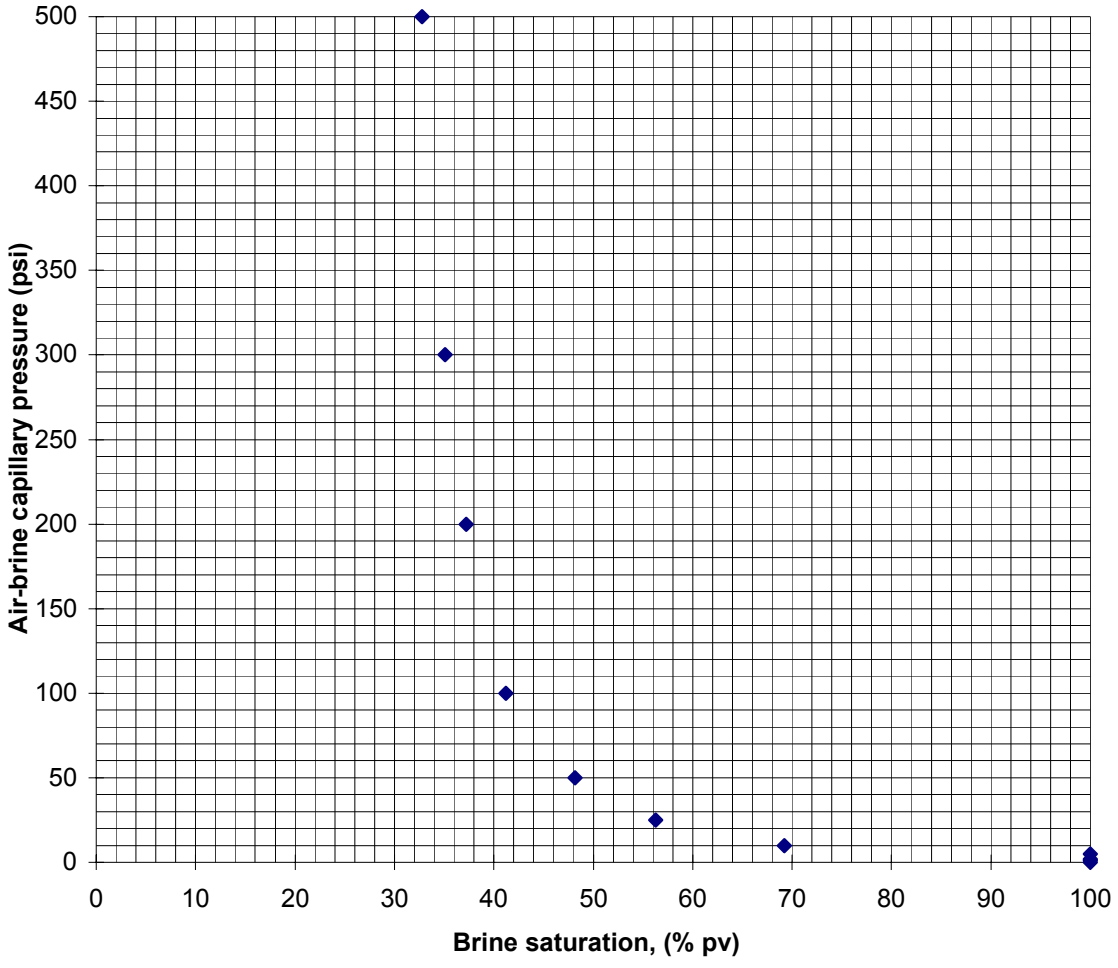
Air-brine capillary pressure by centrifuge at ambient conditions

Sample No.	Depth (m)	Kinf (md)	Kair (md)	Porosity (%)	Capillary pressure (psi)	Brine saturation (%pv)
27	2179.50	2.35	3.11	18.4	0	100.0
					1	100.0
					2	85.2
					5	69.3
					10	58.4
					25	48.9
					50	44.0
					100	40.6
					200	38.2
					300	37.2
					500	36.1



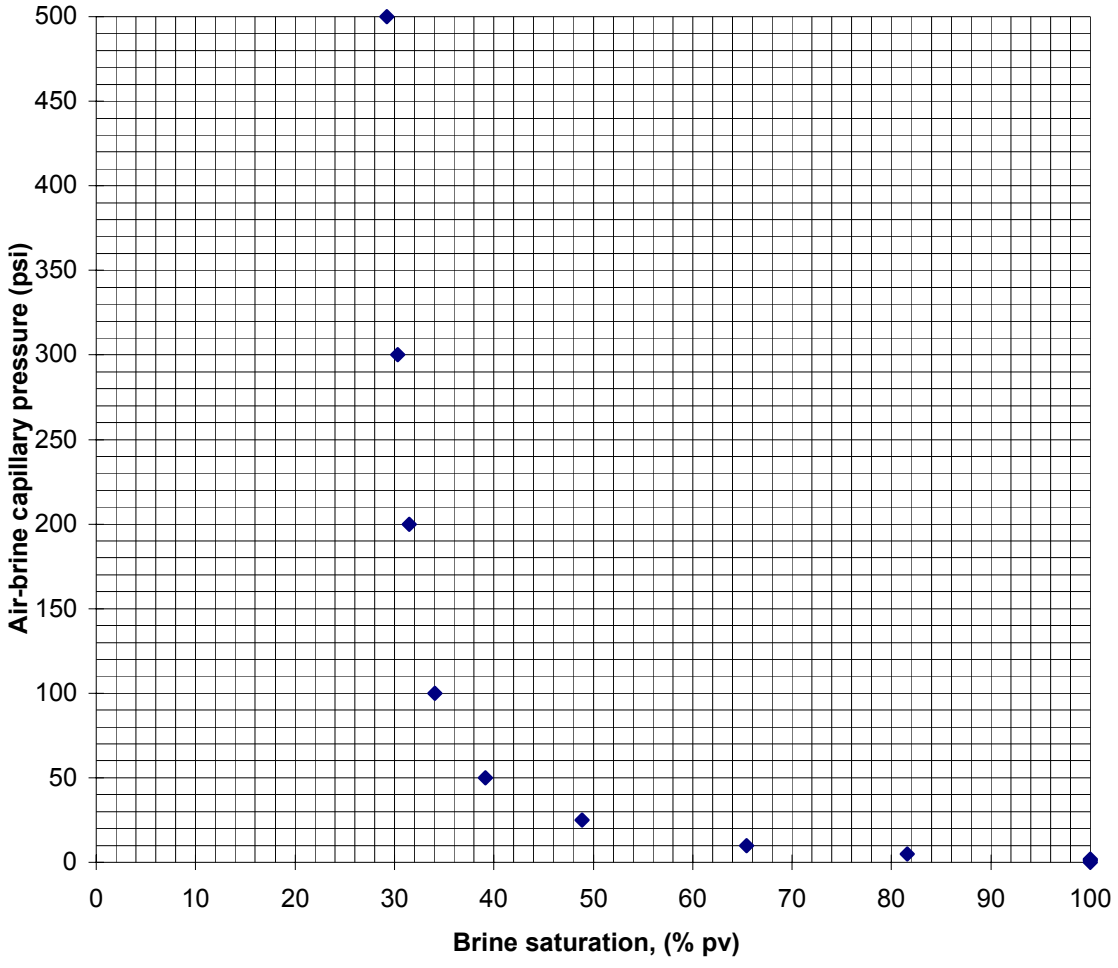
Air-brine capillary pressure by centrifuge at ambient conditions

Sample No.	Depth (m)	Kinf (md)	Kair (md)	Porosity (%)	Capillary pressure (psi)	Brine saturation (%pv)
44	2185.55	0.439	0.677	15.3	0	100.0
					1	100.0
					2	100.0
					5	100.0
					10	69.2
					25	56.3
					50	48.2
					100	41.2
					200	37.2
					300	35.1
					500	32.8



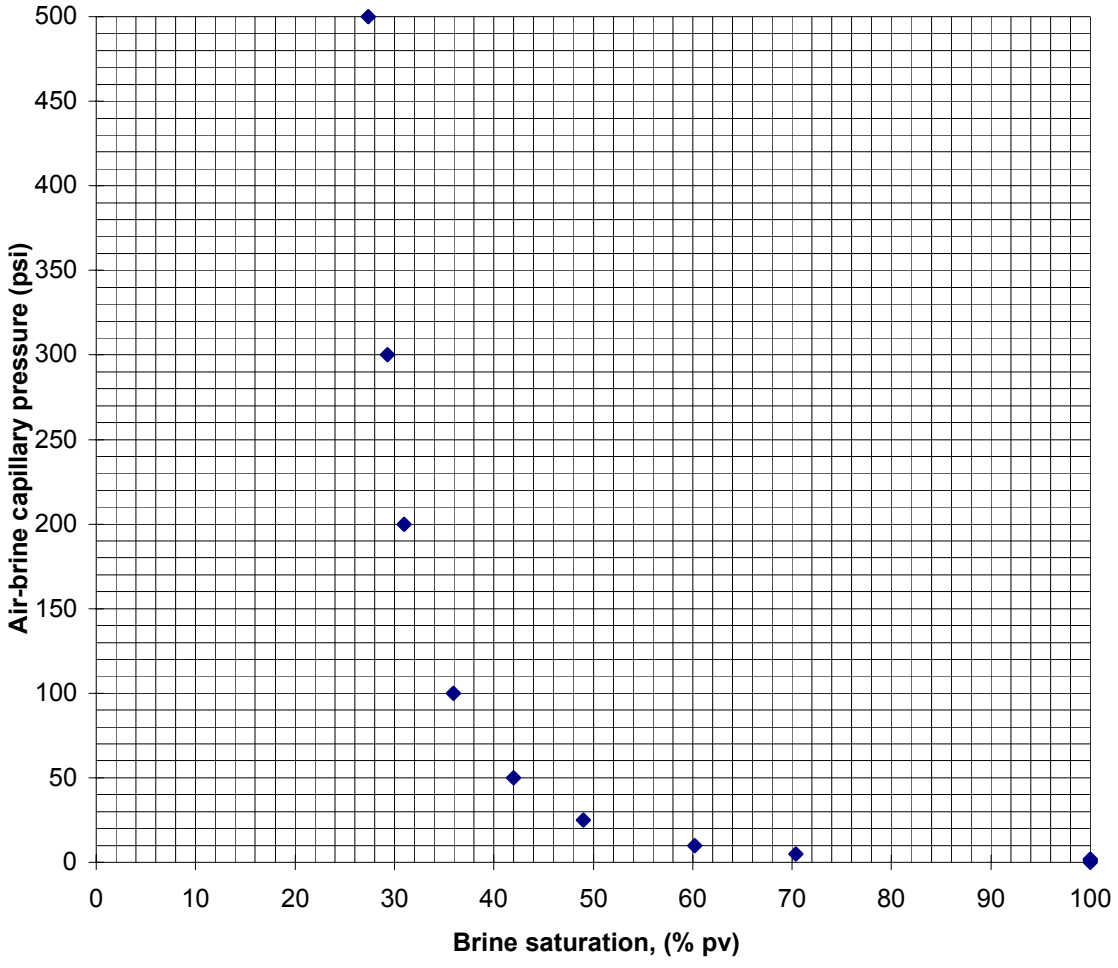
Air-brine capillary pressure by centrifuge at ambient conditions

Sample No.	Depth (m)	Kinf (md)	Kair (md)	Porosity (%)	Capillary pressure (psi)	Brine saturation (%pv)
76	2196.75	5.15	6.44	21.1	0	100.0
					1	100.0
					2	100.0
					5	81.6
					10	65.4
					25	48.9
					50	39.2
					100	34.0
					200	31.5
					300	30.4
					500	29.2



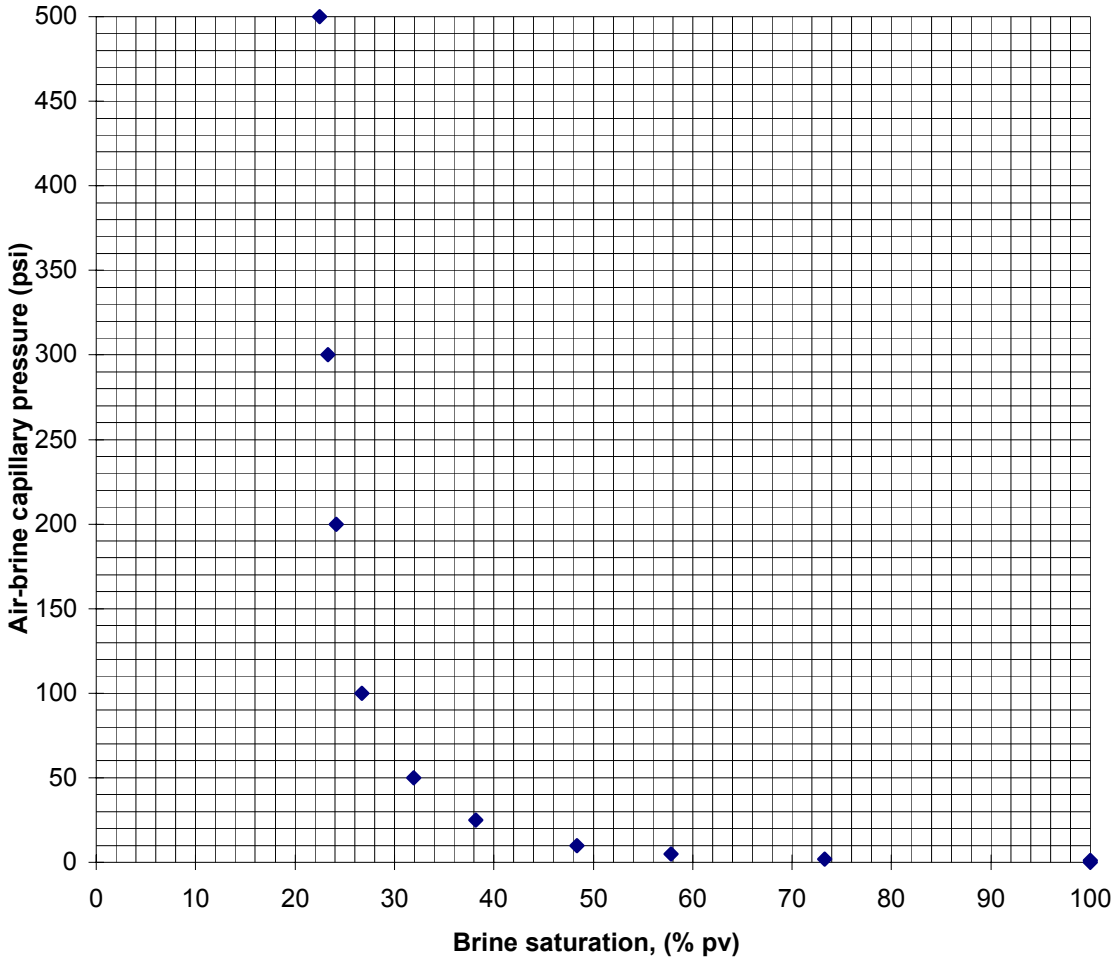
Air-brine capillary pressure by centrifuge at ambient conditions

Sample No.	Depth (m)	Kinf (md)	Kair (md)	Porosity (%)	Capillary pressure (psi)	Brine saturation (%pv)
93	2206.55	6.62	7.97	17.8	0	100.0
					1	100.0
					2	100.0
					5	70.4
					10	60.2
					25	49.0
					50	42.0
					100	35.9
					200	31.0
					300	29.3
					500	27.3



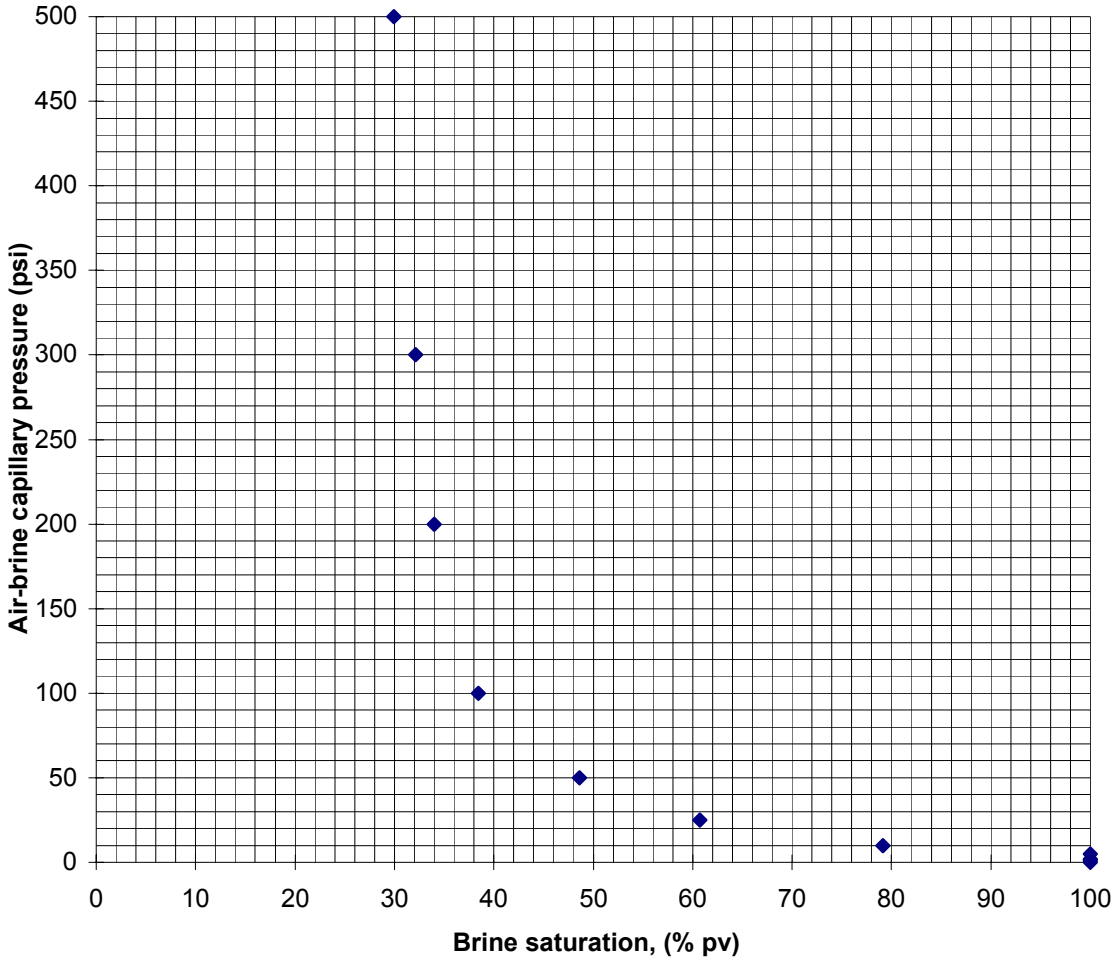
Air-brine capillary pressure by centrifuge at ambient conditions

Sample No.	Depth (m)	Kinf (md)	Kair (md)	Porosity (%)	Capillary pressure (psi)	Brine saturation (%pv)
97	2207.84	22.1	24.9	22.0	0	100.0
					1	100.0
					2	73.3
					5	57.8
					10	48.4
					25	38.2
					50	31.9
					100	26.7
					200	24.1
					300	23.3
					500	22.5



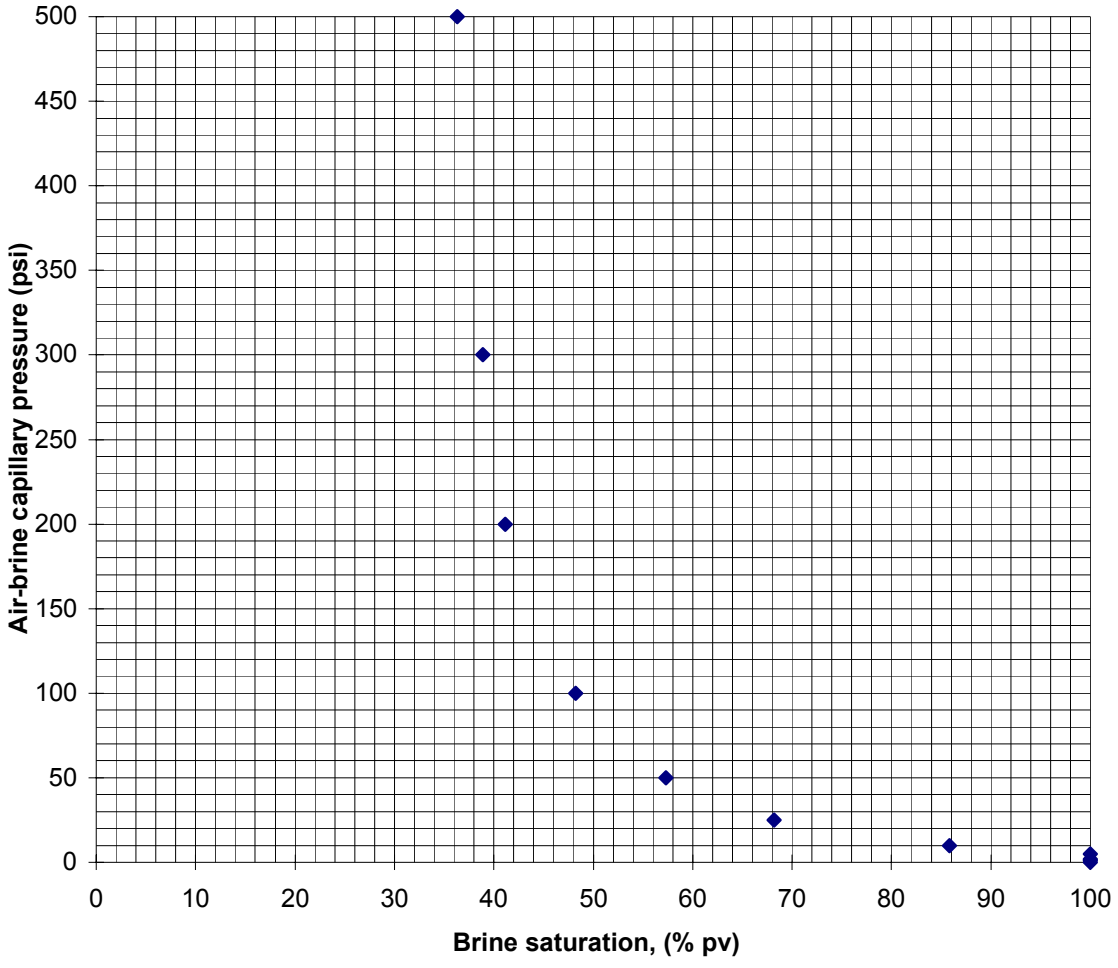
Air-brine capillary pressure by centrifuge at ambient conditions

Sample No.	Depth (m)	Kinf (md)	Kair (md)	Porosity (%)	Capillary pressure (psi)	Brine saturation (%pv)
118	2215.15	2.79	3.60	15.0	0	100.0
					1	100.0
					2	100.0
					5	100.0
					10	79.1
					25	60.7
					50	48.6
					100	38.4
					200	34.0
					300	32.1
					500	30.0



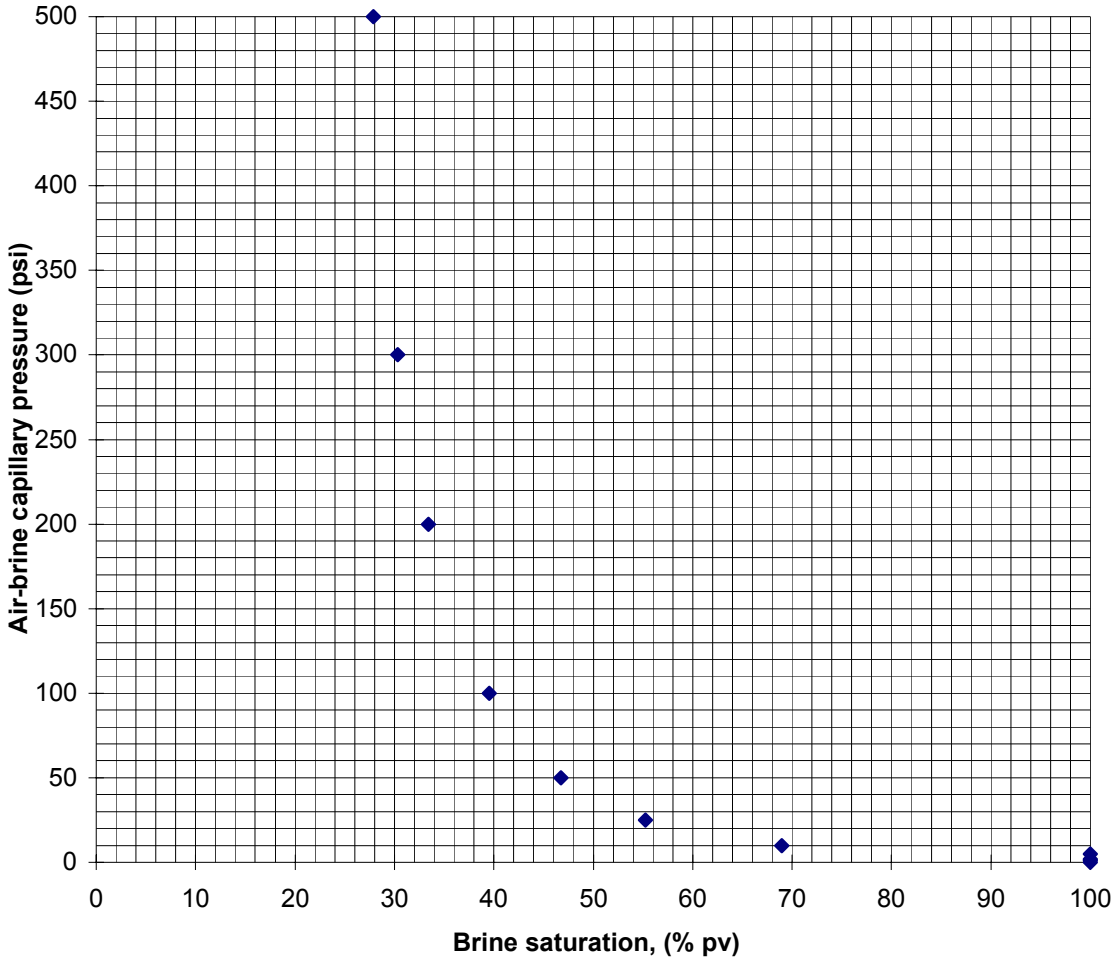
Air-brine capillary pressure by centrifuge at ambient conditions

Sample No.	Depth (m)	Kinf (md)	Kair (md)	Porosity (%)	Capillary pressure (psi)	Brine saturation (%pv)
128	2218.40	0.303	0.427	11.6	0	100.0
					1	100.0
					2	100.0
					5	100.0
					10	85.8
					25	68.2
					50	57.3
					100	48.2
					200	41.2
					300	38.9
					500	36.3



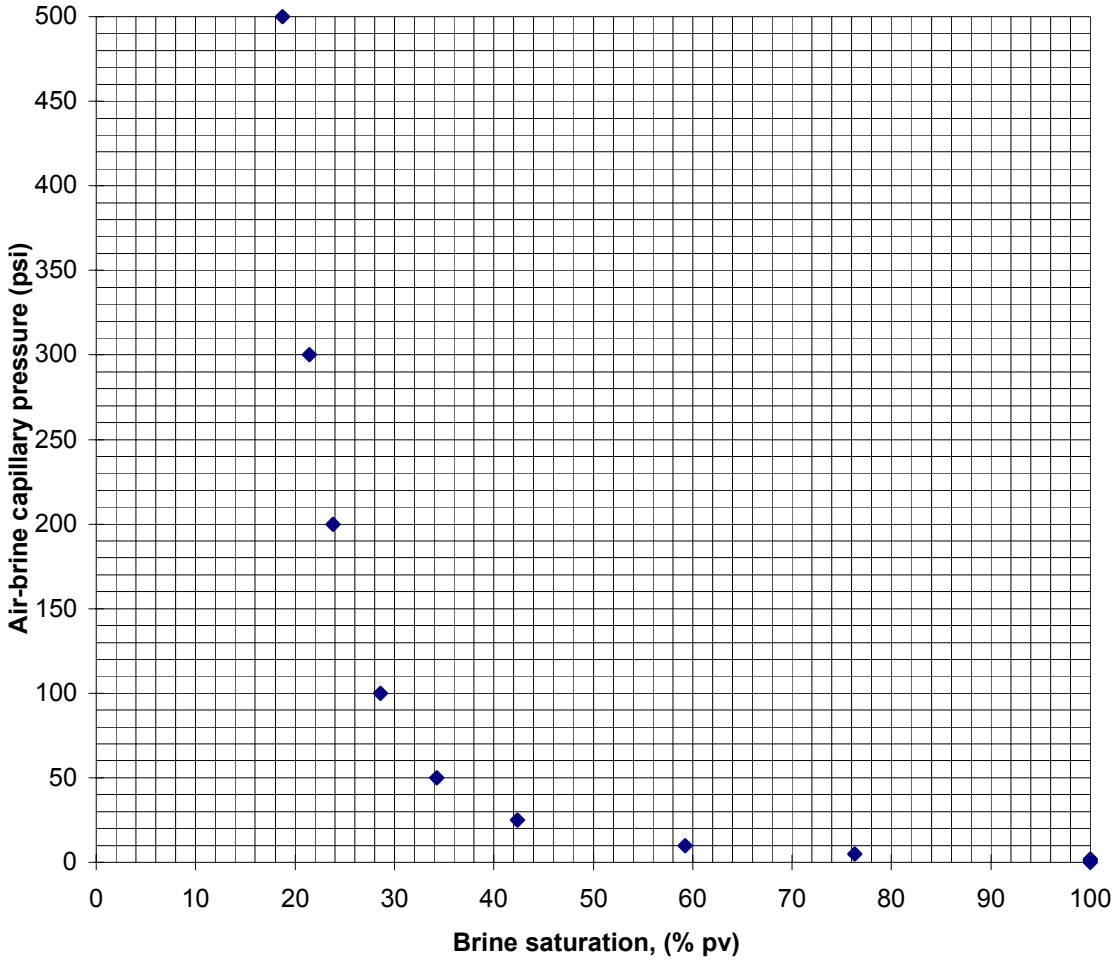
Air-brine capillary pressure by centrifuge at ambient conditions

Sample No.	Depth (m)	Kinf (md)	Kair (md)	Porosity (%)	Capillary pressure (psi)	Brine saturation (%pv)
146	2225.12	1.38	1.89	15.5	0	100.0
					1	100.0
					2	100.0
					5	100.0
					10	69.0
					25	55.3
					50	46.7
					100	39.5
					200	33.4
					300	30.3
					500	27.9



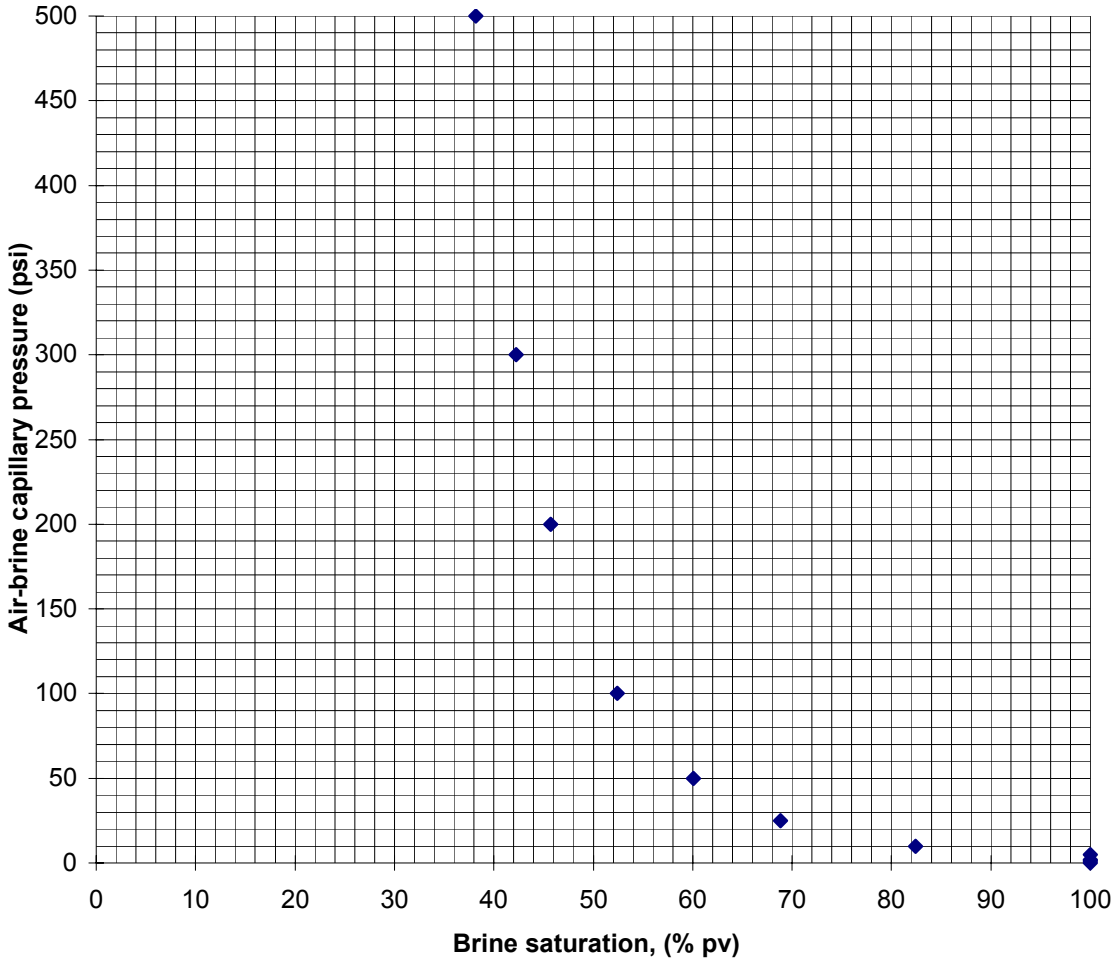
Air-brine capillary pressure by centrifuge at ambient conditions

Sample No.	Depth (m)	Kinf (md)	Kair (md)	Porosity (%)	Capillary pressure (psi)	Brine saturation (%pv)
181	2249.85	7.16	8.87	19.5	0	100.0
					1	100.0
					2	100.0
					5	76.3
					10	59.2
					25	42.4
					50	34.2
					100	28.6
					200	23.8
					300	21.4
					500	18.8



Air-brine capillary pressure by centrifuge at ambient conditions

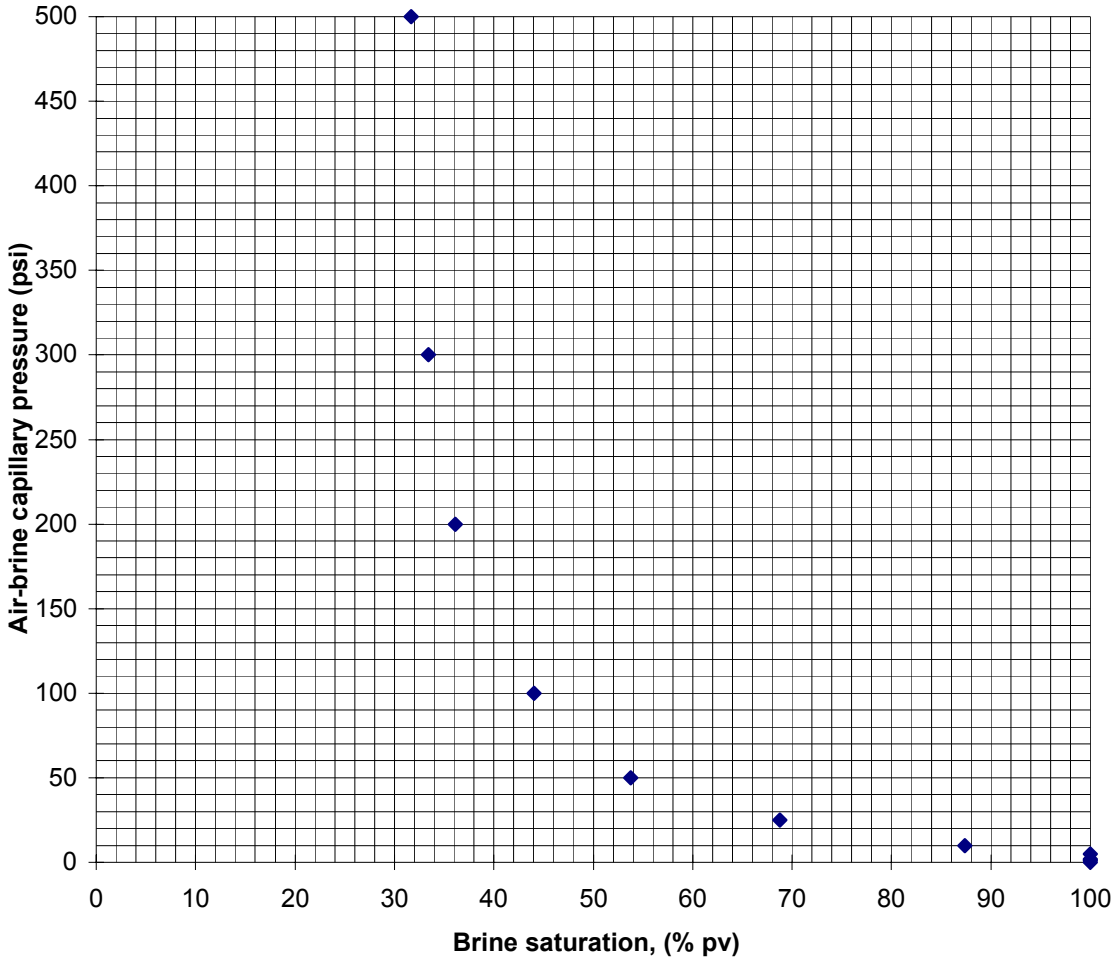
Sample No.	Depth (m)	Kinf (md)	Kair (md)	Porosity (%)	Capillary pressure (psi)	Brine saturation (%pv)
186	2251.20	0.517	0.787	14.7	0	100.0
					1	100.0
					2	100.0
					5	100.0
					10	82.4
					25	68.8
					50	60.1
					100	52.4
					200	45.7
					300	42.2
					500	38.2



CORE LABORATORIES AUSTRALIA - 2002

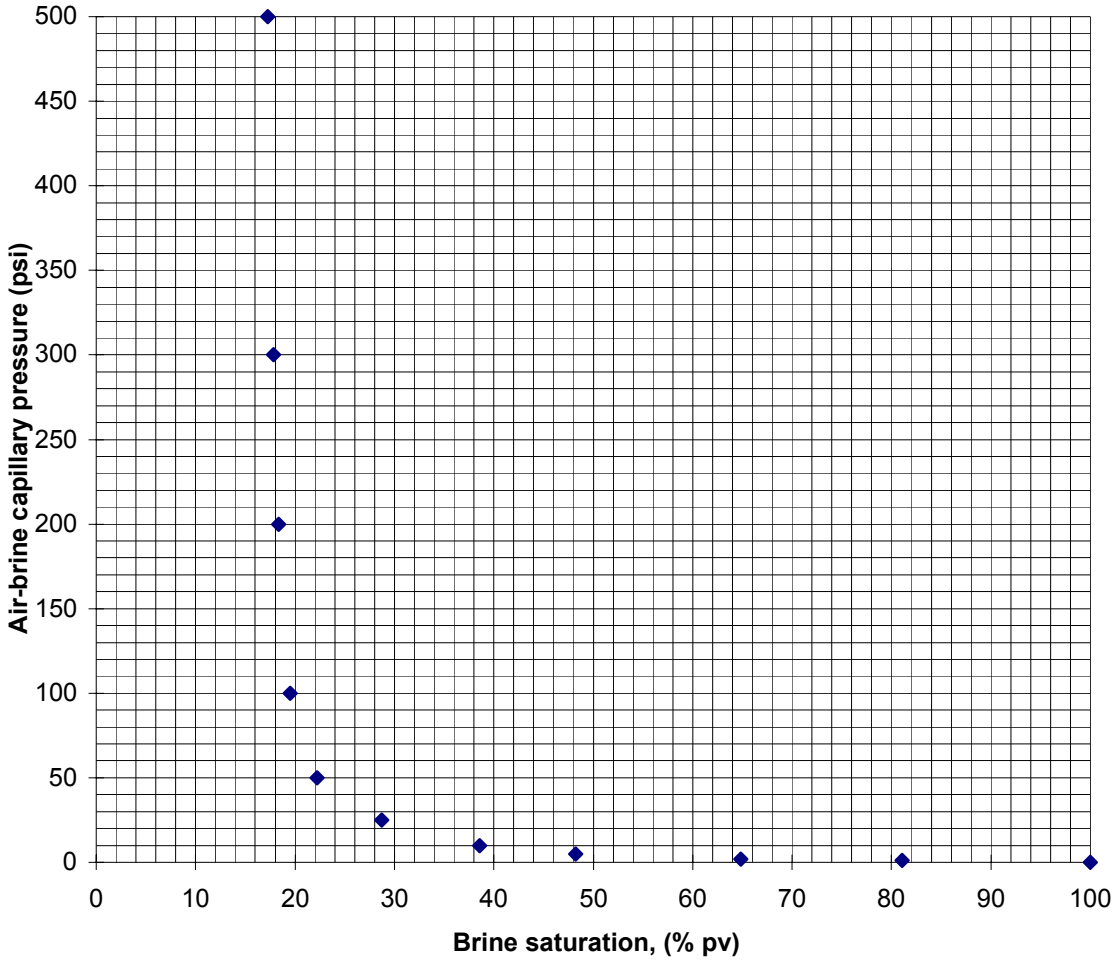
Air-brine capillary pressure by centrifuge at ambient conditions

Sample No.	Depth (m)	Kinf (md)	Kair (md)	Porosity (%)	Capillary pressure (psi)	Brine saturation (%pv)
187	2251.59	0.758	1.12	16.8	0	100.0
					1	100.0
					2	100.0
					5	100.0
					10	87.4
					25	68.8
					50	53.8
					100	44.1
					200	36.1
					300	33.4
					500	31.7



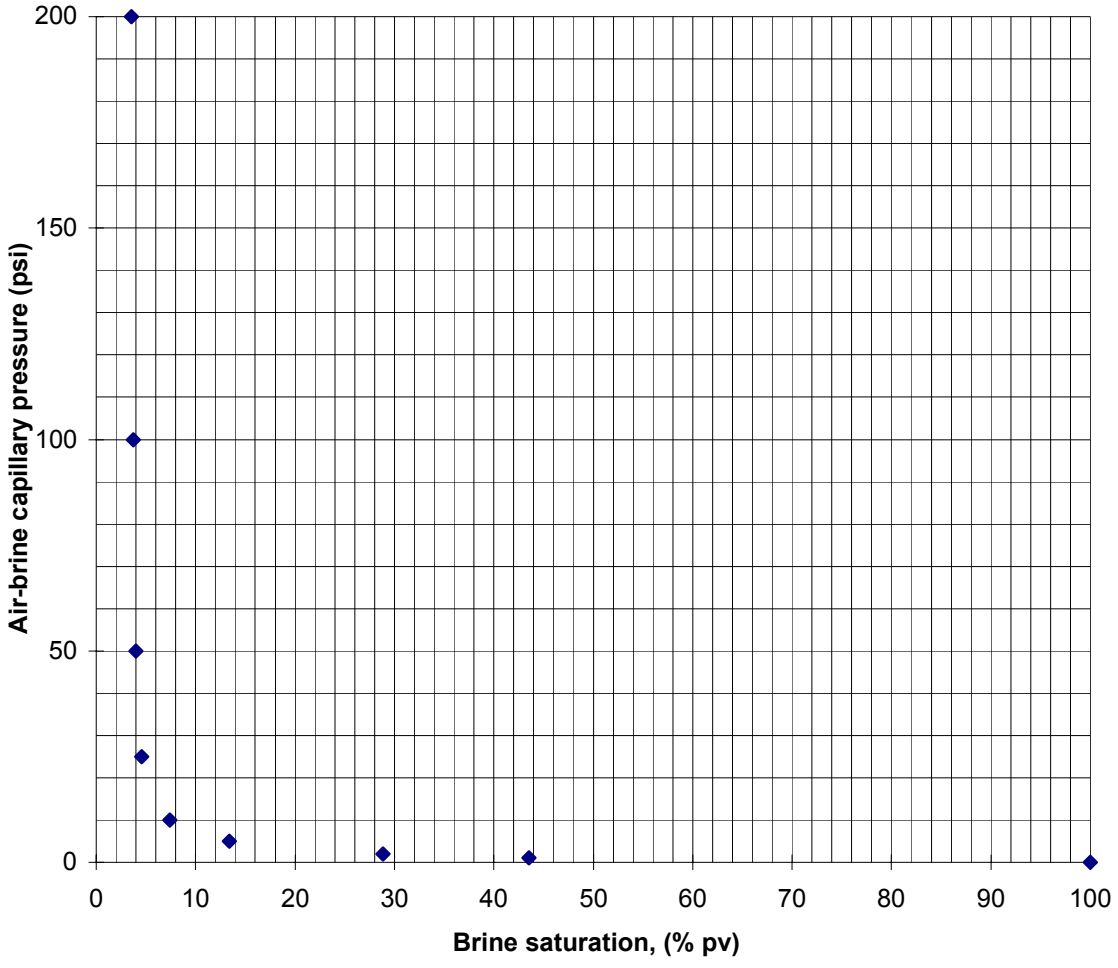
Air-brine capillary pressure by centrifuge at ambient conditions

Sample No.	Depth (m)	Kinf (md)	Kair (md)	Porosity (%)	Capillary pressure (psi)	Brine saturation (%pv)
205	2275.17	174	191	19.7	0	100.0
					1	81.0
					2	64.8
					5	48.2
					10	38.6
					25	28.7
					50	22.2
					100	19.5
					200	18.3
					300	17.8
					500	17.3



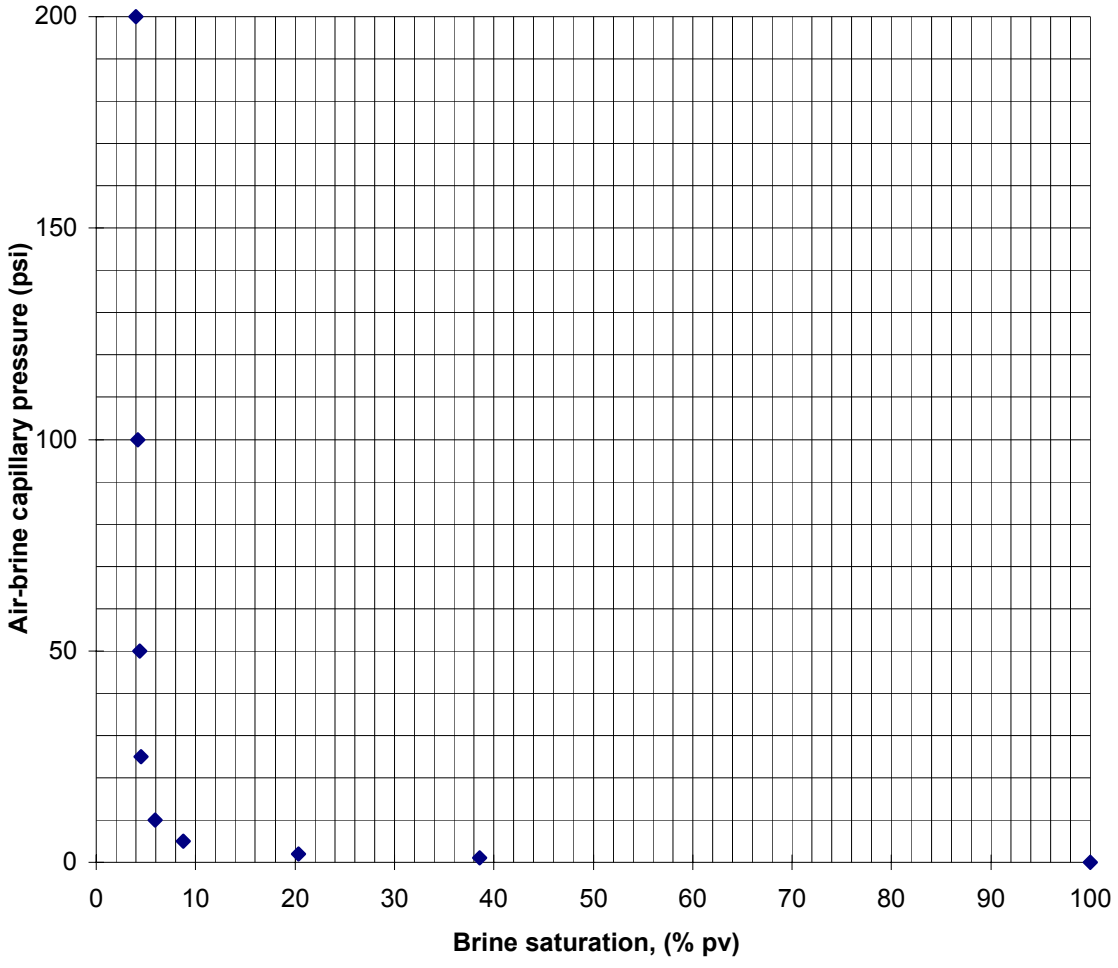
Air-brine capillary pressure by centrifuge at ambient conditions

Sample No.	Depth (m)	Kinf (md)	Kair (md)	Porosity (%)	Capillary pressure (psi)	Brine saturation (%pv)
234	2296.94	5010	5510	24.7	0	100.0
					1	43.5
					2	28.9
					5	13.4
					10	7.42
					25	4.59
					50	3.99
					100	3.74
					200	3.51



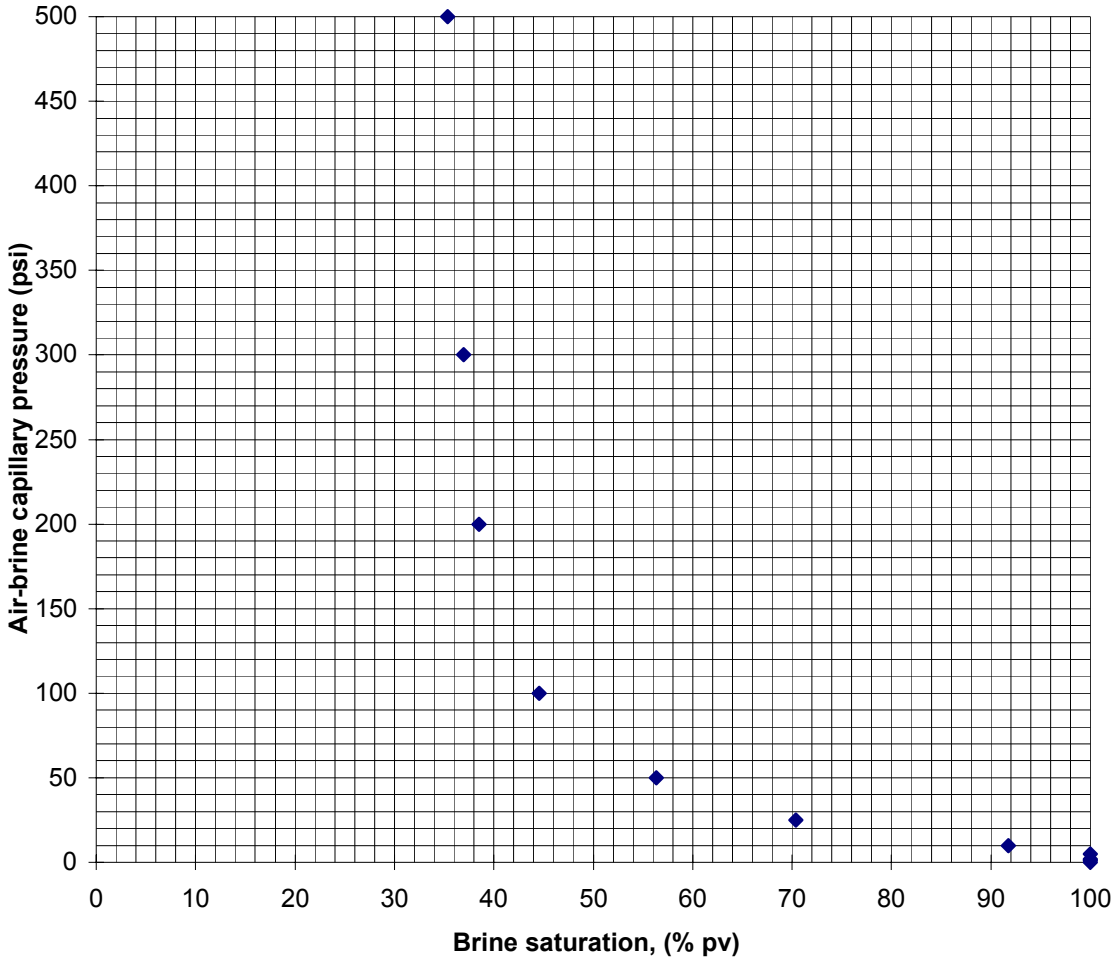
Air-brine capillary pressure by centrifuge at ambient conditions

Sample No.	Depth (m)	Kinf (md)	Kair (md)	Porosity (%)	Capillary pressure (psi)	Brine saturation (%pv)
241	2299.40	5750	6680	21.8	0	100.0
					1	38.6
					2	20.3
					5	8.77
					10	5.94
					25	4.54
					50	4.36
					100	4.19
					200	4.02



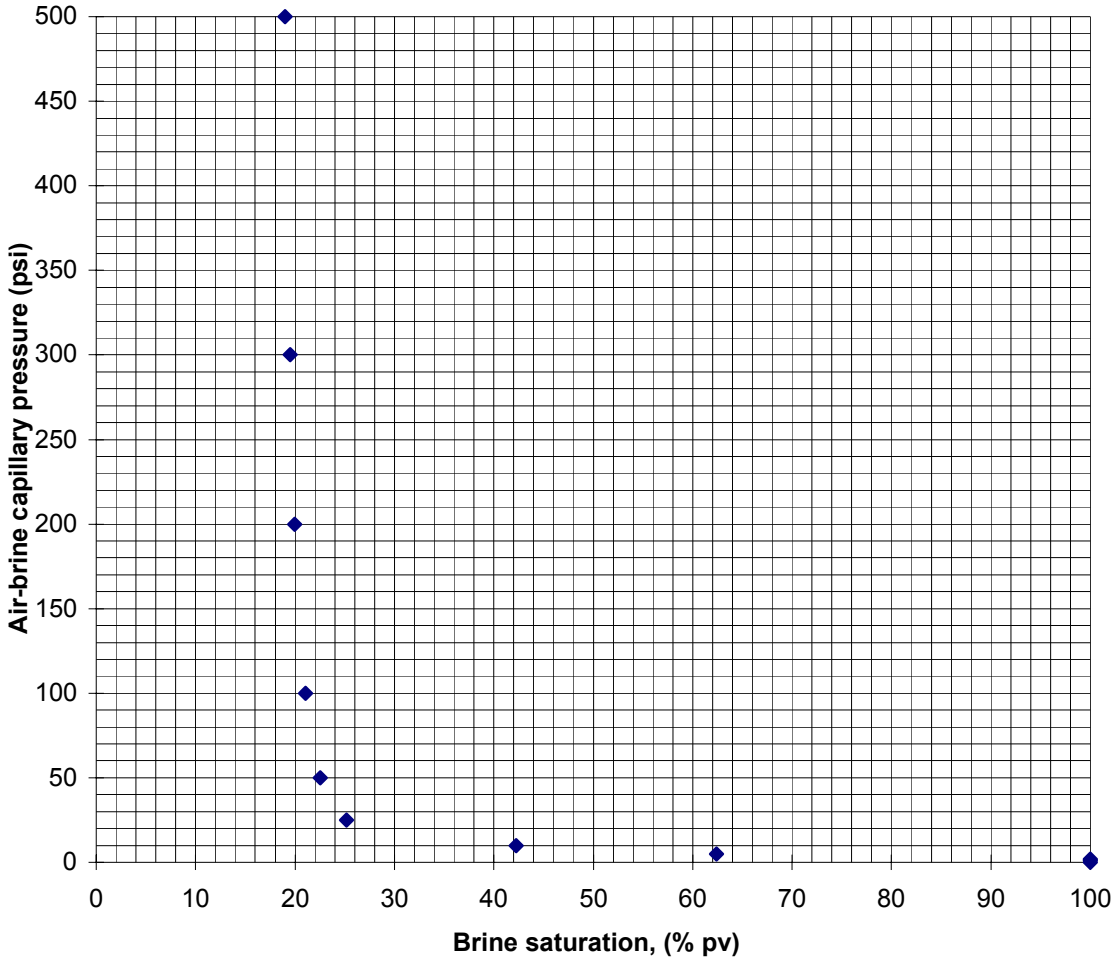
Air-brine capillary pressure by centrifuge at ambient conditions

Sample No.	Depth (m)	Kinf (md)	Kair (md)	Porosity (%)	Capillary pressure (psi)	Brine saturation (%pv)
244	2300.20	0.526	0.816	12.3	0	100.0
					1	100.0
					2	100.0
					5	100.0
					10	91.7
					25	70.4
					50	56.4
					100	44.5
					200	38.5
					300	36.9
					500	35.3

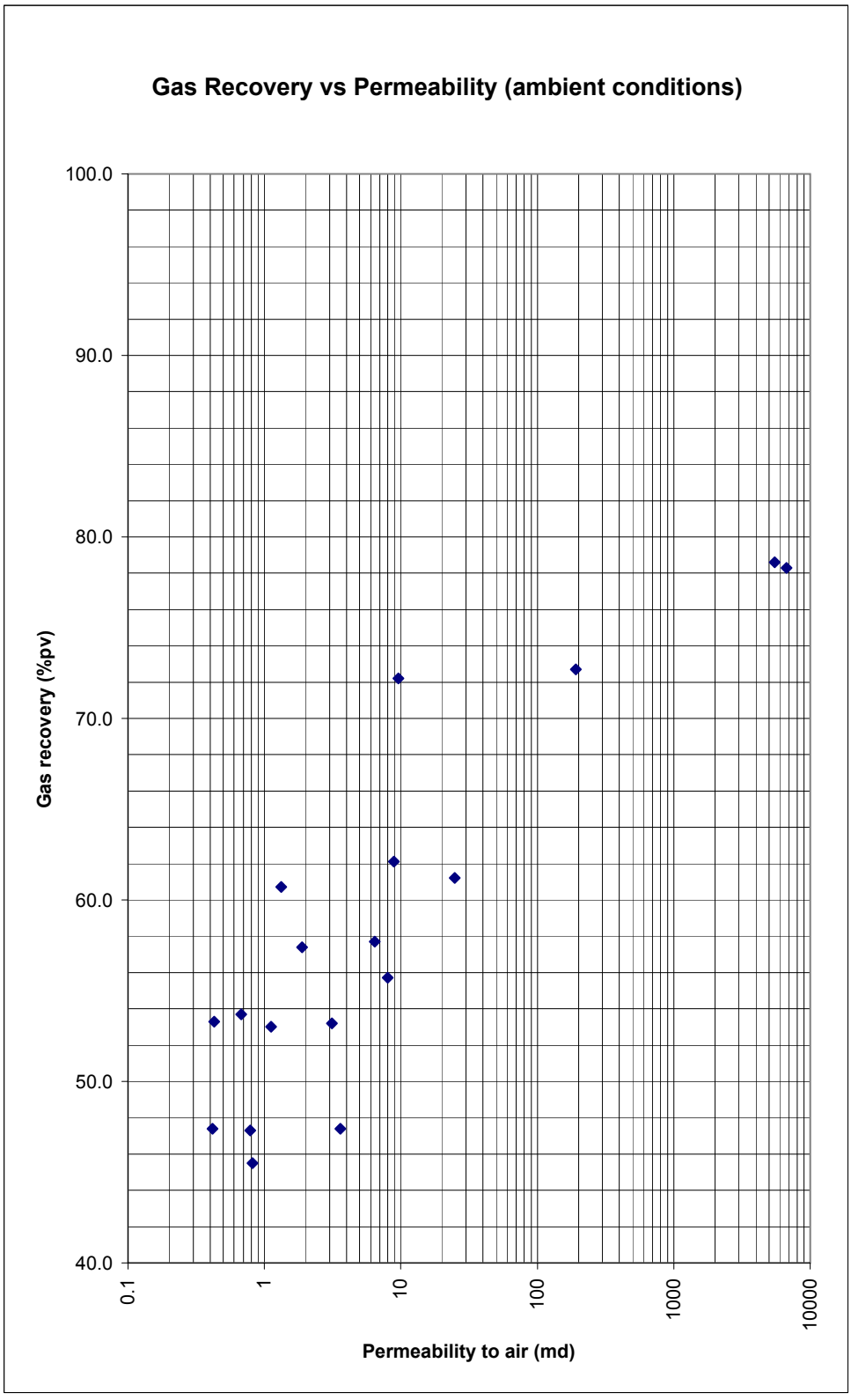


Air-brine capillary pressure by centrifuge at ambient conditions

Sample No.	Depth (m)	Kinf (md)	Kair (md)	Porosity (%)	Capillary pressure (psi)	Brine saturation (%pv)
246	2300.80	7.73	9.61	15.8	0	100.0
					1	100.0
					2	100.0
					5	62.4
					10	42.2
					25	25.2
					50	22.6
					100	21.0
					200	20.0
					300	19.5
					500	19.0



SECTION 4
RELATIVE PERMEABILITY


Gas Recovery vs Permeability (ambient conditions)
100.0
90.0
80.0
70.0
60.0
50.0
40.0
Gas recovery (%pv)
0.1
1
10
100
1000
10000
Permeability to air (md)

Summary of WATER-GAS relative permeability by centrifuge (end-point) at ambient conditions.

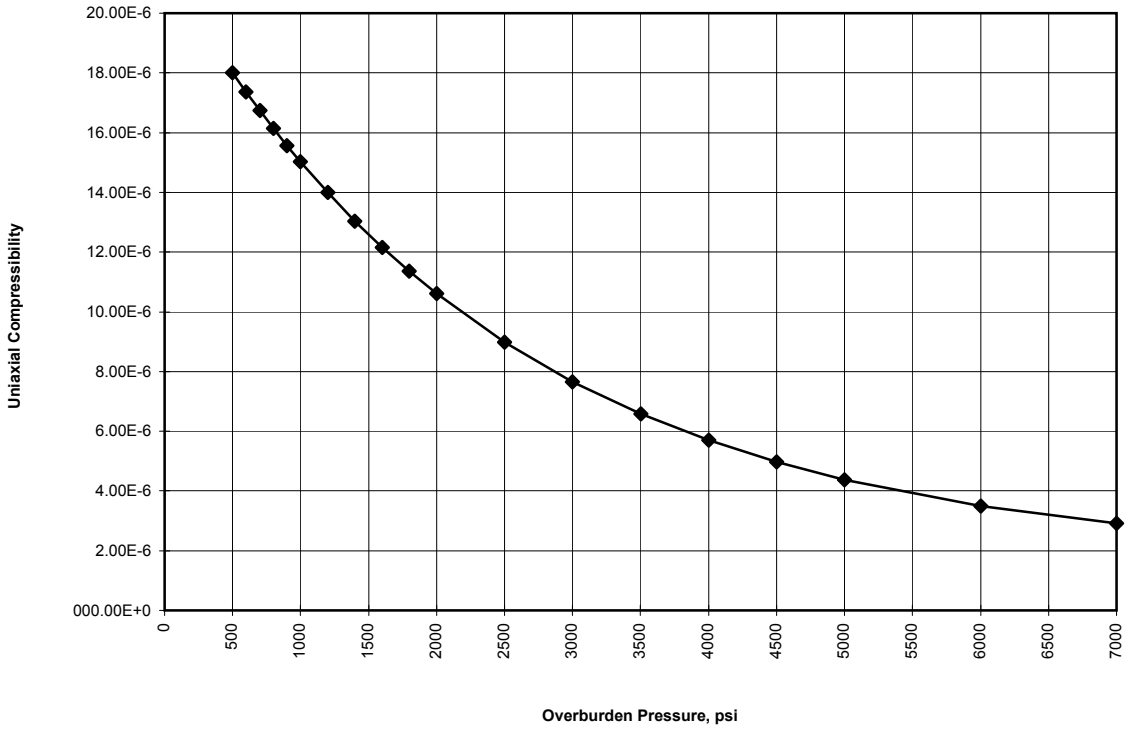
Sample No.	Depth	AMBIENT CONDITIONS		INITIAL CONDITIONS			TERMINAL CONDITIONS			
		Kair	Porosity	Average Swi	Initial gas in place	Kgas at Swi	Sgr	Gas Recovery		Kw at Sgr
	(m)	(md)	(%)	(% pv)	(% pv)	(md)	(% pv)	(% pv)	(% IIGP)	(md)
5	2153.10	0.415	13.8	47.3	52.7	0.300	5.3	47.4	89.9	0.068
12	2174.20	1.33	17.7	33.6	66.4	0.831	5.7	60.7	91.4	0.297
27	2179.50	3.11	18.4	39.1	60.9	1.55	7.7	53.2	87.4	0.685
44	2185.55	0.677	15.3	39.5	60.5	0.346	6.8	53.7	88.8	0.139
76	2196.75	6.44	21.1	33.6	66.4	4.47	8.7	57.7	86.9	1.64
93	2206.55	7.97	17.8	32.5	67.5	5.37	11.8	55.7	82.5	1.72
97	2207.84	24.9	22.0	25.5	74.5	16.92	13.3	61.2	82.1	4.42
118	2215.15	3.60	15.0	47.3	52.7	2.50	5.3	47.4	89.9	0.795
128	2218.40	0.427	11.6	41.4	58.6	0.283	5.3	53.3	91.0	0.098
146	2225.12	1.89	15.5	35.0	65.0	1.18	7.6	57.4	88.3	0.577
181	2249.85	8.87	19.5	25.8	74.2	6.61	12.1	62.1	83.7	2.59
186	2251.20	0.787	14.7	44.0	56.0	0.453	8.7	47.3	84.5	0.162
187	2251.59	1.12	16.8	38.9	61.1	0.455	8.1	53.0	86.7	0.226
205	2275.17	191	19.7	18.4	81.6	115	8.9	72.7	89.1	38.0
234	2296.94	5510	24.7	3.0	97.0	4003	18.4	78.6	81.0	2165
241	2299.40	6680	21.8	3.8	96.2	5056	17.9	78.3	81.4	1505
244	2300.20	0.816	12.3	41.2	58.8	0.513	13.3	45.5	77.4	0.325
246	2300.80	9.61	15.8	20.9	79.1	6.93	6.9	72.2	91.3	3.86

SECTION 5
ROCK (PORE VOLUME) COMPRESSIBILITY

Rock (Pore Volume) Compressibility

Sample number 5A
Depth, metres 2153.02
Permeability to air , md 2.66
Porosity, % 16.6
Grain Density, gm/cc 2.651

Confining Stress (psi)	Porosity (%)	Compressibility (pv/pv/psi)	
		Hydrostatic	Uniaxial *
400	16.6	-	-
500	16.5	29.51E-6	18.00E-6
600	16.5	28.46E-6	17.36E-6
700	16.5	27.44E-6	16.74E-6
800	16.4	26.47E-6	16.14E-6
900	16.4	25.53E-6	15.57E-6
1000	16.3	24.63E-6	15.02E-6
1200	16.3	22.94E-6	13.99E-6
1400	16.2	21.38E-6	13.04E-6
1600	16.2	19.94E-6	12.16E-6
1800	16.1	18.61E-6	11.35E-6
2000	16.1	17.39E-6	10.61E-6
2500	15.9	14.73E-6	8.98E-6
3000	15.9	12.56E-6	7.66E-6
3500	15.8	10.78E-6	6.58E-6
4000	15.7	9.33E-6	5.69E-6
4500	15.7	8.15E-6	4.97E-6
5000	15.6	7.18E-6	4.38E-6
6000	15.5	5.74E-6	3.50E-6
7000	15.5	4.78E-6	2.91E-6

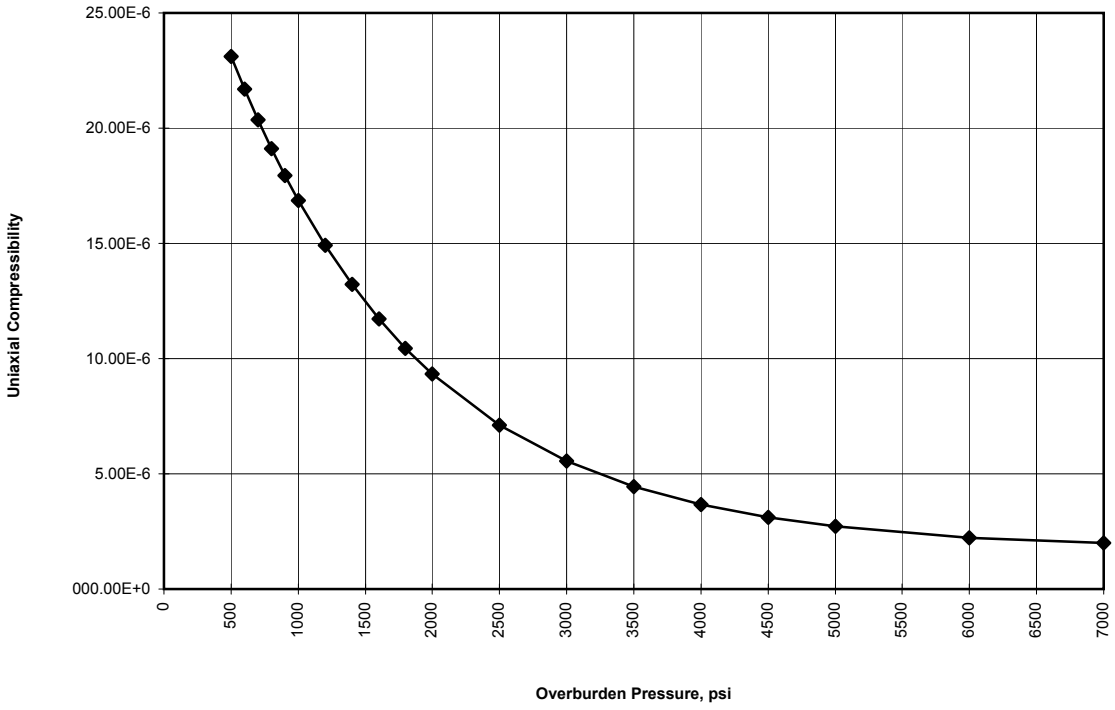


Compressibility under uniaxial loading conditions, transformed from hydrostatic data as per Teeuw, Dirk : "Prediction Of Formation Compaction From Laboratory Compressibility D
Trans: AIME (1971) 251, 263-271

Rock (Pore Volume) Compressibility

Sample number 76A
Depth, metres 2196.80
Permeability to air , md 7.98
Porosity, % 21.2
Grain Density, gm/cc 2.740

Confining Stress (psi)	Porosity (%)	Compressibility (pv/pv/psi)	
		Hydrostatic	Uniaxial *
400	21.2	-	-
500	21.1	37.91E-6	23.12E-6
600	21.0	35.56E-6	21.69E-6
700	21.0	33.38E-6	20.36E-6
800	20.9	31.33E-6	19.11E-6
900	20.9	29.43E-6	17.95E-6
1000	20.8	27.65E-6	16.87E-6
1200	20.7	24.45E-6	14.91E-6
1400	20.7	21.66E-6	13.21E-6
1600	20.6	19.23E-6	11.73E-6
1800	20.6	17.12E-6	10.44E-6
2000	20.5	15.28E-6	9.32E-6
2500	20.4	11.66E-6	7.11E-6
3000	20.3	9.10E-6	5.55E-6
3500	20.2	7.28E-6	4.44E-6
4000	20.2	6.00E-6	3.66E-6
4500	20.1	5.09E-6	3.11E-6
5000	20.1	4.45E-6	2.71E-6
6000	20.0	3.67E-6	2.24E-6
7000	19.9	3.27E-6	1.99E-6

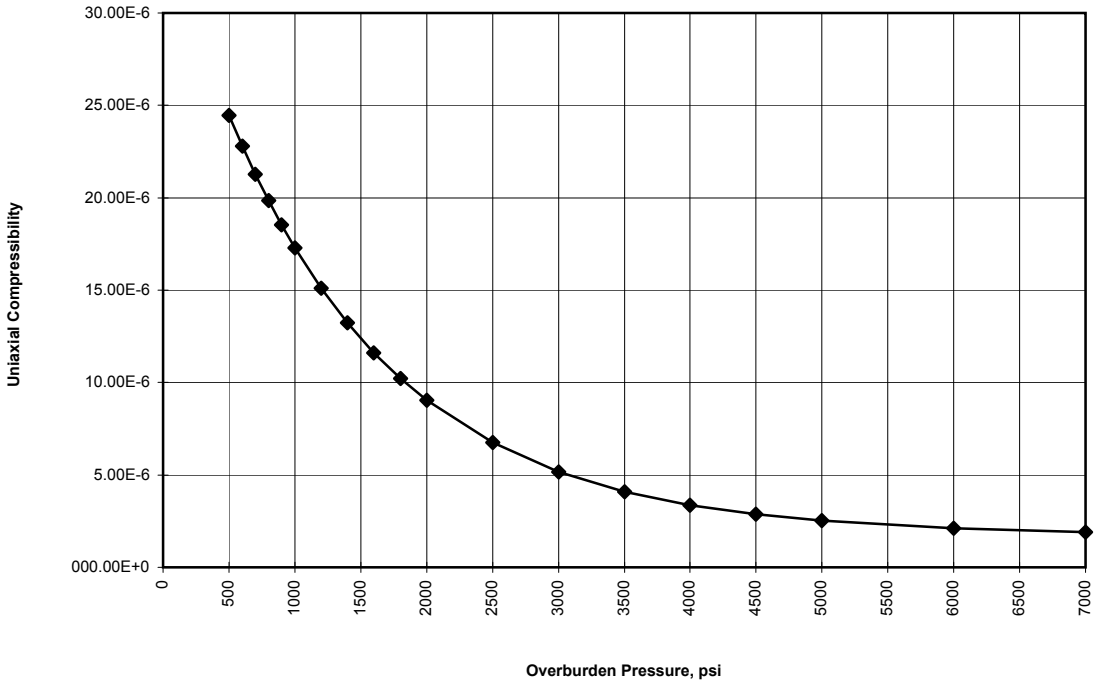


Compressibility under uniaxial loading conditions, transformed from hydrostatic data as per Teeuw, Dirk : "Prediction Of Formation Compaction From Laboratory Compressibility D
Trans: AIME (1971) 251, 263-271

Rock (Pore Volume) Compressibility

Sample number	97A
Depth, metres	2207.90
Permeability to air , md	8.310
Porosity, %	16.8
Grain Density, gm/cc	2.774

Confining Stress (psi)	Porosity (%)	Compressibility (pv/pv/psi)	
		Hydrostatic	Uniaxial *
400	16.8	-	-
500	16.7	40.11E-6	24.47E-6
600	16.6	37.39E-6	22.81E-6
700	16.6	34.87E-6	21.27E-6
800	16.5	32.53E-6	19.84E-6
900	16.5	30.36E-6	18.52E-6
1000	16.5	28.35E-6	17.30E-6
1200	16.4	24.77E-6	15.11E-6
1400	16.4	21.69E-6	13.23E-6
1600	16.3	19.04E-6	11.62E-6
1800	16.3	16.77E-6	10.23E-6
2000	16.2	14.82E-6	9.04E-6
2500	16.1	11.06E-6	6.75E-6
3000	16.1	8.49E-6	5.18E-6
3500	16.0	6.73E-6	4.10E-6
4000	16.0	5.52E-6	3.37E-6
4500	15.9	4.69E-6	2.86E-6
5000	15.9	4.13E-6	2.52E-6
6000	15.8	3.47E-6	2.11E-6
7000	15.7	3.15E-6	1.92E-6



Compressibility under uniaxial loading conditions, transformed from hydrostatic data as per Teeuw, Dirk : "Prediction Of Formation Compaction From Laboratory Compressibility D
Trans: AIME (1971) 251, 263-271

Rock (Pore Volume) Compressibility

Sample number 118A

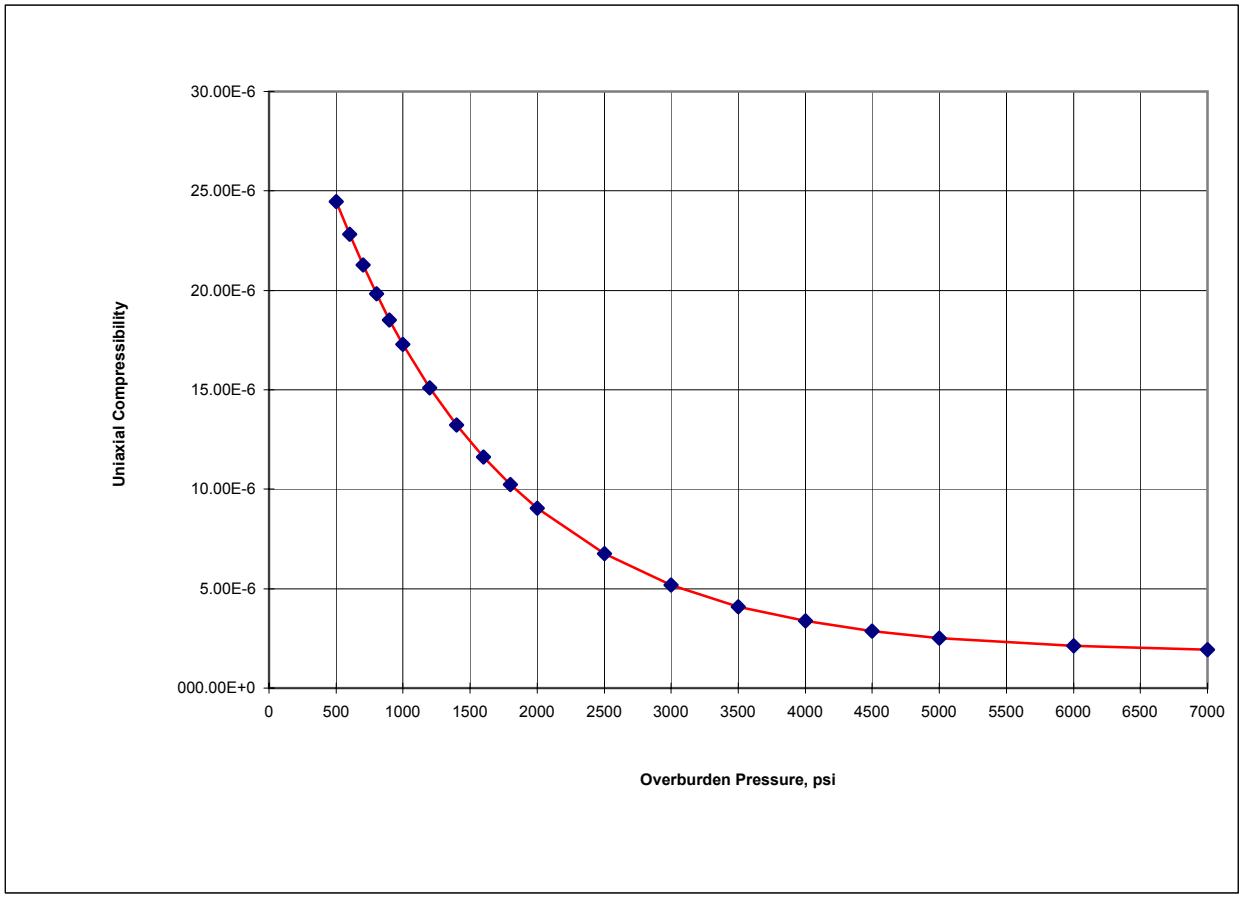
Depth, metres 2215.10

Permeability to air , md 3.64

Porosity, % 15.0

Grain Density, gm/cc 2.653

Confining Stress (psi)	Porosity (%)	Compressibility (pv/pv/psi)	
		Hydrostatic	Uniaxial *
400	15.0	-	-
500	14.9	40.11E-6	24.47E-6
600	14.8	37.39E-6	22.81E-6
700	14.8	34.87E-6	21.27E-6
800	14.7	32.53E-6	19.84E-6
900	14.7	30.36E-6	18.52E-6
1000	14.6	28.35E-6	17.30E-6
1200	14.6	24.77E-6	15.11E-6
1400	14.5	21.69E-6	13.23E-6
1600	14.4	19.04E-6	11.62E-6
1800	14.4	16.77E-6	10.23E-6
2000	14.4	14.82E-6	9.04E-6
2500	14.3	11.06E-6	6.75E-6
3000	14.2	8.49E-6	5.18E-6
3500	14.1	6.73E-6	4.10E-6
4000	14.1	5.52E-6	3.37E-6
4500	14.0	4.69E-6	2.86E-6
5000	14.0	4.13E-6	2.52E-6
6000	13.9	3.47E-6	2.11E-6
7000	13.9	3.15E-6	1.92E-6



Compressibility under uniaxial loading conditions, transformed from hydrostatic data as per Teeuw, Dirk : "Prediction Of Formation Compaction From Laboratory Compressibility D
Trans: AIME (1971) 251, 263-271

APPENDIX-1

SUMMARY OF LABORATORY PROCEDURES

SUMMARY OF LABORATORY PROCEDURES

Sample selections were made by Mr Jon Kelly of Woodside in an attachment to an e-mail dated 29th April 2002. These samples had originally undergone routine core analysis and so had been cleaned, dried and stored at ambient conditions following analysis.

All samples were screened visually initially, to determine if they were of suitable shape and size. Visual screening was followed by computerised tomography (CT) to detect any fractures or other heterogeneities which would render the samples unsuitable for analysis. Samples which failed the screening stage were replaced. Selected replacements were agreed by Woodside and they also underwent visual and CT screening.

For rock (pore volume) compressibility tests, additional duplicate samples (suffix “A”) were drilled adjacent to the selected routine core analysis plugs. Following visual and CT screening, these duplicate samples were cleaned in methanol to remove residual salts. These samples were dried at 90°C in a non-humidified oven prior to measurement of porosity and air permeability at ambient conditions (no applied overburden pressure).

All routine core analysis samples which had been selected for analysis were also re-dried at 90°C and porosity, permeability, grain density values re-checked and compared to originally measured values.

A complete list of samples eventually selected for analysis and samples which failed screening is contained in SECTION 1 of this report.

Saturation

All samples undergoing analysis were evacuated and pressure saturated with a simulated formation brine of 13,500 ppm concentration (comprising 80% NaCl and 20% KCl). All samples were weighed after saturation to check measured pore volumes.

Formation Resistivity

Each fully saturated sample was loaded into a coreholder at the reservoir equivalent NOBP and the electrical resistivities measured on consecutive days until they were stable, indicating ionic eqilibrium in the pore spaces. Formation factor (FRF) and cementation exponent (“m”) values were then calculated.

Two samples (#12 and #93) were selected for BQv measurements by multiple salinity method. Several brines were flowed through each sample in decreasing salinity from 200,000 ppm, 110,000 ppm, 50,000 ppm and finally the 13,500 ppm simulated formation brine. For each salinity at least 10 pore volumes throughput was used before measurement of Co. These Co measurements were repeated on successive days until stable – several days were often required at each brine salinity for ionic equilibrium to occur. From the data acquired, formation resistivity factor values were calculated. Co versus Cw values were plotted for each sample and a line regressed through the data points to enable calculation of "F*" from the slope of the line and "BQv" from the intercept of the line.

Each sample was then de-saturated at incrementally increasing pressures using humidified air as the displacement medium. Electrical resistivities of each sample were measured at the incrementally decreasing partial saturations. When each sample had attained electrical equilibrium at each incremental desaturation stage, values of resistivity index (RI) and saturation exponent ("n") were calculated.

The trimmed-ends of the plugs which underwent FRF and RI measurements were cleaned in toluene and methanol, dried at 60°C in a non-humidified oven and then subjected to determinations of cation exchange capacity (CEC) using the ammonium acetate wet chemistry technique on crushed sample. These CEC values were in turn used to calculate idealised "m*" and "n*" values using Waxman-Smits-Thomas equations.

All electrical resistivity data are presented in SECTION 2.

Following the resistivity index analysis, the samples were resaturated with the simulated formation brine for the capillary pressure analysis.

Air-brine capillary pressure by centrifuge.

Samples were each loaded into individual centrifuge coreholders. Samples were spun at incremental rotational speeds effecting capillary pressure. Each speed (RPM) was maintained for a minimum of 24 hours until production was stable. The speed was then raised to the next higher speed. Volumes of brine produced were monitored using a stroboscope.

Capillary pressure and end-face saturation data were then calculated from the raw data using data reduction techniques developed by Hassler-Brunner. These results are presented within SECTION 3 of this report.

Capillary pressure and end-face saturation data were then calculated from the raw data using data reduction techniques developed by Hassler-Brunner. These results are also presented in SECTION 3.

Water-gas relative permeability (end-point) analysis by centrifuge.

Following the air-brine capillary pressure analyses by centrifuge, each sample was removed from the centrifuge core holders and loaded into a hydrostatic core holder with the minimal 400 psi confining pressure (to seat the sample against the rubber boot) applied. Humidified nitrogen was flowed through each sample and the effective permeability to gas (Kgas) at Swi was determined.

Each sample was next loaded into individual brine-filled centrifuge cups. The samples were then spun at a maximum imbibition brine displacing air, capillary pressure to determine the end-point residual gas saturation (Sgr). The samples were removed from the centrifuge cups and the residual gas saturations were determined gravimetrically.

Each sample was then loaded into a hydrostatic core holder at 400 psi confining stress. Brine was flowed through the samples and effective permeability to brine at Sgr was then determined. Results from the water-gas relative permeability (end-point) by centrifuge are presented in SECTION 4 of this report.

Rock (pore volume) compressibility.

Four samples were selected to undergo rock (pore volume) compressibility analysis.

Each sample was evacuated and pressure saturated with the simulated formation brine. Samples were then loaded into a hydrostatic core holder and allowed to equilibrate at a low net overburden pressure. The net overburden pressure was then raised incrementally and the corresponding pore volume reductions monitored. The overburden pressure was raised to the next higher pressure only when pore volume reduction stabilised.

Hydrostatic compressibility data were then calculated from pore volume reduction data versus increasing overburden pressure. These data were converted to equivalent uniaxial loading following procedures outlined by Dirk Teeuw of Shell Research.

Results are presented in SECTION 5.

APPENDIX-2

RAWDATA FROM ELECTRICAL PROPERTIES, CAPILLARY PRESSURE AND ROCK COMPRESSIBILITY TESTS

RESISTIVITY MEASUREMENTS - RAWDATA

Sample	5
PV (NOBP),cc	5.852
Porosity (NOBP).%	13.4
Length,cm	4.01
Diameter,cm	3.76
Brine density,g/cc	1.007
Brine Rw.ohm-m	0.415

Saturation %PV	Rt ohm-m
84.9	24.36
72.6	30.64
67.3	36.69
61.9	39.12
54.9	44.12

Sample	12
PV (NOBP),cc	8.387
Porosity (NOBP).%	17.2
Length,cm	4.41
Diameter,cm	3.79
Brine density,g/cc	1.007
Brine Rw.ohm-m	0.415

Saturation %PV	Rt ohm-m
74.6	24.39
71.0	25.29
62.4	29.14
55.8	37.53
44.2	49.51

Sample	27
PV (NOBP),cc	8.368
Porosity (NOBP).%	17.9
Length,cm	4.37
Diameter,cm	3.73
Brine density,g/cc	1.007
Brine Rw.ohm-m	0.415

Saturation %PV	Rt ohm-m
74.3	18.67
58.3	27.17
45.4	41.82
40.4	49.60
37.4	54.36

Sample	44
PV (NOBP),cc	6.927
Porosity (NOBP).%	14.9
Length,cm	4.22
Diameter,cm	3.78
Brine density,g/cc	1.007
Brine Rw.ohm-m	0.415

Saturation %PV	Rt ohm-m
82.8	19.74
78.3	23.97
67.0	31.05
52.0	45.69
43.1	56.08

Sample	76
PV (NOBP),cc	9.700
Porosity (NOBP).%	20.7
Length,cm	4.21
Diameter,cm	3.786
Brine density,g/cc	1.007
Brine Rw.ohm-m	0.415

Saturation %PV	Rt ohm-m
60.3	24.74
56.2	27.85
52.0	31.24
41.4	46.03
35.2	56.12
31.0	64.58

Sample	93
PV (NOBP),cc	8.188
Porosity (NOBP).%	17.3
Length,cm	4.24
Diameter,cm	3.79
Brine density,g/cc	1.007
Brine Rw.ohm-m	0.415

Saturation %PV	Rt ohm-m
70.1	25.70
60.8	30.04
53.9	39.69
49.0	49.35
41.5	64.45

RESISTIVITY MEASUREMENTS - RAWDATA

Sample	97
PV (NOBP),cc	10.289
Porosity (NOBP).%	21.6
Length,cm	4.26
Diameter,cm	3.79
Brine density,g/cc	1.007
Brine Rw.ohm-m	0.415

Saturation %PV	Rt ohm-m
58.5	23.12
48.1	30.53
41.7	37.12
32.8	53.48
26.8	74.70

Sample	118
PV (NOBP),cc	6.978
Porosity (NOBP).%	14.5
Length,cm	4.3
Diameter,cm	3.79
Brine density,g/cc	1.007
Brine Rw.ohm-m	0.415

Saturation %PV	Rt ohm-m
72.8	25.29
55.2	43.01
47.9	52.94
43.5	62.29
38.3	70.60

Sample	128
PV (NOBP),cc	5.396
Porosity (NOBP).%	11.2
Length,cm	4.29
Diameter,cm	3.79
Brine density,g/cc	1.007
Brine Rw.ohm-m	0.415

Saturation %PV	Rt ohm-m
80.8	33.05
71.4	41.06
65.8	47.49
60.1	52.77
52.6	65.93

Sample	146
PV (NOBP),cc	7.684
Porosity (NOBP).%	15.1
Length,cm	4.55
Diameter,cm	3.80
Brine density,g/cc	1.007
Brine Rw.ohm-m	0.415

Saturation %PV	Rt ohm-m
61.0	39.23
51.9	48.69
48.1	58.87
44.2	65.68
36.4	84.01

Sample	181
PV (NOBP),cc	8.661
Porosity (NOBP).%	19.1
Length,cm	4.07
Diameter,cm	3.78
Brine density,g/cc	1.007
Brine Rw.ohm-m	0.415

Saturation %PV	Rt ohm-m
61.1	27.84
55.0	34.68
45.3	50.55
41.7	57.56
34.4	79.16

Sample	186
PV (NOBP),cc	5.516
Porosity (NOBP).%	14.3
Length,cm	4.18
Diameter,cm	3.79
Brine density,g/cc	1.007
Brine Rw.ohm-m	0.415

Saturation %PV	Rt ohm-m
78.2	26.26
72.9	30.80
65.4	35.03
59.4	43.45
54.9	49.95
47.3	62.69

RESISTIVITY MEASUREMENTS - RAWDATA

Sample	187
PV (NOBP),cc	7.805
Porosity (NOBP).%	16.5
Length,cm	4.23
Diameter,cm	3.78
Brine density,g/cc	1.007
Brine Rw.ohm-m	0.415

Saturation %PV	Rt ohm-m
70.6	21.93
62.9	26.44
56.6	32.70
50.2	37.12
45.1	42.84

Sample	244
PV (NOBP),cc	6.518
Porosity (NOBP).%	11.9
Length,cm	4.88
Diameter,cm	3.79
Brine density,g/cc	1.007
Brine Rw.ohm-m	0.415

Saturation %PV	Rt ohm-m
70.9	37.56
58.3	65.10
53.6	75.21
41.0	99.96
34.7	141.15

Sample	246
PV (NOBP),cc	7.931
Porosity (NOBP).%	15.5
Length,cm	4.57
Diameter,cm	3.79
Brine density,g/cc	1.007
Brine Rw.ohm-m	0.415

Saturation %PV	Rt ohm-m
59.8	44.23
51.6	58.35
46.6	69.01
32.0	126.40
25.7	159.18

Sample	241
PV (NOBP),cc	11.16
Porosity (NOBP).%	21.2
Length,cm	4.77
Diameter,cm	3.80
Brine density,g/cc	1.007
Brine Rw.ohm-m	0.415

Saturation %PV	Rt ohm-m
62.0	17.78
41.0	30.46
31.8	46.59
27.4	63.25
23.0	90.27
16.6	155.64
15.2	169.08

Sample	205
PV (NOBP),cc	9.898
Porosity (NOBP).%	19.3
Length,cm	4.61
Diameter,cm	3.79
Brine density,g/cc	1.007
Brine Rw.ohm-m	0.415

Saturation %PV	Rt ohm-m
77.1	14.76
53.4	28.59
48.2	37.15
42.9	46.22
37.6	57.52
27.1	87.80
19.7	121.22

Sample	234
PV (NOBP),cc	12.045
Porosity (NOBP).%	24.1
Length,cm	4.54
Diameter,cm	3.79
Brine density,g/cc	1.007
Brine Rw.ohm-m	0.415

Saturation %PV	Rt ohm-m
67.0	12.09
59.8	13.89
53.6	16.21
46.4	19.74
32.1	39.13
28.5	52.95
11.5	235.36

Centrifuge Air-Brine Capillary Pressure - RAWDATA

Sample	5
Pore Vol	6.13
Length	4.01

RPM	Fluid Out (cc)
440	0
630	0
1000	0
1560	0
2250	0.33
3180	0.83
4500	1.33
6370	1.86
8430	2.33
10500	2.66

Sample	12
Pore Vol	8.742
Length	4.41

RPM	Fluid Out (cc)
440	0
630	0
1000	0
1560	0
2250	0.83
3180	2.33
4500	3.49
6370	4.33
8430	4.99
10500	5.59

Sample	27
Pore Vol	8.675
Length	4.37

RPM	Fluid Out (cc)
440	0
630	0
1000	0.60
1560	1.33
2250	2.40
3180	3.00
4500	3.99
6370	4.83
8430	5.09
10500	5.19

Sample	44
Pore Vol	7.216
Length	4.22

RPM	Fluid Out (cc)
440	0.00
630	0.00
1000	0.00
1560	0.66
2250	2.00
3180	2.66
4500	3.33
6370	3.99
8430	4.26
10500	4.39

Sample	76
Pore Vol	10.032
Length	4.21

RPM	Fluid Out (cc)
440	0.00
630	0.00
1000	0.00
1560	1.33
2250	3.00
3180	3.99
4500	5.39
6370	5.99
8430	6.49
10500	6.66

Sample	93
Pore Vol	8.382
Length	4.24

RPM	Fluid Out (cc)
440	0.00
630	0.00
1000	0.66
1560	1.50
2250	2.73
3180	3.33
4500	4.33
6370	4.99
8430	5.49
10500	5.66

Centrifuge Air-Brine Capillary Pressure - RAWDATA

Sample	97
Pore Vol	10.501
Length	4.26

RPM	Fluid Out (cc)
440	0.00
630	0.83
1000	1.33
1560	3.66
2250	4.99
3180	5.99
4500	6.66
6370	7.32
8430	7.66
10500	7.82

Sample	118
Pore Vol	7.262
Length	4.30

RPM	Fluid Out (cc)
440	0.00
630	0.00
1000	0.00
1560	1.00
2250	1.66
3180	2.50
4500	3.33
6370	4.16
8430	4.49
10500	4.66

Sample	128
Pore Vol	5.815
Length	4.29

RPM	Fluid Out (cc)
440	0.00
630	0.00
1000	0.00
1560	0.63
2250	1.00
3180	1.33
4500	1.83
6370	2.66
8430	3.16
10500	3.33

Sample	146
Pore Vol	8.091
Length	4.55

RPM	Fluid Out (cc)
440	0.00
630	0.00
1000	0.00
1560	0.16
2250	1.33
3180	3.00
4500	3.73
6370	4.49
8430	4.99
10500	5.26

Sample	246
Pore Vol	8.143
Length	4.57

RPM	Fluid Out (cc)
440	0.00
630	0.00
1000	0.33
1560	1.00
3180	4.99
4500	5.99
6370	6.33
8430	6.39
10500	6.46

Sample	181
Pore Vol	8.978
Length	4.07

RPM	Fluid Out (cc)
440	0.00
630	0.00
1000	0.16
1560	1.00
3180	4.16
4500	5.33
6370	5.99
8430	6.46
10500	6.66

Centrifuge Air-Brine Capillary Pressure - RAWDATA

Sample	186
Pore Vol	7.347
Length	4.23

RPM	Fluid Out (cc)
440	0.00
630	0.00
1000	0.00
1560	0.16
2250	0.66
4500	2.00
6370	3.16
8430	3.66
10500	3.83

Sample	187
Pore Vol	8.176
Length	4.23

RPM	Fluid Out (cc)
440	0.00
630	0.00
1000	0.00
1560	0.00
2250	0.66
3180	1.66
4500	2.83
6370	3.99
8430	4.66
10500	4.99

Sample	205
Pore Vol	10.156
Length	4.61

RPM	Fluid Out (cc)
440	0.00
630	1.00
1000	2.50
1560	4.83
3180	6.72
4500	7.66
6370	8.06
8430	8.16
10500	8.19

Sample	234
Pore Vol	12.439
Length	4.54

RPM	Fluid Out (cc)
440	5.33
630	6.99
1000	8.82
1560	9.99
3180	11.52
4500	11.85
6370	11.85

Sample	241
Pore Vol	11.156
Length	4.77

RPM	Fluid Out (cc)
440	4.33
630	7.32
1000	8.99
1560	10.15
3180	10.55
4500	10.62
6370	10.65

Sample	244
Pore Vol	6.783
Length	4.88

RPM	Fluid Out (cc)
440	0.00
630	0.00
1000	0.00
1560	0.33
2250	0.66
3180	1.33
4500	2.63
6370	3.49
8430	3.83
10500	3.99

Rock Compressibility - RAWDATA

Company : **WOODSIDE ENERGY LIMITED**
Well : **THYLACINE-2**

Sample	5A		
Pore Vol.	8.163		
Porosity	16.6		
Bulk Vol.	49.199	**Grain Vol.**	41.036
Length	4.380		
Diameter	3.790		
Area	11.283		

OB (psi)	Pore Volume	Bulk Volume	Porosity (%)
400	8.163	49.199	16.6
500	8.129	49.165	16.5
600	8.106	49.142	16.5
700	8.084	49.120	16.5
800	8.062	49.098	16.4
900	8.041	49.077	16.4
1000	8.021	49.057	16.4
1200	7.982	49.018	16.3
1400	7.947	48.983	16.2
1600	7.913	48.949	16.2
1800	7.882	48.918	16.1
2000	7.853	48.889	16.1
2500	7.788	48.824	16.0
3000	7.733	48.769	15.9
3500	7.687	48.723	15.8
4000	7.649	48.685	15.7
4500	7.616	48.652	15.7
5000	7.588	48.624	15.6
6000	7.546	48.582	15.5
7000	7.516	48.552	15.5

Sample	76A		
Pore Vol.	9.88		
Porosity	21.2		
Bulk Vol.	46.660	**Grain Vol.**	36.78
Length	4.180		
Diameter	3.800		
Area	11.343		

OB (psi)	Pore Volume	Bulk Volume	Porosity (%)
400	9.880	46.660	21.2
500	9.826	46.606	21.1
600	9.787	46.567	21.0
700	9.753	46.533	21.0
800	9.723	46.503	20.9
900	9.695	46.475	20.9
1000	9.671	46.451	20.8
1200	9.627	46.407	20.7
1400	9.588	46.368	20.7
1600	9.555	46.335	20.6
1800	9.524	46.304	20.6
2000	9.496	46.276	20.5
2500	9.436	46.216	20.4
3000	9.385	46.165	20.3
3500	9.341	46.121	20.3
4000	9.302	46.082	20.2
4500	9.266	46.046	20.1
5000	9.234	46.014	20.1
6000	9.178	45.958	20.0
7000	9.128	45.908	19.9

Rock Compressibility - RAWDATA

Sample	97A		
Pore Vol.	8.279		
Porosity	16.8		
Bulk Vol.	49.369	Grain Vol.	41.09
Length	4.390		
Diameter	3.800		
Area	11.343		

OB (psi)	Pore Volume	Bulk Volume	Porosity (%)
400	8.279	49.369	16.8
500	8.237	49.327	16.7
600	8.202	49.292	16.6
700	8.173	49.263	16.6
800	8.147	49.237	16.5
900	8.123	49.213	16.5
1000	8.102	49.192	16.5
1200	8.065	49.155	16.4
1400	8.033	49.123	16.4
1600	8.004	49.094	16.3
1800	7.979	49.069	16.3
2000	7.956	49.046	16.2
2500	7.907	48.997	16.1
3000	7.866	48.956	16.1
3500	7.830	48.920	16.0
4000	7.799	48.889	16.0
4500	7.771	48.861	15.9
5000	7.746	48.836	15.9
6000	7.702	48.792	15.8
7000	7.665	48.755	15.7

Sample	118A		
Pore Vol.	6.603		
Porosity	15.0		
Bulk Vol.	44.107	Grain Vol.	37.504
Length	3.930		
Diameter	3.810		
Area	11.402		

OB (psi)	Pore Volume	Bulk Volume	Porosity (%)
400	6.603	44.107	15.0
500	6.558	44.062	14.9
600	6.522	44.026	14.8
700	6.492	43.996	14.8
800	6.466	43.970	14.7
900	6.443	43.947	14.7
1000	6.422	43.926	14.6
1200	6.387	43.891	14.6
1400	6.356	43.860	14.5
1600	6.330	43.834	14.4
1800	6.307	43.811	14.4
2000	6.287	43.791	14.4
2500	6.243	43.747	14.3
3000	6.207	43.711	14.2
3500	6.177	43.681	14.1
4000	6.151	43.655	14.1
4500	6.128	43.632	14.0
5000	6.107	43.611	14.0
6000	6.071	43.575	13.9
7000	6.041	43.545	13.9

Origin Energy

THYLACINE 2
COMPOSITE WELL LOG

Well Location Map



Well Data Card

Name	Thylacine 2
Well Type	Vertical Exploration
Rig Name	Ocean Monarch
Spud	19 Jun 01
Status	Suspended
Location	115 km SW of Perth
Latitude	33° 41' 14.61" S (GDA94) 33° 41' 14.61" S (GDA94)
Longitude	114° 55' 48.36" E (GDA94) 114° 55' 48.36" E (GDA94)
Grid	MGA Zone 50
Water Depth	1,014 m (LAT) 1,014 m (LAT)
Total Depth	4,100 m (MD) 4,100 m (MD)
Total Depth	4,100 m (TVD) 4,100 m (TVD)
Penetration	3,086 m 3,086 m
Bottom Hole Temperature	124 °C (at 4,100 m MD)
Max Deviation	0.5° (at 2,400 m MD)
Rig Floor Height	23 m (above MSL)
Kelly Bushing	23 m (above MSL)
Ground Level	-991 m (above MSL)
Total Depth	4,100 m
Total Depth	4,100 m
Total Depth	4,100 m